THE ROLE OF THE HEDGEHOG SIGNALLING PATHWAY IN ACUTE MYELOID LEUKAEMIA

Victoria L Campbell

FRCPath MRCP MBBS BSc (Hons)

Submitted in fulfilment of the requirements for the degree of Doctor of Philosophy

December 2017

Section of Experimental Haematology
Institute of Cancer Sciences
College of Medical, Veterinary and Life Sciences
University of Glasgow

Abstract

Acute myeloid leukaemia (AML) encompasses a group of aggressive haematological neoplasms. It is a cancer stem cell (CSC) disorder. The Hedgehog (Hh) signalling pathway is one of the self-renewal pathways, highly conserved across species and important in determining stem cell fate, affecting a number of clinically important downstream targets including the Bcl-2 family. Abnormal Hh signalling has been associated with a diverse range of human malignancies. In myeloid malignancies, Hh signalling has been found to be vital in the maintenance and expansion of the CSC.

Primary immotile cilia regulate canonical Hh signal transduction. These highly specialised organelles are present in single-celled eukaryotes through to humans, with defective primary cilia expression being linked to disease.

It is unclear whether haematopoietic cells, normal or malignant, express primary cilia and the role the Hh pathway plays in the pathophysiology of AML. We sought to answer these questions, and further, to determine whether the Hh signalling pathway represented a therapeutic target in AML.

Analysis of primary human AML mononuclear cells (MNCs) (n=76) showed the Hh pathway to be deregulated. *SMO* was significantly deregulated ($p<0.0001$) with two divergent cohorts identified. *GLI-1*, indicative of pathway activity, was detected in 52.6% of samples. Sanger sequencing (n=36) did not identify a mutation in *SMO* to account for the pathway deregulation though a number of silent and missense mutations were identified (mean 1; range 1-3). 25% of our AML samples (9/37) showed expression of GLI-1 in >10% of cells by immunohistochemistry (IHC) on formalin fixed paraffin embedded (FFPE) primary human bone marrow trephines (BMTs) compared to none of our normal controls (n=10) ($p<0.0001$). GLI-1 expression was independent of SMO and PTCH-1. SHH was significantly down-regulated ($p<0.001$) within the blast population whilst secreted SHH, measured by enzyme-linked immunosorbant assay, was up-regulated suggesting paracrine activity. Impaired post-translational modification of SHH was demonstrated with protein located within the nuclei by IHC and immunocytochemistry (ICC). Nuclear expression of SHH was limited to primitive (CD34+) haematopoietic cells and absent from mature haematopoietic (CD14+, CD15+) cells. This correlated with a 20-fold reduction in *HHAT,* the acetyltransferase involved in Hh processing, in normal primitive haematopoietic cells compared to normal MNCs ($p<0.01$). There was no correlation between subtype, mutational profile or clinical outcome and any of the components of the Hh pathway.

Primary immotile cilia were identified in all AML (n=23), and 20% of normal (n=10) primary human FFPE BMTs by ICC. Primary cilia were not identified in AML cell lines (n=7) or primitive (n=4) or mature haematopoietic cells (n=6) isolated from peripheral blood, suggesting they are lost once cells migrate from the bone marrow (BM) microenvironment.

In vitro, SMO inhibition with 20μM cyclopamine reduced cell proliferation by trypan blue exclusion in select, genetically diverse AML cell lines (HL-60, Kasumi-1, KG1a, MOLM-13, MV4-11, OCI-AML3 and THP-1). No change in early or late apoptosis was seen in HL-60, KG1a, MV4-11, OCI-AML3 and THP-1 by flow cytometry (FACS). In contrast an increase in the number of dead cells by trypan blue exclusion was seen in Kasumi-1 ($p<0.01$) and MOLM-13 ($p<0.05$) with apoptosis confirmed by FACS (both $p<0.05$). Culture of the OCI-AML3 cell line with cyclopamine led to cell cycle arrest with an increase in G0-G1 cells ($p<0.05$), and a 3-fold reduction in cell division by CFSE (p=ns); striking morphological changes were seen with an increase in cytoplasm, granules and vacuoles and loss of nucleoli, with FACS analysis demonstrating increased expression of CD11b ($p<0.001$) and CD11c ($p<0.0001$) consistent with a more mature phenotype. Early haematopoietic markers *NAB2, GATA1, EGR2, SCL, IRF8* and *EGR1* were down-regulated whilst *PU1, GCSF* and *MPO* involved in differentiation and maturation were up-regulated (p=ns) in cyclopamine treated cells.

Colony forming cell (CFC) assays showed a statistically significant reduction in the more pluripotent CFU-GM ($p=0.006$) colonies and an increase in omnipotent CFU-G ($p=0.013$) colonies following culture with cyclopamine 20μM.

There is extensive evidence supporting Bcl-2 is altered in malignancy; its role in AML cell maintenance and survival, is well recognised. Further, Bcl-2 is a key downstream target of the Hh signalling pathway. Complete linkage analysis found key members of the Bcl-2 family and cell cycle regulators to cluster with components of the Hh signalling pathway. Sensitivity to the BH3 mimetic ABT-199 was not solely dependent on the expression of Bcl-2, rather a complex interplay between the pro-apoptotic and anti-apoptotic family members. Targeting Bcl-2 had a variable effect on KG1a, MOLM-13, MV4-11, OCI-AML3 and THP-1 cells; combination treatment with ABT-199 and Ara-C showed a highly synergistic effect on cell death in MOLM-13 cells (Chou-Talalay CI<0.47 (range 0.13-0.47) and DRI>2 (range 2-70) for all dose combinations).

We show the Hh signalling pathway to be deregulated in AML, expression of components of the pathway changing with myeloid maturation. We demonstrate primary cilia on haematopoietic cells within the BM, with an increased frequency observed in AML. Their absence when cells migrate from the BM fits with their function and suggests a 'switching off' of canonical signalling on maturation. In the absence of primary cilia, we show the Hh pathway remains active, suggesting a role for non-canonical signalling in AML. Pharmacological inhibition led to both apoptosis and differentiation; preliminary results suggest the effect is dependent upon the degree of SMO inhibition. We believe further work is required to determine the role of the Hh signalling pathway in normal and malignant haematopoiesis but that our data, considered especially in context with other recently published studies provides a rationale to continue to explore SMO or downstream Bcl-2 pathway inhibition as potential therapies in AML.

Table of Contents

Abstract
Table of contents
List of Tables
List of Figures
Related publications
Acknowledgements
Author's declaration
List of abbreviations

1. Introduction

    1.1 Stem cells
        1.1.1 Stem cell niche
        1.1.2 Haematopoiesis and the haematopoietic stem cell
        1.1.3 Bone marrow microenvironment

    1.2 Cancer
        1.2.1 Cancer stem cells
        1.2.2 Leukaemic stem cell

    1.3 Leukaemia
        1.3.1 Acute myeloid leukaemia (AML)
        1.3.2 Pre-leukaemia
        1.3.3 Clonal haematopoiesis of indeterminate potential
        1.3.4 Chemoresistance
        1.3.5 Investigational therapies

    1.4 Hedgehog signalling pathway
        1.4.1 Canonical signalling
        1.4.2 Non-canonical signalling
            1.4.2.1 Type I (Smo-independent)
            1.4.2.2 Type II (Gli-independent)
        1.4.3 Hedgehog signalling in haematopoiesis
        1.4.4 Hedgehog signalling in malignancy
            1.4.4.1 Hedgehog signalling in AML
        1.4.5 Targeting the hedgehog signalling pathway
            1.4.5.1 Targeting the hedgehog signalling pathway in haematological malignancies
        1.4.6 Primary cilia
        1.4.7 Downstream targets

    1.5 B-cell lymphoma 2 (Bcl-2) Family
        1.5.1 Bcl-2 induced apoptotic cell death cascade
            1.5.1.1 Bcl-2 and necrosis
            1.5.1.2 Bcl-2 and autophagy
            1.5.1.3 Bcl-2 and haematopoiesis
            1.5.1.4 Bcl-2 and malignancy
            1.5.1.5 Bcl-2 in AML

1.6 ATP-Binding Cassette (ABC) transporters
1.6.1 ABC transporters and haematopoiesis
1.6.2 ABC transporters and malignancy
1.6.3 ABC transporters in AML

Aims

2. Materials and Methods

2.1 Materials
2.1.1 Tissue culture
2.1.2 Molecular Studies:
2.1.2.4 Reverse transcription
2.1.2.5 Polymerase chain reactions
2.1.2.8 Fluidigm qRT-PCR
2.1.2.9 Sanger Sequencing
2.1.2.10 Next-generation sequencing
2.1.3 Protein expression
2.1.4 Western Blotting
2.1.5 Immunocytochemistry
2.1.6 Immunohistochemistry
2.1.7 Flow cytometry
2.1.8 Electron microscopy

2.2 Methods

2.2.1 Tissue culture
2.2.1.1 Drugs and reagents
2.2.1.2 Cell culture
2.2.1.2.1 AML cell lines
2.2.1.2.1.1 Cell line recovery post cryopreservation
2.2.1.2.1.2 Passaging AML cell lines
2.2.1.2.2 Stromal cell lines
2.2.1.2.2.1 Passaging stromal cell lines
2.2.1.2.3 Cryopreservation of cell lines
2.2.1.2.4 Isolation of mononuclear cells (MNCs)
2.2.1.2.5 Primary cell recovery post cryopreservation
2.2.1.2.6 Primary AML cell culture
2.2.1.2.7 Mesenchymal stem cells derived from human BM samples
2.2.1.2.7.1 Isolation of MSCs from human BM samples
2.2.1.2.7.2 Passage of MSCs
2.2.1.2.8 Cryopreservation of primary AML and MSCs
2.2.1.2.9 Processing of patient plasma
2.2.1.3 Resazurin assay
2.2.1.4 Luciferase assay
2.2.1.5 Cell counting and viability assessment
2.2.1.7 Synergy studies
2.2.1.8 ß-Galactosidase Cell staining
2.2.1.9 Colony Forming Cell assay
2.2.1.10 Cellular transfection

2.2.2 Molecular studies
- 2.2.2.1 RNA extraction and quantification
- 2.2.2.2 cDNA synthesis
- 2.2.2.3 Polymerase chain reaction (PCR)
  - 2.2.2.3.1 RT-PCR
  - 2.2.2.3.2 Quantitative Real-Time PCR (qRT-PCR) by Fluidigm®
    - 2.2.2.3.2.1 Pre-amplification
    - 2.2.2.3.2.2 qRT-PCR
- 2.2.2.4 Gene expression array
- 2.2.2.5 DNA extraction and quantification
- 2.2.2.6 Sequencing
  - 2.2.2.6.1 Sanger sequencing
    - 2.2.2.6.1.1 DNA template amplification and purification by PCR
    - 2.2.2.6.1.2 Cycle sequencing
    - 2.2.2.6.1.3 Sequencing reaction purification by ethanol precipitation
    - 2.2.2.6.1.4 Capillary electrophoresis
- 2.2.2.7.2 Next-generation sequencing
  - 2.2.2.7.2.1 Ion AmpliSeq PGM™
  - 2.2.2.7.2.2 Illumina TruSight®

2.2.3 Protein studies
- 2.2.3.1 Protein extraction and quantification
- 2.2.3.2 Sodium dodecyl sulfate polyacrylamide gel electrophoresis Western blotting
- 2.2.3.3 Immunocytochemistry on cultured cells
- 2.2.3.4 Immunocytochemistry on fresh frozen, paraffin-embedded (FFPE), EDTA-decalcified bone marrow trephines (BMTs)
- 2.2.3.5 Immunohistochemistry on FFPE BMTs
- 2.2.3.7 Enzyme-linked immunosorbant assay

2.2.4 Flow cytometry
- 2.2.4.1 Apoptosis assessment
  - 2.2.4.1.1 Annexin/7AAD staining
  - 2.2.4.1.2 Tetramethylrhodamine methyl ester staining
- 2.2.4.2 Proliferation studies
  - 2.2.4.2.1 Propidium Iodide staining
  - 2.2.4.2.2 Carboxyfluorescein succinimidyl ester staining
  - 2.2.4.2.3 Cell Trace™ Violet staining
- 2.2.4.4 Detection of surface antigen expression
- 2.2.4.5 Intracellular antibody staining
  - 2.2.4.5.1 pBcl-2

2.2.5 Electron microscopy
- 2.2.5.1 Electron microscopy

2.2.6 Statistical analysis

List of Tables

Table 1.1: WHO Classification
Table 1.2: Current Phase III clinical trials for untreated AML
Table 1.3: Characteristics of older and younger adults with AML
Table 1.4: Recently presented investigational therapies and proposed mechanism of action
Table 1.5: Hedgehog inhibitors
Table 1.6: Clinical trials involving hedgehog inhibitors
Table 1.7: ABC transporter families and their functions

Table 2.1.1.1: Plastics for Tissue Culture and Suppliers
Table 2.1.1.2: Reagents for Tissue Culture and Suppliers
Table 2.1.1.3: All-inclusive 'Kits' for Tissue Culture and Suppliers
Table 2.1.1.4: Equipment for Tissue Culture and Suppliers
Table 2.1.1.5: AML Cell Lines and Characteristics
Table 2.1.1.6: Stromal Cell Lines and Characteristics
Table 2.1.1.7: Cell Line Culture Conditions
Table 2.1.1.8: 10% Media for Cell Line Culture
Table 2.1.1.9: 20% Media for Cell Line Culture
Table 2.1.1.10: Media for M210-B4 Culture
Table 2.1.1.11: Media for SL-SL Culture
Table 2.1.1.12: Media for TM3 Culture
Table 2.1.1.13: Media for Cell Line Cryopreservation
Table 2.1.1.14: Media for Primary AML Cell Culture
Table 2.1.1.15: Media for MSC Culture
Table 2.1.1.16: Media for Thawing Primary Samples
Table 2.1.1.17: Freezing media for Primary AML and MSC Samples
Table 2.1.1.18: Reagents for CFC Assay
Table 2.1.1.19: SFM for primary cell culture
Table 2.1.1.20: SFM with high concentration growth factor cocktail
Table 2.1.1.21: Drugs Tested and Suppliers

Table 2.1.2.1: Plastics for Molecular Studies and Suppliers
Table 2.1.2.2: Molecular Reagents and Suppliers
Table 2.1.2.3: Molecular Equipment and Programmes and Suppliers
Table 2.1.2.4.1: Reverse transcription master mix Step 1
Table 2.1.2.4.2: Reverse transcription master mix Step 2
Table 2.1.2.4.3: Reverse Transcription Cycling Conditions
Table 2.1.2.5.1: GoTaq® reverse transcription PCR (RT-PCR) mastermix
Table 2.1.2.5.2: GoTaq® RT-PCR Mastermix Cycling Conditions
Table 2.1.2.6: Taqman® Probes aware this needs completing
Table 2.1.2.7: Primers
Table 2.1.2.8.1: Pre-amplification mix - Primer
Table 2.1.2.8.2: Pre-amplification mix – Probe (Taqman®)
Table 2.1.2.8.3: Pre-amplification Cycling Conditions
Table 2.1.2.8.4: Exonuclease treatment mix for use after primer pre-amplification
Table 2.1.2.8.4.1: Exonuclease treatment Cycling Conditions
Table 2.1.2.8.5: Assay mix for Fluidigm qRT PCR - Primer
Table 2.1.2.8.5.1: Sample mix for Fluidigm qRT PCR - Primer
Table 2.1.2.8.6: Assay mix for Fluidigm qRT PCR - Probe
Table 2.1.2.8.6.1: Sample mix for Fluidigm qRT PCR - Probe
Table 2.1.2.8.7: Fluidigm qRT PCR Cycling Conditions
Table 2.1.2.9.1: *SMO* Primers

Table 2.1.2.9.2: *SMO* RT-PCR Master mix
Table 2.1.2.9.3: *SMO* RT-PCR
Table 2.1.2.9.4: *SMO* RT-PCR Product Clean Up
Table 2.1.2.9.5: *SMO* Sequencing Master mix
Table 2.1.2.9.6: *SMO* Cycle Sequencing
Table 2.1.2.10.1: Targets for Ion AmpliSeq™ Research genes panel
Table 2.1.2.10.1.1: Ion AmpliSeq™ Sequencing Conditions
Table 2.1.2.10.2: Targets for Illumina TruSight® Myeloid Sequencing panel
Table 2.1.2.10.2.1: Illumina TruSight® Sequencing Conditions
Table 2.1.3.1: Reagents for Protein Preparation
Table 2.1.3.2: Solution for Protein Extraction
Table 2.1.4.1: Reagents and Suppliers
Table 2.1.4.2: Equipment and Suppliers
Table 2.1.4.3: 5% Sample Buffer
Table 2.1.4.4: 10X TBS Buffer pH 7.5
Table 2.1.4.5: 1X TBS Buffer pH 7.5
Table 2.1.4.6: 1X TBSN Buffer
Table 2.1.4.7: 10X SDS Page Running Buffer
Table 2.1.4.8: 1X SDS Page Running Buffer
Table 2.1.4.9: 10X Semi-Dry Transfer Buffer Stock
Table 2.1.4.10: 1X Semi-Dry Transfer Buffer
Table 2.1.4.11: Running Gel
Table 2.1.4.12: 5% Stacking Gel
Table 2.1.4.13: 5X BSA Blocking solution
Table 2.1.4.14: Antibody Conditions for Western blots

Table 2.1.4.5: 1X TBSN Buffer
Table 2.1.4.6: SDS Page Running Buffer
Table 2.1.4.7: Running Gel
Table 2.1.4.8: 5% Stacking Gel
Table 2.1.4.9: 5X BSA Blocking solution
Table 2.1.4.10: Antibody Conditions for Western blots
Table 2.1.5.1: Reagents and Suppliers for Immunocytochemistry
Table 2.1.5.2: Equipment for Immunocytochemistry
Table 2.1.5.3: 5X Block
Table 2.1.5.4: Antibody Conditions for Immunocytochemistry
Table 2.1.6.1: Reagents and suppliers for Immunohistochemistry
Table 2.1.6.2: Equipment for Immunohistochemistry
Table 2.1.6.3: Antibody Conditions for Immunohistochemistry
Table 2.1.7.1: Plastics for Flow Cytometry
Table 2.1.7.2: Equipment for Flow Cytometry
Table 2.1.7.3: Reagents for Flow Cytometry
Table 2.1.7.4: 1X HBSS
Table 2.1.7.5: FACS Buffer – FBS / 2% PBS
Table 2.1.7.6: Quenching solution for CFSE assay
Table 2.1.7.7: Antibodies for Flow Cytometry

Table 4.1.3.1: IC_{50} values for cyclopamine in seven, genetically diverse, AML cell lines as determined by the resazurin assay
Table 5.3.2.1: *BAX*/*BCL-2* and *BAK*/*BCL-2* expression ratios in seven genetically diverse AML cell lines
Table 5.3.3.1: IC_{50} values for ABT-199, HA14-1 and TW37 (select BH3 mimetics) in five genetically diverse AML cell lines as determined by the resazurin assay

Tables 5.3.4.1A&B: IC_{50}, and ED_{50}, for ABT-199 and Ara-C in the MOLM-13 and OCI-AML3 cell lines following culture for 72hrs
Table 5.3.9.1: *BAX*/*BCL-2* and *BAK*/*BCL-2* expression ratios following culture of the MOLM-13 and OCI-AML3 cell lines with ABT-199, Ara-C and the combination of ABT-199 and Ara-C for 72hrs

List of Figures

Figure 1.1: Stem cell hierarchy
Figure 1.2: Human haematopoietic hierarchy
Figure 1.3: Schematic illustrating the differences between the classical and redefined models of the haematopoietic hierarchy
Figure 1.4: Bone marrow microenvironment
Figure 1.5: Cancer cell model
Figure 1.6: Canonical Hh signalling
Figure 1.7: Non-canonical Hh signalling
Figure 1.8: Primary cilium
Figure 1.9: Model demonstrating how primary cilia have been linked to cancer
Figure 1.10: Downstream targets of the Hh signalling pathway
Figure 1.11: The Bcl-2 family
Figure 1.12: Schematic illustrating the role of Bcl-2 in cell death pathways

Figure 2.1: Luciferase activity of the Gli luciferase reporting TM3$^{(GLI\text{-}Luc)}$ cell line following culture with increasing concentrations of cyclopamine
Figure 2.2: Representative ICC image depicting cilia on the mucosal surface of the trachea from a mouse
Figure 2.3: Representative FSC / SSC and Annexin V/ 7AAD plots for the OCI-AML3 cell line
Figure 2.4: Diagrammatic representation of the cell cycle
Figure 2.5: Representative histogram showing a progressive reduction in CFSE fluorescence intensity with each successive cell division in the OCI-AML3 cell line

Figure 3.1.2.1: Variance in the baseline gene expression of members of the Hh signalling pathway in an unselected cohort of *de novo* primary human AML samples (n=76)
Figure 3.1.2.2: Variance in expression of components of the Hh pathway between normal bulk MNCs, CD34+ selected PB and CD34+ selected BM cells
Figure 3.1.2.3: *SMO* expression in an unselected cohort of *de novo* primary AML MNCs relative to normal CD34+ selected cells
Figure 3.1.2.4: *SMO* expression in an unselected cohort of *de novo* primary AML MNC samples (n=76) relative to normal unselected MNCs and normal CD34+ selected cells
Figure 3.1.3.1: Heatmap showing heterogeneous expression of components of the Hh pathway in primary human AML MNCs
Figure 3.1.4.1 A, B&C: Expression of the Hh ligands in a cohort of primary, *de novo* AML samples as determined by IHC showing SHH to be significantly down-regulated in AML BMTs
Figure 3.1.4.2: SHH in primary human (A) colon (control tissue) at x4 magnification, (B) normal BMT at x10 magnification and (C) AML BMT at x20 magnification showing cytoplasmic and nuclear expression. (Bi & Ci) are magnified images showing cytoplasmic (Bi) and nuclear and cytoplasmic staining (Ci)
Figure 3.1.4.3: Expression of PTCH1 and GLI-1 in a cohort of primary *de novo* AML BMTs relative to normal BMTs
Figure 3.1.5.1: *HHAT* expression in HSCs relative to normal bulk MNCs
Figure 3.1.5.2: SHH concentration within serum from primary, *de novo* AML and normal subjects by ELISA
Figure 3.2.2.1: Representative confocal images depicting primary cilia within normal human and primary, *de novo* human AML BMTs and a computer generated image depicting fluorescence signal
Figure 3.2.2.2: Representative SEM and TEM images depicting primary cilia within primary human *de novo* AML BMTs
Figure 3.2.2.3: Representative ICC images at x100 magnification depicting an absence of primary cilia in circulating haematopoietic cells
Figure 3.3.2.1 A: Representative Sanger sequencing chromatographs

Figure 3.3.2.1 B: Schematic highlighting the type and position of genetic abnormalities in *SMO* in an unselected cohort of primary *de novo* human AML samples
Figure 3.4.2.1: Expression of genes associated with chemoresistance, and poor survival, according to *SMO* expression
Figure 3.4.2.2: Expression of *NUMB* according to *SMO* expression
Figure 3.4.2.3: Expression of *HOXA3* and *HOXA9* according to *SMO* expression
Figure 3.4.3.1: 'Risk', according to the ELN Prognostic system [1], according to *SMO* expression
Figure 3.4.4.1: Spectrum, and absolute number, of pathological somatic mutations in a cohort of primary, *de novo* AML samples according to sequencing panel
Figure 3.4.4.2: Spectrum, and absolute number, of SNPs and percentage of cases expressing SNPs according to sequencing panel
Figure 3.4.4.3: Spectrum, and absolute number, of mutations categorised according to *SMO* expression

Figure 4.1.2.1: A marked variance in the mRNA expression of components of the Hh pathway was demonstrated in seven genetically diverse AML cell lines
Figure 4.1.2.2: mRNA expression of components of the Hh pathway varied between normal bulk MNCs, CD34 select PB and CD34 select BM cells
Figure 4.1.2.3: mRNA expression of components of the Hh pathway varied between AML cell lines, normal bulk MNCs, CD34 select PB and CD34 select BM cells
Figure 4.1.2.4: Expression of *SMO* varied between, and within, seven genetically diverse AML cell lines according to the harvest conditions
Figure 4.1.3.1: Cell viability in seven genetically diverse AML cell lines following exposure to incremental doses of cyclopamine (μM)
Figure 4.1.3.2: Cyclopamine caused a time and concentration dependent reduction in cell viability in the OCI-AML3 and Kasumi-1 cell lines
Figure 4.1.3.3: Cyclopamine caused a statistically significant, though variable, reduction in proliferation not explained by apoptosis in select, genetically diverse, AML cell lines
Figure 4.1.3.4: Cyclopamine caused apoptosis in select, genetically diverse, AML cell lines
Figure 4.1.4.1: Culture of OCI-AML3 cells with cyclopamine for 72hrs increased the percentage of inactive, non-cycling (G0-G1) cells by PI staining
Figure 4.1.4.2: Culture of OCI-AML3 cells with cyclopamine for 72hrs blocked cell proliferation by CFSE analysis
Figure 4.1.4.3: Culture of Kasumi-1 cells with cyclopamine for 72hrs resulted in a reduction in proliferating cells, with a concomitant increase in dying cells by PI staining
Figure 4.1.4.4: Culture of Kasumi-1 cells with cyclopamine for 72hrs did not affect cell division by CFSE staining
Figure 4.1.5.1: Culture of select, genetically diverse, AML cell lines with cyclopamine for 72hrs did not induce cellular senescence
Figure 4.1.6.1: Culture with cyclopamine for 72hrs resulted in an increase in cell granularity in select, genetically diverse AML cell lines, though not others
Figure 4.1.6.2: Culture of MOLM-13 cells with cyclopamine for 72hrs resulted in apoptosis and increased granularity
Figure 4.1.6.3: Culture of OCI-AML3 cells with cyclopamine for 72hrs resulted in a more mature morphological appearance by Diff-Quik® staining
Figure 4.1.6.4: Culture of OCI-AML3 cells with cyclopamine for 72hrs resulted in a change in CD marker expression profile
Figure 4.1.6.5: Culture of OCI-AML3 cells with cyclopamine for 72hrs resulted in a change in the mRNA expression of early lineage genes and those intrinsically involved in cellular maturation
Figure 4.1.6.6: Culture of OCI-AML3 cells with cyclopamine for 72hrs resulted in a change in colony morphology but not the absolute colony number at day 12
Figure 4.1.6.7: Culture of OCI-AML3 cells with cyclopamine for 72hrs induced a reversible change in cell granularity as determined by the SSC profile generated by flow cytometry
Figure 4.1.7.1: A shRNA against human *SMO* resulted in variable knockdown in Kasumi-1 cells

Figure 4.1.7.2: Cell viability, as determined by trypan blue dye exclusion, in a 50% *SMO* KD in the Kasumi-1 cell line
Figure 4.1.7.3: Proliferation, as determined by CTV staining, in a 50% *SMO* KD in the Kasumi-1 cell line
Figure 4.1.7.4: SSC profile of a 50% *SMO* KD in the Kasumi-1 cell line
Figure 4.1.7.5: Cell viability, as determined by trypan blue dye exclusion, in an 80% *SMO* KD in the Kasumi-1 cell line
Figure 4.1.7.6: SSC profile of an 80% *SMO* KD in the Kasumi-1 cell line
Figure 4.1.8.1: Variance in the mRNA expression of components of the Hh pathway in seven genetically diverse AML cell lines following culture with cyclopamine (5μM, 10μM and 20μM) for 72hrs
Figure 4.1.9.1: Gene expression profiles for genes involved in apoptosis, autophagy and cell cycle, following culture with cyclopamine (5μM, 10μM and 20μM) for 72hrs
Figure 4.1.9.2: Expression of genes involved in autophagy in seven genetically diverse, AML cell lines, following culture with cyclopamine (5μM, 10μM and 20μM) for 72hrs
Figure 4.1.9.3: mRNA expression of the anti-apoptotic members of the Bcl-2 family in seven genetically diverse, AML cell lines, following culture with cyclopamine (5μM, 10μM and 20μM) for 72hrs
Figure 4.1.9.4: mRNA expression of pro-apoptotic members of the Bcl-2 family in seven genetically diverse AML cell lines, following culture with cyclopamine (5μM, 10μM and 20μM) for 72hrs
Figure 4.1.9.5: mRNA expression of genes involved in cell cycle regulation and differentiation in seven genetically diverse AML cell lines, following culture with cyclopamine (5μM, 10μM and 20μM) for 72hrs
Figure 4.1.10.1: Metabolic activity, as a measure of cell viability, in the MOLM-13 and OCI-AML3 cell lines following culture with incremental doses of glasdegib (μM) for 72hrs, as determined by the resazurin assay
Figure 4.1.10.2: Cell viability and cell cycle kinetics following culture of the OCI-AML3 cell line with glasdegib (2.67μM, 5.34μM and 10.68μM; clinically achievable concentrations) for 72hrs
Figure 4.1.10.3: SSC MFI, and representative FACS plot, following culture of the OCI-AML3 cell line with glasdegib (2.67μM, 5.34μM and 10.68μM; clinically achievable concentrations) for 72hrs
Figure 4.1.10.4: Cell viability and cell cycle kinetics following culture of the MOLM-13 cell line with glasdegib (2.67μM, 5.34μM and 10.68μM; clinically achievable concentrations) for 72hrs
Figure 4.1.10.5: SSC MFI, and representative FACS plot, following culture of the MOLM-13 cell line with glasdegib (2.67μM, 5.34μM and 10.68μM; clinically achievable concentrations) for 72hrs
Figure 4.1.11.1: Gene expression profiles for genes involved in apoptosis, autophagy and cell cycle, following culture of the MOLM-13 and OCI-AML3 cell lines with glasdegib (2.67μM, 5.34μM and 10.68μM) for 72hrs
Figure 4.1.12.1: Schematic of the experimental layout used to determine the relationship between glasdegib and Ara-C in the MOLM-13 and OCI-AML3 cell lines using the Chou-Talalay method
Figure 4.1.12.2: Combination indices for the OCI-AML3 and MOLM-13 cell lines according to experimental conditions according to the Chou-Talalay method
Figure 4.1.12.3: Representative plots generated according to the Chou-Talalay method following culture of the OCI-AML3 and MOLM-13 cell lines with specific concentrations of glasdegib and Ara-C for 72hrs
Figure 4.1.13.1: Cell viability, as determined by trypan blue dye exclusion, in one primary AML sample following culture with select concentrations of cyclopamine for 72hrs
Figure 4.1.13.2: Cell viability, as determined by trypan blue dye exclusion, in primary, *de novo*, AML MNCs (n=4) following culture with select concentrations of cyclopamine for 72hrs
Figure 4.1.13.3: Cell viability, as determined by trypan blue dye exclusion, in primary, *de novo*, AML MNCs (n=4) following culture with sonidegib (25nM, 100nM and 500nM) alone, Ara-C (250nM and 500nM) alone and sonidegib 500nM in combination with Ara-C (250nM and 500nM) for 72hrs

Figure 4.1.13.4: Cell viability, as determined by Annexin V / 7AAD staining, in primary, de novo, AML MNCs (n=4) following culture with sonidegib (25nM, 100nM and 500nM) alone, Ara-C (250nM and 500nM) alone and sonidegib 500nM in combination with Ara-C (250nM and 500nM) for 72hrs
Figure 4.1.13.5: Cell viability, as determined by trypan blue dye exclusion, following culture with glasdegib, alone and in combination with Ara-C, in primary, *de novo* AML MNCs (n=4) for 72hrs
Figure 4.1.13.6: Cell viability, as determined by Annexin V / 7AAD staining, in primary, de novo AML MNCs (n=4) following culture with Ara-C (100nM), cyclopamine (20mM), glasdegib (2.67μM) and the combination of Ara-C (100nM) and glasdegib (2.67μM) for 72hrs
Figure 4.1.13.7: Cell cycle kinetics, as determined by PI staining, in primary, de novo, AML MNCs (n=4) following culture with Ara-C (100nM), cyclopamine (20mM), glasdegib (2.67μM) and the combination of Ara-C (100nM) and glasdegib (2.67μM) for 72hrs
Figure 4.1.13.8: Total number of colonies, normalised to the NDC, at day 14 following culture of a primary, *de novo* AML MNC sample (n=1) with Ara-C (100nM), cyclopamine (20μM), glasdegib (2.67μM) and the combination of Ara-C (100nM) and glasdegib (2.67μM)

Figure 5.1.1: Schematic depicting recognised interactions between the self-renewal pathways
Figure 5.1.1.1: Variance in mRNA expression both within, and between, select genes in an unselected cohort of bulk primary AML MNCs
Figure 5.1.2.1 A&B: Expression of key downstream targets in a cohort of primary, *de novo*, AML BMTs relative to a cohort of normal BMTs as determined by IHC
Figure 5.1.2.2: Expression of BCL-2 and BMP4 in a cohort of primary, *de novo* AML BMTs relative to a cohort of normal BMTs as determined by IHC
Figure 5.1.2.3: Heatmap showing expression of members of the Bcl-2 family, cell cycle regulators, select ABC transporters and components of the Hh signalling pathway, clustering highlighted by complete linkage analysis in an unselected cohort of primary, *de novo* human AML samples
Figure 5.2.1.1: mRNA expression of select ABC transporters in an unselected cohort of primary, *de novo*, human AML MNC samples (n=76) relative to a normal control (n=10).
Figure 5.2.2.1: Variance in the expression of *ABCA2, ABCB1* and *ABCC1* in seven, genetically diverse, AML cell lines
Figure 5.2.3.1: Metabolic activity, as a measure of cell viability, in three genetically diverse AML cell lines following culture with incremental concentrations of select ABC transport inhibitors (μM)
Figure 5.2.3.2: Metabolic activity, as a measure of cell viability, in three genetically diverse AML cell lines following culture with incremental concentrations of Ara-C (μM)
Figure 5.2.3.3: Metabolic activity, as a measure of cell viability, in three genetically diverse AML cell lines following culture with incremental concentrations of select ABC transport inhibitors (μM) and Ara-C 500nM
Figure 5.3.1.1: mRNA expression of the Bcl-2 family in an unselected cohort of primary, *de novo* human AML MNC samples
Figure 5.3.2.1: Baseline gene expression of members of the Bcl-2 family in seven, genetically diverse AML cell lines
Figure 5.3.2.2: Representative Western blot showing expression of BCL-2 in select, genetically diverse AML cell lines, a glioblastoma cell line and erythroid BC-CML cell line.
Figure 5.3.3.1: Metabolic activity, as a measure of cell viability, in five genetically diverse AML cell lines following culture with incremental doses of select BH3 mimetics / Bcl-2 inhibitors (μM)
Figure 5.3.4.1: Schematic of the experimental layout used to determine the relationship between ABT-199 and Ara-C in the MOLM-13 and OCI-AML3 cell lines using the Chou-Talalay method
Figure 5.3.4.2: Representative plots generated according to the Chou-Talalay method following culture of the OCI-AML3 and MOLM-13 cell lines with specific concentrations of ABT-199 and Ara-C for 72hrs

Figure 5.3.5.1: Proliferation and apoptosis, as determined by the trypan blue dye exclusion and Annexin V / 7AAD staining, following culture of the OCI-AML3 and MOLM-13 cell lines with select, and differing, concentrations of ABT-199 and Ara-C for 72hrs
Figure 5.3.6.1: Cell cycle kinetics, as determined by PI staining, following culture of the OCI-AML3 and MOLM-13 cell lines with select, and differing, concentrations of ABT-199 and Ara-C for 72hrs
Figure 5.3.7.1: Mitochondrial membrane potential, as measured by TMRM, following culture of the OCI-AML3 and MOLM-13 cell lines with select, and differing, concentrations of ABT-199 and Ara-C for 72hrs
Figure 5.3.7.2: Representative Western blot showing BCL-2 expression following culture of the OCI-AML3 and MOLM-13 cell lines with select concentrations of ABT-199 and Ara-C for 72hrs.
Figure: 5.3.7.3: pBCL-2 expression, as determined by flow cytometry, following culture of the OCI-AML3 and MOLM-13 cell lines with select, and differing, concentrations of ABT-199 and Ara-C for 72hrs
Figure 5.3.8.1: Representative Western blot showing MCL-1 expression following culture of the OCI-AML3 and MOLM-13 cell lines with select concentrations of ABT-199 and Ara-C for 72hrs.
Figure 5.3.9.1: Expression of members of the Bcl-2 family following culture of the OCI-AML3 and MOLM-13 cell lines with select concentrations of ABT-199 and Ara-C for 72hrs
Figure 5.3.10.1: Proliferation, as determined by the trypan blue dye exclusion, following culture of an unselected cohort of primary, *de novo* AML MNCs (n=3) with ABT-199 (19.5nM and 1.15μM) and Ara-C (100nM) alone, and in combination for 72hrs
Figure 5.3.10.2: Apoptosis, as determined by Annexin V / 7AAD staining, following culture of an unselected cohort of primary, *de novo* AML MNCs (n=3) with ABT-199 (19.5nM and 1.15μM) and Ara-C (100nM) alone, and in combination for 72hrs
Figure 5.3.10.3: Cell cycle kinetics, as determined by the PI assay, following culture of an unselected cohort of primary, *de novo* AML MNCs (n=3) with ABT-199 (19.5nM and 1.15μM) and Ara-C (100nM) alone, and in combination for 72hrs
Figure 5.3.11.1: Proliferation, as determined by the trypan blue dye exclusion, following culture of an unselected cohort of primary, *de novo* AML MNCs (n=4) with ABT-199 (19.5nM) and glasdegib (2.67μM) alone, and in combination, for 72hrs
Figure 5.3.11.2: Apoptosis, as determined by Annexin V / 7AAD staining, following culture of an unselected cohort of primary, *de novo* AML MNCs (n=4) with ABT-199 (19.5nM) and glasdegib (2.67μM) alone, and in combination, for 72hrs
Figure 5.3.11.3: Cell cycle kinetics, as determined by the PI assay, following culture of an unselected cohort of primary, *de novo* AML MNCs (n=4) with ABT-199 (19.5nM) and glasdegib (2.67μM) alone, and in combination, for 72hrs

Publications

Dasatinib for the treatment of chronic phase chronic myeloid leukaemia. V Campbell, M Copland. Clinical Practice. 2013 July;10(4):415-425.

Hedgehog signaling in cancer stem cells: a focus on hematological cancers. V Campbell, M Copland. Stem Cells and Cloning: Advances and Applications. 2015 Jan;8:27-38.

Successful Aortic aneurysm Repair in a Woman with Severe von Willebrand (Type 3) Disease. VL Campbell, K Marriott, R Stanbridge, A Shlebak. Case Reports in Haematology. 2015 March;703803.

Deregulated hedgehog pathway signalling is inhibited by the smoothened antagonist LDE225 (Sonidegib) in chronic phase myeloid leukaemia. DA Irvine, B Zhang, R Kinstrie, A Tarafdar, H Morrison, VL Campbell, HA Moke, Y Ho, C Nixon, PW Manley, H Wheadon, JR Goodlad, TL Holyoake, R Bhatia, M Copland. Scientific Reports. 2016 May:6:25476.

Inhibition of Interleukin-1 Signaling Enhances Elimination of Tyrosine Kinase Inhibitor Treated CML Stem Cells. B Zhang, S Chu, P Agarwal, VL Campbell, Hopcroft L, H Jorgensen, A Lin, T Holyoake, R Bhatia. Blood. 2016 September:128(23):2671-2682.

Presentations

Profiling the Hedgehog Pathway in Acute Myeloid Leukaemia. Keystone Symposium: Developmental Pathways and Cancer: Wnt, Notch and Hedgehog. V Campbell, A Tarafdar, E Dobbin, J Goodlad, H Wheadon, M Copland. Banff, Canada. February 2014.

Comparison of self-renewal expression in stromal *in vitro* and *in vivo* microenvironmental models – critical differences and their impact on hematopoietic support function. V Campbell, GA Horne, H Wheadon, T Holyoake, M Copland. European School of Hematology: The tumour microenvironment in hematological malignancies and its therapeutic targeting. May 2015.

Comparison of self-renewal expression in stromal *in vitro* and *in vivo* microenvironmental models – critical differences and their impact on hematopoietic support function. V Campbell, GA Horne, H Wheadon, T Holyoake, M Copland. European Hematology Association: Hematopoiesis, stem cells and microenvironment. June 2015.

The Role and Therapeutic Potential of the Hedgehog Signaling Pathway in Acute Myeloid Leukemia. V Campbell, E Dobbin, J R Goodlad, H Wheadon, M Copland. European School of Hematology: Acute Myeloid Leukaemia "Molecular and Translational": Advances in Biology and Treatment. October 2015.

Unravelling the Complexities of Hedgehog Mediated Signal Transduction in Acute Myeloid Leukaemia and Normal Haematopoiesis. V Campbell, A Tarafdar, E Dobbin, G A Horne, L Park, C Nixon, J R Goodlad, H Wheadon, M Copland. 58th American Society of Haematology Annual Meeting and Exposition. San Diego, USA. December 2016.

Understanding the role and therapeutic potential of the hedgehog signalling pathway in acute myeloid leukaemia. V Campbell, E Dobbin, J R Goodlad, H Wheadon, M Copland. Institute for Translational Medicine & Therapeutics (ITMAT). Edinburgh, UK. March 2017.

Acknowledgements

This work was supported by the Wellcome Trust Scottish Translational Medicine and Therapeutics Initiative, to this collaboration, and Professor D Webb I am indebted.

Firstly I would like to thank Professor Tessa Holyoake who sadly passed away in August 2017, during the write up of this PhD. Tessa offered support throughout my PhD; I will be forever grateful I had the opportunity to meet and work with such an inspirational woman. I am also hugely grateful to my supervisors Professor Mhairi Copland and Dr Helen Wheadon for their guidance, support and kindness. You have enabled me to develop professionally and personally, thank you. I am also thankful for the help and advice offered by Dr Karen Keeshan, Dr Alison Michie and Dr Heather Jorgenson.

I would also like to thank my colleagues in the Paul O'Gorman, many of whom have become valued friends for their support, help and teaching, making my PhD truly memorable. I will not forget this journey, the sacrifices, the successes and failures, the frustrations, the late nights and early mornings, the banter and the laughter. In particular I would like to mention: Dr Ana Tarafdar who taught me how to hold a pipette, and so much more, Dr Edwina Dobbin and Dr Rachel Dakin for their support and help, going above and beyond to help with my sequencing data, Miss Jen Cassells for all of her FACs expertise, Dr Alan Hair for his help with primary samples and his amazing early morning coffee, Mrs Karen Dunn for her help dissecting murine tracheas, Mr Colin Nixon for all his help optimising my primary cilia work, Mrs Margaret O'Prey for her help capturing confocal images, Dr John Goodlad and Mr Tim Ingman for all their help with IHC and Mrs Margaret Mullin for all her help and expertise in EM. I also wish to thank Mrs Diane Verrecchia, Angela Newlands and Ms Michelle Bradley, always so kind and helpful. And to my group, thank you. In particular thank you Dr Gillian Horne, for 'Gilloria', it has been a privilege to work with you, Miss Heather Morrison, for your friendship, help and advice, Dr Ross Kinstrie and Dr Chris Estelle for never failing to make me blush and Dr Susan Rhodes, whom I started this journey with.

To my clinical colleagues, thank you for your support and understanding.

I would also like to thank the AML patients for providing samples for research purposes. Without their generous support this project would not have been possible.

To my friends, many of whom I have neglected during this time, thank you for your understanding. Most importantly I would like to thank my husband, Johann, and my mum; you have both helped and supported me in so many ways, without which this would not have been possible. You both keep asking if it is finished yet – it is! And finally my boys, Ruben (aged 4 years) and Otto (aged 2 years) - at points it felt as though those two blue lines were the only positive results to come from this research! You have been the first in nursery and last out, hidden round a corner while I 'just finish an experiment' and had articles read to you instead of bedtime stories! That you think my favourite animal is a hedgehog says it all! I love you both.

Author's declaration

I declare that, except where explicit reference is made to the contribution of others, that this dissertation is the result of my own work and has not been submitted for any other degree at the University of Glasgow or any other institution.

Victoria Campbell

2018

List of abbreviations

7AAD	7-Aminoactinomycin D
ABCA2	ATP-Binding Cassette, Sub-Family A (ABC1), Member 2
ABCB1	ATP-Binding Cassette, Sub-Family B (MDR/TAP), Member 1 Alternatively referred to as P-gp: P-glycoprotein
ABCC1	ATP-Binding Cassette, Sub-Family C (CFTR/MRP), Member 1 Alternatively referred to as MRP1: Multi drug resistance protein
ABCG1	ATP-Binding Cassette, Sub-Family G (WHITE),
ABCG2	ATP-Binding Cassette, Sub-Family G (WHITE), Member 2 (Junior Blood Group) Alternatively referred to as BCRP: Breast cancer resistance protein
AML	Acute myeloid leukaemia
AML-NOS	Acute myeloid leukaemia not otherwise specified
APC	Allophycocyanin
APML	Acute promyelocytic leukaemia
APS	Ammonium Persulfate
Ara-C	Cytarabine; trade name: Cytosar-U®
As_2O_3	Arsenic trioxide
ASCO	American Society Clinical Oncology
ASH	American Society of Haematology
ATCC	American Type Culture Collection
BCC	Basel cell carcinoma
BCL-2	B-cell lymphoma 2
BCL2L1	BCL2-like 1 isoform 1 Alternatively referred to as BCL-XL: B-cell lymphoma-extra large
BDT	Abi Prism Big Dye V1.1
BM	Bone marrow
BSA	Bovine Serum Albumin
Ca^{2+}	Calcium
CD	Cluster of differentiation
cDNA	Complimentary Deoxyribonucleic acid
CFC	Colony forming cell
CFSE	Carboxyfluorescein succinimidyl ester
CFU	Colony forming unit

CFU-S	Colony forming units within the spleen
CFU-GM	Colony forming unit-granulocyte monocyte Alternatively referred to as GMP
CHiP	Clonal haematopoiesis of indeterminate potential
CI	Combination index
CLL	Chronic lymphocytic leukaemia
cm^3	Cubic centimetre
CML	Chronic myeloid leukaemia
CML-BC	Blast crisis chronic myeloid leukaemia
CMP	Common myeloid progenitor
CN-AML	Cytogenetically normal AML
CO_2	Carbon dioxide
CR	Complete remission
CT	Cycle threshold
CTGF	Connective tissue growth factor
CTV	Cell Trace™ Violet
ΔCT	Delta CT
ΔΔCT	Delta delta CT
DA	Daunorubicin + cytarabine
DAPI	4',6-diamidino-2-phenylindole
ddNTP	2',3' dideoxynucleotides
DFS	Disease free survival
DHH	Desert hedgehog
DIFP	Diisopropyl fluorophosphate
DLBCL	Diffuse large B cell lymphoma
DMEM	Dulbecco's Modified Eagle's Medium
DMEM/F12	Dulbecco's Modified Eagle's Medium/Nutrient Mixture F12
DMSO	Dimethylsulfoxide
DNA	Deoxyribonucleic acid
DNAse	Deoxyribonuclease
DNMT3A	DNA (Cytosine-5-)-Methyltransferase 3 Alpha
dNTP	Deoxynucleotide Triphosphate

DSMZ	Leibniz-Institut Deutsche Sammlung von Mikroorganismen und Zellkulturen
ECL	Enhanced chemiluminescence
EDTA	Ethylenediamine tetra-acetic acid
ELISA	Enzyme-linked immunosorbent assay
ESC	Embryonic stem cell
EU	European Union
FAB	French–American–British classification
FACS	Fluorescence-activated cell sorting
FBS	Foetal Bovine Serum
FCS	Foetal Calf Serum
FITC	Fluorescein Isothiocyanate
FL	Follicular non-Hodgkin lymphoma
FLAG-IDA	Fludarabine + high dose cytarabine + idarubicin + G-CSF
FLT3-ITD/TKD	Fms-like tyrosine kinase 3-internal tandem duplication/tyrosine kinase domain
FSC	Forward scatter
g	Grams
G	Gauge
G0	‘Resting phase’ of the cell cycle
G1	‘Growth phase’ of the cell cycle
G2	Pre-mitotic phase of the cell cycle
G418	Geneticin
GFP	Green fluorescent protein
GLI1-3	GLI family zinc finger 1-3
GM-CSF	Granulocyte-macrophage colony-stimulating factor
GMP	Granulocyte/macrophage progenitor
GSE	Genomic Spatial Event
HBSS	Hank's Balanced Salt Solution
HCl	Hydrogen chloride
HH	Hedgehog
HHAT	Hedgehog Acyltransferase
HHIP	Hedgehog interacting protein

HMA	Hypomethylating agents
HPC	Haematopoietic progenitor cells
HSC	Haematopoietic stem cells
HSPC	Haematopoietic stem progenitor cells
IC50	Median inhibition concentration
ICC	Immunocytochemistry
IHC	Immunohistochemistry
IHH	Indian hedgehog
IL-	Interleukin-
IMDM	Iscove's Modified Dulbecco's Medium
IU	International unit
KDa	Kilodaltons
KIT	Stem cell growth factor receptor
KL	Kit ligand
LIF	Leukaemia inhibitory factor
LSC	Leukaemia stem cells
LTC	Long term culture
MCL-1	Myeloid leukaemia cell 1
MDR	Multi drug resistant
MDS	Myelodysplastic syndrome
2-ME	2-Mercaptoethanol
MFI	Mean fluorescence intensity
Mg^{2+}	Magnesium
MgCl	Magnesium Chloride
MINS	Minutes
µL	Microlitre
µM	Micromolar
ML	Millilitre
mM	Milimolar
MM	Multiple myeloma
MNC	Mononuclear cells

MPN	Myeloproliferatve neoplasm
mRNA	Messenger Ribonucleic acid
MSC	Mesenchymal stem cell
MW	Molecular weight
N/A	Not applicable
NaCl	Sodium chloride
NaOH	Sodium hydroxide
NCRI	National Cancer Research Institute
NFW	Nuclease free water
NGS	Normal goat serum
NPM1	Nucleoplasmin 1
nM	Nanomolar
OS	Overall survival
p	Probability
PB	Peripheral blood
PBS	Phosphate buffered saline
PCR	Polymerase chain reaction
PE	Phycoerythrin
PE-Cy5	Phycoerythrin-Cy5 Tandem
PE-Cy7	Phycoerythrin-Cy7 Tandem
PerCP-Cy5.5	Phycoerythrin Chlorophyll Protein-Cy5.5 Tandem
PFTE	Polytetrafluoroethylene
pH	Poer of hydrogen
PI	Propidium iodide
PKCα	Protein kinase C α
P/S	Penicillin-Streptomycin
PTCH	Patched
rh	Recombinant human
RNA	Ribonucleic acid
RPMI	RPMI (Rosewell Park Memorial Institute) -1640 medium
R/R	Relapsed / refractory

RT	Room temperature
RT-PCR	Reverse transcriptase polymerase chain reaction
SC	Stem cell
SCF	Stem cell factor
SCID	Severe combined immune deficiency
SCT	Stem cell transplant
SD	Standard deviation
SDS	Sodium Dodecyl Sulphate
SECS	Seconds
SHH	sonic hedgehog
siRNA	Small interfering RNA
SMO	Smoothened
SRB	Sequencing Reaction Buffer
SSC	Side scatter
STIL	SCL-interrupting locus
SUFU	Suppressor Of Fused Homolog
TBS	Tris-Buffered Saline
TBSN	Tris-Buffered saline NP40
TE	Tris EDTA Buffer
TEMED	N,N,N',N'-Tetramethylethylenediamine
TGCA	The Cancer Genome Atlas
t-MN	Therapy-related myeloid neoplasms
US	United States
USC	Umbilical stem cell
USUT	Unstained untreated
V	Volts
WHO	World Health Organisation
xg	Gravity
XIAP	X-Linked Inhibitor of Apoptosis, E3 Ubiquitin Protein Ligase

1. Introduction

1.1 Stem cells

Irrespective of stage in life or tissue of origin, stem cell (SCs) are unique, undifferentiated cells defined by three key properties: long life, multipotency, and the capacity to self-renew [2,3]. SC phenotype and potential being defined by characteristics intrinsic to the SC and environmental influences [3].

The first experimental evidence of the SC, and thus of cellular hierarchy in the haematopoietic system, was in 1961, in a murine model [4]. The haematopoietic system was eradicated by whole-body radiation, donor blood cells injected via the tail vein, and assays performed to determine the cell number capable of restoring a functioning haematopoietic system. Colonies of cells were seen within the spleen. Further, some of these were capable of producing all of the mature, differentiated haematopoietic cells required to sustain life following transplantation into secondary recipients [4]. Whilst experimental models have evolved, the principle remains the same: to demonstrate the cardinal properties of the SC - self-renewal and differentiation.

SCs are broadly defined by origin into three groups: embryonic stem cells (ESCs), umbilical stem cells (USCs) and somatic stem cells (SSCs) [5]. As their name would suggest, ESCs derive from an embryo, USCs from cord blood and SSCs are found in all postnatal organs. Additionally, they are defined by their developmental plasticity or potency with SCs being characterised as: totipotent, pluripotent and multipotent. Totipotent cells are capable of producing any cell type, indeed producing all the cells required for the developing embryo and extra-embryonic tissues including the placenta; the term is therefore limited to those cells found within the zygote and morula. Pluripotent cells are able to produce cells from any of the embryonic germ layers: endoderm, mesoderm and ectoderm, these cells compose the inner cell mass of the blastocyst [6]. These primitive cell types develop into all tissues of the body [6]. Multipotent cells, whilst retaining the key characteristics that define a SC, are capable of differentiating into a limited number of cells. These SCs are responsible for both tissue development and maintenance throughout life [7].
Figure 1.1: Schematic diagram depicting stem cell hierarchy.

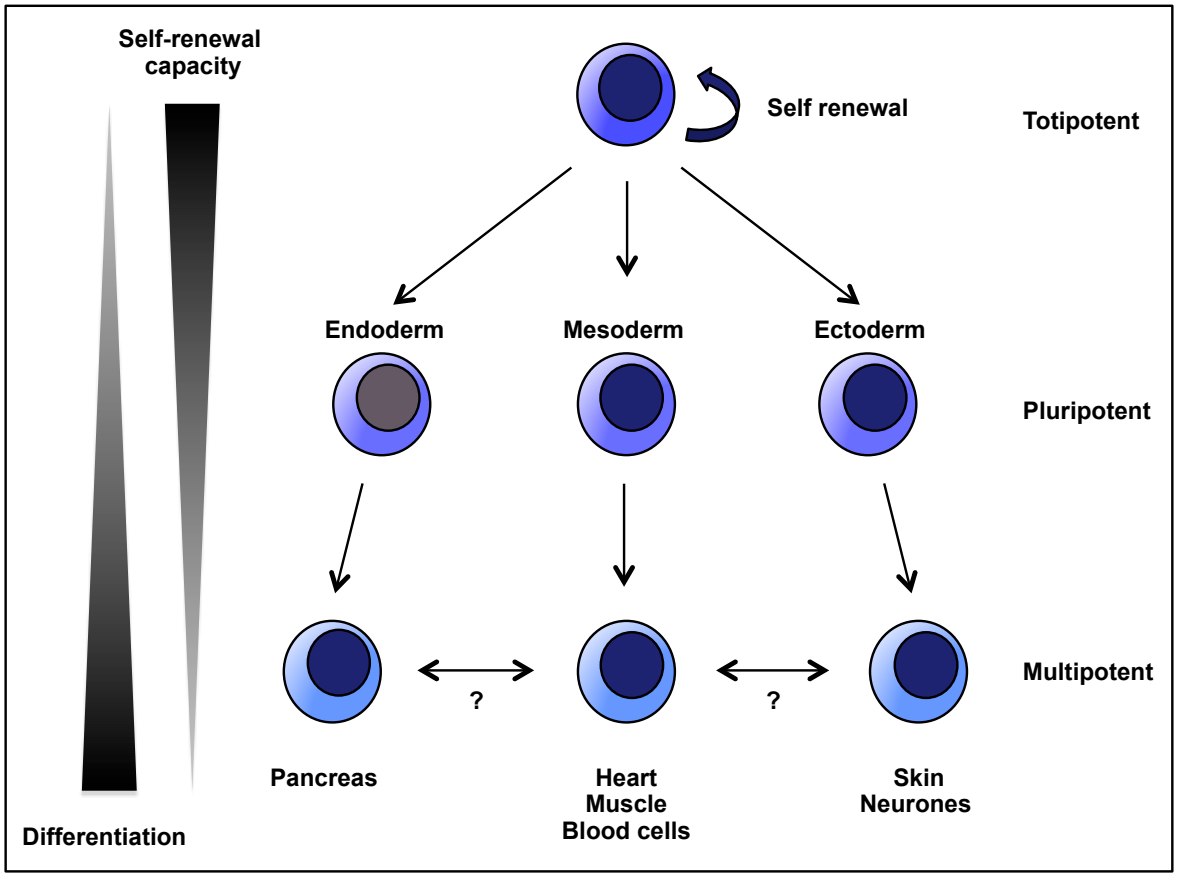

Figure 1.1: Stem cell hierarchy
Stem cells are defined by their self-renewal and multilineage differentiation capacities, placing them at the top of a cellular hierarchy within a given tissue.

SCs are slow cycling, capable of self-renewal cell division, producing another SC with the same development and replication potential, and differentiation, producing tissue-specific specialised cells [8]. This process is tightly regulated, ensuring the maintenance of the SC pool specific to that tissue, and enabling the SC to respond to both local and systemic proliferation signals whilst preventing uncontrolled growth [9].

Whilst classically SC fate was believed to be controlled by growth factors, more recently work has shown it to be controlled by a complex interaction between highly conserved embryonic signalling pathways, transcription factors, and the surrounding extracellular matrix (ECM) or 'stem cell niche' [10-14], discussed in more detail below in Section 1.1.1. Further, deregulated SC interactions have been shown to be fundamental in disease pathogenesis [11,15-17].

Much of what we know about extrinsic regulators of SC fate comes from bulk population studies. It is however increasingly evident that cell fate decisions are made at the level of individual cells [18-20], with researchers currently seeking to address this recognised flaw in our understanding of SC biology through advances in technology and computational skills. Utilising single cell gene expression analysis, researchers have begun to understand the transcriptional programmes underpinning SC behaviour, whilst electrical impedance spectroscopy has allowed for the quantitative analysis of each SC's cellular processes [18,19,21,22].

Finally, despite regulatory systems, cell division carries the risk of aberrant mitosis. SCs being no exception, though the implications are far graver. Further, SCs may be at greater risk as they are long-lived, and therefore exposed to more genotoxic events [23,24]. Fortunately, whilst mutations occur, most are inconsequential. A low frequency may accumulate however, eventually leading to an array of diseases including cancer. Most mutations resulting in cancer have been shown to affect cell division, DNA damage, and signal transduction thereby conferring a survival and proliferation advantage to the transformed SC [25].

1.1.1 Stem cell niche

The concept of the SC niche was considered almost in parallel to the discovery of the SC, in 1968 [26,27]. Research, building upon that of Till and McCulloch, demonstrated the importance of the niche in preserving the reconstituting ability of SCs [28]. This work recognised the inferior ability of the SCs isolated from colony-forming units within the spleen (CFU-S) to reconstitute haematopoiesis in irradiated animals compared to those of the bone marrow (BM). Additionally, heterotrophic transplantation of BM cells had shown these cells to not only form a bony capsule but to be capable of supporting the production of haematopoietic cells of recipient origin [29-31]. Further work determined these BM cells to be fibroblasts, referred to as colony-forming unit-fibroblasts (CFU-F) [32]. Additional work analysing the media collected following CFU-F *in vitro* culture demonstrating their ability to produce haematopoietic growth factors [33-35]. In 1986, work confirmed purified BM-derived fibroblasts were able to support haematopoiesis [36].

Currently the term mesenchymal stem cell (MSC) is preferentially used when referring to these CFU-F / multipotent BM stromal cells. MSCs are defined by the International Society of Cellular Therapy (ISCT) as: plastic adherent, multipotent fibroblast-like cells which express CD73 and CD105, are negative for CD14, CD34 and CD45, and are capable of differentiating into osteoblasts, chondrocytes and adipocytes [37]. However these properties are also shared by CFU-Fs. Whilst more recent work analysing the expression of SSEA-1, SSEA-4 and GD2 appears to suggest a hierarchy of mesenchymal differentiation; at present it is not possible to definitively differentiate between MSCs and CFU-Fs [38-43]. For the purpose of this thesis the term MSC will be used.

The SC niche is defined by anatomy and function as a local tissue microenvironment that regulates and supports the tissue-specific SCs and progenitor cells [14,44,45]. Although the SC niche remains incompletely defined it is clear there is considerable variation in niche design, and therefore possibly importance. SCs that support tissues undergoing constant cellular renewal, for example the haematopoietic system, being shown to be dependent upon the niche and the specific intercellular interactions and cellular organisation it provides [14,46]. In contrast, muscle SCs for example, which are normally quiescent, appear content in relative isolation, residing on the basal lamina of the muscle fibre unit they support [47].

1.1.2 Haematopoiesis and the haematopoietic stem cell

'All mammals make blood in their bones' David T Scadden, E Donnall Thomas Lecture, ASH, San Diego, USA, December 2016.

The site of blood cell production changes through the early stages of development. Primitive haematopoiesis occurs first in the yolk sac whereas definitive haematopoiesis occurs later with the first HSCs originating from the aorta-gonad-mesonephros region, these HSCs subsequently migrate to the placenta, foetal liver and spleen [48,49]. During bone cavity formation the HSCs begin to migrate to the endosteum, forming the BM, with migration completing after birth [50].

After birth, and throughout life, haematopoiesis, in the healthy state, occurs within this BM. In response to stress however, haematopoiesis can occur in extramedullary sites such as the spleen. It is a highly metabolically active system, and it is estimated that greater than $1x10^8$ blood cells are produced every minute in the average healthy adult.

Haematopoiesis is an incredibly dynamic and highly organised hierarchy, homeostasis being maintained by self-renewing HSCs. These rare, multipotent cells produce a population of more committed, progenitor cells. In turn, through successive cell divisions and a complex series of differentiation steps, progenitor cells give rise to terminally differentiated mature blood cells of all lineages [51]. Within this model common myeloid progenitors (CMPs) represent the critical progenitor cell from which the myeloid, megakaryocyte and erythroid cell lineages are ultimately derived, Figure 1.2: Haematopoietic hierarchy in humans.

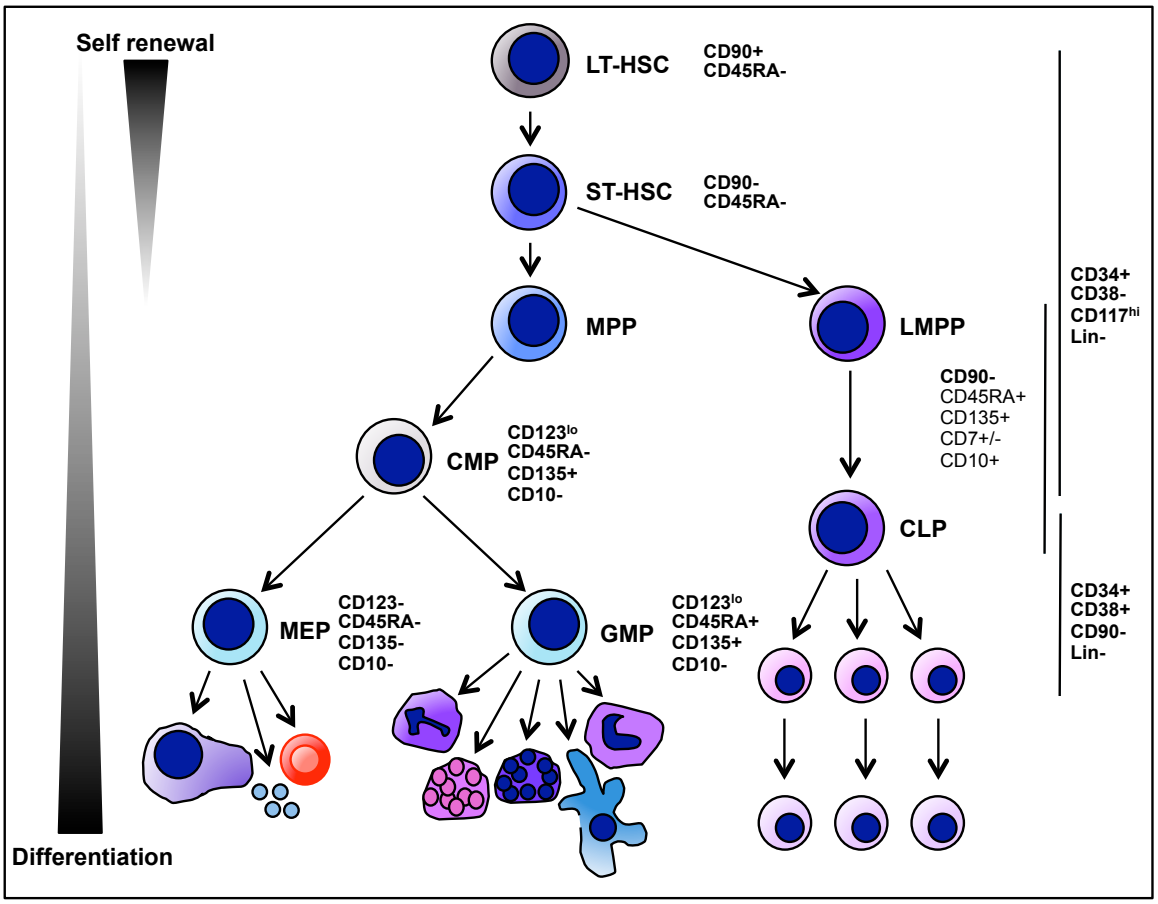

Figure 1.2: Human haematopoietic hierarchy
Long-term self-renewing multipotent haematopoietic stem cells (HSCs) are at the apex of the hierarchy. HSCs are followed by a series of progenitor cells (HPCs) with increasingly limited differentiation and self-renewal potential and finally by terminally differentiated mature haematopoietic cells. Distinct populations can be identified by their surface marker expression (as shown) and functional properties.
HSC, haematopoietic stem cell; LT-, long-term repopulating;;ST-, short-term repopulating; MPP, multipotent progenitor; CMP, common myeloid progenitor; GMP, granulocyte–macrophage progenitor; MEP, megakaryocyte–erythrocyte progenitor; LMPP, lymphoid-primed MPP; CLP, common lymphoid progenitor.

Investigation of haematopoietic hierarchical transitions, from a stem to progenitor to precursor state, through cell purification, transcriptional studies and functional clonal assays has however, provided insight into the cellular and molecular mechanisms underlying haematopoiesis, challenging the previously accepted model [52]. These studies hypothesised that common myeloid progenitors (CMPs) are functionally heterogeneous unipotent progenitors, derived from putative multilineage HSPCs. Further, results suggest oligopotent progenitors may be a negligible component, the human haematopoietic hierarchy behaving rather as a ‘two-tier’ system: a top

tier containing multipotent cells such as HSCs and multipotent progenitors (MPPs), and a bottom tier composed of cells committed to myeloid, erythroid and megakaryocyte lineages. It is, perhaps, the megakaryocyte lineage which has been the most challenged, recent studies suggesting megakaryocytes do not transit through a multipotent or oligipotent progenitor stage; additional evidence suggesting a subset of HSCs to have biased megakaryocyte potential, megakaryocytes directly arising from these HSCs [53]. Whilst much of our understanding of haematopoiesis has derived from the classical model the refined model, perhaps, lends itself more to the notion of the HSPC as the progenitor cell in AML.

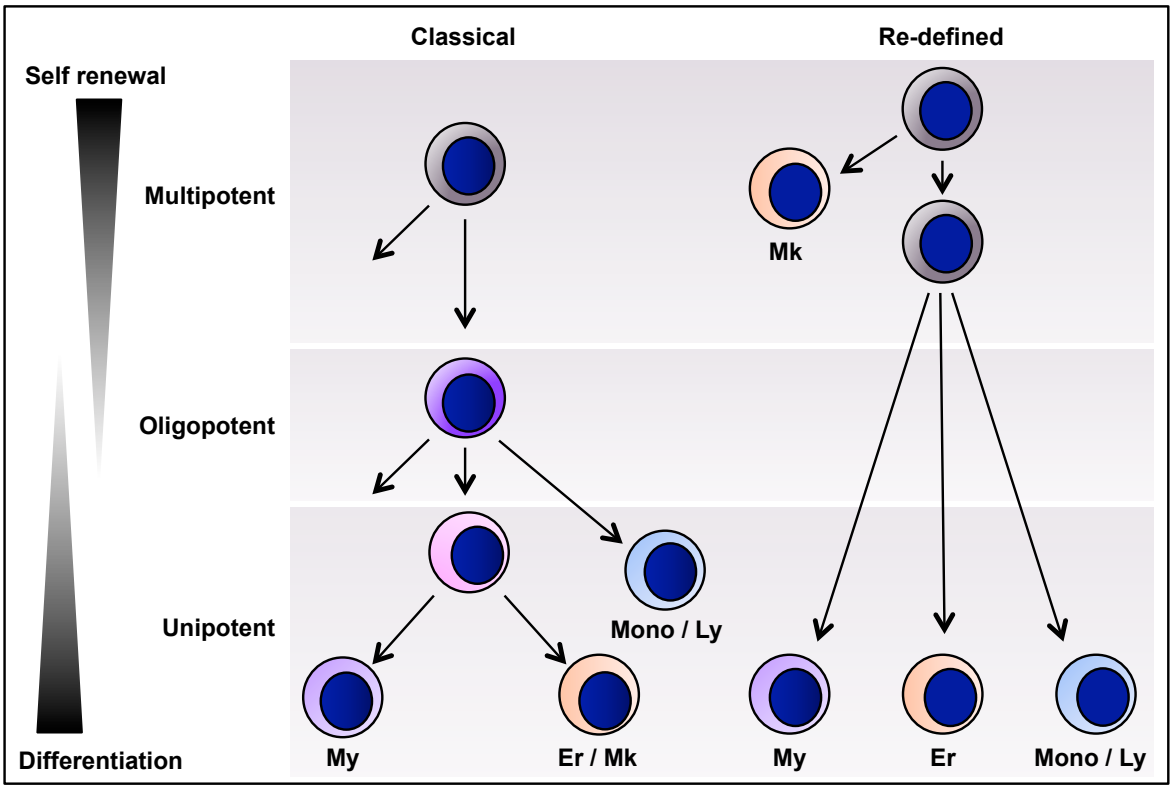

Figure 1.3: Schematic illustrating the differences between the classical and redefined models of the haematopoietic hierarchy.
The classical model, proposes that many HSPCs are multipotent, defining a population of oligopotent progenitors, such as CMP, from which myeloid, erythroid and megakaryocyte differentiation originates. The redefined model proposes a developmental shift in the progenitor cell architecture with development. In this model, haematopoietic hierarchy is thought to follow the classical model in utero but by adulthood the replicative potential of the progenitor population has narrowed considerably whereby it is only the SCs which are multipotent, progenitors becoming unipotent.
The planes represent theoretical tiers of differentiation.
Mk, megakaryocyte; Mono, monocyte, Ly, lymphoid; My, myeloid; Er, erythroid.

Finally, recent work has shown that although their phenotype is tightly defined, these HSCs are functionally heterogeneous. The HSC compartment, in fact, comprising a limited number of distinct subtypes intrinsically biased in their lineage production [51,54,55]. These subtypes reside in close proximity within the BM microenvironment, each with its own epigenetically determined differentiation and proliferation programme [56-60]. Further, recent research utilising single cell gene expression analysis has begun to unravel the structure and function of transcriptional programmes underpinning haematopoiesis in the adult and the process of blood development in the embryo [61] with HSCs being shown to be heterogeneous at a gene expression level [62,63].

It is therefore apparent that it is not just the HSC that is responsible for healthy haematopoiesis but a series of complex communications between these cells and the BM microenvironment within which they reside [11,13].

1.1.3 Bone marrow microenvironment

'In the two hundred million years since fish diverged from our evolutionary tree, animals with blood and bones have made blood in their BM. This lengthy co-evolution has made the BM a special place where multiple non-haematopoietic cells contribute to the orderly regulation of blood cell production.' David T Scadden, E Donnall Thomas Lecture, ASH, San Diego, USA, December 2016.

The BM niche is an interactive system; complex regulatory relationships operating between the haematopoietic, mesenchymal, endothelial and neural cells residing within it, with HSCs distributed throughout. It is this microenvironment that is responsible for supporting and influencing HSC fate. Regulatory signals provided by cytokines, ECM proteins and cues provided through cell-cell contact all influencing SC behaviour down to the level of single stem and progenitor cells; Figure 1.4.

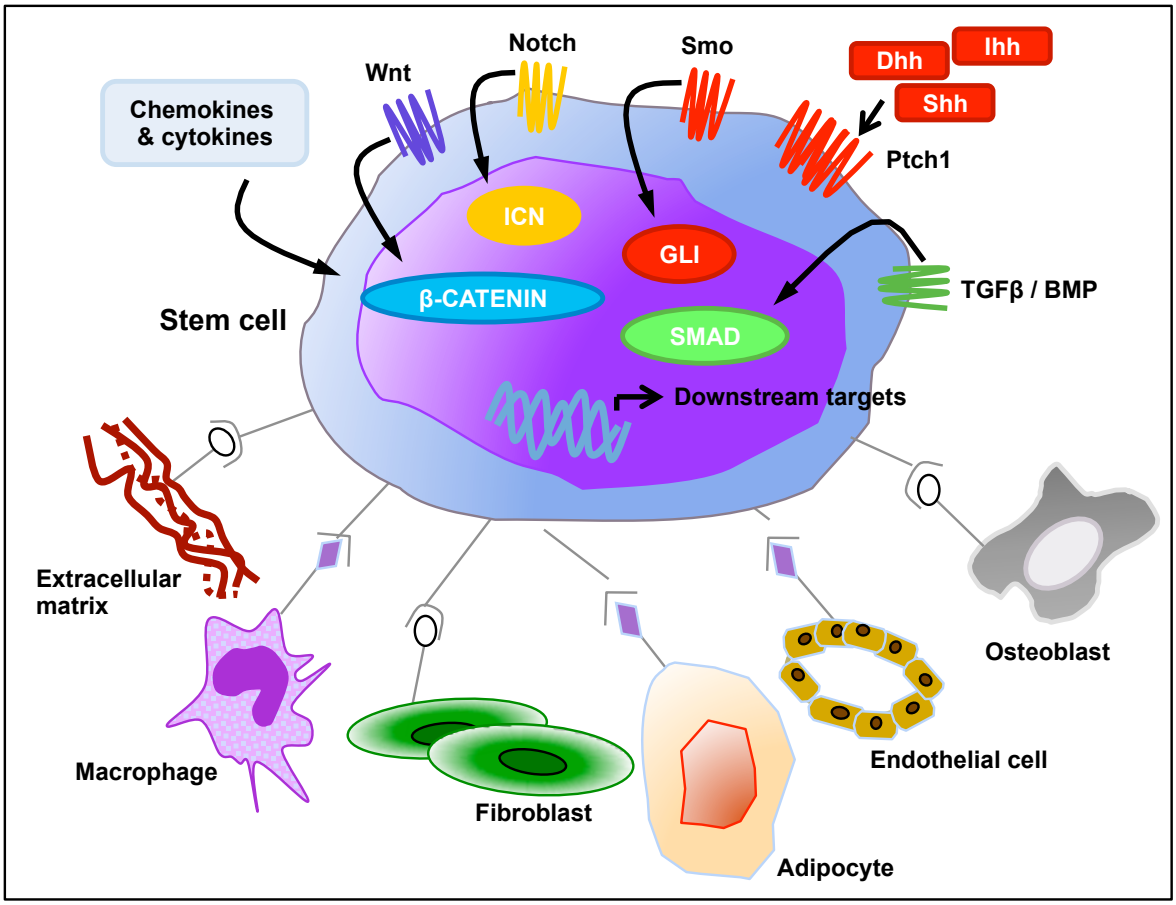

Figure 1.4: Bone marrow microenvironment
The bone marrow (BM) is a specialised microenvironment referred to as the SC niche where HSCs reside, their fate being determined by a complex interplay of extrinsic and intrinsic signals including cytokines, chemokines .and the self-renewal signalling pathways. The BM contains at least two distinctive HSC supportive niches: an endosteal osteoblastic niche, which appears to support quiescence and self-renewal and the perivascular niche that appears to promote HSC proliferation and differentiation.

The cellular identity of the cells that regulate HSCs within the BM niche has been a contentious issue for the past decade. The endosteal region, as an anatomical location for HSCs, is well documented, with many types of cells existing in close proximity within this region: osteoblasts, osteoclasts and endosteal monocytes or macrophages have all been demonstrated to influence SC fate [64,65]. However, whilst osteoblastic cells were the first cell population shown to influence HSC frequency [66,67] more recent work raised concern this may be an artifact of the experimental

method. *In vivo* imaging studies found few HSCs in contact with osteoblastic cells [68-70]. Additionally, manipulation of osteoblast cell numbers had no acute effect on HSC frequency [71-73]; HSC proliferation and differentiation being altered following the genetic modification of primitive osteolineage cells but not mature osteoblasts [74]. Finally, less than 20% of HSCs are located within 10μm of the endosteum; most HSCs being found in the trabecular region of the BM [69,71,75,76]. The location of large numbers of HSCs in the trabecular region implies osteolineage cells do have a role in HSC fate, and that it is not experimental artifact [68,77-79]. The precise nature of this role however remains to be determined.

More recent work has focused on the perivascular area [12,80]. Perivascular MSCs have been shown to express a number of markers directly involved in HSC maintenance including CD146 [78], CXCL12 [70,81,82] and Nestin [83]. Perivascular stromal cells in culture have been shown to both promote HSC maintenance [84] and long-term expansion [85,86]. Further, HSC quiescence was enhanced and self-renewal potential increased in an *E-selectin* knock out model, with HSCs also showing increased resistance to irradiation [87]. Interestingly, HSCs are five times more likely than other haematopoietic cells to be located adjacent to a sinusoid [71,76,88]. Many cell types are thought to directly or indirectly regulate the perivascular niche; for example the sympathetic nervous system has been shown to regulate Cxcl12 expression and thus HSC retention in the BM [12,89,90]. Additionally blood may serve to transport long-range signals integrating HSC activity with overall physiology [91].

Current data suggests there are specialised niches, composed of many cell types, for distinct haematopoietic stem and progenitor cell (HSPC) functions [92]. Further, some stromal cells affect SCs while others affect more mature, lineage-restricted cells, with niche composition and function thought to change under different physiological conditions. Finally, it is apparent stromal sub-populations participate in the malignant process. The extent that malignancies disrupt the SC niche and the ability to exploit this is an exciting area of ongoing research.

1.2 Cancer

The term ‘cancer’ encompasses a spectrum of diseases resulting from abnormal cell growth and behaviour. Clinically, simplistically, cancer can vary from those that are relatively indolent, not requiring treatment, to those that are highly aggressive necessitating early treatment in order to prevent death, and anything in between.

Two models of cancer have been described, the stochastic model and the hierarchical model, depicted in Figure 1.5: Cancer cell model [93]. The stochastic model suggests tumour cell growth to be dependent on both extrinsic and intrinsic signals, each malignant cell possessing cancer initiating potential. In contrast, the hierarchical model proposes heterogeneity within, with only a select few cancer cells capable of cancer initiation; these cells are termed cancer stem cells (CSCs) [93].

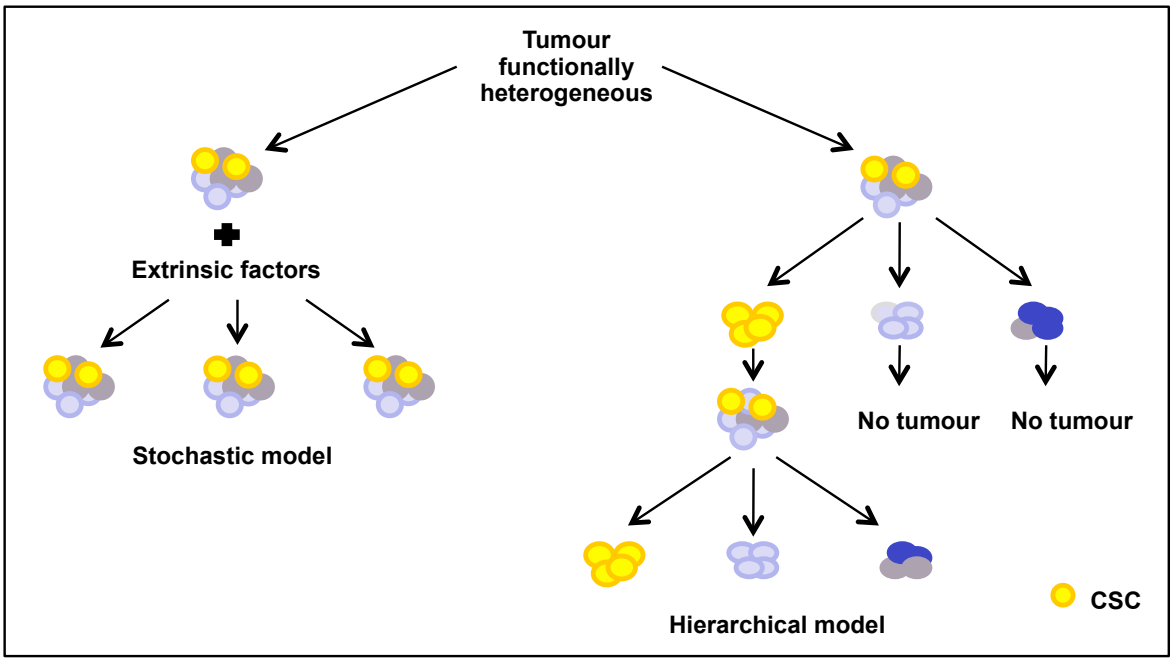

Figure 1.5: Cancer cell model
In the stochastic model all malignant cells have the ability to function as a cancer stem cell (CSC), their ultimate fate being affected by both intrinsic and extrinsic factors. Whilst within the hierarchical model only a small fraction of the malignant cell population have the ability to function as CSCs, to produce both CSCs and progeny with limited self-renewal potential, in other words the cancerous cells are biologically diverse.
CSC, cancer stem cell.

1.2.1 Cancer stem cells

The concept of the CSC was first demonstrated in 1963 [94]. Malignant haematopoietic cells, like their normal counterparts, were demonstrated to be capable of forming splenic colonies when transplanted into irradiated hosts. Definitive evidence, through work in chronic myeloid leukaemia (CML), that a single progenitor cell was capable of driving leukaemia was provided in 1977 [95]. Utilising Glucose-6-phosphate dehydrogenase isoenzymes, CML cell behaviour was studied, the results shaping the future of oncology research. A single pluripotent SC, following transformation, was shown to produce clonal malignant progeny. Further, normal myeloid, lymphoid and erythroid cells and platelets were shown to harbour the same isoenzyme as the malignant population suggesting a common cell of origin / clonal origin [95].

During this period, the concept of a malignant cell hierarchy, and importantly halted differentiation, was established and hence the phase 'oncogeny is blocked ontogeny' was introduced in 1968 [96]. Malignant tissues were shown to resemble foetal tissue, though they strikingly lacked the ability to differentiate into the full complement of mature specialised cells required for functional tissue development [97]. Proliferation studies, within squamous cell carcinoma, demonstrated undifferentiated malignant cells to be capable of producing mature, benign cells [98]; whilst enzymatic studies revealed the similarities, and important differences, between hepatic tumour cells and those within the foetal liver [97].

The CSC theory proposes a cancer to have cellular hierarchy similar to that of the normal tissue, with the CSC reflecting the intrinsic SC's multipotency. The hypothesis is supported by two main experimental findings. First, cancers are intrinsically heterogeneous [99-103]; different cell types demonstrated within a cancer. Second, the cancer cells themselves have been shown to be heterogeneous, with differing phenotypes and varying proliferative potential [99,104,105]. This heterogeneity is thought to be due to genomic instability, interactions with the tumour microenvironment and, to a degree, maintenance of the cellular hierarchy seen in the normal

healthy tissue [106,107]. Additionally, a large number of cancer cells are necessary for a cancer to develop and grow [108,109]. Finally, the progression to cancer is usually associated with genomic instability, generating both clonal and non-clonal populations [110].

There is now extensive evidence to support the CSC theory in a wide array of malignancies [2,111]. These CSCs are understood to exist as a minority population, sharing many properties with normal SCs, including self-renewal and differentiation, and are capable of tumour initiation in secondary transplanted hosts [112].

Malignancies with evidence of CSC origin include haematological cancers [112,113] and several solid tumours including: colon [114], breast [115], prostate [116], pancreas [117], lung [118] and certain neurological malignancies [119].

Classically the CSC was believed to arise from normal SCs; mutations allowing the CSCs to undergo unregulated expansion. In leukaemia, for example, the CSCs were shown to be capable of producing multiple mature lineages and, further, to express certain markers expressed by normal HSCs [120,121]. More recently however, as our ability to identify and distinguish between the primitive cell populations has improved, evidence has shown the CSC can also arise from progenitor cells which have gained the ability to self renew [23,122,123]. This is especially true in haematopoietic malignancies [124,125].

Whilst there is still much to learn in respect of the CSC, various experimental models have shown these cells to be innately less sensitive to treatment, to continually develop genomic and epigenomic changes and to uniquely interact with the SC niche [23,126]. The influence each of these factors has on the CSC's treatment-resistant phenotype is however, unclear. It is therefore vital to continue to seek to unravel the complex and likely intertwined, molecular mechanisms regulating SC fate.

1.2.2 Leukaemic stem cell

Leukaemic stem cells (LSCs) were first demonstrated in acute myeloid leukaemia (AML) in 1994 [112,121]. Using a severe combined immunodeficiency disease (SCID) immunodeficient mouse model and phenotypic cell isolation strategy the proliferation and self-renewal potential of transplanted human AML cell populations were studied [127,128]. This beautifully showed only a subset of cells capable of serial engraftment in recipient mice, these cells were defined as CD34+CD38−. Further work in 2004 used lineage tracing proved that LSCs are not functionally homogeneous, rather LSCs were shown to have a heterogeneous self-renewal potential closely resembling their normal counterparts [129].

More recent studies have expanded the phenotypic definition of the human AML LSC: CD34+CD38−CD90−IL−3R+CD71−HLA−DR−CD117− [130–133].

Whilst initial work appeared to indicate LSCs arose following the transformation of a normal HSC, subsequent work showed the LSC population to resemble haematopoietic progenitor cells (HPCs), rather than the HSC [113,134,135]. This suggested LSCs either arose from HPCs or the differences reflected a change in surface marker expression upon malignant transformation [131,133,136,137]. The weight of evidence from subsequent research however appears to support the idea that LSCs are in fact derived from HPCs.

Initial studies used mouse models to study the effect of leukaemia inducing mutations on myeloid progenitor populations [138,139]. In a transgenic mouse leukaemia model, both HSCs and HPCs transduced with a chimeric minigene encoding *MLL-AF9* (originating from t(9;11)(p22;q23), associated with myelomonocytic AML (FAB M4 / M5) and linked to t-AML resulted in LSCs and leukaemia though many more transduced HPCs had to be transplanted to establish leukaemia compared with HSCs [123,140]. Similar results were demonstrated when the *MLL-ENL* fusion gene

(originating from t(11;19)(q23;p13.3) was expressed in haematopoietic cells, transplantation efficiency shown to progressively fall with cellular differentiation from HSCs to CMPs and finally granulocyte-macrophage progenitors (GMPs) [122,141]. These results suggesting, more committed progenitor cells when transformed, whilst not being as efficient as HSCs retained SC characteristics, notably the experimentally defined ability to give rise to disease following transplantation. Another study assayed the ability of different leukaemogenic genes to transform progenitor populations. CMPs transduced with a *MOZ-TIF2* fusion oncogene (originating from inv(8)(p11q13), associated with FAB M4/5 morphology, involved in histone acetylation [142] [143,144] could be serially replated *in vitro* and induce transplantable AML *in vivo*. However, a *BCR-ABL* (arising from the Philadelphia chromosome, a reciprocal translocation t(9;22)(q34;q11) resulting in a constitutively active tyrosine kinase fusion gene was not able to transform GMPs into LSCs [145,146]. These results suggested that whilst LSCs did arise from HPCs, HPCs required additional mutations to acquire self-renewal ability before they are capable of transforming into LSCs. Further, not all leukaemic cells were capable of giving rise to disease on transplantation, suggesting the LSCs gave rise to both self-renewing and non-self-renewing daughter cells [124,147]. Additional evidence to support HPCs as the cell of origin in myeloid malignancies came from lineage analysis of LSCs in human chronic myeloid leukaemia (CML) [125]. Analysing the colony forming and transplantation potential of different populations of leukaemic cells from patients with CML-blast crisis (BC) revealed those cells with self-renewal potential phenotypically resembled HPCs rather than HSCs [125,148]. Whilst myeloid CML-BC is managed clinically as AML, allowing comparisons to be made, it is important to remember the differences in these entities, not least in the preceding disease and initiating lesion, the heterogeneity of AML precluding such definitive evidence. More recently however two molecularly distinct, hierarchically ordered, populations with stem cell qualities have been identified in CD34+ AML; a $CD34^+CD38^-CD45RA^+$ lymphoid-primed multipotent progenitor (LMPP) population and a more mature $CD34^+CD38^+CD45RA^+$ granulocyte-macrophage progenitors (GMP) population [149]. Interestingly, molecular studies have shown these populations to closely resemble normal progenitor cells suggesting CD34+ AML is a progenitor disease arising following LSC acquisition of abnormal self-renewal potential.

1.3 Leukaemia

The term leukaemia implies a neoplastic process resulting from the uncontrolled expansion of haematopoietic cells, encompassing a broad spectrum of BM disorders. The reality however, is far more complicated, and interesting!

The first case described in the literature was in 1827. The term “leukaemia”, derived from the Ancient Greek meaning white blood however, was not introduced until 1856, and then, in 1889 “acute leukaemia” was used to differentiate rapidly progressive leukaemia from the more indolent chronic forms. Finally, in 1900 the myeloblast was characterised, dividing leukaemia into "myeloid" and "lymphoid" depending on the predominant cell type; 85% of adult leukaemia being myeloid.

1.3.1 Acute myeloid leukaemia

AML encompasses a group of aggressive haematological neoplasms. It arises from impairment in differentiation and over-proliferation of the HPSC compartment, resulting in the accumulation of a clone or clones of abnormal, non-functional, immature myeloid progenitor cells termed myeloblasts. However while substantial progress has been made in understanding AML there are still distinct areas that require major advances.

It is a clinically, morphologically and genetically heterogeneous disease involving one or all of the myeloid lineages [150]. Whole-genome sequencing has shown AML to be polyclonal, with a dominant clone tending to emerge at relapse [151].

AML is the most common malignant myeloid disorder in adults with an annual incidence of approximately 5 per 100,000, increasing progressively with age, to a peak of 21 per 100,000 adults aged 65 years and older [152,153]. Its incidence has increased by 73% since the 1970s, with the largest increase in those aged over 80 years; 2942 new cases were diagnosed in 2013 in the UK alone [152]. This increase is considered to reflect our aging population in addition to improvements in diagnostic techniques and data registration rather than a true increase in disease incidence. It affects all ages, though the median age at presentation is 70 years. Unexplainably, there is a slightly higher incidence in men than women, with a ratio of approximately 1.4:1 [152].

The diagnosis of AML requires a minimum of 20% myeloid blasts within the BM. AML is then classified according to the World Health Organization (WHO) Classification of Tumours of the Haematopoietic and Lymphoid Tissues, defining four major categories; Table 1.1 [154].

Table 1.1: WHO Classification [154]

Name	**Description**
AML with recurrent genetic abnormalities	AML with translocations between chromosome 8 and 21 - t(8;21)(q22;q22); *RUNX1/RUNX1T1* AML with inversions in chromosome 16 - inv(16)(p13.1q22) or internal translocations - t(16;16)(p13.1;q22); *CBFB/MYH11* APL with *PML-RARA* with translocations between chromosome 15 and 17 - t(15;17)(q22;q12); *RARA/PML* AML with translocations between chromosome 9 and 11 - t(9;11)(p22;q23); *MLLT3/MLL* AML with translocations between chromosome 6 and 9 - t(6;9)(p23;q34); *DEK/NUP214* AML with inversions in chromosome 3 - inv(3)(q21q26.2) *GATA2, MECOM* or internal translocations - t(3;3)(q21;q26.2); *RPN1/EVI1* Megakaryoblastic AML with translocations between chromosome 1 and 22 - t(1;22)(p13;q13); *RBM15/MLK1* AML with mutated NPM1 AML with biallelic mutations of CEBPA **PROVISIONAL ENTITY:** AML with *BCR-ABL1* AML with mutated *RUNX1*
AML with myelodysplasia-related changes	This category includes patients with a prior diagnosis of MDS (myelodysplasia) or MPN (myeloproliferative neoplasm), or cytogenetic abnormalities characteristic for this sub-type

	AML with complex karyotype Unbalanced abnormalities: AML with deletions of chromosome 7 - del(7q) AML with deletions of chromosome 5 - del(5q) AML with unbalanced chromosomal aberrations in chromosome 17 - i(17q)/t(17p) AML with deletions of chromosome 13 - del(13q) AML with deletions of chromosome 11 - del(11q) AML with unbalanced chromosomal aberrations in chromosome 12 - del(12p)/t(12p) AML with deletions of chromosome 9 - del(9q) AML with aberrations in chromosome X - idic(X)(q13) Balanced abnormalities: AML with translocations between chromosome 11 and 16 - t(11;16)(q23;q13.3), unrelated to previous chemotherapy or ionizing radiation AML with translocations between chromosome 3 and 21 - t(3;21)(q26.2;q22.1), unrelated to previous chemotherapy or ionizing radiation AML with translocations between chromosome 1 and 3 - t(1;3)(p36.3;q21.1) AML with translocations between chromosome 2 and 11 - t(2;11)(p21;q23), unrelated to previous chemotherapy or ionizing radiation AML with translocations between chromosome 5 and 12 - t(5;12)(q33;p12) AML with translocations between chromosome 5 and 7 - t(5;7)(q33;q11.2) AML with translocations between chromosome 5 and 17 - t(5;17)(q33;p13) AML with translocations between chromosome 5 and 10 - t(5;10)(q33;q21) AML with translocations between chromosome 3 and 5 - t(3;5)(q25;q34)
Therapy-related myeloid neoplasms	This category includes patients who have received prior chemotherapy and/or radiation and subsequently develop AML or MDS.
AML not otherwise categorised	This category includes subtypes which do not fall into the above categories: AML with minimal differentiation AML without maturation AML with maturation Acute myelomonocytic leukaemia

	Acute monoblastic and monocytic leukaemia Acute erythroid leukaemia Acute megakaryoblastic leukaemia Acute basophilic leukaemia Acute panmyelosis with myelofibrosis
Myeloid sarcoma	
Myeloid proliferations related to Down syndrome	Transient abnormal myelopoiesis Myeloid leukaemia associated Down syndrome

This is a revision of the 2008 classification [153]. The classification utilises clinical, morphological and genetic features, developing upon the previous morphologically based French-American-British (FAB) system.

Cytogenetic abnormalities, the majority of which are non-random chromosomal translocations are detected in 50% to 60% of *de novo* AML [155]. The fusion protein being found to primarily alter expression of genes involved in differentiation, proliferation and/or survival.

The WHO subcategory AML with recurrent genetic abnormalities contains a number of clinically relevant onco-fusion proteins [156,157]: runt-related transcription factor 1 (*RUNX1/RUNX1T1)*, CCAAT/enhancer-binding protein ß/Myosin-11 (*CBPß/MYH11)*, retinoic acid receptor α/promyelocytic leukaemia (*RARa/PML)*, mixed lineage leukaemia (*MLLT3/MLL)*, *DEK/NUP214*, ribophorin-1/MDS1 and EVI1 complex locus *(RPN1/EVI1)*, RNA binding motif protein 15/mitogen-activated protein kinase kinase kinase *9 (RBM15/MLK1)*, nucleoplasmin 1 (*NPM1)* and CCAAT/enhancer-binding protein α (*CEBPa)*.

t(8;21), *RUNX1/RUNX1T1* is expressed in 5-12% of AML, whilst *CBPß/MYH11* is found in approximately 8% of AML [158-160]. Both are associated with a favourable prognosis [161,162], and are believed to function as transcriptional repressors. The t(15;17), *RARA/PML* translocation is found in approximately 13% of all AML, and 95% of acute promyelocytic leukaemia (APML) [158]; *RARa/PML* acting as a transcriptional repressor interfering with cellular differentiation, apoptosis, and self-renewal. APML represents a distinct subtype of AML, response to current treatments exceeding 90% [163,164], thus serving as the first malignancy largely cured by targeted therapies. *MLLT3/MLL* is found in 5-10% of AML [158,165,166]. The fusion protein thought to act as an oncogene, conferring a variable prognosis [165]. inv(3)/t(3;3), *RPN1/EVI1* occurs in 1-2% of AML, is involved in cellular differentiation, proliferation and apoptosis, and is characterised by a poor clinical outcome [167,168]. t(6;9) *DEK/NUP214* is found in approximately 1% of AML, increasing cellular proliferation, and conferring a poor prognosis [158]. The t(1;22), *RBM15-MKL1* is found in <0.5%, being found almost exclusively in infants and children, and associated with acute megakaryoblastic leukaemia (FAB M7). It is also associated with a poor prognosis [167,169,170].

NPM1 and *CEBPa* mutations affect cell proliferation and survival [171]. *NPM1* has been detected in approximately 35% of AML, and is associated with a favourable outcome [172-174]. Several mechanisms of action have been proposed including regulation of the tumour suppressor p53 and components of the cell cycle [175,176]. *CEBPa* is found in 5 to 14% of AML, with biallelic but not monoallelic mutations being strongly associated with a favourable prognosis [177]. *CEBPa* is involved in cell differentiation and has been found to serve as a tumour suppressor [178,179].

40% to 50% of AML cases have a normal karyotype, classified as intermediate risk by the WHO Classification. However, these cases are clinically highly diverse, reflecting the genetic heterogeneity seen within this subgroup. The mutations found are broadly defined by function: class I affect cellular proliferation and/or survival, whilst class II result in impaired differentiation. Class I mutations include stem cell growth factor receptor *c-KIT*, fms-like tyrosine kinase 3 (*FLT3)*, neuroblastoma RAS viral oncogene homolog *(NRAS)* and kirsten rat sarcoma viral oncogene homolog *(KRAS)*. Studies have shown activating *KIT* mutations to be associated with a higher incidence of relapse and significantly lower survival, negating favourable prognostic genetic abnormalities including *RUNX1/RUNX1T1* and *CBPB/MYH11*. *FLT3*, a receptor tyrosine kinase vital in determining HSC cell fate, is one of the most frequently encountered mutations in AML being found in approximately 30% of AML [180]; the prognostic impact dependent on the nature of the mutation and its genetic context [181]. *FLT3* mutations can be divided into two categories: internal tandem duplications (*FLT3-ITD*) in or near the juxtamembrane region [182] or point mutations within the activation loop of the tyrosine kinase domain (*FLT3-TKD*) [183]. Both result in constitutive tyrosine kinase activity in the absence of ligand, which signal through different mechanisms, thereby accounting for the biological differences. *FLT3-ITD* typically associates with *NPM1* or *DNMT3a* mutations [181]; studies demonstrating an *NPM1* mutation to mitigate the negative prognostic effect of *FLT3-ITD* [184,185]. *FLT3-ITD* occurs in approximately 25% of *de novo* AML cases. Gene expression profiling has confirmed *FLT3-ITD* to be an independent poor risk factor in AML with trials such as the NCRI AML 19 [186] stratifying patients bearing the FLT3-ITD mutation as high risk [187]. Interestingly the incidence of *FLT3-ITD* varies with age, being relatively rare in paediatric AML [188]. *FLT3-TKD* is less frequent, occurring in approximately 7% of patients, being more common in favourable risk AML [189]. A number of FLT3 tyrosine kinase inhibitors (TKIs) have been developed, being trialled clinically either as a monotherapy or in combination with other agents [190]. Mutations in *NRAS* and *KRAS* occur in approximately 10% and 5% of AML, respectively.

Class II mutations include *MLL* and Wilms tumor gene (*WT-1*). *MLL* fusion genes are found in 5-10% of AML [191]; abrogating p53 function [192]. 11q23 abnormalities are associated with a poor prognosis, whilst t(9;11)(p22;q23) is associated with a more favourable outcome. *WT-1* mutations occur as secondary events, being found in approximately 14% of AML; the significance is dependent on preceding mutations [193].

Novel small molecule inhibitors to target a number of these mutations are in development [181,194,195]. Interestingly, considering other therapeutic approaches, a WT1 peptide vaccination has been trialed in a small number of patients with myelodysplasia (MDS) and/or AML. Whilst the numbers are small, and the cases heterogeneous vaccination has been shown to be safe and feasible, and further clinical responses have been reported [196]. Larger, randomised clinical trials are however needed to further determine the role of WT1 peptide vaccination, and other immunotherapeutic approaches in the management of AML.

AML with myelodysplasia-related changes is a heterogeneous disorder defined by morphologic, genetic and clinical features. It has an adverse prognosis, with many cases preceded by MDS or a myeloproliferative neoplasm (MPN) [154].

Therapy-related myeloid neoplasms (t-MN) occur as a late complication following chemotherapy and or radiotherapy, though the mechanism remains unclear [197,198]. Within this category there is considerable heterogeneity - distinct clinical and cytogenetic subtypes being well recognised. Clonal chromosome abnormalities are found in the majority; abnormalities of chromosome 5, 7 or both account for approximately 75% of cases with an abnormal karyotype [199]. The latency ranges from a few months to several years, dependent upon the nature of the preceding treatment, intensity and cumulative dose [198].

AML not otherwise specified encompasses the cases not belonging to the other categories. It utilises the FAB classification to morphologically sub-categorise each case. Interestingly, FAB M0 was independently associated with an inferior overall survival (OS) and reduced likelihood of

achieving a complete remission (CR) compared with FAB M1, M2, M4, M5, and M6 [200]. However this prognostic significance was lost when the *NPM1* and *CEBPa* mutational status was accounted for [200]. With our ever expanding knowledge and ability to molecularly define AML it will be interesting to see how, or even if, morphological sub-classification, once so vital, provides any clinical benefit in the future.

In keeping with the heterogeneity of the disease, many factors govern treatment decisions and crucially the patient's prognosis – including those that determine the patient's WHO subtype and patient age [201,202]; cytogenetics being the most important prognostic factor for predicting OS, remission and relapse [154,155,158,165].

However, despite advances in understanding of the pathophysiology the basic therapeutic approach to AML has changed little over the last few decades. The approach to adults aged 18–60 years with AML classically involves two phases: achieving CR, defined as a BM with less than 5% blasts, a neutrophil count greater than 1000/μL, and a platelet count greater than 100 000/μL [203] and prolonging / maintaining remission. The standard treatment for AML, excluding patients with APML, consists of 3 days of an anthracycline and 10 days of cytarabine ("3+10") [201]. A number of clinical trials have sought to intensify treatment or minimise toxicity; these trials have used alternative anthracyclines such as idarubicin, added or substituted high-dose cytarabine, or added etoposide. While these alternative regimes have been tolerated, whether they offer OS benefit has yet to be proven. Table 1.2 shows select current phase III trials for previously untreated AML, categorised according to patient age. It does not show investigational therapies and early phase trials, these are discussed later, in Section 1.3.5.

Table 1.2: Current Phase III clinical trials for untreated AML

Funder **Sponsor (where applicable)** **Trial name**	**Treatment**
18-60, and those >60 years for whom intensive therapy is considered appropriate	
HOVON **132 AML**	DA/IA followed by high dose consolidation +/- lenalidomide (immunomodulatory agent)
CR-UK **Cardiff University** **NCRI AML19**	FLAG-Ida vs DA +/- GO (anti-CD33 immunoconjugate) High risk: FLAG-Ida vs CPX-351 followed by allogeneic SCT Standard risk: +/- Ganetespib (Heat shock protein 90 inhibitor) FLT3+: +/- AC220 (FLT3 inhibitor) APML - AIDA
Sprycel	DA + Histone deacetylase (HDAC) inhibitor +/- Dasatinib (dual ABL/SRC inhibitor) in CBF-AML
SWOG	DA vs IA vs IA + Vorinostat (HDAC) inhibitor
>60 years fit for intensive therapy	
EORTC **1301**	DA vs Decitabine followed by allogeneic SCT
HOVON **97 AML**	+/- Azacitadine (DNA methyltransferase inhibitor) maintenance
Bloodwise **Cardiff University** **NCR1 LI-1**	Low dose Ara-C Low dose Ara-C + AC220 Low dose Ara-C + Tosedostat (aminopeptidase inhibitor) Low dose Ara-C + Selinexor (selective inhibitor of nuclear export) Low dose Ara-C + Lenalidomide
CR-UK **Cardiff University** **NCRI AML 18**	DA +/- GO CR & MRD negative after #1: 2 vs 3 cycles DA Lack of CR or MRD positive after #1: DA vs DAC or FLAG-Ida followed by non-intensive allogeneic SCT +/- AC220 +/- Ganetespib

Abbreviations: DA: daunorubicin + cytarabine; DAC: daunorubicin + cytarabine + cladribine; IA: idarubicin + cytarabine; FLAG-Ida: fludarabine + high dose cytarabine + idarubicin + granulocyte colony-stimulating factor (G-CSF); GO: Gemtuzumab ozogamicin; AC220: Quizartinib; SCT: stem cell transplant; AIDA: all-*trans* retinoic acid + idarubicin; HDAC: Histone deacetylase inhibitor; Ara-C: cytarabine; CR: complete remission; MRD: minimal residual disease.

In the UK, eligible, consenting patients are treated within a clinical trial. For those aged between 18 and 60 years and those aged over 60 years for whom intensive therapy is considered appropriate, there is the recently opened National Cancer Research Institute (NCRI) AML19 trial. This large, multi-centered randomised trial seeks to build on previous trial data combining cytogenetic and mutation status with emerging new treatments to improve outlook for younger patients. Briefly, it aims to compare four induction schedules (DA plus Gemtuzumab ozogamicin (GO) / DA plus GOx2 / fludarabine, high dose cytarabine, idarubicin, granulocyte colony-stimulating factor (G-CSF) (FLAG-Ida) plus GO / FLAG-Ida plus GOx2), provided adverse cytogenetics are not already known. Patients are subsequently segregated according to molecular / genetic characteristics, and a validated risk score [204]. For those with adverse cytogenetics the trial seeks to compare the novel treatment agent CPX-351 against FLAG-Ida. CPX-351 is a liposomal formulation of cytarabine and daunorubicin designed to deliver synergistic drug ratios. High-risk, or refractory (resistant disease or <50% reduction in blast percentage) patients will receive allogeneic stem cell transplant providing a suitable donor is available.

Standard treatment regimens however, are associated with considerable morbidity and mortality. Further, although treatment results in a favourable response, with high remission rates of 60-80% in younger patients, only 30-40% survive 5 years (45% of those achieving CR) [205].

Outlook for the older population, those most affected, however remains poor with a median survival of a few months. Patients over 60 years have a 40%–60% chance of CR, with only 5%–15% surviving 5 years [201,202]. Further, whilst those over 70 years can attain a CR with intensive therapy, the chance is reduced yet further to 30%, with <10% of treated patients remaining alive at one year. The difference in prognosis is a reflection of co-morbidities associated with ageing and disease biology [202]. Older adults with AML are also considered more likely to have HSCs with a reduced proliferative capacity [206], which may affect blood count recovery following chemotherapy. Table 1.3 is modified from the American Society of Haematology (ASH) Education handbook demonstrating some of the key differences between young and old AML biology [207].

Given that for 85-95% of older patients any treatment will ultimately be palliative the balance between the potential for cure or survival prolongation and quality of life must be carefully considered in this population. Treatment options include supportive care (transfusion support and antibiotics), low-dose chemotherapy (hydroxycarbamide or low-dose cytarabine), hypomethylating agents (HMAs; azacitidine), high-dose chemotherapy (“3+10”) and novel agents within clinical trials.

In summary, AML is a hugely complex disease both from the perspective of the scientist seeking to improve current understanding and thus patient outlook, and from the clinician treating each individual patient they are faced with. It is however a hugely exciting time to work within this field, work already being translated into improved sub-classification [154], new terminology discussed below, and an expanding armory of small molecule inhibitors and strategies for evaluating emerging treatments.

Table 1.3: Characteristics of older and younger adults with AML [207, 720]

Characteristic	≥60 years	18-60 years
Incidence (rate per 100,000)	52.7	5.8
Secondary AML	24–56%	8%
Favourable cytogenetics		
t(8;21)	2%	9%
inv 16 or t(16;16)	1–3%	10%
t(15;17)	4%	6–12%
Unfavourable cytogenetics		
−7	8–9%	3%
+8	6–10%	4%
Complex	18%	7%
MDR1 expression	71%	35%
CR	40-50%	60-70%
Treatment-related mortality	25–30%	5–10%
DFS	5–15%	30%

CR: complete remission; DFS: disease free survival

1.3.2 Pre-leukaemia

'The evolutionary history of most types of leukaemia starts years before clinical presentation, during a prolonged pre-leukemic stage', Scott A Armstrong, Cell of Origin and Leukaemic Transformation, ASH, San Diego, USA, December 2016.

This concept, of pre-leukaemia, has arisen following work studying the nature, order and consequences of well recognised and frequently occurring mutations within the haematopoietic hierarchy [208-210]. Interestingly, long before this work, research into paediatric ALL provided evidence of an initiating event, a 'first hit', being detectable months or years prior to the clinical development of ALL. Researchers retrospectively analysed neonatal blood spots (Guthrie spots) of patients who had developed ALL carrying the *MLL-AF4* gene rearrangement between the ages of five months and two years [211]. The leukaemic specific molecular abnormality (*MLL-AF4*) was identified in all cases providing definitive evidence ALL in its simplest is a two-step process with an initiation and a driver mutation required for disease development.

More recently, next-generation DNA sequencing has shown AML to be associated with, on average, five somatic mutations in recurrently mutated genes. Particularly interesting is that there appears to be distinct patterns of mutation acquisition; mutations in genes regulating the epigenome (histone modifiers, DNA methylation) occurring early, whilst those involved in proliferative signal transduction (*FLT3, RAS*) occur late [100,212]. Further, these patterns appear to correlate with distinct diagnostic features and clinical outcomes [212].

Whilst the mechanisms that underlie the sequential acquisition of mutations in a specific cell type are not fully understood, evidence suggests the initiating events occur in a leukaemic HSC or more committed progenitor cell [210]; the *NPM1* mutation is found to originate in GMP cells [173]. Further, these pre-leukaemic cells whilst maintaining multi-lineage differentiation potential acquire an increased 'fitness' compared to wild type HSC, gradually becoming the major clone

over time. Fractions of this pre-leukaemic population are at risk of acquiring additional mutations and evolving into overt leukaemia. Whether this knowledge can be harnessed clinically is an exciting area of intense research.

1.3.3 Clonal haematopoiesis of indeterminate potential

Another emerging and interesting concept, related to the concept of pre-leukaemia, is clonal haematopoiesis of indeterminate potential (CHiP). In CHiP, a clone carrying one, or occasionally several, somatic mutations is identified, arising from the expansion of HSPCs [213,214]. These mutations may be those described in pre-leukaemia or distinct. This concept is in its infancy however, with opinion divided whether this state precedes pre-leukaemia or is a distinct entity. Whether ChiP is a consequence of age or a means of 'coping' with age also remains unclear. Interestingly, population-based studies have detected mutations recurrent in haematological malignancies, including *DNMT3A* and *TET2*, in the PB of individuals with no previous haematological disease history [213,214]. Further, long-term follow-up appears to indicate these cases have an increased risk of developing a haematological disease [213,214].

Importantly, irrespective of terminology, the existence of a pre-leukaemic HSC raises the possibility of early detection, prior to the development of AML potentially allowing for intervention therapy and disease prevention.

1.3.4 Chemoresistance

Chemoresistance is the term used to describe a cell, or cells, resistant to cytotoxic agents, with proposed mechanisms proving to be increasingly diverse and complex with our expanding knowledge. Understanding these mechanisms, and how genomic alterations result in different cancer phenotypes is vital when considering current treatment strategies and designing novel therapies. 90% of treatment failures are attributed to chemoresistance [215].

CSCs have been shown to be innately less sensitive to treatment, potentially explaining MRD, relapse and disease progression, highlighting the need to target these cells in order to effect a cure [23,126]. Current chemoresistance hypotheses include microenvironmental cellular interactions, epigenetic changes and deregulation of the self-renewal pathways, and cell proteostasis. Whilst the influence each of these factors has on the CSCs treatment-resistant phenotype is unclear, in reality, it is likely to be a complex interplay between some or all of these factors that enables the CSC to evade cell death. Interestingly, whilst mechanisms of chemoresistance appear common, their function and significance appears to differ depending on the driving genomic alterations [216,217].

The role of each mechanism is beyond the scope of this thesis. For the purpose of context I have chosen to touch upon select mechanisms, discussed below, those intrinsic to my thesis will be discussed in greater depth later.

Altered expression of ATP-binding cassette (ABC) transporters by CSCs is seen as one mechanism of chemoresistance, with anthracyclines key in the treatment of AML, being effluxed by more than one ABC transporter [218]. Clinical trials have sought to overcome this mechanism of chemoresistance through the use of specific ABC transporter inhibitors. Zosuquidar, the multidrug resistance inhibitor was combined with DA in a Phase II clinical trial [219] whilst verapamil, a general ABC transporter was utilised in combination with standard treatment for multiple myeloma (MM) [220]. These studies were discontinued due to their limited efficacy. Nanoparticle drug-delivery attempting to overcome this form of drug resistance has shown promise in both murine and *in vitro* models [221,222]. It remains to be seen if this can be translated clinically. ABC transporters therefore represent a major mechanism of chemoresistance; whilst

early attempts to overcome this mechanism of resistance showed limited efficacy, work continues, and the results are keenly awaited. The European Union (EU) Clinical Trials register [223] presently lists 8 open trials studying the effect of the ABC inhibitors whilst ClinicalTrials.gov, a service of the United States Institutes of Health, lists 48 open trials.

Another mechanism of chemoresistance is the B-cell lymphoma-2 (Bcl-2) protein family, members being identified as critical for the development and growth of many, if not all malignancies [224]. The Bcl-2 proteins play a critical role in regulating apoptosis and proliferation (discussed in Section 1.5 below). Levels of the anti-apoptotic Bcl-2 protein have prognostic significance in a number of malignancies including lymphoid [225] and myeloid malignancies [226]; in AML Bcl-2 has been shown to be over-expressed in 71% of patients, associating with a reduction in DFS [226]. In addition, evidence suggests these proteins can effect chemoresistance through induction of other signalling pathways such as Akt1 [227,228], protein kinase C α (PKCα) [229], extracellular signal-regulated kinase 1/2 (Erk1/2) [230], c-Src and aurora-A [231]. Whilst early drugs struggled with off target effects, ABT-737 a first generation BH3-mimetic causing dose limiting thrombocytopenia through its binding to B-cell lymphoma-extra large (Bcl-xL) [232], the second generation Bcl-2 inhibitors have demonstrated striking clinical efficacy with early phase clinical trials in both solid and haematological malignancies [233]. ABT-199, a BH3-mimetic was subsequently granted breakthrough designation by the United States Food and Drug Administration (FDA) for relapsed or refractory chronic lymphocytic leukaemia (CLL) with 17p deletion in April 2016 (https://www.fda.gov/newsevents/newsroom/pressannouncements/ucm495253.htm). The EU Clinical Trials register [223] presently lists 12 open trials studying the effect of Bcl-2 inhibition whilst ClinicalTrials.gov lists 27 open trials.

Several signalling pathways, with their diverse roles within malignancy, have also been linked to chemoresistance.

Epithelial–mesenchymal transition (EMT) is the process of cell reprogramming from an epithelial to mesenchymal-like phenotype. Whilst a role for the EMT pathway in solid malignancies is well established, [234–239] recent work has shown components of the pathway including Twist1, Snail and Slug to be deregulated in haematological malignancies [236,240,241]. Twist1 being shown to increase Bmi1, a member of the Polycomb family has been linked to leukaemogenesis and prognosis [242]; whilst gain-of-function mouse models have shown deregulation of Snail and Slug pathways to result in an irreversible increase in haematological malignancies, particularly the acute leukaemias [243–246]. A *slug* knockout mouse model has shown Slug to govern cell survival by inhibiting the pro-apoptotic activity of *puma* (Bcl-2 Binding Component 3 (BBC3)). Further, patterns of deregulation have been shown to associate with different AML sub-types, clinical phenotypes and treatment response [240] and to distinguish normal and malignant myeloid precursors excluding myeloid maturation dependence [247]. Interestingly, the HIF-related network has been shown to be differentially expressed in APML relative to other AML subtypes. Further expression of *ITGB2*, *HMOX1*, *IGFBP2* and *MMP2* was reversed upon cellular differentiation following treatment of APL-derived NB4 cells with all-trans retinoic acid [247].

Abnormal activation of the Hh pathway has been reported in a number of CSC models [248], with pathway inhibition sensitising CSCs from a number of malignancies including CML [249–255], gastric [248,256,257], pancreatic [257–261], lung [257,262,263], ovarian [264,265] and prostate [266–268] cancer. The Hh signalling pathway is discussed in considerable detail in Section 1.4.

Chemical activation of the Wnt pathway enhanced chemoresistance within hepatocellular HPSCs whilst a lentiviral *β-catenin* knockdown reversed this resistance, the link being confirmed in other models [269], and malignancies [270]. Interestingly up-regulation of the ABC transporters is considered as one mechanism by which the Wnt pathway mediates chemoresistance; activation of the Wnt pathway, in neuroblastoma cells, being demonstrated to induce the ATP-Binding Cassette, Sub-Family B (ABCB1), conferring chemoresistance [270]. Further, in ovarian CSCs,

chemoresistance was demonstrated to be mediated by the ATP-binding cassette sub-family G member 2 (*ABCG2*), expression and chemoresistance reversed by a *β-catenin* small interfering (siRNA) knockdown [271]. The ABC transporters are recognised as key downstream targets of a number of other signalling pathways, including Hh, and therefore representing an appealing therapeutic target, though as discussed above this has yet to be translated clinically.

The Notch signalling pathway has also been shown to contribute to chemoresistance, primarily through its over activation [272] in a number of malignancies: T-acute lymphoblastic leukaemia [273], AML [274], lung [275,276], breast [277,278], ovarian [279] and certain neurological tumours [280,281]. Further, in glioma, colon and ovarian malignancies, treatment up-regulated and activated the Notch pathway, with a siRNA *Notch 1* knockdown or γ-secretase inhibitor preventing chemoresistance, sensitising these cells to the effects of treatment [279,282]. Interestingly, Notch activation has also been shown to mediate chemoresistance through the ABC transporter ABCC1 in prostate cancer [283].

The Phosphatidylinositol 3-kinase Protein kinase B (PI3K-Akt) and extracellular signal-related kinases (ERK) signalling pathways have also been linked to chemoresistance in gastric [284], endometrial [285], oeophageal [286] and colon cancer [287]. Whilst the mechanisms of resistance are not fully understood, research has shown these pathways down regulate p53 and up-regulate c-Myc [288], ABCB1 and ribonucleotide reductase catalytic subunit M1 (RRM1) [289].

Finally, studies have shown constitutive activation of the nuclear factor kappa B (NFκß) pathway, within ovarian and breast CSCs, correlates with chemoresistance [290-292], whilst inhibition induced cell death [290,293].

The complex relationship existing between these signalling pathways is becoming increasingly apparent, each pathway communicating with others, and converging on key downstream targets. It is not surprising then that small molecule inhibitors targeting isolated components are seeing limited clinical efficacy. Their role in combination with other agents or in targeting specific disease subsets is an area of ongoing work with the results eagerly anticipated.

Another mechanism of chemoresistance is an enhanced DNA damage response, genomic instability being a common feature of cancer with DNA damage induced by chemotherapy and radiotherapy a key factor in cancer treatment. An enhanced DNA damage response therefore correlates with chemoresistance. These cellular DNA damage responses are tightly coordinated by numerous protein kinases: the checkpoint kinases (Chks), cyclin-dependent kinases (Cdks), aurora kinases (Aurk) and polo-like kinases (Plks). These proteins protect cells through cell cycle regulation and the promotion of DNA damage repair and cell death if necessary [294-297].

The Chks are targets of two distinct pathways: ataxia telangiectasia mutated (Atm) and Atm and rad-3-related (Atr). Atr targets checkpoint kinase 1 (Chk1) whilst Atm targets checkpoint kinase 2 (Chk2), with drug development demonstrating Chk1 to be more important in cell protection [296,298]. Somatic mutations, polymorphisms and epigenetic silencing of *ATM* have been demonstrated in ALL [299], CLL [300], breast [301], colorectal [302] and lung cancer [303]. Whilst mutations within *ATR* and *CHK1* are less frequent, they have also been observed in a number of malignancies including colon, stomach and endometrial cancers [304-307]. Aberrant expression of both pathways has been found to confer a poor prognosis in certain malignancies [307,308]. The Cdks bind cyclins, forming an active kinase complex vital in the regulation of cell cycle progression. At least nine Cdks have been discovered with over-expression being demonstrated in a number of malignancies including sarcoma [309,310].

The Aurks regulate spindle assembly, function of centrosomes and cytoskeleton and cytokinesis with aberrant expression linked to tumourigenesis [311,312]. Three kinases have been discovered (A, B and C), with deregulated expression of Aurora A consistently associated with malignancies including breast and gastric cancer [311,313-315]. Research into Aurora kinase inhibitors as therapeutic agents has shown mixed results with their importance and involvement in normal

cell cycle regulation raising concerns regarding toxicity; however to date this fear has not been realised [316].

Epigenetics refers to heritable changes in gene expression [317]. Examples include DNA and histone modifications; deregulated epigenetic mechanisms being shown to have an important role in the pathogenesis of AML [318,319]. Further, epigenetic modifications are frequently reversible and found to be early events in leukaemogenesis [210], making them appealing therapeutic targets.

Mutations in *DNMT3A*, one of the *de novo* DNA methyltransferases, are found in 6% to 36% of AML cases [320]. Whilst the mechanism by which these mutations contribute to leukaemogenesis is not fully understood, recent work suggests DNMT3A R882H promotes chemoresistance [321]. Mutations in *TET2* are observed in 8% to 27% of patients with AML, conferring a poor prognosis in intermediate-risk AML [322] and chemoresistance in prostate cancer. Mutations in the mutually exclusive isocitrate dehydrogenase 1/2 (*IDH1/2*) are found in 5-19% of AML cases [323-325].

Histone acetylation and deacetylation is the process of acetyl group transfer to and from lysine residues in histone proteins governed by histone lysine acetyltransferases (HATs) and histone deacetylases (HDACs), respectively. Acetylation of lysine residues results in open chromatin confirmations, whereas deacetylation results in condensed and closed chromatin. Methylation of histone lysine residues can result in mono-, di-, or trimethylation; this is processed by lysine methyltransferases (KMTs). Acetylation is associated with chemoresistance in pancreatic [326] and colon tumours [327], whilst deacetylation and methylation are associated with chemoresistance in ovarian cancer [328].

In reality, the role each mechanism has in chemoresistance will vary, dependent on the cell of origin and other genetic alterations within the CSC.

1.3.5 Investigational therapies

Given the complexity of the disease, it is not surprising that single agent therapies, in the large part, have failed to achieve more than limited improvements in patient survival. Further, whilst currently AML is risk stratified according to cytogenetic analysis [154], with a dramatic difference in clinical outcome seen between different groups [201,202] this risk stratification is limited, lacking precision.

Progress in our understanding of cancer biology and the mechanisms involved in leukaemogenesis now sees us entering a new era, where research based innovations are being directly translated into patient care. We are shifting towards a time of comprehensive genomic assessment at diagnosis to determine patient classification and prognosis, an awareness of functional AML subsets informing treatment strategies.

A challenge posed by recent advances, including novel molecularly targeted therapies however is the comparatively low incidence of the disease and its intrinsic heterogeneity, making interpretation of results challenging. That said, as a clinician treating patients in an era with an ever increasing armory of new agents is hugely exciting; there are presently 271 Phase I-III open clinical trials listed by the EU Clinical Trials register [223] and 556 by ClinicalTrials.gov. Table 1.4 shows select investigational therapies, and their proposed mechanism of action. These were selected on the basis of their presentation at the following high impact international meetings, ASH and American Society of Clinical Oncology (ASCO) in 2015 and 2016.

Table 1.4: Recently presented investigational therapies and proposed mechanism of action

Sponsor **NCT trial number**	**Phase**	**Patient characteristics**	**Treatment**	**Mechanism of action of novel agent**
Seattle Genetics, Inc. **NCT01902329**	Phase I	>18yrs Untreated CD33+ AML	SGN-CD33A +/- HMA	Antibody-drug conjugate (ADC) targeting CD33
Seattle Genetics **NCT01902329**	Phase I	>18yrs AML relapsed within 3mths of intensive therapy / untreated / low intensity	SGN-CD33A	ADC targeting CD33
BerGenBio AS **NCT02488408**	Phase I	>18yrs R/R AML & high-risk MDS	BGB324 + LDAC	Selective Axl kinase inhibitor
Celdara Medical, LLC **NCT02203825**	Phase I	>18yrs >18yrsAML & MDS	NKG2D	Chimeric antigen receptor-T cells
Bio-Path Holdings, Inc. **NCT01159028**	Phase I	R/R AML & MDS & CML-BC	BP1001 + LDAC	Liposomal Grb2 inhibitor
ADC Therapeutics SARL **NCT02588092**	Phase I	>18yrs R/R CD25+ AML	ADCT-301	ADC targeting CD25 conjugated to SG3199 a pyrrolobenzodiazepine dimer cytotoxine
Celgene Corporation **NCT01915498** **AG221-C-001**	Phase I-II	>18yrs Untreated and R/R *mIDH2*+ AML	AG-221	Inhibits mutant IDH2 specifically within the mitochondria
Celgene Corporation **NCT01915498** **ADH*ENTIFY* trial**	Phase III	≥60yrs *De novo* & seconday R/R *mIDH2*+ AML	AG-221 vs conventional care	Inhibits mutant IDH2 specifically within the mitochondria
Celgene Corporation **NCT02223052**	Phase I-II	>18yrs Untreated / R/R / secondary AML	Extended dosing CC-486	Oral azacitidine
Genentech, Inc. **NCT02287233**	Phase I-II	≥65yrs Untreated AML not eligible for intensive tx	Venetoclax + LDAC	BH3-mimetic
NCI consensus study **NCTO1266083**	Phase II	>18yrs AML in CR1	SLS-001	Multivalent WT1 peptide vaccine

Astellas Pharma Global Development, Inc. **NCT02014558**	Phase II	>18yrs R/R AML	ASP2215	Inhibitor of FLT3 & Axl with activity against FLT3-ITD and FLT3-TKD
Astellas Pharma Global Development, Inc **NCT02421939**	Phase III	>18yrs Primary refractory or first relapse FLT3-ITD+ AML	ASP2215 vs salvage chemotherapy	Inhibitor of FLT3 & Axl with activity against FLT3-ITD & FLT3-TKD
MEI Pharma Inc **NCT01873703**	Phase II	≥65yrs Untreated & unsuitable for intensive tx & poor cytogenetics	Pracinostat & Azacitidine	Oral HDAC inhibitor
Alliance C11001	Phase II	>60yrs Untreated FLT3-ITD/TKD+AML	DA & Sorafenib tosylate	Multi-kinase inhibitor
University of Ulm **AMLSG 16-10** **NCT01477606**	Phase II	18-70yrs Untreated FLT3-ITD+ AML	Induction & consolidation & Midostaurin	Tyrosine kinase inhibitor
Daiichi Sankyo Inc. **NCT02039726** **QuANTUM**	Phase III	18-75yrs Untreated FLT3-ITD+ AML	Induction & consolidation & + AC220 vs placebo	Tyrosine kinase inhibitor
Celator Pharmaceuticals Inc. **NCT01696084**	Phase III	60-75yrs Untreated secondary AML	CPX-351 vs DA	Liposomal DA

HMA: hypomethylating agents (azacitidine / decitabine); CD: Cluster domain; R/R: relapsed/refractory; MDS: myelodysplasia; ADC: antibody drug conjugate; LDAC: low dose cytarabine; tx: treatment; *mIDH2*: mutant Isocitrate Dehydrogenase NADP+ 2; FLT3: Fms Related Tyrosine Kinase 3; ITD: internal tandem duplication; TKD: tyrosine kinase domain; Axl: member of the Tyro3-Axl-Mer receptor tyrosine kinase subfamily; HDAC: histone deacetylase; DA: daunorubicin + cytarabine 7+3.

1.4 Hedgehog signalling pathway

The Hh signalling pathway was initially discovered in 1980 by Nüsslein-Volhard and Weischaus whilst studying embryonic patterning in the Drosophila fruit fly; absence of the Hh protein giving the Drosophila a characteristic 'hairy' or 'prickly' appearance [329,330]. Subsequent work has shown the Hh pathway to be highly conserved across species and vitally important in embryogenesis, performing the function of patterning during the early stages of development through the expansion and contraction of SC numbers. In adult organisms, through its ability to affect SC behaviour in responsive tissues, it is involved in aspects of tissue maintenance and regeneration - proliferation, apoptosis, chromatin modelling, and self-renewal, acting in concert with other stimuli and the SC niche [257].

1.4.1 Canonical signalling

Classically the Hh signalling pathway is believed to be ligand-dependent. Three Hh ligands (Sonic (Shh), Indian (Ihh) and Desert (Dhh)) have been identified in vertebrates, affecting SC behaviour in a time- and concentration-dependent manner [331]. Shh is widely expressed, particularly during embryogenesis, with Shh deficiency being embryonically lethal [330]. Ihh is produced in haematopoietic cells, bone and cartilage [332], whilst Dhh is found in the peripheral nervous system and testes [333]. Hh ligands are initially synthesised as an inactive 45kDa precursor, undergoing post-translational modifications to form a 19kDa amino-terminal active signalling molecule [334]. This cholesterol and palmitoyl modification, catalysed solely by Hedgehog acyltransferase (Hhat), not only enhances ligand activity but also modifies its diffusion capacity [335,336]. The Hh ligands bind to the 12 trans-membrane receptor protein Patched 1 (Ptch1), causing its internalisation and removing its repression of the 7-span trans-membrane protein Smoothened (Smo), allowing pathway activity [337]. In vertebrates, activity of the Hh pathway is intrinsically related to primary immotile cilia; in the absence of ligand, Ptch1 is located within the primary cilia. Following ligand binding, and the internalisation of Ptch1, Smo is able to concentrate in the primary cilia where it interacts with Gli, maintained in an inactive yet stable state complexed to Suppressor of fused (Sufu), shifting the balance towards pathway activation [337].

Whilst the intricacies of this interaction remain poorly understood, studies suggest these receptors do not physically interact, rather Ptch1 is thought to regulate Smo through an intermediary, with studies suggesting that oxysterols, including vitamin D3, are involved [338].

The Sufu-Gli complexes ensure appropriate delivery of Gli proteins to the primary cilium where they dissociate from Sufu, allowing their activation in response to Hh signalling [339]. This dissociation, and subsequent activation, is inhibited if the Sufu-Gli complex cannot travel to the cilium as observed in Kif3a$^{-/-}$ cells [340]. Protein kinase A (Pka) localised at the base of cilia [341] has been shown to control trafficking of the Sufu-Gli complexes to cilia independent of Smo, suggesting a novel mechanism for Hh inhibition. Whether Hh pathway activity regulates Pka however, remains unclear. One hypothesis is that local inhibition of Pka enables interaction between active Smo and Sufu-Gli complexes at the cilia. However, it is likely that additional events are required to transmit the signal from active Smo to the Sufu-Gli complex.

Smo subsequently causes accumulation of the full length active form of the zinc transcription factors Gli-2 and Gli-3 in the nucleus, and potentiates the activity of other positive regulators of the pathway including serine threonine kinase 36 (Stk36) and kinesin family member 7 (Kif7), resulting in transcription of key downstream targets such as *Gli-1* (amplifying output of the pathway) [342,343] and *Ptch1* (preventing uncontrolled pathway activation), regulators of chromatin formation, cell cycle activity including *N-MYC* and *Cyclin D1*, cell mobility and apoptosis, e.g. bone morphogenetic protein 4, forkhead box protein M1 and *WNT2a* [344]; Figure 1.6A: Hh signalling pathway in the active state.

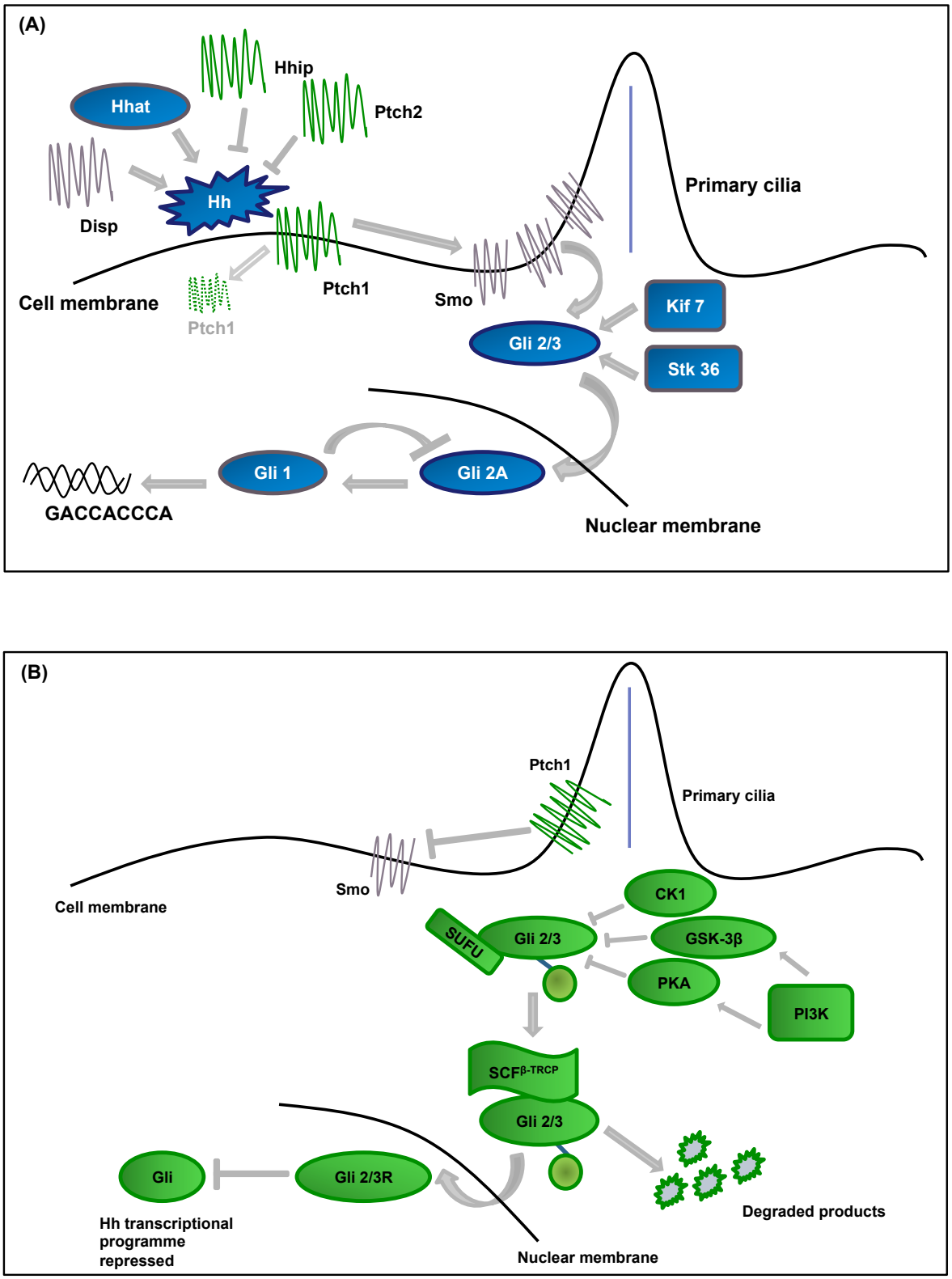

Figure 1.6: Canonical Hh signalling
(A) The Hh pathway is activated by the binding of Hh ligands (Sonic [Shh], Indian [Ihh] or Desert [Dhh]) to the 12 transmembrane protein receptor Patched1 (Ptch1), causing its internalisation and removing repression of the 7-span trans-membrane protein Smoothened (Smo). Smo causes accumulation of the active form of the zinc transcription factors Gli-2 and Gli-3 in the nucleus, and potentiates the activity of other positive regulators of the pathway resulting in transcription of key downstream targets and regulators of chromatin formation, cell cycle activity, cell mobility and apoptosis.
(B) In the inactive state the transcription factors Gli-2 and Gli-3 are non-specifically phosphorylated by casein kinase (CSI), glycogen synthase kinase 3ß (GSK3ß) and protein kinase A (PKA) and retained in the cytoplasm in a protein complex associated with the inhibitory molecule, suppressor of fused (SUFU). This complex undergoes E3 ubiquitin mediated proteolysis to the truncated repressor form which, on translocating to the nucleus, strongly inhibits the Hh pathway.

Of the transcription factors, Gli-1 functions as a positive regulator, Gli-3 a transcriptional repressor, and Gli-2 both a positive and negative transcriptional regulator, determined by post-transcriptional and post-translational modifications [345]. It is the balance between these transcription factors, their active and repressed state, which determines pathway activity [342].

Alternatively, the Hh ligands can bind to several membrane-associated glycoproteins: Patched 2 (Ptch2), Hh-interacting protein (Hhip) and Dispatched (Disp). Ptch2, although structurally similar to Ptch1, has distinct functional properties and a notably different tissue distribution. Ptch1 is broadly expressed whilst Ptch2 is primarily restricted to the skin and testes. Hhip is an endogenous Hh ligand inhibitor, with a binding affinity comparable to Ptch1, preventing pathway activation [346]. Disp is a twelve trans-membrane receptor protein, not involved in Hh ligand synthesis or processing but rather in facilitating ligand movement, thereby modulating canonical pathway activity.

In the inactive state the transcription factors Gli-2 and Gli-3 are retained in the cytoplasm in a protein complex associated with the inhibitory molecule, suppressor of fused (Sufu) [347] and non-specifically phosphorylated by casein kinase (Ck1), glycogen synthase 3ß (Gsk3ß) and Pka. This complex subsequently undergoes E3 ubiquitin-mediated proteolysis by the Skp1-Cullin1-F-box protein ($Scf^{\beta\text{-}TRCP}$) to the truncated repressor form which, on translocating to the nucleus, strongly inhibits the Hh pathway [348]; Figure 1.6B: Hh signalling pathway in the inactive state.

It is the complex interplay between the active and inactive state of the pathway and the positive and negative feedback loops that maintains the careful balance of Hh signalling in normal tissue.

1.4.2 Non-canonical signalling

The notion of non-canonical signalling has arisen following observations that the Hh pathway response does not always appear to follow the classical canonical signalling paradigm. Recent work showing Ptch1 to regulate cell proliferation and apoptosis independent of Smo and Gli and, further Smo to modulate actin cytoskeleton-dependent processes particularly within the nervous system. This data appearing to indicate non-canonical signalling is not only involved, but important, in health and disease. Two broad scenarios of non-canonical Hh signalling are currently recognised, Figure 1.7: Non-canonical Hh signalling [349,350]. In reality, it is likely the canonical and non-canonical pathways act in parallel.

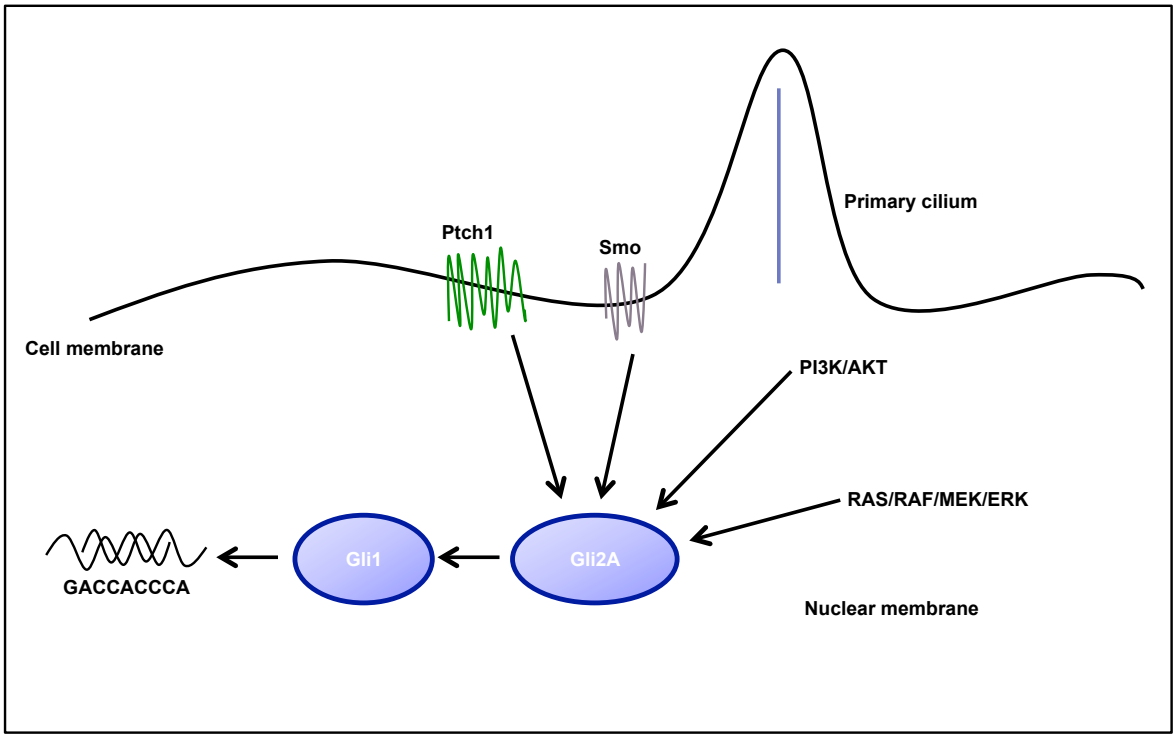

Figure 1.7: Non-canonical Hh signalling
The Hh pathway can be activated directly through PTCH1 or SMO, or via alternative pathways including the PI3K/AKT and RAS/RAF/MEK/ERK signalling cascades.

1.4.2.1 Type I (Smo-independent)

There is considerable evidence to support Hh ligands and Ptch1 can act independently of Smo. Cell culture experiments have shown all three Hh ligands to have an anti-apoptotic effect that was not blocked by Smo antagonists and was independent of Gli transcriptional activity. Further, the effect could not be replicated by genetic or chemical over-expression of Smo [351]. *Ex vivo* and *in vitro* assays have shown Ptch1 to function as a dependence receptor, regulating cell survival in a ligand-dependent manner [352,353], with over-expression inducing apoptosis [353]. Finally, Ptch1 has been shown to regulate the cell cycle through cyclin B1 and Grk2, this association being modulated by Shh and independent of Smo [354,355].

1.4.2.2 Type II (Gli-independent)

Hh pathway activity in the absence of Gli activity, in particular regulating the actin cytoskeleton and axonal guidance is also well recognised. The Hh ligands have been shown to regulate activity of the Rho family of small GTPases in a Smo-dependent manner, promoting actin stress fibre formation and tubulogenesis [351,356]. Further, it is now established that Shh can also act, in a Smo-dependent manner as a commissural axon guide stimulating the phosphorylation of the Src family kinase (Sfk) members Src and Fyn, inhibition of Sfk activity completely blocking Shh-induced axon movement [357,358]. In both situations, the rapid response demonstrated following exposure to Hh ligands, absence of Gli-dependent transcriptional activity, and inability of Gli-3 to attenuate these processes indicates this mechanism functions in a Gli-independent manner. Additionally, cell-based screens analysing components of the canonical Hh signalling process have failed to identify Src and Fyn [359,360] and *Src* and *Fyn* double-mutant mice have been shown not to exhibit phenotypes suggestive of deregulated canonical Hh signalling [361].

1.4.3 Hh signalling in haematopoiesis

In vertebrates, haematopoiesis is broadly divided into two major phases, primitive (embryonic) and definitive. The Hh signalling pathway has a complex role in both embryonic and adult haematopoiesis. This role appears dependent on developmental stage, cell lineage and whether the haematopoietic system is under regenerative pressure [344,362]. Whilst evidence has shown the Hh signalling pathway to be vital for early haematopoietic development [332] there remains controversy over its role in normal haematopoiesis in adult organisms [253,362-364], although some of this may be explained by experimental method. Interestingly, recent early phase clinical trials looking at Smo inhibition have shown little or no haematopoietic toxicity, potentially indicating Hh signalling may be dispensable in certain situations [365]. Importantly, abrogation of canonical Hh signalling by knockout of *Smo* does not adversely affect steady state normal haematopoiesis [363,366].

1.4.4 Hh signalling in malignancy

Crucially, abnormal Hh signalling has been associated with diverse human malignancies including basal cell carcinoma (BCC) [367], medulloblastoma [368], pancreatic [259] and lung cancer [262]; data suggests different mechanisms of action in the various tumour environments. Constitutive pathway activation through loss-of-function mutations [367], epigenetic modifications [258] reduced expression of the negative regulators Ptch, Hhip and Sufu [369]; or gain-of-function mutations and epigenetic changes [370] in the positive regulator Smo have been observed in a number of solid malignancies [371]. To date, no mutations have been identified in haematological malignancies, however epigenetic modifications have been observed in a cohort of paediatric AML patients, correlating with disease status [372]. Ligand-dependent, canonical pathway activation, involves autocrine or paracrine Hh signalling [373]. Autocrine Hh signalling has been identified in MM [374], prostate [266] and lung cancer [263]. Paracrine Hh signalling has been observed in lymphoma [364], colon and pancreatic cancer [265].

1.4.4.1 Hh signalling in AML

In myeloid malignancies, Hh signalling has been found to be vital in the maintenance and expansion of the CSC or LSC, either as a survival and proliferation signal or through direction of the LSC fate [252,344,375-377].

There is considerable evidence to support the role of the Hh signalling pathway in AML. Leukaemic cell lines and primary AML cells have been shown to express *Shh, Gli-1* and *Gli-2*, indicative of active Hh signalling [69]; *Gli-1* expression correlating with cytogenetic risk, inferior EFS and a reduced OS, with *Gli-1* conferring drug resistance through UGT1A-dependent glucuronidation [378,379]. Further, genetic and pharmacological inhibition of Gli-1 caused anti-leukaemic effects and overcame associated chemoresistance [378,379]. Gli-1 expression has also been shown to predict poor remission status and reduced OS in secondary AML [379,380] whilst *Gli-2* has been shown to be a negative prognostic indicator in a number of microarray studies in leukaemia [381,382]. Additionally, aberrant Hh signalling has been linked to drug resistance with inhibition of the pathway restoring chemosensitivity in AML [349,377]. Further, pathway inhibition with PF-04449913 sensitised AML cell lines and primary cells to cytarabine with inhibition of *Smo* being shown to modulate cell cycle and self-renewal signalling [383]. In paediatric AML the hypo- and hypermethylation of pathway promoters was highly associated with AML diagnosis and relapse [372]. The complex interplay between the intrinsic and extrinsic signals governing LSC behaviour may however, mean targeting a single pathway, such as the Hh is insufficient.

1.4.5 Targeting the Hh signalling pathway

As discussed in Section 1.4.4.1, there is increasing evidence to support the role of the Hh signalling pathway in AML, with components representing viable therapeutic targets. Targeting components of the Hh pathway is therefore a very attractive potential treatment strategy. From a drug development perspective, inhibition of Smo and Gli-1 can be readily achieved; Table 1.5.

Table 1.5: Hedgehog inhibitors

Product name	**Mechanism of inhibition**
Arsenic trioxde [384]	Inhibits GLI proteins Degradation of PML-RARA fusion protein
AY9944 [385]	Inhibits Hh pathway, possibly by several mechanisms
Ciliobrevin A [386]	Hh pathway antagonist, inhibits ciliogenesis
Cyclopamine [387]	Smo antagonist
GANT58 [388]	Inhibitor of GLI-1 induced transcription
GANT61 [388]	Inhibitor of GLI-1 and GLI-2-induced transcription
HPI-1 [389]	Inhibits Hh pathway
Itraconazole [390]	Smo antagonist Triazole antifungal
Jervine [385]	Inhibits Hh pathway
JK184 [391]	Prevents GLI transcriptional activity
MRT-10 [392]	Smo antagonist
PF-5274857 [393]	Smo antagonist
Robotnikinin [394]	Inhibits SHH
RU-SKI 43 hydrochloride [395]	Hh acetyltransferase inhibitor
SANT [387]	Smo antagonist
SMANT hydrochloride [396]	Inhibits SHH-induced accumulation of SMO
U18666A [397]	Inhibits Hh pathway
Clinical grade	
BMS-833923 [398]	Smo antagonist
GDC-0449 (Vismodegib) [399]	Specific Hh inhibitor FDA approval 30th January 2012
IPI-926 (Saridegib) [400]	Cyclopamine analogue
LDE225 (Erismodegib) [401]	Smo antagonist
LY2940680 [402]	Specific Hh inhibitor
PF-04449913 [403]	Smo antagonist

Finally, although the primary cilium does not autonomously drive or prohibit oncogenesis, it potentially represents a therapeutic target in those malignances that show dependence upon its activity. Whether we can 'switch off' primary cilia is another area of exciting research.

1.4.5.1 Targeting the Hh signalling pathway in haematological malignancies

There are presently a number of Phase III trials utilising Hh inhibition in solid tumours, with vismodegib being licensed for use in BCC in 2012. The rationale for Hh inhibition in haematological malignancies is to target the CSC, and potentially modulate the protective effect of the tumour microenvironment, with a view to affecting a cure. Whether Hh antagonism will be therapeutically useful however, not only depends on its ability to target the diseased cells but also on the anticipated level of toxicity, both haematological and systemic, although to date, there appears to be few grade 3-4 toxicities reported [127].

Whether Hh inhibition can deliver meaningful clinical results in haematological malignancies is an area of active research; Table 1.6. Excitingly, results of the Phase II NCT01546038 study presented at ASH 2016 show the addition of glasdegib to LDAC significantly increased OS when compared to LDAC alone in patients with AML or high-risk MDS who were ineligible for intensive chemotherapy (HR: 0.501, 80% CI: 0.384, 0.654, one-sided log rank p-value 0.0003) [651].

Table 1.6: Clinical trials in haematological malignancies involving Hh inhibitors

Drug **Sponsor**	**Condition**	**Phase**	**Trial**	**Status**
Dasatinib combined with BMS-833923 Bristol-Myers Squibb	CML with resistance/ suboptimal response to a prior TKI	Phase I/II	NCT01218477	Completed [404]
Dasatinib alone or in combination with BMS-833923 Bristol-Myers Squibb	Newly diagnosed Ph+ CP CML	Phase II	2011-000083-10	Completed [405]
GDC-0449 (Vismodegib) The Lymphoma Academic Research Organisation/Roche Pharma AG	Refractory or relapsed B-cell Lymphoma or CLL	Phase II	NCT01944943	Terminated (Lack of efficacy)
GDC-0449 (Vismodegib) after autologous SCT NCI	Multiple Myeloma	Phase Ib	NCT01330173	Completed
Ribavirin, GDC-0449 (Vismodegib) and/or Azacitidine Sarit Assouline	Adult AML	Phase II	NCT02073838	Recruiting
Vismodegib NCI/Genentech	Patients with Steroid-Refractory Chronic Graft-versus-Host Disease	Pilot	NCT02337517	Recruiting
IPI-926	Primary/secondary MF	Phase II	NCT01371617	Completed [406]
LDE225 and INC424 Novartis Pharmaceuticals	MF	Phase Ib/II	NCT01787552	Ongoing but not recruiting

LDE225 Novartis Pharmaceuticals	Patients with PTCH1 or SMO Mutated Tumors	Phase II	NCT02002689	Terminated (Low enrolment)
Azacitidine or decitabine and LDE225 Novartis Pharmaceuticals	Myeloid malignancies	Phase I/Ib	NCT02129101	Ongoing but not recruiting
PF-04449913 Pfizer	Haematological malignancies	Phase I	NCT00953758	Completed [407]
PF-04449913 alone or in combination with LDAC, Daunorubicin or Cytarabine Pfizer	Japanese patients with: AML MDS	Phase I	NCT02038777	Recruiting
PF-04449913 in combination with Intensive Chemotherapy, LDAC or Cytarabine or Decitabine or Daunorubicin Pfizer	AML and high risk MDS	Phase I/II	NCT01546038/ 2012-000684-24	Ongoing but not recruiting [651]
PF-04449913 Pfizer	Acute leukaemia with high risk of post-allogeneic SCT relapse	Phase II	NCT01841333	Recruiting
PF-04449913 Pfizer	MDS CMML	Phase II	NCT01842646	Ongoing but not recruiting

(AML: acute myeloid leukaemia; MDS: myelodysplastic syndromes; CMML: chronic myelomonocytic leukaemia; MF: Myelofibrosis; MPN: myeloproliferative neoplasms; CML chronic myeloid leukaemia; CLL: chronic lymphoid leukaemia; SCT: stem cell transplant; Ph+: Philadelphia chromosome positive (BCR-ABL); TKI: tyrosine kinase inhibitor; LDAC: low dose Ara-C; NCI: National Cancer Institute)

Erivedge® (vismodegib) was the first orally bioavailable clinical grade Smo inhibitor to be approved for the treatment of locally advanced and metastatic BCC. The FDA approved it in January 2012. Vismodegib has been studied in relapsed / refractory (R/R) AML (NCT01880437). Analysis of two study cohorts was planned: single agent vismodegib, followed by vismodegib in combination with cytarabine. The study was terminated following an interim data review due to a lower than expected efficacy of single agent vismodegib, combination with cytarabine was therefore not undertaken. Vismodegib with ribavirin with or without decitabine (NCT02073838) is currently recruiting patients with R/R AML who are either M4 or M5 morphologically or have been shown to have high levels of the oncogene eIF4E. ElF4e has been shown to be a direct transcriptional target of NFκβ and preferentially dysregulated in AML with an M4 or M5 phenotype [408]; with ribavirin acting as a competitive inhibitor of eIF4e. Further, the Hh pathway has been linked to the methyltransferases, reports showing inhibition of the Hh pathway to enhance the effects of the hypomethylating agents (HMAs) - azacitidine / decitabine [512].

Glasdegib® (1-((2R,4R)-2-(1H-benzo[d]imidazol-2-yl)-1-methylpiperidin-4-yl)-3-(4-cyanophenyl)urea; PF-04449913) is a potent orally bioavailable clinical grade Smo inhibitor [403]. Glasdegib® was recently reported to improve sensitivity to cytarabine in AML cell lines and primary human AML cells [383]. These promising *in vitro* results led to the NCT01546038 trial studying PF-04449913 in combination with LDAC in untreated AML and high-risk MDS cases ineligible for intensive chemotherapy. Results, presented at ASH 2016, suggest the addition of glasdegib to LDAC improves OS when compared to single agent LDAC (8.3months and 4.9 months respectively). Improved OS persisted irrespective of subgroup, although those with good / intermediate risk appeared to gain greater survival benefit (12.2 months vs 6 months for LDAC) compared to those with poor risk (4.4 months vs 2.3 months) [407]. This is the first Smo inhibitor to show clinical benefit in AML. Glasdegib is currently being studied as first line therapy in patients with intermediate-2 and high risk MDS, AML and chronic myelomonocytic leukaemia (NCT02367456).

Odomzo® (sonidegib, LDE225) is a potent orally bioavailable clinical grade Smo inhibitor. Sonidegib gained FDA approval in July 2015 and EU approval in August 2015 for locally advanced BCC based on the Phase II BOLT study showing a durable objective response in 56% of patients (NCT 01327053) [409-411]. The Copland group has previously studied the effect of sonidegib in CML. They showed sonidegib alone, and in combination with nilotinib, was able to reduce the self-renewal capacity of CD34+ CP-CML cells *in vitro*, and consequently, upon administration to EGFP(+)/SCLtTA/TRE-BCR-ABL mice, the combination reduced leukaemia development. No effect on normal HSCs was seen [412]. Within AML, the NCT01826214 trial, which completed in 2016, failed to show a clinical benefit in patients with R / R AML treated with single agent sonidegib. Sonidegib in combination with azacitidine or decitabine in MDS and AML patients is an ongoing, but not recruiting, study (NCT02129101), the results of which are awaited with interest considering recent work showing silencing of *SHH, SMO* and *GLI-3* sensitised cells to the HMAs [413]. At present Novartis are not actively pursuing sonidegib in haematological malignancies.

1.4.6 Primary cilia

Primary immotile cilia are highly specialised organelles present in single-celled eukaryotes through to humans, first reported by Alexander Kowalevsky in 1867 [414]. They are distinct from motile cilia, lacking the central pair of microtubules and radial spokes required for motility; motile cilia were first described in protozoa in 1675 by Anthony van Leeuwenhoek [415].

Primary cilia are regulated by the cell cycle, with ciliation and cell division being mutually exclusive [416,417]. These organelles contain a long microtubular axoneme with a 9+0 configuration, surrounded by an external membrane continuous with the plasma membrane, extending from the basal body [418-420]. The basal body is formed from a centriole, providing the nine-fold symmetric template to build the axonemal structure [418,421,422]. It is the contention for the centriole that balances ciliation and the cell cycle; primary cilia may only be formed when cells are quiescent [416,417].

The basal body, located at the apical plasma membrane, determines cellular position, in accordance with cell polarity, and governs protein entry into the cilium. Protein synthesis is absent in the axoneme, ciliary components therefore need to be constantly imported and exported to render cilia functional. This function appears to be highly dependent, but not exclusively restricted to the intraflagellar transport (IFT) mechanism.

Primary cilia are constructed and maintained by the evolutionarily conserved IFT mechanism, a specialised transport process mediated by a large multiprotein complex [423]. Bidirectional movement of IFT particles is performed by the anterograde kinesin (Kif3a, Kif3b, and Kif3c) and retrograde dynein motors [419,420,424,425], Figure 1.8. It is not yet clear which IFT components are essential, or dispensable, for cilia formation.

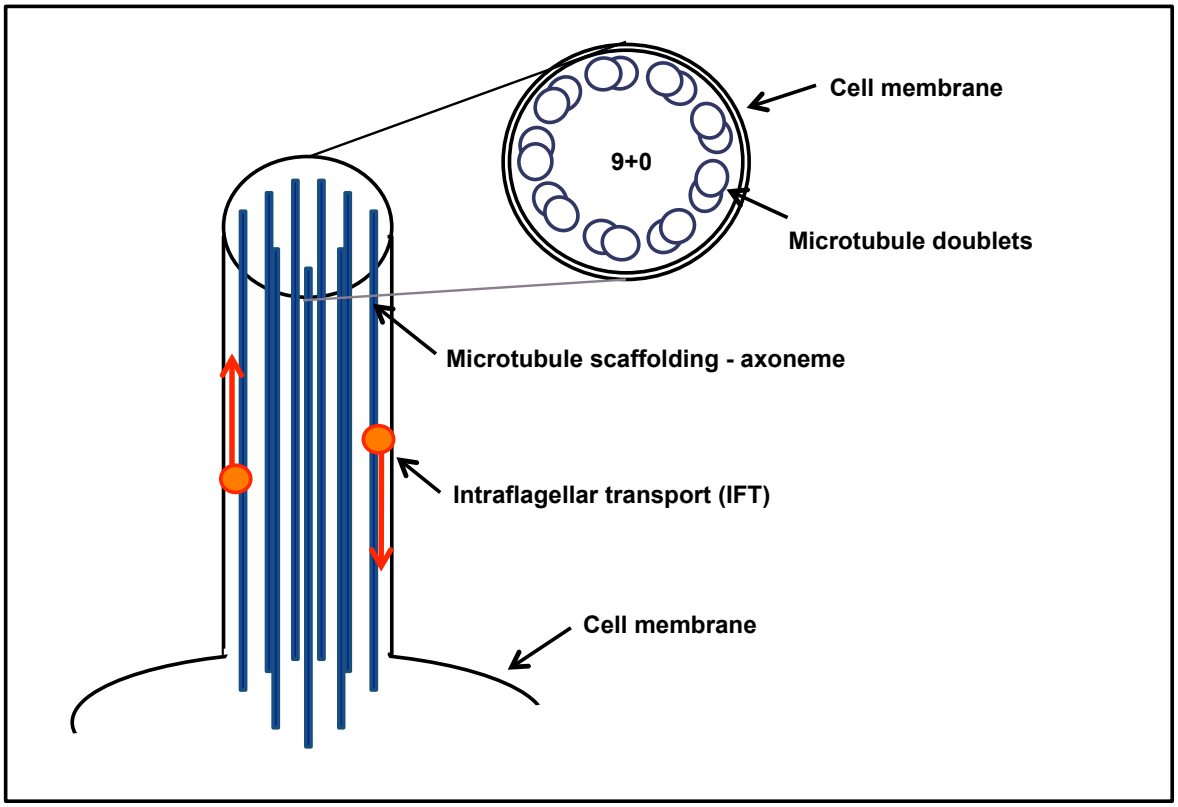

Figure 1.8: Primary cilium

Primary cilia are thought to be present on virtually every mammalian cell, exceptions including ciliated cells and most haematopoietic cells [416]. However recent work in T cells has shown the immunological synapse to be highly dependent on IFT proteins and, therefore considered a functional homolog of the primary cilium[426].

These sensory organelles are vital for tissue development and homeostasis [427-429] being involved in cell-to-cell and cell-to-environment communication. Large-scale genetic, proteomic, and genotype-phenotype studies have generated an evolving list of ciliary associated proteins. Presently, it is thought greater than one thousand proteins comprise the ciliome [418], being synthesised in the cytoplasm and transported to cilia by IFT [430].

These multi-function proteins include membrane receptors (including platelet derived growth factor receptor [PDGFR]) [431,432], components of signalling pathways and transcription factors [417,433]. Consequently, cilia functions have been shown to range from mechanosensation to the transduction of signalling pathways; disruption of the primary cilium being associated with a number of pathologies collectively known as ciliopathies, including Bardet-Biedl syndrome and polycystic kidney disease [434,435]. These ciliopathies are pathologically diverse, the clinical phenotypes ranging from mild to highly complex and severe multi-organ failure syndromes incompatible with neonatal life. Presently, mutations have been recovered in more than fifty ciliopathies.

Considering the ability of cilia to influence cell cycle and their involvement in signalling pathways including Hh, Hippo and Wnt, researchers have begun to question whether primary cilia have a role in oncogenesis. One hypothesis, based on the observation certain tumour phenotypes resemble ciliopathies and given cilia disassembly is a prerequisite for cell proliferation, is that cilia loss is required for tumour progression. Converse to that is the hypothesis that malignancies require, or even up-regulate, cilia.

Although research in this area is in its infancy, data would appear to suggest a role for cilia in oncogenesis [436]. In breast cancer, the cilia-related genes, *GLI-1*, *RPGRIP1* and *DNAH9*, are frequently mutated [437,438] whilst *NPHP9* (*NEK8*), which modulates cilia length and activates the oncogenic transcription factor TAZ is up-regulated [439,440]. *Aurora A (*cilia disassembly promoter), *GLI-3* and *ATPKD1* are frequently mutated in colorectal cancer [441,442]. In melanoma, pancreatic ductal adenocarcinoma, ovarian and renal carcinomas cilia have been shown to be lost through tumour progression [443]; with cilia reduced in breast cancer tissue and cell lines compared to normal breast tissue [444]. In each instance, Ki67 positivity has shown this to be independent of increased proliferation [445,446].

Current work therefore appears to support a model where cilia can promote or repress malignant transformation *in vivo*. Loss of cilia however, does not appear sufficient to drive oncogenesis. Selection for the retention or disposal of cilia by malignancies, therefore, seeming dependent on the underlying oncogenic event; cancer driven by mutations in components dependent upon the primary cilia being cilia-dependent [447,448] whilst in those malignancies driven by deregulation of components downstream of cilia, cilia are obsolete. Interestingly, cancers that depend on cilia retention appear to have better survival statistics [448]. This notion of cilia dependence and independence is supported by the absence of an oncogenic predisposition in many of the ciliopathies, Senior-Loken syndrome (SLNS), Leber congenital amaurosis (LCA) and nephronophthisis (NPHP), though reduced life expectancy may mask true malignant predisposition. *JBN/AHI1* sensitizes tissue for Wnt activation, with consequent over-proliferation: oral hamartomas have been associated with Joubert Syndrome-related disorders [449]. Figure 1.9.

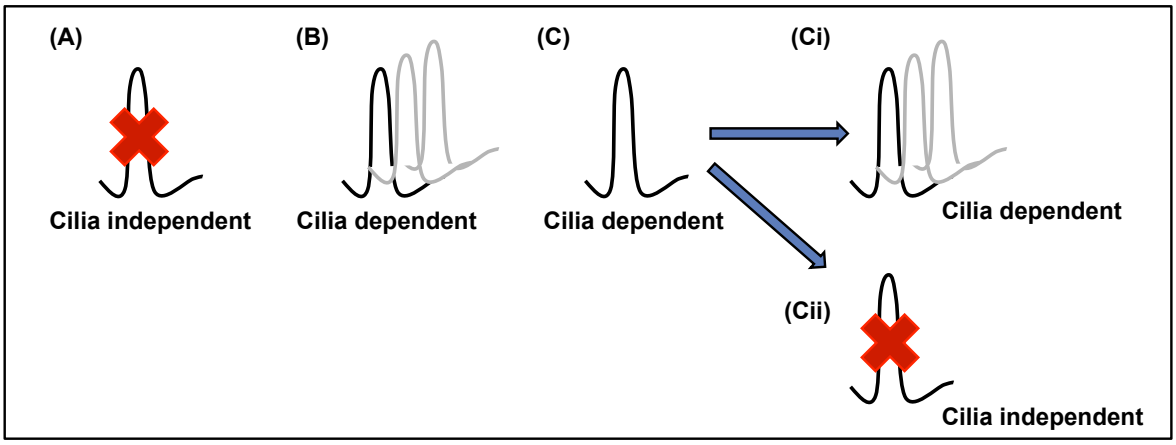

Figure 1.9: Diagrammatic representation of how primary cilia have been linked to cancer
(A) Cilia are lost to enable oncogenic transformation, (B) Cilia are required / up-regulated in the initial transforming event, (C) Cilia are required / up regulated in the initial transforming event, these cells then (Ci) select for cilia retention remaining cilia-dependent or (Cii) further develop into a cilia-independent cancer.

The strong connection between primary cilia and the Hh pathway, and thereby vertebrate development was first revealed by genetic experiments using mouse ethylnitrosourea mutants [450]. Following on from these discoveries, notable components of the Hh pathway have been shown to localise to the cilium: the receptors Ptch1 and Smo, the Gli transcription factors and proteins involved in regulating Gli activity (Pka and Sufu) [451,452]. Ptch1 and Smo localise in a ligand-dependent manner [337,453,454] whilst the Gli proteins localise in a partially ligand-dependent manner: in the absence of Hh ligand, they are present at the ciliary tip in low concentration [430], accumulating within the ciliary tip in response to Hh stimulation [337,451,454]. Sufu is shown to traffic in and out of primary cilia [455]. Mice lacking functional cilia display patterning defects attributable to the loss of Gli [450,456,457], and mutant forms of Smo that fail to localise to the cilium cannot activate the pathway [453,454].

Whilst there is conflicting evidence regarding the effect of mutations in components of the IFT machinery on Hh signalling [458,459] it is now widely accepted that vertebrate canonical Hh signalling requires primary cilia [417]. The relationship between cilia and the Hh pathway is exemplified by mouse knockout models of *Kif3a* or *Ift88*, with consequent inhibition of cilia function, showing phenotypic overlap with those bearing Hh mutations [460]; with developmental processes which depend upon Hh signalling, such as neural tube patterning and limb development, also demonstrating phenotypic overlap between cilia deficient and manipulated pathway models [417,450,455,457].

It is however noteworthy that primary cilia are only present in sensory neurons and sperm, and irrelevant to Hh signalling in Drosophila [461], the organism in which the Hh pathway was first discovered, indicating a unique role for primary cilia in mammalian Hh signalling.

1.4.7 Downstream targets

There are numerous downstream targets of the Hh pathway including Bcl-2, the ABC transporter family members, the Cdks and components of the EMT, Wnt and Notch signalling pathways, Figure 1.10: Downstream targets of the Hh signalling pathway.

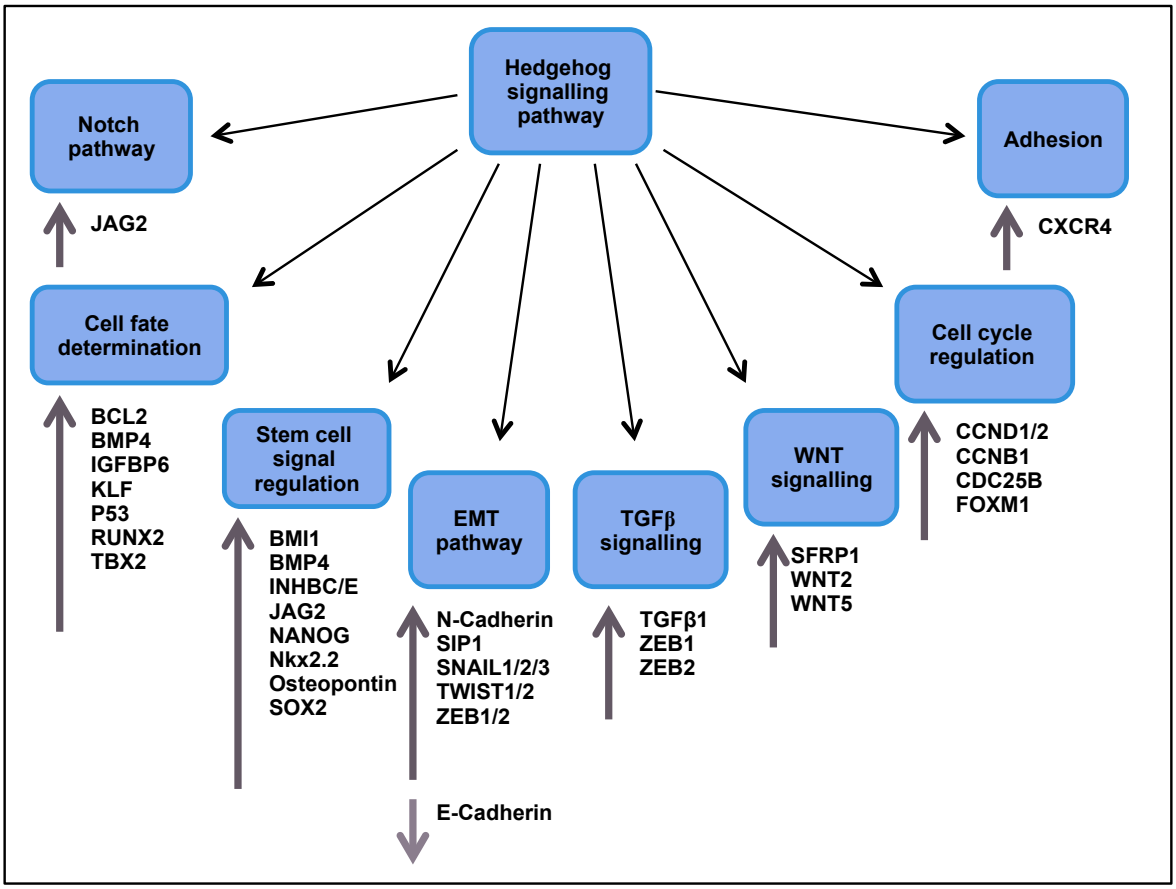

Figure 1.10: Downstream targets of the Hh signalling pathway

There is already evidence to show up-regulation and involvement of many of these pathways in chemoresistance in human malignancies [462,463]. Additionally, studies have highlighted several of these downstream targets to be over-expressed in both AML and CML, with expression linked to chemoresistance and poorer survival [464]. For further discussion please refer to Section 1.3.4.

1.5 Bcl-2 Family

Bcl-2 was the first anti-apoptotic gene discovered, in 1986; deriving its name from its discovery in B cell non-Hodgkin's lymphoma [465,466]. Its oncogenic potential was discovered in 1988, activation endowing B cells with a survival advantage, promoting their neoplastic expansion [467]. The Bcl-2 family regulates all major types of cell death [468]. Approximately twenty members have been identified, both pro- and anti-apoptotic [469]; Figure 1.11: Bcl-2 family.

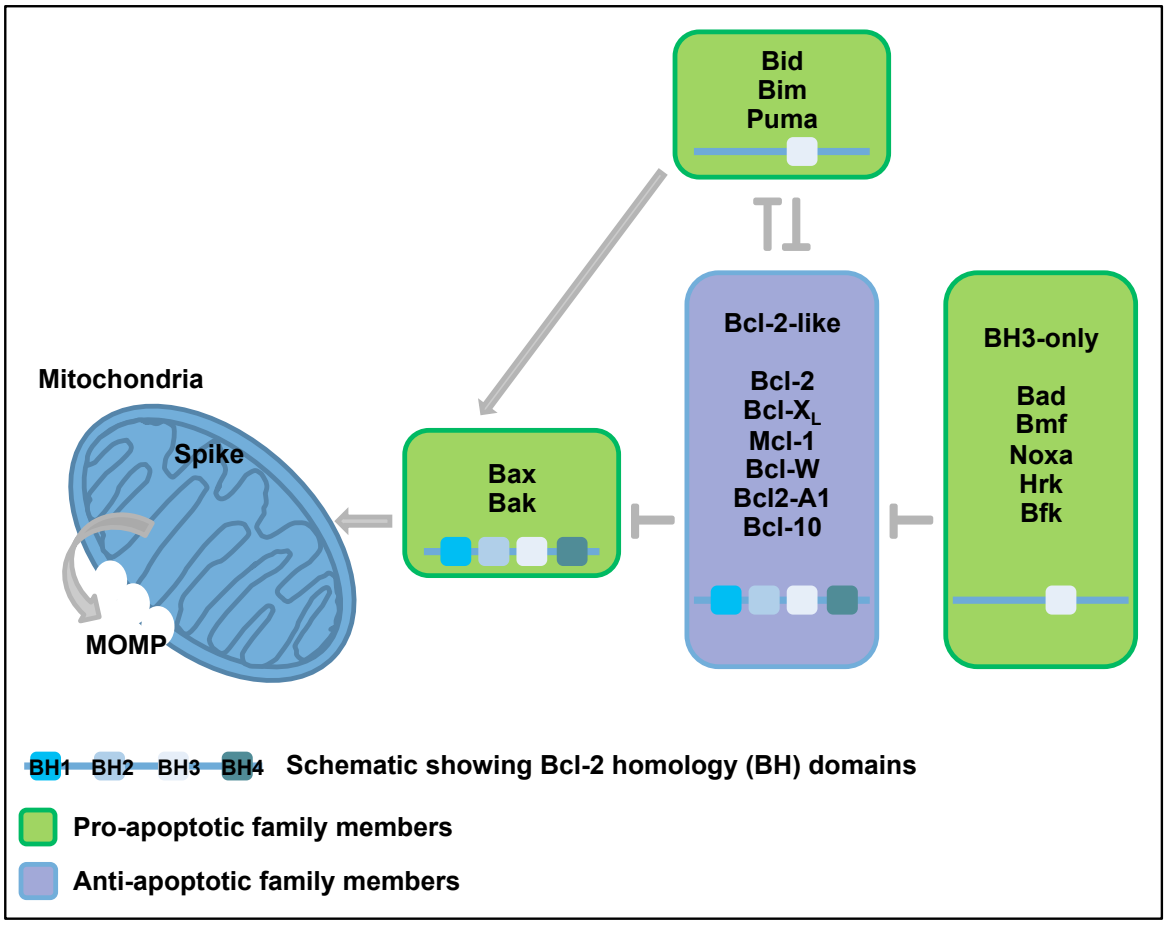

Figure 1.11: Diagrammatic representation of the Bcl-2 family.

The Bcl-2 family members are related by regions of sequence and structural homology; members sharing at least one of the four functionally vital Bcl-2 homology domains (BH1, BH2, BH3 and BH4). Most family members also have a transmembrane domain, most notably allowing their close relationship with the mitochondria.

Within the Bcl-2 family, there are three functionally and structurally distinct subgroups: the apoptosis initiating BH3-only proteins, the pro-survival proteins, and the pro-apoptotic effector proteins. There are six pro-survival family members, Bcl-2, Bcl-xL, Bcl-2-like protein 2 (Bcl2l2/Bcl-w), myeloid cell leukaemia sequence 1 (Mcl-1), Bcl-2-related protein A1 (Bcl2-A1) and Bcl-2-like protein 10 (Bcl2l10) and three pro-apoptotic, pre-activated, effector proteins Bcl-2-associated X protein (Bax), Bcl-2 homologous antagonist/killer (Bak) and BCL-2-related ovarian killer protein (Bok). These proteins share four BH domains adopting a structure consisting of seven amphipathic α-helices surrounding a central hydrophobic helix. Within this structure is a hydrophobic surface groove, responsible for interaction with other family members BH3 domain [470,471]. Interestingly, the BH3-only domain proteins are structurally disordered as discussed below [472].

The pro-apoptotic family members all contain a BH3 domain, some containing only this domain, others sharing BH1, BH2 and / or BH4. It is the BH3 domain that is vital in the promotion of cell apoptosis. Interestingly, although some BH3-only proteins, Bcl-2-like protein 11 (Bim), BH3 interacting-domain death agonist (Bid) and Bbc3, can bind to and neutralise all pro-survival proteins, and vice versa, others Bcl-2-associated death promoter (Bad) and Pmaip1 (Phorbol-12-myristate-13-acetate-induced protein 1 (Noxa)), bind only a limited subset [473,474]. This is thought to be due to subtle differences in the BH3 domains.

In the resting, healthy state, the anti-apoptotic proteins maintain, or guard, the mitochondrial outer membrane. Bak is inhibited predominantly by Mcl-1, Bcl-A1 and Bcl-xL, with Bcl-2 contributing in certain situations [474-476]. Bax can be inhibited by all of the pro-survival proteins [477]. This is noteworthy when considering members of the Bcl-2 family as potential therapeutic targets.

In health, adult tissue homeostasis is critical, cell life and death being carefully orchestrated, with the Bcl-2 family playing a pivotal role [478-480].

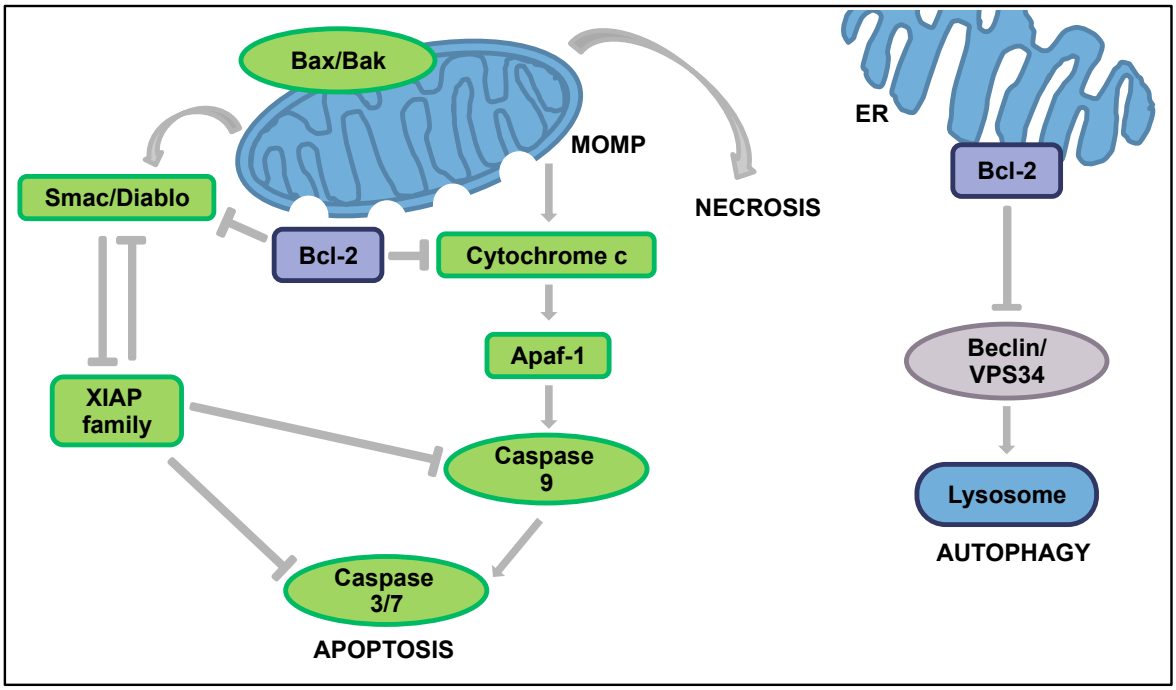

Figure 1.12: Schematic illustrating the role of Bcl-2 in cell death pathways

1.5.1 Bcl-2 induced apoptotic cell death cascade

Apoptosis is the process of programmed cell death. In the presence of various cytotoxic stresses, intracellular damage, or oncogenes, the apoptotic cell death cascade is initiated inducing the transcription or post-translational modification of the BH3-only family members [480]. These BH3 proteins operate by two mechanisms: the direct activation of the pro-apoptotic proteins, and the neutralisation of the pro-survival proteins [481-484]. When sufficient apoptosis inducing BH3-only proteins have been stimulated, the balance is shifted in favour of apoptosis. In addition, p53 has been shown to induce apoptosis through the activation of Bak and Bax [485]. Once activated Bak and Bax undergo conformational change, to form oligomers that subsequently translocate to, and permeabilise, the mitochondrial outer membrane. This process, referred to as mitochondrial outer membrane permeabilisation (MOMP), results in the release of proteolytic proteins, most notably cytochrome c, into the cytosol [486]. Thus, the proteolytic cascade, which will ultimately result in cell apoptosis, is initiated.

Simplified, caspase activation occurs through the scaffold protein apoptotic protease-activating factor 1 (Apaf-1) [487-489], and neutralisation of endogenous inhibitors such as X-linked inhibitor of apoptosis protein (Xiap) through second mitochondria-derived activator of caspases (Smac) [490,491]. Apoptosis can be initiated through other pathways, referred to as the death receptor or 'extrinsic' pathways, for example those controlled by tumour necrosis factor-family death receptors, such as Fas. In certain situations however, this pathway interacts with the 'intrinsic' pathway, for example, through caspase-mediated cleavage and activation of Bid [492].

1.5.1.1 Bcl-2 and necrosis

Necrosis is the process of unprogrammed cell death. It results in autolysis of the cell usually through the action of external factors and often leads to inflammation. It is interesting that despite the significant differences in the apoptotic and necrotic pathways, and the fundamental role of the Bcl-2 family in apoptosis, research has found members of the Bcl-2 family, specifically Bcl-2 and Bcl-xL, to modulate necrosis [493,494]. This is an interesting concept when considering the Bcl-2 family as a therapeutic target.

1.5.1.2 Bcl-2 and autophagy

Autophagy, meaning 'self-eating' is a physiological, regulated, process ensuring homeostasis during periods of cellular stress. It is a mechanism through which cells disassemble unnecessary or dysfunctional components enabling a rebalance of sources of energy when required by cells. Beclin 1, the essential inducer of autophagy, has been shown to interact with the pro-survival proteins, Bcl-2 and Bcl-xL, through a region bearing remarkable resemblance to a BH3 domain on the endoplasmic reticulum (ER). These complexes inhibit autophagy [495].

1.5.1.3 Bcl-2 and haematopoiesis

Bcl-2 is expressed to variable degrees in all haematopoietic lineages [496]. In the normal, healthy BM, Bcl-2 expression appears topographically restricted to areas housing long-lived cells [496]. Further studies have shown a complex highly regulated process exists between pro- and anti-apoptotic factors within HSPCs ensuring a balance between cell death and survival [497-500].

Within the BM, megakaryocytes have the highest level of expression. In the myeloid lineage, there is a progressive down-regulation through the stages of differentiation, expression being at its highest in the promyelocytes and myelocytes, and virtually absent in terminally differentiated granulocytes [496]. The reverse is seen within the lymphoid cells, Bcl-2 expression increasing with maturation. Further, within the myeloid series the opposite pattern to that seen for Bcl-2 was seen for the pro-apoptotic protein Bak, expression being highest within terminally differentiated granulocytes [501].

Analysing the haematopoietic progenitor populations, HSCs and early progenitor cells, studies have shown Bcl-2 expression to be up-regulated on transition from immature (CD34+CD38- population) to more committed progenitor cells (CD34+lin-) [198,225,502,503]; with low levels of Bcl-2 expression limited to the quiescent CD34+CD38-/low cells [502]. Further, these haematopoietic progenitors have been shown to express low levels of the pro-apoptotic proteins Bak, Bad and Bax, with levels increasing with differentiation [502]. It is important to note that analysis of CD34+ cells following culture for 10 days with a standard growth factor cocktail resulted in up-regulation of both the pro-survival and pro-apoptotic proteins, the former to a greater degree [502]. This must be considered when interpreting *in vitro* studies manipulating members of the Bcl-2 family and extrapolating the data to an *in vivo* situation.

1.5.1.4 Bcl-2 and malignancy

There is extensive evidence supporting Bcl-2 to be altered in malignancy [504-508]; elevated expression thought to occur in approximately half of all malignancies [504-508]. Deregulation has been shown to occur through changes in gene expression, copy number, hypomethylation [509] and loss of repressive microRNAs [510]. Data also supports the deregulation of other family members [225,501,511]; *Mcl-1* being highly expressed in lung, prostate, breast, ovarian, renal, and glioma cancer cell lines, whilst Bcl-2 and Bfl-1 are highly expressed in leukemia/lymphoma and melanoma cell lines respectively [505,512]. Further, CSCs in glioblastoma, colon and pancreatic cancer have been shown to depend on multiple-pro survival Bcl-2 family members [513].

1.5.1.5 Bcl-2 in AML

The importance of Bcl-2 in AML cell maintenance and survival has long been established. Early work in the 1990s demonstrated Bcl-2 to be heterogeneously over-expressed in AML. One study reporting Bcl-2 to be present in 87.3% of *de novo* cases and 100% of relapses, with greater than 20% over-expression in 68.3% and 90% of cases respectively [514], whilst another reported a mean of 23% (range 0-95%) [515]. However, evidence regarding the association between Bcl-2 expression in newly diagnosed, untreated AML patients, FAB subtype, blast percentage and CR is conflicting. Some studies report a clear correlation [464,515,516], whilst others demonstrate no association with blast count or percentage, FAB classification, patient demographics or cytogenetic abnormality [514]. It is postulated that these results may simply reflect the heterogeneity of the disease, though study size was sufficiently powered. High BCL-2 was however convincingly shown to be an independent prognostic factor and predictor of remission, suggesting differing roles dependent on genetic abnormalities [517]. It remains to be determined if there are specific genetic alternations responsible for Bcl-2 over-expression in AML as seen in other diseases such as CLL [518].

These early studies looked at bulk leukaemic cells, with more recent work concentrating on expression within defined cell populations. Interestingly in contrast to their normal counterparts, quiescent CD34+CD33-CD13- AML cells have been shown to highly express Bcl-2 [519,520]. Bcl-2, Bcl-xL and Bad being differentially expressed in the CD34+ and progenitor populations [521], with levels up-regulated in the leukaemic cell populations compared to normal donors. Further Bcl-2 and Bcl-xL have been shown to be up-regulated following induction chemotherapy and to be expressed on MRD cells [521] with pharmacological inhibition of Bcl-2 being shown to selectively eradicate quiescent AML LSCs [520]. This increased functional reliance upon Bcl-2 of leukaemic cells, in comparison to normal haematopoietic cells, makes it an exciting therapeutic target which to date appears to translate to the clinic. In 2015 a phase Ib, open-label, non-randomised, dose-escalation trial of venetoclax with decitabine or azacitidine in 22 treatment-naïve elderly patients with AML reported an objective response (CR/CR with incomplete marrow recovery/partial remission (CRi)) in 73% (16/22) (NCT02203773). None of those demonstrating an objective response experienced relapse. The safety profile was acceptable [522,523]. The US FDA subsequently granted ABT-199 a breakthrough therapy designation in January 2016 for use in combination with HMAs in patients aged over 65 years who are not eligible for standard therapy. In October 2016 a phase II, single-arm study evaluating venetoclax in 32 patients with high-risk relapsed AML or those unfit for intensive chemotherapy was reported. The overall response rate (ORR) was 19% (6/32), with an additional 19% (6/32) demonstrating a partial response and incomplete hematologic recovery; safety profile was acceptable [524]. In February 2017 a phase III randomised, double blind, placebo-controlled study (NCT02993523) began recruiting. This study aims to assess venetoclax plus azacitidine compared with placebo plus azacitidine in treatment-naïve elderly and adult patients with AML ineligible for standard induction therapy [525]. The result of this ongoing study is eagerly awaited.

1.6 ABC transporters

The ABC family consists of 49 functionally distinct transmembrane proteins subdivided across seven subfamilies (ABCA through ABCG) [526]. The majority of these transporters comprise of 2 nucleotide-binding folds and 12 transmembrane domains. They play an important role in normal physiology, and are present in virtually all cells, normal and malignant. These transporters are responsible for the transport, or efflux, of a huge variety of compounds from nutrients to cytotoxic agents, across plasma and intracellular membranes, Table 1.7.

Table 1.7: ABC transporter families and their functions

Family	Function
ABCA	Lipid trafficking [527]
ABCB	'MDR (multi-drug resistance) family of ABC transporters' [528]; located within blood-brain barrier and liver; toxin transport
ABCC	Diverse activities – ion and toxin transport, cell surface receptor, multidrug resistance; subfamily includes the cystic fibrosis gene (*ABCC7*) [528]
ABCD	Expressed in peroxisomes, endoplasmic reticulum and lysosomes; transport of lipids, bile acids and vitamin B12; associate with peroxisomal disorders [529]
ABCE	No transmembrane domain therefore unlikely to have transporter function; single family member; promotes interferon activity [513]
ABCF	No transmembrane domain therefore unlikely to have transporter functions; involved in inflammatory processes [513]
ABCG	Transport of hydrophobic compounds; multidrug resistance [530]

1.6.1 ABC transporters and haematopoiesis

ABC transporter function is believed to play an important role in determining HSC fate. An association between *ABCB1*, encoding multi-drug resistance gene (P-gp or MDR1), and *ABCG2* encoding breast cancer resistance protein (BCRP), and immature haematopoietic cells being well recognised [531], with expression being down-regulated upon differentiation. More recently, work has identified an additional 20 ABC transporters that are highly expressed in the normal human CD34+CD38− sub-population and, also down-regulated upon differentiation into CD34+CD38+ expressing cells. Further, it is the drug-effluxing capacity of the ABC transporters that was initially used experimentally to isolate HSCs.

1.6.2 ABC transporters and malignancy

Drug resistance is one of the primary causes of treatment failure and disease relapse [215,532]. Cells exposed to cytotoxic agents have been shown to develop chemoresistance through a number of mechanisms, including reduced uptake and accelerated efflux, altered drug pharmacokinetics, mutations, deregulated cell cycle kinetics and modified death pathways [533]. Often cells can possess several of these mechanisms, potentially affording them MDR.

To date increased expression of thirteen of the ABC transporters (ABCA2, ABCB1, ABCB4, ABCB11, ABCC1–6, ABCC10, ABCC11 and ABCG2) have been linked to chemoresistance [218,526,534]. ABCB1, ABCC1 and ABCG2 are the best characterised. ABCB1 was discovered over 25 years ago, conferring resistance to amphipathic drugs including paclitaxel, anthracyclines, and vinca alkaloids [526,535,536], whilst ABCG2 was identified almost 20 years ago in multidrug resistant breast cancer cells [537,538]. ABCG2 has been linked to resistance to mitoxantrone, topotecan derivatives, anthracyclines, bisantrene and etoposide. ABCB1 differs in that its activity is dependent upon the presence of glutathione. It has been shown to confer resistance to a broad range of drugs including doxorubicin, daunorubicin and vincristine [539-542].

Whilst chemoresistance is primarily mediated through ATP-dependent drug efflux, the substrate being removed through channels formed by transmembrane domains, alternative mechanisms have been proposed. These include impaired substrate entry through hydrophobic and hydrophilic membrane interactions (termed the flippase model) and substrate removal before reaching the cytoplasm (the vacuum cleaner model) [543].

1.6.3 ABC transporters in AML

Chemoresistance has been demonstrated in AML at diagnosis, to arise during treatment, and to be present on relapse. *ABCB1* has been shown to be an independent adverse prognostic factor in *de novo* AML and, expression has been shown to be up-regulated in the poor prognostic WHO subgroups – t-AML and AML with MDS related changes [540,544]. *ABCG2* has been shown to associate with high-risk AML, being found in approximately one third of cases, appearing to therefore confer an independent poor prognostic factor [537]. Whilst the association between *ABCB1* and chemoresistance is recognised, its impact on prognosis remains to be determined [539-541].

Subsequently, research into the role of ABC transporter expression in AML has provided conflicting results: work demonstrating both normal haematopoietic and leukaemic CD34+CD38- cells to express similar patterns of the ABC transporters whilst other work has shown expression to be more heterogeneous in AML CD34+CD38- cells [539,540,545].

AML encompasses a group of aggressive haematological neoplasms; it a clinically, morphologically and genetically heterogeneous disease involving one or all of the myeloid lineages [150]. It is a CSC disorder [112,121,130-133], and whilst our knowledge and understanding is rapidly expanding there is still much to discover. Although the heterogeneity of this disease is, in part, why research is so challenging, it is also why work in this field is so interesting. Despite this heterogeneity however, it is important to remember each case is derived from a LSC. It is this LSC that is thought to be responsible for MRD, resistance and relapse. Further, whilst classically it was cytokines and chemokines which were thought to influences HSC fate more recent work has highlighted the importance of the self renewal pathways including the Hh signalling pathway in determining the behaviour of these LSCs. Further, work at both a gene and protein level has shown the complex tangled web of interactions between the different self-renewal pathways and, particularly interestingly, far removed downstream targets such as the ABC transporters. In essence it is a highly complex yet exciting field of research which promises to no doubt deliver some unexpected results on our journey of knowledge, and quest to translate our advances into the clinic.

Aims

That AML is a CSC disorder is well recognised, with our knowledge and understanding evolving rapidly. The importance of the highly conserved self-renewal pathways in determining CSC fate has also been clearly demonstrated, with huge efforts being made to target components therapeutically. Whilst the Hh signalling pathway has been studied in both normal and malignant haematopoiesis the evidence is conflicting, especially in AML, and therefore warrants further investigation, to determine how dependent AML CSCs are on Hh signalling.

The overall aim of this PhD was to gain a deeper understanding of the role of the Hh signalling pathway in normal haematopoiesis and AML and further whether Smo represents a viable therapeutic target in AML.

The following questions are therefore dealt with sequentially within the relevant results chapters.

1) The role of the canonical Hh signalling pathway in haematopoietic cells, both normal and malignant;

2) The efficacy of the Smo inhibitors, cyclopamine, sonidegib and glasdegib in targeting select, genetically diverse, AML cell lines and primary AML MNCs *in vitro*;

3) The effect of Smo inhibition (apoptosis, senescence, differentiation) and whether this is the same for different AML sub-types;

4) The effects of Bcl-2 inhibition on select AML cell lines and primary AML MNCs *in vitro*.

Each chapter begins with a brief introduction appropriate for the data presented. All results are summarised and discussed at the end of each chapter. Final conclusions and future work is presented in the final discussion chapter.

It is important to note our aims changed during this PhD, in response to published data, results generated and a deeper understanding of the topic. Notably, Novartis suspended work on their Smo inhibitors in haematological malignancies whilst Pfizer published exciting results following the use of their Smo inhibitor PF-04449913 with Ara-C.

2 Materials and Methods

2.1 Materials

2.1.1 Tissue culture

Table 2.1.1.1: Plastics for Tissue Culture and Suppliers

Plastics	Supplier
8-well Lab-Tek II chamber slides	Thermo Scientific Nunc. Massachusetts, USA
Cryovial	Fisher Scientific, Loughborough, UK
Eppendorf tubes (0.5/1.5ml)	Life technologies, Paisley, UK
Falcon tubes (15ml, 50ml)	Fred Baker Scientific, Cheshire, UK
Flat bottomed culture plates (6/12/24/96-well)	Greiner bio one, Gloucestershire, UK; Thermo Scientific Nunc. Massachusetts, USA
5100 Cryo -1^{o}C freezing container, Nalgene, 'Mr Frosty'	Sigma-Aldrich, Dorset, UK
Haemocytometer	Hawksley, Sussex, UK
Pasteur pipette (3ml)	Greiner bio one, Gloucestershire, UK
Pipette tips (p10/20/100/200/1000)	Greiner bio one, Gloucestershire, UK
Single use filter unit (0.22/0.45µm)	Sartorius Stedim Biotech, Epsom, UK
Sterile cell strainer (100µM)	Fisher Scientific, Loughborough, UK
Suspension dish with lid and vent (10x35mm)	Thermo Scientific Nunc. Massachusetts, USA
Syringes (5/10/20/50ml)	Greiner bio one, Gloucestershire, UK
Tissue culture flasks (25/75/300cm^{3}; non-adherent)	Greiner bio one, Gloucestershire, UK
Tissue culture flasks (25/75/300cm^{3}; adherent)	Thermo Scientific Nunc. Massachusetts, USA
Vacubottle	Fisher Scientific, Loughborough, UK
White opaque culture plates (96-well; flat bottomed)	Greiner bio one, Gloucestershire, UK

Table 2.1.1.2: Reagents for Tissue Culture and Suppliers

Reagent	Supplier
BIT 9500 Serum Substitute	Stem Cell Technologies, Grenoble, France
Bright Glo Luciferase system	Promega, Madison, USA
Diff-Quik®	Hergestelit von Fabrique, Dudingen, Switzerland
Dimethylsulphoxide (DMSO)	Sigma-Aldrich, Dorset, UK
DNAse I Solution (1mg/ml) – Bovine Pancreatic Deoxyribonuclease I	Stem Cell Technologies, Grenoble, France
Dulbecco's Modified Eagle Medium	Life technologies, Paisley, UK
Dulbecco's Modified Eagle Medium: Nutrient Mixture F12	Life technologies, Paisley, UK
Dulbecco's Modified Eagle Medium High Glucose	Life technologies, Paisley, UK
Dulbecco's Modified Eagle Medium Low Glucose + glutamax	Life technologies, Paisley, UK
Dulbecco's phosphate buffered saline (without Ca^{2+} and Mg^{2+})	Life technologies, Paisley, UK
Ethanol 100% molecular grade	Sigma-Aldrich, Dorset, UK
Foetal bovine serum	Life technologies, Paisley, UK
Geneticin	Life technologies, Paisley, UK
Ham's F-12	Life technologies, Paisley, UK
Heparin (stock 5000IU/ml)	NHS
Histopaque-1077	Sigma-Aldrich, Dorset, UK
Horse serum	Life technologies, Paisley, UK
Human albumin solution (5%)	NHS, UK
Hyclone FBS - HZSH3007003H	Fisher Scientific, Loughborough, UK
Hygromycin	Life technologies, Paisley, UK
Iscove's Modified Dulbecco's Medium	Life technologies, Paisley, UK
L-glutamine (200mM)	Life technologies, Paisley, UK
Luciferase	Promega, Madison, USA
2-mercaptoethanol (0.1μM)	Sigma-Aldrich, Dorset, UK
Methocult™ H4034	Stem Cell Technologies, BC, Canada

Myelocult 5100	Stem Cell Technologies, BC, Canada
Penicillin-streptomycin (10,000U/ml)	Life technologies, Paisley, UK
Purmorphamine	Santa Cruz, USA
hFLT3L (stock – 100µg/ml)	Peprotech, New Jersey, USA
hIL-3 (stock – 100µg/ml)	Peprotech, New Jersey, USA
hIL-6 (stock – 100µg/ml)	Peprotech, New Jersey, USA
hSCF (stock – 100µg/ml)	Peprotech, New Jersey, USA
HS-5 conditioned media	Made in-house
Resazurin **(7-Hydroxy-3H-phenoxazin-3-one-10-oxide sodium salt)** (R7017)	Sigma-Aldrich, Dorset, UK
RPMI 1640 medium	Life technologies, Paisley, UK
StemSpan 2	Stem Cell Technologies, Grenoble, France
Trypan blue solution (0.4%)	Sigma-Aldrich, Dorset, UK

Table 2.1.1.3: All-inclusive 'Kits' for Tissue Culture and Suppliers

Kit	**Supplier**
Senescence β-Galactosidase Staining Kit #9860	Cell Signalling, MA, USA
Sonic Hedgehog Human ELISA Kit (ab100639)	Abcam, Cambridge, UK

Table 2.1.1.4: Equipment for Tissue Culture and Suppliers

Equipment	**Supplier**
CompuSyn software	ComboSyn, Inc., New Jersey, USA
Multi-channel pipettor	Thermo Scientific Nunc. Massachusetts, USA
Spectramax M5 plate reader	Molecular Devices, California, USA
SoftMax Pro software	Molecular Devices, California, USA

Table 2.1.1.5 AML Cell Lines and Characteristics

Cell line	Disease	Characteristics	Supplier
HL60 [546]	AML FAB M3 or M2 (debated)	Hypotetraploid karyotype with hypodiploid sideline and 1.5% polyploidy - 82-88<4n>XX, -X, -X, -8, -8, -16, -17, -17, +18, +22, +2mar, ins(1;8)(p?31;q24hsr)x2, der(5)t(5;17)(q11;q11)x2, add(6)(q27)x2, der(9)del(9)(p13)t(9;14)(q?22;q?22)x2, der(14)t(9;14)(q?22;q?22)x2, der(16)t(16;17)(q22;q22)x1-2, add(18)(q21) – side line with: -2, -5, -15, del(11)(q23.1q23.2) High expression of c-Myc Derived from PB leucocytes obtained by leukopheresis from a 36yr old female in 1976	In house
Kasumi-1 [547]	AML with recurrent genetic abnormalities	Hypodiploid karyotype - 45<2n>X, -Y, -9, -13, -16, +3mar, t(8;21)(q22;q22), der(9)t(9;?)(p22;?), der(15)t(?9;15)((?q11;?p11) CD34+ Carries the t(8;21) leading to the *AML1-ETO* fusion gene and the KIT mutation N822 Derived from the PB of a 7yr old Japanese male (in 2nd relapse after bone marrow transplantation) in 1989	DSMZ
KG1a [548]	AML	Near-diploid karyotype with 5% polyploidy - 46(44-47)<2n>X/XY, +8, +11, -12, -17, -20, der(5;17)(q10;q10)del(5)(q?11q?13), del(7)(q22q35), i(8q), der(8)t(8;12)(p11;q13)add(8)(q24), i(11q), add(16)(q13/21), der(19)t(14;19)(q11;q13), add(20)(p13) CD34+ Expresses *OP2-FGFR1* fusion gene Established from the BM of a 59yr old male with erythroleukemia that developed into AML; KG-1a is a subclone of the AML cell line KG-1 described as an "undifferentiated variant"	In house
MOLM-13 [549]	AML FAB M5a at relapse after initial RAEB	Human hyperdiploid karyotype with 4% polyploidy - 51(48-52)<2n>XY, +8, +8, +8, +13, del(8)(p1?p2?), ins(11;9)(q23;p22p23 *FLT3 ITD*+ at gene level only; *CBL* deltaExon8 mutant; carries occult insertion effecting *MLL-AF9* fusion Established from PB of a 20yr old male with RAEB	DSMZ

		that developed into AML in 1995	
MV4-11 [550]	**B**iphenotypic B-myelomoncytic leukaemia	Hyperdiploid karyotype - 48(46-48)<2n>XY, +8, +18, +19, -21, t(4;11)(q21;q23) FLT3 ITD+ at gene and protein level Established from a 10yr old male at diagnosis	DSMZ
OCI-AML3 [551]	AML FAB M4	Hyperdiploid karyotype - 48(45-50)<2n>X/XY, +1, +5, +8, der(1)t(1;18)(p11;q11), i(5p), del(13)(q13q21), dup(17)(q21q25) *NPM1* gene mutation (type A) and the DNMT3A R882C mutation Established from the PB of a 57yr old male at diagnosis in 1987	DSMZ
THP-1 [552]	AML FAB M5b	Human near tetraploid karyotype - 94(88-96)<4n>XY/XXY, -Y, +1, +3, +6, +6, -8, -13, -19, -22, -22, +2mar, add(1)(p11), del(1)(q42.2), i(2q), del(6)(p21)x2-4, i(7p), der(9)t(9;11)(p22;q23)i(9)(p10)x2, der(11)t(9;11)(p22;q23)x2, add(12)(q24)x1-2, der(13)t(8;13)(p11;p12), add(?18)(q21) t(9;11)(p21;q23) leading to *MLL-AF9* fusion gene Established from a 1yr old at relapse in 1978	In house

Table 2.1.1.6: Stromal Cell Lines and Characteristics

Cell line	**Origin**	**Supplier**
HS-5 [553]	Human marrow stromal cell line – fibroblast; established from a 30yr old male Expresses Granulocyte colony-stimulating factor (G-CSF), granulocyte-macrophage colony-stimulating factor (GM-CSF), macrophage colony-stimulating factor M-CSF, *Kit* ligand (KL), macrophage-inhibitory protein-1α (MIP-1α), interleukin- (IL-) IL-1α, IL-1β, interleukin-1 receptor antagonist (IL-1RA), IL-6, IL-8, IL-11, and leukaemia inhibitory factor (LIF) Supports proliferation of haematopoietic progenitor cells when co-cultured in serum-deprived media with no exogenous factors	In house
M210-B4 [554,555]	BM stromal cells derived from C57BL/6J X C3H/HeJ) F1 mouse genetically engineered to produce hIL-3 and hG-CSF Support human and murine myelopoiesis in long term culture (LTC)	In house
SL/SL [555,556]	Stromal cell line derived from SL/SL mouse genetically engineered to produce hIL-3 and hSCF	In house

	Support human and murine myelopoiesis in LTC	
TM3 [557] (GLI-Luc) [558]	Murine leydig tumour cell line with intact Hh signalling transfected with a retroviral vector carrying 8 Gli-responsive elements and a luciferase gene	In house

Table 2.1.1.7: Cell Line Culture Conditions

Cell line	Media conditions
HS-5	DMEM High Glucose and 10% ES grade FBS and 10% HS-5 conditioned media
Kasumi-1	RPMI, 20% FBS, 1mM L-Glutamine, 1% Pen/Strep,
KG1a	RPMI, 20% FBS, 1mM L-Glutamine, 1% Pen/Strep
MOLM-13	RPMI, 10% FBS, 1mM L-Glutamine, 1% Pen/Strep
MV4-11	RPMI, 20% FBS, 1mM L-Glutamine, 1% Pen/Strep
M210-B4	DMEM, 10% FBS, 1mM L-Glutamine, 1% Pen/Strep G418 (to give a final concentration of 400μg/ml), Hygromycin B (to give a final concentration of 62.5μg/ml)
OCI-AML3	RPMI, 20% FBS, 1mM L-Glutamine, 1% Pen/Strep
SL/SL	RPMI, 15% FBS, 1mM L-Glutamine, 1% Pen/Strep G418 (to give a final concentration of 800μg/ml), Hygromycin B (to give a final concentration of 125μg/ml)
THP-1	RPMI, 10% FBS, 1mM L-Glutamine, 1% Pen/Strep
TM3	DMEM/F-12, 10% horse serum, 1mM L-Glutamine and Geneticin (100μg/ml)
To minimise proliferation of untransduced wild type SL/SL and M210-B4 cells, these were dosed on alternate weeks with medium supplemented with hygromycin B and G418	

Table 2.1.1.8: 10% Media for Cell Line Culture

Reagent	Volume
FBS	50ml
L-Glutamine (1MM)	5ml
Pen/Strep (1%)	5ml
RPMI	440ml

Table 2.1.1.9: 20% Media for Cell Line Culture

Reagent	Volume
FBS	100ml
L-Glutamine (1MM)	5ml
Pen/Strep (1%)	5ml
RPMI	390ml

Table 2.1.1.10: Media for M210-B4 Culture

Reagent	Volume
DMEM	390ml
FBS	50ml
L-Glutamine (1MM)	5ml
Pen/Strep (1%)	5ml

Table 2.1.1.11: Media for SL-SL Culture

Reagent	Volume
DMEM	415ml
FBS	75ml
L-Glutamine (1MM)	5ml
Pen/Strep (1%)	5ml

Table 2.1.1.12: Media for TM3 Culture

Reagent	Volume
DMEM/F-12	445ml
Geneticin	100μl/10ml
Horse serum	50ml
L-Glutamine (1MM)	5ml

Table 2.1.1.13: Media for Cell Line Cryopreservation

Reagent	Volume
DMSO	5ml
FBS	45ml

Table 2.1.1.14: Media for Primary AML Cell Culture

Reagent	Volume
hFLT3L (stock – 100µg/ml)	5µl
hIL-3 (stock – 10µg/ml)	50µl
hIL-6 (stock – 100µg/ml)	5µl
hSCF (stock – 100µg/ml)	5µl
HS-5 conditioned media	5.5ml
Myelocult	5ml (5%)
StemSpan 2	45ml
All cytokines are made up in filter sterilized PBS and BSA (0.1%)	

Table 2.1.1.15: Media for MSC Culture

Reagent	Volume
D-MEM Low Glucose + glutamax	440ml
Hyclone FCS (10%)	50ml
L-glutamine (100mM)	5ml
Pen/Strep	5ml

Table 2.1.1.16: Media for Thawing Primary Samples

Reagent	Volume
DNAse I (1mg/ml)	1ml
ES FCS (20%)FBS	100ml
Heparin (5000IU/ml)	4ml (20,000IU)
IMDM (Iscoves)	390ml
L-glutamine (200mM)	5ml

Filter sterilized through 0.22μM syringe filter

Table 2.1.1.17: Freezing media for Primary AML and MSC Samples

Reagent	Volume
DMSO	10ml
FBS	35ml
Human albumin solution 5%	5ml

Table 2.1.1.18: Reagents for CFC Assay

Reagent	Composition	Supplier
Methocult™ H4034	IMDM, methylcellulose, BSA, FBS, 2-mercaptoethanol, rhSCF, rhGM-CSF, rhG-CSF, rhIL-3, rhEPO	Stemcell Technologies, Grenoble, France
Serum free media (SFM) with high growth factor cocktail	IMDM, BIT, β-mercaptoethanol, penicillin-streptomycin, L-glutamine Flt3-L, SCF, IL-3, IL-6, G-CSF	Made in house in Vacubottle and filter sterilised

Table 2.1.1.19: Serum free media (SFM) for primary cell culture

Reagent	Volume
IMDM	97.25ml
BIT (BSA, insulin, transferrin)	25ml
L-Glutamine	1.25ml
Pen/Strep	1.25m
Β-Mercaptoethanol (200mM)	250µl (400µM)
Filter sterilise through 0.22µm filter before use	

Table 2.1.1.20: SFM with high concentration growth factor cocktail

Reagent	Supplier	Volume	Final concentration
SFM	Made in house (2.1.1.18)	10mL	-
IL3 (10µg/mL)	Stem Cell Technologies, Grenoble, France	20µl	20ng/mL
IL6 (10µg/mL)	Stem Cell Technologies, Grenoble, France	20µl	20ng/mL
GCSF (10µg/mL)	Chugai Pharma, London, UK	20µl	20ng/mL
SCF (10µg/mL)	Stem Cell Technologies, Grenoble, France	100µl	100ng/mL
Flt3L (10µg/mL)	Stem Cell Technologies, Grenoble, France	100µl	100ng/mL
Filter sterilise through 0.22µm filter before use			

Table 2.1.1.21: Drugs Tested and Suppliers

Drug	Mechanism of action	Supplier
Venetoclax (ABT-199; GDC-0199) [559]	Bcl-2 selective inhibitor with no activity against Mcl-1	Xcess Biosciences Inc, San Diego, USA
Ara-C	Antimetabolic agent and DNA synthesis inhibitor	Sigma-Aldrich, Dorset, UK
Arsenic (III) oxide	Causes degradation of PML-RAR α Acts on the intracellular environment to influence apoptosis, differentiation, growth arrest, and angiogenesis - further research is required to determine the exact pathways through which the cytotoxic actions are mediated	Sigma-Aldrich, Dorset, UK
Cyclopamine (11-Deoxojervine) [560]	Smo inhibitor	Selleckchem.com, Suffolk, UK
Elacridar hydrochloride (*N*-[4-[2-(3,4-Dihydro-6,7-dimethoxy-2(1*H*)-isoquinolinyl)ethyl]phenyl]-9,10-dihydro-5-methoxy-9-oxo-4-acridinecarboxamide hydrochloride)	P-gp/ABCG1 and BCRP/ABCG2 inhibitor	Tocris Bioscience, R&D systems, Abingdon, UK
Glasdegib (PF-04449913)	Smo inhibitor	Selleckchem.com, Suffolk, UK
HA14-1 (2-Amino-6-bromo-α-cyano-3-(ethoxycarbonyl)-4H-1-benzopyran-4-acetic acid ethyl ester)	Bcl-2 inhibitor - binds to surface pocket; disrupts Bax/Bcl-2 interaction; binds Bcl-XL and Bcl-w	Tocris Bioscience, R&D systems, Abingdon, UK
Reversan (*N*-[3-(4-Morpholinyl)propyl]-5,7-diphenylpyrazolo[1,5-*a*]pyrimidine-3-carboxamide)	Selective inhibitor of MRP1 and P-gp Does not sensitize MRP2, MRP3, MRP4 or MRP5 transporters to known substrates	Tocris Bioscience, R&D systems, Abingdon, UK
Tomatidine hydrochloride (3β-Hydroxy-5 α-tomatidane hydrochloride)	Steriodal alkaloid structurally similar to Cyclopamine	Santa Cruz, Texas, USA

TW37 (N-[[2-(1,1-Dimethylethyl)phenyl]-2,3,4-trihydroxy-5-[[2-(1-methylethyl)phenyl]methyl])	Inhibits Bcl-2 and Bcl-XL Inhibits the activation of Notch-1 and Jagged-1	Tocris Bioscience, R&D systems, Abingdon, UK
Zosuquidar hydrochloride ((α*R*)-4-[(1aα,6α,10bα)-1,1-Difluoro-1,1a,6,10b-tetrahydrodibenzo[*a*,*e*]cyclopropa[*c*]cyclohepten-6-yl]-α-[(5-quinolinyloxy)methyl]-1-piperazineethanol trihydrochloride)	P-gp inhibitor	Tocris Bioscience, R&D systems, Abingdon, UK

2.1.2 Molecular Studies:

Table 2.1.2.1: Plastics for Molecular Studies and Suppliers

Equipment	**Supplier**
Fluidigm dynamic Array integrated fluidic circuit (FLEXsix/48.48/96.96)	Fluidigm, San Francisco, USA
MicroAmp Optical Adhesive Film	Applied biosystems, Warrington, UK
Nucleotide free tips, eppendorfs and PCR tubes	Applied biosystems, Warrington, UK
8/12-Cap MicroAmp Optical strips	Applied biosystems, Warrington, UK
96 and 384 MicroAmp Optical Well Plates	Applied biosystems, Warrington, UK

Table 2.1.2.2: Molecular Reagents and Suppliers

Reagent	**Supplier**
3130 Pop-7 Polymer	Life technologies, Paisley, UK
5X Buffer	Promega, Madison, USA
Abi Prism Big Dye® V1.1	Thermo Fisher Scientific, Loughborough, UK
Assay loading reagent (2x)	Fluidigm, San Francisco, USA
cDNA reverse transcription kit	Applied Biosystems, Warrington, UK
Diisopropylfluorophosphate (1mM)	Sigma-Aldrich, Dorset, UK
DNA binding dye (20x)	Fluidigm, San Francisco, USA
DNAeasy Blood and Tissue Kit (69504)	Qiagen, Crawley, UK
DNAse I	Qiagen, Crawley, UK

dNTP	Sigma-Aldrich, Dorset, UK
EDTA Running Buffer (10x)	Life technologies, Paisley, UK
Exonuclease I (E. coli)	New England BioLabs, Hitchin, UK
Exonuclease I reaction buffer	New England BioLabs, Hitchin, UK
Gene expression master mix	Applied Biosystems, Warrington, UK
GE Sample Loading Reagent (20x)	Fluidigm, San Francisco, USA
GoTaq	Promega, Madison, USA
Hi-Di Formamide	Life technologies, Paisley, UK
Illustra Exo-ProStar	Thermo Scientific Nunc. Massachusetts, USA
$MgCl_2$	Promega, Madison, USA
Molecular biology grade 100% Ethanol	Qiagen, Crawley, UK
Molecular biology grade water	Qiagen, Crawley, UK
Nuclease free water	Qiagen, Crawley, UK
OligoDTs	Qiagen, Crawley, UK
PCR Master Mix (1.5mM $MgCl_2$)	Thermo Scientific Nunc. Massachusetts, USA
Pre-amplification master mix	Applied Biosystems, Warrington, UK
Primers – see Table 2.1.2.7	Integrated DNA Technologies, Leuven, Belgium
1X Quickstart Bradford Dye Reagent	Bio-Rad, Hertfordshire, UK
RNeasy Plus Mini kit (74134)	Qiagen, Crawley, UK
RNaseOUT™ recombinant ribonuclease inhibitor	Life technologies, Paisley, UK
Sequencing Reaction Buffer	Thermo Fisher Scientific, Loughborough, UK
SsoFast™ EvaGreen Supermix with low ROX	Bio-Rad, Hertfordshire, UK
Superscript® III reverse transcriptase	Life technologies, Paisley, UK
Taqman Gene Expression Assay (20x)	Fluidigm, San Francisco, USA
Taqman Probes – see Table 2.1.2.8	Applied Biosystems, Warrington, UK
Taqman Universal PCR Master Mix (2x)	Fluidigm, San Francisco, USA
TE Buffer pH8.0	Applied Biosystems, Warrington, UK

Table 2.1.2.3: Molecular Equipment and Programmes and Suppliers

Equipment	Supplier
Alamut Mutational Surveyor	Interactive Biosoftware, Rouen, France
Biomark Real-Time PCR Analysis	Fluidigm, San Francisco, USA
ChemiDoc™ MP System	Bio-Rad, Hertfordshire, UK
Fluidigm Biomark Analyser	Fluidigm, San Francisco, USA
Nanodrop spectrophotometer 2100	Nanodrop technologies, Wilmington, USA
Quantity-One 1-D Analysis Software	Bio-Rad, Hertfordshire, UK
Sorval Legend-T Centrifuge	DJB Labcare Ltd, Buckinghamshire, UK
Taqman 7900 machine	Applied biosystems, Warrington, UK
Techne Thermal Cycler TC-412	Bibby Scientific Limited, Staffordshire, UK

2.1.2.4 Reverse transcription

Table 2.1.2.4.1: Reverse transcription master mix Step 1

Reagent	Volume
dNTPs	1µl
Oligo dT	1µl
RNA	500ng
RNase free water	11µl – RNA volume

Table 2.1.2.4.2: Reverse transcription master mix Step 2

Reagent	Volume
Reverse transcription master mix 1	13µl
5x buffer	4µl
DTT	1µl
RNase	1µl
Superscript III	1µl

Table 2.1.2.4.3: Reverse Transcription Cycling Conditions

	Step 1	Step 2	
Temperature (°C)	65	55	70
Time	5mins	60mins	15mins

2.1.2.5 Polymerase chain reactions

Table 2.1.2.5.1: GoTaq® reverse transcription PCR (RT-PCR) mastermix

Reagent	Volume
cDNA	2µl
dNTPs (10mM)	0.5µl
Forward primer	0.2µl
GoTaq® DNA polymerase	0.1µl
Green GoTaq® Flexi Buffer (5X)	5µl
$MgCl_2$ (25MM)	3 µl
Reverse primer	0.2µl
RNAse free water	14µl

Table 2.1.2.5.2: GoTaq® RT-PCR Mastermix Cycling Conditions

	Stage 1: Initial denature	Stage 2: Cycling conditions 30 cycles			Stage 3: Final extension	Hold
		Denaturing	Annealing	Extension		
Temperature (°C)	95	95	60	72	72	4
Time	2mins	30secs	60secs	60secs	5mins	∞

Table 2.1.2.6: Taqman® Probes

Probe	Life Technologies Identifier	Probe	Life Technologies Identifier
ABCA2	Hs00242232_m1	*ATP5B*	Hs00969569_m1
ABCB1	Hs00184500_m1	*ATR*	Hs00992123_m1
ABCC1	Hs01561483_m1	*AXIN1*	Hs00394718_m1
ABCC3	Hs00978452_m1	*AXIN2*	Hs00610344_m1

ABCG2	Hs01053790_m1	*B2M*	Hs00984230_m1
APC	Hs01568269_m1	*BAD*	Hs00188930_m1
ATG5	Hs00169468_m1	*BAK1*	Hs00832876_g1
ATG7	Hs00197348_m1	*BAX*	Hs00180269_m1
ATM	Hs005892_m1	*BBC3*	Hs00248075_m1
BCL2	Hs00608023_m1	*DVL*	Hs00182896_m1
BCL2A1	Hs00187845_m1	*ENOX2*	Hs00197268_m1
BCL2L1	Hs00236329_m1	*ETV6*	Hs00231101_m1
BCL2L10	Hs00368095_m1	*FOS*	Hs00170630_m1
BCL2L11	Hs00708019_s1	*FOSL1*	Hs00759776_s1
BID	Hs00609632_m1	*FOXM1*	Hs01073586_m1
BIRC2	Hs01112284_m1	*FOXN1*	Hs00919266_m1
BIRC5	Hs04194392_s1	*FRZD*	Hs00201853_m1
BMI1	Hs00995536_m1	*GAPDH*	Hs02758991_g1
BMP4	Hs00370078_m1	*GLI1*	Hs01110766_m1
BRACHYURY	Hs00610080_m1	*GLI2*	Hs01119974_m1
CCND1	Hs00765553_m1	*GLI3*	Hs00609233_m1
CCND2	Hs00153380_m1	*GUSB*	Hs00939627_m1
CD44	Hs01075864_m1	*HES1*	Hs00172878_m1
CCDH1	Hs00765553_m1	*HES5*	Hs01387463_g1
CCDH2	Hs00153380_m1	*HHAT*	Hs00911326_m1
CDX1	Hs00156451_m1	*HHIP*	Hs01011015_m1
CDX2	Hs01078080_m1	*HOXA3*	Hs00601076_m1
CDX4	Hs00193194_m1	*HOXA9*	Hs00365956_m1
C-JUN	Hs01103582_s1	*HOXB4*	Hs00256884_m1
CPA3	Hs00157019_m1	*IGF1R*	Hs00609566_m1
CXCR4	Hs0007978_s1	*IHH*	Hs00745531_s1
CXXC4	Hs00228693_m1	*JAGGED*	Hs00171432_m1
DHH	Hs0036830_m1	*KISS1*	Hs00158486_m1
DKK1	Hs00183740_m1	*KIT*	Hs00174029_m1

DISP2	Hs00394338_m1	*KLF4*	Hs00358836_m1
DMP1	Hs01009391_g1	*KREMEN1*	Hs00230750_m1
DNMT1	Hs00945875_m1	*LEF1*	Hs01547250_m1
DNMT3a	Hs01027162_m1	*LMO2*	Hs00153473_m1
DNMT3b	Hs00171876_m1	*MAML2*	Hs00418423_m1
MAML3	Hs00298519_s1	*SFRP1*	Hs00610060_m1
MAP1LC3B	Hs00797944_s1	*SFRP2*	Hs00293258_m1
MCL1	Hs01050896_m1	*SFRP4*	Hs00180066_m1
MECOM	Hs00602795_m1	*SHH*	Hs00179843_m1
MEIS1	Hs00180020_m1	*SMAD2*	Hs00998186_m1
MMP2	Hs01548727_m1	*SMO*	Hs01090242_m1
MMP3	Hs00968305_m1	*SNAIL1*	Hs00195591_m1
MMP9	Hs00957562_m1	*SNAIL2*	Hs00161904_m1
MMP13	Hs00942584_m1	*SNAIL3*	Hs01018996_m1
MYB	Hs00920556_m1	*SOX2*	Hs01053049_s1
MYC	Hs00153408_m1	*SUFU*	Hs00960520_m1
NANOG	Hs02387400_g1	*STIL*	Hs00161700_m1
NLK	Hs00939681_m1	*TBP*	Hs99999910_m1
NODAL	Hs00415442_m1	*TCF3*	Hs00162613_m1
NUMB	Hs01105433_m1	*TCF4*	Hs00162613_m1
P53	Hs01034249_m1	*TCF7*	Hs01556515_m1
P73	Hs01056231_m1	*TWIST1*	Hs01675818_s1
PARP1	Hs00242302_m1	*TYW1*	Hs00936867_m1
PAX6	Hs01088114_m1	*UBE2D2*	Hs00366152_m1
PBX1	Hs00231228_m1	*VIMENTIN*	Hs00958111_m1
PECAM1	Hs01065279_m1	*WIF*	Hs00183662_m1
PP2CA	Hs01056778_g1	*WNT4*	Hs01573505_m1
PPP2R1A	Hs01026388_m1	*WNT5a*	Hs00998537_m1
PTCH1	Hs00181117_m1	*YWHAE*	Hs00356749_g1
PTCH2	Hs0018404_m1	*XIAP*	Hs00745222_s1

ROR1	Hs00938677_m1	*ZEB1*	Hs01566408_m1
ROR2	Hs00896176_m1		

Table 2.1.2.7 Primers

Primer	Forward sequence	Reverse sequence
APAF-1	TCT CTG TGA GCC GGA AAC TT	CGG GAA AGA TTC GTG ATG TT
ATG5	GGC ACA CCA CTG AAA TGG C	GAT GTT CCA AGG AAG AGC TGA AC
ATG7	CTG ATG TTT GGA GAT TGG TTC C	CAA CCC ATC AAC GTC CTA GC
ATP5B	TCC ATC CTG TCA GGG ACT ATG	ATC AAA CTG GAC GTC CAC CAC
B2M	TTG TCT TTC AGC AAG GAC TGG	ATC CGG CAT CTT CAA ACC TCC
BAD / BCL-XL	AGC TCC GGA GGA TGA GTG AC	CAC CAG GAC TGG AAG ACT CG
BAK	ACG CTA TGA CTC AGA GTT CC	TGA TGC CAC TCT CAA ACA GG
BAX	GCT GAC ATG TTT TCT GAC GG	ATG ATG GTT CTG ATC AGT TCC
BBC3	GAC CTC AAC GCA CAG TAC GA	CTA ATT GGG CTC CAT CTC G
BCL2	ATC GCC CTG TGG ATG ACT GAG T	GCC AGG AGA AAT CAA ACA GAG GC
BCL2L1	GCA TCG AAC AAC GAG AAT CA	GCT GGT CTC CAG GTA ACG AA
BCL-W / BCL2L2	AAG TGC AGG AGT GGA TGG TG	GTC CTC ACT GAT GCC CAG TT
BFK / BCL2L15	TTC AAC GGA GAA TTG GAA GC	AAT CCT GAG CAC ACC AGG TC
BID	GGA ACC GTT GTT GAC CTC AC	GAG GAG CAC AGT GCG GAT
BIK	GAG GTT CTT GGC ATG ACT GAC	CTG AGG CTC ACG TCC ATC TC
BIM	CAG CAC CCA TGA GTT GTG AC	CTT GGG CGA TCC ATA TCT CT
BMF	GAA CCC CAG CGA CTC TTT TA	TTT CGG GCA ATC TGT ACC TC
BMP4	CAG CAC TGG TCT TGA GTA TCC T	AGC AGA GTT TTC ACT GGT CCC
BOK	CAA GGT GGT GTC CCT GTA TG	GCT GAC CAC ACA CTT GAG GA
CASPASE 3	TGT GGA AGA ACT TAG GCA TC	TTT GCT CAC ACT TTC TCT CA
CASPASE 7	TCT TTT GTG CTG CTT CTT TG	CCC ACT CCT ATC TTA CTC CA
CASPASE 8	CTG GTC CCT GCT AAC ATT TG	CTG GTC CCT GCT AAC ATT TG
CASPASE 9	CCT GGA GTC TAG TTG GCT	TCA TAT GGG GCC TGA ACA

CCNA1	CTC GTA GGA ACA GCA GCT ATG C	GCT AGA ACT TTC AGA AGC AAG TGT TC
CCNA2	ACC CTG GAA AGT CTT AAG CCT	GTG TCT CTG GTG GGT TGA GG
CCNB1	CAG CTC TTG GGG ACA TTG GTA AC	ACT GGC ACC AGC ATA GGT ACC
CCNC1	TTT GCT GAG CTT TCT GTG GA	AAT GGT TGC CAT CTC TTT TCT C
CCND1	TGC ATC TAC ACC GAC AAC TCC	CGG ATG ATC TGT TTG TTC TCC G
CCND2	CCG CAG TGC TCC TAC TTC AA	GCC AAG AAA CGG TCC AGG TA
CCND3	CCT CCT ACT TCC AGT GCG TG	AGG CCA GGA AAT CAT GTG CA
CCNE2	CAA GTT GAT GCT CTT AAA GAT GCT CC	GCA GCA GTC AGT ATT CTG TAC TGG
CFLAR	CAC AGC TCA CCA TCC CTG TA	GGC AGA AAC TCT GCT GTT CC
CDH1	TTT GAC GCC GAG AGC TAC AC	GTC CTT TGT CGA CCG GTG CA
CDH2	CTG CTT CAG GCG TCT GTA GA	GCC TGT CCT TCA TGC ACA TC
CKIT	GCA TTC AAG CAA ATG GCA C	CCA ATC AGC AAA GGA GTG AA
CXCR4	TTA CCA TGG AGG GGA TCA GT	GTA GAT GGT GGG CAG GAA GA
CYCTO - C	ACT CTT ACA CAG CCG CCA AT	CCT TCT TCT TAA TGC CGA CAA
DIABLO	AGA TGA AGT GTG GCA GGT GA	GCT GCC ATC TCT GAA AGA CC
FAS	GGA TTG CTC AAC AAC CAT GC	CCT CAA TTC CAA TCC CTT GG
FASL1	GCA CAC AGC ATC ATC TTT GG	CAT AGG TGT CTT CCC ATT CC
ENOX2	GAG CTG GAG GGA ACC TGA TTT	CAC TGG CAC TAC CAA ACT GCA
FOS	AGG AGA ATC CGA AGG GAA AGG	TAG TTG GTC TGT CTC CGC TTG
FOXM1	TCA AAA CCG AAC TCC CCC TG	GCA GCA CTG ATA AAC AAA GAA AGA
GAPDH	ACG GAT TTG GTC GTA TTG GG	ATT TTG GAG GGA TCT GCT C
GLI1	AGC CAA GCA CCA GAA TCG G	TCT TGA CAT GTT TTC GCA GCG
GLI2	CTC CTA TGG TCA CTT ATC TGC AAG T	TGA ACC TAA GCT CTG TTG TCG G
GLI3	TCC ATA CCT TGA CCA GCT TG	GCA GAT TGT CTC TGG ATC TC
HHIP	GCC ATT CAG TAA TGG TCC TTT GG	CCA CTG CTT TGT CAC AGG AC
HSP 60	AGT GGA AAT CAG GAG AGG TA	AGA GGA GGA ATG AGA GAA GG
HSP 70	ATG CCA TGT ACT TCT CTT GG	ATA CAG AAC ATC TCC CAC CT
HSP 90	CAC CAC CCC AAA TAT CTT CT	TAG CTC CTC ACA GTT ATC CA
IHH	GGA CGC TAT GAA GGC AAG ATC G	CAG CGA GTT CAG GCG GTC CTT

LC3B	CGA TAC AAG GGT GAG AAG CA	GCC TGA TTA GCA TTG AGC TG
MCL1	CTT ACG ACG GGT TGG GGA TG	TCC TGC CCC AGT TTG TTA CG
MCM2	ACC CGA AGC TCA ACC AGA TG	TGC GGA TCA TGG ACT CGA TG
MCM3	GAA GTG ATG GAG CAG GGT CG	CAG TGA GTC CTG TAG CCC AA
MCM4	TGA CCG TTA CCC TGA CTC AA	GGG AAT CAG CTG GGA TGT CC
MCM5	CAT CTC TAT CCA GTG CCG CA	GCA TTT GTC GGG CAT GAT GA
MCM6	AAT TTG TCA GCT CCC ATC ATG T	TGA ATG CAA ATC TAC TAT GCG CC
MCM7	GCA TGA AAA TCC GGG GCA AC	GTA AGC CCC ACT CCT GAG GA
MCM8	GGA GGA AGC CAG AAA TAC GC	CCA CAA ACA TAC ACG CCA CG
MCM9	CCA GTC CCT TTC TCA GCC TG	ACT TGT TCG AAT CAC TGT CCC A
MCM10	TCT GGG GAA ACG ACT CAA CC	TCG GCC GGT CAT TTT CTT GT
MDM2	TGT TTG GCG TGC CAA GCT TCT C	CACAGATGTACCTGAGTCCGATG
MYC	GAC TCT GAG GAG GAA CAA GA	TTG GCA GCA GGA TAG TCC TT
NUMB	CCA AAC CAG TGA CAG TGG TGG C	CCC AAG GGT TGG TTT CAC GC
P53	CAG TCA GAT CCT AGC GTC GA	TGT TCA ATA TCG TCC GGG GA
PARP	AGA AGT ACG TGC AAG GGG TG	CCA GCG GTC AAT CAT GCC TA
PMAIP	AAG AAG GCG CGC AAG AAC	TCA GGT TCC TGA GCA GAA GAG
PTCH1	ACA TTT GTG TTA CAA ATC AGG AGA GC	CTG TCC CAG ACT GTA ATT TCG C
PTCH2	TGT GGT GGG AGG CTA TCT G	GCA TGG TCA CAC AGG CAT AG
RPA1	TGC GAA TCC TGA CAT CCC AG	TGG TGT TAC TCC CTC CGA CT
RPA2	CAG ACA TGT GTT TCA GCT GGT	CAG GAA TGA GTG AAG CAG GGA
SHH	CGA GCG ATT TAA GGA ACT CAC C	GCG TTC AAC TTG TCC TTA CAC C
SMO	CTG ACC GCT TCC CTG AAG G	CGT CCT CGT ACC AGC TCT TGG
STIL	GAC ACA GTG CAA GCT GGA AGA C	AGT CAG GCT CTT GAT CCT CAC C
SUFU	CTC CAG GTT ACC GCT ATC GTC A	TGC TCA GGG ATG TTG GCA GAA G
SURVIVIN	TCC GCA GTT TCC TCA AAT TC	GTT GCG CTT TCC TTT CTG TC
TYW1	ATT GTC ATC AAG ACG CAG GGC	GTT GCG AAT CCC TTC GCT GTT
UBE2D2	CCA TGG CTC TGA AGA GAA TCC	GATAGGGACTGTCATTTGGCC
VIMENTIN	GGA GAA ATT GCA GGA GGA GA	TGC GTT CAA GGT CAA GAC GT
XIAP	AGA AAT CCA TCC ATG GCA GA	CAG TTA GCC CTC CTC CAC AG

2.1.2.8 Fluidigm qRT-PCR

Table 2.1.2.8.1: Pre-amplification mix - Primer

Reagent	Volume
Qiagen Multiplex PCR master mix	2.5µl
Pooled assay Taqman mix (x2)	1.25µl
RNase free water	1.5µl
cDNA	1.25µl

Table 2.1.2.8.2: Pre-amplification mix – Probe (Taqman®)

Reagent	Volume
Qiagen Multiplex PCR master mix	2.5µl
Pooled primer mix	0.5µl
RNase free water	0.75µl
cDNA	1.25µl

Table 2.1.2.8.3: Pre-amplification Cycling Conditions

	Stage 1: Initial denature	Stage 2: Cycling conditions 14-18 cycles			Stage 3: Final extension	Hold
		Denaturing	Annealing	Extension		
Temperature (°C)	94	94	60	72	72	4
Time	15mins	30secs	60secs	40secs	5mins	∞

Table 2.1.2.8.4: Exonuclease treatment mix for use after primer pre-amplification

Reagent	Volume
RNase free water	1.4µl
Exonuclease I reaction buffer	0.2µl
Exonuclease I (E. coli)	0.4µl

Table 2.1.2.8.4.1 Exonuclease treatment Cycling Conditions

Temperature	37˚C	80˚C
Time	30mins	15mins

Table 2.1.2.8.5 Assay mix for Fluidigm qRT PCR - Primer

Reagent	**Volume**
2x Assay loading reagent	3µl
TE buffer	0.3µl
Mixed forward and reverse primer	2.7µl

Table 2.1.2.8.5.1: Sample mix for Fluidigm qRT PCR - Primer

Reagent	**Volume**
20x DNA binding dye	0.3µl
SsoFast™ EvaGreen Supermix with low ROX	3µl
Pre-amplified sample	2.7µl

Table 2.1.2.8.6 Assay mix for Fluidigm qRT PCR - Probe

Reagent	**Volume**
2x Assay loading reagent	3µl
Taqman probe	3µl

Table 2.1.2.8.6.1: Sample mix for Fluidigm qRT PCR - Probe

Reagent	**Volume**
20x DNA binding dye	0.3µl
SsoFast™ EvaGreen Supermix with low ROX	3µl
Pre-amplified sample	2.7µl

Table 2.1.2.8.7: Fluidigm qRT PCR Cycling Conditions

	Stage 1: Initial denature	Stage 2: Cycling conditions 40 cycles		Hold
		Denaturing	Annealing	
Temperature (°C)	95	95	60	4
Time	60secs	5secs	20secs	∞

Melt curve when primers used: 60˚C to 95˚C with a 1˚C increase every 3 seconds

2.1.2.9 Sanger Sequencing

Table 2.1.2.9.1: *SMO* Primers

Primer	Sequence
Exon1F_1	GTAGCGCGACGGCCAGT**CAACAAAGGAGCCGGGTC**
Exon1R_1	CAGGGCGCAGCGATGA**CCCGCCAACTCAGCAAAAG**
Exon1F_2	GTAGCGCGACGGCCAGT**CTGAGTTGGCGGGGTTGG**
Exon1R_2	CAGGGCGCAGCGATGA**CCCATCTTACCGCGGCAC**
Exon1F_3	GTAGCGCGACGGCCAGT**GGATTCTCTGGGCGCACA**
Exon1R_3	CAGGGCGCAGCGATGA**CCAGGCACACGTTGTAGC**
Exon2F	GTAGCGCGACGGCCAGT**GAGGACAGGGGTGAAGCTG**
Exon2R	CAGGGCGCAGCGATGA**CACTGGACCCTGCCCTATAC**
Exon3F	GTAGCGCGACGGCCAGT**CCCTGCCATGCTACCTAGAT**
Exon3R	CAGGGCGCAGCGATGA**CTCTCTTCCCACGTTCCAGG**
Exon4F	GTAGCGCGACGGCCAGT**GGCTCAGTTAAGGGTGTCTG**
Exon4R	CAGGGCGCAGCGATGA**TGCCCTGGATCTCGGTTTTA**
Exon5-6_1F	GTAGCGCGACGGCCAGT**GAACCTCCAGACCTCAGCAG**
Exon5-6_1R	CAGGGCGCAGCGATGA**CTCACAGAGTCCCCATCCAC**
Exon5-6_2F	GTAGCGCGACGGCCAGTT**ACTTCCACCTGCTCACCTG**
Exon5-6_2R	CAGGGCGCAGCGATGA**TGGGGTTTCAGCATGGGG**
Exon7-8_1F	GTAGCGCGACGGCCAGTT**CCAGAGCCTTAGGACCCTC**
Exon7-8_1R	CAGGGCGCAGCGATGA**ACTACCACCTACACACACCC**
Exon7-8_2F	GTAGCGCGACGGCCAGTT**GGGACAAGTTAGCCATAGGG**
Exon7-8_2R	CAGGGCGCAGCGATGA**GGTGGAGGTGGGTGTCTTTA**

Exon7-8_3F	GTAGCGCGACGGCCAGT**GACTTCGGTCTGAGGTCCTG**
Exon7-8_3R	CAGGGCGCAGCGATGA**AGGAGAGAGTCTGCCCCACT**
Exon9F	GTAGCGCGACGGCCAGT**GGCCCTTCCCAAGATTTGAT**
Exon9R	CAGGGCGCAGCGATGA**CTGGGAGAGACTAGCACAT**
Exon10-11F	GTAGCGCGACGGCCAGT**CATCGCTCACACACCCATTC**
Exon10-11R	CAGGGCGCAGCGATGA**TCCTTCCTCTTCCTCCTCCT**
Exon12_1F	GTAGCGCGACGGCCAGT**CAGGTTAAGTGCTCCCAGGG**
Exon12_1R	CAGGGCGCAGCGATGA**CCCCATGGAGATGTTAGGCT**
Exon12_2F	GTAGCGCGACGGCCAGT**AGTTCTGGATGTCTGGCTCA**
Exon12_2R	CAGGGCGCAGCGATGA**AGCTCTGGGTCCTCATCAAC**
Exon12_3F	GTAGCGCGACGGCCAGT**GGGGCCATGTCCTCTCTTAA**
Exon12_3R	CAGGGCGCAGCGATGA**CTTGAACCCAGGAGACGGAG**

Universal forward tail: GTAGCGCGACGGCCAGT; Universal reverse tail: CAGGGCGCAGCGATGA

Table 2.1.2.9.2: *SMO* RT-PCR Master mix

Reagent	**Volume**
DNA in a 20µl reaction.	1µl
Forward primer (5pmol/µl)	0.5µl
Reverse primer (5pmol/µl)	0.5µl
PCR Master Mix (1.5mM)	18µl

SMO PCR primers were diluted to 5µM (5pmol/µl) from 100µM stock

Table 2.1.2.9.3: *SMO* RT-PCR

	Stage 1: Initial denature	**Stage 2: Cycling conditions 35 cycles**			**Stage 3: Final extension**	**Hold**
		Denaturing	**Annealing**	**Extension**		
Temperature (°C)	95	94	56	72	72	4
Time	2min	30secs	45secs	90secs	5mins	∞

Table 2.1.2.9.4: *SMO* RT-PCR Product Clean Up

	Step 1	Step 2	Step 4
Temperature (°C)	37	80	4
Time	15mins	15mins	∞

Table 2.1.2.9.5: *SMO* Sequencing Master mix

Reagent	Volume
Big Dye® Terminator	0.5µl
Nuclease free water	7.5µl
Sequencing forward OR reverse primer	1µl
Sequencing Reaction Buffer	1µl

Sequencing primers were diluted to 3.3µM (3.3pmol/µl) from 100µM stock

Table 2.1.2.9.6: *SMO* Cycle Sequencing

	Stage 1: Initial denature	Stage 2: Cycling conditions 35 cycles			Stage 3: Final extension	Hold
		Denaturing	Annealing	Extension		
Temperature (°C)	96	96	50	60	60	4
Time	1min	10secs	5secs	4mins	4mins	∞

2.1.2.10 Next-generation Sequencing

Table 2.1.2.10.1: Targets for Ion AmpliSeq™ Research genes panel

Gene	Target	Gene	Target
ASXL1	Exon 12	***IDH1***	Exon 4
BRAF	COSMIC mutation, COSM476	***IDH2***	Exon 4
CBL	Exon 8,9	***JAKL2***	Exon 14
CEBPA	All coding exons	***KIT***	Exons 8, 10, 11, 17
DNMT3A	All coding exons	***KRAS***	Exons 2, 3
FLT3	Codons 676, 830-850	***NPM1***	Exon 12
GATA2	All coding exons	***NRAS***	Exons 2, 3

PTPN11	Exons 3, 7, 8, 13	***TP53***	All coding exons
RUNX1	Exons 3-8	***WT1***	Exons 7, 9
TET2	All coding exons		

Table 2.1.2.10.1.1: Ion AmpliSeq™ Sequencing Conditions

	Stage 1: Initial denature	**Stage 2: Cycling conditions 20 cycles**		**Hold**
		Denaturing	**Annealing & Extension**	
Temperature (°C)	99	99	60	10
Time	2 mins	15 secs	4 mins	∞

Table 2.1.2.10.2: Targets for Illumina TruSight® Myeloid Sequencing panel

Gene	**Target**	**Gene**	**Target**
ABL1	Exons 4-6	***IDH2***	Exon 4
ASXL1	Exon 12	***IKZF1***	Full
ATRX	Exons 8-10. 17-31	***JAK2***	Exons 12, 13
BCOR	Full	***JAK3***	Exon 4
BCORL1	Full	***KDM6A***	Full
BRAF	Exon 15	***KIT***	Exons 2, 8-11, 13, 17
CALR	Exon 9	***KRAS***	Exons 2, 3
CBL	Exon 8, 9	***MLL***	Exons 5-8
CBLB	Exons 9, 10	***MPL***	Exon 10
CBLC	Exons 9, 10	***MYD88***	Exons 3-5
CDK2NA	Full	***NOTCH1***	Exons 26-28, 34
CEBPA	Full	***NPM1***	Exon 12
CSF3A	Exons 14-17	***NRAS***	Exons 2, 3
CUX1	Full	***PDGFRA***	Exons 12, 14, 18
DNMT3A	Full	***PHF6***	Full
ETV6/TEL	Full	***PTEN***	Exons 5,7
EZH2	Full	***PTPN11***	Exons 3, 13
FBXW7	Exons 9, 10, 11	***RAD21***	Full

FLT3	Exons 14, 15, 20	***RUNX1***	Full
GATA1	Exon 2	***SETBP1***	Exon 4 (partial)
GATA2	Exons 2-6	***SF3BP1***	Exons 13-16
GNaS	Exons 8, 9	***SMC1A***	Exons 2, 11, 16+17
HRAS	Exons 2, 3	***SMC3***	Exons 10, 13, 19, 23, 25+28
IDH1	Exon 4	***SRSF2***	Exon 1
STAG2	Full	***U2AFI***	Exons 2+6
TET2	Exons 3-11	***WT1***	Exons 7, 9
TP53	Exons 2-11	***ZRSR2***	Full

Table 2.1.2.10.2.1: Illumina TruSight® Sequencing Conditions

	Stage 1: Initial denature	**Stage 2: Cycling conditions 25 cycles**			**Hold**	
		Denaturing	**Annealing**	**Extension**		
Temperature (°C)	95	95	66	72	72	10
Time	3 mins	30 secs	30 secs	30 secs	5mins	∞

2.1.3 Protein expression

Table 2.1.3.1: Reagents for Protein Preparation

Reagent	**Supplier**
50mM Tris-HCL pH7.5	Made in house
NaCl	Sigma-Aldrich, Dorset, UK
1% Nonidet p40	Sigma-Aldrich, Dorset, UK
10% Glycerol	Sigma-Aldrich, Dorset, UK
5mM Ethylenediamine Tetraacetic acid (EDTA)	Sigma-Aldrich, Dorset, UK
1mM Sodium Orthovanadate	Sigma-Aldrich, Dorset, UK
1mM Sodium Molybdate	Sigma-Aldrich, Dorset, UK
1mM Sodium Fluoride	Sigma-Aldrich, Dorset, UK
PMSF (stock – 80mg/ml in DMSO)	Sigma-Aldrich, Dorset, UK
Pepstatin A (stock – 1.4mg/ml in methanol)	Sigma-Aldrich, Dorset, UK

Aprotinin (stock – 20mg/ml)	Sigma-Aldrich, Dorset, UK
Leupeptin (stock – 20mg/ml)	Sigma-Aldrich, Dorset, UK
Soyabean trypsin inhibitor (stock – 20mg/ml)	Sigma-Aldrich, Dorset, UK

Table 2.1.3.2: Solution for Protein Extraction

Protein Solubilisation Buffer	**Phosphatase and Protease Inhibitor Concentrations**
50mM Tris-HCL pH 7.5	1mM Sodium Orthovanadate
150mM NaCl	1mM Sodium Molybdate
1% Nonidet P40	1mM Sodium Fluoride
10% Glycerol	4µg/mL Phenylmethylsulphonyl Fluoride
	0.7µg/mL Pepstatin A
	10µg/mL Aprotinin
	10µg/mL Leupeptin
	10µg/mL Soybean trypsin inhibitor

2.1.4 Western Blotting

Table 2.1.4.1: Reagents and Suppliers

Reagent	**Supplier**
Acrylamide	Sigma-Aldrich, Dorset, UK
APS APS (10%) - 0.1g APS in 1000µL MilliQ ultrapure water	Sigma-Aldrich, Dorset, UK
BSA Fraction V	Roche, West Sussex, UK
Chemiluminescent HRP Substrate	Millipore, Livingston, UK
Glycine	Sigma-Aldrich, Dorset, UK
HCl	In house
2-ME	Sigma-Aldrich, Dorset, UK
MilliQ ultrapure water	In house
NaCl	Sigma-Aldrich, Dorset, UK
NP40	Sigma-Aldrich, Dorset, UK

NP40 (10%) - 25ml NP-40 in 250mL MilliQ ultrapure water	
Ovalbumin	Sigma-Aldrich, Dorset, UK
PageRuler Plus Pre-stained Protein ladder	Thermo Fisher Scientific, Loughborough, UK
SDS SDS (10%) - 10g SDS in 91mL MilliQ ultrapure water	Sigma-Aldrich, Dorset, UK
Sodium azide	Sigma-Aldrich, Dorset, UK
TEMED	Sigma-Aldrich, Dorset, UK
Tris-HCl pH 6.8 60.6g Trisma base in 500mL MilliQ ultrapure water, Hcl added dropwise to correct pH	In house
Tris-HCl pH 8.8 60.6g Trisma base in 500mL MilliQ ultrapure water, NaOH added dropwise to correct pH	In house
Trizma base	Sigma-Aldrich, Dorset, UK

Table 2.1.4.2: Equipment and Suppliers

Equipment	**Supplier**
Amersham Protran Premium 0.2 Nitrocellulose membranses	Sigma-Aldrich, Dorset, UK
Exposure cassette Carestream® Kodak® BioMax®	Sigma-Aldrich, Dorset, UK
Konica Minolta SRX-101A developer	Konica Minolta, Sunderland, UK
Mini-PROTEAN® System Glass Plates	Bio-Rad, Hertfordshire, UK
Mini-PROTEAN® Tetra Handcast Systems	Bio-Rad, Hertfordshire, UK
NanoDrop Spectrophotometer	Thermo Fisher Scientific Nunc, Massachusetts, USA
PowerPac™ Basic Power Supply	Bio-Rad, Hertfordshire, UK
Trans-Blot® SD Semi-Dry Transfer Cell	Bio-Rad, Hertfordshire, UK

Table 2.1.4.3: 5% Sample Buffer

Reagent	Concentration
ß-Mercaptoethanol reducing agent (50µl/ml)	5% (v/v)
Bromophenol blue	Sigma-Aldrich, Dorset, UK
MilliQ ultrapure water	10% (W/v)
Glycerol	50% (v/v)
SDS	10% (w/v)
Tris-HCl pH 6.8	200mM

Table 2.1.4.4: 10X TBS Buffer pH 7.5

Reagent	Volume / weight
MilliQ ultrapure water	1000ml
NaCl	87.6g
Trizma base	24.2g

Table 2.1.4.5: 1X TBS Buffer pH 7.5

Reagent	Concentration
NaCl	150mM
Tris-HCl pH 7.5	20mM

100ml 10X TBS Buffer pH 7.5 in 900ml MilliQ ultrapure water

Table 2.1.4.6: 1X TBSN Buffer

Reagent	Concentration
NaCl	150mM
NP40	0.05% (v/v)
Tris-HCl pH 7.5	20mM

100ml 10X TBS Buffer pH 7.5 in 900ml MilliQ ultrapure water with 4ml NP40

Table 2.1.4.7: 10X SDS Page Running Buffer

Reagent	Volume / Weight
Glycine	149.2g
MilliQ ultrapure water	1000ml
SDS	0.1% (w/v)
Trizma base	30g

Table 2.1.4.8: 1X SDS Page Running Buffer

Reagent	Concentration
Glycine	192mM
SDS	10g
Trizma base	25mM

100ml 10x SDS Page Running Buffer in 900ml MilliQ ultrapure water

Table 2.1.4.9: 10X Semi-Dry Transfer Buffer Stock

Reagent	Weight / Volume
Glycine	29.3g
MilliQ ultrapure water	1000ml
SDS	3.75g
Tris base	58.1g

Table 2.1.4.10: 1X Semi-Dry Transfer Buffer

Reagent	Volume
10X Semi-Dry Transfer Buffer	100ml
Methanol (20%)	200ml
MilliQ ultrapure water	1000ml

Table 2.1.4.11: Running Gel

Reagent	Volume		
	7.5%	**10%**	**15%**
Acrylamide (30%)	3.75ml	5ml	7.5ml
APS (10%)	100µl	100µl	100µl
MiliQ dH2O	5.6ml	4.35ml	1.85ml
SDS (10%)	250µl	250µl	250µl
TEMED	20µl	20µl	20µl
Tris-HCl pH 8.8	5.6ml	5.6ml	5.6ml

Table 2.1.4.12: 5% Stacking Gel

Reagent	Volume
Acrylamide (30%)	1.67ml
APS (10%)	50 µl
MilliQ dH2O	6ml
SDS (10%)	150µl
TEMED	10 µl
Tris-HCl pH 6.8	1.25ml

Table 2.1.4.13: 5X BSA Blocking solution

Reagent	Concentration
BSA	1% (w/v)
Ovalbumin	1% (w/v)
Sodium azide	0.01% (w/v)

Dissolved in 1XTBS pH 7.5

Table 2.1.4.14: Antibody Conditions for Western blots

Antibody	Species	Dilution	Diluent	Manufacturer (Catalogue number)
BCL-2	Rabbit	1/1000	1X BSA	Cell signalling, MA, USA, (#2876)
MCL-1	Rabbit	1/1000	1X BSA	Cell signalling, MA, USA, (#4572)
SMO	Rabbit	1/1000	1X BSA	Abcam, Cambridge, UK, (ab72130)

2.1.5 Immunocytochemistry

Table 2.1.5.1: Reagents and Suppliers for Immunocytochemistry

Reagent	Supplier
Acetylated α-tubulin mouse monoclonal	Sigma-Aldrich, Dorset, UK
Alexa fluor 488-labelled goat anti-mouse IgG1	Life technologies, Paisley, UK
Alexa fluor 568-labelled goat anti-mouse IgG2b	Life technologies, Paisley, UK
BSA	Sigma-Aldrich, Dorset, UK
DAPI	Invitrogen, Paisley, UK
Ethanol 100% molecular grade	Sigma-Aldrich, Dorset, UK
Formaldehyde solution	Sigma-Aldrich, Dorset, UK
Γ-tubulin mouse monoclonal	Sigma-Aldrich, Dorset, UK
Nail polish	Local pharmacy
Normal Goat serum	Dako, Cambridgeshire, UK
Ovalbumin	Roche, West Sussex, USA
Poly-L-Lysine (0.5mg/ml)	Sigma-Aldrich, Dorset, UK
PBS (w/o Ca^{2+} or Mg^{2+}) (1X)	In house
100X Sodium Citrate Retrieval Buffer pH6	Thermo Fisher Scientific Nunc, Massachusetts, USA
Sodium Tetraborate (100mM)	Sigma-Aldrich, Dorset, UK
TBS pH 7.5 (1X)	In house
Triton-X (0.2%)	Sigma-Aldrich, Dorset, UK

Tween	BDH Merck, Dorset, UK
Xylene	Ganta Medicals, York, UK

Table 2.1.5.2: Equipment for Immunocytochemistry

Equipment	**Supplier**
Dako pen	Dako, Cambridgeshire, UK
10 well Multispot microscope slides	Hendley, Essex, UK
Pt Module	Thermo Fisher Scientific Nunc, Massachusetts, USA
Tinfoil	Local supermarket

Table 2.1.5.3: 5X Block

Reagent	**Concentration**
BSA	5%
Ovalbumin	1%
Triton-X	0.2%

Dissolved in 1X TBS pH 7.5

Table 2.1.5.4: Antibody Conditions for Immunocytochemistry

Antibody	**Species**	**Dilution**	**Diluent**	**Manufacturer** **(Catalogue number)**
Acetylated α-tubulin	Mouse	1/500	5% NGS in 1X PBS	Sigma-Aldrich, Dorset, UK (T6793)
DAPI		1/1000	5% NGS in 1X PBS	Thermo Fisher Scientific Nunc, Massachusetts, USA (D1306)
DHH	Goat	1/200	5% NGS in 1X PBS	Santa Cruz, Texas, USA, (N-19; sc-1193)
γ-tubulin	Mouse	1/100	5% NGS in 1X PBS	Sigma-Aldrich, Dorset, UK (T5326)
GLI-1	Rabbit Rabbit	1/100 1/100	5% NGS in 1X PBS	Cell Signalling, MA, USA, (25345) Abcam, Cambridge, UK (ab92611)

GLI-2	Rabbit Goat	1/100 1/100	5% NGS in 1X PBS	Santa Cruz, Texas, USA, (H-300; sc-28674) Santa Cruz (G-20; sc20291)
GLI-3	Rabbit	1/100	5% NGS in 1X PBS	Santa Cruz, Texas, USA, (H-280; sc-20688)
IHH	Rabbit	1/100	5% NGS in 1X PBS	Abcam, Cambridge, UK (ab39634)
PTCH-1	Rabbit	1/100	5% NGS in 1X PBS	Santa Cruz, Texas, USA, (H-267; sc-9016)
Acetylated α-tubulin SHH	Rabbit Rabbit	1/100 1/100	5% NGS in 1X PBS	Millipore, Livingston, UK (06-1106). Santa Cruz, Texas, USA, (H-160; sc-9024)
SMO	Rabbit	1/100	5% NGS in 1X PBS	Abcam, Cambridge, UK (ab72130)
Secondary antibodies				
Alexa Fluor 568-labelled anti-mouse IgG2b	Goat anti-mouse IgG1	1/500	5% NGS in 1X PBS	Life technologies, Paisley, UK, Invitrogen (A21144)
Alexa Fluor 488-labelled anti-mouse IgG1	Goat	1/100	5% NGS in 1X PBS	Life technologies, Paisley, UK, Invitrogen (A21121)

2.1.6 Immunohistochemistry

Table 2.1.6.1: Reagents and suppliers for Immunohistochemistry

Reagent	Supplier
Antibodies – see Table 2.1.5.3	
BOND Dewaxing agent	Leica Biosystems, Newcastle, UK (AR9222)
BOND Polymer refine Detection kit	Leica Biosystems, Newcastle, UK (DS9800)
BOND Primary Antibody Diluent	Leica Biosystems, Newcastle, UK (AR9352)
BOND Wash Solution 10X Concentrate	Leica Biosystems, Newcastle, UK (AR9590)
Epitope Retrieval 1 (ER_1) solution	Leica Biosystems, Newcastle, UK (AR9961)
Epitope Retrieval 2 (ER_2) solution	Leica Biosystems, Newcastle, UK (AR9640)

Table 2.1.6.2: Equipment for Immunohistochemistry

Equipment	Supplier
Coverslips	Leica Biosystems, Newcastle, UK
Leica Bond III	Leica Biosystems, Newcastle, UK
Microscope slides	Leica Biosystems, Newcastle, UK

Table 2.1.6.3: Antibody Conditions for Immunohistochemistry

Antibody	Control material	Dilution	Epitope retrieval (Time in mins)	Supplier (Catalogue number)
Anti-BCL-2	Tonsil	1:200	ER_1 (20)	Millipore, Livingston, UK, (05-729)
Anti-BMP4	Colon cancer	1:100	ER_2 (20)	Millipore, Livingston, UK, (MAB1049)

Anti-CD44	Multi tissue control comprising tonsil, breast, small bowel and skin	1:100	ER_2 (20)	Millipore, Livingston, UK, (04-1123)
Anti-CCND1	Tonsil	1:80	ER_1 (20)	Millipore, Livingston, UK, (05-362)
Anti-DHH	Testes	1:1000	EZ_1 (10)	Millipore, Livingston, UK, (04-967)
Anti-GLI-1	Brain	1:100	ER_1 (20)	Abcam, Cambridge, UK, (ab92611)
Anti-IHH	Colon cancer	1:1000	ER_2 (20)	Millipore, Livingston, UK, (MABF23)
Anti-PTCH-1	Cardiac muscle	1:300	ER_1 (30)	Abcam, Cambridge, UK, (ab53715)
Anti-SMO	Kidney	1:200	ER_2 (20)	Abcam, Cambridge, UK, (ab72130)
Anti-SHH	Colon cancer	1:100	ER_1 (20)	Millipore, Livingston, UK, (06-1106)
Anti-WNT5a	Cardiac muscle	1:100	EZ_1 (10)	Millipore, Livingston, UK, (06-1058)

Both ER_1 and ER_2 solutions are specific for heat-induced epitope retrieval; ER_1 is optimal at pH 6, ER_2 optimal at pH 9. EZ: enzyme retrieval.

2.1.7 Flow cytometry

Table 2.1.7.1: Plastics for Flow Cytometry

Plastic	**Supplier**
FACS tubes	Greiner bio one, Gloucestershire, UK

Table 2.1.7.2: Equipment for Flow Cytometry

Equipment	Supplier
BD FACSAria™ III	BD Biosciences, Oxford, UK
BD FACSCanto™ II	BD Biosciences, Oxford, UK
BD FACSDiva™ Software	BD Biosciences, Oxford, UK
FlowJo	Ashland, Oregon, USA

Table 2.1.7.3: Reagents for Flow Cytometry

Reagent	Supplier
Antibodies – see Table 2.1.7.7	BD Biosciences, Oxford, UK
CellTrace Violet cell proliferation kit	Life technologies, Paisley, UK
CellTrace Carboxyfluorescein diacetate succinimidyl (CFSE) cell proliferation kit	Life technologies, Paisley, UK
Ethanol 100% molecular grade	Sigma-Aldrich, Dorset, UK
FACS flow solution	BD Biosciences, Oxford, UK
FACS clean solution	BD Biosciences, Oxford, UK
Fix & Perm cell fixation and permeabilisation kit	Life technologies, Paisley, UK
Foetal bovine serum (FBS)	Life technologies, Paisley, UK
Formaldehyde solution 36.5%	Sigma-Aldrich, Dorset, UK
Hank's Balanced Salt Solution (HBSS)	Life technologies, Paisley, UK
1X PBS (w/o Ca^{2+} or Mg^{2+})	Life technologies, Paisley, UK
Propidium iodide (PI)	BD Biosciences, Oxford, UK
Sodium azide	Sigma-Aldrich, Dorset, UK

Table 2.1.7.4: 1X HBSS

Reagent	Volume
1X HBSS	5ml
Sodium azide	0.01% (w/v)
Sterile water	45ml

Table 2.1.7.5: FACS Buffer – FBS / 2% PBS

Reagent	Volume
1X PBS	48ml
FBS	2ml
Sodium azide	0.01% (w/v)

Table 2.1.7.6: Quenching solution for CFSE assay

Reagent	Volume
1X PBS	40ml
FBS	10ml
Sodium azide	0.01% (w/v)

Table 2.1.7.7: Antibodies for Flow Cytometry

Primary antibody	Fluorochrome	Catalogue reference BD Biosciences, Oxford, UK unless otherwise specified
7AAD	PerCP	BD 559776
Annexin V	FITC	BD 556419
CD3	PeCy5 FITC	BD 555341 BD 555332
CD4	PerCP-PeCy5	BD 560650
CD8	PeCy7	BD 557750
CD10	APC	BD 655404
CD11b	FITC	BD 562793
CD11c	FITC PE	BD 555392 Dako F0173
CD14	PE PeCy7	BD 555398 Miltenyi Biotech, Surrey, UK 130094364
CD15	FITC	BD 565236
CD16	APC	BD 561304

	FITC V500	BD 555406 BD 561394
CD20	APC BV421	BD 559776 BD 562873
CD33	PeCy7 PE PeCy5	BD 333952 BD 555450 BD 551377
CD34	PeCy5 APC PeCy7	BD 555823 BD 555824 BD 334881
CD45	APC-Cy7 PE V450	BD 557833 BD 555483 BD 560367
CD73	PE	BD 550257
CD90	PE PeCy7	BD 555596 BD 561558
CD105	PerCP-cy5.5	BD 560819
Lin-	FITC	BD 340546

2.1.8 Electron microscopy

Table 2.1.8.1: Equipment for Electron microscopy

Equipment	**Supplier**
DIATOME diamond knife 45˚	Diatome, Hatfield, PA, USA
Double sided conductive tape	Agar Scientific, Essex, UK
GATAN Micrograph Imaging software	**Gatan Inc.,** Pleasanton, CA, USA
GATAN Multiscan camera 794	**Gatan Inc.,** Pleasanton, CA, USA
FEI Tecnai T20 TEM	FEI, Oregon, USA
Flat bed moulds	Agar Scientific ltd, Essex, UK
100mesh formvar coated copper grids	Agar Scientific ltd, Essex, UK
JEOL6400 SEM	Jeol, Tokyo, Japan

LEICA Ultracut UCT	Leica Microsystems, Milton Keynes, UK
Olympus Scandium Universal SEM Imaging Platform	Olympus Soft Imaging Solutions, Münster, Germany
POLARON E3000 CPD	Quorum Technologies, East Sussex, UK
Quorum 150T High vacuum Sputter coating system	Quorum Technologies, East Sussex, UK
SEM support stubs	Agar Scientific ltd, Essex, UK

Table 2.1.8.2: Reagents for Electron microscopy

Reagent	**Supplier**
Araldite/epon 812 resin	TAAB Laboratories Equipment Ltd., Berkshire, UK
Distilled water	In house
Ethanol (30%, 50%, 70%, 90% and 100%)	VWR Chemicals, Leicestershire, UK
Glutaraldehyde (2.5%)	Sigma-Aldrich, Dorset, UK
Methanolic uranyl acetate (2%) - 2g Uranyl Acetate in 100ml Annalar Methanol	Fisher Scientific, Leicestershire, UK Prepared in house
Osmium Tetroxide (1%)	Oxkem, Oxfordshire, UK
Paraformaldehyde (2%)	Agar Scientific ltd, Essex, UK
Propylene oxide	VWR Chemicals, Leicestershire, UK
Reynolds lead citrate – Lead nitrate 1.33g, Sodium Citrate 1.76g, 30ml distilled water	Agar Scientific ltd, Essex, UK; Fisher Scientific, Leicestershire, UK Prepared in house
Sodium Cacodylate (0.1M)	Agar Scientific ltd, Essex, UK
Uranyl Acetate (0.5%)	Agar Scientific ltd, Essex, UK

2.2 Methods

2.2.1 Tissue culture

2.2.1.1 Drugs and reagents

Details of all drugs used are described in Materials Table 2.1.1.13. 10mM stock solutions were prepared in DMSO and stored at -20°C. As_2O_3 was dissolved in 1M NaOH to a concentration of 100mM. Dilutions of stock solutions were freshly prepared prior to each experiment in appropriate cell culture media. Growth factors were reconstituted according to manufacturer's instructions and stored in single use aliquots at -80°C.

2.2.1.2 Cell culture

All cell culture experiments were performed using sterile technique in a laminar airflow hood. All cells were cultured in their specific culture media at 37°C in a humidified atmosphere with 5% CO_2 (standard culture conditions).

2.2.1.2.1 AML cell lines

That AML is a heterogeneous, clonal disorder with a range of morphologic, immunophenotypic, cytogenetic, and molecular characteristics is reflected in the number of cell lines available; with over 50 available from one biological resource centre alone [561-564]. A comprehensive understanding of the cell line studied being paramount to interpreting and translating results.

Whilst the rationale for cell line choice will be discussed at the appropriate stage through this thesis; initially we sought to profile the Hh pathway and key downstream targets in a number of cell lines. These cell lines were chosen because they carry common mutations, represent a subtype for which there is a clinical need or which is easily definable, as our aim was for this work to carry from bench to bedside. In addition to clinical need, frequency and identifiability, publicly available datasets were mined to determine if any disease phenotypes had an association with deregulated Hh signalling or key downstream targets. The following publicly available datasets were analysed, Valk (GSE1159) [381], Mile (GSE13159) [565], and Stierwalt (GSE9476) [382].

The following cell lines have been studied through this thesis:

The OCI-AML3 cell line carries an NPM1 and DNMT3A R882C mutation, two of the more common mutations identified in AML. Further it belongs to the FAB M4 subgroup, myelomonocytic AML previously shown to respond to Hh inhibition and to potentially benefit from escalation of induction therapy [379,381].

The Kasumi-1 cell line is a CD34+ expressing AML previously shown to respond to Hh inhibition [377].

KG1a is a CD34-expressing selectively cultured variant of the KG1 cell line. KG1 was derived from a patient with erythroleukaemia in myeloblastic relapse. KG1a in contrast has lost the majority of its myeloid features, expressing only one myeloid antigen, instead expressing markers associated with T cells and T-ALL [548]. Additionally, a study has shown, through ICC, that the CD34-expressing cell lines KG1 and its subline KG1a, possess primary cilia and therefore the potential for canonical Hh signalling to be active within the cells [566].

Recent work has also shown the CD34+ cell lines, Kasumi-1 and KG1a, containing more CD34+ cells, to express higher levels of *GLI-1*. Further, inhibition of GLI-1 with GANT61 induced

apoptosis in the CD34+ KG1a and Kasumi-1 cell lines, whilst causing differentiation in the U937 and NB4 cell lines, with a relative absence of CD34+ cells. A positive correlation between CD34 and GLI-1 at a protein level was confirmed by immunohistochemistry (IHC) in primary AML MNCs, with GANT61 enhancing the cytotoxic effects of cytarabine in CD34+ primary AML cells [567].

The MV4-11 and MOLM-13 cell lines express *MLL* and *FLT3-ITD*. FLT3-ITD being linked to aberrant Hh signalling and a poor prognosis [381,382]. The MV4-11 cell line expresses the FLT3-ITD mutation at the gene and protein level whilst the MOLM-13 cell line carries the *FLT3-ITD* mutation but does not express the protein.

The HL60 cell line is a promyelocytic cell line. Interestingly inhibition of the pathway through SMO antagonism has been shown not only to induce apoptosis but also induce monocytic differentiation [568].

THP-1 is an acute monocytic cell line. Recent work has shown the clinical grade SMO inhibitors (vismodegib and sonidegib) to have moderate single agent activity on this cell line, and excitingly synergistic activity with a combination index (CI) value of 0.57 in combination with Azacitidine [413].

The disease phenotype of each cell line studied is further defined in Materials: Table 2.1.1.5.

For experiments, cells were seeded at $2x10^5$/ml and harvested at various time points for functional assays, gene and protein analysis, dependent on experimental design.

2.2.1.2.1.1 Cell line recovery post cryopreservation

Cell lines were removed from liquid nitrogen and immediately thawed at 37°C in a water bath. Cells were added to a sterile 15ml falcon tube with a Pasteur pipette and slowly recovered by adding specific culture media drop-wise over 15mins at room temperature (RT) with constant agitation. Cells were centrifuged at 400xg for 5mins, the supernatant poured off, and the pellets resuspended in specific culture media. Following recovery, cell number and viability were assessed by trypan blue dye exclusion. Cells were seeded in standard tissue culture flasks at the appropriate density.

2.2.1.2.1.2 Passaging AML cell lines

AML cell lines were passaged every 2 days, with fresh warmed media, to maintain a cell density of between $1x10^5$ – $1x10^6$/ml. This enabled maintenance at optimal concentration according to ATCC or DSMZ instructions.

Specific culture media is detailed in Materials: Table 2.1.1.7.

2.2.1.2.2 Stromal cell lines

The following stromal cell lines were used through this thesis – TM3 [557], M210-B4 [554], SL-SL [556] and HS-5 [553].

$TM3^{(GLI\text{-}Luc)}$ cells are murine Leydig tumour cells, stably transfected with a retroviral vector selectable by geneticin sensitivity, whereby luciferase expression is dependent on GLI activity.

The M210-B4 and SL-SL cell lines, both murine bone marrow-derived stromal cell lines, were chosen as these are frequently used in LTC-IC assays. M210-B4 has been genetically engineered

to produce human IL-3 and G-CSF [554,555]; SL/SL from the SL/SL mouse has been genetically engineered to produce human IL-3 and SCF [555,556].

HS-5 stromal cells are human-derived, allowing comparison between a human and murine stromal environment. Furthermore, through this PhD, we derived a protocol utilising HS-5 stromal cells and their conditioned media (CM) to support the recovery of primary AML cells on thawing.

2.2.1.2.2.1 Passaging stromal cell lines

Cells were cultured in 20ml specific culture media in a 75cm^3 flask in standard culture conditions. Cells were passaged when approximately 85-90% confluent. Media was removed and cells washed in 1x PBS twice then detached with 5ml Trypsin/EDTA buffer (warmed to 37^{o}C). Once detached, the reaction was neutralised with FBS. Cells were collected, centrifuged at 400xg for 5mins and the supernatant discarded or filtered, aliquoted and frozen for future use. The pellet was resuspended in 10ml culture media, counted and 0.75x10^6 transferred to a 75cm^3 flask.

200µl geneticin (1%) was added at each passage to the TM3 cells.

SL-SL and M210-B4 cells were treated with geneticin and hygromycin B every 14 days at a final concentration of 400mg/ml, 62.5mg/ml and 800mg/ml, 125mg/ml respectively.

Cell line characteristics are further defined in Materials: Table 2.1.1.5.

Media conditions are outlined in Materials: Table 2.1.1.10-12.

2.2.1.2.3 Cryopreservation of cell lines

Cells were resuspended at a concentration of 4-6x10^6/2ml in freezing solution (Materials: Table 2.1.1.13) and aliquoted into cryotubes. Cryotubes were placed in a 5100 Cryo -1^{o}C freezing container to provide controlled temperature reduction at -1^{o}C/min. Cells were stored at -80^{o}C for short term use, and transferred to liquid nitrogen for long term storage at -185^{o}C.

2.2.1.2.4 Isolation of mononuclear cells (MNCs)

All samples, PB and BM material, were obtained with informed consent, in accordance with the declaration of Helsinki, with Greater Glasgow and Clyde NHS Trust Ethics Committee approval from patients with newly diagnosed AML and normal healthy volunteers. See Appendix 1 for the biological characteristics of the patients from whom the samples were collected.

All samples were brought to RT before processing. PB was diluted in a 1:1 ratio with sterile 1X PBS. 15ml of the diluted PB was carefully layered onto 10ml of Histopaque-1077 per 50ml Falcon tube and centrifuged at 400xg for 30mins at RT. After centrifugation, the opaque interface (containing the MNCs) was carefully aspirated using a pastette and transferred into a clean 15ml Falcon tube and the volume made up to 12ml using sterile 1X PBS. Following centrifugation at 200xg for 10mins the supernatant was discarded. For the second and third washes the pellets were resuspended in 1X PBS to a total volume of 12ml, centrifuged at 400xg for 5mins and the supernatant discarded. Finally, the pellets were combined by resuspending in 10ml AML culture media (Materials: Table 2.1.1.14) and counted.

BM samples were first passed through a cell strainer to remove bone particles and then diluted in a 1:3 ratio with sterile 1X PBS. Processing was otherwise as described for PB.

Cells used for deoxyribonucleic acid (DNA), ribonucleic acid (RNA) and protein preparation were spun at 230xg for 5mins at RT, resuspended in 1ml 1X PBS containing diisopropyl fluorophosphates (DIFP) (1mM) and incubated on ice for 30mins.

2.2.1.2.5 Primary cell recovery post cryopreservation

50ml aliquots of thawing media (Materials: Table 2.1.1.16) were pre-warmed at 37°C prior to adding 1ml DNAse and filter sterilising (0.2µm single use filter unit). Primary AML cells were removed from liquid nitrogen and immediately thawed at 37°C and gently transferred to the bottom of a 50ml Falcon tube using a 3ml Pasteur pipette. 15mls of thawing media was added drop wise to the cells over a 20min period at RT to enhance the DNAse activity with constant, gentle agitation to prevent clumping. The cells were then passed through a 100µm sterile cell strainer, centrifuged at 200xg for 5mins and the media carefully poured off. The cells were gently resuspended and the remaining 35ml of thawing media added. Following 3hrs at RT, the cells were pelleted at 220xg for 15mins, and resuspended in primary AML culture media supplemented with 10% HS-5 CM at a concentration not greater than $1x10^6$/ml. The cells were then co-cultured on HS-5 cells (at approximately 80% confluence) overnight at 37°C. The flask was gently rocked to release AML cells from the stromal layer and the media containing the cells transferred into a 50ml Falcon tube. The flask was washed x3 using sterile 1X PBS to harvest the remaining AML cells. Cells were centrifuged at 200xg for 5mins, and pellets resuspended in AML culture media; cell number and viability was assessed by trypan blue dye exclusion. A recovery of 25-70% of the cryopreserved cell number was expected.

2.2.1.2.6 Primary AML cell culture

Cells were plated at $1\text{-}2x10^5$/ml on a 24 well collagen coated plate pre-treated with 200µl fibronectin (15µl/ml/5µg/cm^2). Cells were cultured in primary AML culture media (Materials Table 2.1.1.14) for various time periods, with and without defined drug treatments before being harvested for functional assays and gene and protein analysis, dependent on experimental design.

2.2.1.2.7 MSCs derived from human BM samples

MSCs can be isolated from various tissues including adipose, BM, umbilical cord and muscle, expanded i*n vitro* and, due to their self-renewal potential passaged many times without significant alteration of their major properties.

Cultured MSCs are defined by several characteristics. Morphologically they are fibroblast-like, they express a panel of markers: positive for Sca-1, CD105, CD90, CD73 and CD29, and negative for CD11b, CD31, CD34 and CD45 and they have the potential to differentiate into adipocytes, chondrocytes and osteoblasts [37].

MSCs secrete molecules and extracellular vesicles with both local and distant effects. It is these secretions that are believed to be responsible for their anti-inflammatory, immune modulating, anti-tumour and regenerative properties [569-571]. Both supernatant harvested from cultured MSCs and the MSCs themselves were therefore studied in a bid to determine whether there is a role for paracrine Hh signalling in both normal and malignant haematopoiesis.

2.2.1.2.7.1 Isolation of MSCs from human BM samples

The plastic adherence method was used. Briefly, MSCs were derived from BM samples (BM was processed as per Methods; Table 2.2.1.4). $20x10^6$ cells were resuspended in 8ml MSC culture media (Materials: Table 2.1.1.9). Suspended cells were transferred to a $25cm^3$ NUNC flask and cultured in standard culture conditions. Non-adherent cells were removed and media replaced after 72hrs. Fresh media was added every 3-4 days until cells reached approximately 80-90% confluency when they were passaged.

2.2.1.2.7.2 Passage of MSCs

Cells were passaged when approximately 80-90% confluent. Media was removed and cells washed in 1X PBS twice then detached with 5ml Trypsin/EDTA buffer (warmed to 37°C). Once detached, the reaction was neutralised with FBS. Cells were collected, centrifuged at 400xg for 5mins and the supernatant discarded or filtered, aliquoted and frozen for future use. The pellet was resuspended in 10ml culture media, counted and reseeded at a density of $1\text{-}2x10^3$ cells/cm^2. Fresh media was added every 3-4 days until further passage was required. Cells at passage 3 to 6 were used for experiments.

2.2.1.2.8 Cryopreservation of primary AML and MSCs

Cells were resuspended at a concentration of $20x10^6$/ml to $100x10^6$/ml in freezing solution (Materials: Table 2.1.1.17) and aliquoted into cryotubes. Cryotubes were placed in a 5100 Cryo - 1°C freezing container at -80°C to provide controlled temperature reduction at -1°C/min and consequently better cell viability. Cells were cryopreserved in liquid nitrogen at -185°C until use.

2.2.1.2.9 Processing of patient plasma

Plasma was collected prior to processing samples for MNC isolation. All samples were collected in Ethylenediaminetetraacetic acid (EDTA) collector tubes. Samples were centrifuged at 400xg to preserve cell integrity whilst allowing collection of patient plasma. Plasma was snap frozen in liquid nitrogen before storing at -80˚C until use. Plasma samples were used to quantitatively measure human SHH in normal and AML patients.

2.2.1.3 Resazurin reduction assay

The resazurin (7-Hydroxy-3H-phenoxazin-3-one-10-oxide sodium salt) reduction assay is a method of measuring cell viability. It employs bio-reduction of the dye by metabolising cells to reduce the amount of the oxidized form, concomitantly increasing the fluorescent intermediate; fluorescence being proportional to the number of viable cells. The assay therefore allows the rapid assessment of cell viability to a wide range of drug concentrations.

Briefly, cells (at a concentration of $1x10^4$ cells per well) were cultured for 72hrs in 96 well plates in the presence of serially diluted concentration of each drug, allowing for 12 different concentrations of each drug. Following culture, 50μM resazurin was added to each well and incubated at 37°C for 4-6hrs. Plates were read at 535_{ex} and 590_{em} on a Spectramax M5 plate reader and analysed using SoftMax Pro software.

2.2.1.4 Luciferase assay

The aim of this assay was to determine the degree of SMO inhibition by the test drug.

TM3$^{(GLI\text{-}Luc)}$ cells were collected as described in Methods Table 2.1.1.12. Cells were then seeded at a concentration of 2x10^5/ml in the required number of wells of an opaque, white 96 well culture plate. Cells were left for 6hrs in standard culture conditions to allow adherence then incremental concentrations of the test drug resuspended in 5µl culture media added to make a final volume in each well of 100µl. Purmorphamine, a Smo agonist served as the positive control at a concentration of 5nM (previously determined optimal concentration by Dr D Irvine within the Copland laboratory as past of his thesis [572]). Following 48hrs culture, 100µl luciferase was added per well and the degree of luminescence measured at 1500nm on a Spectramax M5 plate reader and analysed using SoftMax Pro software.

Whilst it was quickly established that the IC50 of AML cells to Smo inhibitors was considerably higher than that of TM3$^{(GLI\text{-}Luc)}$ cells, this assay was utilised to ensure each new stock of the Smo inhibitors, cyclopamine, LDE225 and glasdegib, were comparable in efficacy, Figure 2.1.

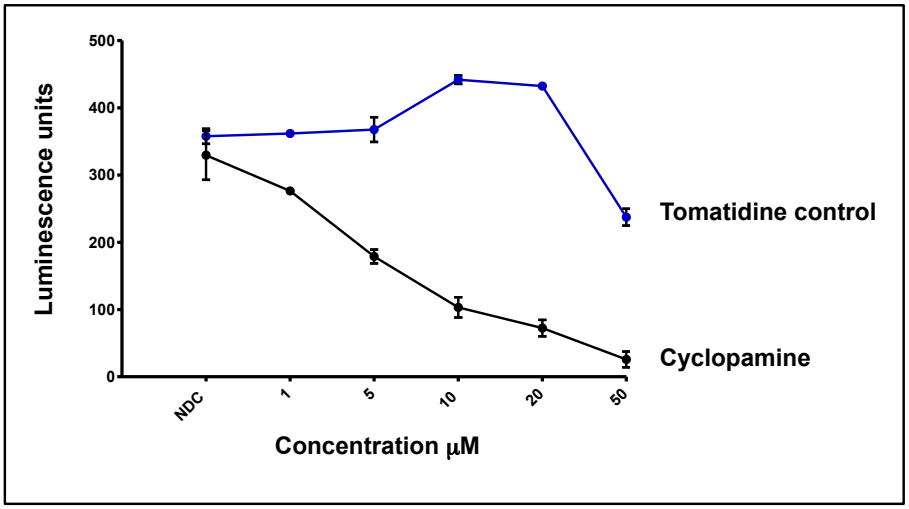

Figure 2.1: Luciferase activity of the Gli-luciferase reporting TM3$^{(GLI\text{-}Luc)}$ cell line following culture with cyclopamine for 72hrs.
Graph showing luciferase activity, as determined by luminescence, of the Gli-luciferase reporting TM3$^{(GLI\text{-}Luc)}$ cell line following culture with incremental concentrations of cyclopamine for 72hrs. Each point represents the mean of four independent experiment with the error bars indicating the standard deviation (SD).

2.2.1.5 Cell counting and viability assessment

Cell counts were performed using a haemocytometer; cell viability assessed by trypan blue exclusion. 10µl of trypan blue solution was added to 10µl of cells to give a 1:2 dilution from which 10µl was transferred to the haemocytometer. Cells were visualised with an inverted microscope using the x10 objective. Live and dead (blue) cells were counted allowing the absolute number of alive and dead cells per ml to be calculated. A minimum of 100 cells were counted per condition.

Within the haemocytometer each 1mm^2 square equates to a volume of 0.1µl. The absolute cell count per ml was therefore calculated by counting the number of live cells per mm^2, dividing by the number of squares counted, multiplying by the trypan blue dilution factor (standardly 2) and then 10^4.

2.2.1.7 Synergy studies

Synergism is the process by which two or more drugs are used in combination to achieve an additional end effect, for example greater cell death. The drugs may target the same molecule or pathway through different mechanisms, or independent molecules or pathways. The end result, irrespective of drug mechanism of action, is greater efficacy. Further, drug synergism may allow for the use of lower doses of each drug within the combination, potentially reducing adverse reactions within the clinical setting.

In order to determine synergism, the combination effect must be greater than that which is expected from the individual drug's potencies. We used the Chou-Talalay method for drug combination, utilising computer software to analyse dose-effect. The formula is based on the median-effect equation, encompassing the Michaelis-Menten Hill, Henderson-Hasselbalch and Scatchard equations. The resulting combination index (CI) provides a quantitative definition for additive effect (CI = 1), synergism (CI < 1), and antagonism (CI > 1) in drug combinations [573].

Cells were seeded in 96 well plates at $0.2x10^5$/ml in media containing the test drug at varying concentrations. Two-fold serial dilutions were made with two concentration points above and below the IC_{50} value; a constant ratio was therefore maintained. Cells were cultured for varying times (24, 48 and 72hrs) then counted using a haemocytometer after being mixed in a 1:2 ratio with trypan blue solution. Biological duplicates were performed. Data analysis was performed with Compusyn software using the Chou-Talalay CI method [573].

2.2.1.8 β-Galactosidase Cell staining

The principle of this experiment was to determine cell senescence; senescent cells express increased levels of lysosomal ß-galactosidase termed senescence-associated ß-galactosidase.

Cells were treated within the experimental arms then fixed and stained overnight according to manufacturer's protocol. Briefly, cells (at a concentration of $1x10^4$ cells per well) were cultured for 72hrs in 6 well plates in the presence or absence of the test drug. Following culture, cells were washed in 1X PBS before 1X fixative solution was added and the cells left for 15mins at RT. Cells were then washed twice with 1X PBS before adding ß-galactosidase staining solution and incubating overnight at 37°C in a dry incubator (without CO_2). This is a simple colorimetric assay, in the presence of increased levels of ß-galactosidase, cells stain blue-green. Cells were scored under bright light microscopy. Alkali conditions (pH10) were used as a positive control.

2.2.1.9 CFC assay

The CFC assay is an *in vitro* assay designed to quantify haematopoietic progenitor cells. The assay is based on the ability of haematopoietic progenitor cells to proliferate and differentiate into colonies in semisolid media with adequate cytokine support. These colonies can be enumerated and characterised according to their unique morphology [574].

Methylcellulose was thawed at 4°C overnight. For each experimental arm, a 3ml aliquot was placed into a sterile plastic vial using a 20ml syringe and brought to RT prior to use. Cell counts were performed to allow calculation of the volume of cell suspension required for $4x10^3$ cells (primary samples) and $2x10^3$ (cell lines) within each experimental arm. Cells were washed and resuspended in 200μl serum free media then pipetted onto the 3ml methylcellulose aliquot and thoroughly mixed. Due to the viscosity of the methylcellulose, to ensure equal division, 1.3ml was added to a 35mm tissue culture dish in duplicate. An additional 35mm culture dish containing sterile water was added to prevent culture plates from drying out. Samples were incubated for 10–14 days prior to characterising and counting the number of viable colonies.

The capacity of an individual colony to re-plate is used experimentally as a measure of the self-renewal potential of the parent haematopoietic progenitor cell [575]. Re-plating assays are therefore used to assess drug treatment effects specifically on self-renewal capacity of haematopoietic progenitors.

For re-plates, 100μl of Methocult was added to each well of a 96-well plate, with the exception of the peripheral wells, which were filled with sterile water to prevent culture drying. 50 colonies were then harvested from each experimental arm and resuspended in 10μl serum free media prior to being added to the Methocult and thoroughly mixed. Plates were cultured for a further 10-14 days prior to the number of viable colonies being counted.

2.2.1.10 Cellular transfection

A hairpin against human *SMO* in a PLKO.1 plasmid (Open Biosystems; TRCN0000014367:CGGCCTGACTGTGAGATCAAGAATCTCGAGATTCTTGATCTCACAGTCAGGTTTT) was previously validated within the Copland laboratory. The short hairpin RNA (shRNA) was cut using NdeI and SpeI restriction enzyme digestion and ligated into PLKO.1 with a green fluorescent protein (GFP) tag. PLKO.1 with a non-targeting hairpin sequence was used as a control. HEK293 cells were transfected overnight at 37°C in T75cm^3 flasks when approximately 75% confluent, using calcium chloride with HIV-1 and VSV-g as accessory plasmids. Virus was collected in DMEM supplemented with 20% FBS and the Kasumi-1 cell line was cultured in viral medium supplemented with 4mg/ml Polybrene. This was repeated every 3-4hrs. Following 48hrs of viral transduction the Kasumi-1 cells were washed and resuspended in normal media. After overnight culture, the GFP positive cells were sorted using the BD FacsAria for RNA and protein studies, and resuspended in fresh media allowing recovery for 24hrs before further experiments were undertaken.

2.2.2 Molecular studies

2.2.2.1 RNA extraction and quantification

Cells were harvested, lysed and RNA extracted using the RNeasy RNA Plus Mini and Micro Kits as per manufacturer's instructions.

Briefly, cells were suspended in the recommended volume for cell number of guanidine-thiocyanate-containing lysis buffer and homogenised using a 26G needle. The homogenised lysate was passed through a genomic DNA removal column to remove DNA contamination. Following ethanol precipitation, the sample was added to a silica spin column that selectively binds RNA prior to washing, with provided buffers to remove impurities. The column was then dried by centrifugation to remove ethanol and allow for a clean elute. RNAse-free water was used to elute the RNA.

RNA concentration and quality were determined using a Nanodrop Spectrophotometer, using 2μl of the sample. 260nm quantifies nucleic acids. Absorbance was also recorded at 230nm and 280nm to determine purity (as a ratio to 260nm). Contamination was primarily due to protein, phenol or carbohydrate contamination. Concentration was automatically calculated; pure RNA has an expected ratio of 2. RNA was stored at -80°C until required.

2.2.2.2 cDNA synthesis

500ng of RNA was reverse transcribed to complementary DNA (cDNA) using the high fidelity reverse transcriptase Superscript III according to protocol as per manufacturer's instructions.

Briefly, this is a two-step reaction, as reverse transcriptase cannot initiate synthesis *de novo*. The first step enables oligo(dTs) to bind to the mRNA through the poly-A tail thus priming the DNA (Materials Table 2.1.2.4.1 Reverse transcription Mastermix Step 1; Materials Table 2.1.2.4.3 Reverse transcription cycling conditions Step1). The second step involves second strand DNA synthesis. 7µl of reverse transcription mix 2 (Materials Table 2.1.2.4.2 Reverse transcription Mastermix Step 2) is added to each sample giving a total volume of 20µl and cycled as outlined in Materials Table 2.1.2.4.3 Reverse transcription cycling conditions Step 2.

Oligo(dT) primers were used due to their specificity for mRNA and non-specific nature enabling different targets to be studied. The cDNA produced for each gene is therefore proportional to the mRNA from which it was produced.

The integrity of cDNA was assessed by performing RT-PCR for *GN2BL* as a housekeeping gene using Promega GoTaq® DNA polymerase.

2.2.2.3 Polymerase chain reaction (PCR)

RT-PCR and qRT-PCR are methods to detect mRNA expression, with qRT-PCR able to quantify mRNA expression. The reactions can be performed using Taqman® probes or primers.

Primers were designed in-house using National Center for Biotechnology Information (NCBI)/ Primer-Blast. Briefly, the cDNA sequences of each gene of interest were identified through a Pubmed search and used to design primers. We aimed to design primers of approximately 20 base pairs with the forward and reverse primers having similar melting temperatures, ideally 60^{o}C.

2.2.2.3.1 RT-PCR

RT-PCR is a method to detect mRNA expression in a sample following its reverse transcription into cDNA. This is a qualitative analysis of expression. The method cannot quantify expression for a number of reasons: PCR products do not accurately reflect input cDNA since they are analysed following the exponential stage of amplification having reached a plateau, and ethidium bromide is a relatively insensitive stain. Gel electrophoresis separates products according to size.

Briefly, the reaction involved mixing 2µl of the transcribed cDNA with the GoTaq® RT-PCR master mix (Materials Table 2.1.2.5.1). Cycling details are outlined in Table 2.1.2.5.2.

PCRs were then run by gel electrophoresis using a 1.5% agarose gel. The gel was prepared with 1.5g agarose powder in 100ml of 1X TBE buffer with ethidium bromide (10mg/ml). This was heated in a microwave until the agarose powder was fully dissolved, then poured into a casting tray with a comb to create the wells. The gel was left for approximately 30mins until fully set. 12µl of PCR product was added to each well. 6µl of a 100bp DNA ladder was loaded into one lane of each gel for reference. PCR products were visualised due to the presence of ethidium bromide using the ChemiDoc MP System and analysed using the Quantity One 1-D Analysis Software.

2.2.2.3.2 Quantitative Real-Time PCR (qRT-PCR) by Fluidigm®

Real-time quantitative PCR (qRT-PCR) enables relative and absolute quantitation of gene expression.

Briefly the Taqman® assay uses oligonucleotide probes that are fluorescently labelled at their 5' end, with a non-extendable 3' end containing a quencher dye. In the absence of the target sequence, the quencher dye neutralises the fluorescence emitted by the reporter dye. In the presence of the target sequence, the annealed probe is cleaved by Taq® DNA polymerase, separating the reporter dye from the quencher dye. With each cycle, additional reporter dye molecules are cleaved from their respective probes, resulting in an increase in fluorescence intensity proportional to the amount of amplicon produced. The same principle applied when primers were used, although in this instance Bio-Rad Ssofast Evagreen Supermix served as the fluorescent label.

The abundance or frequency of a gene of interest is measured by setting a threshold level of fluorescence. When the signal emitted by the reporter dye molecules for each gene of interest cross this point a positive, or real, signal is recorded. This is termed the cycle threshold (CT). The CT therefore represents the stage within the PCR reaction when real signal is detected over a background level. High frequency genes which cross the threshold early (after a low number of PCR cycles) will have a low CT value, with the reverse being true for low copy number genes that therefore have a high CT value.

Comparison between gene expression can be made, and statistical analysis performed, once variation in input cDNA is taken into account. Briefly, for each gene of interest, the DeltaCT (ΔCT) is calculated by subtracting the CT value of between 3 and 6 housekeeping (control) genes from the CT recorded the gene of interest. The $2^{-\Delta\Delta CT}$ method can then be used to show the relative expression of the gene of interest relative to control, where normal is expressed as 1 [576].

2.2.2.3.2.1 Pre-amplification

Due to the low level expression of some target genes of interest, a pre-amplification step was carried out to increase the quantity of cDNA targets prior to gene expression analysis.

Briefly cDNA was incubated with a pre-amplification mastermix, containing a pool of primers or probes specific to the cDNA of interest (Table 2.1.2.8.1 Primer Pre-amplification Mastermix; Table 2.1.2.8.2 Probe Pre-amplification Mastermix). Pre-amplification was performed for target and reference genes as per manufacturer's instructions. Cycling conditions are detailed in Table 2.1.2.8.3 The pre-amplified cDNA was then diluted 1:5 in Tris-EDTA (TE) buffer and stored at -20°C until required.

When primers were used, residual unused primers were removed using an exonuclease (Table 2.1.2.8.4). Cycling conditions are detailed in Table 2.1.2.8.4.1. Exonuclease is used as it specifically digests single stranded DNA.

2.2.2.3.2.2 qRT-PCR

qRT-PCR was performed using Fluidigm® Biomark technology and data collected as per manufacturer's instructions. The chip design was chosen dependent upon experiment design – those used were 48:48, 96:96 and FLEXsix Dynamic Array chips.

Briefly, each sample was run in technical triplicate, and a no template control included with each chip. The chip was first primed with line control fluid before the assays (Tables 2.1.2.8.5

Primer & 2.1.2.8.6 Probe) and samples (Tables 2.1.2.8.5.1 Primer & 2.1.2.8.6.1 Probe) were loaded within 60mins. The FLEXsix has 6 12x12 partitions that can be run independently or simultaneously; this chip is only primed once, prior to the first run. Separate partitions can be used for up to 3 months following first use.

Each chip is designed such that each sample is cycled with each probe/primer from loading into a single well. The FLEXsix generates 144 x 6 data points, the 48:48 chip 2304 data points and the 96:96 chip 9216 data points. Internal sample control was ensured subtracting the average of selected housekeeping genes (ATP5S, *B2M, ENOX2, GAPDH, GUSB, TYW1 and UBE2D2*) from each gene of interests CT value.

2.2.2.4 Gene expression array

The purpose of this array was to evaluate changes within a large number of genes between the most primitive HSC compartment, and the early progenitor populations, MPP, CMP, GMP and MEP. The gene expression microarray (GSE 47927) was performed and analysed by the Copland laboratory prior to this study's initiation [577].

Briefly, patient samples were sorted using multi-parameter fluorescence-activated cell sorting (FACS). Samples were run on the Affymetrix GeneChip Human Gene 1.0ST array system, enabling 28,869 transcript targets to be detected. The annotated raw fluorescence intensity (.CEL) files were analysed using Partek Genomics Suite. Following log transformation, a one-way ANOVA was performed [578].

2.2.2.5 DNA extraction and quantification

Cells were harvested, lysed and DNA extracted using the DNAeasy Blood and Tissue Kit as per manufacturer's instructions.

Briefly, cells were directly lysed using Proteinase K before being passed through a silica spin column that selectively binds DNA, prior to washing with provided buffers to remove impurities. Buffer AE (a Tris-CL, EDTA, pH 9 buffer) was used to elute the RNA.

DNA concentration was determined on a Nanodrop Spectrophotometer using 2µl of the sample, at 280nm. Absorbance was also recorded at 230nm and 260nm to determine purity (as a ratio to 280nm). Impurities were primarily due to protein, phenol or carbohydrate contamination. Concentration was automatically calculated using a correction factor for differing base composition; pure DNA has an expected ratio of >1.8. DNA was stored at -80^{o}C until required.

2.2.2.6 Sequencing

2.2.2.6.1 Sanger sequencing

DNA polymerases synthesise DNA from deoxyribonucleotides. They can also incorporate analogues of nucleotide bases: dideoxyribonucleotides (ddNTPs). ddNTPs are perfectly functioning dNTPs, however once they are incorporated the DNA polymerase cannot progress any further since they lack the 3'-hydroxyl group. This is the basis of the Sanger sequencing method developed in 1977: the ddNTPs serving as specific chain-terminating inhibitors of DNA polymerase enabling the DNA sequence to be determined by reading the end ddNTP from each fragment generated by the sequencing cycle [579].

This process was further developed in the 1990s. Fluorescently based cycle sequencing labels each of the four ddNTPs with a different colour dye and the fragments are separated by capillary electrophoresis to determine the DNA sequence.

Sanger sequencing was performed to determine the mutational status of *SMO* in an unselected primary patient cohort, *SMO* mutations being found in a number of solid malignancies [367,580–582].

2.2.2.6.1.1 DNA template amplification and purification by PCR

SMO PCR primers, detailed in Table 2.1.2.9.1, were diluted to 5μM (5pmol/μl) from 100μM stock with RNAse-free water before use. All *SMO* PCR primers where universally tailed.

The *SMO* RT-PCR reaction was run using a mastermix as documented in Table 2.1.2.9.2, with a different reaction tube for each primer. 1μl DMSO was added to exon 1_1, 1_2 and 1_3 reactions as these regions are GC rich and therefore difficult to amplify. Cycling details are outlined in Table 2.1.2.9.3. To ensure clean sequencing 5μl of the sequencing PCR reaction was transferred to fresh tubes with 2μl of EXO-Star. Cycling details outlined in Table 2.1.2.9.4.

2.2.2.6.1.2 Cycle sequencing

A Big Dye® mastermix was prepared as documented in Table 2.1.2.9.5. 10μl was dispensed into each well then approximately 0.2μl of PCR product added. Sequencing primers were diluted to 3.3μM (3.3pmol/μl) from 100μM stock. Cycling conditions are outlined in Table 2.1.2.9.6.

2.2.2.6.1.3 Sequencing reaction purification by ethanol precipitation

Following this, 2μl 3M sodium acetate and 28μl 100% ethanol was added to each well, the plate vortexed, mixed by inversion and spun at 3000xg for 30mins. The solution was then discarded. Complete removal of solution at each step was essential for good performance, so the plate was inverted and spun at 3000xg for 20secs. Then, 75μl of 70% ethanol was added to each well, the plate vortexed, mixed by inversion and spun at 3000xg for 10mins. At this stage, the plate was stored at -20 ^{o}C.

2.2.2.6.1.4 Capillary electrophoresis

Sequencing was performed on a Tetrad 3130/3130xl Genetic Analyser within NHS Lothian, 15μl of Hi-Di Formamide was added immediately before the plate was run. Analysis was performed using Alamut mutational surveyor.

This work was accomplished in collaboration with NHS Lothian, in particular Dr Edwina Dobbin. I am indebted to her for her time, help and expertise.

2.2.2.7.2 Next-generation Sequencing

Non-random, clonal chromosome aberrations are detectable in approximately 55% of AML cases, and are important when considering disease classification and treatment algorithms; 45% of cases however remain unclassified, leading to difficulties in risk stratification and treatment decisions [156,165].

In 2013, the Cancer Genome Atlas Research Network listed 23 significantly mutated genes in AML [583]. Following this, several AML research gene panels have been commercially developed, two have been used in this PhD.

2.2.2.7.2.1 Ion AmpliSeq PGM™

The Ion AmpliSeq™ covers 19 genes, 14 described by the Cancer Genome Atlas Research Network [583], Table 2.1.2.10.1.

Ion semiconductor sequencing is a method of DNA sequencing based on the detection of hydrogen ions released during the polymerization of DNA. This is a method of sequencing by synthesis, a complementary strand being built on the sequence of a template strand. If the introduced dNTP is complementary to the leading template nucleotide, it is incorporated into the growing complementary strand. This causes the release of a hydrogen ion that triggers an ion-sensitive field-effect transistor ion sensor, in which the reaction is measured.

The assay was performed as per manufacturer's instructions, Table 2.1.2.10.1: Ion AmpliSeq™ Sequencing Conditions.

This work was accomplished in collaboration with NHS Lothian, in particular Dr Edwina Dobbin and Dr Nicola Carroll. I am indebted for their time, help and expertise.

2.2.2.7.2.2 Illumina TruSight®

The Illumina TruSight® Myeloid panel covers 54 genes, 15 in their entirety and an additional 39 targeted to cover oncogenic hotspots, Materials 2.1.2.10.2.

Illumina dye sequencing also uses a sequence by synthesis approach.

Briefly, purified dsDNA is cleaved by transposons generating random lengths of DNA. The cut ends are repaired and adapters, (indices which enable up to 96 samples to be run simultaneously), primer binding sites, and terminal sites (necessary for the DNA strand to attach to the flow cell) are added to each strand of DNA. The modified DNA is loaded onto a specialised chip, termed a flow cell, for amplification and sequencing. Hundreds of thousands of oligonucleotides are anchored to the bottom of the flow cell. These serve to bind DNA strands with complementary sequences.

Once the fragments have attached, cluster generation begins through bridge amplification. This step makes approximately one thousand identical copies of each single template molecule in very close proximity, termed a cluster. Sequencing by synthesis is initiated using a sequencing primer; a single fluorescently tagged modified dNTP being added to the chain with each sequencing cycle. Each of these nucleotides has a reversible 3' terminator that acts as a terminator for polymerisation; ensuring only one nucleotide is added per cycle. After each round of synthesis, the base is determined by the wavelength of the fluorescent tag. Each of the four bases has a unique emission. This cycle is repeated 150 times until the full DNA molecule is sequenced. The purpose of the cluster is to ensure a strong fluorescence signal. The sequence data is analysed using the MiSeq reporter [584].

The assay was performed as per manufacturer's instructions, Materials 2.1.2.10.2.1: Illumina TruSight® Sequencing Conditions.

This work was accomplished in collaboration with NHS Greater Glasgow and Clyde, in particular Dr Rachel Dakin. I am indebted for her time, help and expertise.

2.2.3 Protein studies

2.2.3.1 Protein extraction and quantification

1-5x10^6 cells were harvested and washed x3 in ice-cold 1X PBS without Ca^{2+} or Mg^{2+} and pelleted at 220xg. After the third wash, pellets were lysed in ice-cold solubilisation buffer containing phosphatase and protease inhibitors at a concentration of 2x10^6/10µl solubilisation buffer, Table 2.1.3.2. This suspension was left on ice for 30mins then centrifuged at 20000xg for 10mins to pellet all cell debris. The supernatant was transferred to a fresh eppendorf and stored at -80°C.

Protein concentration was quantified using the 1x Quick Start™ Bradford Dye Reagent and compared to a standard curve prepared using Quick Start™ Bovine Serum Albumin (BSA) protein. This is a colorimetric protein assay based on the binding of Coomassie Brilliant Blue G-250 dye to protein, and the associated colour change from brown to blue this causes. This can be measured by visual absorbance on the Spectramax M5 plate reader at 595nm using SoftMax Pro software.

2.2.3.2 Sodium dodecyl sulfate polyacrylamide gel electrophoresis Western blotting

Gel solutions were prepared as per Tables 2.1.4.7 & 2.1.4.8. 10% gels were used to separate proteins smaller than 50kDa; 7.5% gels to separate those larger than 50kDa. All stacking gels were 5%.

10-20µg of cell lysates were denatured at 100°C with Sodium dodecyl sulfate (SDS) and ß-mercaptoethanol for 5mins. Samples were run in 1x Running Buffer at 80Volts (V) for 15mins then 180V for 45mins. The semi-dry transfer method was used to transfer separated proteins to nitrocellulose membranes. Briefly, membranes and nitrocellulose were saturated in 1X semi-dry transfer buffer, the gel placed on top of the membrane and sandwiched between eight 9cm x 6cm Whatman paper strips. Transfer was performed at 40mA/gel for 60mins and confirmed using Ponceau S Solution staining. Membranes were washed in 1X TBS to remove Ponceau S prior to blocking with 5% BSA for 1hr to prevent non-specific binding. Following blocking, the membrane was incubated in primary antibody and resuspended in 1X blocking solution overnight with gentle agitation on a rocker. Unbound antibody was washed with 1X TBS-N, pH 7.5, 4 times for 10mins per wash. Secondary antibodies, conjugated to horseradish peroxidise (HRP), were used at a dilution of 1:10,000 and incubated for 1hr. Secondary antibody was washed with 1X TBS-N followed by three 1X TBS washes, 10mins for each. Protein was visualised by placing membranes in 2ml chemiluminescent HRP substrate for 3mins, then placed in a cassette before being exposed to X-ray for varying time periods. X-ray film was developed using a Konica Minolta SRX-101A developer in a dark room.

2.2.3.3 Immunocytochemistry on cultured cells

Immunocytochemistry (ICC) was performed on multispot polytetrafluoroethylene (PTFE) coated glass microscope slides if cells were non-adherent, and within 8-well Lab-Tek II chamber slides if adherent, allowing cellular morphology to be maintained. To ensure optimal fixing, the PTFE microscope slides were pre-coated with 5µg/ml Poly-L-Lysine in borate buffer. Cells were at a density of 6x10^4cells/well if non-adherent, and maintained at approximately 80% confluency if adherent. If non-adherent, cells were harvested at 3rd or 4th passage in optimal growing conditions (resuspended in fresh media 24hrs before harvesting at a density of 2-3x10^5/ml). Cells were washed once in 1X PBS, fixed for 10mins (non-adherent) or 30mins (adherent) with 4% paraformaldehyde, washed a further three times with 1X PBS then permeabilised over 15mins with 0.5% Triton-X100. Adherent cells were blocked in 5% normal goat serum (NGS) or 5% normal

rabbit serum (NRS) depending on which species the staining antibodies were raised in. Non-adherent cells were blocked in 5% BSA/1% Ovalbumin in 1X PBS with 0.2% Triton-X100. Cells were blocked for a minimum of 30mins before the primary antibody was added and incubated overnight at 4^{o}C; Table 2.1.4.10 shows primary antibody concentrations. 1:200 dilutions of appropriate secondary antibody (Alexa Fluor 488 or 594; mouse, goat or rabbit) were added after washing slides x3 in 1X PBS, and then incubated for 1hr at RT. Antibody master mixes were prepared for each experiment. 4',6-diamidino-2-phenylindole (DAPI) mounting solution was used to fix and seal the slides with cover slips. Negative (no primary antibody, NPA) controls were included with each experiment. For each antibody, microscope settings were kept constant between cell lines and samples. The slides were visualised on a Zeiss TS 100 inverted microscope and pictures taken using Axio-vision software.

2.2.3.4 Immunocytochemistry on fresh frozen, paraffin-embedded, EDTA-decalcified bone marrow trephines

Whilst the protocol for identifying primary cilia in cultured cells is well recognised, there are no reports in the literature using fresh frozen, paraffin-embedded (FFPE) tissue.

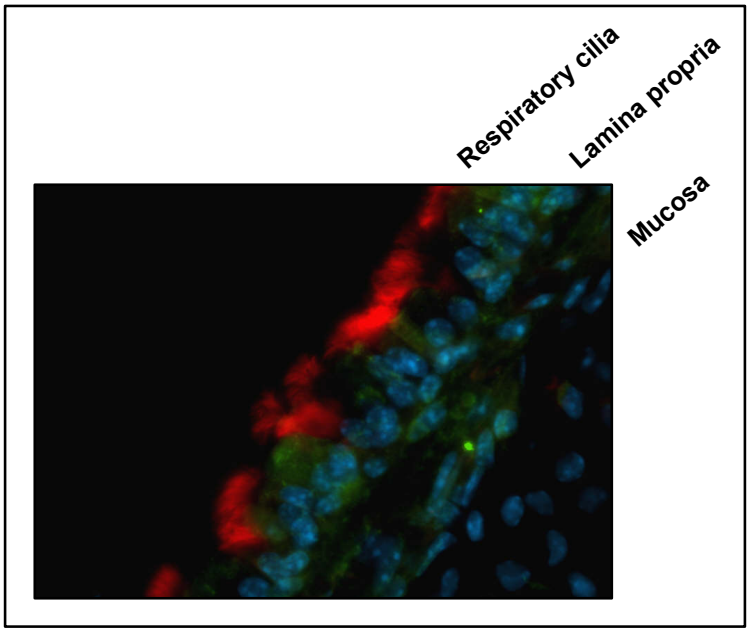

Figure 2.2: Representative ICC cross sectional image, x40 magnification, depicting cilia on the mucosal surface of the trachea from a mouse.
Tracheas were dissected, cut and mounted from sacrificed mice by Karen Dunn. Antibodies were added serially, at a range of concentrations. Images were visualised with a Zeiss TS100 inverted microscope. Respiratory cilia, composed of α-tubulin are stained with α-tubulin (red); γ-tubulin, composing cell cytoskeleton is shown in green. Cell nuclei are stained with DAPI (blue).

There are a number of well-recognised technical issues when performing ICC on FFPE, in particular auto fluorescence. The technique was therefore optimised on FFPE human BCC sections. These were chosen as BCC cells have been reported to have primary cilia [447], aberrant Hh pathway activity and, from a practical perspective, the tissue was easily accessible. The specificity of the antibodies was confirmed on mouse trachea sections, motile cilia being found on the surface of the trachea in large numbers, with both motile and primary cilia being composed of a microtubule-based cytoskeleton, Figure 2.2.

BM trephine (BMT) sections were cut at 3-4μM, from embedded blocks, floated onto a warm (42°C) water bath then picked up onto Superfrost plus slides (performed by John O'Connor, NHS Lothian). To preserve antigenicity, sections were stored at 4°C. Prior to staining, sections were placed in a 60°C oven for 1hr, followed by 5mins in xylene to remove the paraffin. Sections were rehydrated with 2x 1min wash in 100% ethanol followed by a single 1min wash in 70% ethanol and finally 5mins in deionised water. Antigen retrieval was performed on the Thermo Scientific™ PT Module with pH6 sodium citrate retrieval buffer solution at 98°C for 25mins. Sections were subsequently washed in PBS/Tween (1:2000) twice (4mins each) before serially adding antibodies and incubating for an hour at RT or overnight at 4°C, (Table 2.1.5.4 Immunocytochemistry antibody details). Finally, sections were washed x2 in PBS/Tween, before DAPI at a concentration of 1:1000 was added, coverslip applied and fixed. Stained sections were visualised with a Zeiss 710 confocal scanning microscope with 60× oil immersion optics. Laser lines at 405, 488 and 543 for excitation of DAPI, acetylated α-tubulin and γ-tubulin, respectively, were provided by an argon laser. Detection ranges were set to eliminate crosstalk between fluorophores. Positive (BCC cases) and NPA controls were included with each experiment; settings were adjusted between samples.

2.2.3.5 Immunohistochemistry on FFPE BMTs

This work was accomplished in collaboration with NHS Lothian, in particular John O'Connor, Tim Ingman and Dr John Goodlad. I am indebted for their time, help and expertise.

Sections were cut at 3-4μM, from embedded blocks, floated onto a warm (42°C) water bath then picked up onto Superfrost plus slides (performed by John O'Connor, NHS Lothian). To preserve antigenicity sections were stored at 4°C. Sections were dewaxed prior to antigen retrieval using the proprietary antigen retrieval solutions ER1 and ER2 and the Leica Bond III platform. ER1 is a ready-to-use citrate-based pH6.0 solution; ER2 is a ready-to-use EDTA based pH 9.0 solution. Single antibody detection was accomplished using a Leica Bond III immunostainer (performed by Tim Ingman, NHS Lothian). All antibodies were optimised prior to use on control material as specified by product datasheet. Selected antibodies, optimal dilutions, control material and epitope retrieval method is documented in Table 2.1.6.3.

Protein expression was estimated at x10 magnification by two investigators in a blinded fashion. A previously described score system with minor modifications was used [585]. The staining intensity was semi-quantitatively classified as negative, weakly positive and over-expressed; staining was considered negative if <10% of cells were positive.

2.2.3.6 Enzyme-linked immunosorbant assay

A commercially developed enzyme-linked immunosorbant assay (ELISA) for SHH was used to quantitatively measure SHH expression; the assay employing an antibody specific for the N-terminus of human SHH.

To determine SHH ligand expression by various cell lines, conditioned media was collected, filtered using a 0.45μM filter and snap frozen. Plasma was collected from primary samples and processed as described in Section 2.2.1.2.9.

The assay was performed as per manufacturer's instructions. Briefly, the kit supplied a 96-well plate, pre-coated with an antibody specific for human SHH. Standards and samples were pipetted into wells and incubated for 2½hrs at RT. SHH present in a sample was consequently bound by the immobilised antibody. Wells were then washed x4 with 1X wash solution (provided in the kit and used throughout) and biotinylated anti-Human SHH antibody added and incubated with gentle agitation at RT for 1hr. Following further washes (x4) HRP-conjugated streptavidin

was added and the plate incubated at RT for 45mins. Following the final washes (x4) a TMB substrate solution was added to each well and the plate incubated at RT in the dark for 30mins. The reaction was stopped immediately by the addition of stop solution, colour being proportional to the amount of SHH bound. The reaction was quantified by absorbance measured at 450nm on a scanning plate reader immediately after the stop solution was added. The quantity of SHH present was determined from the standard curve.

2.2.4 Flow cytometry

Flow cytometry is a quantitative technique that enables characterisation of cells at a single cell level using fluorophore labelled antibodies and dyes. Simply, cells are suspended in a stream of fluid, passed through at least one laser exciting the fluorophore, causing the emission of light of a specific wavelength (colour). Each fluorophore has a different excitation and emission spectra. Multiple fluorophore-labelled antibodies can be used simultaneously provided they emit at different wavelengths (colours). The BD Biosciences FACSCanto™ II can detect up to 8 colours simultaneously using 3 lasers.

All flow cytometry was performed on a FACSCanto™ II flow cytometer, data acquired using FACS Diva software and analysed using FlowJo software. Appropriate isotype controls, to determine the emission of non-specific binding, positive controls to offset spectral overlap between fluorophores, and an unstained sample were utilised to set voltages and compensation when required. Compensation was set using the linear-log scale for each antibody used. Viable cell populations, when required, were gated using FSC and SSC characteristics, with FSC measuring cell size, and SSC cytoplasmic granularity. A minimum of 10,000 events was collected for all experiments.

2.2.4.1 Apoptosis assessment

Apoptosis is a normal physiological process, essential for tissue homeostasis. It is characterised by certain features, including loss of membrane integrity, condensation of the cytoplasm and nucleus and inter-nucleosomal DNA cleavage.

During the early stages of apoptosis there is loss of membrane asymmetry with phospholipid phosphatidylserine (PS) translocating from the inner to the outer leaflet of the plasma membrane. It is this feature by which Annexin V can identify apoptotic cells. Annexin V, a calcium dependent phospholipid-binding protein, has a high affinity for PS, binding to cells with exposed PS. When conjugated to fluorochromes, it can thereby identify cells undergoing apoptosis by flow cytometry.

7-Amino-Actinomycin (7AAD) is a nucleic acid stain distinguishing between viable and dead cells on the basis of loss of membrane integrity, and is excluded from live cells.

Tetramethylrhodamine, methyl ester (TMRM) is a cell-permeant fluorescent dye that is sequestered by active mitochondria. This stain therefore allows changes in mitochondrial membrane potential, an indirect consequence of MOMP, to be assessed.

2.2.4.1.1 Annexin / 7AAD staining

The principle of this experiment was to quantitatively determine the percentage of viable, early apoptotic, late apoptotic and dead cells (Figure 2.3); cellular staining of Annexin V and 7AAD recording cell membrane integrity as a measure of cell viability. This assay is however unable to distinguish between necrotic and apoptotic cell death.

Cells were harvested, washed twice with 1X HBSS (Table 2.1.7.4) and resuspended in 1X HBSS. Fluorophore-conjugated Annexin V and 7AAD were added (2µl of each per 100µl 1X HBSS) and mixed well prior to incubation for 15mins in the dark at RT. 300µl of 1X HBSS was then added and the samples analysed immediately. Analysis was performed using the BD FACSCanto II. Isotype controls and an unstained sample were utilised to set voltages and compensation.

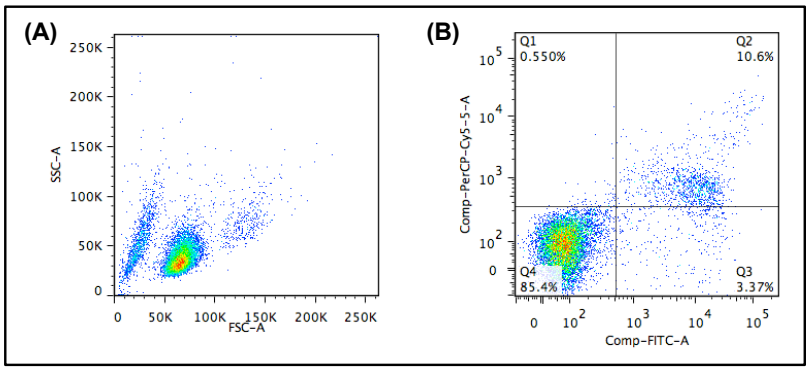

Figure 2.3: Representative FSC / SSC and Annexin V / 7AAD plots for the OCI-AML3 cell line. OCI-AML3 cells were harvested, washed with 1X HBSS. Fluorophore-conjugated Annexin V and 7AAD were added prior to incubation for 15mins. 1X HBSS was then added and the samples analysed immediately. Analysis was performed using the BD FACSCanto II. (A) Representative FSC / SSC plot for the OCI-AML3 cell line; (A) Representative plot showing live / early apoptotic / late apoptotic and dead quadrants defined by Annexin V / 7AAD.

2.2.4.1.2 Tetramethylrhodamine methyl ester staining

The principle of this was to quantitatively assess changes in mitochondrial membrane potential, an early feature of the apoptotic process. Cells were harvested, washed twice with FACS buffer (Table 2.1.7.5), resuspended in 1ml of 250nM TMRM in appropriate cell culture media and incubated for 30mins at 37°C. Cells were then washed twice with FACS buffer, and the samples analysed immediately using the BD FACSCanto II. Isotype controls and an unstained sample were utilised to set voltages.

2.2.4.2 Proliferation studies

The cell cycle is a complex series of events tightly governed within a cell leading to its division and duplication, ultimately resulting in two daughter cells [586].

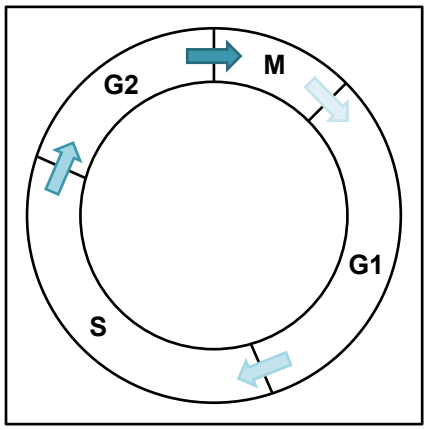

Figure 2.4: Diagrammatic representation of the cell cycle.
M: Mitosis, G1: Growth, S: DNA synthesis and G2: Growth and preparation for mitosis.

2.2.4.2.1 Propidium Iodide staining

The principle of this experiment was to measure the proportion of cells progressing through the different stages of the cell cycle: Interphase (G_1, S, G_2) and Mitosis (M). Propidium iodide (PI) is an intercalating agent, binding double-stranded nucleic acids. PI is therefore capable of showing the increase in cellular DNA as the cell progresses through cell division prior to cell separation.

Cells are fixed in ethanol prior to staining to permeabilise the cell and allow the PI to enter and bind the DNA. Cells were harvested, washed once with FACS buffer, fixed in 1ml 70% ice-cold ethanol whilst gently vortexing to prevent cell clumping, and stored for a minimum of 24hrs at -20^{o}C. Prior to analysis, cells were centrifuged at 400xg for 5mins, resuspended in 250µl PI/RNase staining buffer, vortexed for 30secs and incubated for 15mins at RT in the dark. Analysis was performed immediately using the BD FACSCanto II.

When analysed a histogram, in linear scale, was used to visualise separate cells into G0-G1, S and G2-M phases of the cell cycle, according to the peaks and troughs seen in the control sample. In some experiments, there was not a clear peak for G2-M, in these instances cells were separated into G0-G1 and S-G2-M. The fluorescence of the G2-M peak should be approximately double that of the G0-G1 peak. To ensure accurate analysis for each experiment, this was confirmed using FlowJo software to calculate each peak's mean fluorescence intensity (MFI).

2.2.4.2.2 Carboxyfluorescein succinimidyl ester staining

The principle of this experiment was to follow cell division. Carboxyfluorescein succinimidyl ester (CFSE) is an intracellular fluorescein-based dye that enables cell divisions to be tracked [587]. CFSE fluorescence intensity progressively reduces with each cell division, due to the equal division of the fluorescent stain between daughter cells, allowing the number of divisions to be calculated relative to an undivided control population; Figure 2.5.

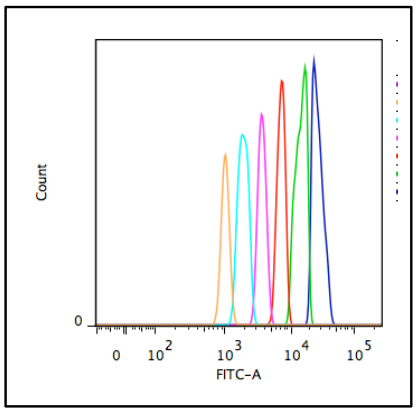

Figure 2.5: Representative histogram showing a progressive reduction in CFSE fluorescence intensity with each successive cell division in the OCI-AML3 cell line.

Cells were harvested and washed twice with FACS buffer. At this stage, an aliquot was removed for the unstained untreated control (USUT). The remainder of the cells were resuspended in 5ml FACS buffer to which CFSE was added, to a final concentration of 1μM, and incubated in a waterbath at 37°C for exactly 10mins. CFSE uptake was stopped immediately by adding ice-cold quenching solution (Table 2.1.7.6) to the cells in a 10:1 ratio. Cells were then washed in FACS buffer before subsequent experiments were set up, and analysis performed at selected time points. For each experiment, an aliquot of CFSE+ cells were treated with 100ng/ml Colcemid, arresting cells in metaphase, serving to determine the position of $CFSE^{max}$ cells.

2.2.4.2.3 Cell Trace™ Violet staining

The principle of this experiment was to follow cell division; Cell Trace™ Violet (CTV) fluorescence intensity progressively reducing with each cell division allowing number of divisions to be calculated relative to a non-dividing control population [588]. CTV was used in place of CFSE staining when studying cell division in the *SMO* knockdown model since these cells were labelled with GFP which is seen in the same channel (FITC) as CFSE.

Cells were harvested and washed twice with FACS buffer. At this stage, an aliquot was removed for the UTUS control. The remainder of the cells were resuspended in 1ml FACS buffer to which 2μL 5mM CTV stock solution in DMSO was added, to give a final concentration of 10μM, and incubated in a waterbath at 37°C for exactly 20mins. CTV uptake was stopped by adding 5x volume of cell-specific culture medium and incubating the cells for a further 5mins. Cells were then washed in FACS buffer before subsequent experiments were set up and analysis performed at selected time points.

2.2.4.4 Detection of surface antigen expression

The principle of this experiment was to determine the cellular phenotype. Expression and absence of a panel of CD markers by primary MSC cells being a key component to their validation [37]. Further, a change in CD markers expression is seen with cell differentiation.

Briefly, cells were harvested, washed twice with 1x PBS and resuspended in FACS buffer. Fluorochrome-conjugated antibodies were added at specified concentrations (Table 2.1.7.7) and mixed well prior to incubation for 30mins in the dark at 4°C. Cells were the washed twice, re-suspended in 400μl FACS buffer and the samples analysed immediately.

2.2.4.5 Intracellular antibody staining

Cells were harvested and washed twice with FACS Buffer. Fixation and permeabilisation was performed using FIX & PERM® Cell Fixation & Permeabilisation Kit as per manufacturer's instructions, with the cells being fixed and stored to allow for intracellular staining at a later time.

2.2.4.5.1 pBcl-2

Briefly, to fix the cells, they were resuspended in 1ml 4% paraformaldehyde solution at 4°C and incubated for 20mins. Cells were then washed twice in FACS buffer and resuspended in 90% FBS/10% DMSO for storage at -80°C until required.

Fixed cells were permeabilised prior to staining: cells were washed twice in FACS buffer to remove DMSO then resuspended in 1ml permeabilising agent (Perm/Wash™ buffer, reagent B) for 15mins. Fixed/permeabilised cells were thoroughly resuspended in 50μl Perm/Wash™ buffer with 2μl pBcl-2 and incubated at 4°C for 30mins. Cells were washed twice in Perm/Wash™ buffer prior to being resuspended in 50μl Perm/Wash™ buffer with 1μl FITC goat anti-rabbit IgG and incubated at 4°C for 15mins. This step was required since the pBCL-2 antibody was not conjugated to a fluorophore. Finally, cells were washed twice with 1ml Perm/Wash™ buffer, resuspended in FACS buffer and analysis performed immediately.

2.2.5 Electron microscopy

Electron microscopy allows the ultrastructure of both tissues and cells to be studied and has classically been used to identify primary cilia within cells [416,428].

Samples were stabilised (fixed), ensuring the ultrastructure of the BM was maintained. Fresh NOD-SCID mouse femurs were fractured and fixed in 2.5% Glutaraldehyde/ 2% Paraformaldehyde/ 0.1MSodium Cacodylate fixative buffer for one hour at RT. Primary human BMT sections were dewaxed and rehydrated as described in 2.2.3.4, then fixed as for the murine bones. Samples were washed for 5mins in 0.1M Sodium Cacodylate buffer solution three times prior to secondary fixation in 1% Osmium Tetroxide/0.1M Buffer for one hour to add contrast. Sections were subsequently washed in distilled water three times (10mins each). Samples were then block stained in 0.5% Uranyl Acetate for one hour in the dark (light sensitive stain) to add contrast. Sections were dehydrated with serial 10min washes in ethanol at 30%, 50%, 70%, 90% and four 5min washes in 100% ethanol. Samples were further dehydrated through 4 washes in absolute ethanol (5mins each). Type 3A molecular sieves were used to dehydrate ethanol producing absolute ethanol – the ethanol must be anhydrous for resin embedding.

For scanning electron microscopy (SEM), samples were delicately dried (referred to as critical point drying) ensuring preservation of the surface structure using a POLARON 3000 CPD to preserve morphology samples. Dried samples were mounted onto SEM support stubs using double-sided conductive tape and silver paint and gold/palladium coated (20nm thickness) using a Quorum 150T High vacuum Sputter coating system. Imaging was performed on a JEOL6400 SEM running at 10kV. Tiff images were captured using Olympus Scandium Software.

For transmission electron microscopy (TEM), samples were washed in propylene oxide three times (5mins each) as this solvent mixes better with resin. Samples were then placed in propylene oxide:araldite/epon 812 (1:1) resin overnight. The propylene oxide evaporates off. The following day, samples were resuspended in pure araldite/epon 812 resin for three hours, the solution poured off and the process repeated twice, including a second overnight incubation.

The following day, samples were placed in fresh resin, embedded in flat bed moulds and polymerised for 48hrs at 60℃. 50-60nm thick ultrathin sections were produced using a LEICA Ultracut UCT and a DIATOME diamond knife at an angle of 6℃. Sections were picked up on 100mesh formvar coated copper grids, then contrast stained with 2% methanolic uranyl acetate for 5mins and, subsequently, Reynolds lead citrate for 5mins. Samples were viewed on a FEI Tecnai T20 TEM running at 200kV. Images were captured using a GATAN Multiscan camera and GATAN Micrograph Imaging software.

Margaret Mullin performed this work, I am grateful for her time, knowledge, perseverance and skill.

2.2.6 Statistical analysis

All statistical analyses were performed using Graphpad Prism 6. When two groups were compared the unequal variances t-test with Welch's correction, Student's t-test, Fisher's exact test and the Chi-Squared test (dependent on experimental design) were used.

Unless otherwise stated, all experiments were performed at least 3 times. Results are expressed as the mean +/- standard deviation (SD), or the median +/- range where appropriate. $P \leq 0.05$ was considered to be statistically significant. All results are expressed to the nearest three decimal places unless more significant, in these instances, results are expressed as $p < 0.001$ or $p < 0.0001$.

3 Hypothesis 'The Hh pathway is deregulated in AML relative to normal haematopoiesis, this deregulation being associated with a poor prognosis and inferior clinical outcome.'

3.1 To determine the activity of the Hh signalling pathway in select AML cell lines and an unselect cohort of primary human AML MNCs

3.1.1 Introduction

AML is a CSC disease, with the LSC believed to be responsible for treatment resistance, MRD and relapse. LSC behaviour is tightly controlled by a complex interplay between intrinsic and extrinsic signals with the Hh signalling pathway implicated as both an intrinsic and extrinsic mediator of CSC function.

Whilst components of the Hh pathway have been shown to be expressed in select AML cell lines [377,379,566] and primary AML MNCs, [378,379,381,382,565,566] no dataset has included all recognised components of the pathway. Further, the role of the Hh pathway in AML remains contentious. We therefore sought to confirm and then evaluate expression of the Hh signalling pathway in select, genetically diverse AML cell lines and within an unselected cohort of primary human AML patients.

3.1.2 Primary human AML MNCs differentially express components of the Hh pathway at the gene level

To determine expression of members of the Hh signalling pathway MNCs from 76 newly diagnosed AML patients were studied. Sample characteristics are listed in Appendix 1.

Whilst in diseases such as CML the LSC is well defined, in AML the phenotype of this primitive cell of origin remains to be determined [52,112,121,129], with recent work challenging previously accepted concepts [52]. Gene expression was therefore performed on unselected PB MNCs (leukaemic blasts), and compared to unselected normal bulk MNCs (n=10) from a range of age groups (age range 22 – 73 years) comparable to our AML cohort. This is in keeping with published work [86,87]. RNA was isolated from cells following culture for 24hrs. A standardised approach was adopted to minimise confounding factors.

To account for input cDNA the ΔCT for each gene was calculated by subtracting the CT value of 6 housekeeping (control) genes from the CT recorded for the gene of interest. *ATP5S*, β*2M*, *ENOX2*, *GAPDH*, *TYW1* and *UBE2D2* were selected as housekeeping genes, CT values ranged from 3 to 13. To ensure accuracy of our results samples were excluded where >2 genes failed due to technical reasons – poor technical triplicate, a signal was detected in the no template control (NTC) or the reaction failed by Fluidigm®. This stringency was applied to all gene expression analysis presented throughout this thesis.

Expression levels of the Hh ligands *SHH, DHH* and *IHH*, the receptors *PTCH1* and *SMO*, the transcription factors *GLI1-3*, and the pathway modulators *PTCH2*, *SUFU*, *HHIP*, *STIL*, *DISP2* and *HHAT* were quantified by qRT-PCR using Fluidigm® technology. Expression is presented as fold change ($2^{-\Delta\Delta CT}$) relative to our normal control cohort. Expression for *DHH* and *GLI-2* are presented as $2^{-\Delta CT}$ as these genes were not expressed by our cohort of normal MNCs (n=10); Figure 3.1.2.1.

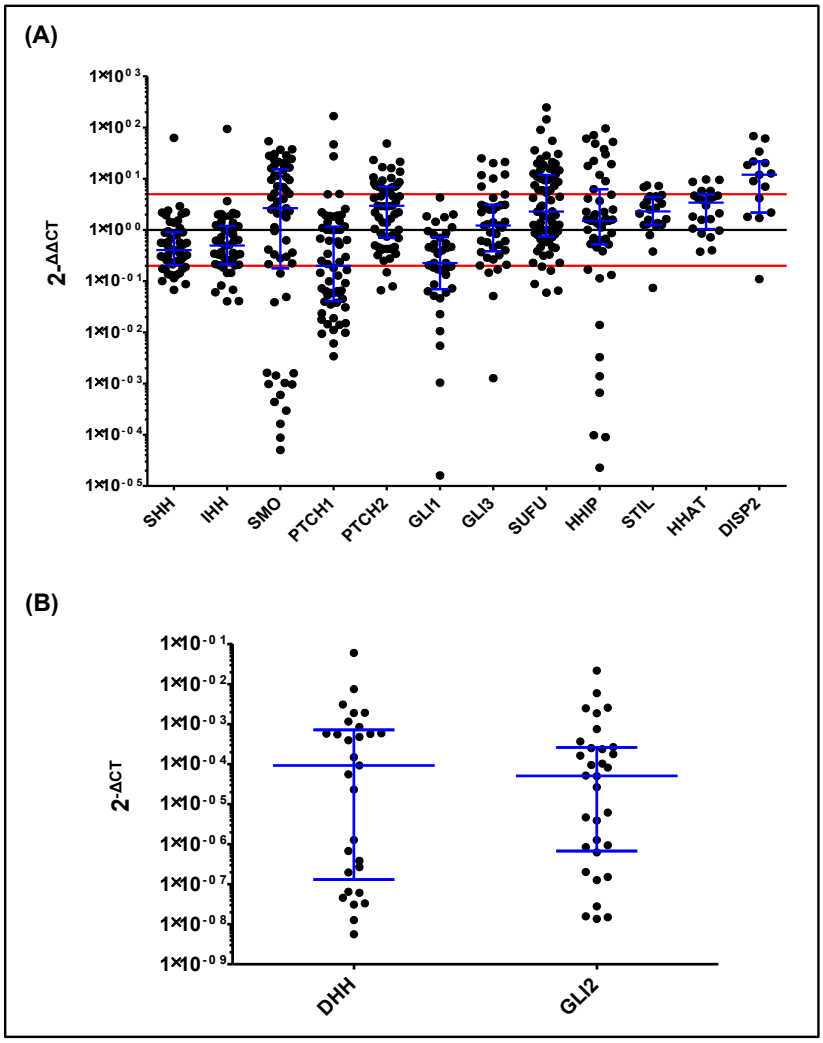

Figure 3.1.2.1: Variance in the baseline gene expression of members of the Hh signalling pathway in an unselected cohort of *de novo* primary human AML samples (n=76).
RNA was extracted from cells harvested following culture for 24hrs. Expression levels were quantified by qRT-PCR using Fluidigm® technology with 6 housekeeping genes – *ATP5S, B2M, ENOX2, GAPDH, TYWI* and *UBE2D2* serving as endogenous control; CT values for these genes ranged from 3 to 13. (A) mRNA expression levels are shown as the fold change ($2^{-\Delta\Delta CT}$) relative to the mean of 10 normal MNC samples. The median is presented with error bars showing interquartile range and demonstrating the variability in baseline expression between individual AML samples. Red lines highlight a 5-fold change taken as our threshold for significance. (B) mRNA expression for *DHH* and *GLI-2* are shown as $2^{-\Delta CT}$, these genes were not expressed by our cohort of 10 normal MNC samples. As in (A) the median is presented with error bars indicating the interquartile range.
For each gene expression was evaluated in the following number of samples: *SHH* (51), *IHH* (49), *DHH* (42), *SMO* (54), *PTCH1* (76), *PTCH2* (76), *GLI-1* (53), *GLI-2* (42), *GLI-3* (53), *SUFU* (76), *HHIP* (76), *STIL* (24), *HHAT* (22) and *DISP2* (22); expression was not determined in all samples *for STIL, HHAT* and *DISP2*. Sample number otherwise varied for technical reasons – poor technical triplicates, signal detected in the no template control or failed reaction by Fluidigm®. Where the number of points on the graph does not total the number of samples in which gene expression was evaluated this is due to the gene not being expressed by that particular sample.

All three Hh ligands, *SHH*, *IHH* and *DHH* were expressed by our AML cohort. mRNA expression was demonstrated in 82.3% (42/51 samples), 83.6% (41/49 samples) and 69% (29/42 samples) for *SHH*, *IHH* and *DHH*, respectively, Figure 3.1.2.1. In contrast *SHH* and *IHH* were expressed in 6/10 normal MNCs whilst *DHH* was not detected. Expression of the receptors *SMO* and *PTCH1* was found in 84.2% (45/54 samples) and 78.9% (60/76 samples) of AML cases, respectively, whilst expression of *GLI-1*, *GLI-2*, and *GLI-3* was detected in 52.6% (28/53 samples), 76.2% (32/42 samples) and 65.8% (35/53 samples) respectively, Figure 3.1.2.1. Finally, *PTCH2* was expressed in 84.2% of cases (64/76 samples), *SUFU* in 94.7% (72 samples), *HHIP* in 67.1% (51/76 samples),

STIL in 91.7% (70 /76 samples), *DISP2* in 68.2% (15/22 samples) and *HHAT* in 27.6% (6/22 samples), Figure 3.1.2.1.

Strikingly, despite the heterogeneity of AML, analysis of an unselected cohort of *de novo* primary human AML samples (n=76) demonstrated deregulation of *SMO* when compared to normal MNCs ($p<0.0001$) with a significant >5-fold up-regulation demonstrated in 43.4% of cases (23/53 samples) and a >5-fold down-regulation in 32.1% of cases (17/53 samples), Figure 3.1.2.1. In contrast *PTCH1* was down-regulated (p=ns) with a >5-fold down-regulation in 39.5% (30/76 samples), Figure 3.1.2.1. This data is particularly interesting given that *PTCH1* has been shown to predict imatinib response and thus a promising molecular marker [251]. Work in AML however has had focused on expression of the Gli transcription factors showing deregulation of the pathway. This data adds to that, providing a rationale for considering utilising the Smo inhibitors in AML.

We acknowledge the Hh pathway is a self-renewal pathway, intrinsic to stem cell function. We therefore studied expression of components of the pathway in normal CD34+ selected cells (BM CD34+ cells were purchased from stem cell technologies; PB CD34+ cells were isolated from normal donors following G-CSF stimulation and apheresis) and normal bulk MNCs to determine if expression differed with cell maturity; Figure 3.1.2.2.

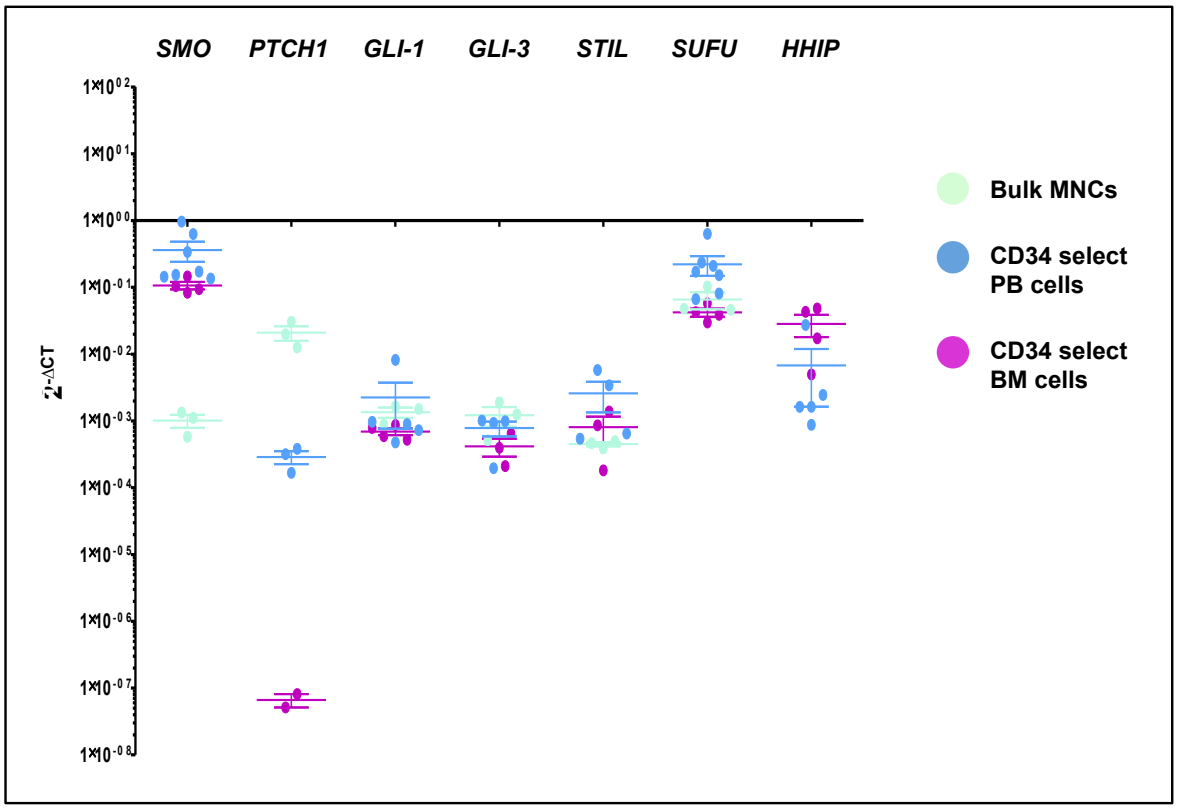

Figure 3.1.2.2: Variance in expression of components of the Hh pathway varied between normal bulk MNCs, CD34 select PB and CD34 select BM cells.
PB CD34+ cells were harvested by G-CSF stimulated apheresis and CD34+ BM cells purchased from Stem Cell Technologies. RNA was extracted from recovered cells following culture for 24hrs. Expression levels were quantified by qRT-PCR using Fluidigm® technology. Expression levels are shown as $2^{-\Delta CT}$, with 6 housekeeping genes – *ATP5S, B2M, ENOX2, GAPDH, TYWI* and *UBE2D2* serving as endogenous control. 3-5 samples were analysed, where the number does not reach this data has been excluded for technical reasons to ensure accuracy. Error bars indicate SD.
This graph clearly shows whilst there is a degree of variance expression is seen to cluster according to cell maturity.

Most striking was the homogeneity seen within the normal samples, the exception being on analysis of the receptors *SMO* and *PTCH1* where a clear distinction between CD34 positive cells and MNCs was demonstrated, Figure 3.1.2.2.

Looking first at *SMO*, there was a statistically significant difference (p=0.019) in expression between the bulk MNC and CD34+ selected cells (both BM and PB derived), the populations being seen to cluster, with the CD34+ selected cells demonstrating a >10-fold increase in level of expression, Figure 3.1.2.2. Expression of *PTCH1* differed markedly between the defined groups, with a statistically significant difference between CD34 select PB and BM cells (p=0.039), and CD34 select BM cells and bulk MNCs (p=0.016), statistical significance was not reached for CD34 select PB cells relative to bulk MNCs (p=0.052) suggesting expression change on cell maturation, Figure 3.1.2.2.

We questioned whether the differential expression of these regulating receptors correlated with pathway activity, hypothesising the pathway was down-regulated or 'switched off' with cell maturation. Interestingly however, expression of *SMO* and *PTCH1* did not correlate with that of *GLI-1*, expression of *GLI-1*, the positive regulator, being relatively homogeneous across our normal cell populations, Figure 3.1.2.2. *GLI-2* is not included within the figure since it was not reliably expressed in any of our normal samples. There was either (1) an absence of signal following 40 PCR cycles or (2) insufficiently robust data generated - poor technical triplicates (greater than 1.5CT difference). Importantly a signal was never detected below a CT of 37 suggesting if the signal was real expression of *GLI-2* in these isolated samples was at a very low level. This is particularly interesting considering its role as both a positive and negative regulator, and proposed close relationship between each of the transcriptional regulators.

Considering the striking difference in *SMO* expression between the CD34 positive cells and bulk MNCs we considered our primary *de novo* AML expression data relative to a population of CD34 positive cells, Figure 3.1.2.3.

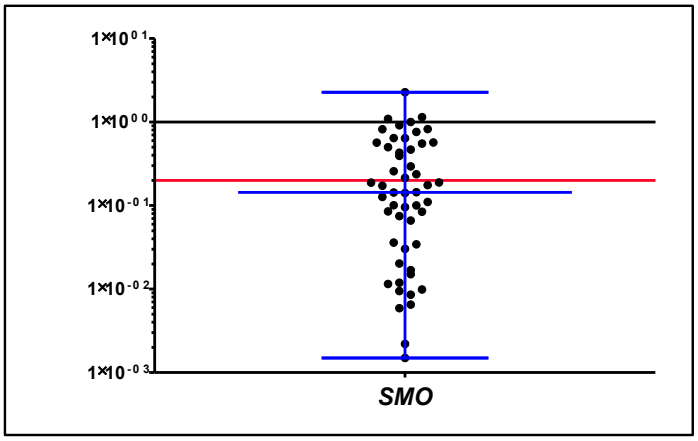

Figure 3.1.2.3: *SMO* expression in an unselected cohort of *de novo* primary AML MNCs relative to normal CD34+ selected cells
PB CD34+ cells were harvested by G-CSF stimulated apheresis and CD34+ BM cells purchased from Stem Cell Technologies. RNA was extracted from cells harvested following culture for 24hrs. Expression levels were quantified by qRT-PCR using Fluidigm® technology. mRNA expression levels are shown as the fold change ($2^{-\Delta\Delta CT}$) relative to the mean of 6 normal CD34+ select cell populations (PB and BM) with 6 housekeeping genes – *ATP5S, B2M, ENOX2, GAPDH, TYWI* and *UBE2D2* serving as endogenous control; CT values for these genes ranged from 3 to 13. The red line highlights a 5-fold change.
The median is presented, showing *SMO* was universally, though variably, down-regulated in the AML bulk MNCs relative to normal CD34+ selected cells (BM and PB). Error bars indicate the interquartile range, demonstrating the degree of variance between samples.

As expected, expression was seen to shift in accordance with the change in calibrator from bulk MNCs to CD34 positive cells. When CD34 positive normal cells (PB and BM) were used as the calibrator *SMO* expression was found to be down-regulated in 93.2% of AML cases, with 45.7% of cases demonstrating a >5-fold down-regulation relative to our cohort of normal CD34 positive cells. This marked difference in relative expression according to calibrator population is highlighted in Figure 3.1.2.4 with 32.1% showing a >5-fold down-regulation and 43.4% showing a >5-fold up-regulation when bulk normal MNCs were used as the calibrator. Recognising AML

arises from impairment in differentiation and a consequent accumulation of immature myeloid progenitor cells the differential expression of a targetable positive regulator with cell maturation makes Smo an interesting therapeutic target. Further, it could explain results from early phase clinical trials showing a reduction in disease burden with a relative sparing of normal haematopoiesis [407], standard therapeutic agents classically being associated with significant, and at times life threatening haematopoietic toxicity. An agent that spares an already compromised haematopoietic system is therefore very attractive in the clinical setting.

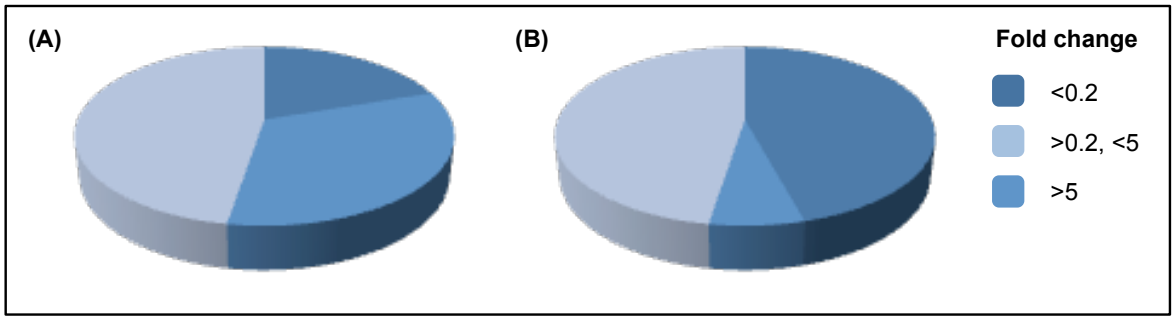

Figure 3.1.2.4: *SMO* expression in an unselected cohort of primary, *de novo*, AML MNC samples (n=76) relative to normal unselected MNCs and normal CD34+ selected cells.
PB CD34+ cells were harvested by G-CSF stimulated apheresis and CD34+ BM cells purchased from Stem Cell Technologies. RNA was extracted from cells harvested following culture for 24hrs. Expression levels were quantified by qRT-PCR using Fluidigm® technology. 6 housekeeping genes – *ATP5S, B2M, ENOX2, GAPDH, TYWI* and *UBE2D2* serving as endogenous control. (A) mRNA expression levels categorised according to fold change ($2^{-\Delta\Delta CT}$) relative to the mean of 10 normal bulk MNC samples. (B) mRNA expression levels categorised according to fold change ($2^{-\Delta\Delta CT}$) relative to the mean of 6 normal CD34+ select cell populations (PB and BM).
A clear difference in relative expression, dependent upon comparator cell population, is demonstrated suggesting a down-regulation of *SMO* on cell maturation in normal haematopoiesis.

Whilst we acknowledge leukaemic blasts are more primitive than mature MNCs arrested differentiation is fundamental to the pathogenesis of AML. To compare unselected AML MNCs with a selected more primitive normal CD34 expressing population has the potential to eliminate fundamental, potentially targetable, differences through population selection. We therefore consider it more accurate to compare AML MNCs, leukaemic blasts, to normal MNCs despite these marked differences. Gene expression of AML MNCs is thus compared with that in normal bulk MNCs throughout this thesis.

3.1.3 *SMO* expression did not define an expression profile within the Hh pathway

Whilst deregulation of the Hh pathway has been reported within AML, no publicly available dataset has studied all components of the pathway. Further, there is no published data analysing the transcriptional relationship between family members within AML. We therefore sought to determine the impact of up-regulation of *SMO* at a transcriptional level on other family members. Expression levels were quantified by qRT-PCR using Fluidigm® technology as outlined above, 3.1.2. Samples were classified according to *SMO* expression, with high expressers defined as those with a ≥5-fold increase in *SMO* relative to normal MNCs. 26 of our cohort of 76 (34.2%) were stratified as high expressers of *SMO*. Gene expression within high expressers was compared to that in a cohort of AML samples demonstrating a <5-fold change in *SMO* relative to normal MNCs. Log transformation of the fold change was performed to analyse expression

patterns within these defined cohorts according to the unsupervised Eisen approach using PermutMatrix software [589]. Figure 3.1.3.1.

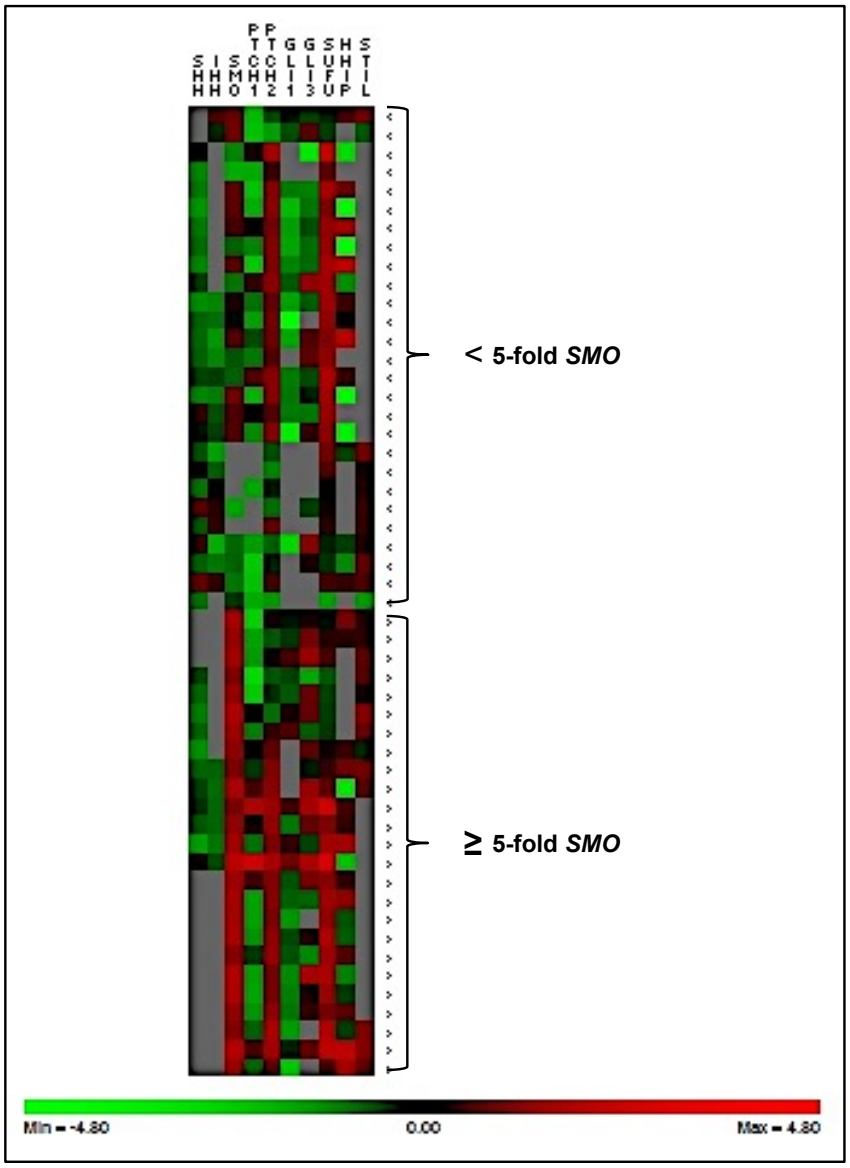

Figure 3.1.3.1: Heatmap showing expression of components of the Hh pathway in primary human AML MNCs according to *SMO* expression.
RNA was extracted from cells harvested following culture for 24hrs. Expression levels were quantified by qRT-PCR using Fluidigm® technology. To account for input cDNA the ΔCT for each gene was calculated with 6 genes – *ATP5S*, *B2M*, *ENOX2*, *GAPDH*, *TYWI* and *UBE2D2* serving as endogenous control. Technical triplicates were performed for each sample. Log transformation of the $2^{-\Delta\Delta CT}$ enabled graphical display of expression patterns according the unsupervised Eisen approach using PermutMatrix software [506], clearly showing expression of components of the Hh pathway to be heterogeneous, and not linked to *SMO* expression.

The expression of components of the Hh pathway is shown for 53 of our 76 samples, with an equal proportion of samples demonstrating a ≥5-fold increase in *SMO* (classified as high expressers; n=26) and a <5-fold increase in *SMO* (n=27). 23 samples were excluded from this heatmap as the expression of ≥4 genes was not available / excluded. Expression values of excluded genes are marked in grey. Clustering was not performed due to missing data points. A heatmap was selected to represent this data since it enables comparison between cohorts and allows the reader to see the expression profile of individual samples and therefore appreciate the degree of heterogeneity.

Whilst a clear expression profile was not demonstrated within *SMO* high expressers, given the degree of heterogeneity and size of our cohort, this observation is not surprising. Interestingly, irrespective of *SMO* expression, *SUFU and PTCH2* were shown to be up-regulated, whilst the ligands *SHH* and *IHH* are shown to be down-regulated relative to normal MNCs.

3.1.4 Components of the Hh pathway are differentially expressed at a protein level in primary human AML

The vast majority of work studying the Hh pathway looks at gene expression, excluding changes that may occur post transcription. We therefore sought to determine native protein expression of components of the Hh pathway and their relationship to each other and further to pathway activity, Gli-1 being recognised as a marker of pathway activity, in an unselected cohort of *de novo* primary human AML and normal subjects.

Western blots were performed though are not presented due to the marked heterogeneity between experiments, raising concerns about the validity of the results, despite considerable time and effort optimising protocols. The quality of antibodies against components of the Hh signalling pathway is recognised by the scientific community to be an issue, protein data often not included in published works. The importance of the BM microenvironment in normal haematopoiesis and AML is also recognised. We had planned to evaluate and compare expression within the AML blast population, as determined by Western blotting, with that within the BM microenvironment, as determined by IHC.

Following optimisation IHC enabled analysis of components of the Hh signalling pathway at the protein level within the BM microenvironment of human AML BMTs (n=37) compared to BMTs from normal age-matched controls (n=10). The expression of PTCH1, SMO, GLI-1 and all three Hh ligands were analysed. Ligand expression was included to determine whether autocrine or paracrine signalling existed in AML. Expression of SHH, DHH, IHH, SMO, PTCH1 and GLI-1 was estimated at x10 magnification by two investigators in a blinded fashion. In addition, a previously described scoring system was referenced [494] - samples were semi-quantitatively classified as positive (or 'expressing') if staining was identified in >10% and negative (or 'non-expressing) in those with expression below this threshold [494]. This work was done with the assistance of Mr T Ingman and Dr J Goodlad. I am indebted for their time, skills and knowledge.

Looking first at the Hh ligands. Expression of SHH was significantly down-regulated (p=0.002) within AML BMTs compared to normal BMTs, whilst there was no significant difference in expression of IHH or DHH between AML and normal subjects, Figure 3.1.4.1 (A,B&C).

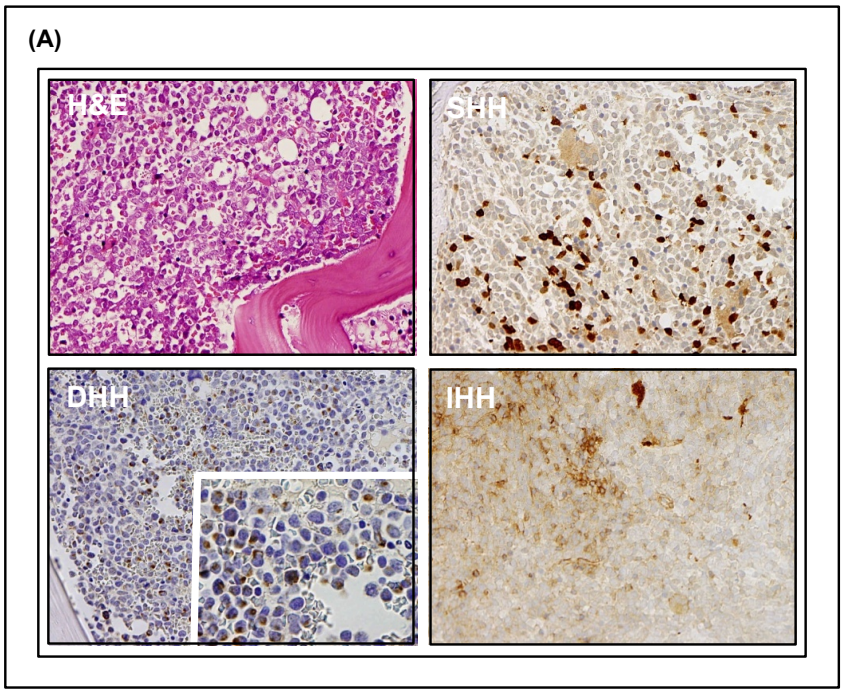
(A)
H&E
SHH
DHH
IHH

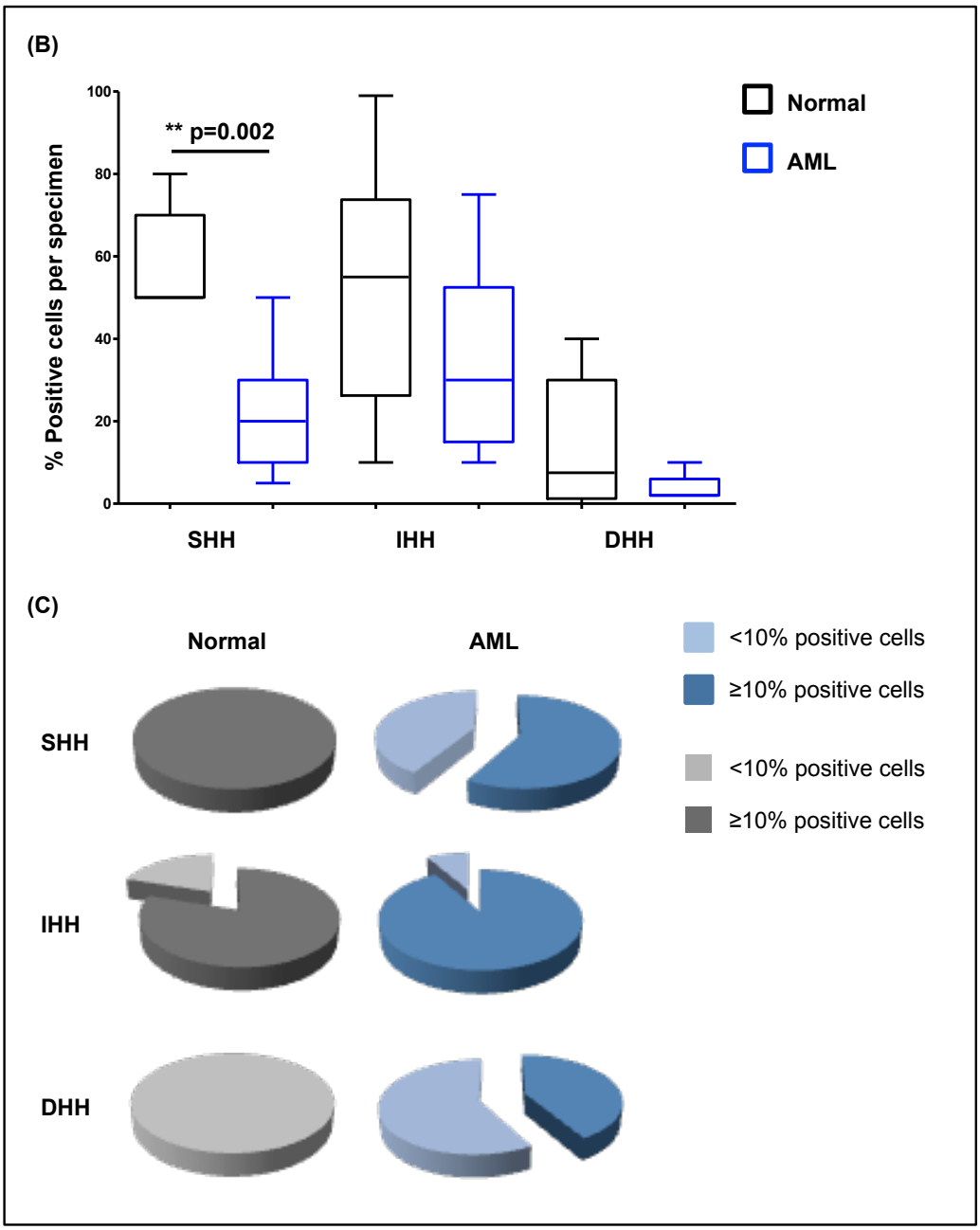

Figure 3.1.4.1 A,B&C: : Expression of the Hh ligands in a cohort of primary, *de novo* AML samples as determined by IHC showing SHH to be significantly down-regulated in AML BMTs.
IHC was performed on human AML BMTs (n=37) and compared to BMTs from normal controls (n=10). Expression of the ligands SHH, IHH and DHH was estimated at x10 magnification by two investigators in a blinded fashion. (A) Representative images at x10 (inlay x40) demonstrating staining patterns for each antibody. (B) Box and whisker plot showing percentage of positive cells per specimen, minimum and maximum values are depicted. (C) Pie charts showing the percentage of samples classified as negative, and the number classified as positive according to a recognised scoring system [494.] by which staining intensity is semi-quantitatively classified as negative and positive (staining was considered negative if <10% of cells were positive).
These graphs show SHH was significantly down-regulated (p=0.002) within AML BMTs compared to normal BMTs. There was no significant difference in expression of IHH or DHH between AML and normal subjects. Statistically significant results are highlighted with p value to the nearest 3 decimal places, those not highlighted are not significant (ns).

In addition, SHH was noted to demonstrate both nuclear and cytoplasmic expression within the AML BMTs but not the normal control BMTs, Figure 3.1.4.2 (B&C). Nuclear staining was seen with two different Shh antibodies, raised in different species. Within a BMT specimen, both nuclear (strong) and cytoplasmic (weak to moderate) staining was demonstrated implying differing levels of production, or reliance, dependent on cell lineage or cell maturity. Further cells within the same BMT specimen were seen to stain with differing intensities, implying variable antigen and therefore protein concentration. Erythroid cells were identified within erythroid islands as negative for SHH, whilst lymphoid cells were strongly positive for SHH.

Interestingly, SHH showed both nuclear and cytoplasmic expression within the colon control, nuclear staining being identified within the colonic crypt bases where colonic SCs reside. Within the AML BMTs positive cells were scattered throughout the marrow, neither localising to the endosteal osteoblastic or peri-sinusoidal regions. This observation was investigated further, presented and discussed in section 3.1.5.

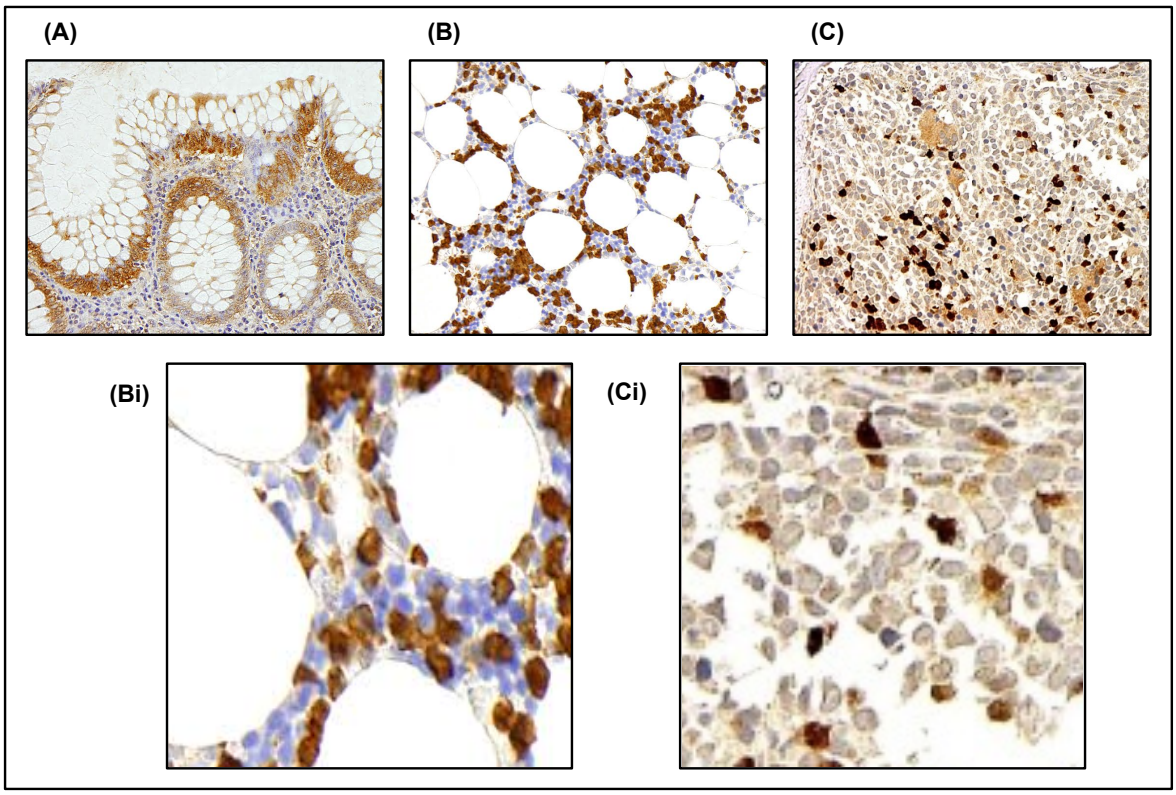

Figure 3.1.4.2: SHH in primary human (A) colon (control tissue) at x4 magnification, (B) normal BMT at x10 magnification and (C) AML BMT at x20 magnification showing cytoplasmic and nuclear expression. (Bi & Ci) are magnified images showing cytoplasmic (Bi) and nuclear and cytoplasmic staining (Ci).
To determine native expression of SHH within the unique BM microenvironment IHC was performed on human AML BMTs (n=37) and compared to BMTs from normal controls (n=10). Each image is representative of those captured and studied for each population cohort, clearly demonstrating the staining pattern of SHH.
The colon control SHH showed both nuclear and cytoplasmic expression, nuclear staining being identified within the colonic crypt bases where colonic SCs reside. Both nuclear and cytoplasmic expression was seen in AML BMTs whilst only cytoplasmic staining was demonstrated in the normalBMTs.

Looking next at SMO, PTCH1 and GLI-1. Whilst a marked difference in the expression of PTCH1 and GLI-1 was seen across both our normal control and AML cohort the difference was not significant due to the degree of variance, Figure 3.1.4.3 (A). Interestingly the mean expression for SMO was similar between our AML cohort and the normal controls.

Referencing the previously described scoring system [494] statistical significance was however seen. 25% of our AML samples were classed as expressing GLI-1 according to this system as opposed to none of our normal controls ($p<0.0001$) whilst 85% of our AML samples expressed PTCH1 as opposed to 50% of our normal controls ($p<0.0001$), Figure 3.1.4.3 (B).

Whilst the scoring system is recognised, and validated, within the scientific community for the purpose of this thesis we chose to present our data in two formats –unmanipulated, showing expression levels, and categorised, highlighting expression patterns, according to the validated scoring system [494].

No relationship between expression levels of these proteins was demonstrated. It is important however, to consider the sensitivity of IHC. IHC does not differentiate between a membranous and cytoplasmic staining pattern and a purely cytoplasmic staining pattern. Classical, canonical signalling is controlled by the internalisation of Ptch1, removing its repression of Smo thereby allowing pathway activity. Whilst the lack of a relationship between SMO and PTCH1 is therefore potentially explained by the inability to determine functional from total protein levels the lack of a relationship between the receptors and GLI-1 raises the question of non-canonical signalling and pathway crosstalk, additional proteins determining GLI-1 expression.

Our work clearly raises further questions: Is SMO an appropriate target given the relative similarity in its expression in normal and AML cases? Should we consider GLI-1 as our target when considering the Hh signalling pathway? Importantly however we have uniquely shown the Hh signalling pathway to be deregulated at a protein level as well as gene level in AML.

This work does however suggest, as with other targeted therapies, that universal targeting of the Hh signalling pathway would not be appropriate, nor necessarily effective since GLI-1 was only expressed in a subset of cases (25%). Expression at a level of 25% in such a heterogeneous disease however is exciting and provides a clear rationale for considering this pathway as a potential therapeutic target. Finally, the marked difference in expression across our cohort of AML samples is also interesting. The phenotype and genotype of these patients in our opinion requires further evaluation in a bid to translate these results into the clinic.

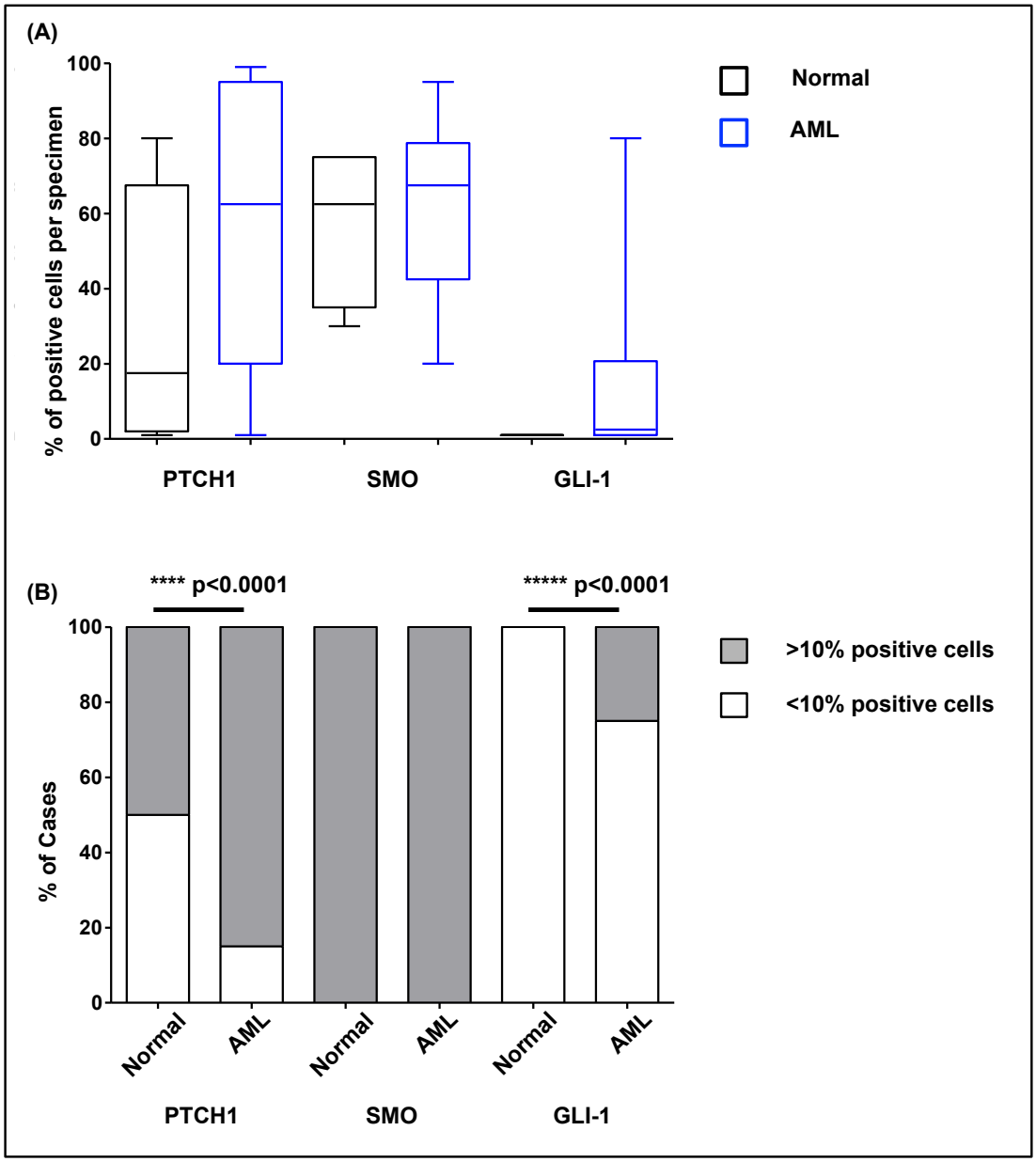

Figure 3.1.4.3: Expression of PTCH1 and GLI-1 in a cohort of primary *de novo* AML BMTs relative to normal BMTs.

IHC was performed on human AML BMTs (n=37) and compared to BMTs from normal controls (n=10). Expression of the receptors PTCH1 and SMO and the positive transcription regulator GLI-1 was estimated at x40 magnification by two investigators in a blinded fashion. (A) Box and whisker plot showing percentage of positive cells per specimen, minimum and maximum values are depicted. Expression of PTCH1, SMO or GLI-1 was not statistically significant due to variance. (B) Bar graph showing the percentage of samples classified as negative and positive according to a recognised scoring system [494] by which staining intensity is semi-quantitatively classified (staining was considered negative if <10% of cells were positive). There was a statistically significant difference seen in the percentage of PTCH1 and GLI-1 positive cells ($p<0.0001$ by the Chi-Squared test). A relationship between the receptors PTCH1, SMO and GLI-1 was not apparent in the normal or AML BMTs.

3.1.5 Post-translational modification of SHH is impaired in AML

As shown in Figure 3.1.4.2 IHC of primary *de novo* human AML BMTs had shown SHH expression to be cytoplasmic, as expected, and, interestingly, also nuclear. A nuclear expression pattern has previously been reported, and recognised in subsets of central nervous system cells [594]. Nuclear staining was also identified within the colonic crypt bases, colon tissue serving as the positive control (Figure 3.1.4.2).

Considering this further, colonic SCs reside within the crypt bases. As colonic SCs differentiate they lose their SC potential and move away from the crypt base towards the villous apex through the transit amplifying and differentiating zones. Additionally, SHH undergoes post-translational modification enhancing its activity and modifying its diffusion capacity.

We hypothesised nuclear expression of SHH reflected attenuated post-translational modification within the SC population. ICC was performed on normal PB MNCs, obtained by G-CSF stimulation and apheresis or venepuncture, and sorted by FACS to allow analysis of patterns of SHH expression in defined cell populations. The following populations were sorted, stained and analysed: uncommitted early progenitor / SC (CD34+), myeloid - mature (CD11b+) and intermediate (CD33+). The pattern and intensity of SHH differed according to cell population. A nuclear location was exclusively seen in the normal HSC / progenitor populations (defined by their expression of CD34 or CD33). No detectable levels of SHH were demonstrated in mature neutrophils.

Hhat is the sole acetyltransferase involved in SHH processing, we therefore sought to determine its expression within the HSC / progenitor populations, Figure 3.1.5.1. There was a 20-fold reduction in *HHAT* in normal HSCs (defined immunophenotypically as CD34+CD38-) compared to normal bulk MNCs (p=0.008).

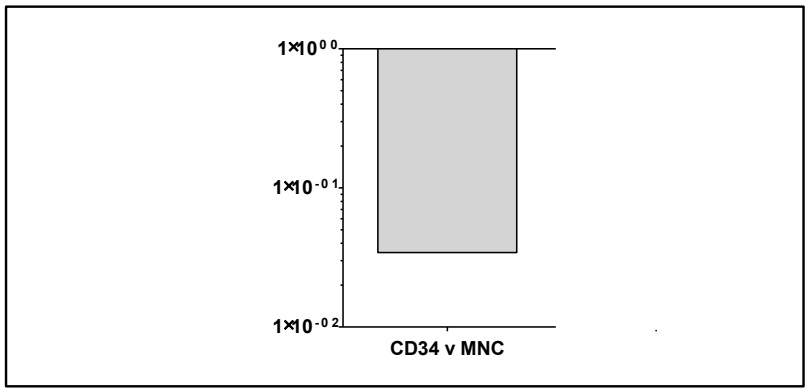

Figure 3.1.5.1: *HHAT* expression in HSCs relative to normal bulk MNCs.
RNA was made from CD34+ selected cells (n=6) and MNCs (n=29). Expression levels were quantified by qRT-PCR using Fluidigm® technology. mRNA expression levels are shown as the fold change ($2^{-\Delta\Delta CT}$) relative to the mean of 6 normal CD34+ samples with 6 housekeeping genes – *ATP5S, B2M, ENOX2, GAPDH, TYWI* and *UBE2D2*.
This data shows *HHAT* to be down-regulated in normal HSCs compared to normal bulk MNCs (p=0.008 according to Fisher's exact test).

To verify our findings, we looked at microarray-based gene expression data previously generated within the Copland laboratory, GSE 47927. This enabled us to compare distinct populations within the haematopoietic hierarchy. Expression of *HHAT* was reduced in normal HSCs (defined immunophenotypically as CD34+CD38-CD90+D45RA-) compared to the more differentiated GMP and MEP populations (p=0.032 and p=0.001 respectively). Aside from normal subpopulations this array focused on CML, looking at expression levels in each sub-population within -CP, -AP and -BC samples. We therefore studied *HHAT* in CML-BC, using this as a paradigm for AML. Interestingly there was a significant difference in expression between normal HSCs and CML-BC HSCs (p=0.001), with expression being lower within the CML-BC samples suggesting a down-

regulation of autocrine Hh signalling. It is however important to acknowledge this microarray had analysed 2 myeloid BC-CML samples. Further, BC-CML is thought to arise due to continued BCR-ABL activity and consequent increased genetic instability, with many patients carrying multiple mutations and chromosomal aberrations. Considering these factors it is important therefore not to overinterrept this result but rather view it with interest and recognise further work is required to confirm and validate this consideration.

We had shown *SHH* to be differentially expressed by leukaemic blasts and normal MNCs, with SHH reduced at a protein level and evidence of impaired post-translational modification through down-regulation of *HHAT* in CD34+ cells relative to bulk MNCs. We had shown the positive regulator *SMO* to be up-regulated and the negative receptor *PTCH1* to be repressed, with pathway activity evidenced by up-regulation of one of the prime transcriptional effectors *GLI-2*. We therefore sought to determine whether, as in B-cell lymphomas [364,595], the Hh pathway was activated in a paracrine fashion, through signals produced by neighbouring cells. Levels of the SHH ligand in the plasma of AML patients (n=11) and normal controls (n=6) was therefore measured by ELISA, Figure 3.1.5.2.

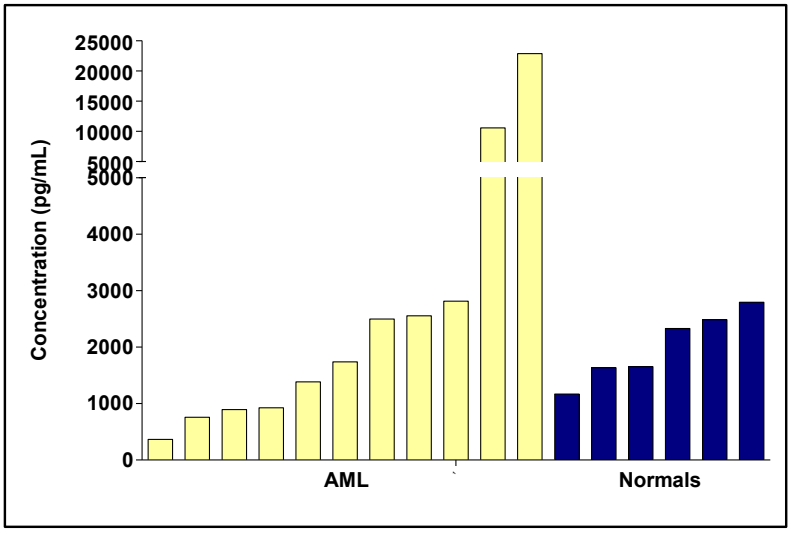

Figure 3.1.5.2: SHH concentration within serum from primary, *de novo* AML and normal subjects by ELISA.
The mean concentration of SHH was determined by ELISA, as described in methods 2.2.3.6, in AML was 4304pg/ml (SD 6769pg/ml) compared to 2010pg/ml (619pg/ml) in normal samples though the results were not statistically significant.

In keeping with the disease, marked heterogeneity in the plasma concentration of SHH was demonstrated across our cohort of AML samples; the SD was 10-fold greater within the AML samples. Interestingly whilst the mean concentration of SHH in AML was 2-fold greater the median was comparable. These results suggest the SHH ligand is increased, indicating paracrine activity, in a subset of AML cases. Had time allowed we would have repeated the experiment to increase statistical power and sought to obtain paired samples enabling parallel measurement of circulating SHH, cellular SHH and gene expression data.

There is already published evidence supporting a role for the Hh signalling pathway in AML - leukaemic cell lines and primary AML cells shown to express *Gli-1* and *Gli-2*, indicative of active Hh signalling [69]. Further, genetic and pharmacological inhibition of Gli-1 has been shown to have anti-leukaemic effects and to be capable of overcoming chemoresistance [378,379]. Through this section we have sought to further understand the role of the Hh signalling pathway in AML and normal haematopoietic cells.

Uniquely we have studied all components of the Hh signalling pathway at the gene level, interestingly showing *SMO* to cluster, with a cohort of both high and low expressers. Additionally whilst gene expression studies simply showed the genetic heterogeneity expected of AML when samples were classified according to *SMO* expression genes associated with poor prognosis and chemoresistance were found to be up-regulated in those samples demonstrating high levels of *SMO*. This is data we are still analysing, in particular referencing it to clinical data where available. We have looked at gene expression relative to both normal bulk MNCs and CD34+ select cells, our data mirroring published data, the results of which vary notably dependent on the comparator cell population and highlighting the difficulties faced when considering gene expression in AML. Additionally we have studied components of the pathway at a protein level, uniquely showing the location of SHH to differ according to cell maturity with *HHAT*, responsible for the post-translational modification of SHH and thus its cellular movement, found to be reduced in CD34+ select cells relative to mature MNCs.

Having confirmed expression of components of the Hh signalling pathway in haematopoietic cells, with expression of GLI-1 serving as evidence of pathway activity, we sought to determine if haematopoietic cells possessed primary cilia, the machinery required to enable canonical Hh signalling and thus provide a rationale for the use of Smo inhibitors in AML.

3.2 To determine whether haematopoietic cells, both normal and leukaemic, possess primary cilia.

3.2.1 Introduction

The strong connection between primary cilia and the Hh pathway was first reported in 2003 [450]. Following on from this, numerous other groups have demonstrated the relationship between components of the pathway and primary cilia [337,430,450-457]. It is now widely accepted that vertebrate canonical Hh signalling requires primary cilia [417]. Additionally, considering the ability of cilia to influence cell cycle and their involvement in signalling pathways, including Hh, Hippo and Wnt, a role for primary cilia in oncogenesis has begun to be hypothesised with early research supporting this theory [436-446].

Haematopoietic cells have however, until recently, been considered to be among the few cells not to possess primary cilia [416,428]. In 2013, the immunological synapse of T cells was shown to be highly dependent on IFT proteins and, therefore considered a functional homolog of the primary cilium [426]. Whilst in 2014, work studying bone mechanotransduction in sheep identified primary cilia in 4% osteocytes, 4.6% bone lining cells, and in approximately 1% of cells within the BM (though these cells were not studied in greater depth) [610]. Finally, in 2016, during the write up of this PhD, primary cilia were shown to be present on human PB and BM haematopoietic cells [566,611]. Further, these primary cilia were shown to be functional and to play a role in Hh signalling. Interestingly, analysis of AML cell lines (KG1, KG1a, and K562) demonstrated primary cilia to be less frequent and frequently dysmorphic [566,611].

During the experimental phase of this PhD, we had questioned the conflicting results seen *in vitro* and *in vivo* with Smo antagonists. Further, whilst work had shown the Hh signalling pathway to be involved in cytotoxic T lymphocyte function, and the immunological synapse to potentially represent a modified cilium [426] whether a haematopoietic cell, normal or malignant possessed primary cilia remained unanswered. We therefore sought to determine whether primary human haematopoietic cells within the BM microenvironment or circulatory system, or AML cell lines possessed primary cilia, and therefore the machinery to enable canonical Hh signalling. We hypothesised HSPC would possess primary cilia within the BM but that these organelles would

become defunct on cell maturation and migration into the PB, this differential expression accounting for differences reported between *in vitro* and *in vivo* studies and the relative absence of haematopoietic toxicity following use of Smo antagonists in early phase clinical trials.

3.2.2 Primary cilia were identified in haematopoietic cells within the bone marrow microenvironment

ICC was performed to determine the presence or absence of primary cilia within the BM microenvironment. Briefly, FFPE BMT sections were deparaffinised and rehydrated prior to antigen retrieval. An unselected cohort of primary *de novo* human AML BMTs (n=25) and a cohort of normal control BMTs (n=10) were analysed. Within our AML cohort, the pathology report of 80% reported sheets of blasts replacing or near replacing (>90%) the marrow space, enabling greater confidence in considering the identified primary cilia to arise within haematopoietic cells. Primary cilia were defined by co-localisation of acetylated α- and γ-tubulin, visualised using a Zeiss 710 confocal scanning microscope (60× oil immersion optics). Confocal microscopy enabled co-localisation of the two antibody signals and therefore proteins to be confirmed through z sections. Additionally, Image J enabled us to generate a model of fluorescence intensity mathematically confirming co-localistaion of the antibody signals [612], removing observer bias / interpretation. Cell morphology and cell location relative to sinusoids and bone trabeculae was recorded. Excitingly, primary cilia were identified in all AML (n=25), and 20% of normal (n=10) BMTs by ICC, Figure 3.2.2.1.

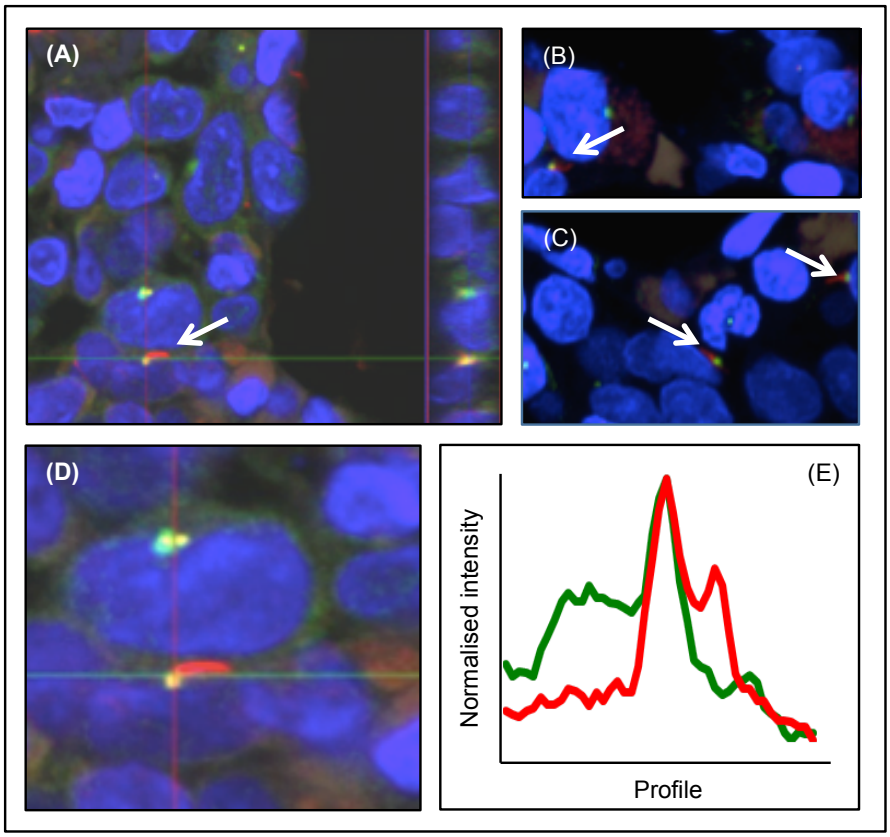

Figure 3.2.2.1: Representative confocal images depicting primary cilia within normal human and primary, *de novo* human AML BMTs and a computer generated image depicting fluorescence signal. FFPE BMT sections were deparaffinised and rehydrated prior to antigen retrieval using the Thermo Scientific™ PT Module. Sections were stained for DAPI, acetylated α-tubulin and γ-tubulin prior to visualisation with a Zeiss 710 confocal scanning microscope (x60 oil immersion optics). Positive and no primary antigen controls were included with each experiment; settings were adjusted between samples.
(A, C & D) Representative confocal images from FFPE AML BMTs (n=25) and (B) normal (n=10) primary human BMTs clearly showing the presence of primary cilia. Primary cilia were defined by co-localisation of acetylated α and γ tubulin, (A) confirmed on z sections and through (E) computer generated models of fluorescence intensity.

Expression of primary cilia within our normal cohort was at a low frequency of <1% cells. In contrast the number of primary cilia identified in our AML cohort varied significantly in keeping with the disease's heterogeneous nature. Whilst technical reasons precluded an accurate absolute number or percentage of cells expressing primary cilia within each specimen the percentage was approximated at <1% to 5% of cells. As an additional comparator we studied the expression of primary cilia within CML, a role for Hh signalling better established in this disease setting [249,251-253,412,613]. In this setting, primary cilia were again identified in a cohort of ten CP-CML BMTs. Expression was uniform, primary cilia being identified in approximately 1% of cells in all samples. The frequency of expression, even within AML, did not allow conclusions to be drawn regards cellular location within the BM – we had considered primary cilia, if limited to the HPSC, would be found preferentially within areas classically considered BM SC niche (in close vicinity to bony trabeculae or vascular sinusoids).

The gold standard technique for identifying primary cilia is EM. Critical to EM is the fixation process, however, fresh human BMTs were not available. EM was therefore performed on human FFPE BMTs following deparaffinisation, rehydration and fixation in glutaraldehyde / paraformaldehyde. A cohort of 3 AML and 3 normal BMTs were studied. In addition, we analysed 4 glutaraldehyde / paraformaldehyde fixed mice femurs. Mice femurs, fixed in optimal conditions for EM, were studied in parallel to the human BMTs since we had concerns tissue

architecture might be distorted during deparaffinisation and rehydration. Margaret Mullen, to whom I am indebted, largely performed this work.

Primary cilia were identified in cells, which morphologically bared all the characteristics of haematopoietic progenitor cells by SEM and TEM [614-616], Figure 3.2.2.2. Included in the figure are accepted and validated SEM and TEM primary cilia images for comparison [615,616].

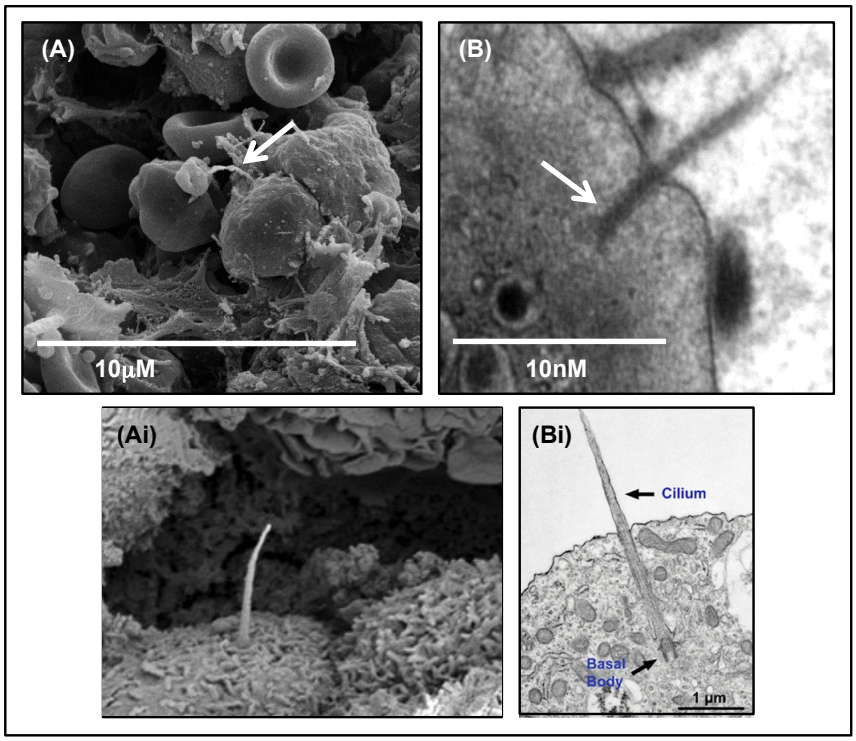

Figure 3.2.2.2: Representative SEM and TEM images depicting primary cilia within primary human *de novo* AML BMTs.
EM was performed as described in methods 2.2.5. (A) Representative SEM image showing a cell independently identified as haematopoietic with a primary cilia and (Ai) SEM image of kidney primary cilium for comparison [614]. (B) Representative TEM image showing a cell independently identified as haematopoietic with a primary cilia and (Bi) cell and its primary cilium [615].

Finally, whilst primary cilia were identified on cells that, morphologically, were medium in size with a high nuclear to cytoplasmic ratio, we were unable to definitively label these cells haematopoietic in origin. In this respect, we tried staining our samples with additional primary antibodies (haematopoietic - CD45, CD34 and mesenchymal – CD44, CD90 and CD105) to confirm or refute their haematopoietic nature. This took considerable optimisation; the antigen retrieval process was felt to potentially damage the CD antigens and there was a need to carefully select our primary and secondary antibody cocktail to ensure specificity, minimise spectral overlap and be detectable using a Zeiss 710 confocal scanning microscope. An antibody cocktail containing acetylated α- and γ- tubulin, CD45 and a nuclear stain (DAPI) was optimised. Samples (human AML BMTs n=5 and normal human BMTs n=3) were mounted on coverslips (1cm in diameter) coated with carbon grids enabling each cell of interest to be 'mapped' for future identification and analysis of the cell's ultrastructure by EM. This process was technically challenging and labour intensive. Difficulties included (1) cutting the sections sufficiently thin to enable EM to be performed, (2) mounting the sections on these small and delicate coverslips, (3) ensuring sections and carbon coating remained adherent to the coverslips during the antigen retrieval process, (4) ensuring optimal staining with four primary antibodies and three fluorochromes, and (5) visualising and mapping the desired cell. Primary cilia were identified within CD34+ cells in one sample, however, the sample was burnt during image capture, before the image had been sufficiently captured. In five samples, the process failed to produce an evaluable specimen

either due to distorted cell architecture (n=2), inadequate fixation - the sample therefore moving under the microscope precluding image capture (n=1) or poor staining quality / significant auto fluorescence (n=2). In two instances, no cilia were identified. For these reasons despite the process being performed on eight samples no images are available.

We had shown primary cilia to be present within the BM, and satisfied ourselves they were present on haematopoietic cells. We therefore sought to determine whether they were present on haematopoietic cells within the circulatory system. ICC was performed on bulk AML MNCs (n=3), normal bulk PB MNCs (obtained by venepuncture (n=3)) and normal FACs sorted cell populations. The following populations were sorted, stained and analysed: uncommitted early progenitor / SC (CD34+, n=2), myeloid - intermediate (CD33+, n=2) and mature (CD11b+, n=3) and lymphoid - T (CD3+) and B (CD19+) (both n=3). In addition, ICC was performed on seven selected, genetically diverse AML cell lines including the KG1a cell line.

Whilst the cytoskeleton was clearly and beautifully demonstrated, and in cases the centrosome and mitotic spindle, primary cilia were not identified within our AML cell lines, AML or normal MNCs or selected populations, Figure 3.2.2.3. The presence of primary cilia on haematopoietic cells within the BM microenvironment and absence on 'circulating' or 'suspension' cells suggests, as we had hypothesised, that primary cilia are lost once haematopoietic cells mature and migrate from the BM microenvironment. Excitingly, the absence of primary cilia, and thus the machinery to enable canonical Hh signalling, on mature / maturing haematopoietic cells potentially explains the differential results seen *in vitro* and *in vivo*, and further the relative sparing of haematopoietic toxicity in clinical trial.

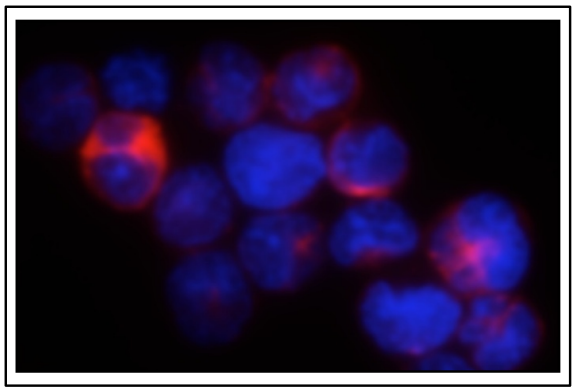

Figure 3.2.2.3: Representative ICC images at x100 magnification depicting an absence of primary cilia in circulating haematopoietic cells.
ICC was performed on normal PB MNCs sorted by FACS (n=3), seven genetically diverse AML cell lines and 3 primary, de novo AML MNC samples. The normal and AML samples were sorted to enable analysis of the following populations: uncommitted early progenitor / SC (CD34+, n=2), myeloid - mature (CD11b+, n=3) and intermediate (CD33+, n=2) and lymphoid - T (CD3+) and B (CD19+) (both n=3) populations were selected. Cells were fixed, permeabilised and stained with α- and γ-tubulin. Nuclei were stained with DAPI. Images were visualised with a Zeiss TS100 inverted microscope.
This representative image of mature CD11b+ myeloid cells clearly shows the absence of primary cilia. Primary cilia were absent from all of the sorted cell populations.

We acknowledge our data conflicts with that now published - Singh *et al*. reporting MNCs isolated from the PB and BM and AML cell lines (KG1, KG1a, and K562) possess primary cilia [566,611]. It is important to note experimental techniques were different – Singh *et al*. analysed PB and BM MNCs directly after isolation without culture, in contrast our samples were cultured for 24hrs prior to analysis. Further, whilst the fluorescence intensity profiles show acetylated α- and γ-tubulin to co-localise, it is important to note, as the authors do, the difference in the shape of the fluorescent signal of acetylated α-tubulin between the mouse embryonic fibroblasts (NIH3T3) used as a positive control and that demonstrated in the haematopoietic cells (PB and BM) and

AML cell lines. Within the NIH3T3 cells, the acetylated α-tubulin was seen as a long, thin projection, arising from the basal body. In contrast, within the primary MNCs (PB and BM) and AML cell lines, the primary cilia were seen to be shorter, the signal from each antibody less distinct.

Considering the identification of primary cilia within haematopoietic cells was challenging, we had determined strict criteria that needed to be fulfilled before we definitively recorded the signal as that of a primary cilium. Signal patterns as shown by Singh *et al.* would not, according to our criteria, derived following extensive review of published images, have been classified as primary cilia. On close inspection of the acetylated α-tubulin images for the PB MNCs the signal is composed of two distinct dots rather than a single tubular projection, the images being more consistent with those of a centrosome. Further, looking at the images for BM MNCs, whilst the acetylated α-tubulin signal appears as a single dot the images for γ-tubulin are significantly impaired by the degree of background signal. Considering the numerous roles acetylated α- and γ-tubulin play within the cell, it is important to establish whether these signals represent true primary cilia or, as shown in cytotoxic T lymphocytes [426], a modified cilium. Our discounted images were not dissimilar to those published by Singh *et al.* Interestingly however, whether true or modified, these organelles are shown to be functional, and haematopoietic cells utilising them to facilitate canonical (ligand-mediated) Hh signalling and pathway activity. Finally, the authors report the presence of primary cilia on virtually all PB and BM MNCs. This conflicts with work published in 2014 identifying primary cilia in approximately 1% of cells within the BM (though these cells were not studied in greater depth, and the work was performed in sheep) [610]. This frequency data is however, more in line with our data. Considering their, and our functional data presented in Chapter 4, perhaps these organelles do represent modified primary cilium and therefore an ongoing ability to respond to Smo inhibition, irrespective of stage of maturation / microenvironment. Whether primary cilia are, with time, accepted to be present on haematopoietic cells, and further those in the circulation or simply those within the BM niche is hugely exciting and remains to be determined.

3.3 To determine whether increased Hh activity resulted from activating mutations within Smo

3.3.1 Introduction

We had shown deregulated mRNA expression of components of the Hh pathway, with pathway activity evidenced by *GLI-2* expression. In addition, we had demonstrated the Hh pathway to be deregulated at a protein level, GLI-1 being up-regulated within the BM microenvironment relative to normal controls in keeping with increased pathway activity. In addition, circulating SHH was demonstrated following analysis of serum from a cohort of AML subjects. Whilst the median concentration was comparable to that demonstrated in normal control subjects, marked variation was observed within the AML cohort indicating an importance, possibly reliance, in a subset of AML cases. These results do not, however, account for the increased Hh activity observed at both a gene and protein level. Constitutive pathway activation through gain-of-function mutations and epigenetic changes in the positive regulator Smo have been observed in a number of solid malignancies [370,371]. Whilst epigenetic modifications have been observed in a cohort of paediatric AML patients, correlating with disease status [372] mutations have not been identified in haematological malignancies [378]. Pathogenic missense mutations in exon 9 and 10 of the *SMO* gene have been demonstrated in BCCs [367]. Further an insertion mutation in exon 1 and missense mutations in exons 9 and 12 of the *SMO* gene have been found in gastric tumours, though these do not appear to be driver mutations [617]. We therefore sought to determine if a mutation or mutations within *SMO* could be responsible for our findings.

3.3.2 Sanger sequencing did not identify a mutation in *SMO* to account for the increased activity in this cohort

Our data, as discussed in the preceding sections, and that published by others [378,381,382,618], clearly shows the Hh pathway to be deregulated in AML. We therefore considered whether a gain-of-function mutation within Smo might account for the increased activity. No mutations had been identified in haematological malignancies, we therefore chose to sequence each of the twelve exons rather than adopt a targeted approach. Once optimised Sanger sequencing was performed on an unselect cohort of primary *de novo* human AML samples (n=36). This work was performed in collaboration with Dr E Dobbin to whom I am indebted for her time, knowledge and expertise.

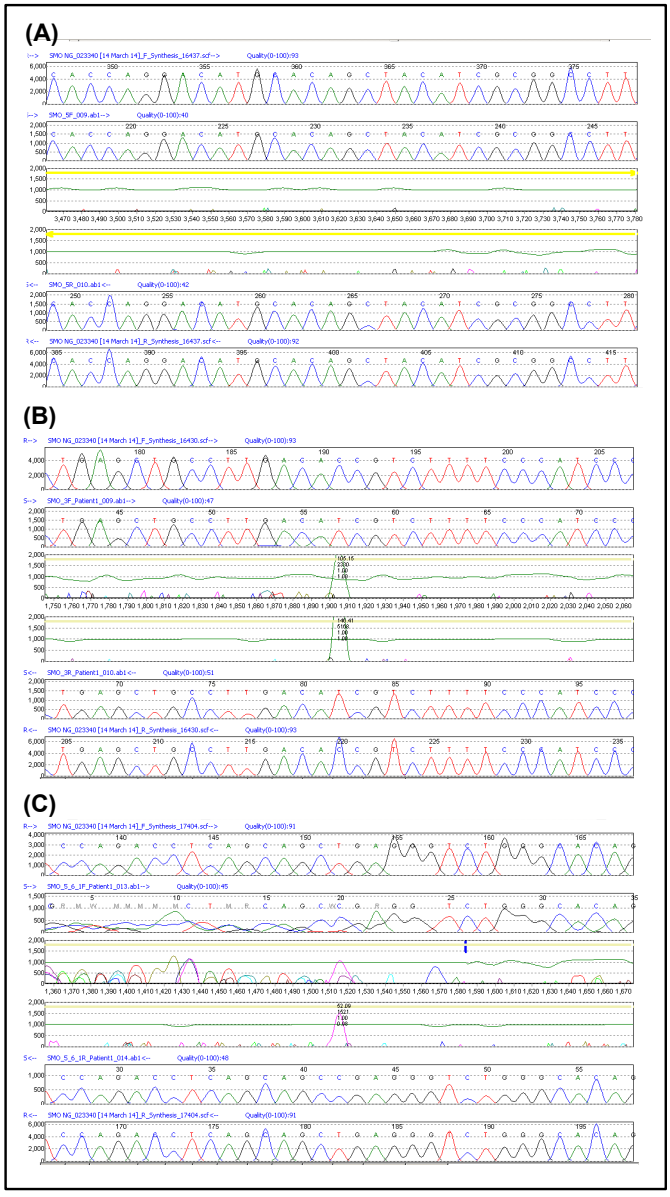

Figure 3.3.2.1 A: Representative Sanger sequencing chromatographs.
Sanger sequencing was performed on an unselected cohort of primary, *de novo* human AML samples (n=36). Each of the twelve exons of *SMO* were sequenced. Select chromatographs are shown, in each case the wild-type sequence (wt) is depicted at the top.
(A) No abnormality, (B) 920+79C>T Intron 4 dbSNP rs2075778 Reference 1000 Genomes Project, clean preparation, (C) 921-84 T>C Intron 4 dbSNP T>C rs2075779 Reference 1000 Genomes Project, poor preparation but still analysable.

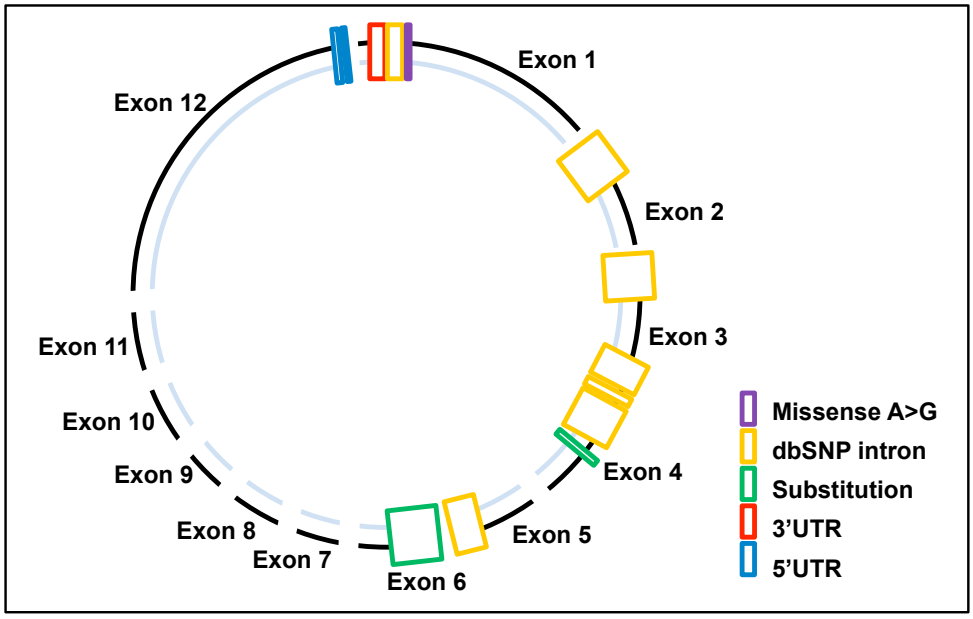

Figure 3.3.2.1 B: Schematic highlighting the type and position of genetic abnormalities in *SMO* in an unselected cohort of primary, *de novo* human AML samples (n=36).
Sanger sequencing was performed to obtain full length coding sequences in a cohort of 36 *de novo* primary human AML samples. The COSMIC database served as mutation reference. Data is diagrammatically represented showing type, position and frequency of genetic abnormalities. The missense mutation was classed as C0 by Align GV, and predicted to be tolerated with a score of 0.81; substitution mutations were synonymous variants.
A mutation was not identified however in keeping with the genetic instability and heterogeneity of AML all samples contained single nucleotide polymorphisms (SNPs) with an average of 4 SNPs detected per sample (range 1-7); the effects of these variants are unknown.

We did not identify a somatic mutation in *SMO* using the COSMIC database as mutation reference in our cohort by Sanger sequencing, Figures 3.3.2.1A&B. In keeping with the genetic instability and heterogeneity of AML, a number of silent and missense mutations were identified (mean 1; range 1-3). All samples were shown to contain single nucleotide polymorphisms (SNPs) (mean 4; range 3-8), though the effects of these SNPs are unknown and deserve further consideration. Whilst we are reluctant to conclude an absence of mutations within *SMO* in AML due to our cohort size we also recognise mutations, albeit at a low level, were identified in a cohort of 39 histologically variable gastric tumors [617]. Additionally, paired RNA / protein and DNA samles were not available precluding correlation with Smo expression and pathway deregulation, this is an area we believe worthy of further investigation – 'is *SMO* the driver of Hh deregulation?'

Looking at those malignancies within which *SMO* mutations have been identified, it is important to recognise the frequency is low in most – within a carefully defined subset of medulloblastomas, recognised to have aberrant Hh activity termed 'sonic-hedgehog-driven medulloblastoma', mutations average approximately 15% [619] whilst the frequency within gastric malignancies is reported as approximately 5% [617]. Further, whilst the frequency within BCC has been reported at up to 50%, this is in those cases demonstrating resistance to Smo inhibitors [620], thereby considered a selected population. It is important therefore to consider our study may have been insufficiently powered to detect a mutation considering the intrinsic heterogeneity of AML

3.4 To determine the association of the Hh pathway on prognosis in AML

3.4.1 Introduction

We had shown components of the Hh pathway to be deregulated at a gene level, in keeping with published data [378,381,382,618], and at a protein level; with pathway activity again demonstrated at both a gene and protein level. In addition, we had shown haematopoietic cells possess primary cilia, enabling canonical Hh signalling within the BM microenvironment. We therefore questioned whether deregulation of components of this pathway had prognostic implications. A number of groups have published on the negative impact of *GLI-2*, and to a lesser extent *GLI-1* [378,381,382]; with a significant association being reported between *GLI-2* and the poor prognostic marker FLT3-ITD [325,378,382]. The impact of other members of the pathway remains to be determined, though co-expression of *SMO* (p=ns) and *GLI-1* (p=0.002) has been shown in *GLI-2* expressers suggestive of canonical pathway activation [378]. The influence of Hh signalling on disease phenotype and, consequently clinical outcome, however remains to be determined. We therefore sought to correlate our expression data with patients' baseline characteristics and clinical outcome.

3.4.2 Genes associated with a poor prognosis were up-regulated in our cohort of samples with high expression of *SMO*

We considered whether, on considering the wide range of downstream targets of the Hh signalling pathway, we could identify a gene expression profile specific to those samples with up-regulated *SMO*. In this respect, whilst there is considerable evidence to support the role of the Hh signalling pathway in AML [69], and its correlation with the FAB classification M4 phenotype [379] and FLT3-ITD mutation [325,378,382] the impact of pathway deregulation on downstream targets and other SC pathways is unknown. A >100-gene signature encompassing a wide range of downstream targets was therefore studied. We selected members of the self-renewal pathways and key downstream targets following a literature review inclusive of both solid and haematological malignancies. Genes selected included the ABC transporters, those involved in 'intrinsic' cell death, cell cycle regulators, components of the BMP, EMT, Notch, TGFß and Wnt pathways, DNA methyltransferases, pluripotency regulators, proteases, transcription factors and tyrosine kinases. Expression was calculated as $2^{-\Delta\Delta CT}$, allowing comparison of levels of mRNA expression between primary AML samples. Samples were classified according to *SMO* expression (high expressers defined as those with a ≥5-fold increase in *SMO* relative to normal MNCs). Gene expression within this cohort was compared to that demonstrated in those AML samples demonstrating a <5-fold change in *SMO* relative to normal MNCs (n=50); Figure 3.4.2.1. We required a gene to be expressed in > 10 samples within each cohort to be considered in our analysis. Expression values were excluded if there was a greater than 1.5CT difference between technical triplicates or two of the technical triplicates failed in either the AML or comparator (normal) sample.

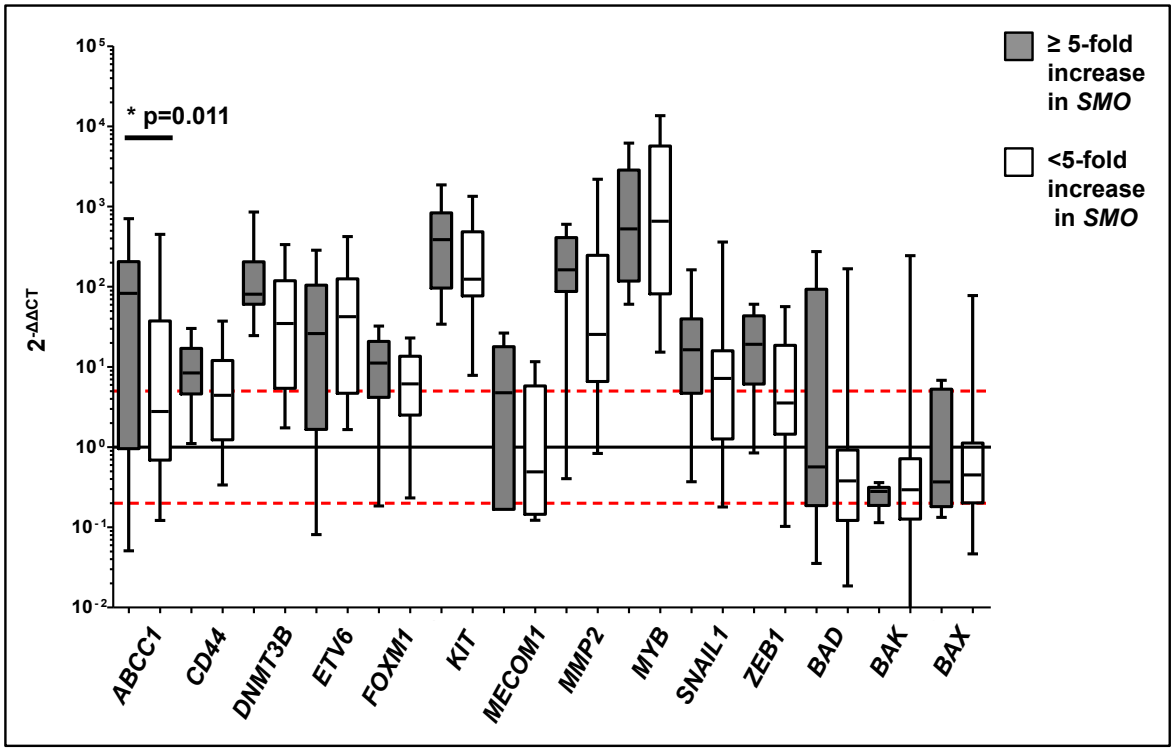

Figure 3.4.2.1: Expression of genes associated with chemoresistance, and poor survival, according to *SMO* expression.
RNA was made from cells harvested following culture for 24hrs. Expression levels were quantified by qRT-PCR using Fluidigm® technology. mRNA expression levels are shown as the fold change ($2^{-\Delta\Delta CT}$) relative to the mean of 10 normal MNC samples with 6 housekeeping genes – *ATP5S, B2M, ENOX2, GAPDH, TYWI* and *UBE2D2* serving as endogenous control. A ≥ 5-fold change relative to normal MNCs (n=10) was categorised as high *SMO* expression. The red lines indicate a 5-fold change. Results are depicted in a box and whisker plot showing median, min and max values.
In addition to the up-regulation of these genes in AML relative to normal MNCs this graph shows the median expression of *CD44, DNMT3B, FOXM1, KIT, MECOM1, MMP2, SNAIL1* and *BAD* to be increased in *SMO* high expressers compared to those demonstrating a <5-fold change in *SMO* relative to normal MNCs. The unpaired t test with Welch's correction demonstrated a statistical significant difference in the expression of *ABCC1* (p=0.011).

There was a >5-fold up-regulation of genes associated with chemoresistance and poor survival in both high and low *SMO* expressing patients relative to our normal cohort. These genes included *ABCC1, CD44, DNMT3B, ETV6, FOXM1, KIT, MECOM, MMP2, MYB, SNAIL1* and *ZEB1*. Further, there was a 4-5-fold reduction in the pro-apoptotic genes *BAK, BAX* and *BAD*. These genes are associated with (1) determining cell behaviour / fate (*FOXM1, KIT, MECOM* and *ZEB1*) (2) chemoresistance (*ABCC1, DNMT3B, KIT, MMP2, SNAIL1* and *ZEB1*) and (3) poor prognosis (*CD44* and *ZEB1*). There was a statistically significant difference in the expression of *ABCC1* (p=0.011), using the unpaired t-test with Welch's correction, between the two cohorts with expression greater in the *SMO* high expressers. Interestingly patients with high levels of *SMO* expression also demonstrated higher levels of *CD44, ZEB1* and *SNAIL1* when compared to the low *SMO* expressing patients. *CD44, ZEB1* and *SNAIL1* are linked to EMT transition, with high *CD44* expression correlating to lower overall survival in AML [590]. The absence of a statistical significance was considered to reflect the degree of variance between samples, and sample size.

It is important to consider a couple of noteworthy observations in greater detail. Published data has shown *NUMB* to be increased in the absence of Smo and, to show an upward trend following pharmacological inhibition of Smo [252]. Our data shows *NUMB* to be decreased in AML relative to our normal cohort. Further there was a difference though this was not statistically significant between our two cohorts of AML with a 2-fold reduction in *NUMB* in patients with high levels of *SMO* expression and a 4-fold reduction in the low *SMO* expressing patients, Figure 3.4.2.2.

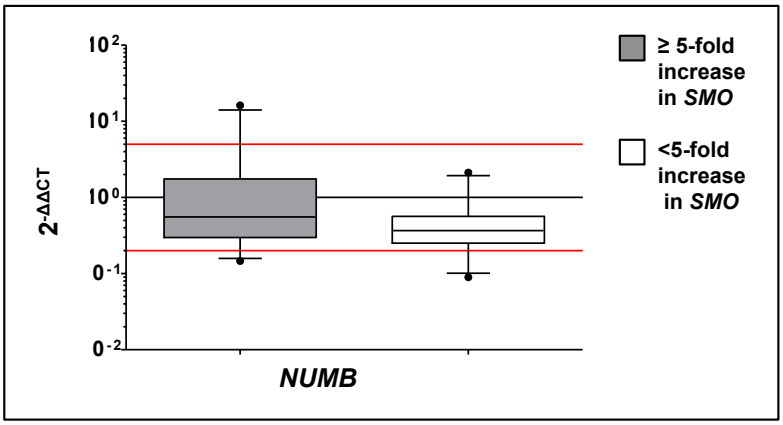

Figure 3.4.2.2: Expression of *NUMB* according to *SMO* expression.
RNA was made from cells harvested following culture for 24hrs. Expression levels were quantified by qRT-PCR using Fluidigm® technology. mRNA expression levels are shown as the fold change ($2^{-\Delta\Delta CT}$) relative to the mean of 10 normal MNC samples with 6 housekeeping genes – *ATP5S*, *B2M*, *ENOX2*, *GAPDH*, *TYWI* and *UBE2D2* serving as endogenous control. A > 5-fold change relative to normal MNCs (n=10) was categorised as high *SMO* expression. The red lines indicate a 5-fold change. Results are depicted in a box and whisker plot showing median, min and max values showing *NUMB* was increased in high *SMO* expressers though this was not significant.

Additionally, *HOXA3* and *HOXA9* were up-regulated within patients with high levels of *SMO* expression relative to the low *SMO* expressing patients though this was not significant, Figure 3.4.2.3. The HOX genes are recognised to play a significant role in haematopoiesis [591], with aberrant expression extensively reported in AML and implicated in the process of malignant transformation [592]. Further, an association between the Hox genes and Hh signalling pathway has been reported [593], both involved in the process of development and cellular patterning. Whilst an association between aberrant Hh signalling and members of the Hox family might therefore be anticipated, it is interesting to consider the role of these expression changes in the malignant transformation process.

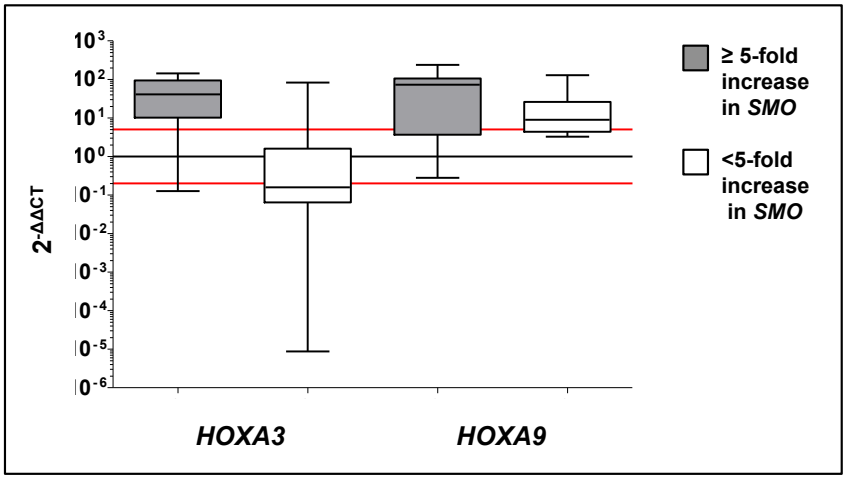

Figure 3.4.2.3: Expression of *HOXA3* and *HOXA9* according to *SMO* expression.
RNA was made from cells harvested following culture for 24hrs. Expression levels were quantified by qRT-PCR using Fluidigm® technology. mRNA expression levels are shown as the fold change ($2^{-\Delta\Delta CT}$) relative to the mean of 10 normal MNC samples with 6 housekeeping genes – *ATP5S*, *B2M*, *ENOX2*, *GAPDH*, *TYWI* and *UBE2D2* serving as endogenous control. A > 5-fold change relative to normal MNCs (n=10) was categorised as high *SMO* expression. The red lines indicate a 5-fold change. Results are depicted in a box and whisker plot showing median, min and max values showing HOXA3 and HOXA9 to be up-regulated in SMO high expressers relative to those with a <5-fold increase in SMO relative to our normal cohort, though the result was not significant.

3.4.3 Increased *SMO* correlated with an increase in high-risk stratification and poor prognostic features

Caldicott approval was obtained prior to hospital records being accessed. Patient demographics, baseline disease characteristics, treatment and clinical outcomes, where available, were recorded for each AML sample analysed, Appendix 1. Of the 76 samples we studied, clinical data was available for 56 samples (73.7%). Samples were classified according to *SMO* expression, with high expressers defined as those with a ≥5-fold increase in *SMO* relative to normal MNCs. 26 of our cohort of 76 (34.2%) were stratified as high expressers. Clinical data within this cohort was compared to the cohort of AML samples demonstrating a <5-fold change in *SMO*.

There was no significant difference between patient demographics (sex and age at diagnosis) between the two cohorts. Considering published data, we considered the FLT3-ITD mutation status of our cohort of *SMO* high expressers. The FLT3-ITD mutation was reported in 5 *SMO* high expresser samples (19.2%), and 7 demonstrating a <5-fold change in *SMO* (26.7%). Whilst these results are in keeping with published data, FLT3-ITD mutations being reported in 15-36% of cases depending on AML subtype [180,188,195,621-623] the result was not as we had expected. We had hypothesised FLT3-ITD would be present at a higher frequency in *SMO* high expressers considering FLT3-ITD has been linked to aberrant Hh signalling [381,382]. Interestingly however, there was an increase in the percentage of patients classified as Internediate-2 (high risk) according to the ELN Prognostic scoring system [1], Figure 3.4.3.1

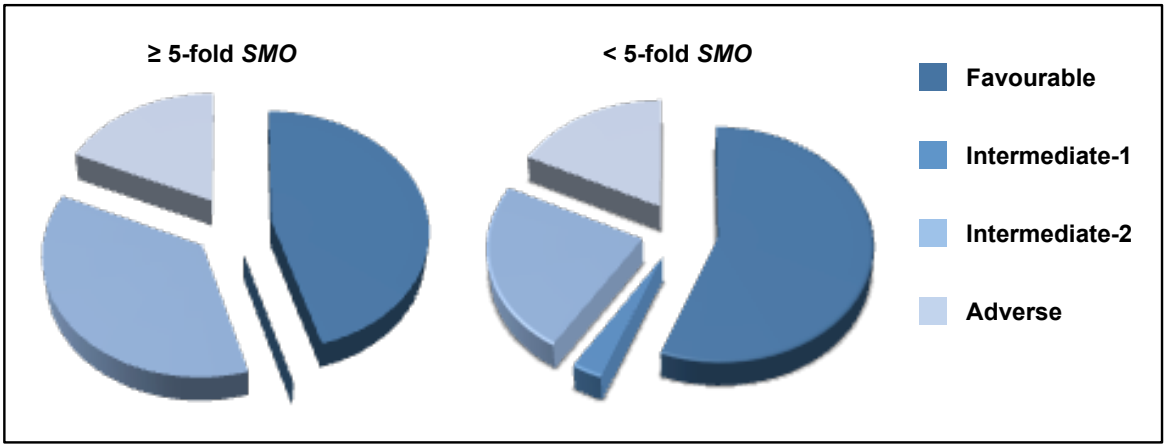

Figure 3.4.3.1: 'Risk', according to the ELN Prognostic system [1], according to *SMO* expression.

3.4.4 Next-generation sequencing confirmed an aggressive phenotype in those classified as *SMO* high expressers

Next-generation DNA sequencing has shown AML to be associated with, on average, five somatic mutations in recurrently mutated genes. Further, non-random, clonal chromosome aberrations are detectable in approximately 55% of AML cases, contributing to disease classification and treatment algorithms. 45% of cases however remain unclassified, leading to difficulties in risk stratification and treatment decisions [156,165]. In 2013, the Cancer Genome Atlas Research Network listed 23 significantly mutated genes in AML [583]. Following this a number of AML research gene panels have been commercially developed, two were used for this section of work: the Ion AmpliSeq™ and the Illumina TruSight® Myeloid panels. Different panels were used as this work was performed in conjunction with the development and evaluation of sequencing services within haematological malignancies within NHS Lothian (Ion AmpliSeq™) and NHS Greater Glasgow and Clyde (Illumina TruSight®).

The Ion AmpliSeq™ covers 19 genes, 14 described by the Cancer Genome Atlas Research Network [583]. In contrast, the Illumina TruSight® Myeloid panel covers 54 genes, 15 in their entirety and an additional 39 targeted to cover oncogenic hotspots. Analysis was performed using Alamut, a software application designed to interpret medical genetic variants. This system integrates data (protein annotations, mutations, polymorphisms and conservation information) from public sources enabling users to study the effects of genetic variants on transcription, splicing and translation. 47 samples were sequenced, 30 by Ion AmpliSeq™. 18 of the 47 samples (38.3%) were classified as *SMO* high expressers, 15/47 (31.9%) demonstrated a <5-fold increase in *SMO* relative to normal MNCs. Gene expression was not available for 14 of the 47 samples (29.8%).

In keeping with AML, marked genetic heterogeneity was demonstrated, with a mean of 4.7 publically documented pathogenic mutations detected by the Illumina TruSight® Myeloid panel (range 1 to 8), and a mean of 1.7 detected by Ion AmpliSeq™ (range 0 to 4). Mutations, and the number of samples within which they were detected are depicted in Figure 3.4.4.1. Those genes / oncogenic hotspots in which no abnormality was found are not shown.

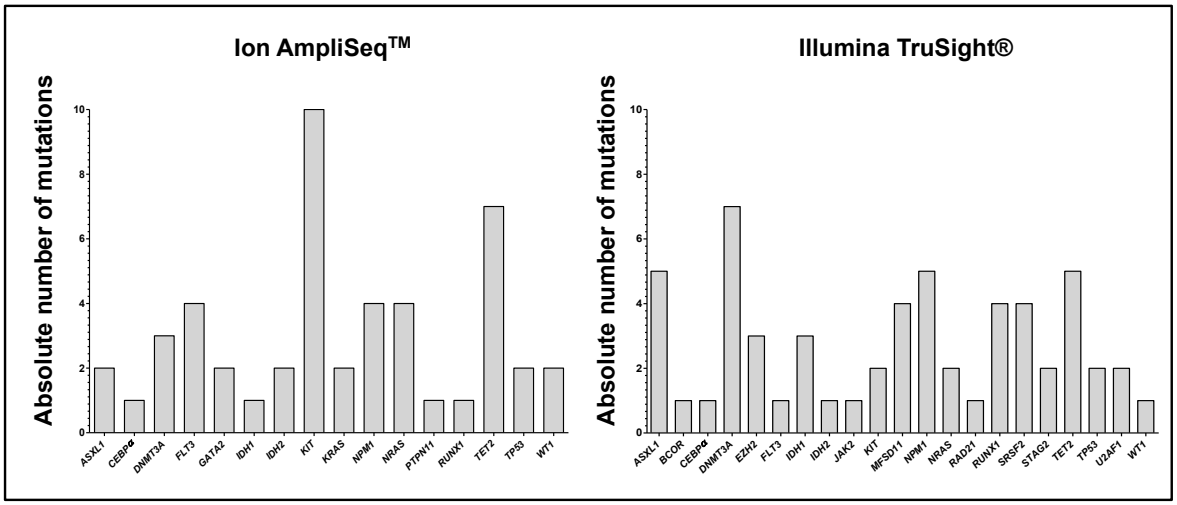

Figure 3.4.4.1: Spectrum, and absolute number, of pathological somatic mutations in a cohort of primary, *de novo* AML samples according to sequencing panel.
Ion AmpliSeq™ covers 19 genes, 14 described by the Cancer Genome Atlas Research Network [582]. In contrast the Illumina TruSight® Myeloid panel covers 54 genes, 15 in their entirety and an additional 39 targeted to cover oncogenic hotspots. Analysis was performed using Alamut. 47 samples were sequenced, 30 by Ion AmpliSeq™. In keeping with AML marked genetic heterogeneity was demonstrated, with a mean of 4.7 pathogenic mutations detected by the Illumina TruSight® Myeloid panel (range 1 to 8), and a mean of 1.7 detected by Ion AmpliSeq™ (range 0 to 4).

All 47 samples were shown to contain SNPs with a mean of 8.2 SNPs detected by the Illumina TruSight® Myeloid panel (range 5 to 13), and a mean of 10.2 detected by Ion AmpliSeq™ (range 7 to 17), Figure 3.4.4.2. The marked difference in mutation frequency is explained by the variant number of targets of each panel; whilst the variance in SNP concordance also reflects analytical differences including read depth and frequency parameters and filters such as the inclusion / exclusion of synonymous and intronic SNPs.

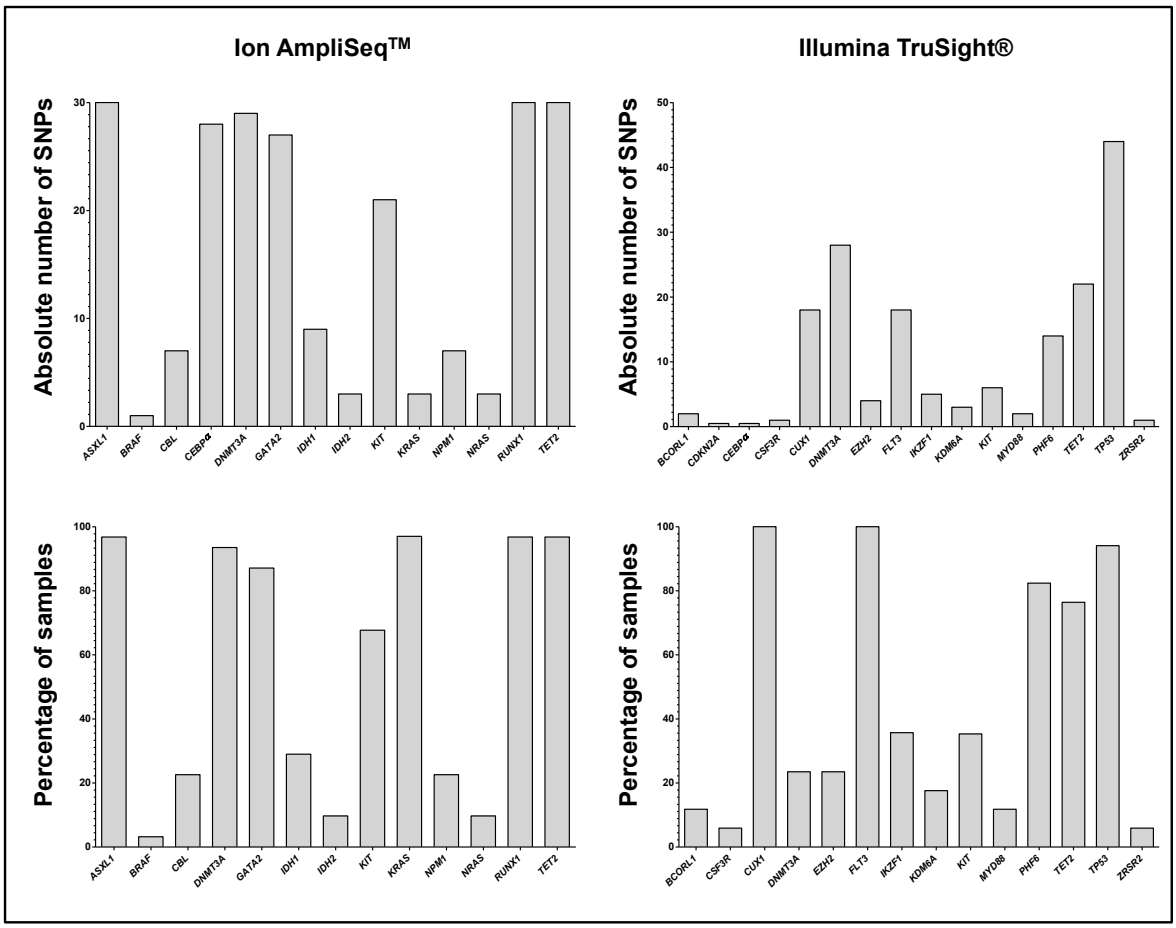

Figure 3.4.4.2: Spectrum, and absolute number, of SNPs and percentage of cases expressing SNPs according to sequencing panel.

Ion AmpliSeq™ covers 19 genes, 14 described by the Cancer Genome Atlas Research Network [582], the Illumina TruSight® Myeloid panel covers 54 genes, 15 in their entirety and an additional 39 targeted to cover oncogenic hotspots. Analysis was performed using Alamut. 47 samples were sequenced. In keeping with AML marked genetic heterogeneity was demonstrated. All 47 samples were shown to contain SNPs with a mean of 8.2 SNPs detected by the Illumina TruSight® Myeloid panel (range 5 to 13), and a mean of 10.2 detected by Ion AmpliSeq™ (range 7 to 17). The marked difference in mutation frequency is explained by the variant number of targets of each panel; whilst the variance in SNP concordance also reflects analytical differences including read depth and frequency parameters and filters such as the inclusion / exclusion of synonymous and intronic SNPs.

Considering those in which *SMO* expression data was available, marked genetic heterogeneity was demonstrated, Figure 3.4.4.3. Whilst a genetic pattern was not demonstrated we found *DNMT3A*, associated with an inferior outcome [320,624], to be present in 25% (4/16) of *SMO* high expressers compared to 6.7% (1/15) in those with a <5-fold increase in *SMO* relative to normal MNCs (p=0.0006). This is particularly interesting considering research showing synergy between sonidegib and vismodegib and azacitidine, and an RNA interference screen which identified several HDAC sensitiser genes including components of the Hh pathway [413]. Additionally, *EZH2, FLT3, GATA2, IDH2, MFSD11, NPM1, NRAS, RUNX1, SRSF2, TET2, TP53* and *WT1* mutations were more frequent in *SMO* high expressers, expression patterns were statistically significant for EZH2, NPM1, NRAS, TP53 (all p<0.0001) and TET2 p=0.015. Statistical analysis was performed using the Chi-Squared test.

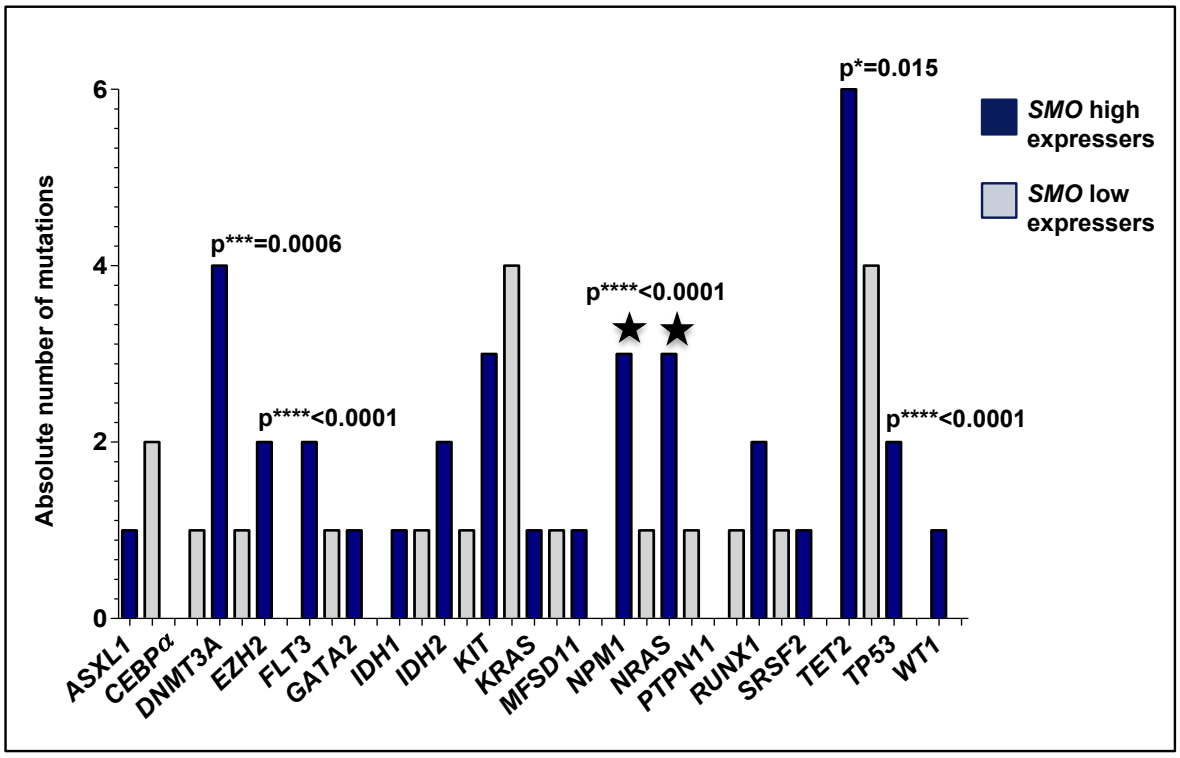

Figure 3.4.4.3: Spectrum, and absolute number, of mutations categorised according to SMO expression.
Samples were sequenced using the Ion AmpliSeq™ and the Illumina TruSight® Myeloid panel with analysis performed using Alamut. 47 samples were sequenced. Samples were categorised according to *SMO* expression. 16 were *SMO* high expressers and 15 demonstrated a <5-fold increase in *SMO* relative to normal MNCs. Gene expression was not available for 16 samples.
This graph shows the sequencing results for those in which *SMO* expression data was available. *DNMT3a* was present in 25% (4/16) of *SMO* high expressers compared to 6.7% (1/15) in those not classed as *SMO* high expressers (p=0.0006). *EZH2, FLT3, GATA2, IDH2, MFSD11, NPM1, NRAS, RUNX1, SRSF2, TET2, TP53* and *WT1* mutations were more frequent in *SMO* high expressers, expression patterns were statistically significant for EZH2, NPM1, NRAS, TP53 (all p<0.0001) and TET2 p=0.015 by the Chi-Squared test.

3.5 Discussion

AML encompasses a group of aggressive haematological neoplasms. It is a clinically, morphologically and genetically heterogeneous disease involving one or all of the myeloid lineages [150]. Within this heterogeneous disease genetic and morphological subtypes have been demonstrated. Published data has linked the Hh pathway both to those carrying the FLT3-ITD mutation and, interestingly, those classified morphologically as M4/5 according to the FAB classification system [381]. These associations are interesting in their clinical utility, being readily defined / detected, and further in their poor prognostic association, our increasing knowledge and understanding of AML suggesting the need for targeted therapies.

We have uniquely shown the Hh pathway to be deregulated at a gene and protein level, pathway activity evidenced by GLI-1 activity. Interestingly, we did not demonstrate a clear relationship between SMO, PTCH1 or the positive regulator GLI-1. It is important however to note that whilst we had analysed expression of GLI-1, we did not assess the expression of GLI-2 or GLI-3, an intricate relationship existing between these transcription factors and pathway activity. The expression of each transcription factor and their relationship with other components of the Hh pathway in our opinion deserves further evaluation. Further we recognise crosstalk exists between the self-renewal pathways, and whilst we had studied the expression of notable downstream targets, key upstream molecules such as members of the Ras/Raf/Mek pathway were not studied.

The lack of a relationship between a key regulator of pathway activity and the receptors SMO and PTCH1 caused us to question whether primary human haematopoietic cells within the BM microenvironment or circulatory system, or AML cell lines possessed primary cilia, and therefore the machinery to enable canonical Hh signalling. Whilst it is widely accepted that vertebrate canonical Hh signalling requires primary cilia [417] until recently haematopoietic cells have been considered to be among the few cells not to possess primary cilia [416,428]. Interestingly in 2013, emphasising the importance of a microtubular structure in enabling canonical Hh signalling, in the absence of a primary cilium the immunological synapse of T cells was shown to serve as a functional homolog of the primary cilium [426]. We hypothesised HSPCs possess primary cilia within the BM but that these organelles become defunct on cell maturation and migration into the PB. During the write up of this PhD, Singh *et al*. reported MNCs isolated from the PB and BM and AML cell lines (KG1, KG1a, and K562) posses primary cilia [566,611]; primary cilia were less frequent and often dysmorphic in the AML cell lines (KG1, KG1a, and K562) [566,611]. Importantly, these primary cilia were shown to be functional and play a role in Hh signalling. We too identified primary cilia in both normal and AML BMTs by ICC, further confirming the primary cilia structure through EM. In contrast however we did not identify primary cilia in PB AML or normal MNCs or AML cell lines. Whilst we have reservations regarding the images, questioning whether they might represent centrosomes rather than primary cilia, the evidence to show these structures are functional, involved in Hh signalling is hugely exciting. Whether primary cilia are, with time, accepted to be present on haematopoietic cells, and further those in the circulation or simply those within the BM niche remains to be determined.

Having shown deregulation of the Hh signalling pathway in AML, and the presence of primary cilia enabling canonical signalling in haematopoietic cells within the BM we considered the role of the Hh ligands. We found SHH to be significantly down-regulated in AML BMTs relative to normal BMTs. We considered whether the expression differences between AML and normal BMTs reflected different cellular composition. Whilst we acknowledge lymphocytes may comprise up to 20% of the normal BM population, with a marked reduction classically seen in AML due to the variable replacement of the normal BM population by blast cells we considered this part of the disease process and therefore important to include in our comparisons.

Considering the differential expression of SHH we analysed *HHAT*, the acetyltransferase responsible for post-translational modification of SHH, finding it to be significantly down-regulated in AML MNCs compared to normal MNCs. Within normal haematopoiesis *HHAT* expression increased with cell maturation, being lowest in HSCs. Further, we noted SHH to be located within the cytoplasm and nuclei of AML blast cells and interestingly, cells located within the colonic crypt bases, colonic tissue being our control material. This was particularly interesting since nuclear expression was not seen in normal BMTs, nor in colonic cells once they had migrated from the crypt base. Considering this data we hypothesised *HHAT*, and therefore SHH activity, was tightly regulated by SCs, potentially controlling canonical signalling and thus pathway activity. We sought to validate this hypothesis by analysing *HHAT* in colonic crypt bases relative to its expression in colonic villi apices, the crypt bases containing colon SCs, and the apices mature, differentiated daughter cells. Whilst the SC niche within the BM microenvironment is recognised it is not so clearly defined, nor identifiable within tissue. We therefore planned to use colon tissue, with its anatomically defined cell maturation as a model for pathway modulating processes within haematopoiesis. Ethical consent was obtained. Six frozen human colon sections were laser dissected. Four colonic crypt bases, and four colonic crypt apices were captured and processed for RNA. Unfortunately samples were destroyed prior to analysis. We plan to repeat this technically very interesting and challenging work in the future.

Pathway activity in the absence of ligand expression within the AML blast cell population led us to consider paracrine activity. Paracrine activity has been shown to determine pathway activity in mature B cell malignancies [364]. Whilst variation might be expected within a heterogeneous disease such as AML the concentration range was particularly interesting. The majority of AML

cases showed a similar expression pattern to our normal age matched control cohort; two samples were shown to be 4- and 10-fold greater. It is tempting to consider whether these results suggest a differential dependence and response, emphasising the importance of sample and subtype selection however this would need to be verified in a larger cohort. The results certainly raise interesting questions however. How does the serum concentration of SHH affect pathway activity? Can serum SHH be used as a biomarker for those cases with increased Smo and or Hh signalling, or to identify the cases most suited to the small molecule Smo antagonists. Particularly interesting is the question of how the serum SHH concentration correlates with SHH with the BM microenvironment given we had shown a statistically significant down-regulation of SHH within AML BMTs. Further if this data is considered in parallel to preliminary data showing stromal cell sensitivity to Smo antagonism to vary depending upon confluence discussed in section 6 could the hypercellular nature of AML inhibit stromal Hh activity? In an attempt to answer this we have begun work harvesting media from MSCs at varying confluence alone and following culture with cyclopamine to determine the impact on levels of secreted SHH. Further, we acknowledge this was a small cohort and plan to increase our numbers, and consequently the study power in the future. We would seek to perform paired analysis enabling correlation of SHH expression in AML BMTs and serum and SHH expression with pathway activity in our blast population.

The absence of a clear relationship between components of the Hh pathway and pathway activity led us to question whether, as in solid malignancies a gain-of-function mutation within Smo might account for the increased activity. An extensive literature search did not find any reports on mutational status within haematological malignancies. However, whilst a number of silent and missense mutations were identified a somatic mutation in *SMO* was not identified. Interestingly a number of SNPs were identified throughout *SMO* though the effects of these are unknown although one could speculate that given the number observed per sample that these might in some way influence protein stability. In the future we would seek to determine if a loss-of-function in *PTCH1* might explain the lack of a relationship between the receptors and pathway activity.

Finally whilst a correlation between *SMO*, clinical characteristics and prognosis was not identified we plan to look at the impact of other components. Interestingly *PTCH1* has been shown to confer a poor outcome in CML. It would therefore be interesting to look at the expression of *PTCH1* in BC-CML and further to contrast this to expression within primary *de novo* AML cases.

4 Hypothesis 'The Hedgehog signalling pathway represents a viable therapeutic target in AML'

4.1 To determine the effect of the Smo inhibitors, cyclopamine, sonidegib and glasdegib, on a diverse array of AML cell lines and primary AML MNCs *in vitro*

4.1.1 Introduction

Hh signalling is vital in the maintenance and expansion of the LSC in myeloid malignancies; serving either as a survival and proliferation signal or through direction of the LSC fate [252,344,375-377].

Work by the Copland group has already shown the Hh pathway to be deregulated in CML stem and progenitor cells. Further, using the clinical grade Smo inhibitor, LDE225 (sonidegib; Novartis Pharma) in combination with nilotinib (second generation TKI; Novartis Pharma), they were able to effectively eliminate CML stem and progenitor cells both *in vitro* and *in vivo* [254,412].

We have shown the Hh signalling pathway to be deregulated in an unselected cohort of primary *de novo* AML samples (Chapter 3) in keeping with published data [378,379,625]. However whilst the evidence of pathway deregulation is increasing, with aberrant signalling linked to drug resistance [349,377] and high levels of the transcription factors *GLI-1* and *GLI-2* shown to confer a poor prognosis [378,379,381,382] the relationship between the Hh pathway and AML, and further its role in disease pathogenesis, is not yet fully understood.

We sought to determine the effect of Smo inhibition in AML. We recognised the morphological, immunophenotypic, cytogenetic, and molecular heterogeneity of AML. We therefore selected seven, genetically diverse, AML cell lines (HL60, Kasumi-1, KG1a, MOLM-13, MV4-11, OCI-AML3 and THP-1). These cell lines were specifically chosen because they (1) carry high prevalence mutations, (2) are easily definable, (3) carry poor risk features or (4) published data indicated a link between characteristics of the chosen cell line and the Hh pathway. The following publically available datasets were analysed: GSE1159 [381], GSE13159 [565] and GSE9476 [382]. These datasets were selected because of the (1) number of samples analysed and, (2) cell populations studied. GSE1159 contains data from 285 AML patients, with data for 13,000 genes derived from PB or BM. Work published using this dataset identified 16 groups of patients on the basis of molecular signatures through **u**nsupervised cluster analyses, *GLI-1* shown to associate with *FLT3-ITD* and the FAB M4 phenotype [381]. GSE13159 presents whole-genome data from 2,096 PB or BM samples [565]. This work was undertaken to assess the clinical utility of gene expression profiling in the diagnosis and classification of myeloid and lymphoid malignancies. Referencing conventional classification definitions investigators reported an accuracy of 92% (median specificity 99.7%), confirmed using a prospective cohort of 1152 (95.6% median sensitivity, 99.8% median specificity) [626]. GSE9476 compares gene expression profiles between normal haematopoietic cells isolated from 38 healthy volunteers - CD34+ selected (n = 18), unselected BM (n = 10) and unselected PB (n = 10) and unselected blast cells from 26 AML patients [382]. Twenty genes were differentially expressed in AML relative to normal haematopoietic cells; expression changes for 13 of the 20 genes were confirmed using the GSE1159 dataset [382].

4.1.2 Components of the Hh signalling pathway are expressed in select AML cell lines and primary AML cells at both a gene and protein level

Components of the Hh pathway have been shown to be expressed in select AML cell lines, yet not in others [377,379,566]. We therefore first screened our chosen AML cell lines. Expression levels of the receptors *PTCH1* and *SMO*, the transcription factors *GLI1-3*, and the pathway modulators *PTCH2*, *SUFU* and *HHIP* were quantified by qRT-PCR using Fluidigm® technology. RNA was extracted from cells harvested in optimal growing conditions (resuspended in fresh media 24hrs before harvesting at a density of 2-3x10^5/ml). To account for input cDNA the ΔCT for each gene was calculated by subtracting the CT value of 6 housekeeping (control) genes from the CT recorded for the gene of interest. *ATP5S, B2M, ENOX2, GAPDH, TYWI* and *UBE2D2* were selected as housekeeping genes, CT values ranged from 3 to 13. To ensure accuracy of our results, samples were excluded where >2 genes failed due to technical reasons – poor technical triplicate, a signal was detected in the no template control (NTC) or the reaction failed by Fluidigm®. This stringency was applied to all gene expression analyses presented throughout this chapter. Expression is presented as $2^{-\Delta CT}$, allowing comparison of levels of mRNA expression between each cell line; Figure 4.1.2.1.

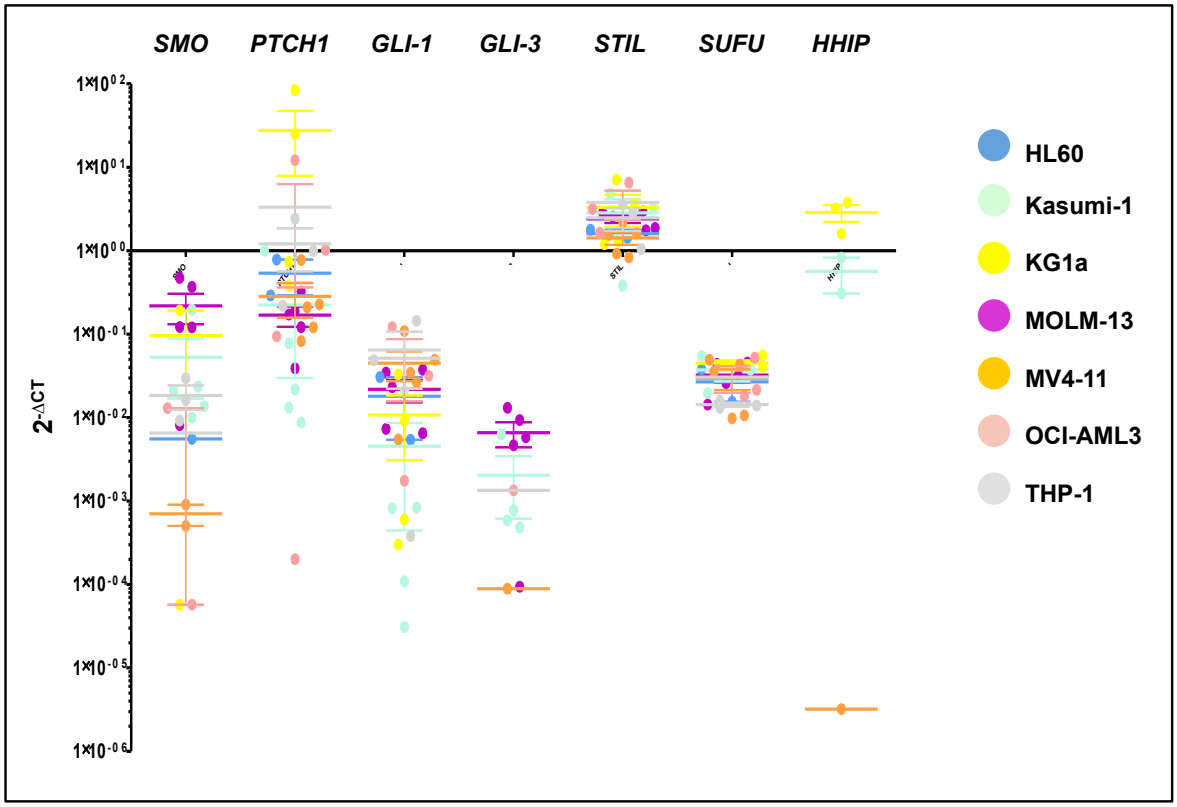

Figure 4.1.2.1: Variance in the mRNA expression of components of the Hh pathway in seven genetically diverse AML cell lines.
RNA was extracted from cells harvested in optimal growing conditions. Expression levels were quantified by qRT-PCR using Fluidigm® technology. Expression levels are shown as $2^{-\Delta CT}$, with 6 housekeeping genes –*ATP5S, B2M, ENOX2, GAPDH, TYWI* and *UBE2D2* serving as endogenous control; CT values for these genes ranged from 3 to 13. The mean of 3-5 samples are presented clearly demonstrating the variability in baseline expression between the cell lines. Error bars indicate SD.

Our chosen cell lines all had complex karyotypes. By FAB classification, four were myelomonocytic (MOLM-13, MV4-11, OCI-AML3 and THP-1). Additionally, two were CD34 expressing (Kasumi-1 and KG1a) and two carried the FLT3-ITD mutation (MOLM-13 and MV4-11). Despite these shared characteristics, striking differences were demonstrated. Of the components analysed; *SMO, PTCH1, GLI-1, STIL* and *SUFU* were expressed by all of our selected cell lines.

GLI-2 was universally not expressed. *GLI-3* was expressed by Kasumi-1, MOLM-13, MV4-11 and OCI-AML3; *HHIP* was expressed by Kasumi-1, KG1a and MOLM-13. It is interesting to note the presence of *GLI-3* in CD34+ Kasumi-1, yet its absence in the CD34+ KG1a cell line, and the expression of *HHIP* by the FLT3-ITD+ MOLM-13 cell line yet its absence in FLT3-ITD+ MV4-11 cell line indicating there is not a simplistic relationship between cell maturity or mutational status and the Hh pathway.

A notable difference in the expression of *SMO* was demonstrated between cell lines, with OCI-AML3 the highest expresser and MV4-11 the lowest. A less pronounced difference in the expression of *PTCH1* was demonstrated between cell lines, with KG1a the highest expresser and Kasumi-1 the lowest. All cell lines showed evidence of pathway activity with expression of *GLI-1*, though heterogeneity persisted with differences in expression seen between THP-1, the highest expresser, and Kasumi-1, the lowest. The absence of *GLI-2* is particularly interesting, if not perplexing, considering *GLI-1* and *-3* and other key members of the pathway were expressed. It would be interesting to investigate this further, to evaluate the presence or absence of *GLI-2* in our selected AML cells lines. Interestingly, there was minimal variance, across all cell lines, in the expression of *STIL* and *SUFU,* components functioning to determine pathway activity through their interactions with *GLI-1*. These results emphasise the need to carefully select potential subtypes of AML for targeted therapies and, when analysing and interpreting results, the importance of correlating functional responses to phenotype and genotype.

Cell lines serve as experimental models, enabling investigation and analysis of primary processes and the effect of manipulating molecular pathways. It is, however, well recognised that cell lines may not always behave in the same manner as, and not always accurately represent, primary cells [627]. Primary cell experiments are therefore required to validate cell line data. In this respect, we studied the expression of components of the pathway in normal CD34+ selected cells (BM CD34+ cells were purchased from stem cell technologies; PB CD34+ cells were isolated from normal donors following G-CSF stimulation and apheresis), normal bulk MNCs and an unselected cohort of 76 primary AML cases. Whilst expression in our normal and primary *de novo* AML cohorts are presented in section 3.1.2 here we consider the differential expression between these cohorts and our selected AML cell lines. RNA was extracted from cells harvested following culture for 24hrs; a standardised approach was adopted to minimise confounding factors. Expression is presented as $2^{-\Delta CT}$, enabling comparison of expression levels; Figure 4.1.2.2.

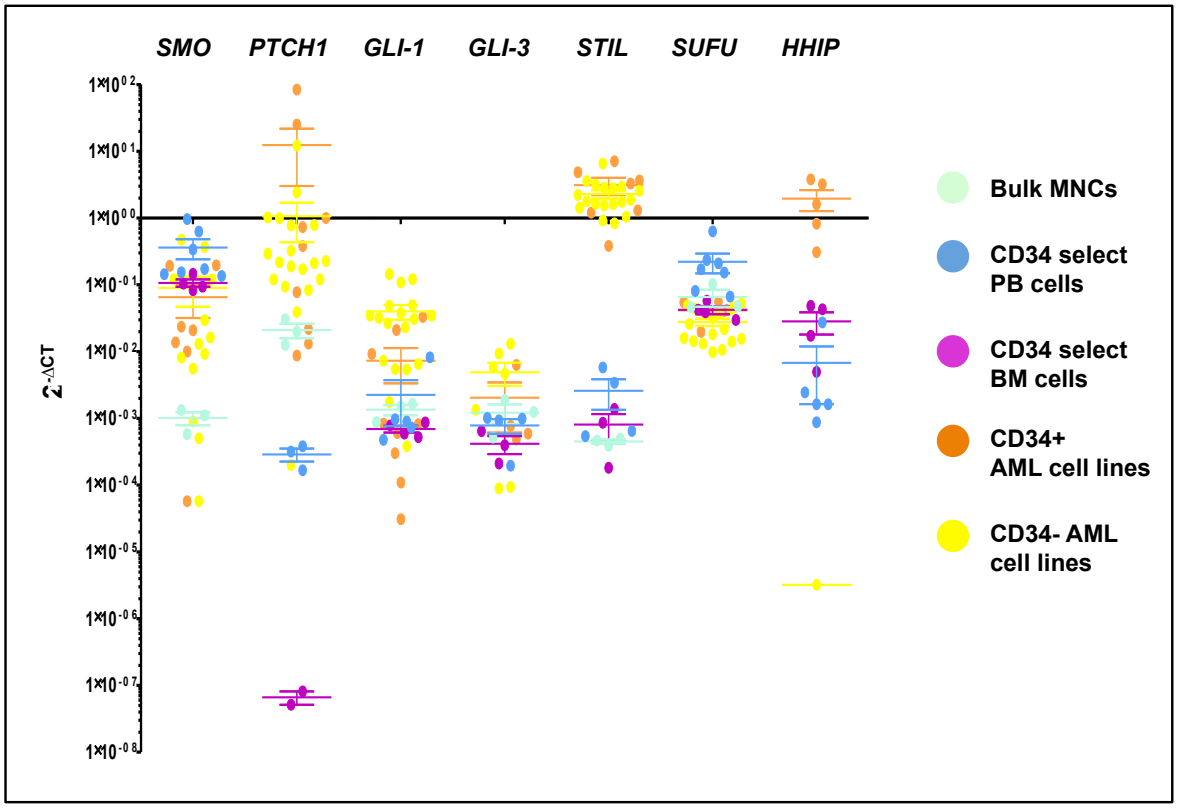

Figure 4.1.2.2: Variance in the mRNA expression of components of the Hh pathway between normal bulk MNCs, CD34+ selected PB and CD34+ selected BM cells.
PB CD34+ cells were harvested by G-CSF stimulated apheresis and CD34+ BM cells purchased from Stem Cell Technologies. RNA was extracted from cells harvested following culture for 24hrs. Expression levels were quantified by qRT-PCR using Fluidigm® technology. Expression levels are shown as $2^{-\Delta CT}$, with 6 housekeeping genes – *ATP5S*, *B2M*, *ENOX2*, *GAPDH*, *TYWI* and *UBE2D2* serving as endogenous control. 3-5 samples were analysed, where the number does not reach this data has been excluded for technical reasons to ensure accuracy. Error bars indicate SD.
This graph clearly shows expression to differ between normal cell populations and AML cell lines for select genes. Interestingly, irrespective of CD34 status, expression of *SMO* within the AML cell lines is comparable to that of the CD34+ PB and BM normal samples whilst expression of *PTCH1* is closer to that seen in bulk MNCs and markedly different from expression within the CD34+ select cell populations.

Looking first at the mRNA expression within our normal cohorts and selected AML cell lines there were notable differences. Expression within the AML cell lines was more heterogeneous. *GLI-1* showed a trend towards up-regulation in our AML cell lines compared to normal cells, irrespective of CD34 status (p=ns). *STIL* and *HHIP* were universally down-regulated in normal cells (p=ns) relative to our selected AML cell lines. Interestingly, expression patterns for the CD34+ AML cell lines did not mirror those of our CD34+ normal cohorts (PB or BM). Irrespective of CD34 status, expression of *SMO* within our selected cell lines was comparable to that of the CD34+ PB and BM normal samples. Whilst expression of *PTCH1* was rather distinct it was closer to that demonstrated in bulk MNCs. This data suggests a differential expression of components of the Hh pathway in normal and malignant progenitor cell populations, accepting the limitations of comparing immortalised cell lines with primary patient samples.

A standardised approach was adopted since earlier experiments had shown marked variation in the mRNA expression of *SMO*, Figure 4.1.2.3. We considered a number of potential factors - passage number, cell density and time relative to media change. We therefore sought to remove any potential confounding factor bias from our results by controlling for these variables. The observed mRNA expression variance fits with the recognised synergistic relationship between the Hh pathway and cell cycle regulators and other pathways including the Notch pathway, which is subject to cis-inhibitory interactions [628]. It would be interesting to consider this in further detail in the future.

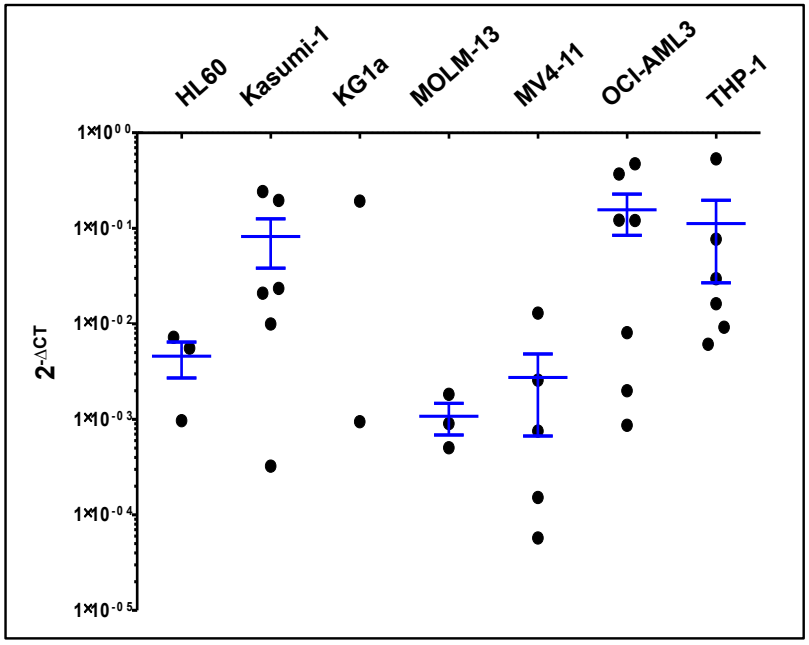

Figure 4.1.2.3: Expression of *SMO* in seven genetically diverse AML cell lines according to harvesting conditions.
RNA was extracted from cells harvested at variable density ($2x10^5$-$1x10^6$/ml), passage number (P2-7) and growing conditions (24-48hrs post media change). Expression levels were quantified by qRT-PCR using Fluidigm® technology. Expression levels are shown as $2^{-\Delta CT}$ with 6 housekeeping genes serving as endogenous control - *ATP5S, B2M, ENOX2, GAPDH, TYWI* and *UBE2D2*. Each data point represents the mean of a technical triplicate. The mean of 5-7 samples are presented with error bars indicating SD clearly demonstrating the variability in baseline expression both within and between the cell lines.

4.1.3 Manipulation of the Hh pathway by Smo inhibition with cyclopamine alters cell proliferation in select cell lines

Cyclopamine is a steroidal alkaloid, isolated from the American corn lily [629,630]. Its effects are caused by inhibition of the Hh pathway through direct inhibition of Smo. Whilst its poor solubility, stability, and moderate activity [631] has impeded its clinical development, a number of analogues have been developed which have progressed to clinical trial as discussed in section 1.4.5. Despite its limitations, however, it continues to be used in research to evaluate the effect of Hh pathway inhibition. Tomatidine, a steroidal alkaloid with structural similarity to cyclopamine, though unable to inhibit Smo, is used experimentally as a negative control [263], serving to give greater confidence that results generated are due to Smo inhibition rather than off-target effects.

We utilised the resazurin assay to determine the effect of a wide range of concentrations of cyclopamine on cell viability following culture for 72hrs for each of our chosen cell lines; Figure 4.1.3.1. A 72hr time point was chosen to allow sufficient time for an effect to be demonstrated, whilst minimising the risk of confounding factors such as nutrient exhaustion, altered environment (pH, electrolyte balance) due to apoptosing cells and cis- and trans- interactions due to increased cell density.

A 50% reduction in luminescence, taken as a crude measure of the half maximal inhibitory concentration (IC_{50}), was universally not seen at doses below 10μM, Figure 4.1.3.1. This is notably higher than that demonstrated following culture of the Gli-luciferase reporting $TM3^{(GLI\text{-}Luc)}$ cell line with cyclopamine for 72hrs, the IC_{50} falling between 5μM and 10μM (Figure 2.1).

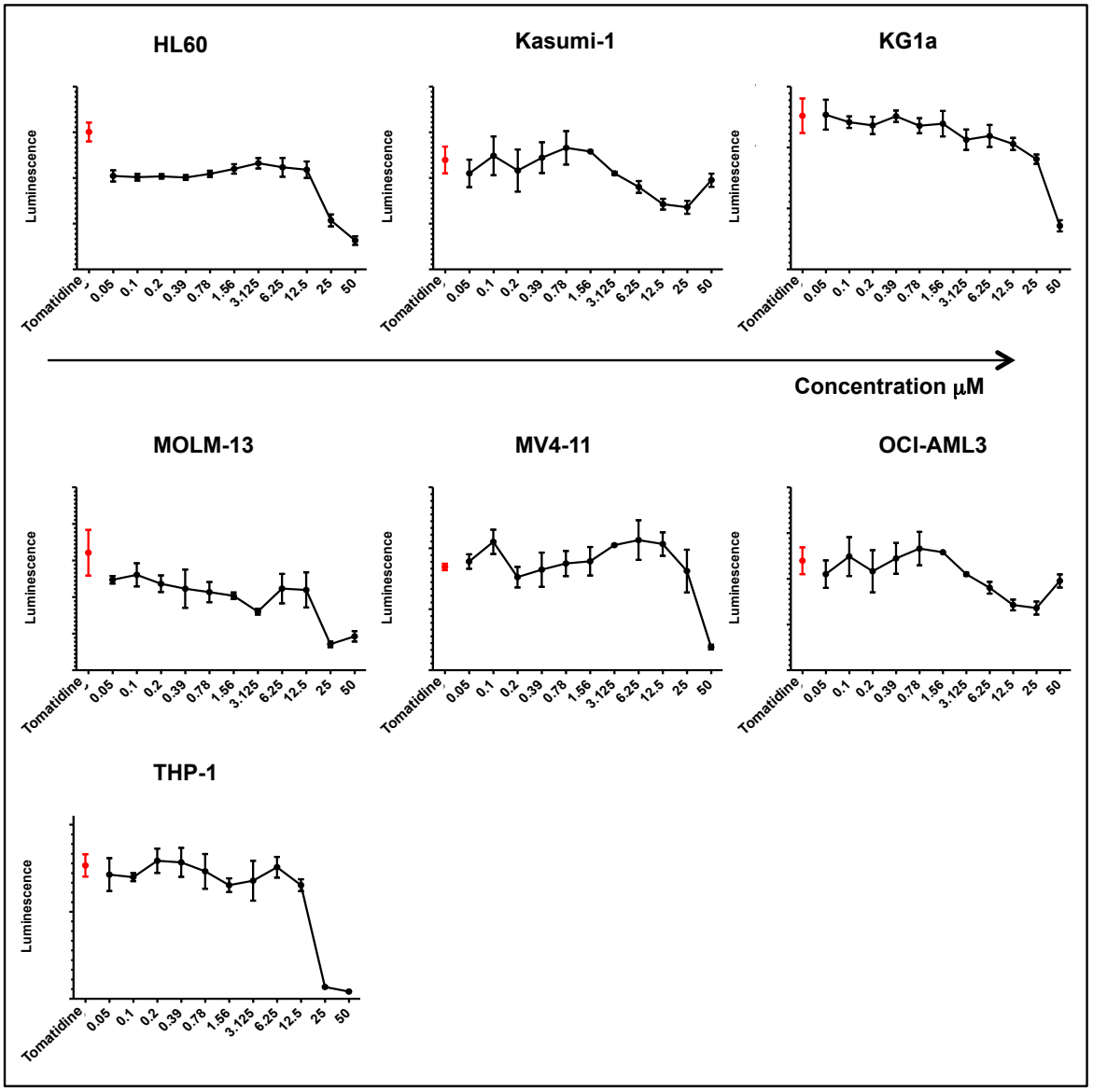

Figure 4.1.3.1: Metabolic activity as a measure of cell viability in seven genetically diverse AML cell lines following culture with incremental doses of cyclopamine (μM) as determined by the resazurin assay.
Cells, at a concentration of $1x10^5$/ml, were exposed to incremental doses of cyclopamine and cultured for 72hrs. Cell viability was determined using the resazurin assay. Results are expressed as the mean luminescence (n=4) with error bars indicating SD. Luminescence in the presence 20μM tomatidine is highlighted in red, serving as the NDC. Luminescence in the presence of tomatidine was comparable to that with media only. Notably, luminescence following culture of the Gli-luciferase reporting $TM3^{(GLI\text{-}Luc)}$ cell line with cyclopamine for 72hrs demonstrated a 50% reduction in luminescence between 5μM and 10μM.

Whilst Graphpad software can enable accurate calculation of the IC_{50}, we chose to record a 'rough range' for the IC_{50} for each cell line, Table 4.1.3.1. This approach was taken considering experimental design - the shape of the curves and limited data points above a concentration of 6.25μM calling into question the accuracy of the Graphpad extrapolated IC_{50} values. Expression of *SMO* did not affect cell response to cyclopamine.

Table 4.1.3.1 Cyclopamine IC_{50} values for our selected AML cell lines as determined by the resazurin assay

Cell line	IC_{50}
HL60	>12.5μM, <25μM
Kasumi-1	>25μM
KG1a	>25μM
MOLM-13	>12.5μM, <25μM
MV4-11	>25μM
OCI-AML3	>25μM
THP-1	>12.5μM, <25μM

Although no significant effect on cell viability was seen below 10μM we acknowledge the limitations of the resazurin assay in assessing the IC_{50}. We therefore elected to perform cell counts and assess cell viability by trypan blue dye exclusion at 24hrs, 48hrs and 72hrs in the genetically diverse Kasumi-1 and OCI-AML3 cell lines using a range of doses including those significantly below the approximated IC_{50}: NDC, 100nM, 1μM, 5μM, 10μM and 20μM to determine if cyclopamine had a time- or concentration-dependent effect on cell kinetics; Figure 4.1.3.2. 20μM as the maximum dose is in keeping with published work in haematological disease [377]. Further, work looking at dose- and route-dependent toxicity and pharmacokinetic profiles using naive female C57BL/6J mice at 12–16 weeks of age reported cyclopamine toxicity to be independent of Cmax or area under curve (AUC) values, with a Cmax of 19.9μM ± 3.15μM, and AUC of 59.6μM ± 4.4μM [631]. Lower doses were included given the self-renewal nature of the Hh signalling pathway, inhibition therefore not necessarily expected to result in apoptosis. These doses were determined by referencing the Gli-luciferase reporting $TM3^{(GLI\text{-}Luc)}$ cell line (Methods 2.2.1.4).

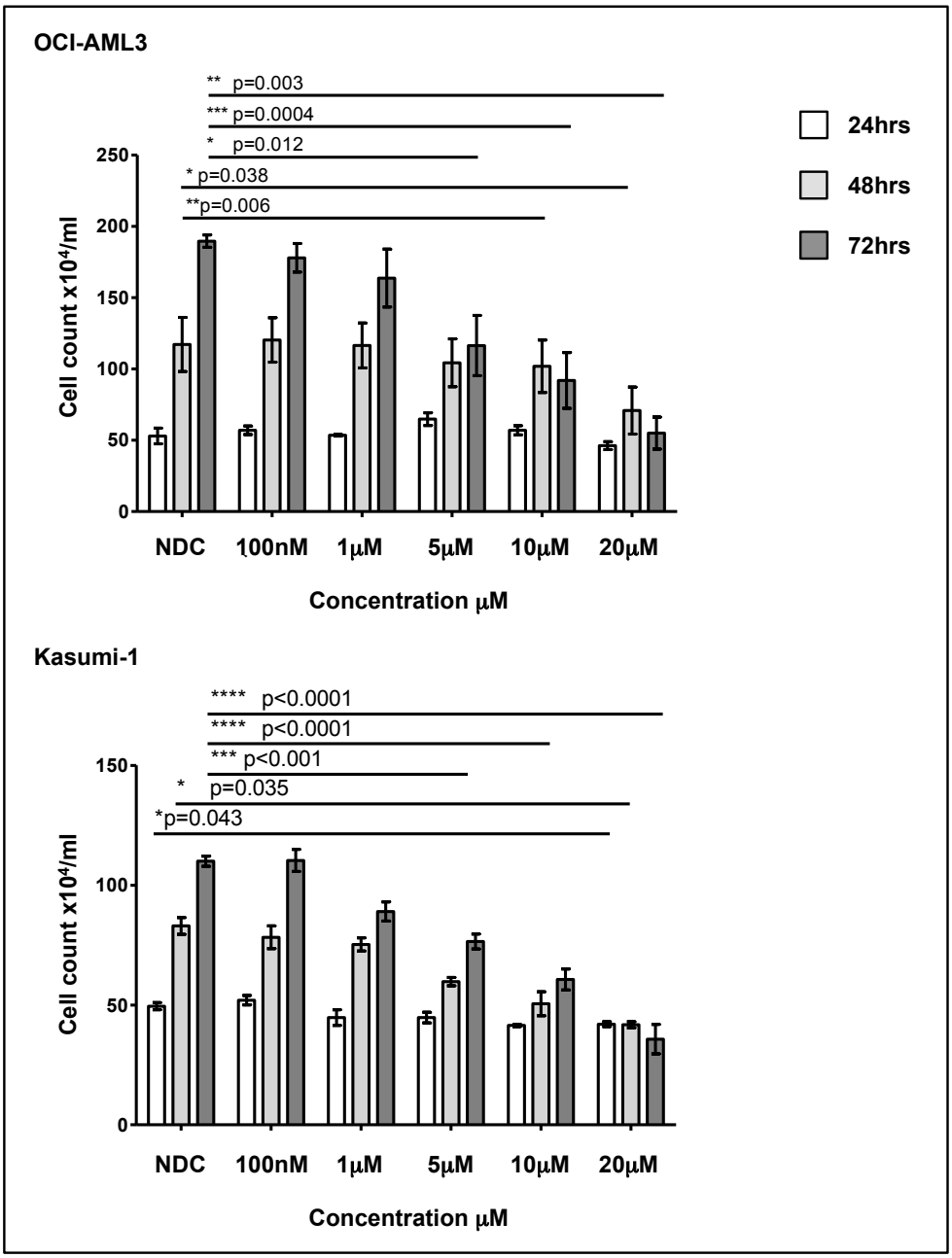

Figure 4.1.3.2: Cell viability, as determined by the trypan blue dye exclusion assay, in the OCI-AML3 and Kasumi-1 cell lines following culture with cyclopamine at increasing concentrations. OCI-AML3 and Kasumi-1 cells were seeded at a concentration of $2x10^5$/ml, exposed to incremental doses of cyclopamine and cultured for 24hrs, 48hrs and 72hrs. Cell counts, live and dead, were determined using the trypan blue dye exclusion assay. Each bar represents the mean cell number x 10^4 from four independent experiments with error bars indicating SD showing culture with cyclopamine caused a time and concentration dependent reduction in cell viability in the OCI-AML3 and Kasumi-1 cell lines. All statistically significant results are highlighted with p value to the nearest 4 decimal places, those not highlighted are not significant (ns).

In the OCI-AML3 cell line there was no difference in cell counts between the NDC and all concentrations of cyclopamine at 24hrs. At 48hrs there was a trend towards a reduction in the number of live cells following culture with 5μM, 10μM and 20μM, reaching statistical significance following culture with 10μM (p=0.006) and 20μM (p=0.038). At 72hrs a statistically significant reduction in live cells was seen following culture with 5μM (p=0.012), 10μM (p<0.001) and 20μM (p=0.003).

In the Kasumi-1 cell line there was a statistically significant difference in the number of live cells following culture with 20μM at 24hrs and 48hrs (p=0.043 and p=0.035 respectively) relative to the NDC. At 72hrs there was a trend towards a reduction in the number of live cells following culture with 1μM, reaching statistical significance following culture with 5μM (p<0.001), 10μM (p<0.0001) and 20μM (p<0.0001).

The range for all future experiments was therefore narrowed to: NDC, 5μM, 10μM and 20μM. In each experiment tomatidine at a maximum dose of 20μM and DMSO at a volume of 1.25μl/ml (volume equivalent to maximum dose of cyclopamine) were used as negative controls (NDC).

In the HL60, KG1a, MV4-11, OCI-AML3 and THP-1 cell lines, cell number by trypan blue dye exclusion showed a statistically significant reduction in live cell number with increasing doses of cyclopamine (statistics following culture with the maximum concentration of 20μM cyclopamine: p=0.008, p=0.006, p=0.006, p=0.047 and p=0.010 respectively). This was not seen in the negative control arms. The total number of dead cells however remained relatively constant (all p=ns). This was confirmed by Annexin V / 7AAD staining which demonstrated no significant change in viable, early apoptotic, late apoptotic or dead cells, suggesting an alteration in cell cycle kinetics rather than apoptosis; Figure 4.1.3.3.

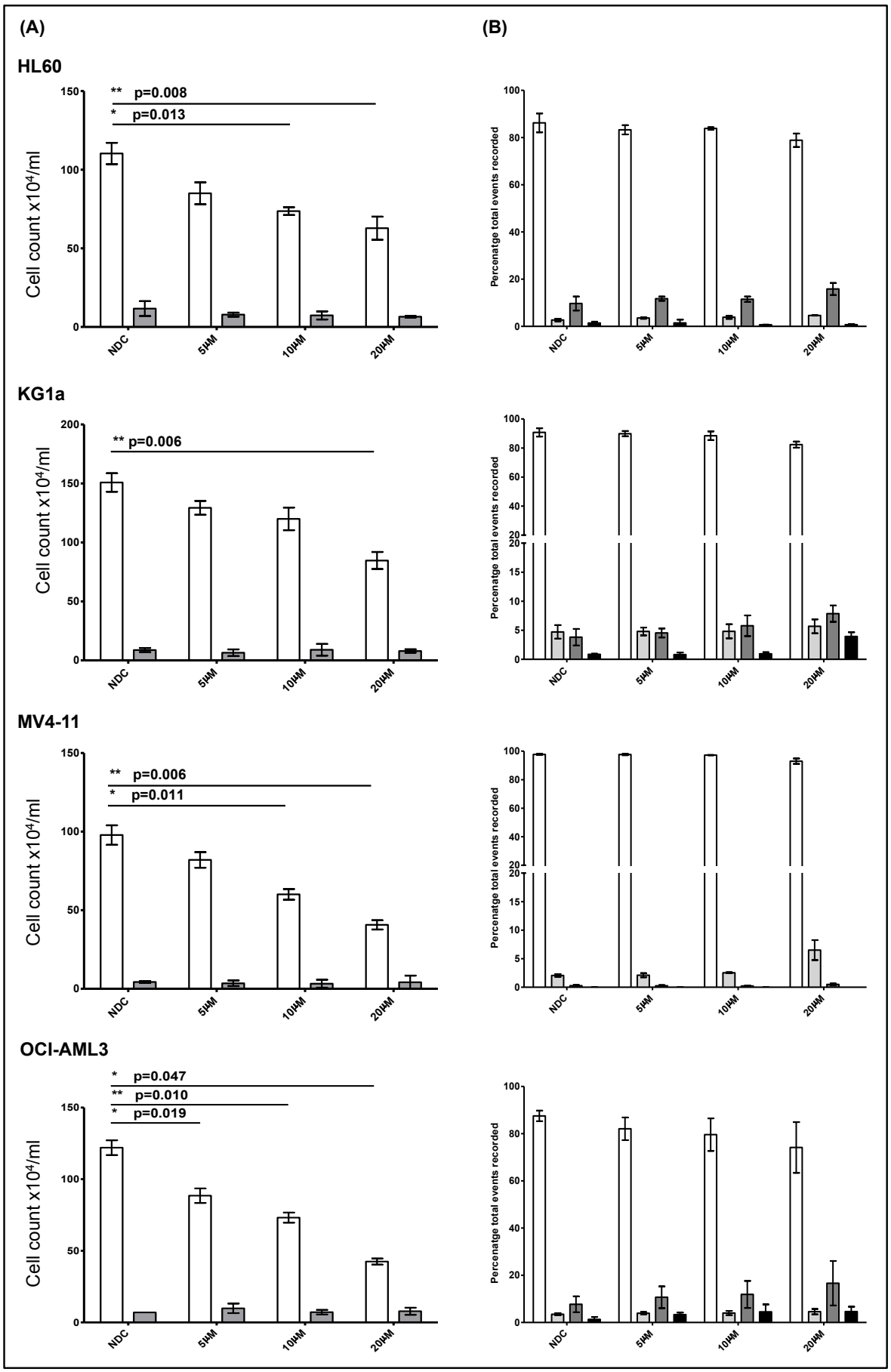
(A)
(B)
HL60
** p=0.008
* p=0.013
Cell count x10⁴/ml
Percenatge total events recorded
NDC
5μM
10μM
20μM
KG1a
** p=0.006
MV4-11
** p=0.006
* p=0.011
OCI-AML3
* p=0.047
** p=0.010
* p=0.019

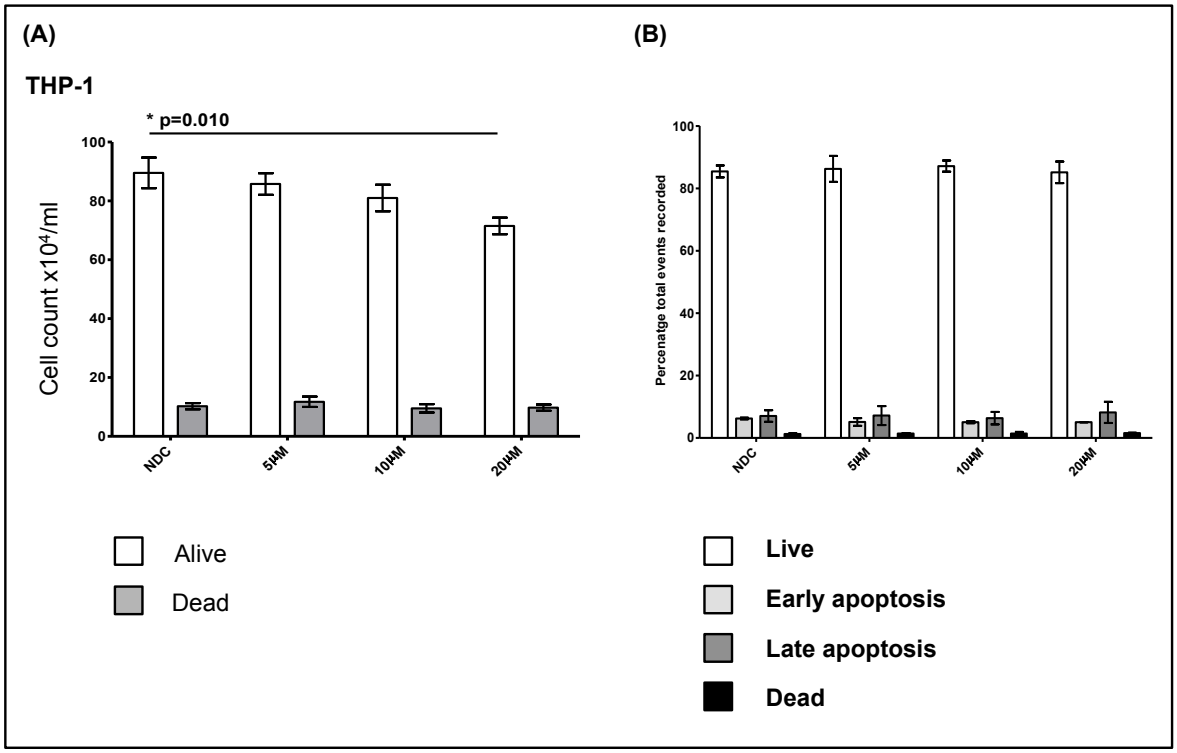

Figure 4.1.3.3: Proliferation, as determined by the trypan blue dye exclusion assay, and apoptosis, as determined by Annexin V / 7AAD staining, in the Kasumi-1 and MOLM-13 cell lines following culture with cyclopamine (5μM, 10μM and 20μM).
Cells from each of the AML cell lines were seeded at a concentration of $2x10^5$/ml, exposed to incremental doses of cyclopamine and cultured for 72hrs. (A) These graphs show cell viability as determined by trypan blue exclusion for each of the AML cell lines. Each bar represents the mean cell number $x10^4/m^l$ from four independent experiments with error bars indicating SD. (B) These graphs indicate the proportion of cells which are viable, in early apoptosis, in late apoptosis or dead as determined by Annexin V / 7AAD staining, and analysis by flow cytometry. The percentages shown indicate the proportion of total events within each of the respective categories as gated on the flow cytometry plots (see Figure 2.3 for gating strategy). Each bar represents the mean percentage from four independent experiments with error bars indicating SD showing cyclopamine caused a statistically significant, though variable, reduction in proliferation not explained by apoptosis in select, genetically diverse, AML cell lines. All statistically significant results are highlighted with p value to the nearest 3 decimal places, those not highlighted are not significant (ns).

In contrast, apoptosis was seen in two genetically diverse AML cell lines: the CD34+ hypo-diploid Kasumi-1 cell line expressing the *AML-ETO* fusion gene and *KIT* mutation and the hyper-diploid, myelomonocytic MOLM-13 cell line carrying the *FLT3-ITD* and *CBL* mutants and the *MLL-AF9* fusion gene; Figure 4.1.3.4. Previous research has indicated an association between *FLT3-ITD* mutational status and Hh pathway activity [381,382], potentially explaining the increased sensitivity of the MOLM-13 cell line to Smo inhibition. Apoptosis was not seen in other myelomonocytic cell lines: MV4-11, OCI-AML3 and THP-1. This is particularly interesting considering both the MV4-11 and MOLM-13 cell lines carry the *FLT3-ITD* and *MLL* mutants, and are derived from paediatric patients. MOLM-13 cells, however, carry the additional genetic abnormality, *CBL*, and interestingly, do not express FLT3-ITD at the protein level. Further, we demonstrated differing results in our two selected CD34-expressing cell lines: Kasumi-1 and KG1a. Whilst increased activity has been shown in more primitive CD34+ AML cells [618] our results highlight the heterogeneity intrinsic to AML. A common phenotypic or genotypic trait to explain the increased sensitivity of the Kasumi-1 and MOLM-13 cell lines could not be identified.

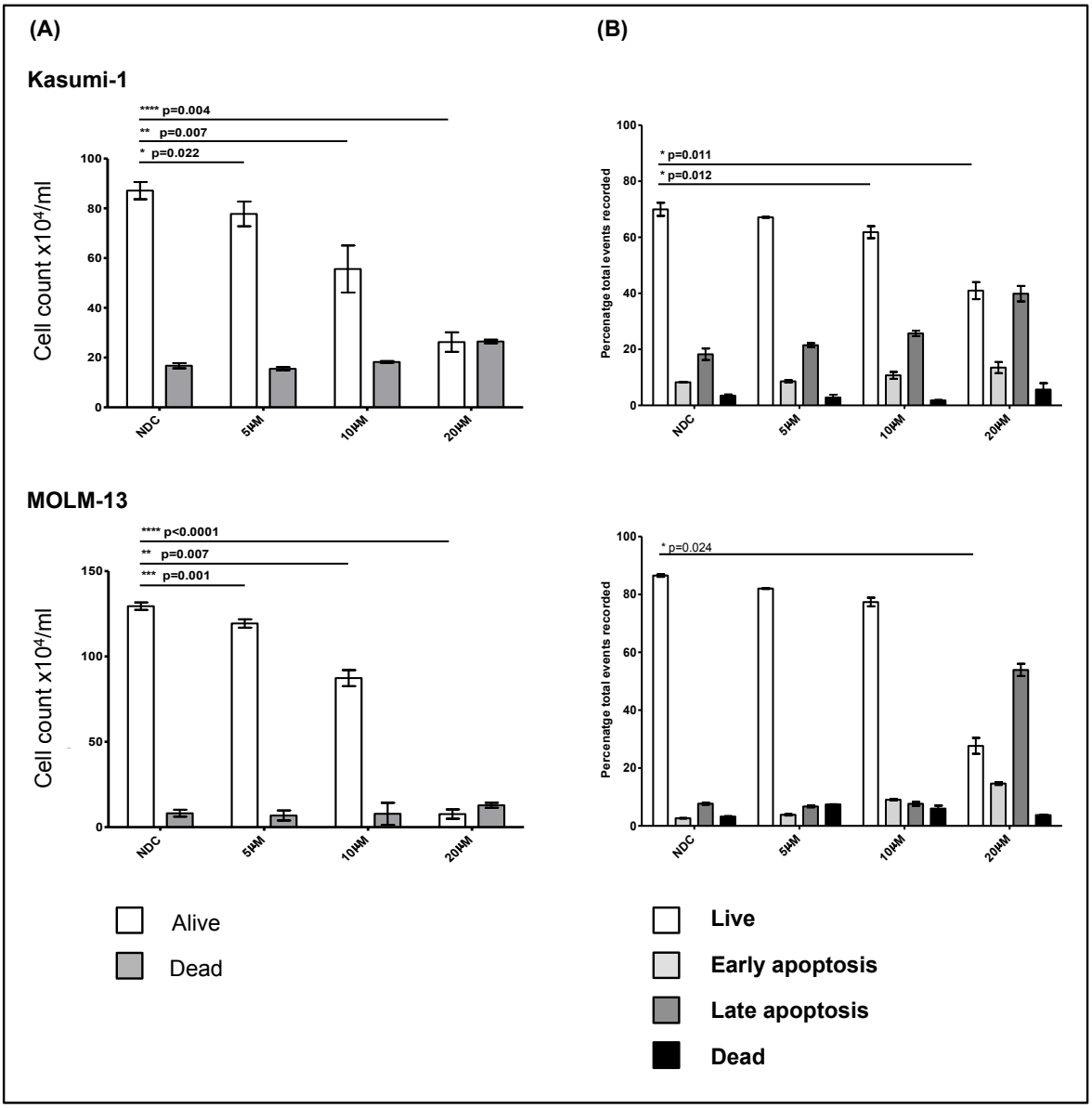

Figure 4.1.3.4: Proliferation, as determined by the trypan blue dye exclusion assay, and apoptosis, as determined by Annexin V / 7AAD staining, in select, genetically diverse, AML cell lines following culture with cyclopamine (5μM, 10μM and 20μM).
Cells from each of the AML cell lines were seeded at a concentration of $2x10^5$/ml, exposed to incremental doses of cyclopamine and cultured for 72hrs. (A) These graphs show cell viability as determined by trypan blue exclusion for each of the AML cell lines. Each bar represents the mean cell number x 10^4 from four independent experiments with error bars indicating SD. (B) These graphs indicate the proportion of cells which are viable, in early apoptosis, in late apoptosis or dead as determined by Annexin V / 7AAD staining, and analysis by flow cytometry. The percentages shown indicate the proportion of total events within each of the respective categories as gated on the flow cytometry plots (see Figure 2.3 for gating strategy). Each bar represents the mean percentage from four independent experiments with error bars indicating SD; graphs showing cyclopamine caused apoptosis in select, genetically diverse, AML cell lines. All statistically significant results are highlighted with p value to the nearest 3 decimal places, those not highlighted are not significant (ns).

For the purpose of further understanding the effect of Smo inhibition, we focused on two cell lines, the Kasumi-1 cell line in which apoptosis was demonstrated, and the OCI-AML3 cell line in which altered cell kinetics in the absence of apoptosis was observed. Reference is however made to other cells lines where informative results are available.

4.1.4 Manipulation of the Hh pathway by Smo inhibition with cyclopamine alters cell cycle kinetics in select AML cell lines

We clearly demonstrated reduced proliferation in the absence of apoptosis in genetically distinct cells lines: HL60, KG1a, MV4-11, OCI-AML3 and THP-1. We therefore sought to determine the underlying mechanism. Cell cycle kinetics were studied by two methods: PI (to enable analysis of cell cycle status) and CFSE (to enable analysis of cellular proliferation). In addition, these assays were performed in the Kasumi-1 cell line, in which cyclopamine had resulted in apoptosis, to enable us to compare and contrast cellular responses.

In the OCI-AML3 cell line, cell cycle arrest was demonstrated with a clear increase in the percentage of inactive, non-cycling cells (G0-G1) (p=0.011) and reduction in the dividing cell fractionss (S-G2-M) compared to the NDC by PI (p=0.009), Figure 4.1.4.1. Considering this further we used CFSE, an intracellular fluorescein-based dye, that enables cell divisions to be analysed [587]; CFSE fluorescence intensity progressively reduces with each cell division, due to the equal division of the fluorescent stain between daughter cells, allowing the number of divisions to be calculated relative to an undivided control population. This data supported that seen with PI, CFSE clearly showing a reduction in cell division with increasing doses of cyclopamine compared to the NDC; Figure 4.1.4.2.

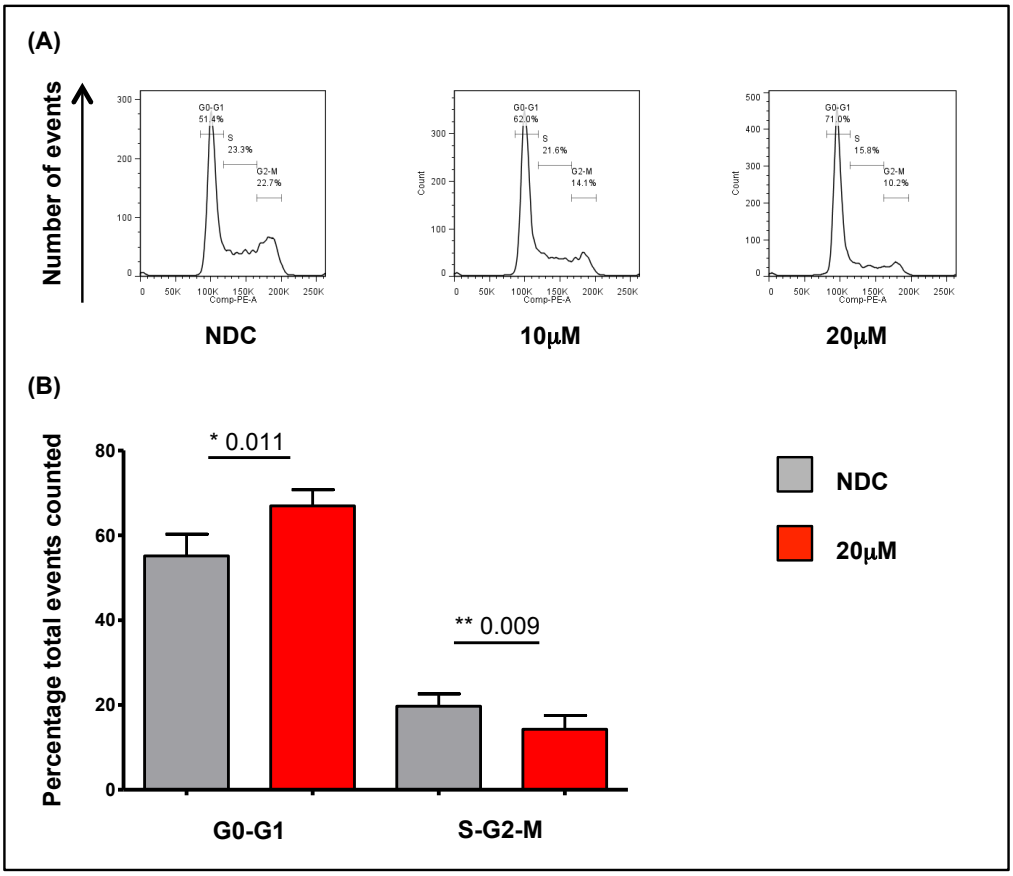

Figure 4.1.4.1: Percentage of inactive, non-cycling (G0-G1) OCI-AML3 cells by PI staining following culture with cyclopamine (10μM and 20μM) for 72hrs.
OCI-AML3 cells were seeded at a concentration of $2x10^5$/ml, exposed to incremental doses of cyclopamine, cultured for 72hrs then harvested and stained with PI prior to analysis by flow cytometry. (A) Representative flow cytometry plots, and gating strategy, following PI staining of OCI-AML3 cells following culture with select doses of cyclopamine for 72hrs. Each plot is representative of data from one experiment of four with similar results. (B) Bar graph indicating the proportion of cells within determined cell cycle phase (G0-G1and S-G2-M) as determined by PI, and analysis by flow cytometry. Each bar represents the mean percentage from four independent experiments with error bars indicating SD. Statistically significant results are highlighted with p value to the nearest 3 decimal places. This figure clearly shows culture of OCI-AML3 cells with cyclopamine for 72hrs to increase the percentage of inactive, non-cycling (G0-G1) cells.

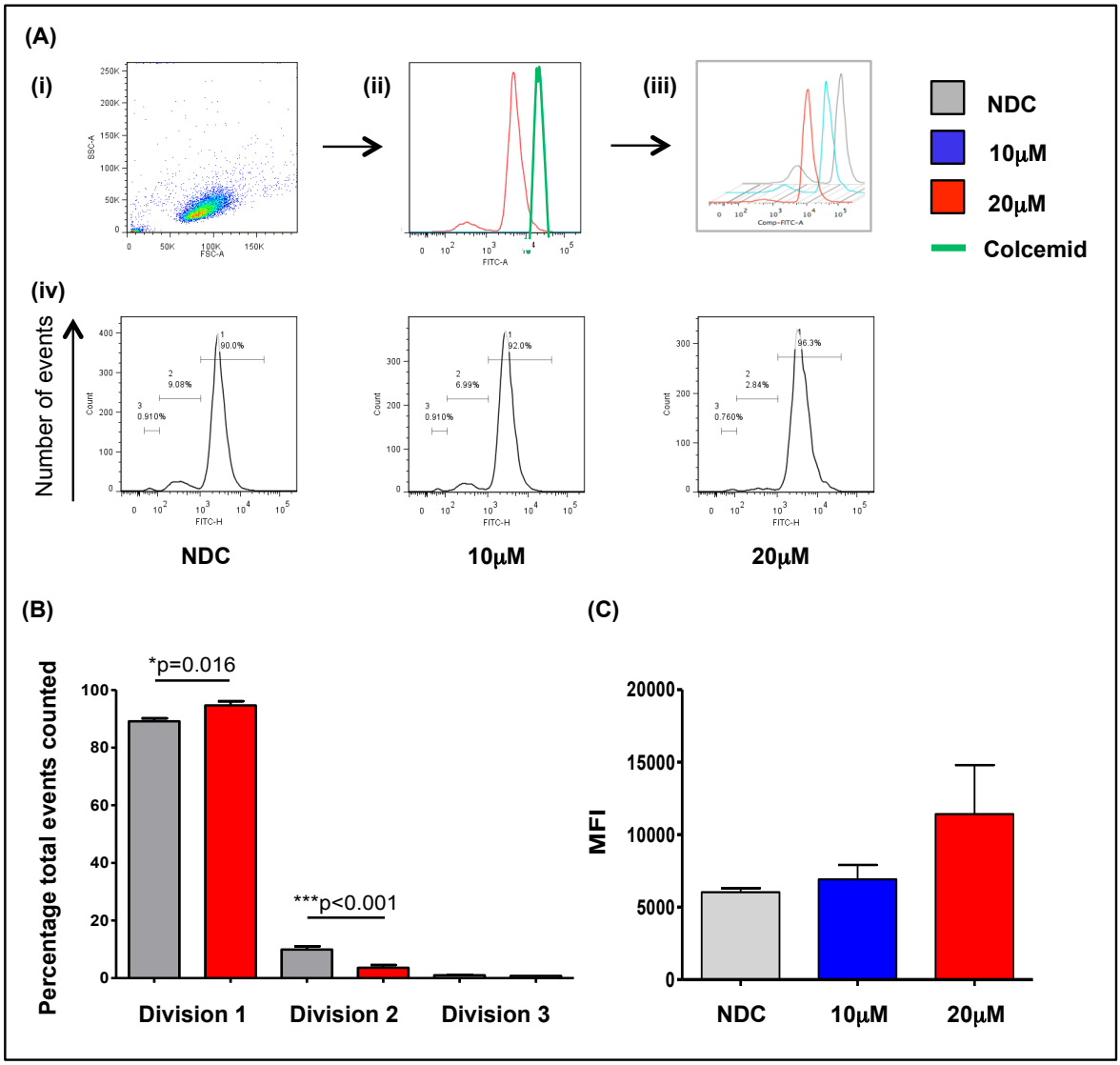

Figure 4.1.4.2: Cellular proliferation, as determined by CFSE in OCI-AML3 cells following culture with cyclopamine (10μM and 20mM) for 72hrs.
OCI-AML3 cells were seeded at a concentration of $2x10^5$/ml, exposed to incremental doses of cyclopamine, cultured for 72hrs then harvested and stained with CFSE prior to analysis by flow cytometry. (A) Representative flow cytometry plots (i) Cell population, (ii) Histogram showing colcemid control (green) relative to CFSE stained population, (iii) Staggered histogram showing NDC, 10μM cyclopamine and 20μM cyclopamine, (iv) Histograms with gating strategy following CFSE staining of OCI-AML3 cells following culture with select doses of cyclopamine for 72hrs. Each plot is representative of data from one experiment of four with similar results. (B) This graph indicates the proportion of cells within each cell division as determined by CFSE and analysis by flow cytometry clearly demonstrating a block in cell proliferation following culture with 20μM cyclopamine for 72hrs. (C) Graph showing the average MFI for each experimental arm showing a progressive increase in the MFI, consistent with reduced proliferation and cell division, following culture with increasing doses of cyclopamine for 72hrs.
Each bar represents the mean percentage from four independent experiments with error bars indicating SD. All statistically significant results are highlighted with p value to the nearest 3 decimal places, those not highlighted are not significant (ns).

In contrast, in keeping with the apoptosis demonstrated by Annexin V / 7AAD, cell cycle analysis by PI in the Kasumi-1 cell line demonstrated a statistically significant reduction in cells undergoing interphase and mitosis, the dividing cell fraction (S-G2-M) (p=0.015), with a concomitant modest increase in dying (sub G0) cells though this was not significant, Figure 4.1.4.3. CFSE demonstrated no significant difference in the rate of proliferation between the NDC and all doses of cyclopamine up to and including 20μM, Figure 4.1.4.4.

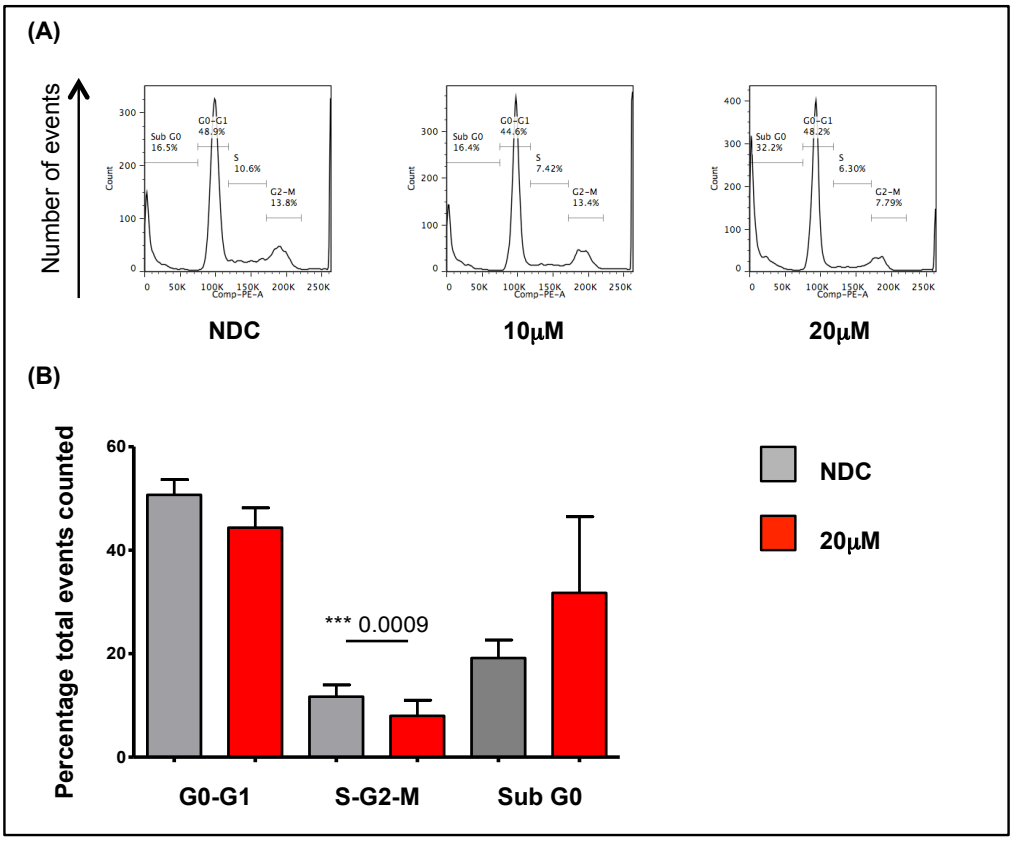

Figure 4.1.4.3: Percentage of inactive, non-cycling (G0-G1) Kasumi-1 cells by PI staining following culture with cyclopamine (10μM and 20μM) for 72hrs.
Kasumi-1 cells were seeded at a concentration of $2x10^5$/ml, exposed to incremental doses of cyclopamine, cultured for 72hrs then harvested and stained with PI prior to analysis by flow cytometry. (A) Representative flow cytometry plots, and gating strategy, following PI staining of Kasumi-1 cells following culture with select doses of cyclopamine for 72hrs. Each plot is representative of data from one experiment of four with similar results. (B) This graph indicates the proportion of cells within determined cell cycle phases (G0-G and, S-G2-M) as determined by PI, and analysis by flow cytometry. Each bar represents the mean percentage from four independent experiments with error bars indicating SD. Statistically significant results are highlighted with p value to the nearest 3 decimal places, those not highlighted are not significant (ns).
This data clearly shows culture of Kasumi-1 cells with cyclopamine for 72hrs resulted in a reduction in proliferating cells, with a concomitant increase in dying cells.

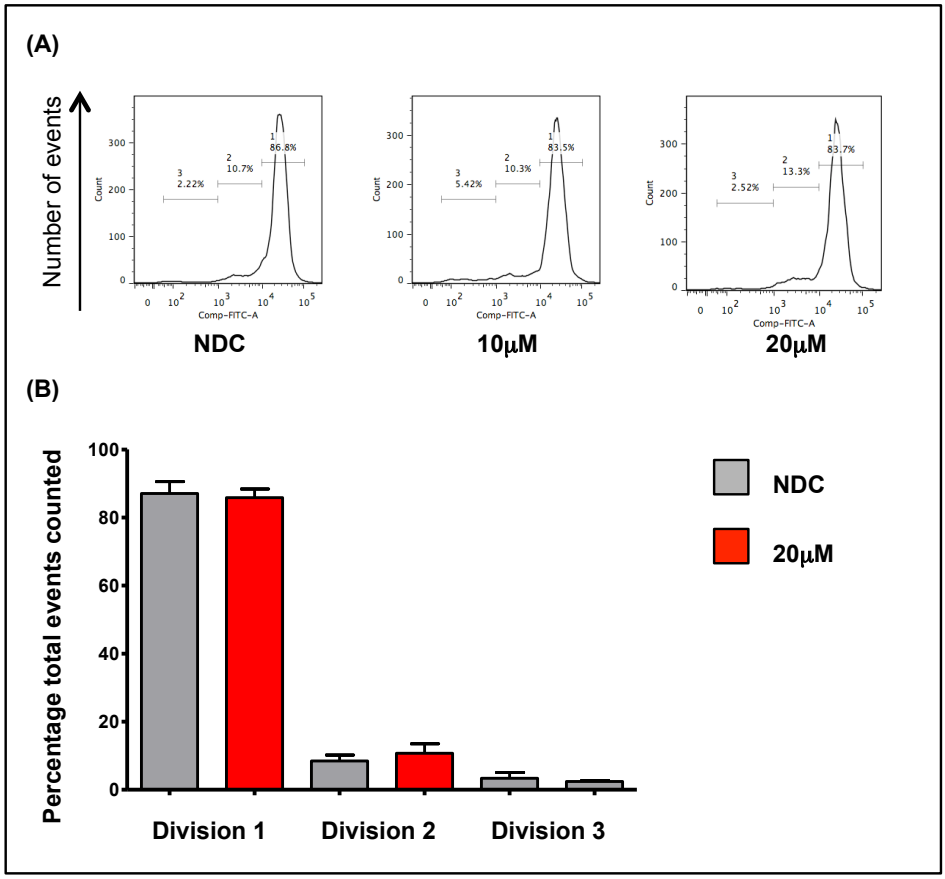

Figure 4.1.4.4: Cellular proliferation, as determined by CFSE in Kasumi-1 cells following culture with cyclopamine (10μM and 20μM) for 72hrs.
Kasumi-1 cells were stained with CFSE, seeded at a concentration of $2x10^5$/ml, exposed to incremental doses of cyclopamine and cultured for 72hrs prior to analysis by flow cytometry. (A) Representative flow cytometry plots, and gating strategy, of CFSE stained Kasumi-1 cells following culture with select doses of cyclopamine for 72hrs. Each plot is representative of data from one experiment of three with similar results. (B) This graph indicates the proportion of cells within each cell division as determined by CFSE, and analysis by flow cytometry, clearly showing culture of Kasumi-1 cells with cyclopamine for 72hrs did not affect cell division by CFSE staining. Each bar represents the mean percentage from three independent experiments with error bars indicating SD. All statistically significant results are highlighted with p value to the nearest 3 decimal places, those not highlighted are not significant (ns).

Whilst the cell kinetic data was in keeping with reduced proliferation in the OCI-AML3 cell line, the mechanism remained unclear. We therefore considered whether culture with cyclopamine resulted in cellular senescence or differentiation in the OCI-AML3 cell line, discussed in the following sections.

4.1.5 Manipulation of the Hh pathway by Smo inhibition with cyclopamine did not induce cellular senescence in select AML cell lines

Cell senescence, as a possible mechanism to explain the altered cell kinetics seen in the OCI-AML3 cell line was determined through measurement of ß-galactosidase activity. ß-galactosidase activity was also measured in the HL60, Kasumi-1, KG1a and MV4-11 cell lines. The Kasumi-1 cell line was included as a comparator given the differing effect Smo inhibition had.

ß-galactosidase activity was measured in each of the cell lines following culture for 72hrs with cyclopamine at a dose of 10μM and 20μM, tomatidine at a dose of 20μM and DMSO at a volume of 1.25μl/ml; Figure 4.1.5.1. No evidence of cellular senescence was demonstrated either in the presence of cyclopamine or the negative controls, the positive control confirmed the assay had worked (development of blue colouration) on each occasion (n=3).

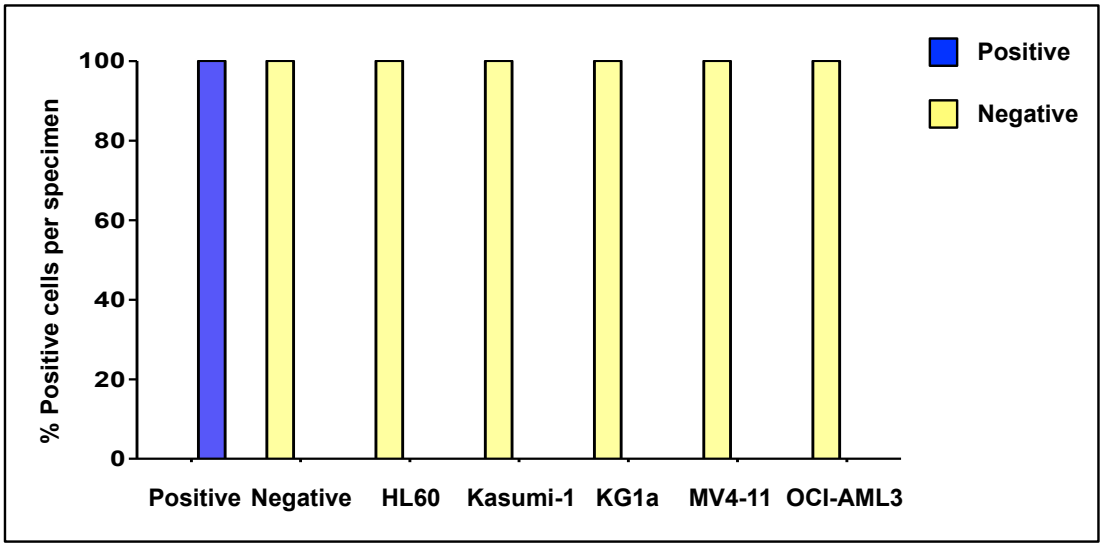

Figure 4.1.5.1: ß-glactosidase activity in select, genetically diverse, AML cell lines following culture with 20mM cyclopamine for 72hrs.
ß-galactosidase activity, a characteristic of senescent cells not found in other cell states eg. quiescent cells was assessed in HL6o, Kasumi-1, KG1a, Mv4-11 and OCI-AML3 cells following culture for 72hrs with cyclopamine at a dose of 10μM and 20μM, tomatidine at a dose of 20μM and DMSO at a volume of 1.25ml/ml. The percentage of senescent cells (staining blue-green) for each of our selected cell lines following culture with cyclopamine 20μM, the negative and positive control is shown. A minimum of 100 cells were counted for each experimental arm. Alkali conditions (pH10) were used as a positive control, all cells within the positive control stained blue-green. There was no evidence of cellular senescence in any of the cell lines across all the experimental arms, with cells remaining colourless (n=3).

4.1.6 Manipulation of the Hh pathway by Smo inhibition with cyclopamine induced differentiation in select AML cell lines

We considered whether cell differentiation could explain the altered cell kinetics demonstrated in previous assays, we had observed a morphological change in cells whilst performing trypan blue dye exclusion cell counts. We therefore studied our flow cytometry plots, specifically looking at the FSC / SSC plots for each experimental condition and each cell line. There was a striking, statistically significant increase in SSC within the HL60, MV4-11, OCI-AML3 and THP-1 cell lines, with cells clearly becoming more granular when cultured for 72hrs with 20μM of cyclopamine when compared to the NDC. A similar, though less significant effect, was seen at 10μM. Interestingly, no morphological change was demonstrated within either of the CD34-expressing cell lines, Kasumi-1 and KG1a; Figure 4.1.6.1.

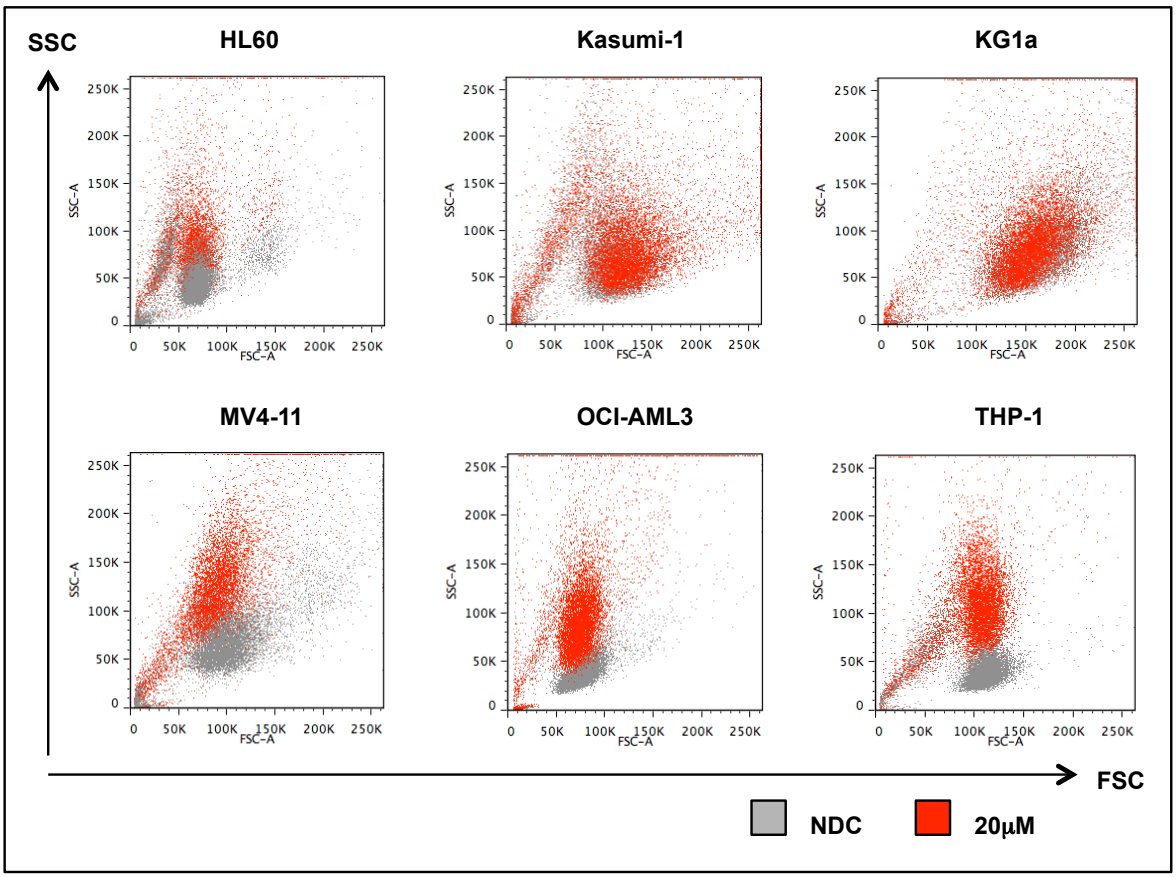

Figure 4.1.6.1: Representative FSC / SSC plots from select, genetically diverse AML cell lines following culture with 20μM cyclopamine for 72hrs.
Cells from each of our seven selected, genetically diverse AML cell lines were seeded at a concentration of $2x10^5$/ml, exposed to incremental doses of cyclopamine and cultured for 72hrs prior to analysis by flow cytometry. Representative FSC / SSC flow cytometry plots are shown. Each plot is representative of data from one experiment of three with similar results and demonstrates the striking increase in SSC (reflecting cell granularity) in the HL60, MV4-11, OCI-AML3 and THP-1 cell lines relative to the NDC; whilst no change is seen in the Kasumi-1 or KG1a cell lines. FSC, forward scatter; SSC, side scatter.

Analysis of the MOLM-13 cell line showed two different effects within the same cell population; Figure 4.1.6.2. As expected there was a population of cells that underwent apoptosis (highlighted in green). However, when these were gated out as shown in Figure 4.1.6.2 (B) two distinct populations of live cells remained (live by Annexin V / 7AAD). These cell populations were distinguishable by their FSC / SSC properties. One population demonstrated no change, plotting in the same region as those from the NDC whilst, interestingly, a second, smaller population showed an increase in SSC in keeping with increased granularity, as seen in the HL60, MV4-11, OCI-AML3 and THP-1 cell lines.

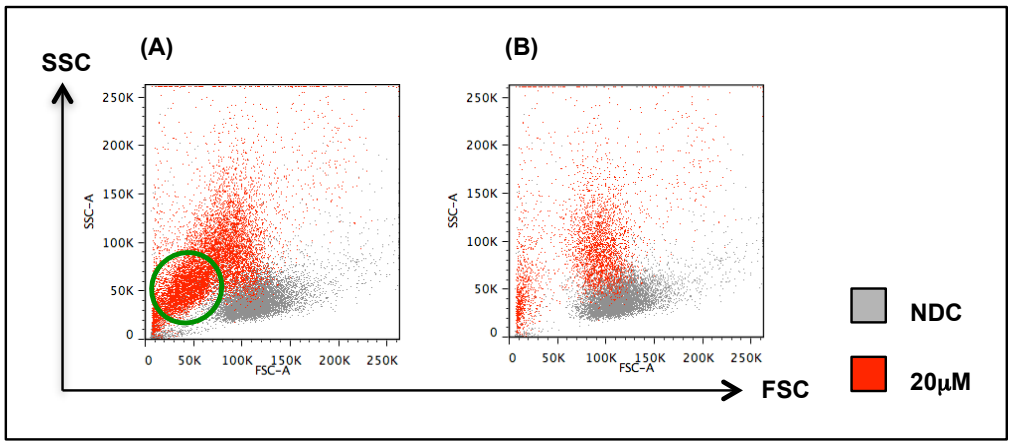

Figure 4.1.6.2: Representative FSC / SSC plots from the MOLM-13 cell line following culture with 20μM cyclopamine for 72hrs.
MOLM-13 cells were seeded at a concentration of $2x10^5$/ml, exposed to incremental doses of cyclopamine and cultured for 72hrs prior to analysis by flow cytometry. Representative FSC / SSC flow cytometry plots are shown. Each plot is representative of data from one experiment of three with similar results. (A) Shows the FSC / SSC plot for the total number of events recorded; Green highlights those events considered as dead / dying cells and cell debris. (B) Shows the FSC / SSC plot following exclusion of the apoptosing cell population clearly showing a smaller but distinct population of cells with increased granularity relative to the NDC. FSC, forward scatter; SSC, side scatter.

We recognise the data obtained from the FACs scatter plots was observational. We therefore sought to validate our observations. Cells were therefore visualised by light microscopy with Diff-Quik® staining. The OCI-AML3 cell line was shown to clearly have a more mature monocytoid appearance with increased cytoplasm, cytoplasmic vacuoles and granules and loss of cytoplasmic basophilia and nucleoli, supporting our observation of a change in cell morphology, Figure 4.1.6.3. All slides were blindly reported and independently verified by Dr M Leach, Consultant Haematologist, NHS Greater Glasgow and Clyde to whom I am indebted for time and expertise. Morphological changes were not seen in the presence of 20μM tomatidine.

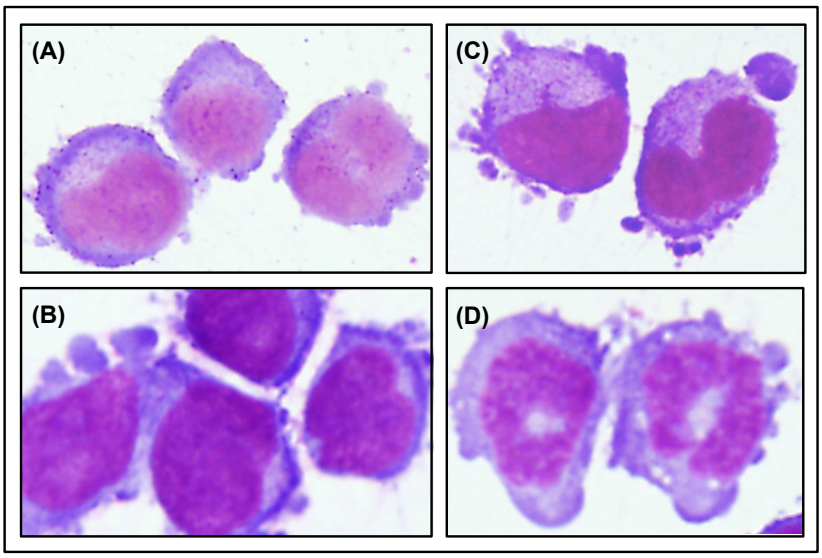

Figure 4.1.6.3: Representative images following Diff-Quik® staining of OCI-AML3 cells following culture with 20mM cyclopamine for 72hrs.
OCI-AML3 cells were seeded at a concentration of $2x10^5$/ml, exposed to incremental doses of cyclopamine and cultured for 72hrs. Freshly harvested cells were spun onto a microscope slide by the use of a cytocentrifuge then stained with Diff-Quik® to enable analysis of cell morphology. Representative images are shown. Each plot is representative of data from one experiment of four with similar results. Following culture with 20μM cyclopamine the OCI-AML3 cells can be seen to have increased cytoplasm, cytoplasmic vacuoles and granules compared to the NDC with their higher nuclear to cytoplasmic ratio, visible nucleoli and basophilic cytoplasm. (A) NDC x60 magnification, (B) NDC x100 magnification, (C-D) Cyclopamine 20μM x100 magnification, showing range of morphological features displayed by the more mature monocytoid cells.

Differentiation was confirmed by CD marker expression in the OCI-AML3 cell line following culture with cyclopamine at concentrations of 10μM and 20μM for 72hrs. A statistically significant increase in the expression of CD11b ($p<0.0001$) and CD11c ($p=0.008$), in keeping with a more mature phenotype was demonstrated following culture with cyclopamine 20μM for 72hrs when compared to the NDC arm; Figure 4.1.6.4. No difference in expression was seen in the following myeloid markers: CD14, CD15, CD16, CD33, CD34 and CD68 (data not shown). CD marker analysis at 24hrs and 48hrs showed a progressive change with time. The effect therefore did not occur on exposure to cyclopamine but rather the progressive morphological change implies a shift in cell division towards differentiation rather than proliferation.

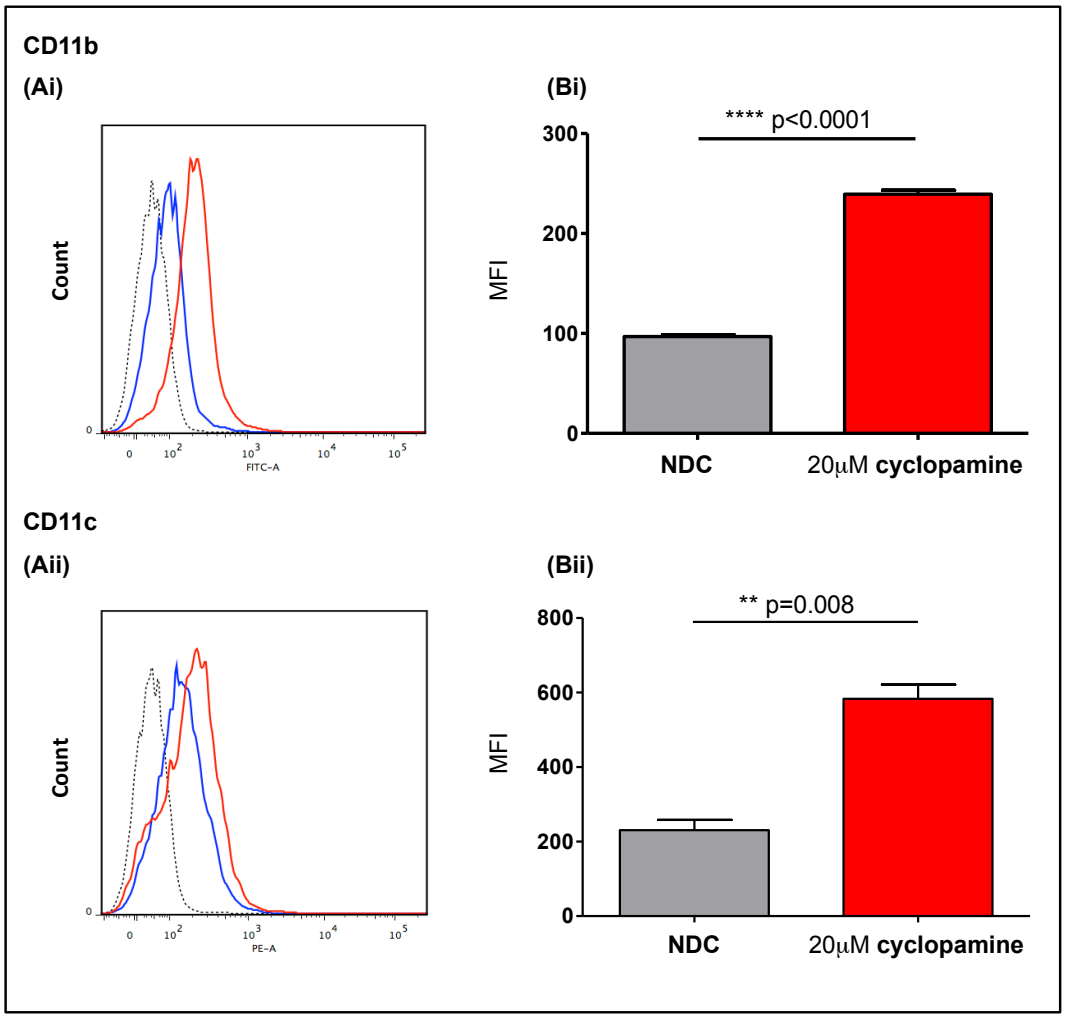

Figure 4.1.6.4: CD marker expression profile on OCI-AML3 cells following with cyclopamine 20μM for 72hrs.
OCI-AML3 cells were seeded at a concentration of $2x10^5$, exposed to incremental doses of cyclopamine and cultured for 72hrs. Freshly harvested cells were stained with an antibody cocktail containing CD11b, CD11c, CD14, CD15, CD16, CD33, CD34 and CD68 prior to analysis by flow cytometry. (A) Representative flow cytometry plots. Each plot is representative of data from one experiment of four with similar results. (B) Graphs show the mean fluorescence intensity (MFI) of the CD markers (CD11b (i) and CD11c (ii)) as determined by flow cytometry showing culture with cyclopamine for 72hrs led to a change in cell CD marker expression profile of OCI-AML3 cells. Each bar represents the mean percentage from four independent experiments with error bars indicating SD. All statistically significant results are highlighted with p value to the nearest 3 decimal places. Unstained untreated (grey dotted line); NDC (blue); 20μM cyclopamine (red).

Gene expression analysis sought to determine a mechanism for cell differentiation. Key genes involved in myelomonocytic and granulocytic regulation and differentiation were studied, levels quantified by qRT-PCR using Fluidigm® technology. Genes were chosen on the basis of their role within early haematopoiesis and myeloid maturation. To account for input cDNA the ΔCT for each gene was calculated by subtracting the CT value of 2 housekeeping (control) genes, *ENOX2* and *UBE2D2*, from the CT of the gene of interest. The $2^{-\Delta\Delta CT}$ method was used to show expression of the gene of interest relative to the NDC, which was expressed as 1.

There was a reduction in the expression of the early lineage markers: *NAB2, GATA1, EGR2, SCL, IRF8* and *EGR1* (p=ns) and an increase in expression seen in genes involved in differentiation and maturation, *PU1, GCSF* and *MPO* (p=ns); Figure 4.1.6.5. Whilst the results support our functional data we had expected the changes to be statistically significant. It is important however, to note that all early haematopoiesis markers were down-regulated and those involved in maturation up-

regulated. To postulate significance might be seen at a later time point does not fit with our functional data showing clear differentiation by 72hrs. We did not study all genes involved in early haematopoiesis and myeloid maturation and may therefore have missed those in which a significant change has occurred. On reflection, however, we propose these relatively minor shifts in gene expression in key behaviour and lineage determinant genes are sufficient to significantly affect cell phenotype, to alter the balance between self-renewal and differentiation, as demonstrated by our functional assays.

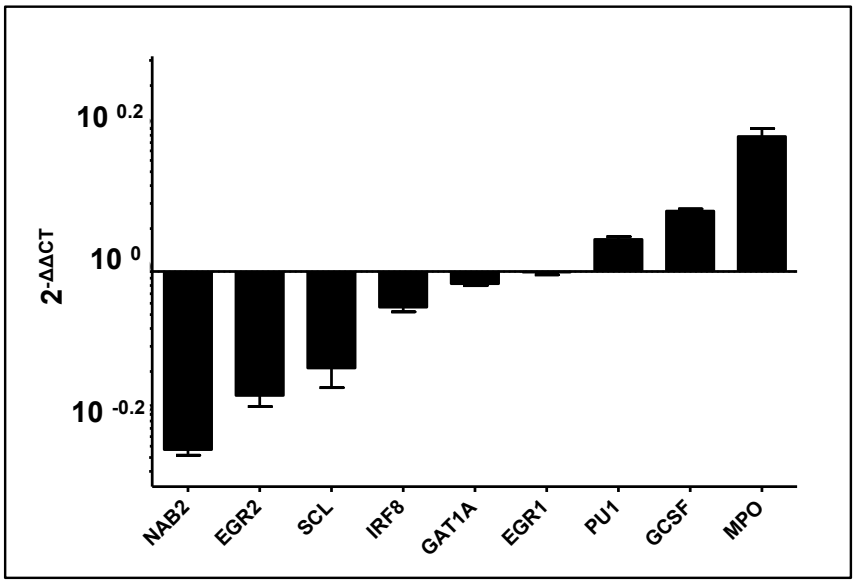

Figure 4.1.6.5: Culture of OCI-AML3 cells with cyclopamine for 72hrs resulted in a change in the mRNA expression of early lineage genes and those intrinsically involved in cellular maturation. OCI-AML3 cells were seeded at a concentration of $2x10^5$/ml, exposed to incremental doses of cyclopamine and cultured for 72hrs. RNA was extracted from freshly harvested cells. A reduction in early lineage markers and an increase in genes involved in differentiation and maturation Is clearly demonstrated though these results were not statistically significant. Expression levels are shown as the fold change ($2^{-\Delta\Delta CT}$) relative to NDC with 2 housekeeping genes (*ENOX2* and *UBE2D2*) serving as endogenous control. Each bar represents the mean fold change from three independent experiments with error bars indicating SD.

Finally, CFC assays were performed to determine the ability of the OCI-AML3 cells to proliferate, and differentiate, into colonies. The CFC assay is an *in vitro* assay based on the ability of haematopoietic progenitor cells to proliferate and differentiate into colonies in semisolid media with adequate cytokine support. These colonies can be enumerated and characterised according to their unique morphology, providing information about differentiation and proliferative qualities [574,632].

We hypothesised culture with cyclopamine, through its ability to cause cell differentiation, would result in fewer colonies by CFC assay. In contrast to our hypothesis, there was no significant difference between absolute colony number across all experimental arms. Further, the absolute colony numbers challenged our previous results, showing no significant difference between total colony numbers, and therefore proliferative capabilities, across each of the experimental arms. When we considered the predominant character of the colonies, as defined by morphology, within each of the experimental arms however an extremely interesting observation was made. Initial culture with 20μM cyclopamine for 72hrs resulted in a statistically significant reduction in the more pluripotent CFU-GM ($p=0.006$) colonies and an increase in omnipotent CFU-G ($p=0.013$) colonies at day 12 compared to the 20μM tomatidine control. Whilst CFU-M colonies were reduced 2-fold following drug treatment the result was not significant; Figure 4.1.6.6. Replates were performed though <3 secondary colonies grew in each of the experimental arms (n=2). We consider this difference in colony morphology to indicate a shift

towards differentiation but not a fully differentiated state, the cells retaining the property of self-renewal. Excitingly these results correlate, and thus strengthen, our *in vitro* functional assays and gene expression data.

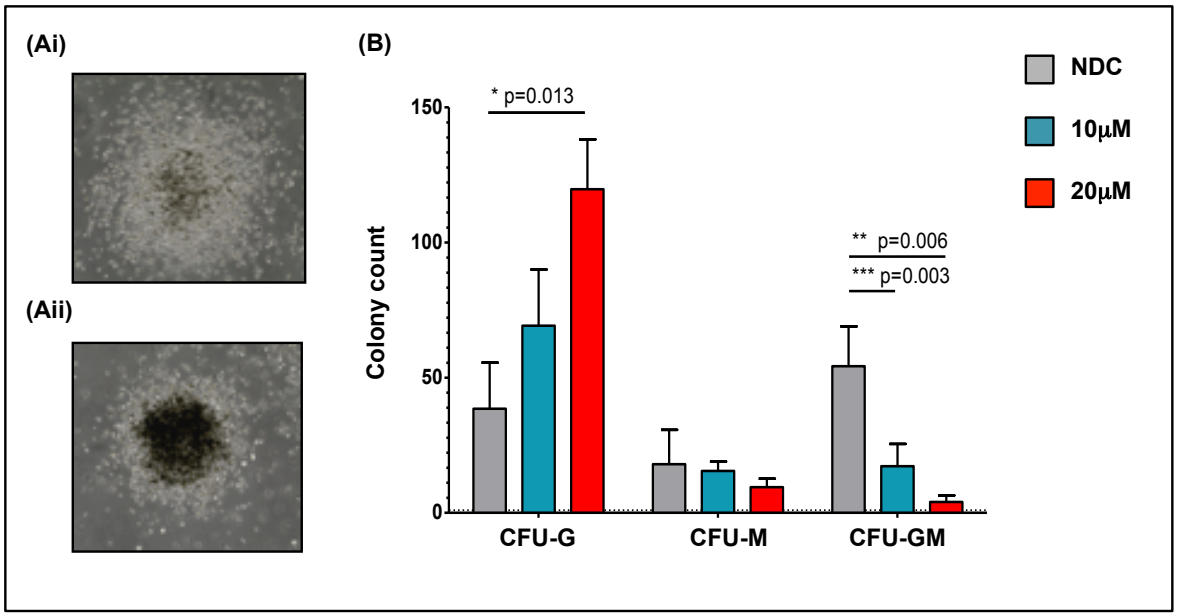

Figure 4.1.6.6: Colony morphology and number at day 12 following culture of OCI-AML3 cells with cyclopamine (10μM and 20μM) for 72hrs.
OCI-AML3 cells were seeded at a concentration of $2x10^5$/ml, exposed to incremental doses of cyclopamine and cultured for 72hrs. Cells, from each experimental arm, at a concentration of $4x10^3$/ ml, were suspended in serum free media (supplemented with a growth factor cocktail), added to methylcellulose media, thoroughly mixed then divided between two 35mm culture dish before being cultured for a further 12 days. (A) Representative images of colonies at day 12 (i) CFU-GM, (ii) CFU-G (B) Graphs show the absolute number of each type of colony showing culture of OCI-AML3 cells with cyclopamine for 72hrs resulted in a change in colony morphology but not the absolute colony number at day 12. Each bar represents the mean percentage from four independent experiments with error bars indicating SD. All statistically significant results are highlighted with p value to the nearest 3 decimal places. CFU-, colony forming unit; GM, granulocyte, macrophage; G, granulocyte; M, macrophage.

Whilst the CFC assay is a recognised and accepted assay for studying cell behaviour, colony morphology and number enabling analysis of a cell's ability to proliferate and / or differentiate, we sought to validate our findings, recognising that this data is observational and thus could be subject to observer bias. We therefore sought to analyse the expression of select CD markers by cells within our colonies using flow cytometry.

Briefly, at day 12, colonies were counted and characterised before being harvested, washed and stained prior to flow cytometry analysis. Expression of CD11b and CD11c were studied as these CD markers had shown significant up-regulation following liquid culture of the OCI-AML3 cells. No difference in expression was seen (n=2; data not shown). It is important however to consider these results in experimental context. Methocult contains a cocktail of growth factors, designed to support the growth and differentiation of HPCs. It would be interesting therefore to study a broader range of CD markers, the mature markers - CD14, CD15, CD16 and CD68, and the more immature markers - CD33 and CD34. In addition, experimental design precluded analysis of individual colonies; if expression changes were not universal they may therefore not have been detected.

Whilst we had demonstrated a statistically significant difference in colony character, suggesting modified differentiation abilities we considered whether this was a reversible phenotype shift. *In vivo* studies have shown rapid clearance of cyclopamine, with serum drug concentrations approaching, or below, the lower limit of quantification 24hrs following bolus administration [631].

'Washout' experiments were therefore performed. Briefly OCI-AML3 cells were cultured for 72hrs with 10μM and 20μM cyclopamine as described previously, washed twice in fresh media prior to resuspending the cells in fresh media and culturing for a further 72hrs in the absence of cyclopamine. Analysis showed loss of cell cycle arrest by PI and a striking and complete reversion of FSC / SSC parameters; Figure 4.1.6.7.

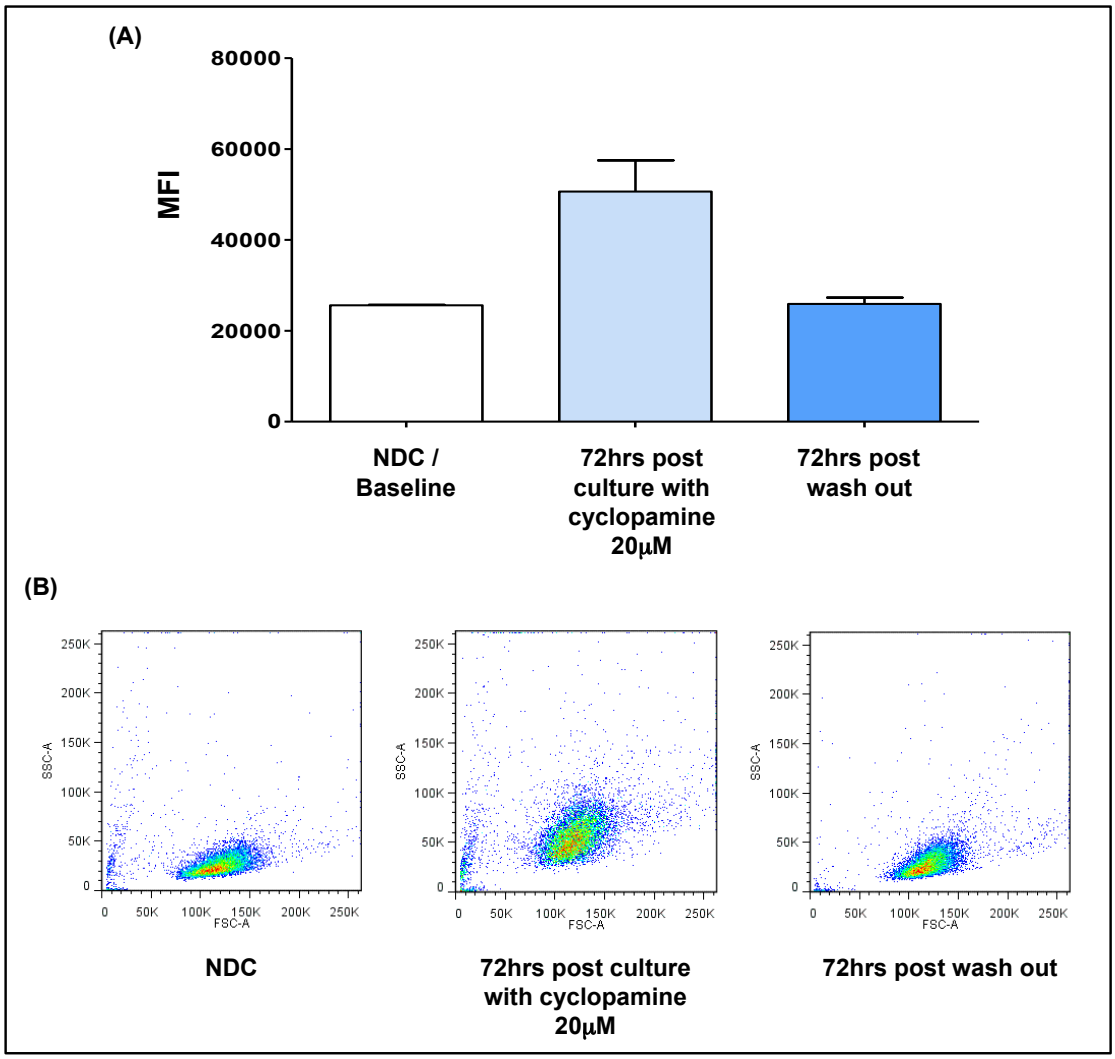

Figure 4.1.6.7: SSC profile of OCI-AML3 cells following culture with 20μM cyclopamine for 72hrs and after a 'wash-out' and further 72hrs in fresh media.
OCI-AML3 cells were seeded at a concentration of $2x10^5$/ml, exposed to incremental doses of cyclopamine and cultured for 72hrs. Cells were then harvested, washed twice in fresh media prior to being resuspended in fresh media and cultured for a further 72hrs in the absence of cyclopamine. (A) Bar graph showing the SSC MFI, reflecting changes in cell granularity, at baseline and following culture with and subsequently without cyclopamine, clearly showing culture of OCI-AML3 cells with cyclopamine induced a reversible change in cell granularity as determined by the SSC profile. Each bar represents the mean percentage from three independent experiments with error bars indicating SD, clearly demonstrating the marked increase in cell granularity following culture with cyclopamine and the subsequent reversal back to baseline following its removal. (B) Representative flow cytometry plots from each experimental stage. Each plot is representative of data from one experiment of three with similar results. Statistically significant results are highlighted with p value to the nearest 3 decimal places, those not highlighted are not significant (ns).

It would be interesting to determine if increased Smo inhibition, through prolonged culture or the addition of fresh drug every 24hrs, equating to a daily or continuous administration within the clinical setting, would cause irreversible differentiation, or go further to modify the cells proliferative abilities.

4.1.7 Gene interference using a *SMO* siRNA in the Kasumi-1 cell line generated differing functional results dependent upon the degree of knockdown achieved (n=2 with technical duplicates)

Whilst tomatidine was used as a negative control to ensure the effects seen with cyclopamine were due to Smo inhibition, we sought to clarify this further. A shRNA against human *SMO* in a PLKO.1 plasmid (Methods 2.2.1.10) was therefore used to generate a Kasumi-1 *SMO* knockdown (KD). The Kasumi-1 cell line was selected since pharmacological inhibition had resulted in apoptosis whilst other cell lines had shown differentiation. We therefore questioned whether apoptosis was an off-target effect or a reflection of sensitivity to cyclopamine.

In parallel to functional assays, the KD efficiency was analysed by RT-qPCR analysis. Compared with the scrambled (SCR) control, the remaining *SMO* expression ranged from 20% to 50%. For clarity, the average and individual results are shown, Figure 4.1.7.1. This experiment was performed twice. For the purpose of my thesis, I have addressed each of the biological replicates in succession as each supports a different hypothesis. I acknowledge this experiment needs to be repeated to achieve at least n=3 not least due to the differing results obtained.

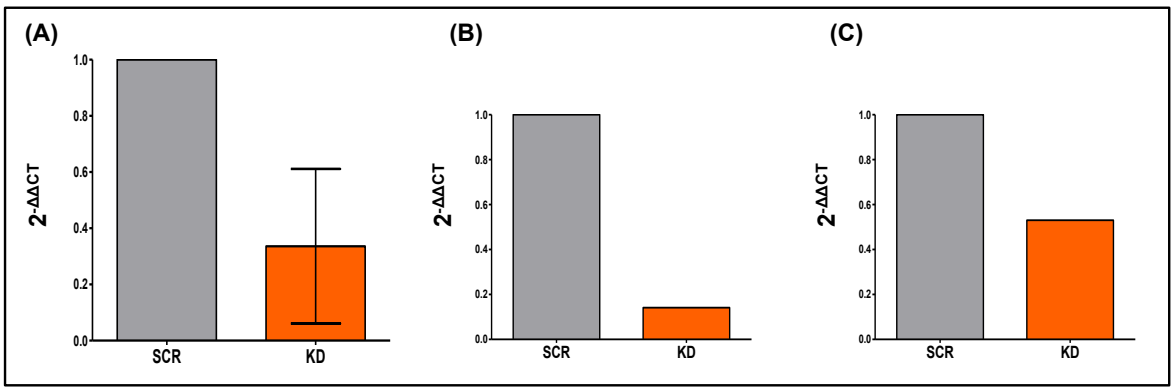

Figure 4.1.7.1: Knockdown efficiency of a shRNA against human *SMO* in Kasumi-1 cells. Kasumi-1 cells were virally transfected with a GFP tagged shRNA, cultured for 24hrs then harvested, RNA extracted and qRT-PCR performed to assess knockdown efficiency. Expression levels are shown as the fold change ($2^{-\Delta\Delta CT}$) relative to NDC with 2 housekeeping genes (*ENOX2* and *UBE2D2*) serving as endogenous control showing variable knockdown of *SMO*. (A) Each bar represents the fold change from two independent experiments with error bars indicating SD; (B&C) Each graph shows fold change from each individual experiment highlighting the variance in knockdown efficiency. SCR, Scrambled; KD, *SMO* knockdown.

In the 50% *SMO* KD model at 72hrs (Figure 4.1.7.1c) there was a 1.5-fold increase in the total number of live cells relative to input number by trypan blue dye exclusion compared to a 2.5-fold increase in the SCR control (Figure 4.1.7.2). Accounting for differences in the input cell number for each of the experimental arms at the 72hr time point, there was 1.8-fold greater number of live cells in the SCR control compared to *SMO* KD. In contrast to the results we had seen following pharmacological Smo inhibition, there was no difference in the number of dead cells by trypan blue dye exclusion between the *SMO* KD and SCR control. We therefore had evidence of reduced proliferation in the 50% *SMO* KD which was not explained by apoptosis.

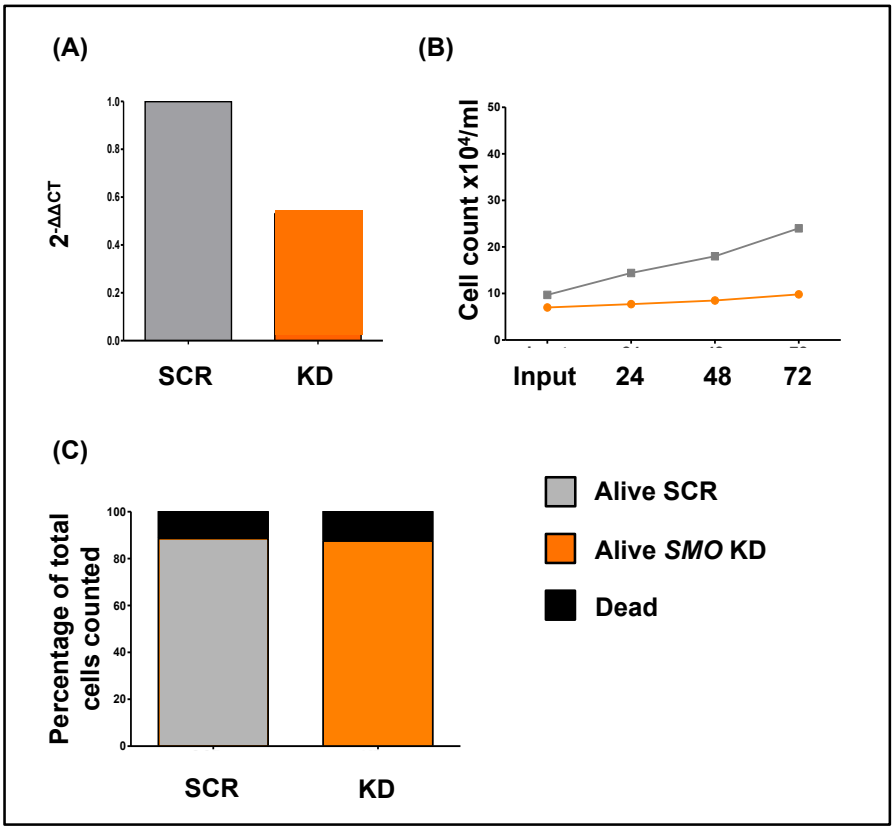

Figure 4.1.7.2: Cell viability, as determined by trypan blue dye exclusion, in a 50% *SMO* KD in the Kasumi-1 cell line.
Kasumi-1 cells were virally transfected with a GFP tagged shRNA. mRNA expression by qRT-PCR demonstrated 50% efficiency. (A) Levels of *SMO* expression following viral transfection expressed as the fold change ($2^{-\Delta\Delta CT}$) relative to SCR control with 2 housekeeping genes (*ENOX2* and *UBE2D2*) serving as endogenous control. (B) Cell number by trypan blue dye exclusion in the *SMO* KD and SCR control. (C) Percentage live and dead cells by trypan blue dye exclusion in the *SMO* KD and SCR control.
Reduced proliferation is demonstrated in the 50% KD compared to the SCR control by trypan blue dye exclusion, with no difference in the percentage of dead cells.

Considering this finding cell proliferation was studied by FACs using CTV to follow cell division; CTV fluorescence intensity progressively reducing with each cell division allowing number of divisions to be calculated relative to a non-dividing control population [588]. CTV was used rather than CFSE as our cells were labelled with GFP, seen in the same channel (FITC) as CFSE.

Interestingly, a reduction in cell proliferation was demonstrated by CTV showing a >2-fold reduction (0.45-fold change) in the MFI at 24hrs in the SCR control compared to a <2-fold reduction (0.67-fold change) in the *SMO* KD, Figure 4.1.7.3. Analysis beyond this time point was limited by the low input numbers and auto-fluorescence generated by the GFP tagged plasmid.

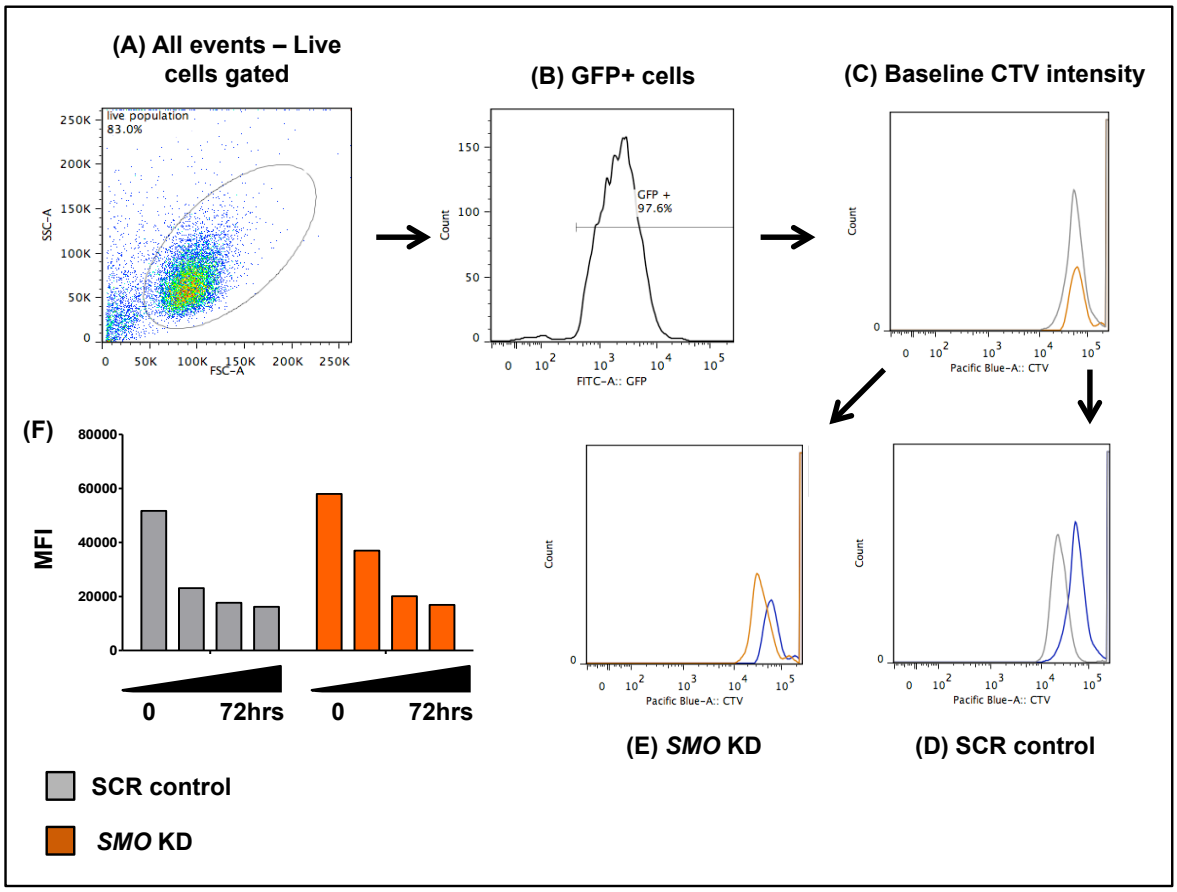

Figure 4.1.7.3: Proliferation, as determined by CTV staining, in a 50% *SMO* KD in the Kasumi-1 cell line.
Kasumi-1 cells were virally transfected with a GFP tagged shRNA. qRT-PCR demonstrated 50% efficiency. Reduced proliferation was demonstrated in the 50% KD compared to the SCR control by CTV staining and flow cytometry analysis. (A) FACS plot showing all events, with the live cell population gating strategy. (B) FACS plot showing GFP status of the live cell population with gating strategy. (C) FACS plot showing baseline (0hrs) CTV staining profile for the *SMO* KD (orange line) and SCR control (grey line). (D) FACS plot showing CTV staining profile following 24hrs culture profile for the SCR control (grey line) relative to baseline (blue line). (E) FACS plot showing CTV staining profile following 24hrs culture for the *SMO* KD (orange line) relative to baseline (blue line). (F) Graph showing the MFI of CTV staining at successive time points (24, 48 and 72hrs) in the *SMO* KD and SCR control clearly showing a reduction in proliferation at 24hrs in the 50% *SMO* KD relative to the SCR control.

Interestingly, as with the OCI-AML3 cell line in which altered cell kinetics were clearly demonstrated, a difference in cell morphology as determined by FSC / SSC parameters was also demonstrated suggesting a partial reduction in *SMO* leads to cell differentiation, Figure 4.1.7.4.

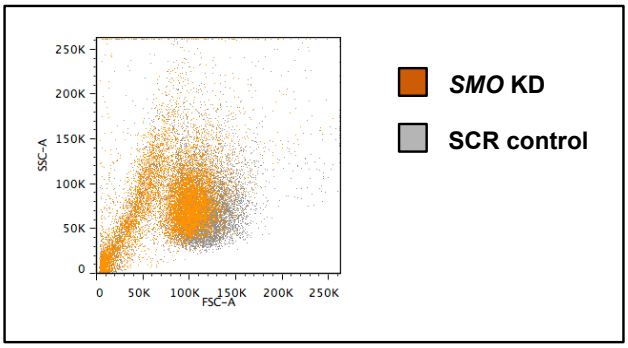

Figure 4.1.7.4: SSC profile of a 50% *SMO* KD in the Kasumi-1 cell line.
Kasumi-1 cells were virally transfected with a GFP tagged shRNA. qRT-PCR demonstrated 50% efficiency. Flow cytometry demonstrated an increase in SSC (reflecting granularity) in the 50% *SMO* KD compared to the SCR control following culture for 24hrs.

In contrast, in the 80% *SMO* KD model there was a 25% reduction in the total number of live cells, and a doubling in the number of dead cells by trypan blue dye exclusion compared to the SCR control at 72hrs. A difference in cell viability between the *SMO* KD and SCR control at 24hrs, 48hrs and 72hrs was confirmed by 7AAD with an increase in dead cells seen in the *SMO* KD relative to SCR control at each time point, Figure 4.1.7.5. Further, in contrast to the results seen with the 50% KD there was no difference in the FSC / SSC parameters between the *SMO* KD and SCR control arm, Figure 4.1.7.6.

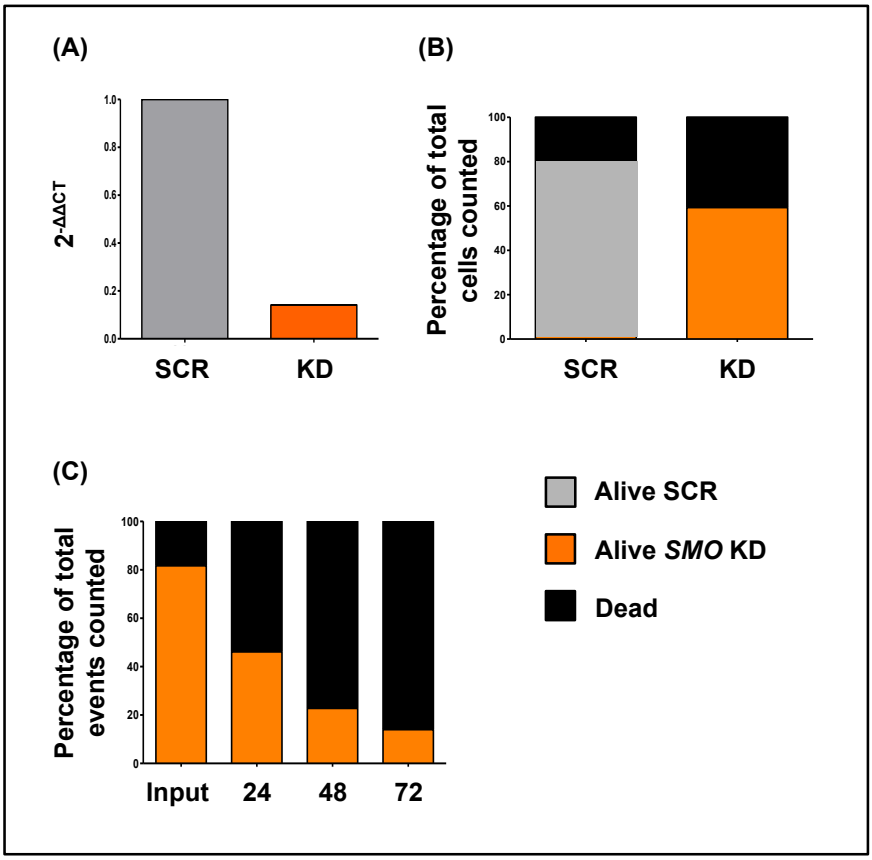

Figure 4.1.7.5: Cell viability, as determined by trypan blue dye exclusion, in an 80% *SMO* KD in the Kasumi-1 cell line.
Kasumi-1 cells were virally transfected with a GFP tagged shRNA. mRNA expression by qRT-PCR demonstrated 80% efficiency. (A) Levels of *SMO* expression following viral transfection expressed as the fold change ($2^{-\Delta\Delta CT}$) relative to SCR control with 2 housekeeping genes (*ENOX2* and *UBE2D2*) serving as endogenous control. (B) Percentage live and dead cells by trypan blue dye exclusion in the *SMO* KD and SCR control. (C) The *SMO* KD showed a progressive reduction in the number of live cells, with an accompanying increase in dead cells by 7AAD.
An increase in cell death was demonstrated in the 80% KD compared to the SCR control by trypan blue dye exclusion and FACs analysis using 7AAD.

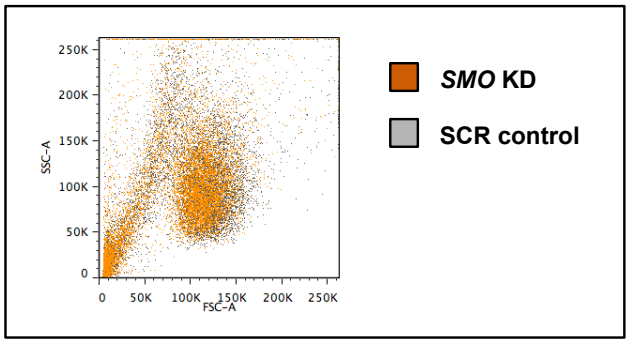

Figure 4.1.7.6: SSC profile of an 80% *SMO* KD in the Kasumi-1 cell line.
Kasumi-1 cells were virally transfected with a GFP tagged shRNA. qRT-PCR demonstrated 80% efficiency. Flow cytometry demonstrated no change in FSC / SSC parameters in the *SMO* KD compared to the SCR control following culture for 24hrs.

Whilst we acknowledge our knockdown model needs to be repeated, it is tempting to compare the contrasting results in our two KD experiments with the differing effects seen between the cell lines dependent upon their IC_{50}. This raises an interesting hypothesis, with exciting translational opportunities - could partial Smo inhibition force the cells to differentiate, whilst complete, or near complete, inhibition cause apoptosis? In the future we plan to validate this hypothesis by repeating the experiment to ensure n≥3 for both the partial *SMO* KD model, and near complete *SMO* KD model, evaluating key members of the Hh signalling pathway and downstream targets at both the gene and protein level. Further, it would be interesting to analyse the cells at a morphological level for evidence of differentiation and also apoptosis - hallmarks of cell apoptosis being cell shrinkage, nuclear DNA fragmentation and membrane blebbing [633]. In addition, it would be very interesting to perform a KD in the OCI-AML3 cell line given the contrasting response to cyclopamine.

There was insufficient material from the limited experiments performed to allow protein analysis by Western blotting. Interestingly, despite the functional changes demonstrated, ICC showed no significant difference in SMO expression between the *SMO* KD and SCR control at 72hrs, This may however reflect basal protein expression, before changes in transcription could be translated to the protein level, the presence of the protein reflecting the rate of protein degradation rather than changes in protein synthesis [634]. Further, Smo is cycled between the membrane and cytoplasm depending on pathway activity. The antibody however cannot discriminate between available (membrane bound) and unavailable (cytoplasmic) protein. Had time allowed, we would have repeated the experiment, performing ICC on cells harvested at both earlier and later time points, to determine the timing and degree of change in SMO protein expression.

4.1.8 Smo inhibition with cyclopamine led to the down-regulation of *GLI-1*, a marker of pathway activity, in select, genetically diverse AML cell lines.

As discussed in Background 1.4.2, whilst classically the Hh pathway was believed to be ligand-dependent, more recent work has considered the notion of non-canonical signalling [349,350,374]. Further, both positive and negative feedback is understood to regulate pathway activity [331,340,345,635,636]. We therefore sought to determine the effects of cyclopamine on the transcription of components of the Hh pathway. RNA was extracted from an aliquot of cells harvested following culture with increasing doses of cyclopamine for 72hrs. The remainder of the cells were used for various functional assays to minimise confounding effects and to ensure gene changes could be accurately correlated with functional change. The $2^{-\Delta\Delta CT}$ method was used to show expression of the gene of interest relative to the NDC, expressed as 1, Figure 4.1.8.1.

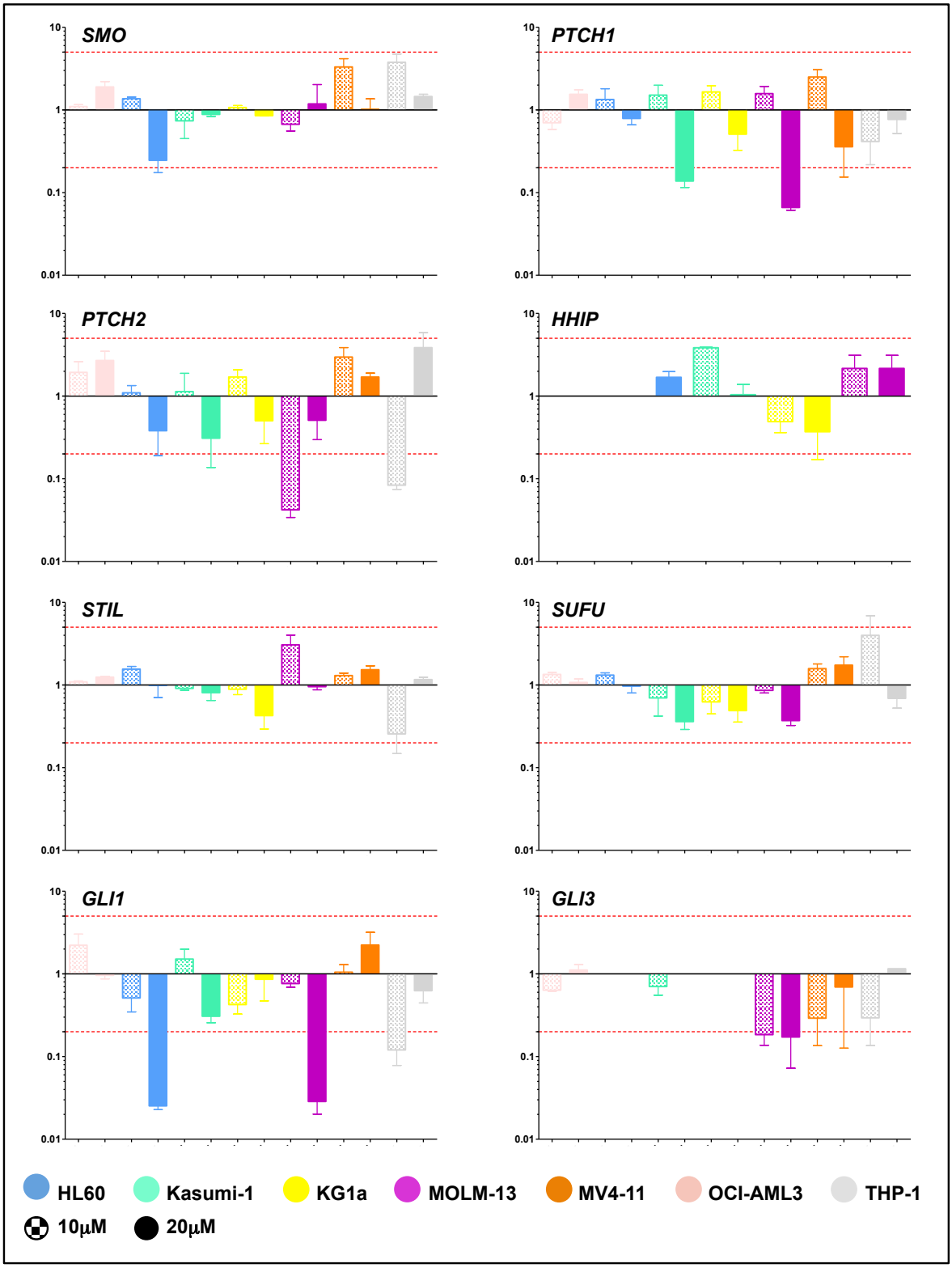

Figure 4.1.8.1: Variance in the mRNA expression of components of the Hh pathway in seven genetically diverse AML cell lines following culture with cyclopamine (10μM and 20μM) for 72hrs. RNA was extracted from an aliquot of cells harvested following culture with cyclopamine at a dose of 10μM and 20μM for 72hrs. Expression levels were quantified by qRT-PCR using Fluidigm® technology. Expression levels are shown as $2^{-\Delta\Delta CT}$, with 6 housekeeping genes genes - *ATP5S*, *B2M*, *ENOX2*, *GAPDH*, *TYWI* and *UBE2D2* serving as endogenous control; CT values for these genes ranged from 3 to 13. The mean of 3 biological replicates, each performed in technical duplicate, are shown with error bars indicating the SD clearly showing a marked variance in the mRNA expression of components of the Hh pathway in our selected AML cell lines.

There was no significant change in the expression of *SMO* in each of our selected cell lines following culture with cyclopamine (10μM and 20μM). *PTCH1* was down-regulated in the genetically diverse Kasumi-1, MOLM-13 and MV4-11 cell lines following culture with 20μM cyclopamine though not 10μM; apoptosis was seen in the Kasumi-1 and MOLM-13 cell lines though not the MV4-11 cell line following culture with cyclopamine. *GLI-1* was down-regulated in the MOLM-13 cell line and, to a lesser degree the Kasumi-1 cell line; it was marginally up-regulated in the MV4-11 cell line. *GLI-2*, previously shown to be absent when cells were harvested following culture for 24hrs at optimal cell density was not detected in any cell line, irrespective of experimental condition. Interestingly, the transcriptional repressor, *GLI-3*, was variably down-regulated in all cell lines, with the effect greater following culture with 20μM cyclopamine. There was minimal change identified in the other negative regulators *HHIP, STIL* and *SUFU* following culture of each of our selected, genetically diverse cell lines with both 10μM and 20μM cyclopamine.

4.1.9 Manipulation of the Hh pathway by Smo inhibition with cyclopamine affects expression of genes involved in apoptosis and autophagy in a cell line-specific manner

We recognise the degree of cross talk between the self-renewal pathways, and the potential for redundancy of individual components, and therefore the limitations of interpreting expression of components of the Hh pathway in isolation. We therefore sought to analyse expression of key downstream targets. Acknowledging the vast array of targets of the pathway, Figure 1.8, we selected key targets and pathways (1) known to be affected by conventional treatment (considering our ultimate objective to evaluate the potential of these small molecule inhibitors in the clinical setting) and (2) in accordance with our functional data.

First line treatment for AML standardly uses Ara-C combined with an anthracycline [201,202]. Research has shown clinical response to Ara-C to depend upon genes including deoxycytidine kinase, cytidine deaminase, cytosolic 5'-nucleotidases, DNA polymerases, topoisomerases, *BCL-2* and *TP53* [533]. However, the exact mechanism, and the pathways involved remain to be determined. Considering the complexity of AML, and the evidence to support pathway redundancy, it is not surprising that small molecule inhibitors, as single agents, have had limited effects. Our functional data, supported by others [377,379], has shown Smo inhibition to result in apoptosis in select cell lines. However, in contrast to these results, reduced proliferation in the absence of apoptosis was demonstrated in other cell lines. This is again supported by research showing the Hh pathway to regulate the cell cycle [362,637]. Additionally, autophagy is a highly controlled proteolytic process that can be induced by cellular stress [638,639], with recent work demonstrating its involvement in oncogenesis, disease progression, treatment resistance and relapse [640]. Interestingly, recent work has shown the Hh pathway to regulate autophagy, though results are conflicting with the Hh pathway being shown to both inhibit and induce autophagy [613,641,642]. Our results had shown evidence of both altered cell cycle kinetics and apoptosis. We therefore sought to determine the effect of cyclopamine at a gene level on apoptosis, autophagy and the cell cycle.

RNA was extracted from cells following culture with cyclopamine at a concentration of 5μM, 10μM and 20μM for 72hrs. 5μM was selected to evaluate whether gene expression was affected by a concentration not shown to affect cell proliferation or cell death by trypan blue dye exclusion. Technical triplicates were performed for each sample. The $2^{-\Delta\Delta CT}$ method was used to show expression of the gene of interest relative to the NDC. Log transformation of the fold change enabled graphical display of expression patterns according to the unsupervised Eisen approach using PermutMatrix software [589]; Figure 4.1.9.1.

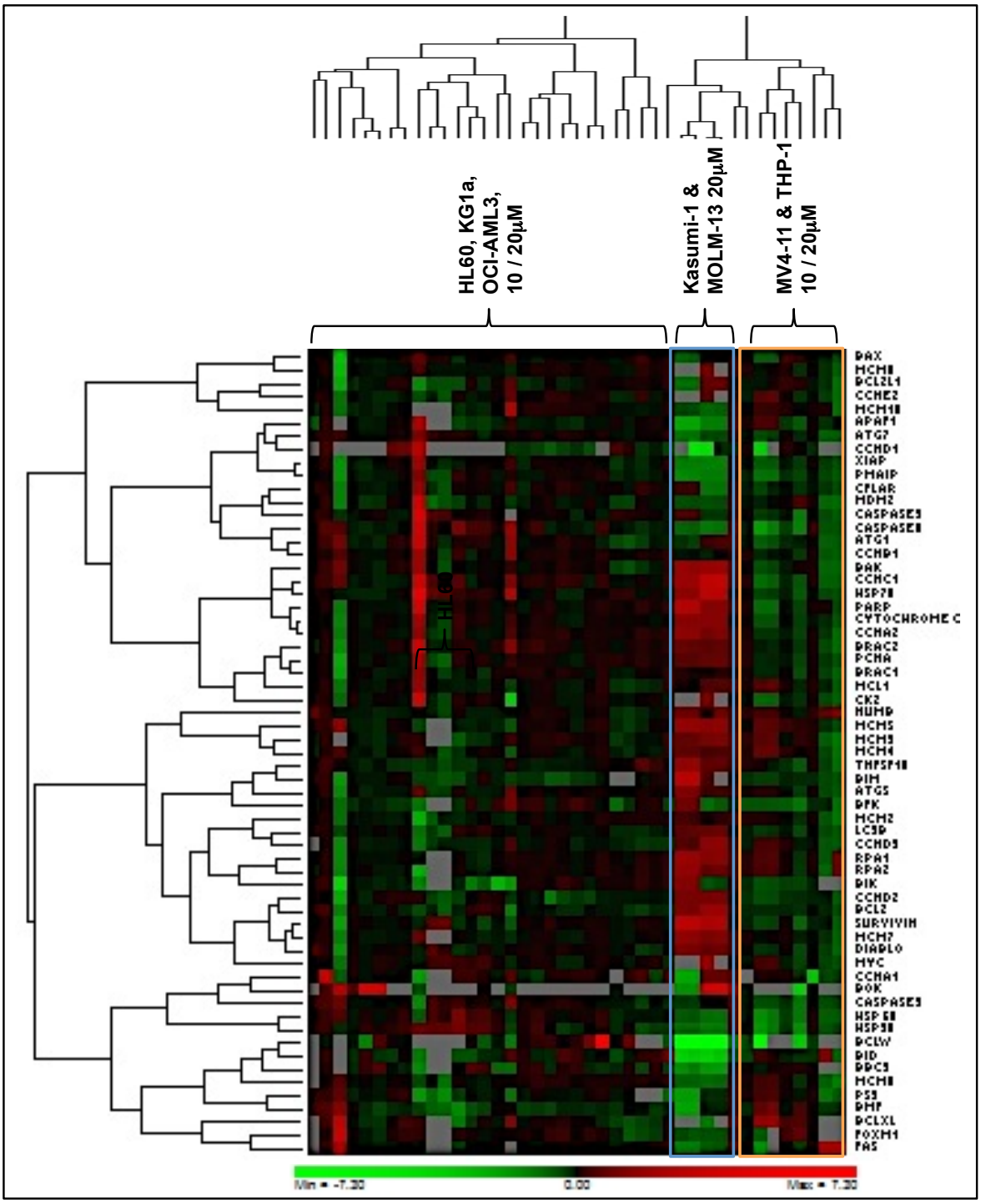

Figure 4.1.9.1: Gene expression profiles for genes involved in apoptosis, autophagy and cell cycle, following culture with cyclopamine (5μM, 10μM and 20μM) for 72hrs.
RNA was extracted from an aliquot of cells harvested following culture with increasing doses of cyclopamine for 72hrs. Expression levels were quantified by qRT-PCR using Fluidigm® technology. To account for input cDNA the ΔCT for each gene was calculated by subtracting the CT value of 6 housekeeping (control) genes (*ATP5S, B2M, ENOX2, GAPDH, TYWI* and *UBE2D2)* from the CT recorded the gene of interest. Technical triplicates were performed for each sample. Log transformation of the $2^{-\Delta\Delta CT}$ enabled graphical display of expression patterns according the unsupervised Eisen approach using PermutMatrix software [506]. Complete-linkage clustering of our selected genes and all experimental conditions are shown. The expression changes and consequent clustering of Kasumi-1 and MOLM-13 following culture with cyclopamine 20μM is highlighted in blue. MV4-11 and THP-1 are also seen to cluster irrespective of cyclopamine concentration, highlighted in orange.

The results generated by PermutMatrix are striking. Complete linkage clustering found marked similarity between the Kasumi-1 and MOLM-13 cell lines (highlighted in blue) suggesting a dependence upon Smo or the Hh pathway or a shared characteristic influenced by the Hh pathway despite their genetic diversity. Interestingly, this similarity in gene expression was restricted to culture with 20μM cyclopamine; expression patterns following culture with cyclopamine at 5μM and 10μM were scattered throughout the heatmap suggesting a threshold effect. It is important however, to consider whether the expression changes within the Kasumi-1 and MOLM-13 cell lines reflect cellular stress, and the apoptotic process, or whether it is these expression changes which result in apoptosis. To investigate this further we would analyse gene expression at successive time points, correlating it with functional data. As striking as this clustering, or similarity, is, is the disparity in the expression patterns of the CD34 positive cell lines: Kasumi-1 and KG1a, and the FLT3-ITD expressing cell lines: MV4-11 and MOLM-13. In our opinion, these varied expression changes highlight the complexity, and to a degree our yet superficial understanding and characterisation, of AML.

A number of findings are now highlighted and discussed in further detail. *LC3B* was up-regulated in the Kasumi-1 and MOLM-13 cell lines following culture with cyclopamine at a concentration of 20μM; Figure 4.1.9.2. This is particularly interesting considering the dual role LC3B plays in regulating autophagy and microtubule assembly [643], microtubules being vital in forming primary cilia and thereby enabling canonical Hh signalling [429,431,454,641]. Apoptosis was observed following culture of the Kasumi-1 and MOLM-13 cell lines with cyclopamine (10μM and 20μM). Interestingly expression changes were not seen following culture of the Kasumi-1 and MOLM-13 cell lines with 10μM cyclopamine. *ULK1*, *ATG5* and *ATG7* were not significantly affected, remaining relatively uniformly expressed following culture with cyclopamine, at a concentration of 10μM and 20μM, relative to the NDC in all cell lines.

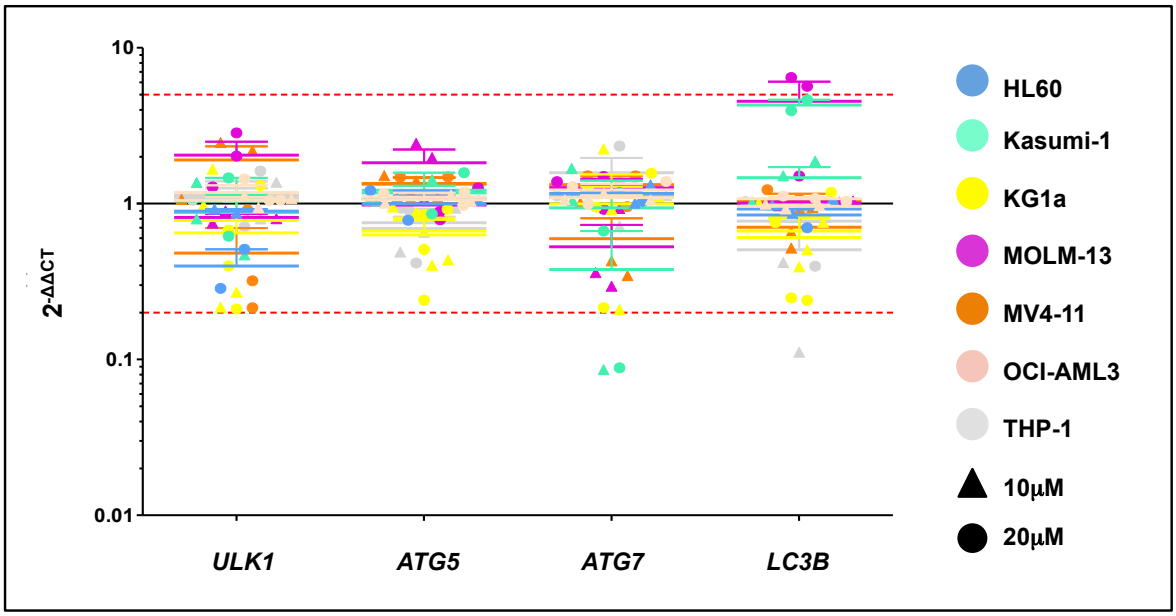

Figure 4.1.9.2: Expression of genes involved in autophagy in seven genetically diverse, AML cell lines, following culture with cyclopamine (10μM and 20μM) for 72hrs.
RNA was extracted from an aliquot of cells harvested following culture with increasing doses of cyclopamine for 72hrs. Expression levels were quantified by qRT-PCR using Fluidigm® technology. Expression levels are shown as $2^{-\Delta\Delta CT}$, with 6 housekeeping genes genes – *ATP5S*, *B2M*, *ENOX2*, *GAPDH*, *TYWI* and *UBE2D2* serving as endogenous control; CT values for these genes ranged from 3 to 13. The mean of 3 biological replicates are shown, each performed in technical duplicate, with error bars indicate SD. With the exception of *LC3B* genes involved in autophagy were uniformly expressed by our selected genetically diverse AML cell lines, irrespective of the concentration of cyclopamine with which they were cultured.

Within the anti-apoptotic genes we had selected, minimal change was seen following culture with cyclopamine (10μM and 20μM) relative to the NDC in all cell lines with a couple of notable exceptions; Figure 4.1.9.3. *BCL-W* was down-regulated in the genetically diverse HL60 and MOLM-13 cell lines (>10-fold), in which our functional data had shown differing results; it was relatively unchanged in the Kasumi-1, KG1a, MV4-11 and OCI-AML3 cell lines. *MCL-1* was consistently up-regulated by MV4-11 following culture with cyclopamine (both 10μM and 20μM; 3-fold and 2.3-fold, respectively) though this was not significant. This is particularly interesting since recent work analysing Bcl-2 inhibitors has highlighted the intricate relationship between Mcl-1 and Bcl-2, either seemingly able to 'rescue' the cell from apoptosis if up-regulated in the absence of the other [232]. We postulate that up-regulation of *MCL-1* might explain the differential results, both functional and at a gene level, seen following culture of our two FLT3-ITD positive cell lines MOLM-13 and MV4-11 with cyclopamine.

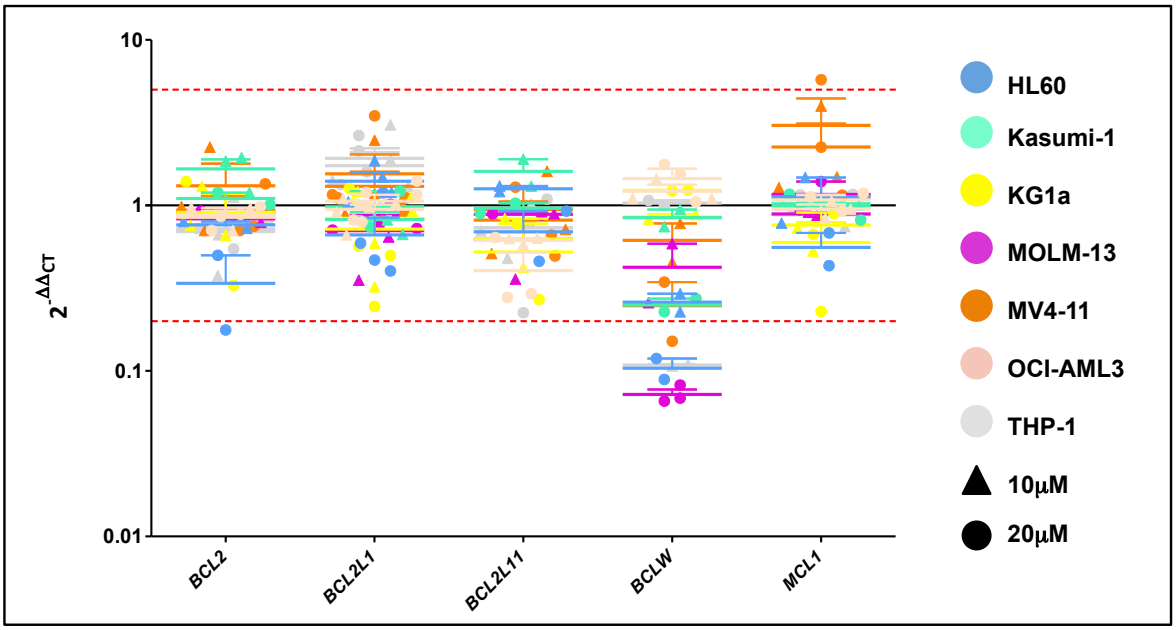

Figure 4.1.9.3: mRNA expression of the anti-apoptotic members of the Bcl-2 family in seven genetically diverse, AML cell lines, following culture with cyclopamine (10μM and 20μM) for 72hrs. RNA was extracted from an aliquot of cells harvested following culture with increasing doses of cyclopamine for 72hrs. Expression levels were quantified by qRT-PCR using Fluidigm® technology. Expression levels are shown as $2^{-\Delta\Delta CT}$, with 6 housekeeping genes genes - *ATP5S, B2M, ENOX2, GAPDH, TYWI* and *UBE2D2* serving as endogenous control; CT values for these genes ranged from 3 to 13. The mean of 3 biological replicates, each performed in technical duplicate, are shown with error bars indicate SD. mRNA expression of the anti-apoptotic members of the Bcl-2 family were tightly regulated with the exception of *BCL-W* in seven genetically diverse AML cell lines following culture with cyclopamine for 72hrs.

Minimal change was seen within our selected pro-apoptotic genes following culture with cyclopamine relative to the NDC in all cell lines (Figure 4.1.9.4); notable exceptions require further discussion. *APAF-1, BBC3* and *BID* were down-regulated in the Kasumi-1 cell line while *TP53* was down-regulated in the HL60 cell line following culture with cyclopamine.

Considering our functional data, the gene expression profiles we observed were not expected - we had anticipated an expression shift in favour of apoptosis in the Kasumi-1 and MOLM-13 cell lines. We propose a number of potential explanations, which, would be interesting to consider in the future: (1) changes occurred at a protein rather than gene level, (2) slight changes in expression of these powerful genes were sufficient to push cells towards apoptosis, (3) caspase-independent pathways were involved, the tumour necrosis factor (TNF) receptor, c-Jun N-terminal kinase (JNK), NF-κB and mitogen-activated protein kinase (MAPK) / ERK [645,646]. It would be interesting to study expression of these genes.

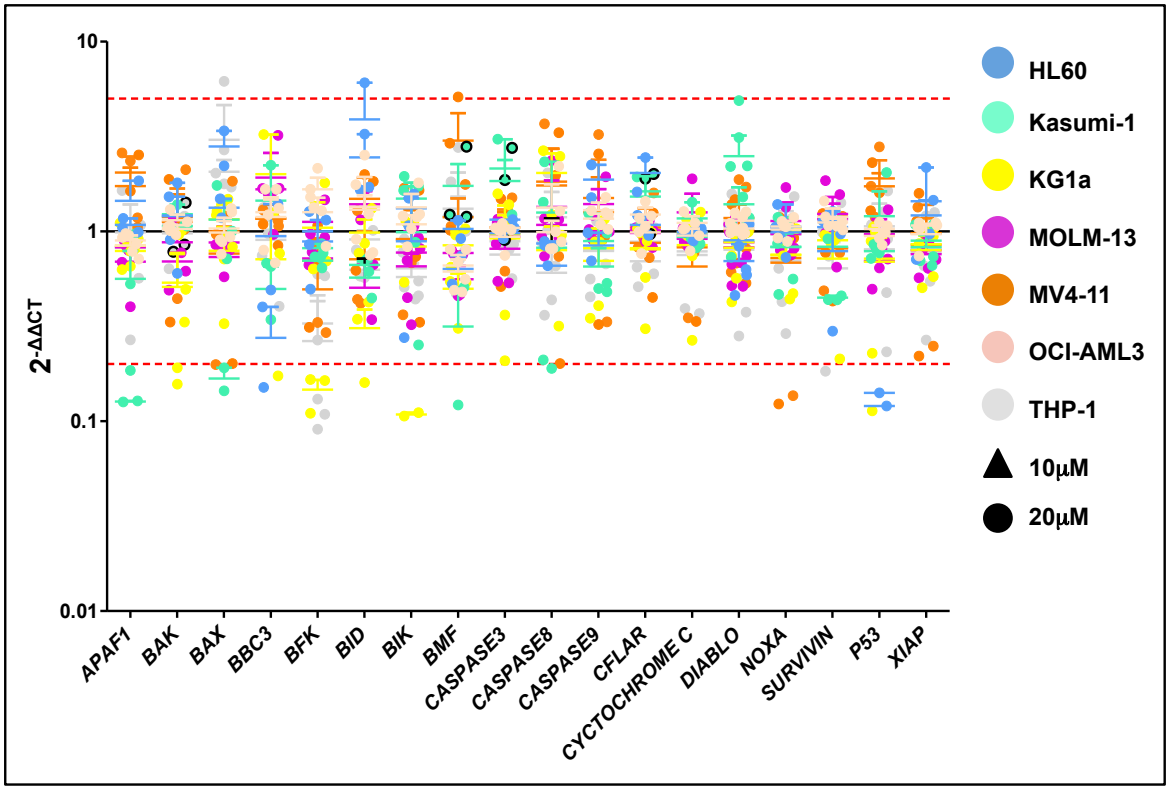

Figure 4.1.9.4: mRNA expression of pro-apoptotic members of the Bcl-2 family in seven genetically diverse AML cell lines, following culture with cyclopamine (10μM and 20μM) for 72hrs.
RNA was extracted from an aliquot of cells harvested following culture with increasing doses of cyclopamine for 72hrs. Expression levels were quantified by qRT-PCR using Fluidigm® technology. Expression levels are shown as $2^{-\Delta\Delta CT}$, with 6 housekeeping genes genes – *ATP5S, B2M, ENOX2, GAPDH, TYWI* and *UBE2D2* serving as endogenous control; CT values for these genes ranged from 3 to 13. The mean of 3 biological replicates, performed in technical duplicate, are shown with error bars indicate SD. Expression of pro-apoptotic genes was tightly regulated, and largely unchanged following culture with cyclopamine across each of our selected AML cell lines.

Within regulators of cell cycle, *CCND1*, required for progression through the G1 phase of the cell cycle, was down-regulated in the Kasumi-1 and MOLM-13 cell lines following culture with 20μM cyclopamine, Figure 4.1.9.5. The uniform up-regulation of *PARP1* is interesting considering its role in differentiation, proliferation and perhaps, more importantly in this context, DNA repair. Further, PARP1 has been shown to be up-regulated in haematological malignancies, with clinical grade PARP inhibitors in early clinical trial in solid and haematological malignancies; the PARP inhibitor Olaparib was approved by the EMA and FDA in 2014 [647-653] for relapsed ovarian cancer. As we have discussed earlier, the use of small molecule inhibitors in isolation is unlikely to change the trajectory of these highly complex and diverse malignancies. Could Smo inhibition induce a stress response thus sensitising AML cells to standard chemotherapeutic agents or other small molecule inhibitors?

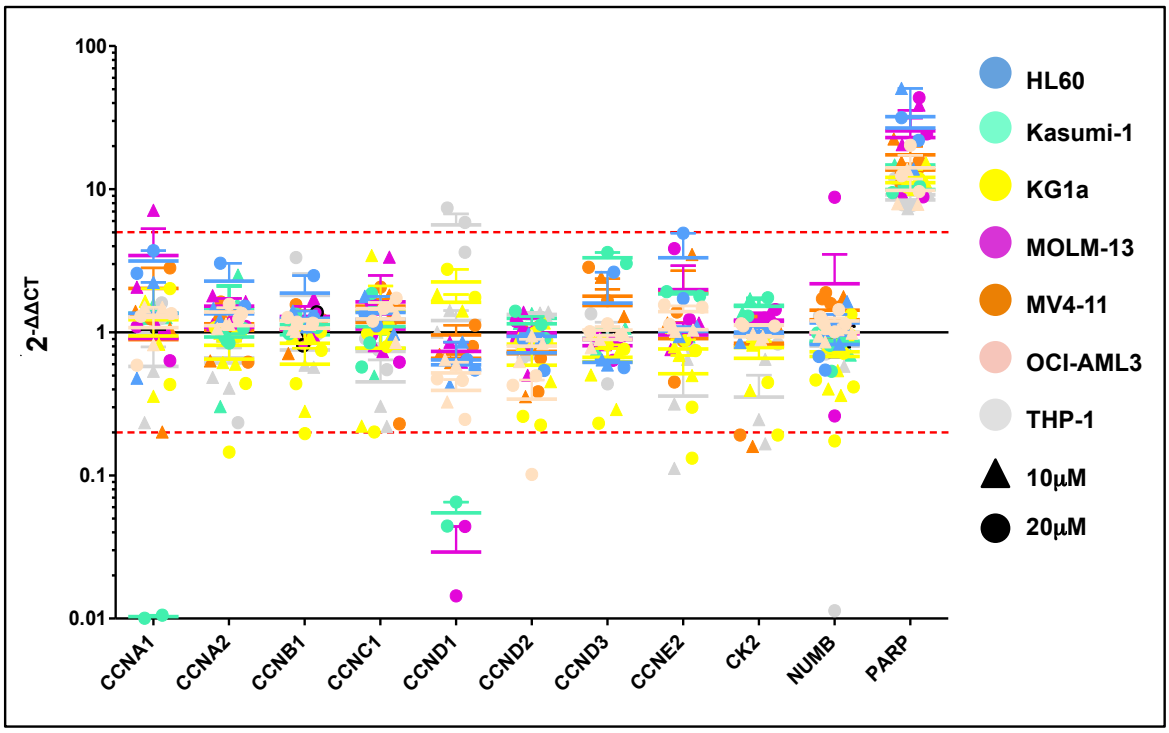

Figure 4.1.9.5: mRNA expression of genes involved in cell cycle regulation and differentiation in seven genetically diverse AML cell lines, following culture with cyclopamine (10μM and 20μM) for 72hrs.

RNA was extracted from an aliquot of cells harvested following culture with increasing doses of cyclopamine for 72hrs. Expression levels were quantified by qRT-PCR using Fluidigm® technology. Expression levels are shown as $2^{-\Delta\Delta CT}$, with 6 housekeeping genes genes – *ATP5S, B2M, ENOX2, GAPDH, TYWI* and *UBE2D2* serving as endogenous control; CT values for these genes ranged from 3 to 13. The mean of 3 biological replicates, performed in technical duplicate, are shown with error bars indicate SD. *PARP* was universally up-regulated following culture with cyclopamine. The cell cycle regulators were otherwise not significantly affected by culture with cyclopamine, irrespective of concentration with the exception of *CCND1* and *CCND2 which* were down-regulated following culture of the Kasumi-1 and MOLM-13 cell lines.

4.1.10 Manipulation of the Hh pathway with glasdegib, a clinical grade SMO inhibitor alters cell proliferation

APML is the success story of AML, a model for precision medicine. In APML ATRA forces the leukaemic blast cells to differentiate, rendering them more susceptible to cytotoxic agents. Evidence of differentiation in select, genetically definable, AML cell lines *in vitro* was, therefore, hugely exciting, suggesting a potential mechanism, and thus role, for Smo antagonism in the clinical management of AML. We hypothesised Smo inhibition would drive a subset of AML cases to differentiate, rendering them more sensitive to cytotoxic therapy. Further, evidence of apoptosis in other, genetically distinct, AML cell lines suggests Smo antagonists have the potential to prove beneficial though perhaps through different mechanisms dependent upon genotype. Considering this and recognising cyclopamine is not suitable for clinical use we studied several clinical grade drugs: Erivedge® (vismodegib, Genentech), Glasdegib® (PF-04449913, Pfizer) and Odomzo® (sonidegib, Novartis), discussed in greater depth in Background 1.4.5.1. The results of our work looking at glasdegib are presented here. The OCI-AML3 cell line was selected to determine whether cellular differentiation was specific to Smo inhibition with cyclopamine or seen in the presence of other, clinical grade, Smo antagonists. In addition, another myelomonocytic cell line, MOLM-13, was studied. MOLM-13 carries the FLT3-ITD mutation, found in approximately 30% of all cases of AML, with published data linking the FLT3-ITD mutation with deregulated Hh signalling, in particular in those historically classed as FAB M4

[379,381]. Further, our functional data had shown evidence of apoptosis, with gene expression studies consistent with cellular stress, following culture with cyclopamine.

We utilised the resazurin assay to determine the effect of a wide range of concentrations of glasdegib on cell viability following culture for 72hrs for each of our chosen cell lines; Figure 4.1.10.1.

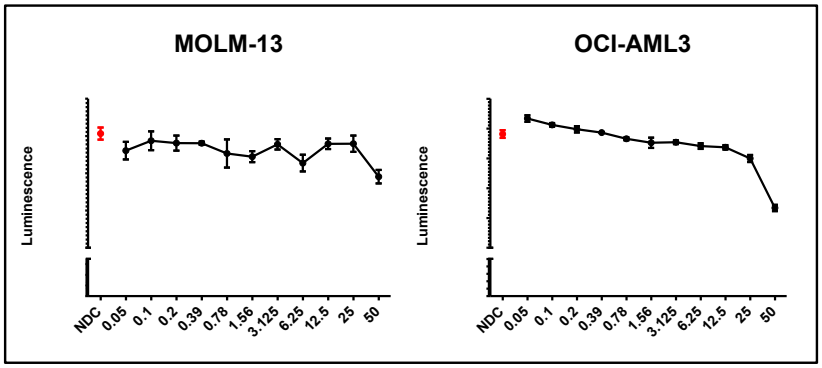

Figure 4.1.10.1: Metabolic activity, as a measure of cell viability, in the MOLM-13 and OCI-AML3 cell lines following culture with incremental doses of glasdegib (μM) for 72hrs, as determined by the resazurin assay.
Cells, at a concentration of $1x10^5$/ml, were exposed to incremental doses of glasdegib (μM) and cultured for 72hrs. Cell viability was determined using the resazurin assay. Results are expressed as the mean luminescence (n=8) with error bars indicating SD. NDC is highlighted in red. Whilst a reduction in luminescence was demonstrated following culture of the OCI-AML3 cell line at concentrations of >25mM no change was seen within the MOLM-13 cell line across all concentrations.

Using the resazurin assay, no significant change in metabolic activity was seen with doses below 25μM in the OCI-AML3 cell line, with no change in metabolic activity across all doses in the MOLM-13 cell line. These results are consistent with those reported showing no notable change following *in vitro* short term culture of the AML cell line Marimo [383] and comparable to results obtained following culture of these cell lines with cyclopamine (section 4.1.3). These results contrasted with those reported following long-term *in vitro* culture and murine studies [383].

We recognise the limitations of the resazurin assay. Further, this assay had suggested minimal effect on metabolic activity following culture of these cell lines with cyclopamine at concentrations below 25μM; whilst trypan blue dye exclusion had demonstrated a statistically significant reduction in the number of live cells following culture with cyclopamine at a concentration of10μM and 20μM. Considering our aim was to compare the effects of the *in vitro* culture of genetically diverse AML cell lines with cyclopamine to those with a clinical grade Smo antagonist we referenced a phase 1 safety and pharmacokinetics study published in 2015 [407] to determine appropriate drug concentrations. Objective responses, suggestive of biological activity, were demonstrated across a range of doses, with the maximum tolerated dose for continuous treatment reported to be 400mg OD [407]. The recommended phase two dose was determined to be ≤200mg OD. No off-target effects were identified. We therefore looked at the median pharmacokinetic area under the plasma concentration-time curve at 0hrs following the administration of 180mg, 270mg and 400mg. Converting ng/ml to μM we determined a dose range of 2.67μM to 10.68μM. A glasdegib concentration of 2.67μM, 5.34μM and 10.68μM was therefore used for all future experiments; we wished to determine the effects of a clinical grade drug at clinically compatible concentrations. Considering our results following culture with cyclopamine we initially performed the following functional assays:

1) Trypan blue dye exclusion (as a measure of cell proliferation and death),

2) Annexin V / 7AAD staining with flow cytometry analysis (to accurately study the process of apoptosis),

3) PI staining with flow cytometry analysis (to analyse cell cycle kinetics) and

4) Analysis of FSC / SSC flow cytometry plots (to assess morphological change).

There was a consistent downward trend in the number of live cells by trypan blue dye exclusion following culture of OCI-AML3 cells with increasing concentrations of glasdegib; with a statistically significant reduction demonstrated following culture with glasdegib at a concentration of 10.68μM ($p=0.049$). There was no change in the number of dead cells by trypan blue dye exclusion, and no evidence of apoptosis by Annexin V / 7AAD. In contrast to results obtained following culture with cyclopamine there was no change in cell cycle kinetics by PI, Figure 4.1.10.2.

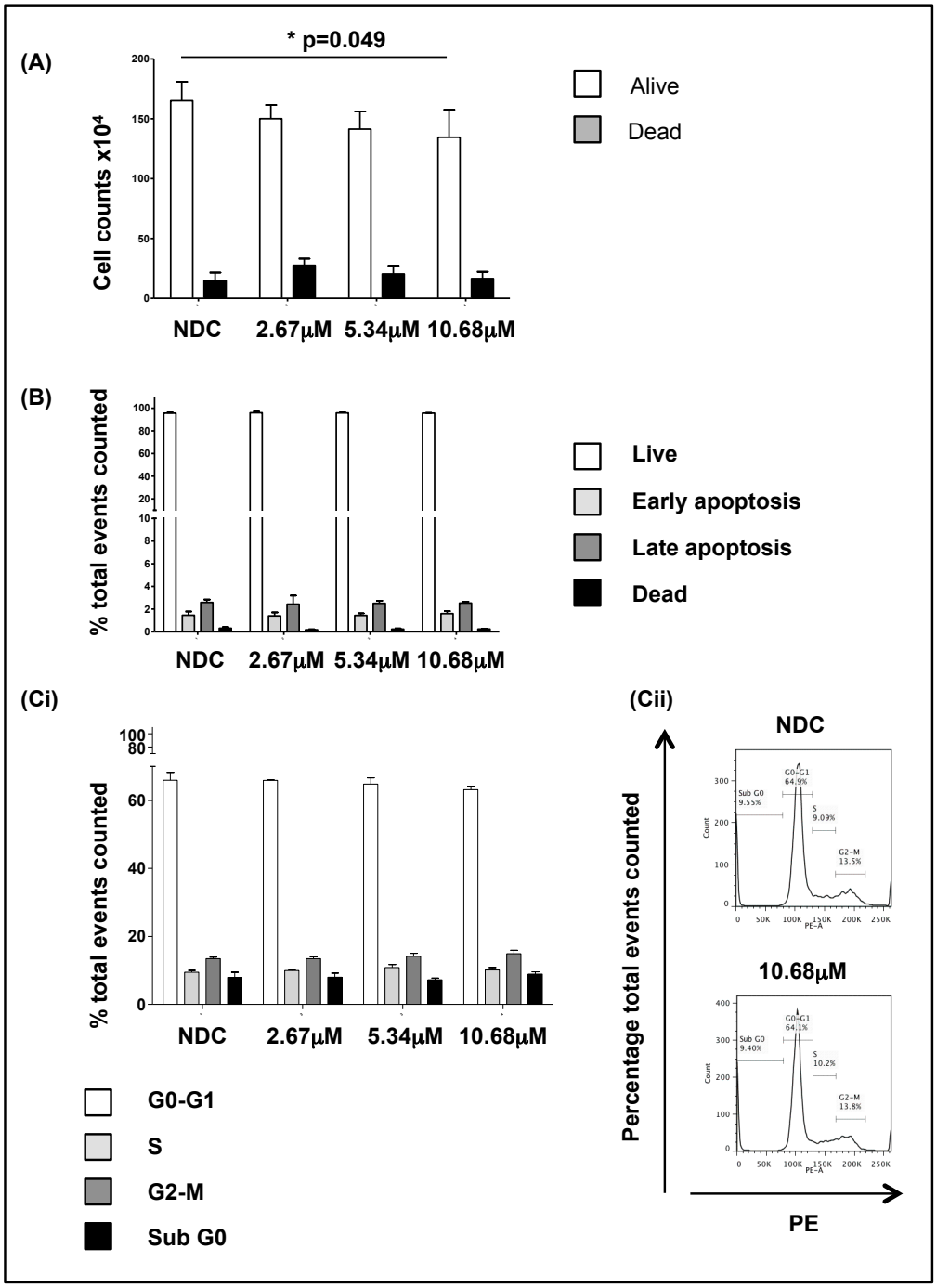

Figure 4.1.10.2: Cell viability and cell cycle kinetics following culture of the OCI-AML3 cell line with glasdegib (2.67μM, 5.34μM and 10.68μM; clinically achievable concentrations) for 72hrs. OCI-AML3 cells were seeded at a concentration of $2x10^5$/ml, exposed to incremental doses of glasdegib, cultured for 72hrs then harvested and stained with trypan blue dye exclusion, Annexin V / 7AAD or PI prior to analysis. (A) Bar graph showing cell viability as determined by trypan blue dye exclusion. Each bar represents the mean cell number $x10^4$/ml from four independent experiments with error bars indicating SD. (B) Bar graph showing the proportion of cells which are viable, in early apoptosis, in late apoptosis or dead as determined by Annexin V / 7AAD staining, and analysis by flow cytometry. The percentages shown indicate the proportion of total events within each of the respective categories as gated on the flow cytometry plots (see Figure 2.3 for gating strategy). Each bar represents the mean percentage from four independent experiments with error bars indicating SD. (Ci) Bar graph indicating the proportion of cells within each cell cycle phase (G0-G1, S, G2-M and Sub G0) as determined by PI staining, and analysis by flow cytometry. Each bar represents the mean percentage from four independent experiments with error bars indicating SD. (Cii) Representative flow cytometry plots, and gating strategy, following PI staining. Each plot is representative of data from one experiment of four with similar results. All statistically significant results are highlighted with p value to the nearest 3 decimal places, those not highlighted are not significant. These graphs showing culture of the OCI-AML3 cell line with glasdegib caused a statistically significant reduction in proliferation not explained by apoptosis or altered cell kinetics.

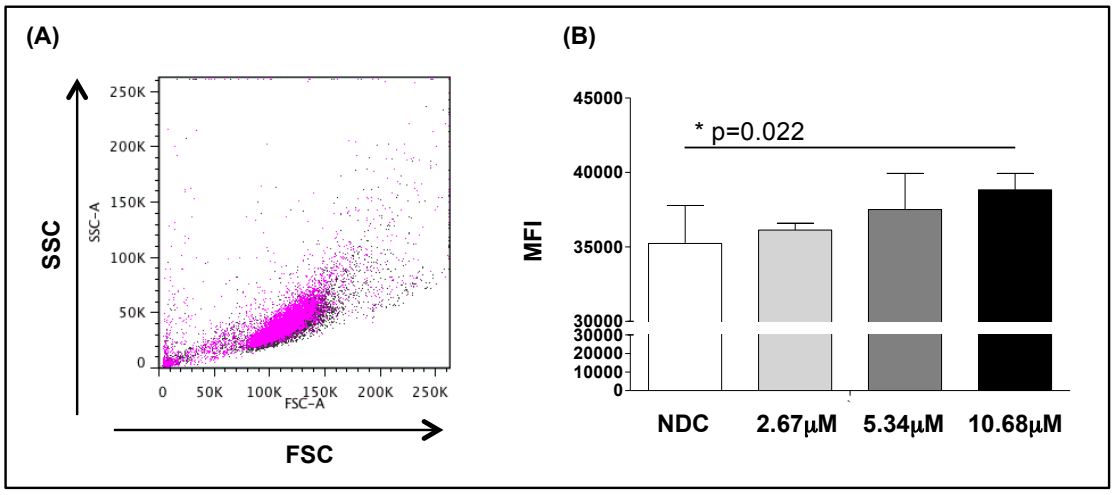

Figure 4.1.10.3: SSC MFI, and representative FACS plot, following culture of the OCI-AML3 cell line with glasdegib (2.67μM, 5.34μM and 10.68μM; clinically achievable concentrations) for 72hrs. OCI-AML3 cells were seeded at a concentration of $2x10^5$/ml, exposed to incremental doses of glasdegib, cultured for 72hrs then harvested prior to analysis by flow cytometry. (A) Representative FSC / SSC flow cytometry plot from one experiment of four with similar results. This demonstrates the increase in SSC (reflecting cell granularity) in OCI-AML3 cell line relative to the NDC. (B) Bar graph showing the MFI of SSC. Each bar represents the mean MFI from four independent experiments with error bars indicating SD. All statistically significant results are highlighted with p value to the nearest 3 decimal places, those not highlighted are not significant. The FACS plot, and bar graph, clearly showing culture of the OCI-AML3 cell line with glasdegib caused a statistically significant increase in the SSC parameter, reflecting increased granularity.

Analysis of the FSC / SSC plots following culture of the OCI-AML3 cell line with glasdegib for 72hrs, whilst not as striking as following culture with cyclopamine, showed a statistically significant increase in the SSC parameter in keeping with increased granularity, Figure 4.1.10.3. This was confirmed when cells were visualised by light microscopy - cells were seen to have a more mature phenotype with cytoplasmic vacuoles and granules and loss of nucleoli. Slides were blindly reported and independently verified by Dr M Leach, Consultant Haematologist, NHS Greater Glasgow and Clyde to whom I am indebted for time and expertise.

Within the MOLM-13 cell line, there was a reduction in the total number of live cells by trypan blue dye exclusion following culture with increasing doses of glasdegib, though this was not significant. In contrast to results following culture with cyclopamine, there was no change in the total number of dead cells by trypan blue dye exclusion, and no evidence of apoptosis by Annexin V / 7AAD staining. It must, however, be acknowledged that whilst a reduction in live cells was seen with increasing concentrations of cyclopamine apoptosis was only apparent following culture with 20μM. Interestingly, PI staining demonstrated cell cycle arrest with a statistically significant increase in the percentage of inactive, non-cycling cells (G0-G1) following culture with glasdegib, 5.35μM (p=0.029) and 10.68μM (p=0.035), compared to the NDC; Figure 4.1.10.4. Further work is required to determine the mechanism of cell cycle arrest. There was no evidence of cellular senescence as determined by measuring ß-galactosidase activity and, there was no change in FSC / SSC parameters seen between the NDC and all concentrations of glasdegib, Figure 4.1.10.5.

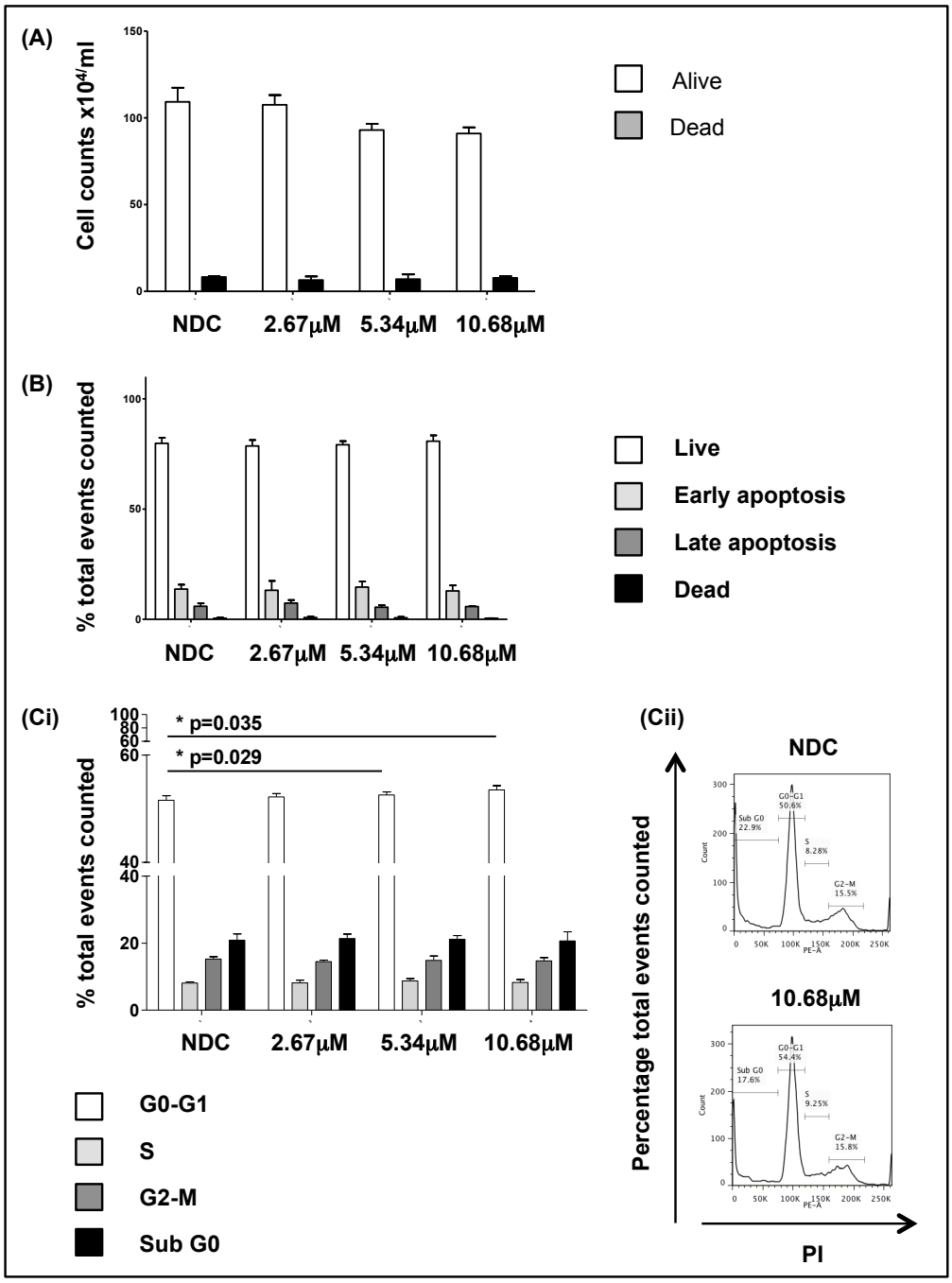

Figure 4.1.10.4: Cell viability and cell cycle kinetics following culture of the MOLM-13 cell line with glasdegib (2.67μM, 5.34μM and 10.68μM; clinically achievable concentrations) for 72hrs. MOLM-13 cells were seeded at a concentration of $2x10^5$/ml, exposed to incremental doses of glasdegib and cultured for 72hrs then harvested and stained with trypan blue dye exclusion, Annexin V / 7AAD or PI prior to analysis. (A) Bar graph showing cell viability as determined by trypan blue dye exclusion. Each bar represents the mean cell number $x10^4$/ml from four independent experiments with error bars indicating SD. (B) Bar graph showing the proportion of cells which are viable, in early apoptosis, in late apoptosis or dead as determined by Annexin V / 7AAD staining, and analysis by flow cytometry. The percentages shown indicate the proportion of total events within each of the respective categories as gated on the flow cytometry plots (see Figure 2.3 for gating strategy). Each bar represents the mean percentage from four independent experiments with error bars indicating SD. (Ci) Bar graph indicating the proportion of cells within each cell cycle phase (G0-G1, S, G2-M and Sub G0) as determined by PI staining, and analysis by flow cytometry. Each bar represents the mean percentage from four independent experiments with error bars indicating SD. (Cii) Representative flow cytometry plots, and gating strategy, following PI staining. Each plot is representative of data from one experiment of four with similar results. All statistically significant results are highlighted with p value to the nearest 3 decimal places, those not highlighted are not significant. This figure clearly showing culture of the MOLM-13 cell line with glasdegib caused a statistically significant increase in inactive, non-cycling cells (G0-G1) by PI staining.

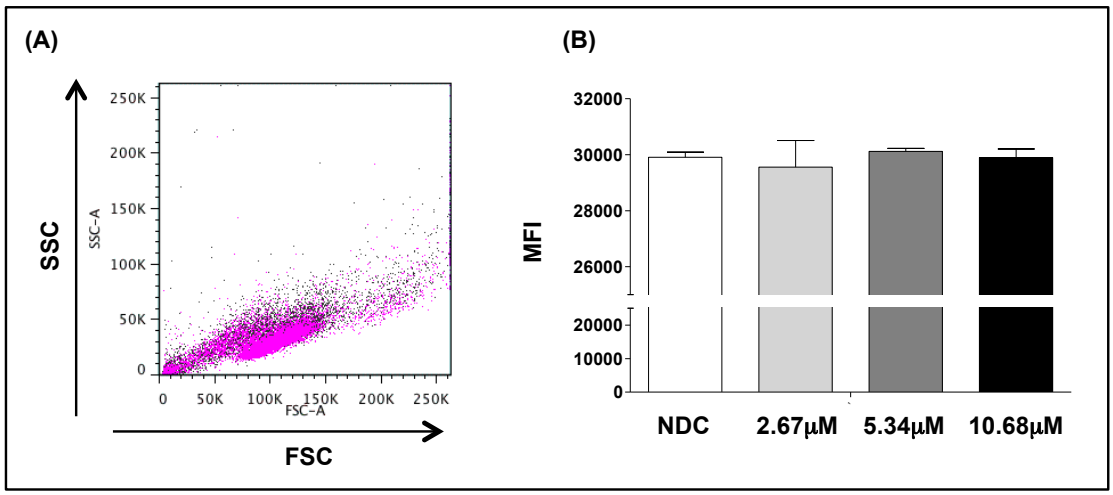

Figure 4.1.10.5: SSC MFI, and representative FACS plot, following culture of the MOLM-13 cell line with glasdegib (2.67μM, 5.34μM and 10.68μM; clinically achievable concentrations) for 72hrs. MOLM-13 cells were seeded at a concentration of $2x10^5$/ml, exposed to incremental doses of glasdegib, cultured for 72hrs then harvested prior to analysis by flow cytometry. (A) Representative FSC / SSC flow cytometry plot from one experiment of four with similar results. This demonstrates no change in the FSC / SSC parameters in the MOLM-13 cell line relative to the NDC. (B) Bar graph showing the MFI of SSC. Each bar represents the mean MFI from four independent experiments with error bars indicating SD. All statistically significant results are highlighted with p value to the nearest 3 decimal places, those not highlighted are not significant. The FACS plot, and bar graph, clearly showing culture of the MOLM-13 cell line with glasdegib did not affect the cells FSC / SSC parameters.

4.1.11 Manipulation of the Hh pathway with glasdegib affected genes involved in apoptosis, autophagy and cell cycle, with a striking difference seen between two myelomonocytic AML cell lines

Expression of genes involved in apoptosis, autophagy and cell cycle were analysed in the MOLM-13 and OCI-AML3 cell lines following culture with glasdegib. These cell behaviour pathways were selected considering published data linking the Hh pathway to apoptosis, autophagy [613,641,642] and cell cycle regulation to determine if glasdegib might render cells more sensitive to treatment with standard agents such as Ara-C. Further these genes had been studied following culture with cyclopamine, enabling us to compare and contrast the effects of different Smo antagonists. RNA was extracted from an aliquot of cells harvested following culture with glasdegib at a concentration of 2.67μM, 5.34μM and 10.68μM for 72hrs. To account for input cDNA the ΔCT for each gene was calculated by subtracting the CT value of 6 housekeeping (control) genes from the CT recorded for the gene of interest. *ATP5S, B2M, ENOX2, GAPDH, TYWI* and *UBE2D2* were selected as housekeeping genes, CT values ranged from 3 to 13. Technical triplicates were performed for each sample. The $2^{-\Delta\Delta CT}$ method was used to show expression of the gene of interest relative to the NDC. Log transformation of the fold change enabled graphical display of expression patterns according to the unsupervised Eisen approach using PermutMatrix software [589]; Figure 4.1.11.1.

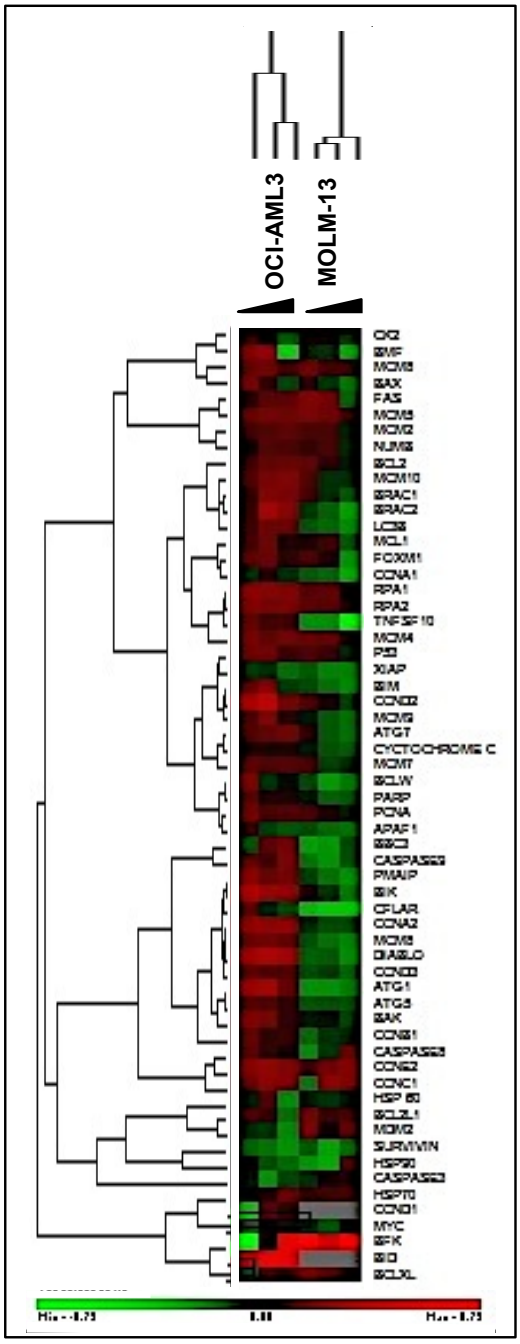

Figure 4.1.11.1: Gene expression profiles for genes involved in apoptosis, autophagy and cell cycle, following culture of the MOLM-13 and OCI-AML3 cell lines with glasdegib (2.67μM, 5.34μM and 10.68μM) for 72hrs.

RNA was extracted from an aliquot of cells harvested following culture with increasing doses of glasdegib for 72hrs. Expression levels were quantified by qRT-PCR using Fluidigm® technology. To account for input cDNA the ΔCT for each gene was calculated by subtracting the CT value of 6 housekeeping (control) genes from the CT recorded for the gene of interest. Technical triplicates were performed for each sample. Log transformation of the $2^{-\Delta\Delta CT}$ enabled graphical display of expression patterns according the unsupervised Eisen approach using PermutMatrix software [506]. Complete-linkage clustering of our selected genes, and all experimental conditions, are shown highlighting the strikingly different expression patterns of our selected genes in these two myelomonocytic cell lines.

The difference in gene expression between the two cell lines is striking though interestingly the concentration of glasdegib with which the cells were cultured was not a significant variable. Expression of select genes is discussed in further detail. Numb, an evolutionally conserved cell fate determinant, has been shown to be increased in the absence of Smo in CML [252]. We demonstrate *NUMB* to be up-regulated following culture of both cell lines with glasdegib, at all concentrations. In contrast to results following culture with cyclopamine *CCNDI* was progressively down-regulated in the OCI-AML3 cell line following culture with increasing doses of glasdegib (2.5-fold reduction); no change was seen in the MOLM-13 cell line. There was no change in *LC3B* in either cell line following culture with glasdegib (at 2.67μM, 5.34μM and 10.68μM) relative to the NDC; there was a progressive down-regulation of *ATG7* in the MOLM-13 cell line with increasing concentrations of glasdegib (2-fold reduction following culture with 10.68μM). Whilst the majority of the Bcl-2 family were largely unchanged, of the pro-apoptotic genes *NOXA* was progressively up-regulated whilst *BID* was progressively down-regulated in the OCI-AML3 cell line following culture with increasing concentrations of glasdegib. *BCL-2* and *BCL2L1* were down-regulated following culture of the MOLM-13 cell line with glasdegib at all concentrations; *BBC3* was up-regulated whilst *BAX, BIM, BMF, BIK* and *Cytochrome C* were down-regulated. These results highlight the complexity involved when interpreting mRNA expression data and the need to correlate results with functional data, and where appropriate determine protein expression. Further, it suggests subgroup analysis, and perhaps even selection, should be considered when considering trial data and the clinical application of Smo antagonists.

4.1.12 Combination treatment with glasdegib and Ara-C showed synergism in both the MOLM-13 and OCI-AML3 cell lines

We had shown glasdegib, at clinically tolerated doses, to cause changes in SSC in OCI-AML3 cells, and to alter cell cycle kinetics in MOLM-13 cells. Whilst subtle, these changes were significant. Further, we had shown, irrespective of concentration, glasdegib resulted in changes in genes involved in apoptosis and the cell cycle. Whilst these expression changes were not reflected in our functional data, we questioned whether glasdegib induced a stress response in AML cells, potentially making them more sensitive to standard chemotherapeutic agents. First line treatment for AML standardly uses Ara-C combined with an anthracycline [201,202] with clinical response dependent upon genes including *BCL-2* and *TP53* [533]. Work has also linked the Hh signalling pathway to the methyltransferases, reports showing inhibition of the Hh pathway to enhance the effects of the HMAs, whilst silencing of *SHH, SMO* and *GLI-3* sensitised cells to the HMAs [413]. Additionally, at the time of this PhD, Pfizer were running an early phase clinical trial looking at glasdegib in combination with Ara-C, presented at ASH 2016 [654]. We therefore elected to determine whether the combination of Ara-C and glasdegib was synergistic *in vitro*. The CompuSyn computer programme employing the Chou-Talalay method (discussed in section 2.2.1.7) was used to quantify synergy between Ara-C and glasdegib in the MOLM-13 and OCI-AML3 cell lines. Briefly cell counts as determined by the trypan blue dye exclusion assay were recorded following culture of the MOLM-13 and OCI-AML3 cell lines with glasdegib, Ara-C and the combination of glasdegib and Ara-C at a range of concentrations for 24hrs, 48hrs and 72hrs. The concentrations and combinations are depicted in Figure 4.1.12.1. We had determined the IC_{50} for each drug initially using the resazurin assay, recognising its limitations but acknowledging it allowed for the rapid evaluation of cell metabolic activity following culture with a wide range of drug concentrations. The trypan blue dye exclusion assay was used to confirm accuracy of this calculated IC_{50} and published work was referenced.

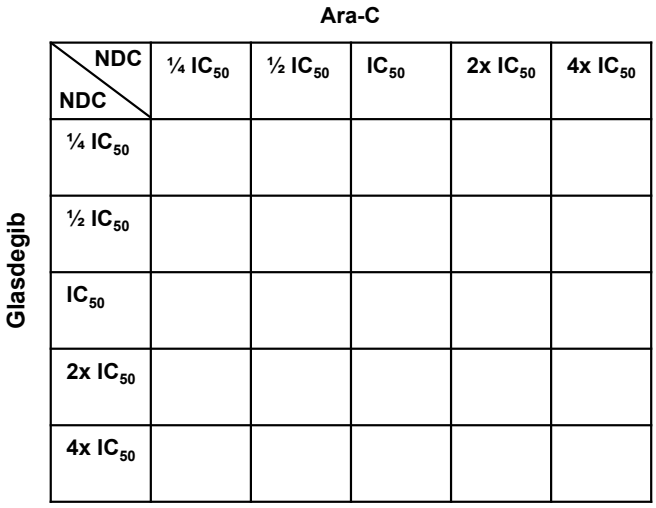

Figure 4.1.12.1: Schematic of the experimental layout used to determine the relationship between glasdegib and Ara-C in the MOLM-13 and OCI-AML3 cell lines using the Chou-Talalay method. MOLM-13 and OCI-AML3 cells were seeded at a density of $2x10^5$/ml, cultured with specific concentrations of each drug as outlined above for 24hrs, 48hrs and 72hrs. Trypan blue dye exclusion was performed to determine the number of live and dead cells for each experimental condition. Technical duplicates were performed, and the experiment performed three times.

The CI was seen to range from 1.779 to 0.0095 and 2.750 to 0.188 in the MOLM-13 and OCI-AML3 cell lines respectively with synergism CI < 1, antagonism CI > 1 and an additive effect CI = 1, Figure 4.1.12.2. However it is important to consider the drug concentrations at which synergism was seen. Within the MOLM-13 cell line interestingly antagonism with a CI ≥1 was demonstrated following culture with Ara-C at ¼ the predetermined IC_{50} irrespective of the concentration of glasdegib. Synergism was seen following culture within all other concentration combinations. The CI for clinically compatible drug concentrations was clearly synergistic ranging from 0.307 to 0.779 (mean 0.545). Within the OCI-AML3 cell line, antagonism, with a CI ≥1 was seen when the concentration of Ara-C was below the calculated IC_{50} irrespective of the concentration of glasdegib. Importantly however, whilst less powerful, synergism was seen at clinically compatible drug concentrations, the CI ranging from 0.683 to 0.821 (mean 0.764). Whilst it must be noted that the drug concentrations differed between the two cell line it is exciting to consider a synergistic effect was seen in these two genetically diverse AML cell lines, Figure 4.1.12.3.

OCI-AML3

Ara-C

Glasdegib \ NDC	¼ IC_{50} (0.125μM)	½ IC_{50} (0.25μM)	IC_{50} (0.5μM)	2 IC_{50} (1.0μM)	4 IC_{50} (2.0μM)
¼ IC_{50} (0.66μM)	2.750	1.968	0.683	0.843	0.256
½ IC_{50} (1.33μM)	2.138	2.242	0.788	0.872	0.276
IC_{50} (2.67μM)	2.120	2.480	0.821	0.815	0.256
2 IC_{50} (5.34μM)	1.310	1.259	1.223	0.521	0.276
4 IC_{50} (10.68μM)	1.578	0.866	0.466	0.344	0.188

MOLM-13

Ara-C

Glasdegib \ NDC	¼ IC_{50} (37.5nM)	½ IC_{50} (75nM)	IC_{50} (150nM)	2 IC_{50} (300nM)	4 IC_{50} (600nM)
¼ IC_{50} (12.5nM)	1.166	1.779	0.638	0.584	0.242
½ IC_{50} (25nM)	1.009	0.539	0.713	0.386	0.256
IC_{50} (50nM)	1.265	1.133	0.779	0.508	0.184
2 IC_{50} (100nM)	1.710	0.589	0.359	0.308	0.095
4 IC_{50} (200nM)	1.124	0.636	0.768	0.330	0.169

Figure 4.1.12.2: Combination indices for the OCI-AML3 and MOLM-13 cell lines according to experimental conditions according to the Chou-Talalay method.
OCI-AML3 and MOLM-13 cells were seeded at a density of $2x10^5$/ml, and cultured with specific concentrations of each drug as outlined in Figure 4.1.12.1 for 24, 48 and 72hrs. Trypan blue dye exclusion was performed to determine the number of live and dead cells for each experimental condition. Technical duplicates were performed, and the experiment performed three times. CompuSyn software was used. CI<1 = synergism (red), CI=1 = additive effect, CI>1 = antagonism (blue).

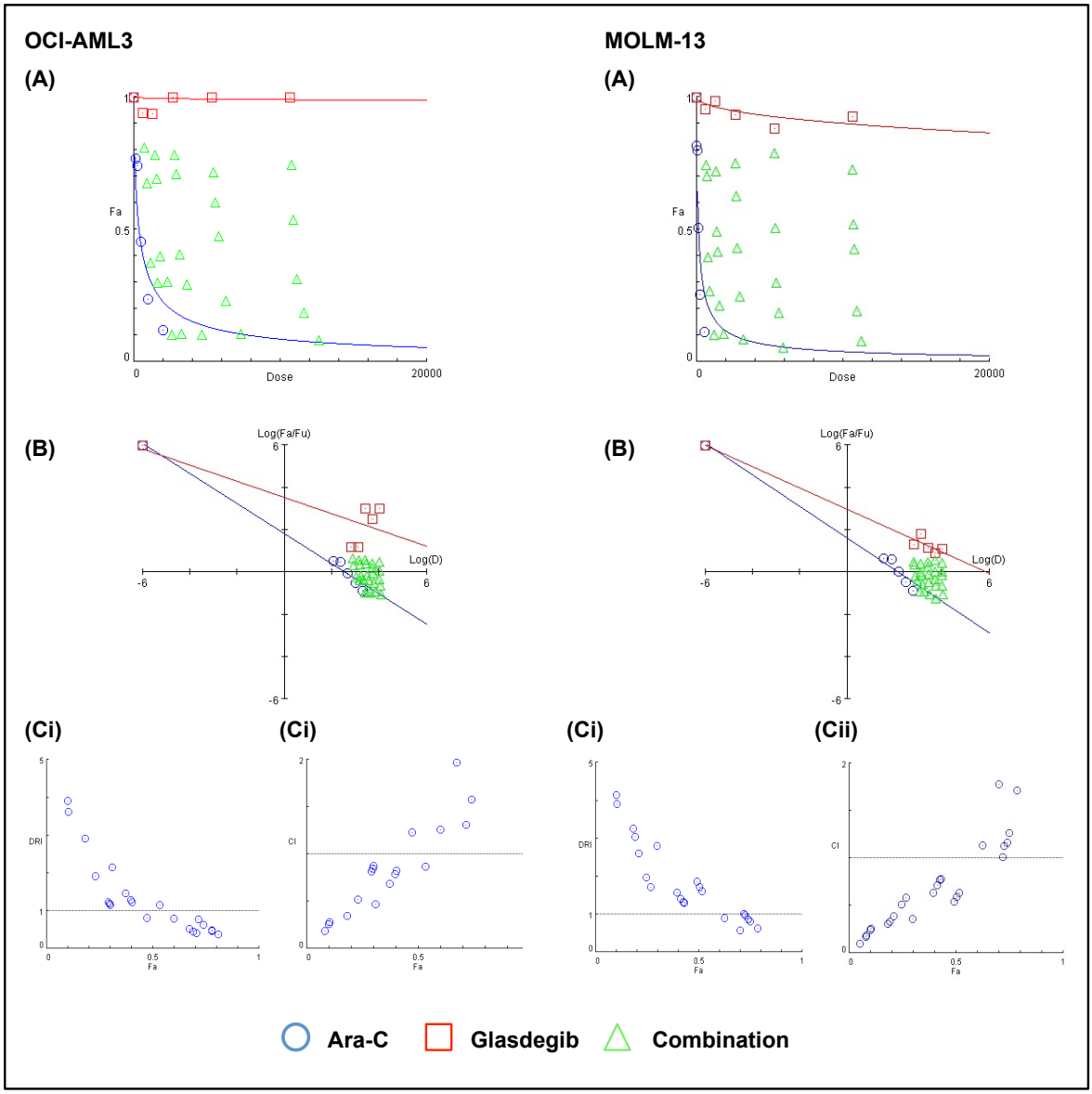

Figure 4.1.12.3: Representative plots generated according to the Chou-Talalay method following culture of the OCI-AML3 and MOLM-13 cell lines with specific concentrations of glasdegib and Ara-C for 72hrs.

OCI-AML3 and MOLM13 cells were seeded at a density of $2x10^5$/ml and cultured with specific concentrations of each drug as outlined in Figure 4.1.12.1 for 24hrs, 48hrs and 72hrs. Trypan blue dye exclusion was performed to determine the number of live and dead cells for each experimental condition. Technical duplicates were performed, and the experiment performed three times. Data for the 72hr time point are shown. (A) Dose-Effect curve, (B) Median-Effect plot and (C) DRI and CI plots for OCI-AML3 and MOLM-13 cells.

These plots clearly show wide variation in effect dependent upon drug concentration. While minimal effect on cell viability was seen with glasdegib alone, in both cell lines the combination of glasdegib and Ara-C, at select doses, was synergistic.

4.1.13 Manipulation of the Hh pathway by Smo inhibition in unselected primary AML samples produced differing results

Whilst cell lines, as experimental models, enable the investigation and analysis of primary processes and the effect of manipulating these, it is well recognised that cell lines may not always behave in the same manner as, and therefore not always accurately represent, primary cells [627]. We therefore sought to determine the effect of Smo inhibition in a cohort of primary AML samples, initially focusing on cyclopamine, then the clinical grade Smo inhibitors glasdegib

and sonidegib, alone and in combination with Ara-C. We sought to determine the effect of combination therapy in primary samples considering we had demonstrated evidence of synergism in genetically diverse AML cell lines.

Primary AML MNCs were isolated from whole PB and BM samples, recovered and cultured as detailed in Methods 2.2.1.2.4-6. An unmanipulated recovered cell population was used.

Considering first cyclopamine, whilst its pharmacokinetics and moderate activity have impeded its clinical development, it continues to be used in research to evaluate the effect of Smo inhibition [631]. Further, these experiments enabled us to compare the results generated by primary AML cells with those from immortalised AML cell lines, the concern being through the process of generating a cell line these cells undergo genotypic and / or phenotypic change. Cells, seeded at a density of $1.5x10^5$/ml, were cultured as NDC and with cyclopamine at the following concentrations - 100nM, 1μM, 5μM, 10μM and 20μM; 20μM tomatidine was used as an additional control as described in Methods 2.2.1.2.6. A broad range of concentrations was used to ensure an effect was not missed. Cell counts and the assessment of cell viability were performed by trypan blue dye exclusion at 24, 48 and 72hrs in technical triplicates using one sample (AML 022) initially, Figure 4.1.13.1. Doses and time points were selected to determine if cyclopamine had a time- or concentration-dependent effect on cell viability and kinetics.

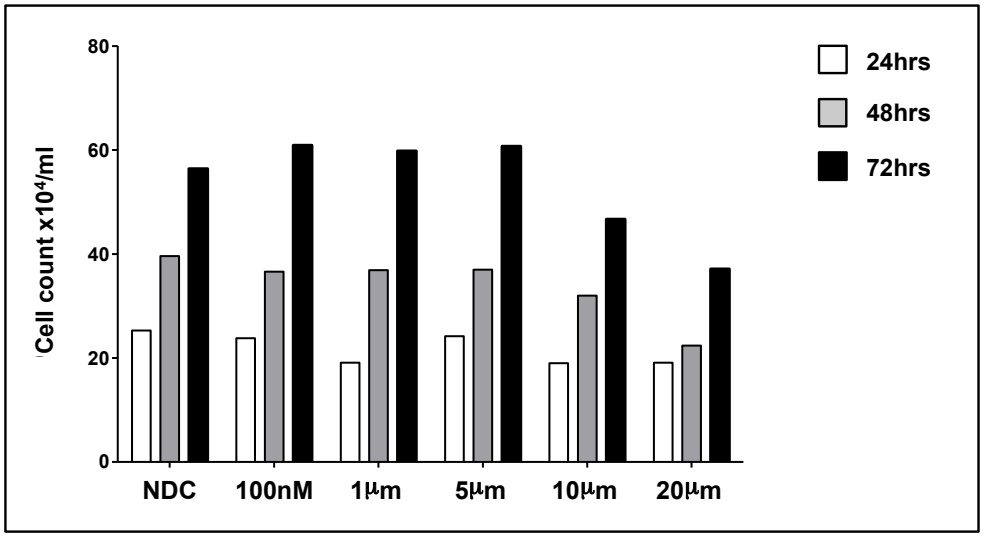

Figure 4.1.13.1: Cell viability, as determined by trypan blue dye exclusion, in one primary AML sample following culture with select concentrations of cyclopamine for 72hrs.
The primary sample AML 022 was recovered as described in Methods 2.2.1.2.5. Recovered cells were seeded at a concentration of $1.5x10^5$/ml, exposed to incremental doses of cyclopamine and cultured for 72hrs as described in Methods 2.2.1.2.6. Each bar represents the mean cell number x 10^4/ml from technical triplicates.
There was no difference in cell count between the NDC and all concentrations of cyclopamine at 24hrs. At 48hrs there was a reduction in the number of live cells following culture with 10μM and 20μM cyclopamine with the effect increased at 72hrs. Statistical analysis was not performed since this graph represents data from n=1.

There was no difference in cell viability between the NDC and all concentrations of cyclopamine at 24hrs. At 48hrs there was a reduction in the number of live cells following culture with 10μM and 20μM with a further reduction demonstrated at 72hrs. The range was therefore narrowed to: 5μM, 10μM and 20μM with a single time point of 72hrs selected for additional primary samples (AML1002, AML 017 and AML 005), Figure 4.1.13.2.

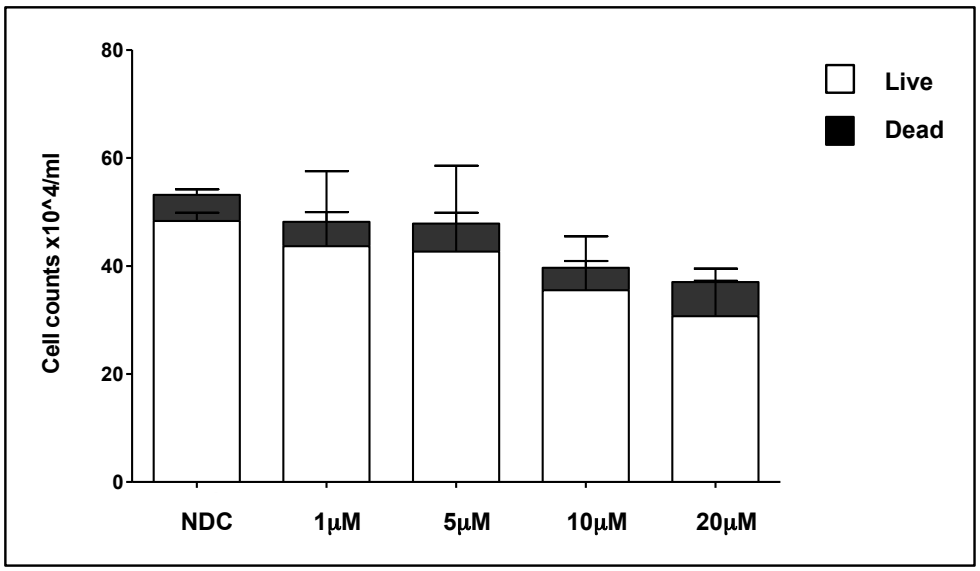

Figure 4.1.13.2: Cell viability, as determined by trypan blue dye exclusion, in primary, *de novo*, AML MNCs (n=4) following culture with select concentrations of cyclopamine for 72hrs.
The primary samples AML 1002, AML 022, AML 017 and AML 005 were recovered as described in Methods 2.2.1.2.5. Recovered cells were seeded at a concentration of $1.5x10^5$/ml, exposed to incremental doses of cyclopamine and cultured for 72hrs as described in Methods 2.2.1.2.6. Each bar represents the mean cell number x 10^4/ml with error bars indicating SD.
There was a trend towards a reduction in the number of live cells following culture with 10μM and 20μM cyclopamine though this was not significant. The number of dead cells did not differ between the NDC and all concentrations of cyclopamine.

Whilst statistical significance was not demonstrated there was a trend towards a reduction in the number of live cells following culture with 10μM, (p=0.065) and 20μM (p0.051). No significant difference in the number of dead cells was seen between the NDC and all concentrations of cyclopamine.

Acknowledging the altered biological properties of primary AML cells and AML cell lines, it is reassuring that a similar trend was seen in both the cell lines and primary samples analysed, with no change in viability seen at 24hrs whilst a reduction was seen at 48hrs, increasing at 72hrs following culture with cyclopamine at concentrations of ≥10μM. Additionally, we had questioned whether an effect might be lost due to the genetic heterogeneity of primary AML cells; this data discounted this. It would be interesting to assess the effect of cyclopamine in defined subtypes of AML. Would statistical significance be reached? Having demonstrated an effect with cyclopamine, recognising its limitations in the clinical setting and the value of our primary AML cell bank as a resource, we sought to determine the effect of two clinical grade Smo antagonists – glasdegib and sonidegib, alone and in combination with Ara-C.

Primary AML samples were seeded at a density of $1.5x10^5$/ml and cultured with sonidegib at the following concentrations - 25nM, 100nM and 500nM alone and in combination with Ara-C 250nM and 500nM as described in Methods 2.2.1.2.6. Sonidegib concentrations were selected following review of data published by the Copland group studying sonidegib in CML [412]. A concentration of 500nM for Ara-C equates to the maximum clinically tolerated. Cell counts and the assessment of cell viability was performed by trypan blue dye exclusion at 72hrs in four samples (AML 018, AML 020, AML 036 and AML 037), Figure 4.1.13.3.

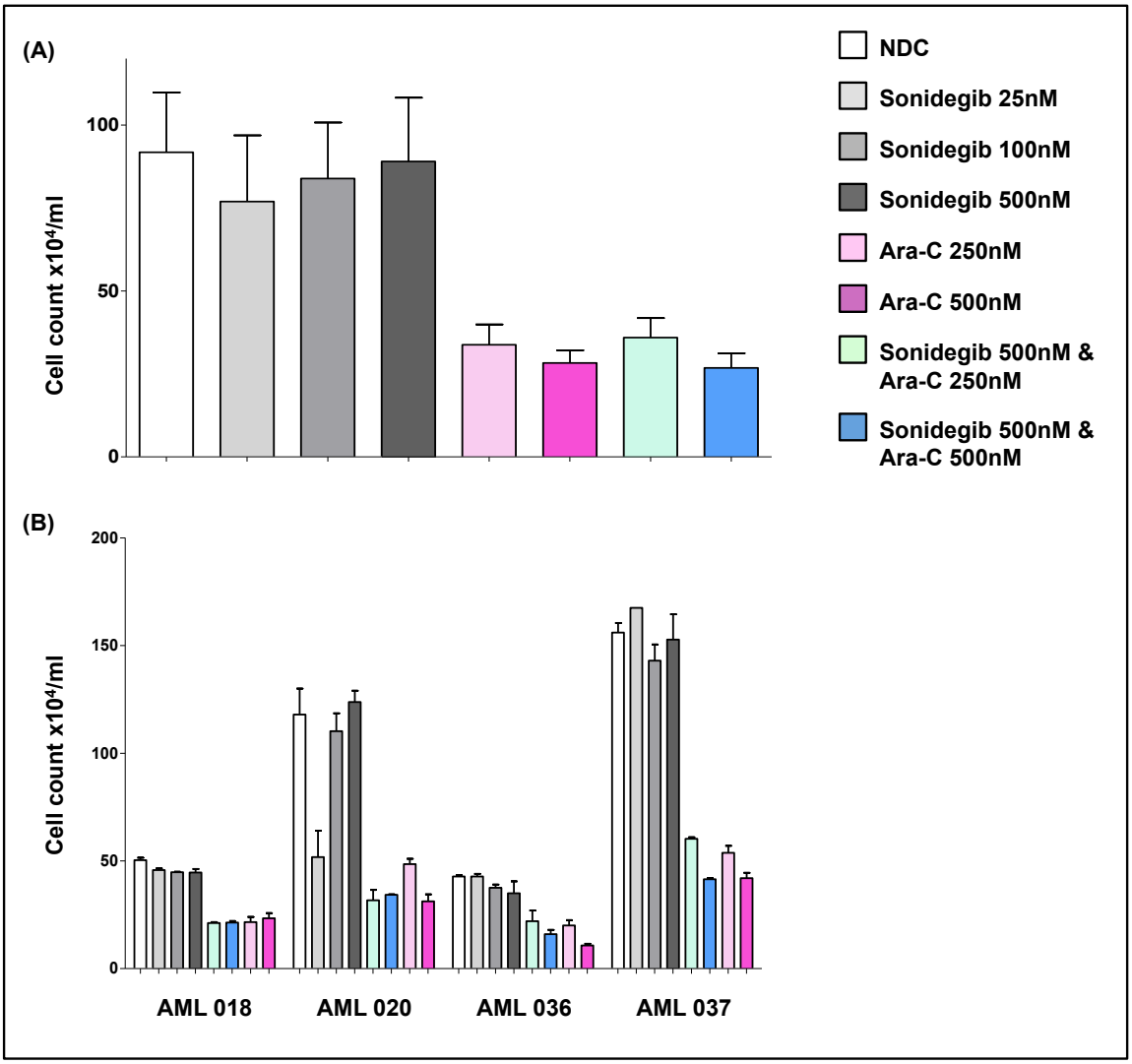

Figure 4.1.13.3: Cell viability, as determined by trypan blue dye exclusion, in primary, *de novo*, AML MNCs (n=4) following culture with sonidegib (25nM, 100nM and 500nM) alone, Ara-C (250nM and 500nM) alone, and the combination of sonidegib 500nM with Ara-C (250nM and 500nM) for 72hrs.

The primary samples AML 018, AML 020, AML 036 and AML 037 were recovered as described in Methods 2.2.1.2.5. Recovered cells were seeded at a concentration of $1.5x10^5$/ml, exposed to incremental concentrations of sonidegib alone and in combination with Ara-C 250nM and 500nM and cultured for 72hrs as described in Methods 2.2.1.2.6. (A) Graph showing the mean cell number $x10^4$/ml with error bars indicating SD in each of the experimental arms. (B) Graph illustrating the variance between samples.

There was no change in cell viability following culture with sonidegib alone. There was a reduction in cell viability following culture with Ara-C 250nM and 500nM. Interestingly there was no difference between the results obtained from these two concentrations. The addition of sonidegib did not enhance the effect of Ara-C.

As expected, there was a reduction in cell viability following culture with Ara-C 250nM and 500nM. Interestingly there was no significant difference between the effect of Ara-C at a concentration of 250nM and 500nM with both reducing cell viability more than 2-fold. There was no change in cell viability following culture with sonidegib. The addition of sonidegib did not enhance the effect of Ara-C. Results following the assessment of apoptosis mirrored the results for cell viability - Annexin V / 7AAD staining and flow cytometry analysis showing a reduction in the live cell population with an increase in early apoptosis following culture with Ara-C alone, and in combination with sonidegib. The addition of sonidegib did not enhance the effect of Ara-C in these short-term assays, Figure 4.1.13.4. Considering the absence of an effect, albeit we had only assessed proliferation and apoptosis in short-term assays, and the concomitant release of

data from the NCT01826214 study evaluating the efficacy and safety of LDE225 (sonidegib) in patients with R/R acute leukaemia [655], we decided not to continue investigating sonidegib.

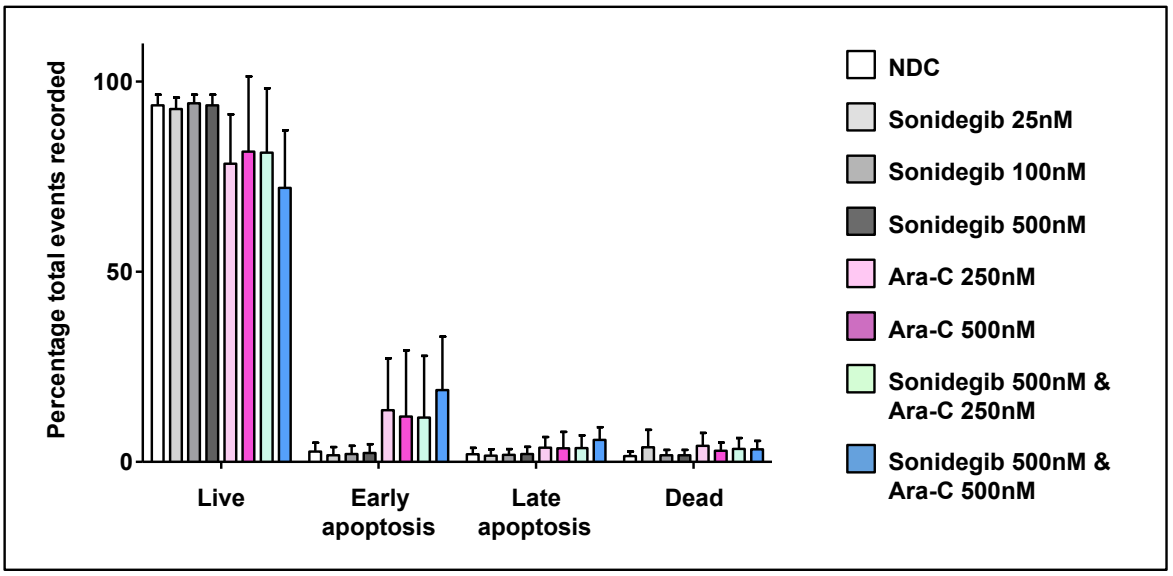

Figure 4.1.13.4: Cell viability, as determined by Annexin V / 7AAD staining, in primary, de novo, AML MNCs (n=4) following culture with sonidegib (25nM, 100nM and 500nM) alone, Ara-C (250nM and 500nM) alone and the combination of sonidegib 500nM with Ara-C (250nM and 500nM) for 72hrs.
The primary samples AML 018, AML 020, AML 036 and AML 037 were recovered as described in Methods 2.2.1.2.5. Recovered cells were seeded at a concentration of $1.5x10^5$/ml, exposed to incremental concentrations of sonidegib alone and in combination with Ara-C 250nM and 500nM and cultured for 72hrs as described in Methods 2.2.1.2.6. Apoptosis was assessed by Annexin V / 7AAD staining and analysis by flow cytometry. The proportion of viable, early apoptosis, late apoptosis and dead cells are shown. Each bar represents the mean total number of events from four independent experiments with error bars indicating SD.
A reduction in the proportion of live cells with a consequent increase in early apoptosis was seen following culture with Ara-C alone, and in combination with sonidegib. Statistical significance was not reached. The addition of sonidegib did not enhance the effect of Ara-C.

Considering glasdegib, we sought to determine its effect on primary cells in liquid culture using clinically achievable concentrations. We accept the limitations of this approach in an *in vitro* system. These concentrations were however selected to enable comparison between primary cells and cell lines and, recognising the degree of crosstalk between pathways, by tailoring our drug concentrations, we sought to limit off-target and supra-therapeutic 'toxic' effects leading to false conclusions. Additionally, considering our data showing a marked reduction in cell viability, explained by apoptosis in primary cells following culture with Ara-C at a concentration of 250nM and 500nM, we choose a concentration of 100nM. We wanted to determine if inhibition of the Hh pathway conferred an additive effect, and ensure an effect was not masked by another, more powerful drug effect. A concentration of 100nM is supported by data studying the IC_{50} for single agent Ara-C in expanded primary AML cells in liquid culture [656] and concentrations utilised in other published primary AML cell *in vitro* studies [657]. Cells were seeded at a density of $1.5x10^5$/ml and cultured as either the NDC or with glasdegib 2.67μM, Ara-C 100nM, glasdegib 2.67μM and Ara-C 100nM or cyclopamine 20μM as described in Methods 2.2.1.2.6. Five primary samples (AML 1002, AML 053, AML019, AML018 and AML 013) with variable *SMO* expression relative to normal MNCs were selected ($2^{-\Delta\Delta CT}$ range 0.626 – 28.700). One sample was excluded from analysis due to poor recovery: AML 019 – this sample was an APML, recovery potentially therefore reflecting cell biology, these blasts classically being hypergranular. Cell counts and the assessment of cell viability was performed by trypan blue dye exclusion at 72hrs in technical duplicate, Figure 4.1.13.5.

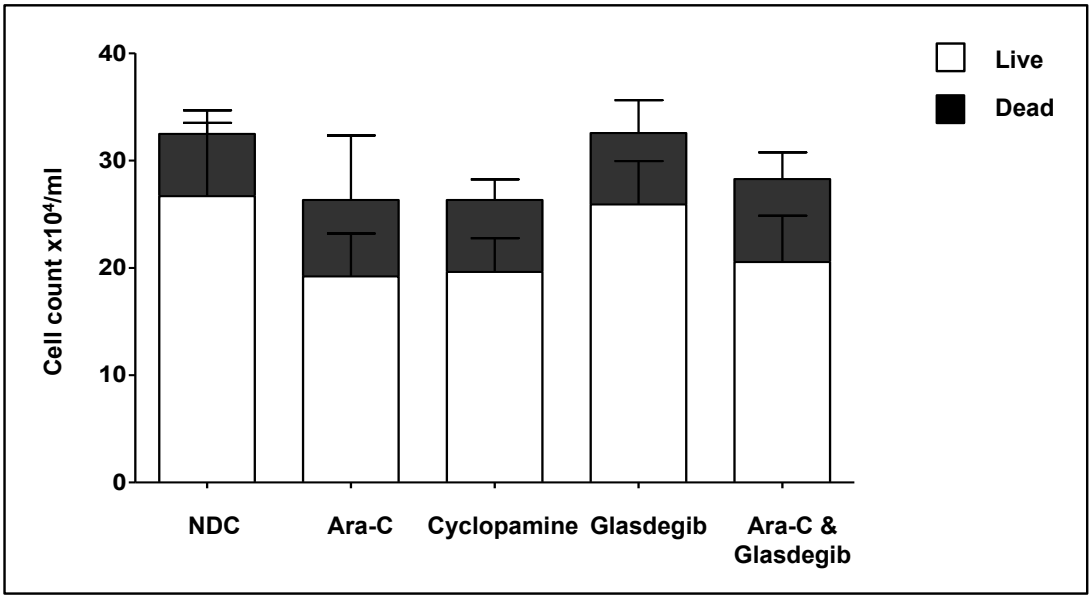

Figure 4.1.13.5: Cell viability, as determined by trypan blue dye exclusion, following culture with glasdegib alone and in combination with Ara-C, in primary, *de novo*, AML MNCs (n=4) for 72hrs.
The primary samples AML 1002, AML 053, AML 019, AML 018 and AML 013 were recovered as described in Methods 2.2.1.2.5. AML 019 was excluded due to poor recovery. Recovered cells were seeded at a concentration of $1.5x10^5$/ml, exposed to glasdegib 2.67μM alone and in combination with Ara-C 100nM and cyclopamine 20μM and cultured for 72hrs as described in Methods 2.2.1.2.6. Cell counts, live and dead, were determined by trypan blue dye exclusion. Each bar represents the mean cell number x 10^4/ ml with error bars indicating SD.
There was no change in cell viability following culture with glasdegib alone. There was a reduction in cell viability following culture with Ara-C 100nM alone and in combination with glasdegib 2.67μM though these results were not significant. The addition of glasdegib to Ara-C did not increase the effect of Ara-C.

There was a reduction in cell viability by trypan blue dye exclusion following culture with Ara-C 100nM alone and in combination with glasdegib 2.67μM though this was not significant (p=0.074 and p=0.089 respectively). As previous experiments had shown, represented in Figures 4.1.13.1&2, there was a reduction in cell viability following culture with cyclopamine, but again, this was not significant (p=0.081). There was no difference in the number of dead cells by trypan blue dye exclusion across all experimental arms relative to the NDC.

We sought to evaluate whether the reduction in cell proliferation was due to cell apoptosis, acknowledging no difference in cell death had been demonstrated. Annexin V / 7AAD staining and flow cytometry analysis showed an increase in apoptosis (early and late) following culture with Ara-C alone though this was not significant (p=0.054). The addition of glasdegib did not enhance this effect.

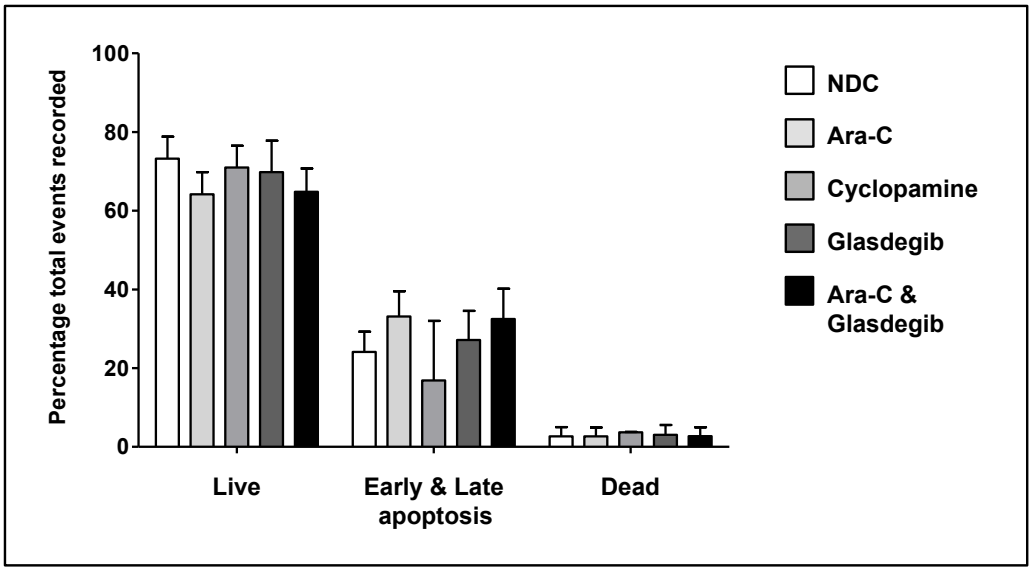

Figure 4.1.13.6: Cell viability, as determined by Annexin V / 7AAD staining, in primary, *de novo* AML MNCs (n=4) following culture with Ara-C (100nM), cyclopamine (20μM), glasdegib (2.67μM) and the combination of Ara-C (100nM) and glasdegib (2.67μM) for 72hrs.
The primary samples AML 1002, AML 053, AML 019, AML 018 and AML 013 were recovered as described in Methods 2.2.1.2.5. AML 019 was excluded due to poor recovery. Recovered cells were seeded at a concentration of $1.5x10^5$/ml, exposed to glasdegib 2.67μM alone and in combination with Ara-C 100nM and cyclopamine 20μM and cultured for 72hrs as described in Methods 2.2.1.2.6. Apoptosis was assessed by Annexin V / 7AAD staining and analysis by flow cytometry. The proportion of viable, apoptotic and dead cells are shown. Each bar represents the mean total number of events from four independent experiments with error bars indicating SD.
There was no significant difference between each of the experimental arms. Considering the high degree of variance between each of the samples we considered the data on an individual basis – a trend towards apoptosis was not apparent across all experimental arms.

The reduction in total cell number by trypan blue dye exclusion in the absence of apoptosis is interesting however. Considering previous results demonstrating cyclopamine to induce differentiation we considered whether this reduction in cellular proliferation was as a consequence of altered cell cycle kinetics. No change in cell cycle kinetics, by PI staining, was seen across all experimental arms relative to the NDC, Figure 4.1.10.7.

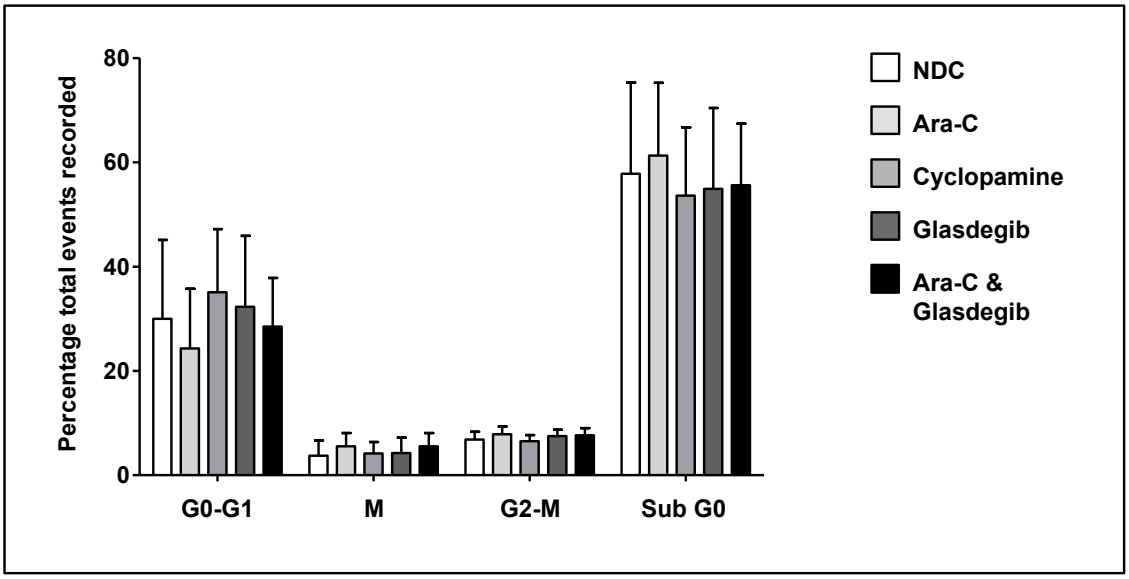

Figure 4.1.13.7: Cell cycle kinetics, as determined by PI staining, in primary, *de novo* AML MNCs (n=4) following culture with Ara-C (100nM), cyclopamine (20μM), glasdegib (2.67μM) and the combination of Ara-C (100nM) and glasdegib (2.67μM)for 72hrs.
The primary samples AML 1002, AML 053, AML 019, AML 018 and AML 013 were recovered as described in Methods 2.2.1.2.5. AML 019 was excluded due to poor recovery. Recovered cells were seeded at a concentration of $1.5x10^5$/ml, exposed to glasdegib 2.67μM alone and in combination with Ara-C 100nM and cyclopamine 20μM and cultured for 72hrs as described in Methods 2.2.1.2.6 before being harvested and stained with PI prior to analysis by flow cytometry. The graph shows the proportion of cells within each cell cycle phase (G0-G1, S, G2-M and Sub G0) as gated on the flow cytometry plots. Each bar represents the mean percentage from four independent experiments with error bars indicating SD. There was considerable variance between these primary samples, as demonstrated by the error bars. Individually, and collectively however, no significant difference in cell cycle kinetics was seen between each of the experimental arms.

Whilst there was no evidence of a change in cell cycle kinetics we accept the limitations of our selected assay. In particular we were not able to differentiate between G0 and G1. We therefore performed CFSE analyses on three primary samples (AML 1002, AML 018 and AML 013) to determine if cell division was affected. For technical reasons, primarily the number of cells available for analysis, the results were inconclusive and are not shown.

Finally, the Hh signalling pathway is a self-renewal pathway, involved in aspects of tissue maintenance and regeneration - proliferation, apoptosis, chromatin modelling, and self-renewal [257]. We recognise we had not studied self-renewal activity in our liquid assays. Whilst, possibly, the most robust assessment of self-renewal activity is through limited dilution xenograft transplantation, *in vitro* assays, as an experimental model, are frequently used. Further these assays have a potential benefit in non-immortalised cells since these cells may only be capable of a limited number of divisions. We therefore sought to perform re-plating of colonies derived from CFC assays.

CFC assays were undertaken on four samples (AML 1002, AML 053, AML 018, AML 013), with a view to perform a re-plate assay to assess self-renewal potential. We plated $4x10^3$/ml, $4x10^4$/ml and $1x10^5$/ml cells following culture with glasdegib 2.67μM alone and in combination with Ara-C 100nM, Ara-C 100nM alone and cyclopamine 20μM. No samples suffered contamination. Irrespective of plating density three samples were not suitable for analysis because (1) an insufficient number of colonies grew (≤2 within the NDC) and / or (2) cell 'clusters' contained insufficient cell numbers to be counted as a colony [658]. The results of one sample are presented, Figure 4.1.13.8.

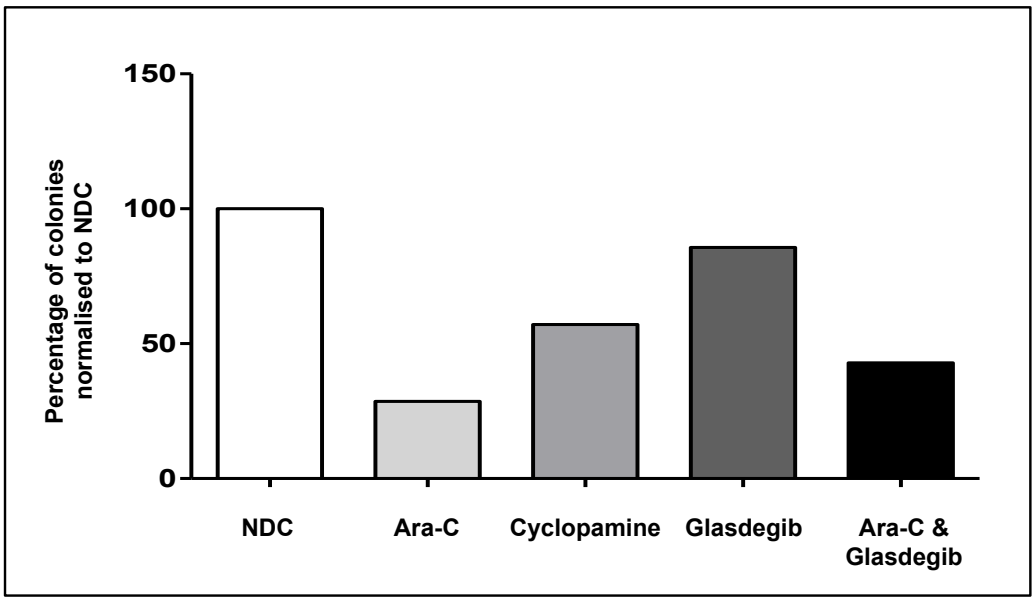

Figure 4.1.13.8: Total number of colonies, normalised to the NDC, at day 14 following culture of a primary, de novo, AML MNC sample (n=1) with Ara-C (100nM), cyclopamine (20μM), glasdegib (2.67μM)and the combination of Ara-C (100nM) and glasdegib (2.67μM).
The primary sample AML 1002 was recovered as described in Methods 2.2.1.2.5. Recovered cells were seeded at a concentration of $1.5x10^5$/ml, exposed to glasdegib 2.67μM alone and in combination with Ara-C 100nM and cyclopamine 20μM and cultured for 72hrs as described in Methods 2.2.1.2.6. Cells were subsequently harvested, washed and resuspended in fresh SFM. $4x10^4$ cells were inoculated into Methocult as described in Methods 2.2.1.9. Colonies were counted after 14 days. Colony number is shown normalised to the NDC.
The graph indicates Ara-C, and cyclopamine reduce colony formation and, to a lesser degree glasdegib. The combination of Ara-C and glasdegib did not further reduce colony forming potential. Statistics are not presented as this graph represents n=1.

Ara-C reduced colony formation as expected; published data showing Ara-C to target committed progenitor cells [659]. Interestingly, cyclopamine and, to a lesser degree glasdegib reduced colony formation suggesting Smo antagonists influence the behaviour of the more mature, committed progenitor cells. The combination of Ara-C and glasdegib did not further reduce colony forming potential. No colonies grew within the NDC arm of our secondary re-plates preventing further analysis.

Referencing literature recommended cell numbers per 35mm plate varied markedly; for CD34+ enriched cells a cell density of $5.0x10^2$/ml- $2.0x10^3$/ml is recommended, for BM $1.0x10^4$/ml – $5.0x10^4$/ml and for PB $1x10^5$/ml – $2x10^5$/ml. Further we had shown colonies with a cell density of $4.0x10^4$. We therefore do not consider our selected cell densities to be the cause of CFC failure. Work in AML, both expression and functional studies, classically uses bulk AML MNCs, does this approach need to be reconsidered when considering the self-renewal pathways? Published work has however shown bulk primary AML MNCs to be capable of forming colonies, though interestingly, cells were either added to MethoCult immediately following thawing, or after a significantly shorter *in vitro* culture period of 24hrs [618,660]. It would be interesting to replicate these experimental designs. Had we simply been unlucky in selecting samples with a low percentage of HSPCs or in which the HSPCs had not survived cryopreservation and storage? Considering experimental design, it would be interesting to compare colony forming potential following culture with supportive stromal cells. Would supportive stromal cells protect the colony forming potential of HSPCs? There is work currently ongoing within the Copland group seeking to optimise our CFC and serial re-plate protocol for primary AML samples to allow evaluation of these small molecule inhibitors on their colony-forming ability and subsequently their self-renewal capacity.

4.1.12 Discussion

AML is characterised by a number of functional changes, including increased proliferation, differentiation block, inhibition of apoptosis and altered cell adhesion and stromal interactions. Pharmacological inhibition of Smo with cyclopamine or glasdegib (PF-04449913) has been shown to abrogate chemoresistance [377-379,618]. Previous work with the Kasumi-1 cell line has shown cyclopamine to induce apoptosis [73]. Uniquely we have shown Smo inhibition with cyclopamine allows cellular differentiation in select, genetically diverse, AML cell lines whilst higher doses induces apoptosis in other genetically diverse AML cell lines, indicating that partial and total inhibition of the pathway may potentiate different responses in AML. Further, we have shown cyclopamine to reduce proliferation in the absence of cell death in a limited unselected cohort of primary AML samples.

Considering the clinical grade Smo antagonists we referenced published work. We demonstrated an absence of effect on proliferative abilities and apoptosis following short-term *in vitro* culture of primary AML cells with sonidegib. A comprehensive exposure-response analysis was recently published reporting pharmacokinetic characteristics of sonidegib within clinical trial [661]. This study reported the Cmin to range from 680.9ng/ml to 1089ng/ml depending upon time point. Converting ng/ml to μM provides a dose range of 1.402μM to 2.243μM. Further daily dosing, as in the clinical trials, led to a log-fold increase in plasma concentration. An absence of effect may therefore reflect our experimental design and selected concentrations. Unfortunately the NCT01826214 study, evaluating the efficacy and safety of LDE225 (sonidegib) in patients with R/R acute leukaemia, returned disappointing results with no CRs and one CRi in the 69 participants treated. Subsequent to this data release Novartis determined it would not pursue LDE225 as a therapy in haematological malignancies.

During the write up of this PhD glasdegib was shown to reduce proliferation in the absence of cell death *in vitro* in the Marimo cell line [618]. The Marimo cell line was developed from a 68 year old female following treatment for essential thrombocythaemia, a MPN, representing a t-AML, with a complex karyotype [662]. This work used a maximum concentration of 5μM of glasdegib [618], comparable to the median concentration used in our work. How the drug was administered was not addressed, however, the time points studied differed from ours - the majority of work focused on a 48hr time point, though the MTT assay was extended to 6 days [618]. As with our data in genetically diverse cell lines, 5μM induced minimal cell death. Interestingly, and in contrast to our work, this study demonstrated a reduction in the quiescent G0 population by Hoechst-33343^{low}/Pyronin-Y^{low} and flow cytometry analysis. Hoechst-33343^{low}/Pyronin-Y^{low} is capable of separating G0 and G1 since Hoechst-33343^{low} is an exclusive DNA dye while Pyronin-Y^{low} reacts with both DNA and RNA [663]. This shift towards cell proliferation was supported by their MTT assay results showing a relative increase in the number of viable cells when cells were cultured with 5μM glasdegib for up to, and including, three days. Interestingly, however, there was a relative reduction in the viable cell number beyond this time point, though the mechanism was not discussed in the paper. Whilst no comment on cell morphology was made, a comprehensive screen of cell surface markers, including CD markers and adherent surface molecules, using the BD Biosciences human cell surface marker screening panel, only recorded a substantial reduction in the expression of CD164, a potent negative regulator of haematopoiesis [664], the significance of which was not discussed. Whether non-significant changes were observed was also not discussed. The shift in cell proliferation is particularly interesting, though not fully developed. These results contrast with ours in which reduced proliferation was demonstrated. Whilst experimental design differed, and may account for some of these differences, it is interesting to consider the different genetics of the cell lines studied; in particular the Marimo cell line carrying the *calreticulin* mutation. Whilst recent work has suggested this cell line is not dependent on JAK/STAT signalling [665], a relationship between the STAT and Hh pathways is well recognised. Could a shift in balance between these two pathways account for the relative increase in early proliferation? Was the loss of effect with time due to drug metabolism or a change in cellular behaviour? Does a more complex relationship exist? It would be interesting to replicate thei

experimental design using our selected cell lines, and further to perform our selected assays on the Marimo cell line in order to determine if the reported effects are due to experimental design or cell line specific - particularly important when seeking to translate results into the clinic.

Our data extends on this published data. Whilst we have also shown reduced proliferation by trypan blue dye exclusion and apoptosis by Annexin V / 7AAD our KD model adds complexity to the picture. Our KD model suggests cellular response to Smo antagonism is dependent upon the degree of Smo inhibition achieved. Whilst we acknowledge the genetic diversity of our selected AML cell lines it is interesting to consider the varied expression of *SMO* within each of these cell lines, and therefore degree of inhibition following exposure to the Smo antagonists, as a determining factor in cellular response. We acknowledge our KD models need to be repeated and, further studies are required to validate this hypothesis.

If we consider these results in parallel to those seen with the clinical grade Smo antagonist glasdegib the therapeutic possibilities become even more exciting. We demonstrated a statistically significant increase in SSC properties in select AML cell lines following culture with glasdegib. Further, a synergistic relationship between glasdegib and Ara-C in select AML cell lines was shown. These results are especially interesting considering the recently presented Phase II NCT01546038 trial, reporting an improved OS in AML, and high-risk MDS patients treated with PF-04449913 (glasdegib) and LDAC compared with LDAC alone [618].

It is not possible to hypothesise that Smo inhibition causes, or allows, cellular differentiation without considering, and learning, from the success story of APML. ATRA is able to induce CR in >90% of patients with APML through *in vivo* differentiation of the blast population. In combination with an anthracycline ATRA results in cure, with relatively mild toxicity, in >90%; in combination with arsenic trioxide cure rates have been shown to reach 100% [164]. The ability of Smo antagonists to allow cellular differentiation in the DNMT3a carrying OCI-AML3 cell line is therefore particularly exciting, especially since a RNA interference screen [413] had shown a number of the Hh family members, including *SMO*, to potentially sensitise cells to the effects of azacitidine. Will detection of the DNMT3a mutation, or those with chromosome 5 or 7 abnormalities, classify a subpopulation of AML which, in the future we will treat differently, with improved outcomes much as detection of PML-RARA determines a subgroup of AML with a significantly better prognosis. This is particularly important as HDAC inhibitors afford a viable treatment option for those less fit patients for whom the outlook is otherwise bleak. Had time allowed we would have sought to determine the functional effect of glasdegib and the HDAC inhibitors on our genetically diverse AML cells lines. It will be interesting therefore to see the results of the NCT02367456 trial, a combination study of glasdegib (PF-04449913) and azacitidine as a first line therapy in patients with MDS, AML and CMML which is currently underway.

Published data however is conflicting, with the variation in results itself a particularly interesting finding. A number of groups have reported a limited effect following short-term *in vitro* culture with the Smo antagonists, whilst also demonstrating changes in long-term culture and murine models [618]. Further, early phase human clinical trials of AML have recently reported promising results [618]. This is not simply explained by the genetic diversity of AML. Considering CML, a genetically homogeneous disease characterised by the t(9;22) chromosomal translocation, the Copland group has previously reported no evidence of effect following short-term culture of CD34+ CP-CML cells with sonidegib, alone and in combination with the TKI nilotinib. Long-term culture-initiating cell assays (LTC-ICs) and replates however showed the number and self-renewal capacity of CML LSCs to be reduced following Smo inhibition and, the combination of sonidegib and nilotinib to reduce CD34+ CP-CML cell engraftment in NOD/SCID/Gamma (NSG) mice [412]. We therefore considered a number of variables, which might contribute to the discrepant results seen following Smo antagonism *in vitro* (short and long-term assays) and *in vivo*:

(1) Genetic heterogeneity

Published data has shown a correlation between the Hh pathway and FLT3-ITD mutational status and those cases with a monocytic phenotype, M4 and M5 according to the FAB classification [381]. Even within these defined groups marked variation is seen; studies therefore require large numbers to ensure sufficient power. An absence of effect may therefore simply reflect sample or cell line selection.

(2) Cell phenotype

There are two important considerations under this category: cell lines versus primary cells and, bulk versus defined populations.

Cell lines serve as experimental models enabling investigation and analysis of primary processes and the effect of manipulating these processes. Cell lines are however immortalised, may not always behave in the same manner as, and therefore not always accurately represent, primary cells [627]. Primary cell experiments are therefore required to validate cell line data. When interpreting primary cell work, it is however important to remember these cells have also been manipulated – they have been harvested, isolated and, in many instances, cryopreserved before utilisation. What is the effect of cryopreserving and thawing these cells? Does this process select specific cell populations, and therefore influence the results generated?

Considering next the cell population being analysed. If we consider CML, work within this disease is able to focus on the more primitive stem and progenitor populations, understood to lead to treatment resistance and disease relapse, and which, within the context of CML are well defined. Within AML however the stem cell phenotype remains to be fully defined. Initially defined as CD34+CD38− further work phenotypically defining the human AML LSC as CD34+CD38−CD90−IL−3R+CD71−HLA−DR−CD117− [112,130-133], with evidence the LSC population resembles, and derives from, HPCs [113,131,133-137,149]. The majority of work within AML uses bulk MNCs derived from the PB or BM. Considering the Hh pathway is defined as a stem cell self-renewal pathway, we consider the cell population to be an important variable in determining response. Indeed the Hh signalling pathway has been shown to be more active in CD34+ primary AML cells than in CD34- primary AML cells [618]. Results must therefore be carefully interpreted for the population in which they have been derived.

(3) Primary cilia

The relationship between primary cilia and the Hh pathway was first reported in 2003 [450]. It is now widely accepted that vertebrate canonical Hh signalling requires primary cilia [337,417,430,450-457]. Haematopoietic cells have however, until recently, been considered to be among the few cells not to possess primary cilia [416,428,566,611]. This data and ours suggests haematopoietic cells possess primary cilia and therefore the machinery to enable canonical Hh signalling though response may differ depending upon cell phenotype; discussed in greater depth in section 3.2.

(4) Influence of the microenvironment

The intricate relationship between the BM microenvironment and HSCs, both normal and malignant, is well established. Recent evidence highlights the importance of the SC niche in governing SC behaviour. Considering experimental design, supportive stromal cells are absent from CFCs and liquid culture. Published data has shown colony growth to occur in >50% of samples though cells were plated either immediately after thawing or following culture for 24hrs. Colonies grew 25% of our samples (1/4). This work is insufficiently powered to consider whether insufficient colonies reflect experimental design or sample selection; it does however raise an interesting question about AML progenitor cell behaviour *in vitro*. When an AML stem cell phenotype is defined it would be fascinating to track this cell and it's behaviour following *in vitro* liquid culture at various time points, would we see a shift towards a more mature, and thus differentiated, phenotype? Considering our *in vitro* data we hypothesise manipulation of the Hh

signalling pathway through Smo antagonism influences leukaemic cell behaviour, encouraging both apoptosis and differentiation, effect potentially dependent upon both intrinsic and extrinsic factors.

The evidence in favour of the use of small molecule Smo inhibitors appears to be ever increasing, the recently presented Phase II NCT01546038 trial particularly encouraging, demonstrating an effect in an unselected cohort of AML and high-risk MDS patients treated with PF-04449913 (glasdegib) and LDAC compared with LDAC alone [618]. Whether Smo antagonists will have a role clinically outwith the trial setting however remains to be determined. Further, whether these drugs, as with other small molecule inhibitors will find their niche, demonstrating increased efficacy in a select subtype or subtypes is an area of great interest.

5 'Key downstream targets of the hedgehog pathway represent therapeutic targets.'

5.1 Introduction

There is considerable data showing the Hh signalling pathway to be intrinsically linked to numerous pathways and downstream targets, both in solid tumours and haematological malignancies, Figure 5.1.1.

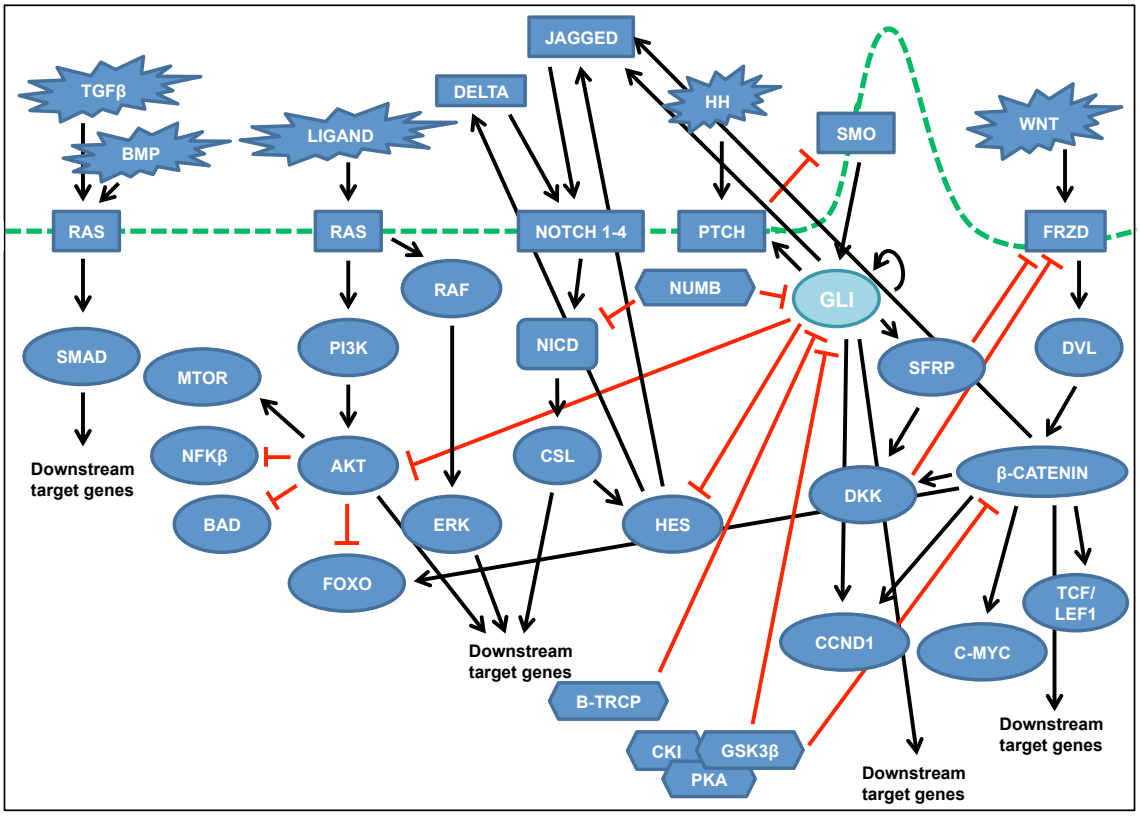

Figure 5.1.1: Schematic depicting recognised interactions between the self-renewal pathways.

5.1.1 Primary human AML MNCs differentially express key downstream components of the Hh pathway at a gene level

Considering the degree of cross talk between the self-renewal pathways – BMP, Hippo, Notch, TGFß and Wnt, and the vast array of downstream targets, as depicted in Figure 1.10, we studied the expression of >100 genes (outlined in 3.4.2) within an unselected cohort of MNCs from primary *de novo* AML samples (n=76). Sample characteristics are listed in Appendix 1. Expression was compared to an unselected cohort of normal bulk MNCs (n=10) for reasons previously discussed (section 3.1.2), and in keeping with published work. Expression levels were quantified by qRT-PCR using Fluidigm® technology. To account for input cDNA the ΔCT for each gene was calculated by subtracting the CT value of 6 housekeeping (control) genes (*ATP5S*, β*2M*, *ENOX2*, *GAPDH*, *TYW1* and *UBE2D2*) from the CT recorded for the gene of interest. Expression is presented as $2^{-\Delta\Delta CT}$, allowing comparison of levels of mRNA expression between each AML sample; Figure 5.1.1.1.

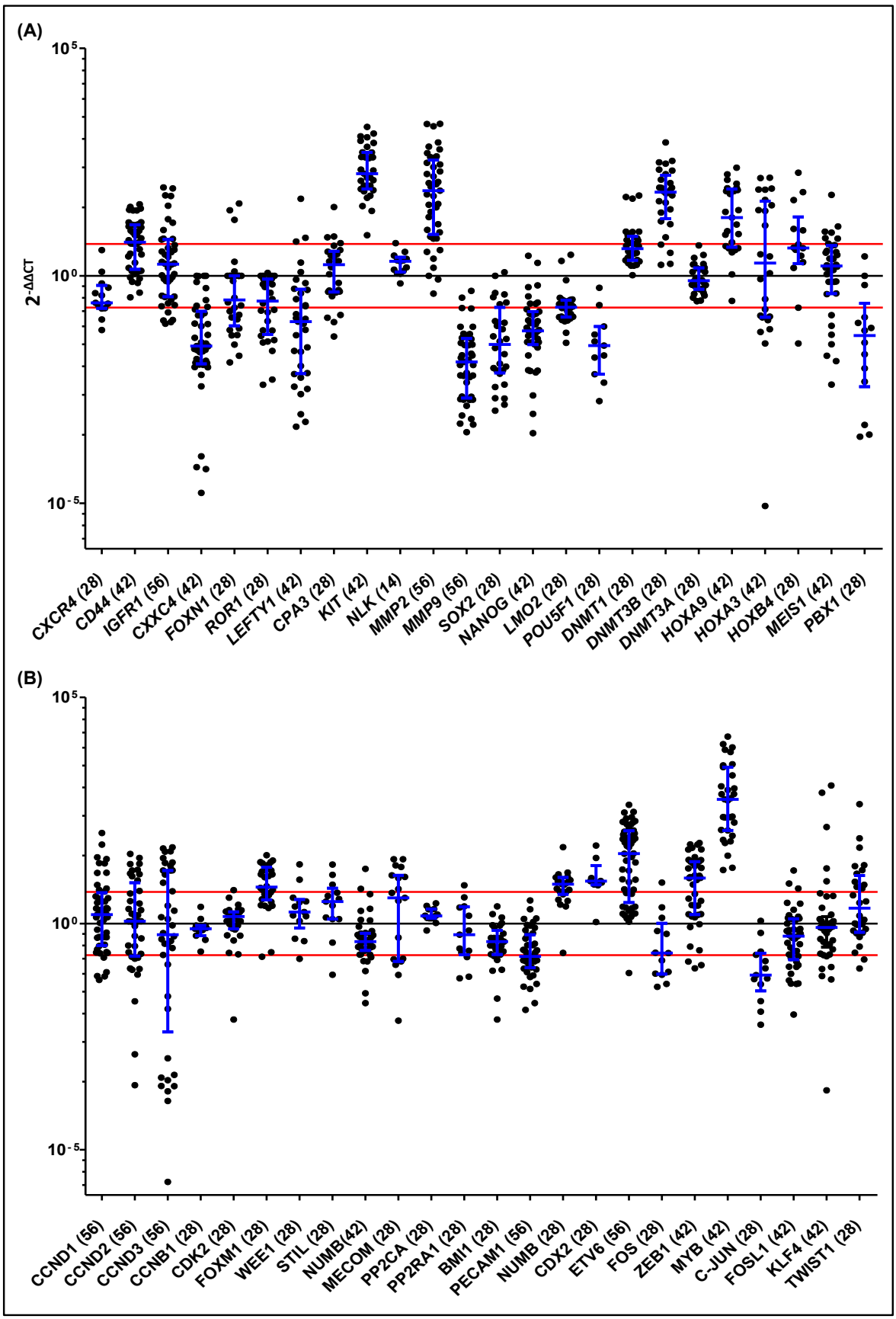
(A)
10^5
10^0
10^{-5}
$2^{-\Delta\Delta CT}$
CXCR4 (28)
CD44 (42)
IGFR1 (56)
CXXC4 (42)
FOXN1 (28)
ROR1 (28)
LEFTY1 (42)
CPA3 (28)
KIT (42)
NLK (14)
MMP2 (56)
MMP9 (56)
SOX2 (28)
NANOG (42)
LMO2 (28)
POU5F1 (28)
DNMT1 (28)
DNMT3B (28)
DNMT3A (28)
HOXA9 (42)
HOXA3 (42)
HOXB4 (28)
MEIS1 (42)
PBX1 (28)
(B)
10^5
10^0
10^{-5}
CCND1 (56)
CCND2 (56)
CCND3 (56)
CCNB1 (28)
CDK2 (28)
FOXM1 (28)
WEE1 (28)
STIL (28)
NUMB(42)
MECOM (28)
PP2CA (28)
PP2RA1 (28)
BMI1 (28)
PECAM1 (56)
NUMB (28)
CDX2 (28)
ETV6 (56)
FOS (28)
ZEB1 (42)
MYB (42)
C-JUN (28)
FOSL1 (42)
KLF4 (42)
TWIST1 (28)

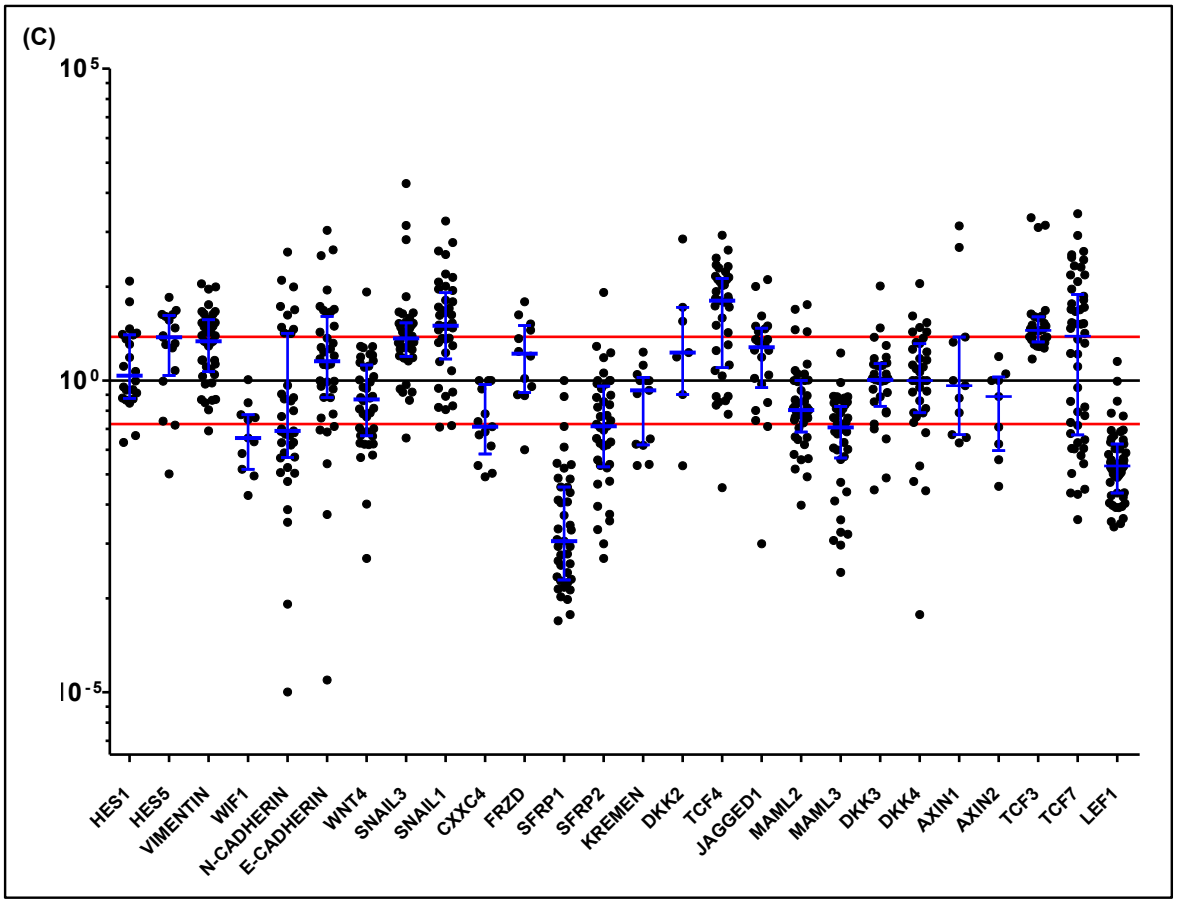

Figure 5.1.1.1: Variance in mRNA expression both within, and between, select genes in an unselected cohort of bulk primary AML MNCs.
RNA was extracted from cells harvested following culture for 24hrs. Expression levels were quantified by qRT-PCR using Fluidigm® technology. mRNA expression levels are shown as the fold change ($2^{-\Delta\Delta CT}$) relative to the mean of 10 normal MNC samples with 6 housekeeping genes – *ATP5S, B2M, ENOX2, GAPDH, TYWI* and *UBE2D2* serving as endogenous control. The median is presented with error bars indicating the interquartile range. Red lines indicate a 5-fold change. A total of 76 primary samples were screened though not for all genes, sample number variance reflects technical issues – poor technical triplicates, signal detected in the no template control or failed reaction by Fluidigm®. (A, B & C) Genes were chosen due to their association with myeloid malignancies and / or the Hh signalling pathway and from self-renewal pathways with which Hh is known to cross-talk in myeloid malignancies.

Whilst the heterogeneity of AML is demonstrated no gene expression patterns were identified - expression was studied both within and across AML subtypes and according to *SMO* expression.

Genes were found to be up- and down-regulated relative to normal MNCs and to not be expressed. Further, within individual genes expression varied markedly (fold change difference across an individual gene ranging from 100 to 10,000). Despite this heterogeneity, considering those genes expressed, interesting trends were noted within our unselected cohort of primary *de novo* human AML samples. Up-regulation of *CDX2, DNMT1, DNMT3B, ETV6, FOXM1, HOXA9, KIT, MECOM, MMP2, MYB, SNAIL1, SNAIL3, TCF3, TCF4, TWIST1* and *Vimentin* was demonstrated whilst down-regulation was seen in *BMI1, CXXC4, FOXN1, LEF1, LEFTY1, LMO2, MAML3, MMP9, NANOG, NUMB, PBX1, PECAM1, POU5F1, ROR1, SFRP, SFRP1* and *SOX2*. Interestingly, there was no significant difference between AML and normal MNCs in the following genes: *CDK2, CPA3, DKK3, DKK4, DNMT3A, FOSL1, HES1, KLF4, NLK, PP2CA* and *WNT4*.

5.1.2 Key downstream targets of the Hh pathway are differentially expressed at a protein level in primary human AML

The BM niche is a highly dynamic system which serves to regulate and support haematopoiesis [14,44,45]. Deregulated interactions have been shown to be fundamental in disease pathogenesis [11,15-17].; within AML interactions between the leukaemic cell and those of the BM are thought to be involved in chemoresistance [596,597]. We sought to determine native protein expression of key downstream targets of the Hh pathway within this unique, highly specialised environment.

IHC was performed on an unselected cohort of *de novo* primary human AML BMTs (n=37) and compared to BMTs from normal controls (n=10). Targets were selected following review of the literature and our gene expression data. Expression of BCL-2, BMP4, CD44, CCND1, Vimentin, and Wnt5a were analysed. GLI-1 and -3 have been shown to transcriptionally regulate BCL-2 in BCC. BCCs are known to express high levels of BCL-2 with deregulated Hh signalling, mediated through SHH, thought to contribute to the up-regulation in BCL-2 [598]. The Gli proteins have been shown to induce BMP expression, specifically BMP-4, during normal bone formation [599], though their relationship in malignancies remains to be determined. CD44 is extensively expressed within the adult BM, shown to play an important role in adult haematopoietic regulation with research showing a number of cell surface ligands including CD44 to be preferentially expressed on the AML LSC compared to the normal HSC [600]. Further, CD44 is recognised to be active alongside the Hh signalling pathway [248]; work showing the GLI transcriptional regulators and CD44 serve as important biomarkers for aggressiveness, survival and recurrence in gastric cancers [601]. A close relationship is also recognised between the Hh signalling pathway and cell cycle regulators, in health [602] and disease [603]. The EMT pathway and its regulation is far less understood, a complex interplay between the Hh, WNT and TGFß signalling pathways presently considered to be key factors in determining this process [604]. Additionally, the Wnt5a ligand is expressed in HSPCs, lymphocytes and stromal cells within the BM [605,606]; Wnt5a being shown to maintain HSCs in a quiescent state, suppressing their proliferation [607]. Expression of these targets is shown in Figure 5.1.2.1.

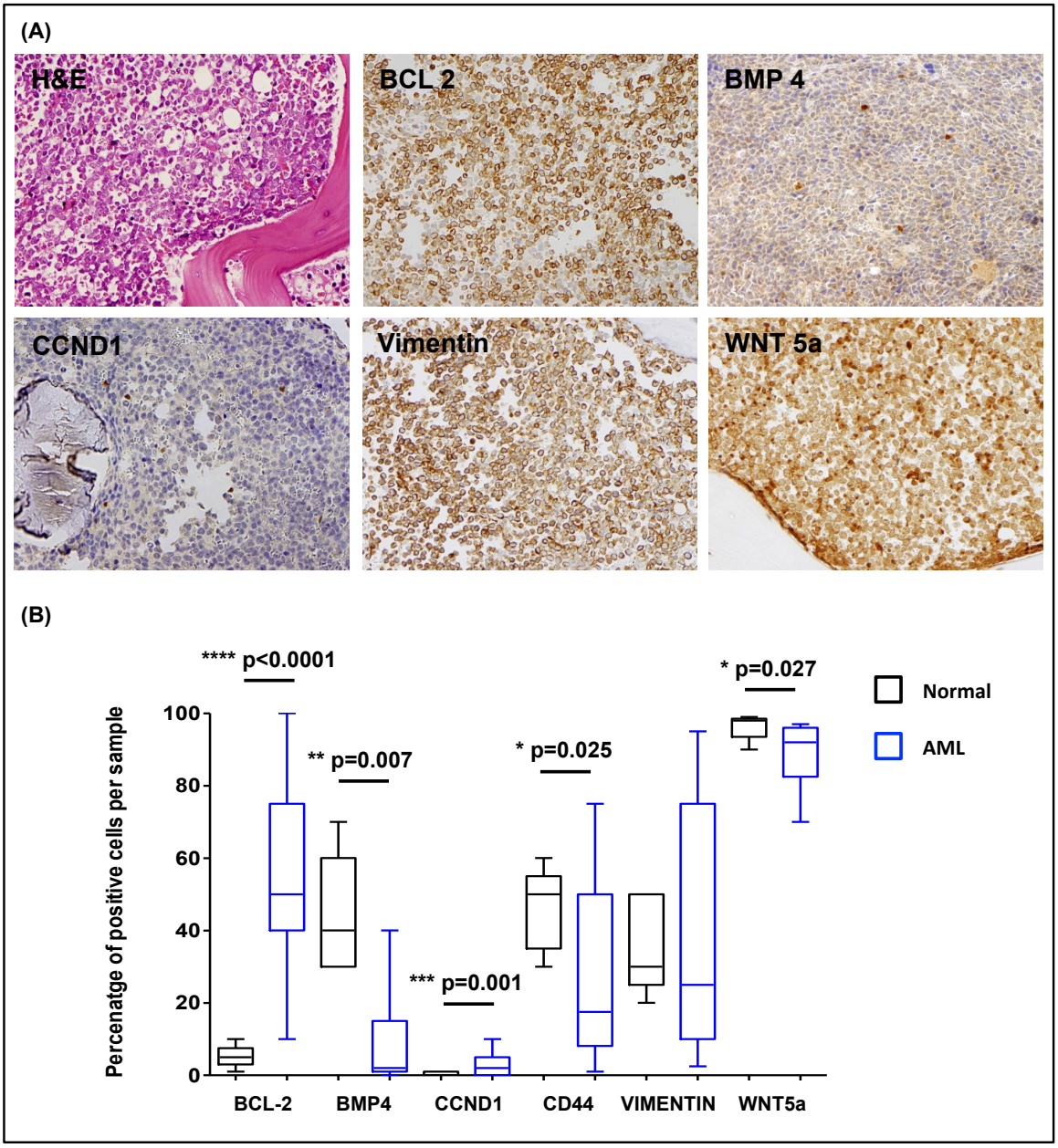

Figure 5.1.2.1 A&B: IHC on a cohort of AML BMTs (n=) demonstrated marked variation in key downstream targets of the Hh signalling pathway; with BCL-2 significantly up-regulated and BMP4 significantly down-regulated in AML.
IHC was performed on human AML BMTs (n=37) and compared to BMTs from normal controls (n=10). Expression was estimated at x10 magnification by two investigators in a blinded fashion.
(A) Representative images at x10 demonstrating staining patterns for each antibody. (B) Box and whisker plot showing percentage of positive cells per specimen, minimum and maximum values are depicted.
There was marked variance in expression within our AML cohort. BCL-2 and CCND1 were significantly up-regulated ($p<0.0001$ and $p<0.001$ respectively) whilst BMP4, CD44 and WNT5a were significantly down-regulated ($p=0.007$, $p=0.025$ and $p=0.027$ respectively) in AML BMTs relative to normal BMTs. Statistics were performed using Fisher's exact test and are highlighted with p values to the nearest 3 decimal places.

As expected there was marked variation in the expression of these targets within our AML cohort, and to a lesser degree our normal cohort. Statistics were performed using Fisher's exact test. Looking first at BCL-2, there was a significant up-regulation within our AML cohort relative to normal controls ($p<0.0001$).

Considering the clinical phenotype of AML, published data and the results of early phase clinical trials targeting Bcl-2 in AML, up-regulation of BCL-2 was expected. It is however, interesting to consider it in parallel with our gene expression data showing *BCL-2* to be deregulated in AML, with an equal percentage of samples demonstrating up- and down-regulation of *BCL-2* relative to our normal cohort, presented in section 5.3.1. BCL-2 however was significantly up-regulated with no overlap between the expression values within our AML and normal cohorts.

BMP4, interestingly, was down-regulated in AML relative to our normal cohort ($p<0.001$). If we consider this alongside our gene expression data we had shown *BMP4* and *SMAD2* to be down-regulated relative to normal MNCs (both the mean and median fold change), and published data reporting AML cells to induce osteogenic differentiation and acquire a growth advantage through BMP-connective tissue growth factor (CTGF) signalling [608]. Interestingly, considering other myeloid malignancies, work in CML has shown the BMP pathway to be deregulated in all subpopulations of CML from immature CD34 positive cells through to mature neutrophils (CD14+/CD15+), lymphocytes (CD3+ and CD19+) and erythroid cells (glycophorin +); high levels of BMP receptor Type 1a&b (*BMPRIa* and *BMPRIb)* and low expression *SMAD1* shown to differentiate between normal and malignant immature cells [609]. Further, BMP4 has been shown to be down-regulated in CML CD34+ cells and up-regulated in MNCs [609]. It would therefore be particularly interesting to study expression of soluble BMP4 and further of the receptor BMPR1a&b at both the gene and protein level in our AML cohort.

CCND1 was shown to be up-regulated at the protein level though expression was consistently ≤10% in both the normal and AML samples; none of the normal control showed expression of >1%, one AML sample was positive for CCND1 in 10% of cells. Interestingly our gene expression data had shown *CNND1* to be both up- and down-regulated relative to normal MNCs (fold change 0.057 to 100.349), Figure 5.1.1.1, suggesting a complex network of interactions regulate protein expression and, further, cell behaviour.

CD44 was down regulated in AML cell relative to our normal cohort though there was marked variance. This result contrasts with what we had expected, CD44 expression linked to a poor prognosis [590], targeting of CD44 with a monoclonal antibody shown to eradicate human AML SCs in a NOD SCID mouse model [600]. Interestingly, however there are a number of variants of CD44, with differential expression seen on progenitor and mature haematopoietic cells and further, some but not all linked with inferior prognosis [590]. The datasheet does not specify which variants are identified by our selected antibody, it would therefore be extremely interesting to repeat IHC on the same samples using antibodies specific to variants associated with AML – CD44v6, and those linked to other haematological malignancies – CD44v9 and CD44v10 [590].

Finally, WNT5a was highly expressed in both the normal and AML BMTs. Interestingly however there was a statistically significant difference in expression; WNT5a was down-regulated in our AML cohort ($p=0.027$). Whilst Wnt5a is classically considered to activate non-canonical signalling it is also recognised to inhibit canonical signalling. It would be interesting to assess expression of the Wnt family receptors downstream targets.

Statistical significance remained for BCL-2 ($p=0.001$) and BMP4 ($p=0.029$) when samples were categorised according to a previously published semi-quantitative scoring system [494] with statistics performed using Fisher's exact test, Figure 5.1.2.1. Importantly statistical significance was lost for CCND1/2, CD44 and WNT5a when this scoring system was applied.

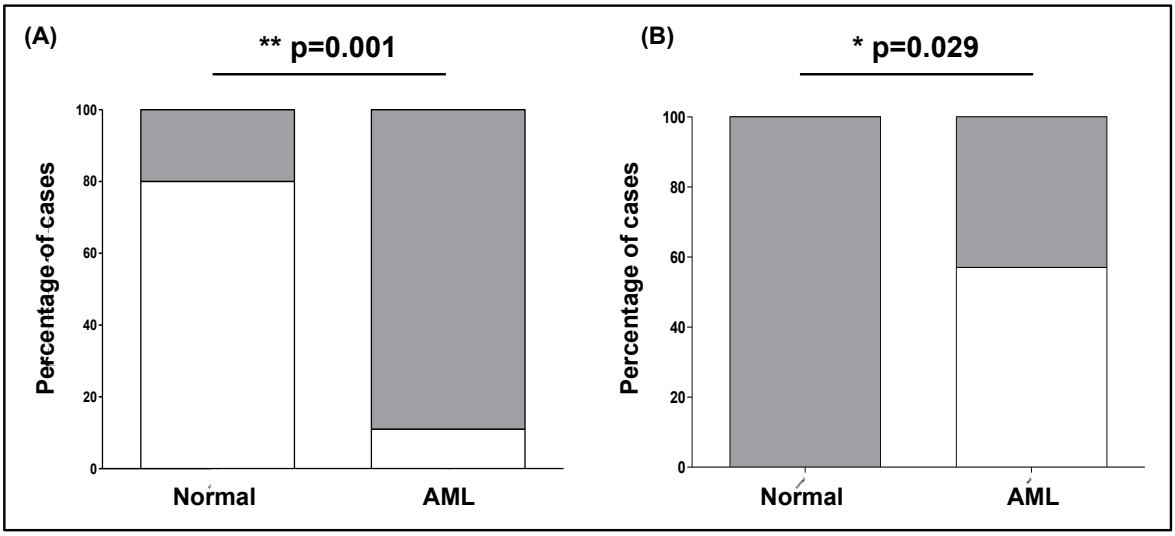

Figure 5.1.2.2: BCL-2 was significantly elevated whilst BMP4 was significantly down-regulated in primary human AML irrespective of subtype.
IHC was performed to assess the expression of (A) BCL-2 and (B) BMP-4 within the BM microenvironment in a cohort of primary human *de novo* AML BMTs (n=37) and compared to expression in BMTs from normal controls (n=10). Protein expression was estimated at x40 magnification by two investigators in a blinded fashion. The staining intensity was semi-quantitatively classified as negative and positive; staining was considered negative if <10% of cells were positive [489].
BCL-2 was significantly up-regulated (p=0.001) whilst BMP4 was significantly down-regulated (p<=.029). Statistics were performed using the Fisher's exact test and are shown to the nearest three decimal places.

This data highlights the importance of analysing downstream targets at a protein level, to consider both translational and post-translational modifiers in determining protein synthesis, and further, the intricate relationship between family members in determining protein expression and ultimately cell fate.

This data combined with our functional data, presented in chapter 4, demonstrating altered cell cycle kinetics, differentiation and apoptosis following Smo inhibition led us to consider the relationship between cell cycle regulators and components of the Bcl-2 family with the Hh signalling pathway. Log transformation of the fold change was performed to enable graphical analysis of our dataset according to the unsupervised Eisen approach using PermutMatrix software [589]. Complete linkage analysis, an agglomerative method of hierarchical clustering found key members of the Bcl-2 family and cell cycle regulators to cluster with components of the Hh signalling pathway, Figure 5.1.2.3. We therefore sought to determine whether Bcl-2 and / or select ABC transporters could be therapeutically targeted in select AML cell lines and primary samples.

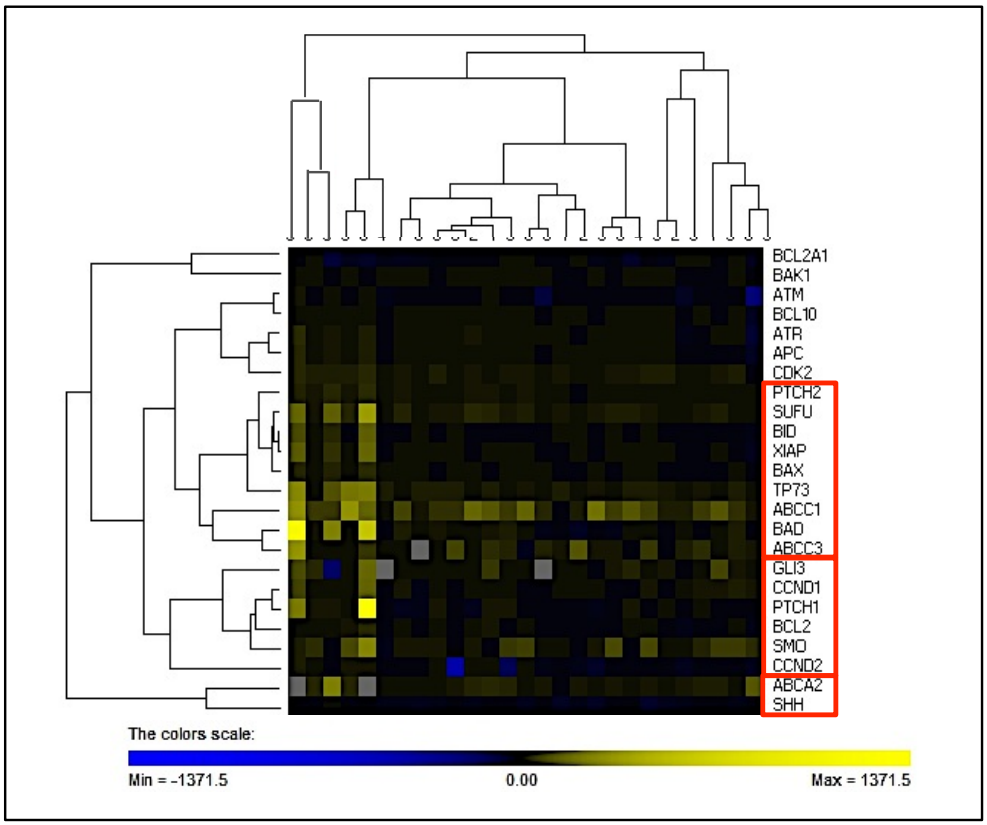

Figure 5.1.2.3: Heatmap showing expression of members of the Bcl-2 family, cell cycle regulators, select ABC transporters and components of the Hh signalling pathway, clustering highlighted by complete linkage analysis in an unselected cohort of primary, *de novo*, human AML samples (n=28). RNA was made from a cohort of 28 *de novo* primary human AML samples relative to normal bulk MNCs (n=10). AML MNCs were derived from PB and BM; the use of AML MNCs is in keeping with published work [86,87]. MNCs were harvested following culture at a density of $1.5x10^5$/ml for 24hrs. To account for input cDNA the ΔCT for each gene was calculated by subtracting the CT value of 6 housekeeping (control) genes from the CT recorded for the gene of interest. *ATP5S*, β*2M*, *ENOX2*, *GAPDH*, *TYW1* and *UBE2D2* were selected as housekeeping genes. Expression levels were quantified by qRT-PCR using Fluidigm® technology. Log transformation of the $2^{-\Delta\Delta CT}$ enabled graphical display of expression patterns according to the unsupervised Eisen approach using PermutMatrix software [588]. Complete linkage analysis finding key members of the Bcl-2 family, cell cycle regulators and ABC transporters to cluster with components of the Hh signalling pathway.

5.2 ABC transporters in AML

5.2.1 Introduction

The ABC family consists of 48 functionally distinct transmembrane proteins subdivided across seven subfamilies (ABCA through ABCG) [526]. They play an important role in normal physiology, being present in virtually all cells, responsible for the transport, or efflux, of a huge variety of compounds, across plasma and intracellular membranes. In addition, they have been linked to a number of disorders including AML, in which they have been demonstrated at diagnosis, arising during treatment and presenting on relapse, conferring an inferior outcome.

Chemoresistance is considered one of the main causes of treatment resistance and disease relapse. Cells exposed to cytotoxic agents have been shown to develop chemoresistance through a number of mechanisms, including deregulated ABC transporter expression. To date increased expression of thirteen of the ABC transporters (*ABCA2*, *ABCB1*, *ABCB4*, *ABCB11*, *ABCC1-6* *ABCC10*, *ABCC11* and *ABCG2*) have been linked to chemoresistance. ABC transporters serving to protect the CSC from a broad range of cytotoxic agents [539,540,666,667], and to confer a survival advantage through altered cholesterol metabolism in AML [668-670]. We therefore studied expression of the ABC transporters *ABCA2, ABCB1, ABCC1, ABCC2* and *ABCG2* in a cohort of *de novo* primary human AML samples relative to normal bulk MNCs (n=10). AML MNCs (leukaemic blasts) were derived from PB and BM; the use of AML MNCs is in keeping with published work [86,87]. RNA was isolated from cells following culture for 24hrs. To account for input cDNA the ΔCT for each gene was calculated by subtracting the CT value of 6 housekeeping (control) genes from the CT recorded for the gene of interest. *ATP5S*, β*2M*, *ENOX2*, *GAPDH*, *TYW1* and *UBE2D2* were selected as housekeeping genes. Expression was quantified by qRT-PCR using Fluidigm® technology. Expression is presented as fold change ($2^{-\Delta\Delta CT}$) relative to our normal control cohort with marked variance between AML samples, seen within each of the ABC transporters and up-regulation of *ABCA2*, *ABCC1*, *ABCG2* and to a lesser degree *ABCC3*; Figure 5.2.1.1. We therefore sought to study the expression of select ABC transporters within our cell lines and, to determine whether these ABC transporters represented therapeutic targets.

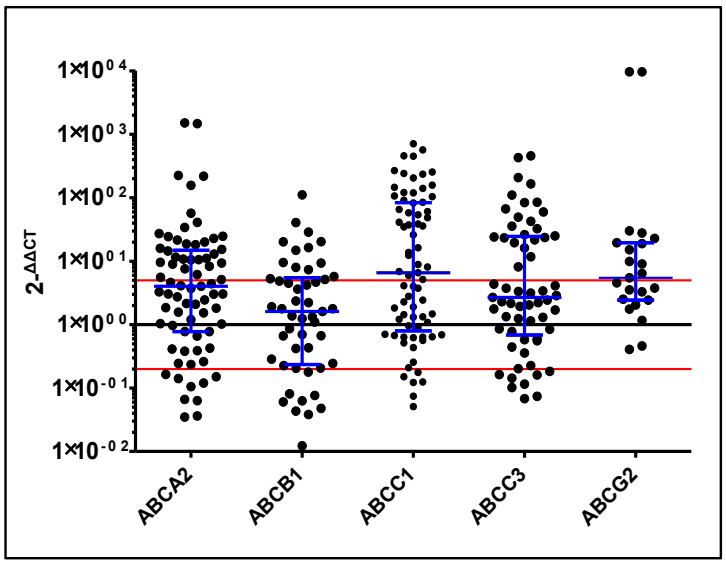

Figure 5.2.1.1: mRNA expression of select ABC transporters in an unselected cohort of primary, *de novo*, human AML MNC samples (n=76) relative to a normal control (n=10).
RNA was made from cells harvested following culture for 24hrs. Expression levels were quantified by qRT-PCR using Fluidigm® technology. Expression levels are shown as $2^{-\Delta\Delta CT}$, with 6 housekeeping genes – *ATP5S, B2M, ENOX2, GAPDH, TYWI* and *UBE2D2* serving as endogenous control; CT values for these genes ranged from 3 to 13. Red lines indicate a 5-fold change. The median is presented, error bars show the SD and demonstrate (1) the variability in baseline expression between individual AML samples, (2) the variance between each of the ABC transporters and, (3) the up-regulation of *ABCA2*, *ABCC1*, *ABCG2* and to a lesser degree *ABCC3*.

5.2.2 The ABC transporters are heterogeneously expressed in AML cell lines

qRT-PCR using Fluidigm® technology was used to determine the baseline mRNA expression of a number of ABC transporters - *ABCA2, ABCB1, ABCC1, ABCC3* and *ABCG2;* selected following a literature search showing them to be linked to chemoresistance in AML. RNA was extracted from cells harvested in optimal growing conditions (resuspended in fresh media 24hrs before harvesting at a density of 2-3x10^5/ml). To account for input cDNA, the ΔCT for each gene was calculated by subtracting the CT value of 6 housekeeping (control) genes from the CT recorded for the gene of interest. *ATP5S*, β2*M*, *ENOX2*, *GAPDH*, *TYW1* and *UBE2D2* were selected as housekeeping genes. Expression is presented as $2^{-\Delta CT}$, allowing comparison of levels of mRNA expression between each cell line, Figure 5.2.2.1.

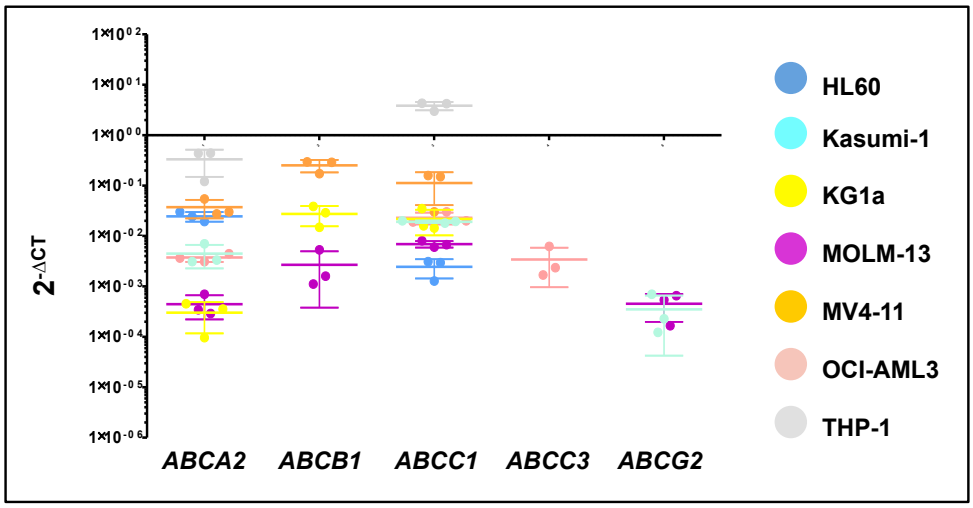

Figure 5.2.2.1: Variance in the expression of *ABCA2*, *ABCB1* and *ABCC1* in seven, genetically diverse, AML cell lines.
RNA was made from cells harvested in optimal growing conditions. To account for input cDNA the ΔCT for each gene was calculated by subtracting the CT value of 6 housekeeping (control) genes from the CT recorded for the gene of interest. *ATP5S*, β*2M*, *ENOX2*, *GAPDH*, *TYW1* and *UBE2D2* were selected as housekeeping genes. Expression levels were quantified by qRT-PCR using Fluidigm® technology and are shown as $2^{-\Delta CT}$. The mean of 3 biological replicates samples are shown with error bars indicating SD. A marked variance in the mRNA expression of *ABCA2*, *ABCB1* and *ABCC1* was demonstrated in seven, genetically diverse AML cell lines.

Genetic heterogeneity is clearly demonstrated. *ABCA2* and *ABCC1* were expressed by all of our selected cell lines. A >100-fold difference in the expression of *ABCA2* was demonstrated between cell lines; THP-1 cells demonstrated the highest expression and Kasumi-1 cells the lowest. A >100-fold difference in the expression of *ABCC1* was also demonstrated between cell lines; OCI-AML3 cells had the lowest expression whilst THP-1 cells were again shown to have the highest expression. This is particularly interesting considering we had shown THP-1 cells to be less sensitive to Ara-C, the IC_{50} by rezarurin assay being > 4-fold higher, than our other selected cell lines (Figure 5.2.3.2). *ABCB1* was detected in the Kasumi-1, KG1a and MOLM-13 cell lines. *ABCC3* was only expressed within the MV4-11 cell line whilst *ABCG2* was expressed by the HL60 and KG1a cell lines. Previous work has shown 22 ABC transporters, including *ABCB1* and *ABCC1*, to be predominantly expressed in CD34+CD38− cells and, to be subsequently down-regulated upon differentiation into the CD34+CD38+ cells [545]; four of our selected ABC transporters were expressed by the CD34+ KG1a cell line, and three by the Kasumi-1 cell line. Interestingly however, whilst the CD34+ cell lines (Kasumi-1 and KG1a) expressed a number of the studied ABC transporters the CD34- cell lines, MOLM-13, MV4-11 and THP-1, were shown to express these genes at significantly higher levels. Both FLT3-ITD+ cell lines, MOLM-13 and MV4-11, expressed three of our selected ABC transporters; this is particularly interesting since *FLT3-ITD* is associated with a poor prognosis.

5.2.3 The ABC transporters elacridar, reversan and zosuquidar confer no additional benefit to Ara-C in select AML cell lines

The ABC inhibitors serve as bio-enhancers, designed to block transport mediated drug efflux. Deregulated ABC transporter expression is well recognised in AML, with chemoresistance a powerful and difficult clinical issue. Despite research into ABC transporters generating exciting hypotheses, clinical trials studying the first (verapamil, quinidine and cyclosporine A) and second (PSC-833 (Valspodar)) generation inhibitors, with and without chemotherapy, showed little clinical benefit. Interestingly, RNA expression indicates high redundancy between the ABC transporters. Further, functional studies appear to suggest a 'rescue effect' from alternative non-targeted transporters in these early studies. The absence of toxicity when these small molecule inhibitors are used clinically, and the high frequency of their expression in AML, does however mean they remain interesting therapeutic targets. We therefore sought to study a number of multifunctional modulators in seven genetically diverse, AML cell lines.

Three ABC transporter drugs were chosen: elacridar which inhibits ABCG1 and ABCG2, reversan which inhibits ABCC1 and ABCG1 and zosuquidar which inhibits ABCG1. We selected these inhibitors for a number of reasons. The roles for ABCG2 and ABCC1 are well established, both up-regulated in our cohort of *de novo* primary human AML samples [667,670]. *ABCC1* and *ABCG2* were differentially expressed in our cell lines enabling us to contrast each cell line's response to the different inhibitors – in order to demonstrate an effect should these inhibitors be used in a selected, targeted manner? Whilst we did not screen our cells lines for expression of *ABCG1,* and its direct involvement in chemoresistance has not yet been demonstrated, this is one of six ABC transporters predominantly expressed by immature haematopoietic cells and associated with a chemoresistant phenotype [534]; *ABCG1* expression shown to be >1000-fold greater in HSCs compared to non-HSCs [531]. We therefore questioned whether this represented a new target.

All inhibitors were tested on KG1a, OCI-AML3 and THP-1 cells alone, and in combination, with 100nM and 500nM Ara-C for 72hrs to ensure time to enable an effect to be measurable yet avoid confounding factors such as nutrient exhaustion, or increased apoptosis due to surrounding cell death and the consequent environment change. A concentration of 500nM Ara-C was selected as this is the maximally tolerated clinical dose; 100nM was selected to assess whether the addition of an ABC transport inhibitor would allow a dose reduction in Ara-C without loss of effect. 100nM is consistent with published work studying the effect of Ara-C in AML *in vitro* [656,657]. Cell lines were chosen according to their phenotype and ABC transporter expression. KG1a is a CD34+ cell line expressing *ABCC3* and *ABCG2*, OCI-AML3 a myelomonocytic cell line expressing neither of our targeted ABC transporters though a number of others, and THP-1, a myelomonocytic cell line with the highest expression of *ABCC1*. Metabolic activity, as a measure of cell viability, was measured using the resazurin assay.

The ABC transport inhibitors were not expected to result in cell death alone. However a reduction in luminescence, reflective of a fall in metabolic activity was demonstrated following culture of the KG1a cell line with increasing concentrations of all three ABC transporter inhibitors. Considering the OCI-AML3 cell line, a progressive decline in metabolic activity was seen following culture with reversan and zosuquidar whilst a marked reduction in viabilty was seen following culture with elacridar at a concentration of greater than 5μM. Finally, looking at the THP-1 cell line, no effect was seen following culture with reversan at all concentrations or zosuquidar until the concentration exceeded 25μM whilst a gradual decline was seen following culture with elacridar. Figure 5.2.3.1. As expected culture of each of these cell lines with increasing concentrations of Ara-C for 72hrs led to a progressive reduction in cell viability; Figure 5.2.3.2.

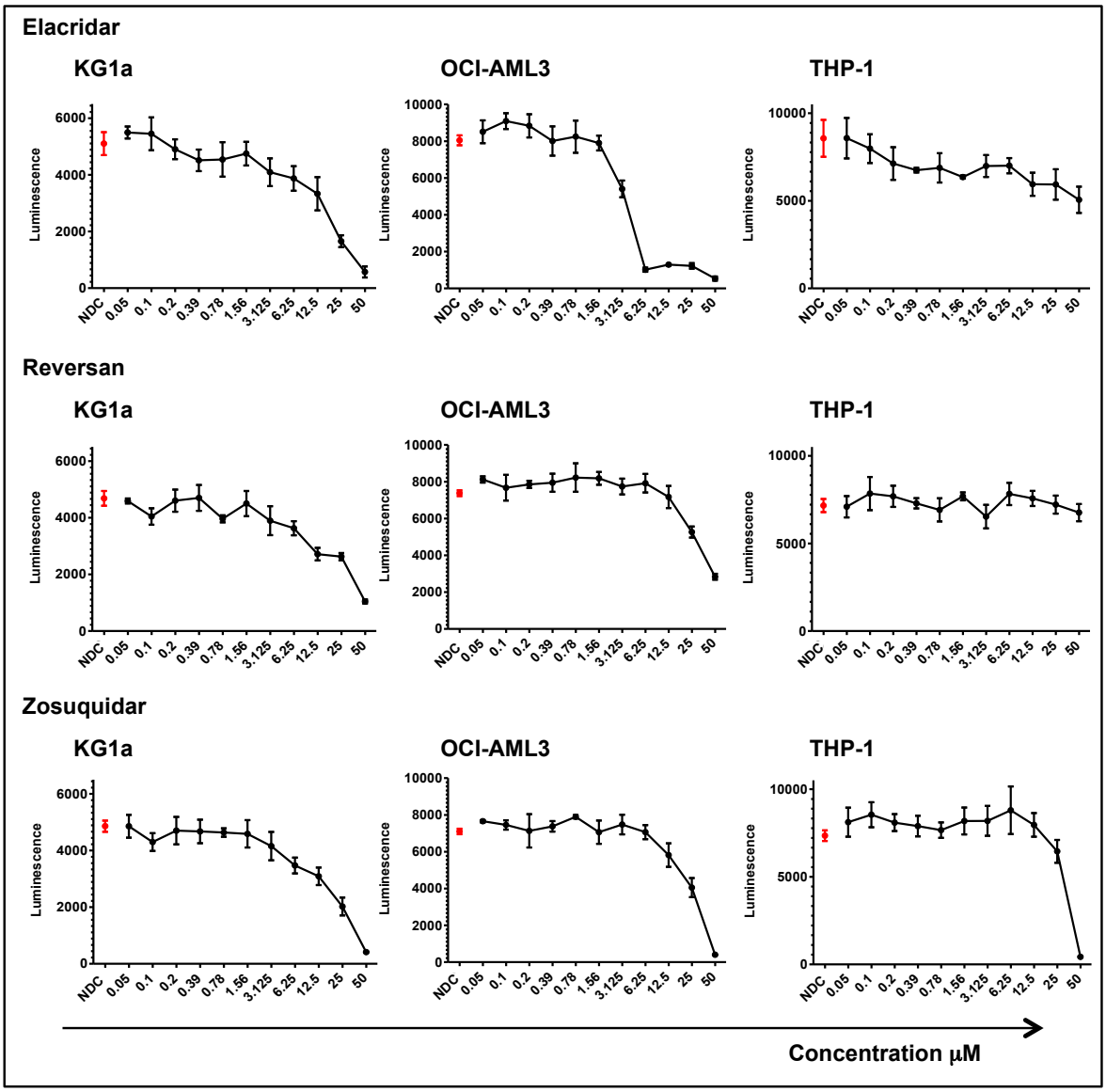

Figure 5.2.3.1: Metabolic activity, as a measure of cell viability, in three genetically diverse AML cell lines following culture with incremental concentrations of select ABC transport inhibitors (μM). Cells, at a concentration of $1x10^5$/ml, were cultured with incremental doses of elacridar, reversan and zosuquidar for 72hrs. Cell viability was determined using the resazurin assay. Results are expressed as the mean luminescence (n=4) with error bars indicating SD. The NDC is highlighted in red.
The ABC transporters had a variable effect on metabolic activity within the selected AML cell lines, this did not appear to reflect ABC transporter expression.

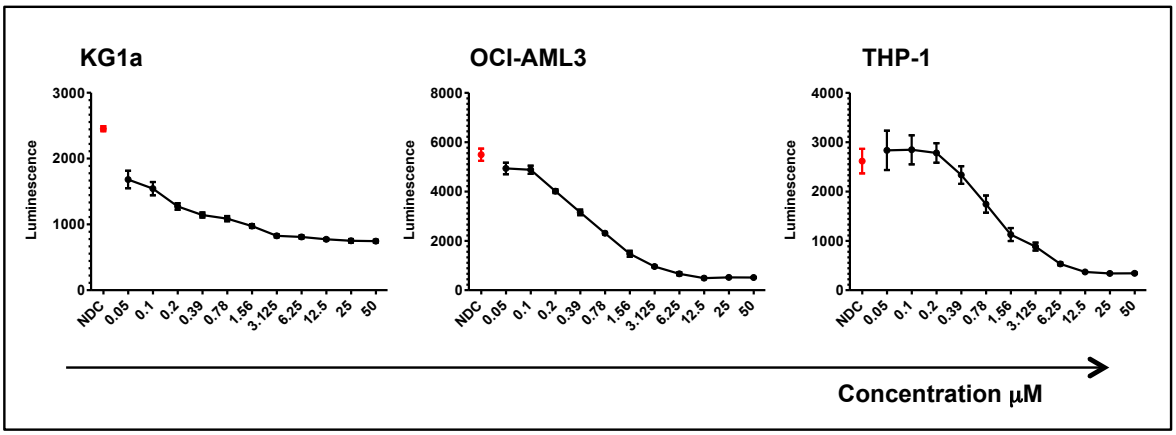

Figure 5.2.3.2: Metabolic activity, as a measure of cell viability, in three genetically diverse AML cell lines following culture with incremental concentrations of Ara-C.
Cells, at a concentration of $1x10^5$/ml, were cultured with incremental concentrations Ara-C for 72hrs. Cell viability was determined using the resazurin assay. Results are expressed as the mean luminescence (n=4) with error bars indicating SD. NDC is highlighted in red. Culture of each of these cell lines with increasing concentrations of Ara-C for 72hrs led to a progressive reduction in metabolic activity.

The addition of our selected ABC transport inhibitors did not enhance the reduction in cell viability seen following culture with Ara-C at both 100nM and 500nM as measured by the resazurin assay. The shape of the graphs, and thus change in metabolic activity, mirrored that seen following culture with the ABC transport inhibitors as single agents, Figure 5.2.3.3. Further, a variable effect, not reflective of ABC transporter expression was demonstrated. There was a progressive decline in metabolic activity following culture of the KG1a cell line with increasing concentrations of all three ABC transporter inhibitors; with no difference in effect was seen between elacridar, targeting ABCG1 and ABCG2, and the other ABC transporter inhibitors. The KG1a cell line expresses *ABCG2* suggesting a degree of redundancy of the ABC transporters. Figure 5.2.3.3.

Despite published work in solid malignancies showing limited clinical impact we had hoped a more targeted approach would enable us to identify a therapeutic window. In light of these findings however the role of ABC transport inhibitors in the treatment of AML was not pursued further during my PhD.

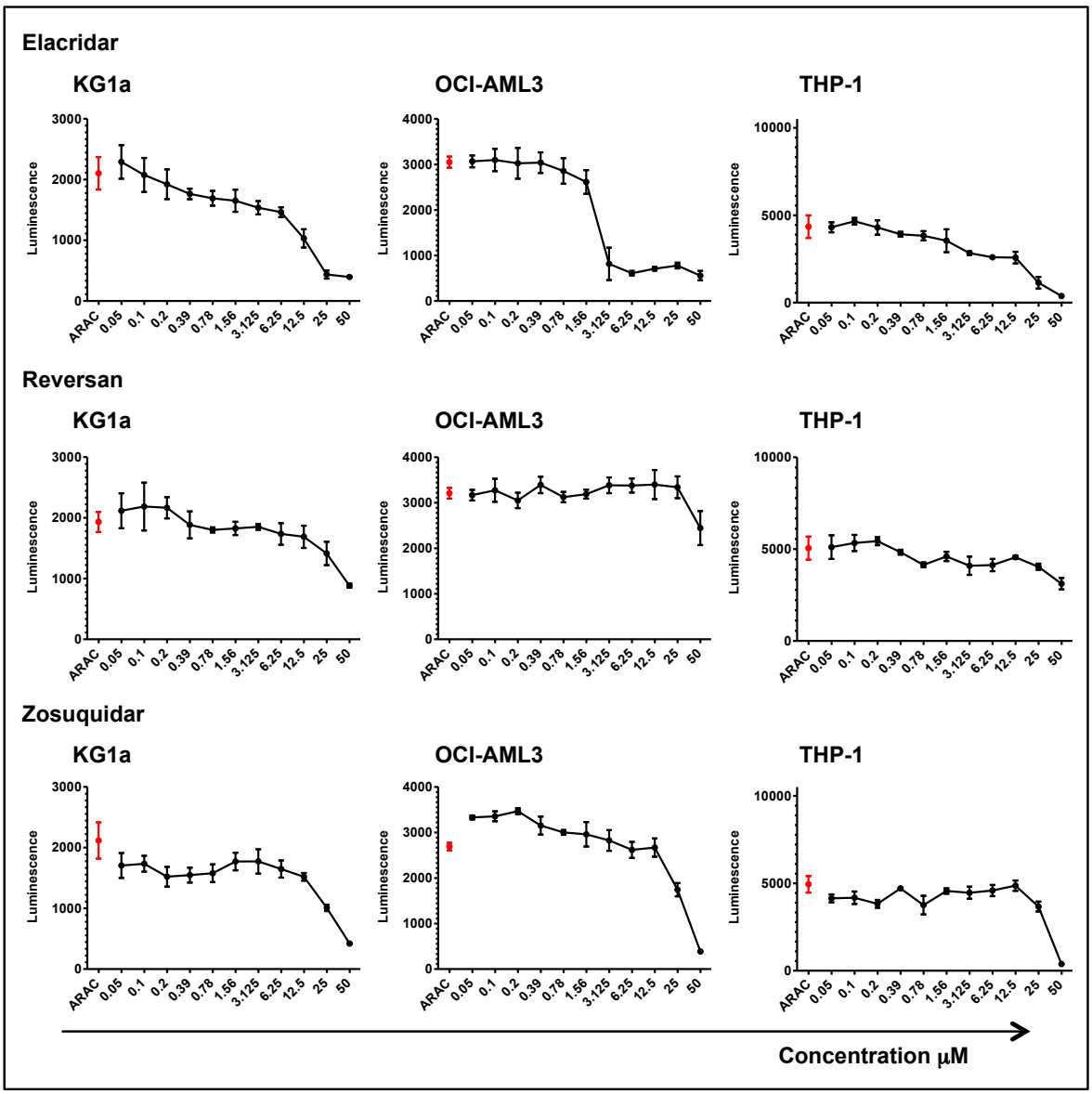

Figure 5.2.3.3: Metabolic activity, as a measure of cell viability, in three genetically diverse AML cell lines following culture with incremental concentrations of select ABC transport inhibitors (μM) and Ara-C 500nM.

Cells, at a concentration of $1x10^5$/ml, were cultured with incremental doses of elacridar, reversan and zosuquidar and Ara-C at a concentration of 500nM for 72hrs. Cell viability was determined using the resazurin assay. Results are expressed as the mean luminescence (n=4) with error bars indicating SD. Highlighted in red is the luminescence (viability) following culture with Ara-C 500nM as a single agent for comparison.

An additive effect between the ABC transport inhibitors and Ara-C was not evident in our selected AML cell lines.

5.3 Bcl-2 inhibition in AML

5.3.1 Introduction

An association between AML and Bcl-2 family has long been recognised, with high Bcl-2 being demonstrated to be an independent prognostic factor and predictor of remission [517]. Further, more recent work analysing expression within sorted populations has shown, in contrast to their normal counterparts, quiescent CD34+CD33-CD13- AML cells highly express Bcl-2 [519,520]. It is these primitive cells, which are believed to be responsible for MRD, and relapsed disease. The increased functional reliance of leukaemic cells upon Bcl-2 in comparison to normal haematopoietic cells makes it an exciting therapeutic target.

We therefore studied expression of the Bcl-2 family in a cohort of *de novo* primary human AML samples relative to normal bulk MNCs (n=10); experimental design as described in section 5.2.1. Expression is presented as fold change ($2^{-\Delta\Delta CT}$) relative to our normal control cohort with members of the Bcl-2 family deregulated in AML compared to normal and interestingly, almost universally down-regulated; Figure 5.3.1.1. We therefore sought to (1) study the expression of the Bcl-2 family within our cell lines, (2) determine whether inhibition of Bcl-2 represented a viable therapeutic and, (3) if cell death was demonstrated to determine the underlying mechanism.

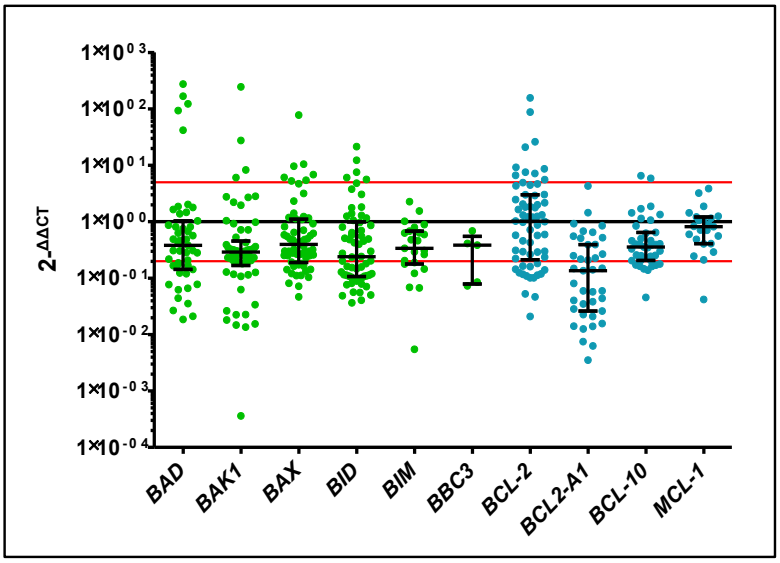

Figure 5.3.1.1: mRNA expression of the Bcl-2 family in an unselected cohort of primary, *de novo*, human AML MNC samples (n=76) relative to our normal cohort (n=10).
RNA was made from cells harvested following culture for 24hrs. Expression levels were quantified by qRT-PCR using Fluidigm® technology. Expression levels are shown as $2^{-\Delta\Delta CT}$, with 6 housekeeping genes – *ATP5S, B2M, ENOX2, GAPDH, TYWI* and *UBE2D* serving as endogenous control; CT values for these genes ranged from 3 to 13. Red lines indicate a 5-fold change. Pro-apoptotic family members are highlighted in green, anti-apoptotic family members in blue. The median is presented, error bars show the SD and demonstrate the variability in baseline expression between individual AML samples; pro-apoptosis genes shown to be down-regulated, with the greatest variance seen in the expression of *BCL-2*.

5.3.2 The Bcl-2 family are heterogeneously expressed in AML cell lines

qRT-PCR using Fluidigm® technology was used to determine the baseline mRNA expression of components of the Bcl-2 family, expressed as $2^{-(DCT)}$, with experimental design as described in section 5.2.2. Genetic heterogeneity is clearly demonstrated, Figure 5.3.2.1. Both pro- and anti-apoptotic family members were deregulated. Despite the phenotypic heterogeneity of our cell lines, expression patterns were relatively homogeneous. Interestingly, both pro- and anti-apoptotic components of the Bcl-2 family were up- and down-regulated, suggesting a complex network of interactions regulate the apoptotic process.

Looking at select genes in more detail, the anti-apoptotic member *MCL-1*, essential for the survival of HSCs [671] and involved in delayed cell cycle progression through interactions with the checkpoint inhibitors and cyclin dependent kinases [672,673] was consistently, and homogeneously, highly expressed in all cell lines suggesting a dependence upon this molecule. *BCL-2* was also up-regulated, though expression was more heterogeneous, the OCI-AML3 and THP-1 cell lines showing consistently lower levels of expression relative to the other cell lines. Of the pro-apoptotic members the expression of *BAK* and *BAX*, the gate-keepers for cytochrome c release, was particularly interesting - *BAK* was shown to be down-regulated whilst *BAX* was up-regulated. Expression of *BAX* was approximately 10-fold greater than that for *BAK*. This divergent expression pattern is particularly interesting considering activation of these proteins is required for mitochondrial driven apoptosis, their activity precisely controlled by the same pathways.

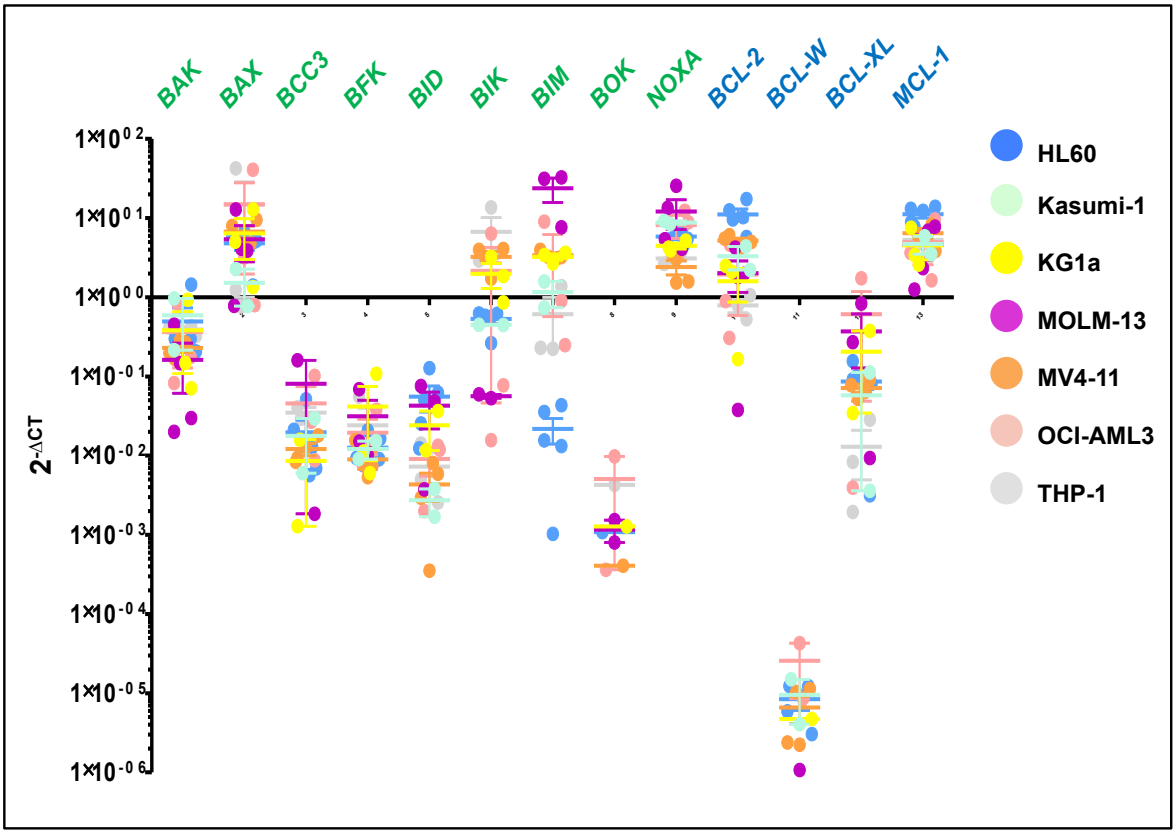

Figure 5.3.2.1: Baseline gene expression of members of the Bcl-2 family in seven, genetically diverse, AML cell lines.
RNA was made from cells harvested in optimal growing conditions. Expression levels were quantified by qRT-PCR using Fluidigm® technology. Expression levels are shown as $2^{-\Delta CT}$, with 6 housekeeping genes - *ATP5S, B2M, ENOX2, GAPDH, TYWI* and *UBE2D2* serving as endogenous control. The mean of 3 samples are presented, with error bars showing the SD. Pro-apoptotic family members are highlighted in green, anti-apoptotic family members in blue. Both pro- and anti-apoptotic components of the Bcl-2 family are shown to be up- and down-regulated. *MCL-1* is consistently, and homogeneously, highly expressed in all cell lines. *BCL-2* is also up-regulated, though expression is more heterogeneous. Of the pro-apoptotic members *BAK* is shown to be down-regulated whilst *BAX* is up-regulated.

Previous work has shown the ratio of *BAX* and / or *BAK* to *BCL-2*, rather than expression of *BAK*, *BAX* and *BCL-2*, to have prognostic and predictive significance in colon and bladder cancer [674,675]. We therefore evaluated the *BAX*/*BCL-2* and *BAK*/*BCL-2* expression ratios for each cell line, Table 5.3.2.1.

Table 5.3.2.1: *BAX*/*BCL-2* and *BAK*/*BCL-2* expression ratios in seven, genetically diverse, AML cell lines

Cell line	***BAK*/*BCL-2* expression ratio**	***BAX*/*BCL-2* expression ratio**
HL60	0.179157	0.461673
Kasumi-1	0.240589	1.60712
KG1a	0.0807	1.250073
MOLM-13	0.044261	1.301589
MV4-11	0.188073	1.34105
OCI-AML3	0.044461	0.432757
THP-1	0.494037	2.630983

This table demonstrates that whilst *BAX* is seen to be up-regulated at a gene level the balance of pro- and anti-apoptotic gene expression favours anti-apoptosis in the majority of cell lines. In those cell lines in which the ratio favours apoptosis – Kasumi-1, KG1a, MOLM-13, MV4-11 and THP-1, with the exception of the THP-1 cell line, this appears to be counteracted by the marked shift in favour of anti-apoptosis when looking at the *BAK*/*BCL-2* expression ratios. It is important to consider however that these ratios do not account for the other family members, or interacting genes, a complex network of interactions determining cell fate – morphologically and functionally these cells were healthy, maintaining their predetermined rate of cell division. Further, gene expression does not necessarily correlate with functional activity, as it does not account for post-transcriptional regulation. For example, although transcriptional control of *BCL-2* by *NFκB* and *SHH* has been reported [598,676], evidence suggests post-transcriptional regulation to be fundamental to its function [677]. We therefore sought to determine the baseline expression of BCL-2 in each of our selected cell lines by western blotting, with SHP2 serving as an endogenous control (n=2), Figure 5.3.2.2.

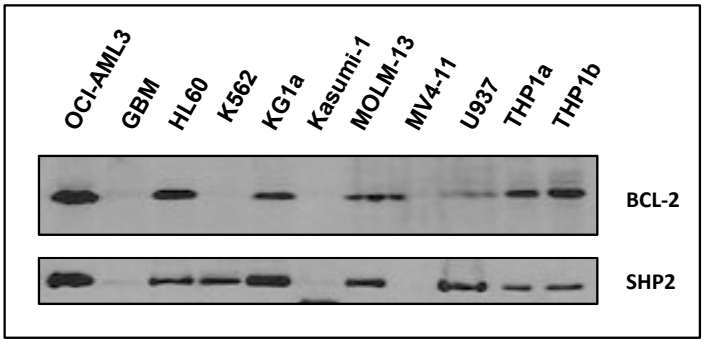

Figure 5.3.2.2: Representative Western blot showing expression of BCL-2 in select, genetically diverse AML cell lines, a glioblastoma cell line and erythroid BC-CML cell line.
Protein was extracted from cells harvested in optimal growing conditions as described in section 2.2.3.1. Western blotting, as described in section 2.2.3.2, enabled quantitative analysis of BCL-2. Representative western blot of two with similar results showing variance in the expression of BCL-2. SHP2 served as an endogenous control. The THP1cell line was run twice for internal control THP1a shows results for 10μg protein, THP1b for 20μg protein.
GBM, glioblastoma multiforme cell line; K562, erythroid CML-BC cell line; U937, monocyte lymphoma cell line.

BCL-2 was present in the HL60, KG1a, MOLM-13, OCI-AML3 and THP-1 cell lines, and absent from Kasumi-1, K562 and MV4-11. K562 was established from a 53 year old female with BC-CML, with studies determining it to be an erythroleukaemia. U937 was derived from a 37 year old male with histiocytic lymphoma, used to study monocyte behaviour. Both were included for interest to consider expression of BCL-2 in other haemaopoeitic cell lineages.

Accounting for the endogenous control the HL60, OCI-AML3 and THP-1 cell lines had the highest amount of protein whilst the KG1a and MOLM-13 had the least. This is particularly interesting as it contrasts with our *BCL-2* expression data, with the OCI-AML3 and THP-1 showing the lowest levels of BCL-2 and HL60 and MV4-11 showing the highest. This difference could be explained by a number of factors including protein stability, processes involved between transcription and translation and the complex network involved in the apoptotic process. This is in keeping with other published work which analysed the correlation between gene and protein expression, finding it to be as low as 40% depending upon the system [678]. It does however highlight the importance of assessing, and measuring, expression of the target when considering the use of small molecule inhibitors.

5.3.3 Targeting Bcl-2 with ABT-199, HA14-1 and TW37 has a variable effect within select, genetically diverse AML cell lines

ABT-199 is a second generation BH3 mimetic, gaining FDA approval for the treatment of relapsed, refractory CLL with 17p deletion in 2016 [522]. HA14-1 and TW37 are small molecule inhibitors of Bcl-2 which also inhibit other Bcl-2-like family members Bcl-XL and Bcl-W [679], and Bcl-W [680,681] respectively. Considering HA14-1, previous work has highlighted the importance of Bcl-XL in platelet survival [232]. Treatment with the first generation BH3-mimetic ABT-263 complicated by dose-limiting severe thrombocytopenia, an issue which led to the development of ABT-199. This is an important consideration given patients with AML frequently present with thrombocytopenia. All drugs were tested on KG1a, MOLM-13, MV4-11, OCI-AML3, and THP-1 cells for 72hrs to enable an effect to be measurable yet avoid confounding factors such as nutrient exhaustion. Cell metabolic activity was measured using the resazurin assay, Figure 5.3.3.1 and Table 5.3.3.1.

Table 5.3.3.1: IC_{50} values for ABT-199, HA14-1 and TW37 (select BH3 mimetics) in five genetically diverse, AML cell lines as determined by the resazurin assay

Cell line	$IC_{50}(\mu M)$		
	ABT-199	HA14-1	TW37
KG1a	0.1-0.2	12.5-25	0.05-0.1
MOLM-13	<0.05	>25	0.39
MV4-11	<0.05	12.5-25	0.2-0.39
OCI-AML3	>25	>25	0.2-0.39
THP-1	12.5-25	>25	0.1-0.2

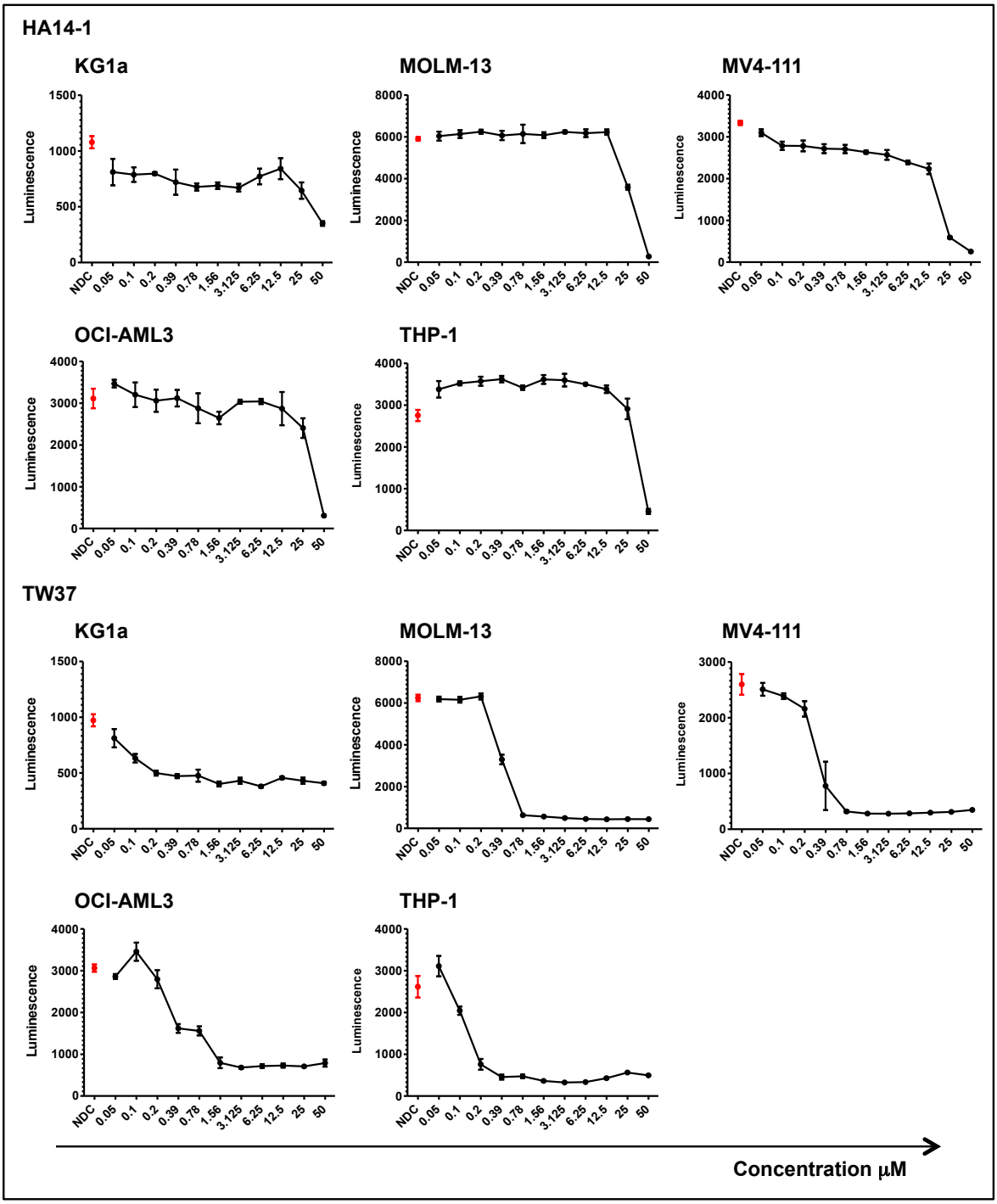
HA14-1
KG1a
MOLM-13
MV4-111
OCI-AML3
THP-1
TW37
KG1a
MOLM-13
MV4-111
OCI-AML3
THP-1
Luminescence
NDC
0.05
0.1
0.2
0.39
0.78
1.56
3.125
6.25
12.5
25
50
Concentration µM

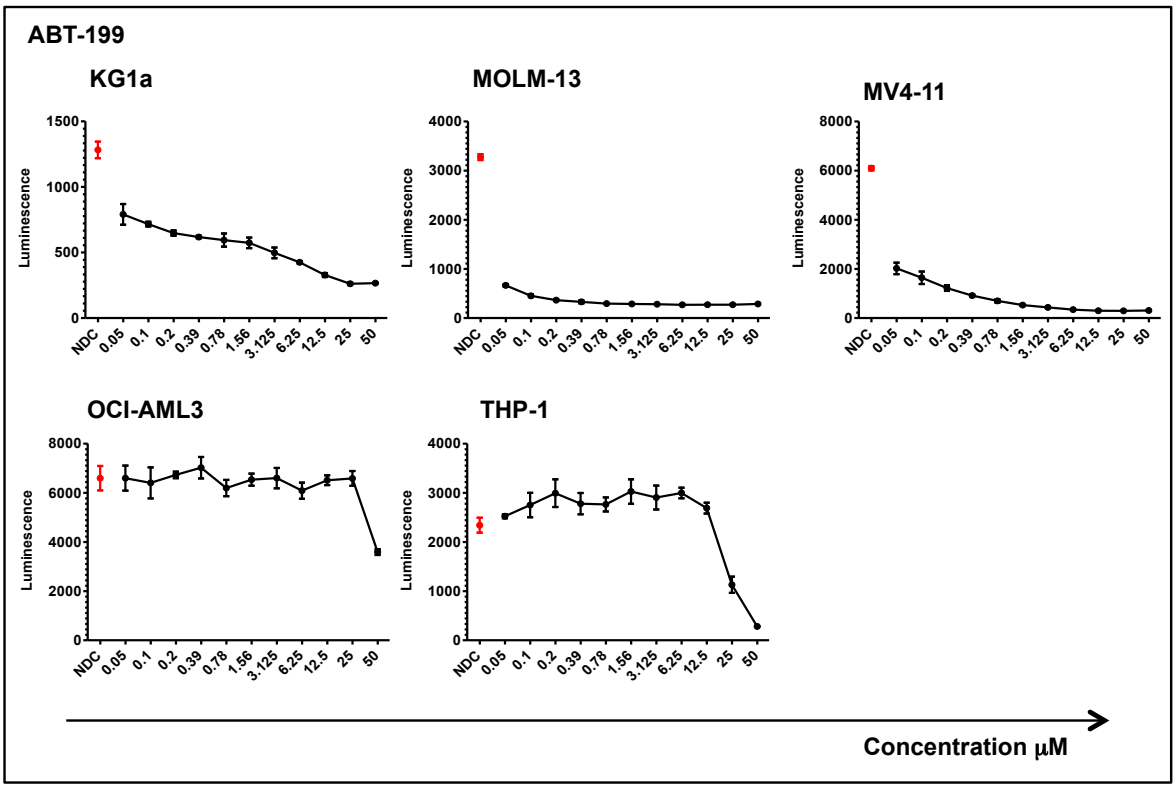

Figure 5.3.3.1: Metabolic activity, as a measure of cell viability, in five genetically diverse AML cell lines following culture with incremental doses of select BH3 mimetics / Bcl-2 inhibitors (μM). Cells, at a concentration of $1x10^5$/ml, were cultured with incremental concentrations of select Bcl-2 inhibitors (HA14-1, TW27 and ABT-199) and cultured for 72hrs. Cell viability was determined using the resazurin assay. Results are expressed as the mean luminescence (n=4) with error bars indicating SD. NDC is highlighted in red. The heterogeneous response both between, and within, our selected cell lines following culture with each of the three Bcl-2 inhibitors is clearly shown.

The heterogeneous response both between, and within, our selected cell lines following culture with each of the three Bcl-2 inhibitors is clearly demonstrated by the dose response curves, Figure 5.3.3.1, and confirmed when looking across the IC_{50} values shown in Table 5.3.3.1. All cell lines were resistant to HA14-1 with no effect seen following culture at concentrations below 6.25μM, an effect only demonstrated following culture at concentrations greater than 25μM in the OCI-AML3 and THP-1 cell lines. Intermediate sensitivity to TW37 was seen in all cell lines, with the IC_{50} ranging between 100nM and 1μM. Two cell lines were sensitive to ABT-199 induced apoptosis, MOLM-13 and MV4-11, with an IC_{50} <50nM, whilst three were highly resistant with an IC_{50} >10μM. As a comparator ABT-199 has been shown to have an inhibitory constant of <0.1nM in CLL. The marked variation in response between each cell line is not unexpected considering the notable differences in Bcl-2 expression at baseline, in addition to the different genetic signatures, and likely differing drug pharmacodynamic profiles. Considering all three compounds are small molecule BH3 mimetics, preventing heterodimerisation, and consequently inactivation, of pro-apoptotic molecules the variable effect is interesting, seemingly pointing to small but fundamental differences in their pharmacological properties. ABT-199 was in early phase clinical trials within AML, we therefore elected to investigate the mechanisms underlying treatment resistance and sensitivity. Further, and rather interestingly, whilst preclinical *ex vivo* data suggested AML cell lines, primary patient samples, and murine primary xenografts are very sensitive to single-agent venetoclax [682] a subsequent early phase clinical trial evaluating venetoclax as a single agent in patients with R/R AML demonstrated responses (CR/CRi) of 19% (6/32 patients) [524]. In contrast in elderly patients with untreated AML venetoclax, in combination with LDAC or HDMAs, showed a response rate of 44% and 76% respectively [523,683]. Whilst these conflicting results may simply reflect eligibility criteria and single versus combination therapy it

may also reflect up-regulation of Bcl-XL and Mcl-1 in AML, particularly in relapsed disease [684]. High BCL-2 correlates with venetoclax sensitivity in CLL [559,685]; with cell line work and xenograft models in CLL and NHL cells suggesting sensitivity to the BH3 mimetics can be predicted by the ratio of anti-apoptotic to pro-apoptotic family members [686,687]. Whether this can be translated into the clinic, and further whether this will be seen in acute or myeloid malignancies remains to be determined. We therefore selected the sensitive MOLM-13 and highly resistant OCI-AML3 cell lines for further analysis. Had time allowed we would have sought to understand the mechanism underpinning the different responses seen across the different BH3 mimetics.

5.3.4 Combination treatment with ABT-199 and Ara-C showed a highly synergistic effect on cell death in MOLM-13 cells

The development and introduction of small molecule inhibitors into the treatment armoury of AML is hugely exciting. *In vitro* and *in vivo* work has however shown these agents to have limited effect in isolation. Recognising this, the majority of current clinical trials are using these new, experimental, small molecule inhibitors in conjunction with established chemotherapeutic agents such as Ara-C and decitabine. We therefore sought to determine if the combination of Ara-C and ABT-199 was synergistic. The Chou-Talalay method (discussed in section 2.2.1.7) was used to quantify synergy between ABT-199 and Ara-C in the MOLM-13 and OCI-AML3 cell lines. Briefly cell counts were performed by trypan blue dye exclusion following culture for 24, 48 and 72hrs. The concentrations and combinations are depicted in Figure 5.3.4.1.

Ara-C

ABT-199 \ Ara-C	NDC	¼ IC_{50}	½ IC_{50}	IC_{50}	2x IC_{50}	4x IC_{50}
NDC						
¼ IC_{50}						
½ IC_{50}						
IC_{50}						
2x IC_{50}						
4x IC_{50}						

Figure 5.3.4.1: Schematic of the experimental layout used to determine the relationship between ABT-199 and Ara-C in the MOLM-13 and OCI-AML3 cell lines using the Chou-Talalay method. MOLM-13 and OCI-AML3 cells were seeded at a density of $2x10^5$/ml and cultured with specific concentrations of each drug as outlined above for 24, 48 and 72hrs. Trypan blue dye exclusion was performed to determine the number of live and dead cells for each experimental condition. Technical duplicates were performed, and the experiment performed three times.

Tables 5.3.4.1A&B show the predetermined IC_{50} for each drug as single agents, and the ED_{50} calculated by the Chou-Talalay method for each drug when used in combination at 24, 48 and 72hrs. Synergism, with a CI<0.47 (range 0.13-0.47) and DRI>2 (range 2-70) for all dose combinations was seen in the MOLM-13 cell line. It is interesting to note the calculated ED_{50} for ABT-199 in MOLM-13 cells was >100-fold greater than that determined for CLL cells for which venetoclax (ABT-199) is clinically approved and licensed. Weak synergism was seen in the OCI-AML3 cell line, Figure 5.3.4.2. However this was using a clinically toxic concentration of ABT-199. All subsequent experiments performed on the OCI-AML3 cell line used the maximum

clinically tolerated concentration of 1.15μM for ABT-199 and 500nM Ara-C. The calculated ED_{50} for both ABT-199 and Ara-C was used for all further experiments with the MOLM-13 cell line. All experiments were terminated at 72hrs. Had time allowed, in addition to using the maximum clinically tolerated dose, we would have performed all experiments on the OCI-AML3 cell line using the same concentrations as for the MOLM-13 cell line. This would enable comparison to be made between a sensitive and resistant cell line at both a functional and molecular level.

Tables 5.3.4.1A&B: IC_{50}, and ED_{50}, for ABT-199 and Ara-C in the MOLM-13 and OCI-AML3 cell lines following culture for 72hrs

(A)

Cell line	**ABT-199**	**Ara-C**
	IC_{50}	
MOLM-13	50nM	150nM
OCI-AML3	10μM	0.5μM

(B)

Cell line	**ABT-199**	**Ara-C**
ED_{50} at 24hrs		
MOLM-13	114.2nM	896.6nM
OCI-AML3	18.770μM	1.334μM
ED_{50} at 48hrs		
MOLM-13	31.7nM	85.1nM
OCI-AML3	18.454μM	211nM
ED_{50} at 72hrs		
MOLM-13	19.562nM	34.487nM
OCI-AML3	7.854μM	77nM

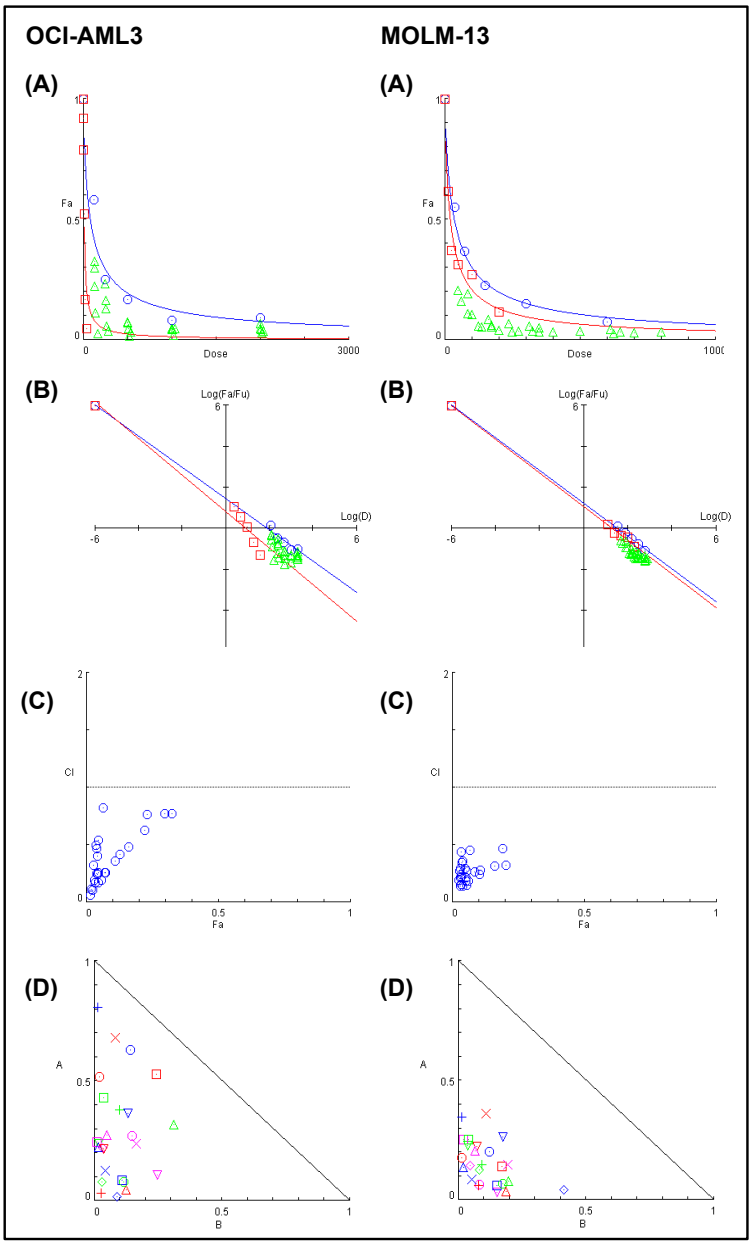

Figure 5.3.4.2: Representative plots generated according to the Chou-Talalay method following culture of the OCI-AML3 and MOLM-13 cell lines with specific concentrations of ABT-199 and Ara-C for 72hrs.

MOLM-13 and OCI-AML3 cells were seeded at a density of $2x10^5$/ml, and cultured with specific concentrations of each drug as outlined in Figure 5.3.4.1 for 24, 48 and 72hrs. Trypan blue dye exclusion was performed to determine the number of live and dead cells for each experimental condition. Technical duplicates were performed, and the experiment performed three times. (A) Dose-Effect curve, (B) Median-Effect plot, (C) CI plot, and (D) Normalised isobologram for OCI-AML3 and MOLM-13 cells. These plots clearly demonstrate strong synergism in the MOLM-13 cell line. Whilst synergism is also seen within the OCI-AML3 cell line this is at clinically toxic concentrations of ABT-199.

5.3.5 Inhibition of Bcl-2 using the BH3 mimetic ABT-199 alters cell proliferation in select AML cell lines

Using the resazurin assay, we had demonstrated OCI-AML3 to be resistant to ABT-199 whilst MOLM-13 was relatively sensitive. The Chou-Talalay method had demonstrated synergism between Ara-C and ABT-199 in the MOLM-13 cell line, and whilst also demonstrating weak synergism in the OCI-AML3 cell line this was at clinically toxic concentrations of ABT-199. We therefore sought to further analyse the effect of ABT-199, Ara-C and the combination of ABT-199 and Ara-C on our selected cell lines.

First we assessed cell proliferation and viability by trypan blue dye exclusion at 72hrs. With the OCI-AML3 cell line, culture for 72hrs with 500nM Ara-C led to a statistically significant decrease in the total number of live cells by trypan blue dye exclusion ($p=0.007$); culture with 1.15μM ABT-199 did not statistically affect the total number of live cells. There was a further decrease in the total number of live cells by trypan blue dye exclusion when cells were cultured with the combination of 500nM Ara-C and 1.15μM ABT-199 ($p=0.003$). There was no statistical difference between the total number of live cells in the Ara-C and ABT-199 arms, however a significant difference was shown between ABT-199 and the combination arm ($p=0.004$). Whilst the number of dead cells by trypan blue dye exclusion was increased in the Ara-C and combination arms this was not significant. Annexin V / 7AAD staining and flow cytometry analysis demonstrated a statistically significant increase in early apoptosis with the Ara-C and combination arms ($p=0.013$ and $p=0.045$ respectively); whilst the total number of live cells counted was lowest in the combination arm, this was not significant due to variance, it was significant in the Ara-C arm ($p=0.030$), Figure 5.3.5.1.

Culture of the MOLM-13 cell line with both 19.5nM ABT-199 and 34.5nM Ara-C as single agents showed a statistically significant decrease in total number of live cells by trypan blue dye exclusion ($p=0.0003$ and $p=0.001$ respectively). This was significantly enhanced when cells were cultured with the combination of 19.5nM ABT-199 and 34.5nM Ara-C ($p<0.0001$). Additionally there was a statistical difference in the number of live cells when comparing ABT-199 and Ara-C ($p=0.013$) and both ABT-199 and Ara-C and the combination arm (both $p<0.0001$). There was an accompanying statistically significant increase in dead cells by trypan blue dye exclusion in the ABT-199 arm ($p=0.002$), further enhanced in the combination arm ($p=0.0006$). A statistical difference in the number of dead cells was demonstrated between ABT-199 and Ara-C ($p=0.002$) and ABT-199 and the combination arm ($p=0.009$). Annexin V / 7AAD staining and flow cytometry analysis supported these results showing a statistically significant reduction in the percentage of live cells following culture with ABT-199 ($p=0.001$), Ara-C ($p=0.006$) with increased significance in the combination arm ($p=0.005$). Early and late apoptosis were increased in all treatment arms (ABT-199, $p=0.001$; Ara-C $p=0.009$; combination $p=0.0008$). Late apoptosis was increased following culture with ABT-199 ($p=0.006$) and the combination ($p=0.007$); Figure 5.3.5.1.

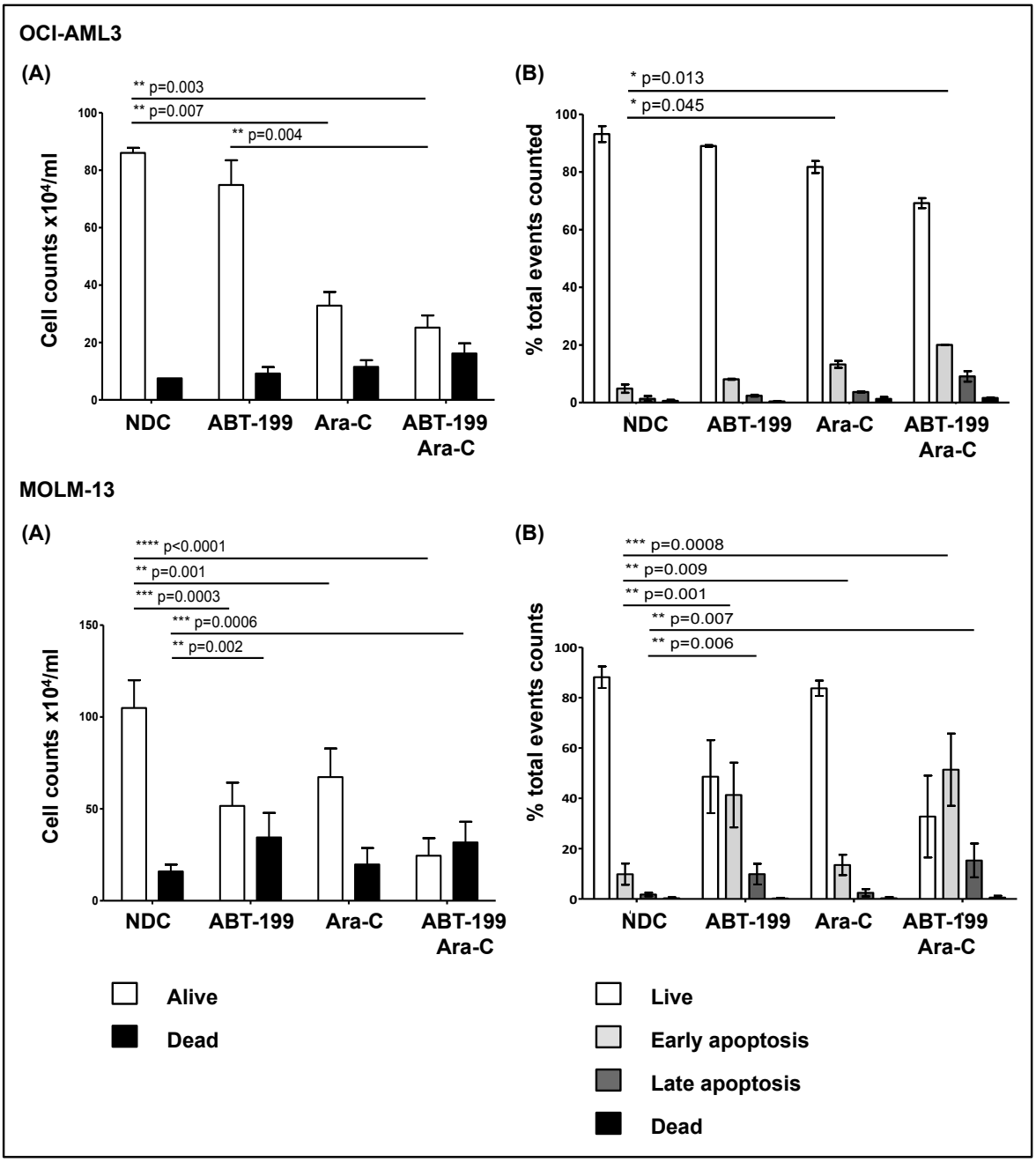

Figure 5.3.5.1: Proliferation and apoptosis, as determined by trypan blue dye exclusion and Annexin V / 7AAD staining, following culture of the OCI-AML3 and MOLM-13 cell lines with ABT-199 (1.15μM and 19.5nM respectively) and Ara-C (34.5nM and 500nM respectively) for 72hrs.
OCI-AML3 cells were seeded at a concentration of $2x10^5$/ml, exposed to ABT-199 (1.15μM), Ara-C (500nM) and ABT-199 (1.15μM) and Ara-C (500nM) in combination and cultured for 72hrs. MOLM-13 cells were seeded at a concentration of $2x10^5$/ml, exposed to ABT-199 (19.5nM), Ara-C (34.5nM) and ABT-199 (19.5nM) and Ara-C (34.5nM) in combination and cultured for 72hrs. (A) These graphs show cell viability as determined by trypan blue dye exclusion. Each bar represents the mean cell number x 10^4 /ml from four (OCI-AML3) and nine (MOLM-13) independent experiments with error bars indicating SD. (B) These graphs indicate the proportion of cells which are viable, in early apoptosis, in late apoptosis or dead as determined by Annexin V / 7AAD staining, and analysis by flow cytometry (see Figure 2.3 for gating strategy). Each bar represents the mean percentage from four (OCI-AML3) and nine (MOLM-13) independent experiments with error bars indicating SD. All statistically significant results are highlighted with p value to the nearest 3 decimal places, those not highlighted are not significant (ns). Within the MOLM-13 cell line a statistically significant reduction in live cells, explained by apoptosis, was seen following culture with ABT-199 and Ara-C, with the significance increased further in the combination arm consistent with drug synergism. ABT-199 did not reduce proliferation, or induce apoptosis, and there was no evidence of synergism in the OCI-AML3 cell line.

5.3.6 Inhibition of Bcl-2 using the BH3 mimetic ABT-199 alter cell cycle kinetics in select AML cell lines

Changes in cell viability following culture of MOLM-13 cells with ABT-199 alone, and in combination with Ara-C, had been shown by trypan blue dye exclusion; with an absence of effect seen in the OCI-AML3 cell line. Ara-C is the backbone of current AML treatment. We therefore sought to determine if, and how, ABT-199 and Ara-C alone, and in combination, affected cell cycle in our selected AML cell lines by PI staining and flow cytometry analysis.

A statistically significant reduction in the percentage of OCI-AML3 cells in G0-G1 was demonstrated following culture with the combination of Ara-C and ABT-199 ($p=0.019$). The shape of the histograms generated following PI staining ($n=6$) precluded separation of the S and G2-M phases. No statistically significant change in cell cycle kinetics was seen following culture with ABT-199 or Ara-C alone; though Ara-C as a single agent was demonstrated to affect cell cycle kinetics in a manner very similar to the combination arm, lack of statistical significance was attributed to variance in the results, Figure 5.3.6.1.

A statistically significant reduction in the percentage of MOLM-13 cells in the G0-G1 fraction was demonstrated when cultured with ABT-199 alone ($p=0.043$) and in combination with Ara-C ($p=0.049$). The percentage of cells within the G0-G1 fraction following culture with Ara-C alone was reduced, though this was not significant. A statistical difference between ABT-199 and the combination of ABT-199 and Ara-C was demonstrated ($p=0.038$). A statistically significant increase in the percentage of cells in the sub G0 fraction was seen following culture with Ara-C alone ($p=0.011$) and in combination with ABT-199 ($p=0.043$). Whilst the percentage of events gated within the sub G0 fraction was 1.5-fold greater in the combination arm relative to ABT-199 this was not statistically significant. There was no significant difference in the percentage of cells within the S or G2-M phases between any of the experimental arms, Figure 5.3.6.1. It would be interesting to analsye cell cycle kinetics at earlier time points, the cells appearing to arrest in G0-G1 and subsequently enter sub G0. It would be interesting to utilise agents such as Hoechst-33343^{low}/Pyronin-Y^{low} to separate the G0 and G1 stages to determine the effect ABT-199 had within this fraction of cells. This data suggests ABT-199 does not affect the cell cycle in the MOLM-13 cell line. Whilst Ara-C has been shown to result in cell cycle inhibition [533] this was not demonstrated in our hands. This may be due to the drug concentrations selected for the purpose of our experiments.

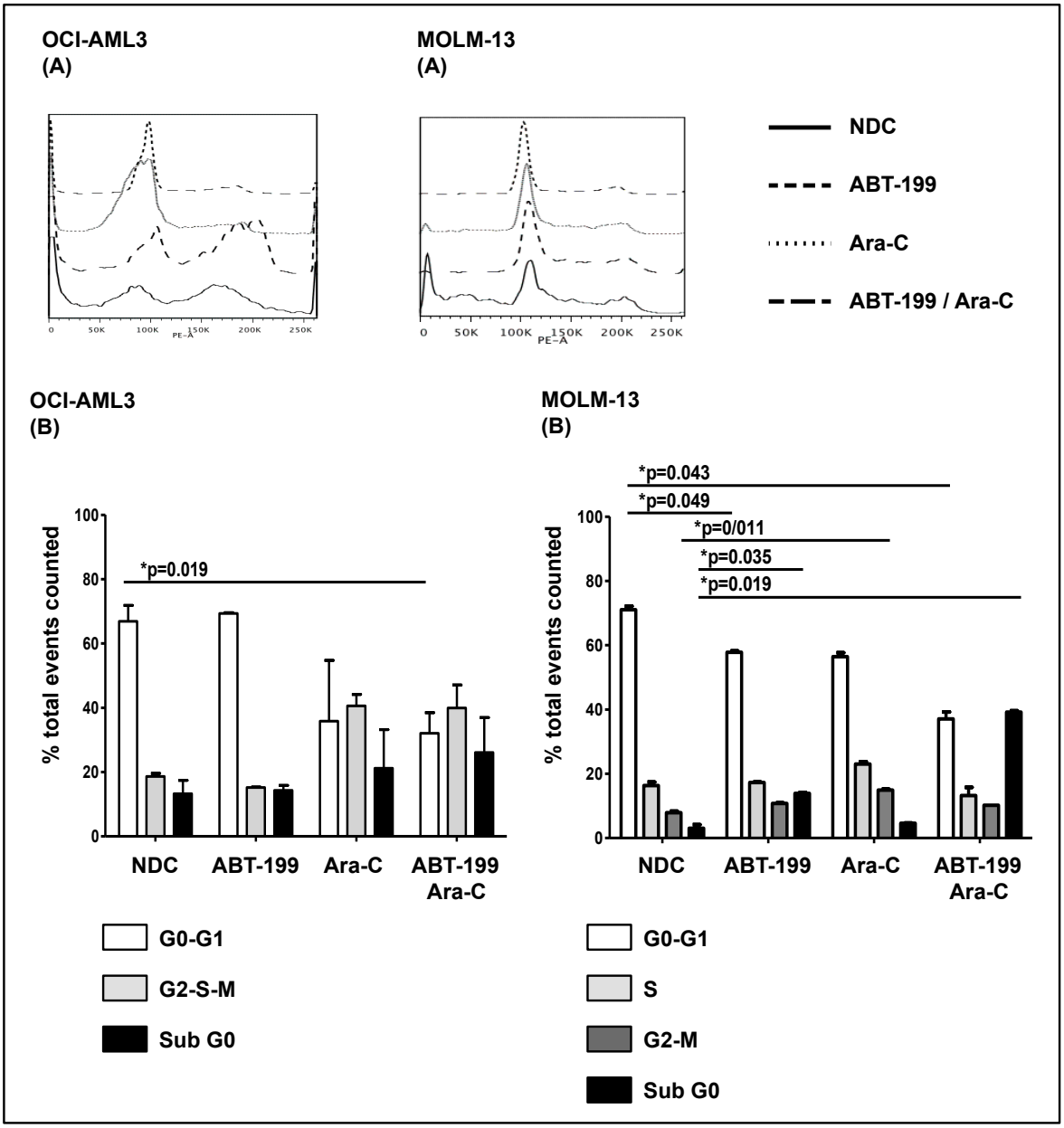

Figure 5.3.6.1: Cell cycle kinetics, as determined by PI staining, following culture of the OCI-AML3 and MOLM-13 cell lines with select, and differing, concentrations of ABT-199 and Ara-C for 72hrs. OCI-AML3 and MOLM-13 cells were seeded at a concentration of $2x10^5$/ml, exposed to ABT-199 (1.15μM and 19.5nM respectively), Ara-C (500nM and 34.5nM respectively) or the combination, cultured for 72hrs then harvested and stained with PI prior to analysis by flow cytometry. (A) Representative staggered histograms showing the PI staining pattern generated with FlowJo software. Each plot is representative of data from one experiment of four with similar results. (B) These graphs indicate the proportion of cells within each cell cycle phase as determined by PI staining, and analysis by flow cytometry. Each bar represents the mean percentage from four independent experiments with error bars indicating SD. All statistically significant results are highlighted with p value to the nearest 3 decimal places, those not highlighted are not significant. ABT-199 is shown to significantly reduce the number of cycling MOLM-13 cells, the addition of Ara-C increasing this effect; ABT-199 did not affect cell cycle kinetics in OCI-AML3.

5.3.7 Inhibition of Bcl-2 using the BH3 mimetic ABT-199 induces apoptosis via the 'intrinsic' cell death pathway

We had shown ABT-199 to induce apoptosis in the MOLM-13 cell line. We sought to determine if this was, as expected, through the 'intrinsic' cell death pathway by affecting mitochondrial membrane integrity, and further, the effect of Ara-C on this process. TMRM is a cell permeant fluorescent dye readily sequestered by active mitochondria. This stain therefore enables the assessment of mitochondrial membrane potential. Loss of mitochondrial membrane potential is an indirect consequence of MOMP, whereby the mitochondrial membrane becomes permeable, with the consequent leakage of intermembrane proteins including cytochrome c, indicative of apoptosis by the 'intrinsic' pathway. When mitochondrial membrane integrity is lost the mitochondria are no longer able to retain TMRM, the dye is therefore redistributed throughout the cell's cytoplasm. This results in a clear fall in fluorescence intensity quantified by flow cytometry.

Mitochondrial membrane potential, using the TMRM stain and flow cytometry analysis, was measured following culture with ABT-199, Ara-C and the combination of ABT-199 and Ara-C for 72hrs, Figure 5.3.7.1. No significant difference in the mitochondrial membrane potential was seen in OCI-AML3 cell line across all treatment arms. Interestingly, considering the absence of effect when OCI-AML3 cells were cultured with ABT-199 and Ara-C as single agents a 25% reduction in mitochondrial membrane potential and 20% increase in cells gated as Annexin V positive was however demonstrated in the combination arm. Whilst this was not significant it does hint at a beneficial effect existing between Ara-C and ABT-199 in this resistant cell line.

There was a statistically significant decrease in mitochondrial membrane potential when MOLM-13 cells were treated with ABT-199 alone (p=0.033) with statistical significance increased in the combination arm (p=0.002). In addition there was an increase in early apoptosis - the percentage of cells gating as Annexin V positive increasing from 40% in the ABT-199 arm to 50% following culture with both Ara-C and ABT-199, Figure 5.3.7.1.

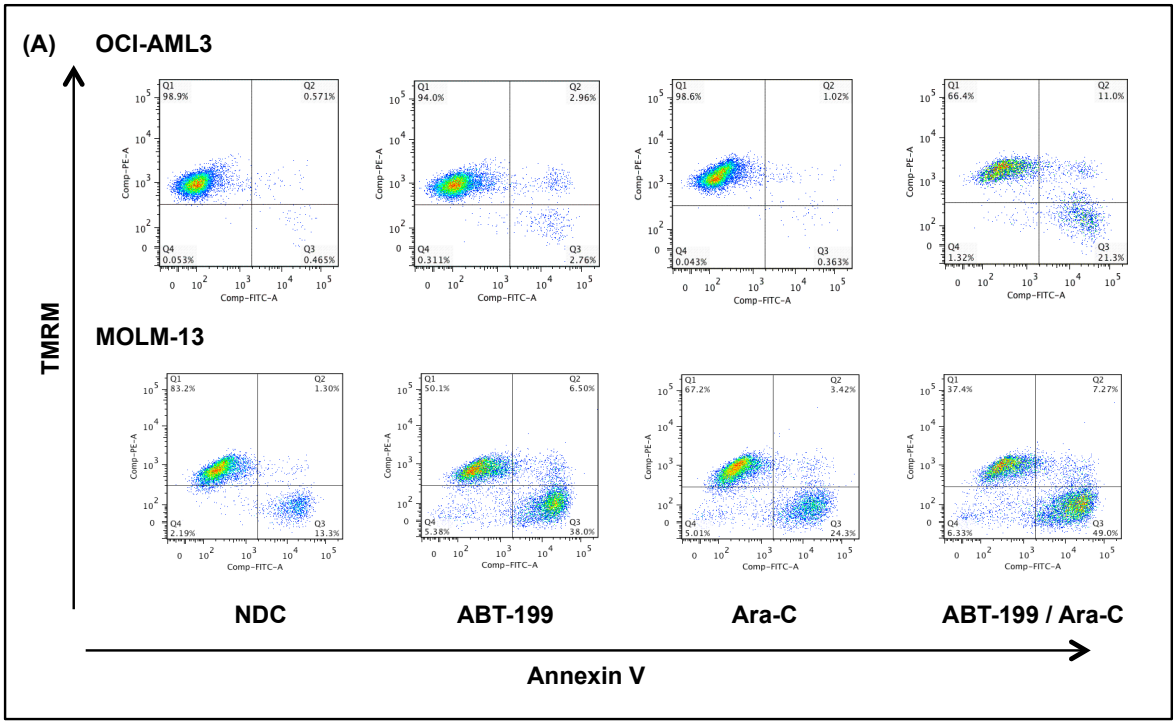

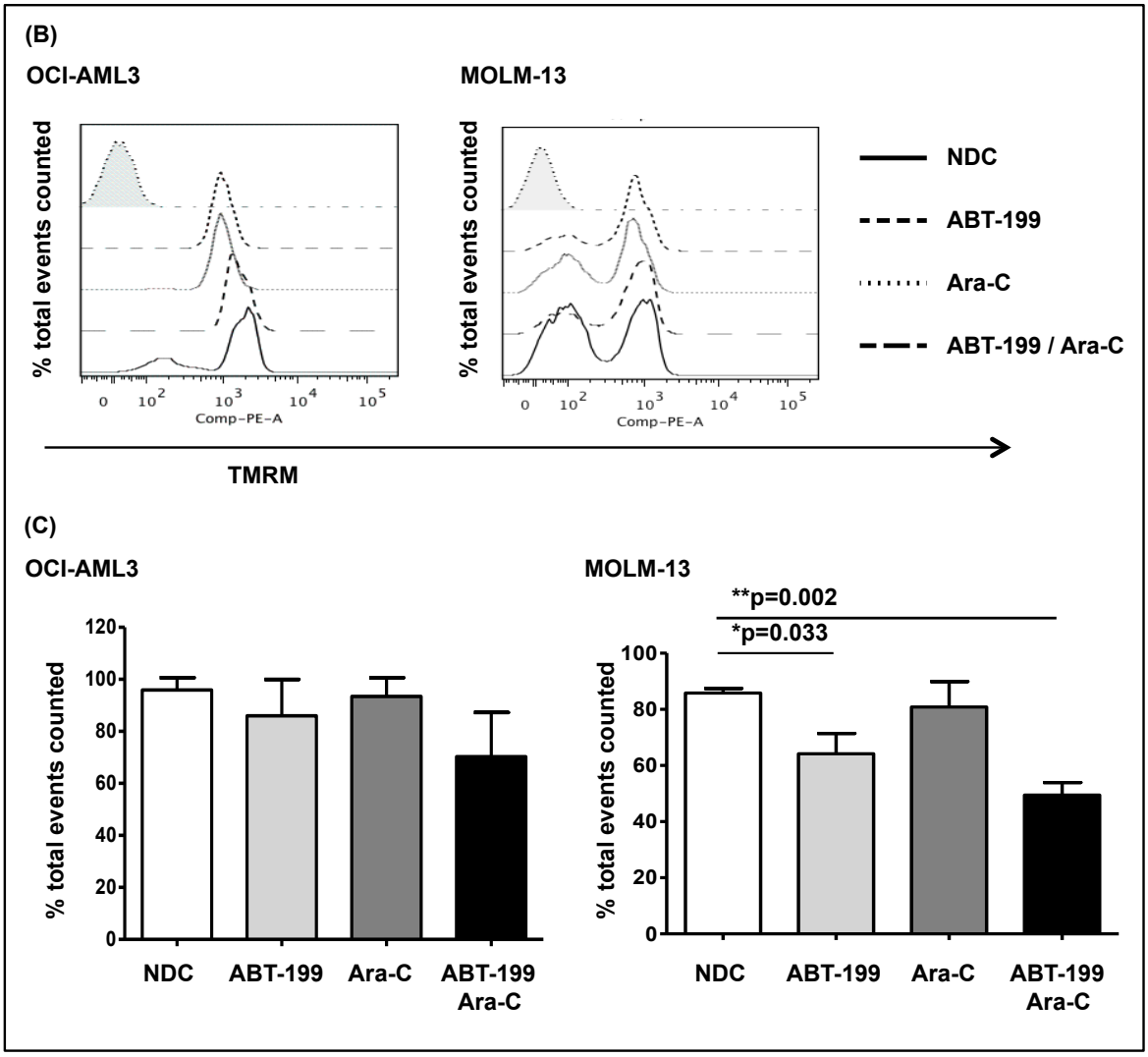

Figure 5.3.7.1: Mitochondrial membrane potential, as measured by TMRM, following culture of the OCI-AML3 and MOLM-13 cell lines with select, and differing, concentrations of ABT-199 and Ara-C for 72hrs.

OCI-AML3 and MOLM-13 cells were seeded at a concentration of $2x10^5$/ml, exposed to ABT-199 (1.15μM and 19.5nM respectively), Ara-C (500nM and 34.5nM) or the combination, cultured for 72hrs then harvested and stained with TMRM and Annexin V prior to analysis by flow cytometry. (A) Representative flow cytometry plots following TMRM / Annexin V staining. Each plot is representative of data from one experiment of four with similar results. (B) Representative staggered histograms showing the TMRM staining pattern, generated using FlowJo software. Each histogram is representative of data from one experiment of four with similar results. (C) These graphs indicate the proportion of cells with preserved membrane potential, gated as TMRM positive by flow cytometry. Each bar represents the mean percentage from four independent experiments with error bars indicating SD. All statistically significant results are highlighted with p value to the nearest 3 decimal places, those not highlighted are not significant.

These figures demonstrate the significant reduction in TMRM (in keeping with loss of mitochondrial membrane integrity) following culture of the MOLM-13 cell line with ABT-199, with the effect strengthened by the addition of Ara-C. Whilst a similar change was seen on culturing OCI-AML3 cells the results were not significant.

The loss of membrane potential is in keeping with the known mechanism of action of ABT-199, a BH3 mimetic, by binding to the hydrophobic groove of multiple anti-apoptotic members of the Bcl-2 family this molecule inhibits the anti-apoptotic function of these proteins enabling apoptosis through the pro-apoptotic family members, Bak and Bax. We consider this balance shift, sensitising cells to cellular stress as the mechanism for the synergism seen between ABT-199 and Ara-C in MOLM-13 cells. Further, it suggests that whilst synergism was not seen in the

resistant OCI-AML3 cell line, the addition of ABT-199 to conventional chemotherapy in an unselected patient cohort may still show clinical benefits.

We had shown loss of mitochondrial membrane potential, recognised to be a consequence of Bak and Bax activity. We therefore sought to confirm activation of the pro-apoptotic Bax protein. Analysis of the conformational change of Bax however, was unsuccessful (n=6). A fluorochrome conjugated antibody is no longer available. Despite trialling a number of primary anti-Bax antibodies (manufactured by the same company against the same epitope and sourced from other companies) a consistent and reliable result could not be obtained precluding accurate interpretation. Had time allowed we would have continued to optimise this experiment to enable the direct measurement of 'intrinsic' pathway activity.

Bcl-2 contains a BH3 motif, the target for ABT-199. We therefore sought to quantify BCL-2 following culture with ABT-199, Ara-C and the combination relative to the NDC. Protein was quantified by western blotting (n=2), with SHP2 serving as an endogenous control, Figure 5.3.7.2.

BCL-2 was shown to be reduced in MOLM-13 cells following culture with ABT-199 and Ara-C in combination for 72hrs. Considering its mechanism of action we would not expect it to affect protein levels. Whilst we considered if this result reflected transcriptional and translational effects of Ara-C, known to target *BCL-2* [533], the absence of this effect following culture with Ara-C alone, does not support this hypothesis. The result may reflect the degree of cellular stress, with a 'switching off' of pro-survival proteins, and shift towards apoptosis in these cells, however this cannot be conclusively determined with this data. In this respect it would be interesting to measure BCL-2 levels at progressive time points, correlating BCL-2 with functional data.

Accounting for endogenous control within the OCI-AML3 cell line, BCL-2 was reduced in all treatment arms. This data is perhaps harder to explain – our functional data showing no evidence of apoptosis following culture with ABT-199 precluding apoptosis as an explanation, and ABT-199 not affecting protein levels, rather disabling the function of BCL-2. In the future we plan to repeat this experiment, to improve statistical power and determine actual protein levels using mass spectrometry.

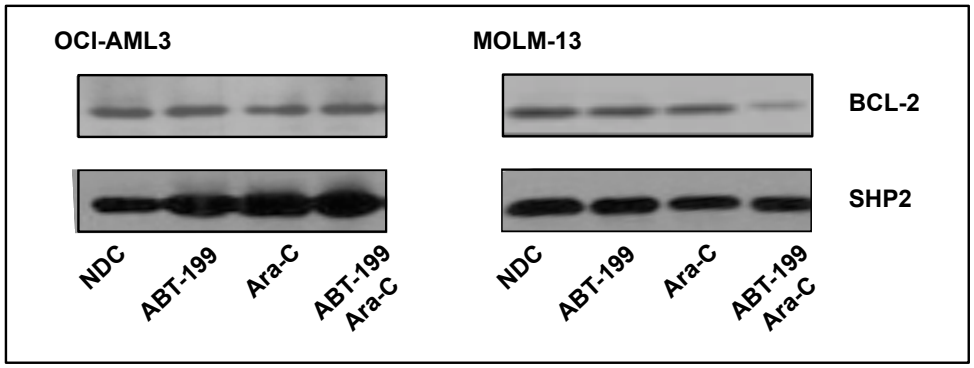

Figure 5.3.7.2: Representative Western blot showing BCL-2 expression following culture of the OCI-AML3 and MOLM-13 cell lines with select concentrations of ABT-199 and Ara-C for 72hrs. OCI-AML3 and MOLM-13 cell lines were seeded at a density of $2x10^5$/ml, exposed to ABT-199 (1.15μM and 19.5nM respectively), Ara-C (19.5nM and 500nM respectively) and the combination of ABT-199 and Ara-C (using the respective concentrations), cultured for 72hrs then harvested. Protein was extracted as described in section 2.2.3.1. Western blotting, as described in section 2.2.3.2, enabled quantitative analysis of BCL-2 within each experimental arm. Representative western blot of two with similar results is shown demonstrating a reduction in BCL-2 following culture of MOLM-13 cells for 72hrs with Ara-C and ABT-199 in combination. SHP2 served as an endogenous control.

Post-translational phosphorylation of BCL-2 is known to regulate its anti-apoptotic function [688,689]. Importantly, phosphorylation of BCL-2 has been shown to induce a structural alteration in the BH3-binding groove [690], with recent work showing this to confer resistance to BH3 mimetics in CLL cells by impeding direct binding [690,691]. pBCL-2 was therefore measured by flow cytometry (n=2). We considered whether a lack of apoptosis within the OCI-AML3 cell line in the presence of a BH3 mimetic could be, in part, due to increased pBCL-2. pBCL-2 is an intracellular protein, therefore cells were fixed and permeabilised prior to staining. Baseline levels of pBCL-2 were first determined. Subsequent to this pBCL-2 levels were measured following culture of MOLM-13 and OCI-AML3 cell lines with ABT-199, Ara-C and the combination of ABT-199 and Ara-C, with results compared to the NDC, Figure 5.3.7.3.

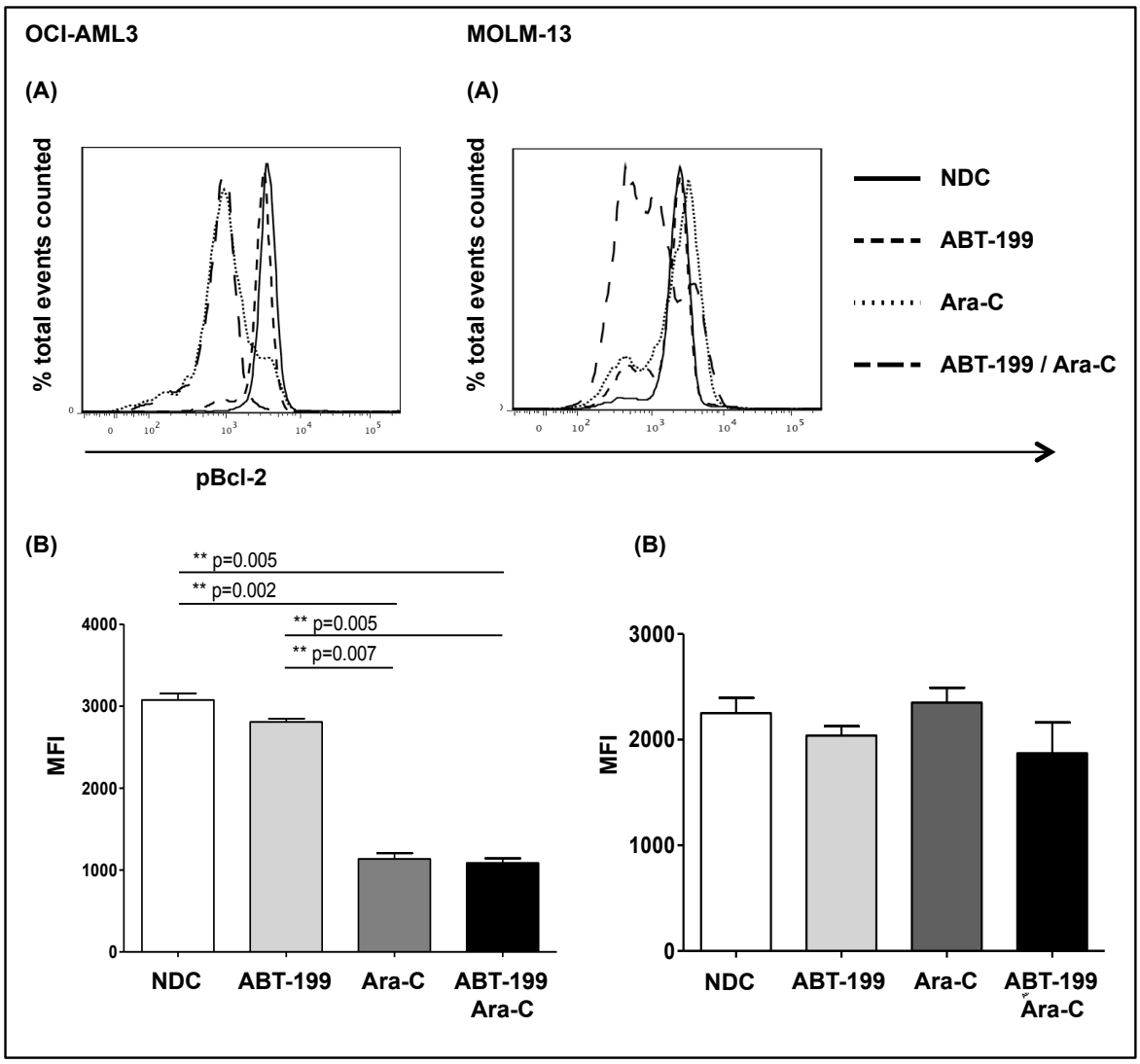

Figure: 5.3.7.3: pBCL-2 expression, as determined by flow cytometry, following culture of the OCI-AML3 and MOLM-13 cell lines with select, and differing, concentrations of ABT-199 and Ara-C for 72hrs.

OCI-AML3 and MOLM-13 cells were seeded at a concentration of $2x10^5$/ml, exposed to ABT-199 (1.15μM and 19.5nM respectively), Ara-C (500nM and 34.5nM) or the combination, cultured for 72hrs then harvested and stained with pBCL-2 prior to analysis by flow cytometry. (A) Representative overlain histograms showing the pBCL-2 staining pattern. Each is representative of data from one experiment of three with similar results. (B) These graphs show the MFI of pBCL-2 within each treatment arm by flow cytometry. Each bar represents the mean percentage from three independent experiments with error bars indicating SD. All statistically significant results are highlighted with p values to the nearest 3 decimal places, those not highlighted are not significant.

A statistically significant decrease in pBCL-2 following culture of OCI-AML3 cells with Ara-C is shown. The addition of ABT-199 did not increase this effect. Whilst a reduction in p-BCL2 is shown following culture of the MOLM-13 cell line with ABT-199 and, further so with the combination of ABT-199 and Ara-C, this was not significant.

The MFI of pBCL-2 was 1.5-fold greater in the OCI-AML3 cells compared to the MOLM-13 cells at baseline, and within the NDC. This may serve as one potential explanation for the marked difference in sensitivity between the two cell lines to ABT-199. Looking within our experimental arms: OCI-AML3 cells demonstrated a statistically significant reduction in p-BCL-2 following culture with Ara-C (p=0.002) and the combination (p=0.005) relative to the NDC. In addition a statistical reduction in pBCL-2 was seen following culture with Ara-C (p=0.007) and the combination (p=0.005) relative to culture with ABT-199 alone. An absence of effect following culture with ABT-199 would support the hypothesis that BH3 mimetic activity is prevented in the presence of pBCL-2. As stated previously, cellular response to Ara-C is dependent upon a number of genes including *BCL-2* [533]. An extensive literature search did not find work reporting on the effect of the BH3 mimetics on pBCL-2. Considering the greatest experience of ABT-199 is in CLL, it would be interesting to assess both total BCL-2 and pBCL-2 following culture of CLL cells with ABT-199. Additionally, considering venetoclax has received FDA approval for the treatment of both CLL (those who have received at least one prior therapy and carry the *TP53* mutation) and AML (those who are not eligible for standard high dose treatment in combination with HMAs) it would be particularly interesting to compare and contrast protein responses in these two very different haematological malignancies.

The MOLM-13 cell line expressed lower levels of pBCL-2 relative to the OCI-AML3 cell line. This indicates the numerous and complex mechanisms involved in determining cell response to Ara-C. If p-BCL2 levels alone were sufficient to sensitise cells to Ara-C we would expect the IC_{50} for OCI-AML3 cells to be lower than that demonstrated in MOLM-13 cells. It is not possible to contrast the differing effects on pBCL-2 levels between the two cell lines following culture with Ara-C since OCI-AML3 cells were exposed to the IC_{50} of Ara-C (500nM), whilst MOLM-13 cells were exposed to 37.5nM as determined by the Chou-Talalay method for drug synergy, a concentration 23% of the IC_{50}. As expected no significant change in levels of pBCL-2 was seen following culture with ABT-199. The reduction in pBCL-2 following culture with ABT-199 and Ara-C is however interesting, though not easily explained. One hypothesis is Ara-C effects the transcription and translation of *BCL-2*, resulting in less BCL-2, whist targeting existing pBCL-2 and ABT-199 binds to the hydrophobic groove within BCL-2, inhibiting phosphorylation of newly translated BCL-2. An alternative explanation is this result reflects the degree of cellular stress, with a shutting down of survival processes and shift towards apoptosis.

5.3.8 Sensitivity to ABT-199 is not solely dependent on the expression of Bcl-2, rather a complex interplay between the pro-apoptotic and anti-apoptotic family members

Whilst we had shown differences in the baseline expression of Bcl-2 at a gene and protein level, and also in the expression of pBCL-2 in the genetically diverse OCI-AML3 and MOLM-13 cell lines we questioned whether other factors contributed to cell sensitivity to the BH3 mimetics. We considered whether the differential response demonstrated arose from (1) a lack of dependence upon the Bcl-2 family, (2) an up-regulation of other anti-apoptotic family members or, (3) recruitment of other survival molecules. In this respect the MCL-1 / BCL-2 ratio has been shown to predict sensitivity of CLL cells to the BH3 mimetics, higher ratios predictive of resistance [690]. We therefore sought to determine levels of MCL-1 at baseline and following culture within each of our experimental arms.

Accounting for endogenous control, no change in MCL-1 was seen across all experimental arms, in both the MOLM-13 and OCI-AML3 cell lines, Figure 5.3.8.1. Whilst a reduction in MCL-1 following culture of the MOLM-13 cell line with ABT-199 and Ara-C could be considered the endogenous control was not sufficiently clean to allow enable conculsions to be drawn. An absence of change was not surprising however. Considering its mechanism of action we did not expect ABT-199 to affect levels of MCL-1. MCL-1 activity has been shown to be largely

determined at a transcriptional level by extrinsic (growth factors [692-694]) and intrinsic (notably transcription factors belonging to the STAT family [695]) signals; whilst the STAT family has clearly been linked with AML, work to date has not shown this family to be a target for Ara-C. Instead, research has looked at the JAK/STAT pathway as a potential molecular target, utilising JAK2 inhibitors alone and with conventional chemotherapy [696]. The currently recruiting NCT02257138 trial is composed of two parts. Part one is designed to determine the maximally tolerated dose of decitabine in combination with the JAK2 inhibitor ruxolitinib in patients with AML. Considering the concept of personalised, or tailored medicine, part two will seek to determine if this combination is clinically beneficial in post myeloproliferative neoplasm AML; the presence of the JAK2 V617F mutation, resulting in constitutive activation of the JAK/STAT pathway, is considered the most important criterion in the diagnosis of BCR-ABL MPNs according to the WHO classification.

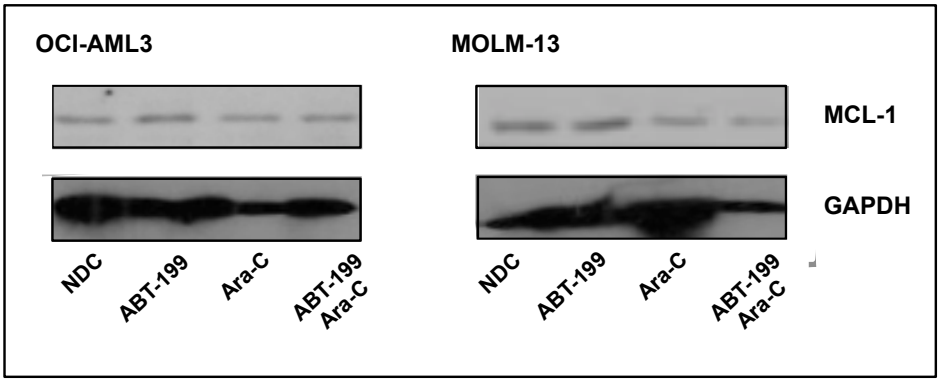

Figure 5.3.8.1: Representative Western blot showing MCL-1 expression following culture of the OCI-AML3 and MOLM-13 cell lines with select concentrations of ABT-199 and Ara-C for 72hrs.
OCI-AML3 and MOLM-13 cell lines were seeded at a density of $2x10^5$/ml, exposed to ABT-199 (1.15μM and 19.5nM respectively), Ara-C (500nM and 34.5nM) and the combination, cultured for 72hrs then harvested. Protein was extracted as described in section 2.2.3.1. Western blotting, as described in section 2.2.3.2, enabled quantitative analysis of MCL-1 within each experimental arm. GAPDH served as an endogenous control.
Representative western blots of two with similar results are shown demonstrating no change in the quantity of MCL-1, accounting for endogenous control, across all experimental arms, and within both cell lines.

In the future it would be interesting to quantitate the level of MCL-1 relative to both BCL-2 and pBCL-2, and further to quantify levels of BAK and BAX and the ratio of these pro-apoptotic proteins to their anti-apoptotic family members.

5.3.9 The BH3 mimetic ABT-199 affects genes involved in apoptosis in a cell line-specific manner

There is extensive work published on the effect of baseline protein levels on the sensitivity and resistance of cells to the BH3 mimetic, ABT-199 [559,685,687], and further the effect of the BH3 mimetics on Bcl-2 family members at a protein level. There is however, little data on the effect of these small molecules at a gene level. We therefore sought to determine gene expression changes of members of the Bcl-2 family, other cell death and apoptosis regulators and the Hh signalling pathway. The $2^{-\Delta\Delta CT}$ method was used to show expression relative to the NDC, with experimental design as described in section 5.2.2.

The difference in gene expression is striking, Figure 5.3.9.1. Considering the OCI-AML3 cell line, we had shown an absence of cell death following culture with ABT-199. At the gene level however both pro- and anti-apoptotic genes were up-regulated suggesting a cellular stress response despite an absence of functional effect. In contrast, culture of the OCI-AML3 cell line, with Ara-C alone, and in combination with ABT-199, resulted in apoptosis; addition of ABT-199

had not enhanced the apoptotic effect demonstrated following culture with Ara-C alone. At a gene level culture with Ara-C in combination with ABT-199 led to a statistically significant up-regulation of *BAK* (p=0.004) whilst culture with Ara-C alone led to a significant up-regulation of *BAX* (p=0.043). Interestingly, the anti-apoptotic genes, *BCL-2* and *MCL-1*, were also up-regulated though the results were not significant. In contrast a universal down-regulation of selected pro- and anti-apoptotic genes was seem in the MOLM-13 cell line, across all experimental arms. *BCL-2* was statistically significantly down-regulated following culture with ABT-199 (p=0.011). Statistical significance was not demonstrated following culture with ABT-199 and Ara-C, this was considered to be due to the high variance in expression.

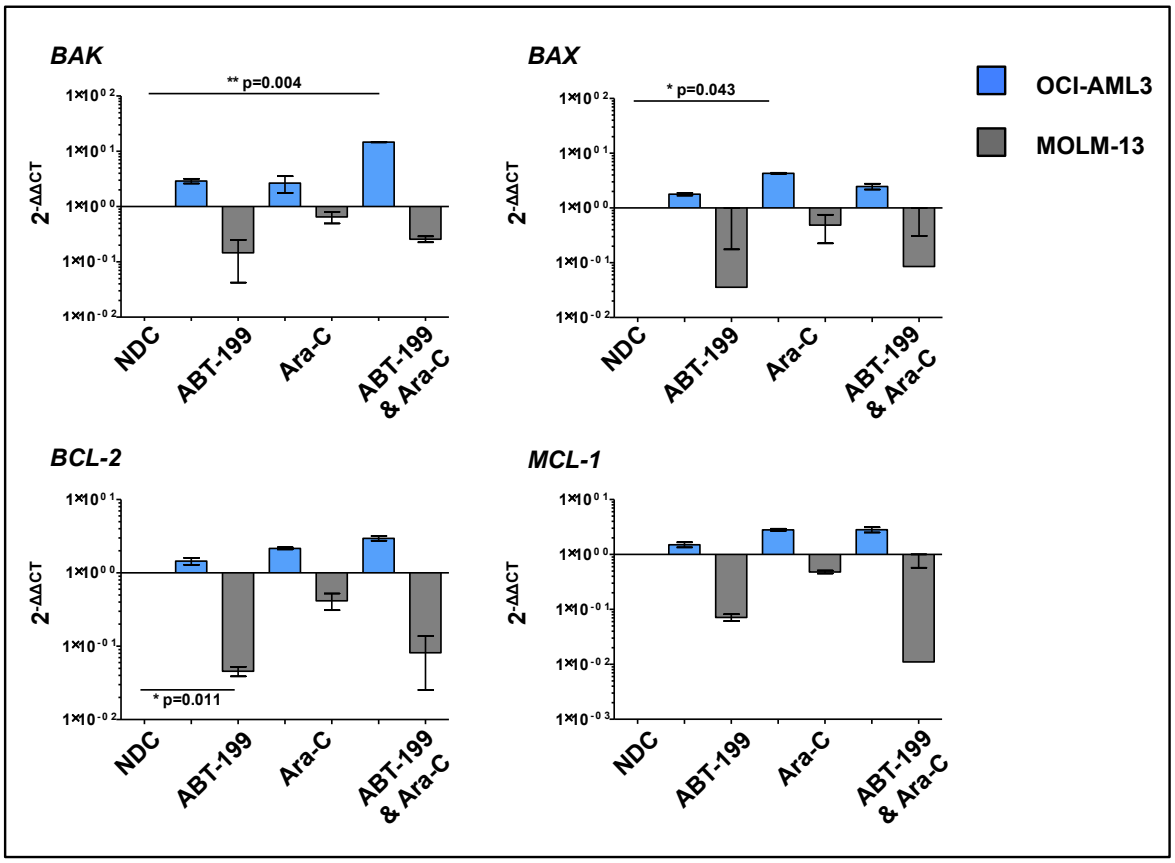

Figure 5.3.9.1: Expression of members of the Bcl-2 family following culture of the OCI-AML3 and MOLM-13 cell lines with select concentrations of ABT-199 and Ara-C for 72hrs.
OCI-AML3 and MOLM-13 cells were seeded at a concentration of $2x10^5$/ml and exposed to ABT-199 (1.15μM and 19.5nM respectively), Ara-C (500nM and 34.5nM respectively) or the combination. Cells were cultured for 72hrs then harvested and RNA extracted. Expression levels were quantified by qRT-PCR using Fluidigm® technology. Expression levels are shown as $2^{-\Delta\Delta CT}$, with 6 housekeeping genes – *ATP5S, B2M, ENOX2, GAPDH, TYWI* and *UBE2D2* serving as endogenous control. The mean of 3 biological replicates, performed in technical duplicate, are shown. Error bars indicate SD.
Both pro- and anti-apoptotic genes were up-regulated in the OCI-AML3 cell line whilst they were down-regulated in the MOLM-13 cell line across all experimental arms suggesting a complex network is involved in determining cell fate.

The ratio of *BAK* and /or *BAX* to *BCL-2* rather than the expression of these genes in isolation is predictive of cell behaviour in solid malignancies [674,675]. We therefore considered the *BAX*/*BCL-2* and *BAK*/*BCL-2* expression ratios, Table 5.3.9.1.

Table 5.3.9.1: *BAX/BCL-2* and *BAK/BCL-2* expression ratios following culture of the MOLM-13 and OCI-AML3 cell lines with ABT-199, Ara-C and the combination of ABT-199 and Ara-C for 72hrs

Experimental arm	*BAK/BCL-2* expression ratio	*BAX/BCL-2* expression ratio
OCI-AML3		
ABT-199	0.101	0.025
Ara-C	0.301	0.226
ABT-199 & Ara-C	0.087	0.029
MOLM-13		
ABT-199	63.780	39.139
Ara-C	6.364	10.329
ABT-199 & Ara-C	180.158	30.345

Interestingly within the OCI-AML3 cell line these expression ratios suggested a shift in expression to support apoptosis across all experimental arms, most notably the combination arm. Whilst in stark contrast results within the MOLM-13 cell line suggested the balance of these pro- and anti-apoptotic genes to favour anti-apoptosis. The differential gene expression between experimental arms is interesting considering ABT-199 inhibits anti-apoptotic protein activity through the competitive, and irreversible, binding of the BH3 domain. Whether these genetic changes translate to the protein level would be an interesting angle to pursue and an interesting concept to consider when investigating drug resistance, especially resistance acquired during therapy.

Considering cell physiology we had expected expression of anti-apoptotic genes to increase in the presence of cellular stress such as culture with cytotoxic agents, with a subsequent increase in pro-apoptotic genes when irreversible cell damage was recognised by the cell. This expression data conflicts with our functional data suggesting a complex, tightly regulated, process involved in determining cell behaviour and fate. It would be interesting to assess genetic changes over a time period to determine if these changes were time-dependent. The up-regulation of *BAK* and *BAX* in the resistant OCI-AML3 cell line is however hugely exciting, suggesting a potential role for the BH3 mimetics in combination with standard chemotherapeutics agents such as Ara-C in AML.

5.3.10 The BH3 mimetic ABT-199 resulted in apoptosis in unselected primary AML samples, with the addition of Ara-C showing an additive effect

We have previously acknowledged the limitations of cell lines as experimental models [627], discussed further in 5.3.11. We therefore sought to determine the effect of the BH3 mimetic ABT-199 in a cohort of primary *de novo* human AML samples, alone and in combination with Ara-C.

Primary AML MNCs were isolated from whole PB and BM samples, recovered and cultured as detailed in Methods 2.2.1.2.4-6. An un-manipulated recovered cell population was used. Four samples were seeded at a density of $1.5x10^5$/ml and cultured with ABT-199 at 19.5nM and 1.15μM, alone and in combination with Ara-C 100nM as described in Methods 2.2.1.2.6. 19.5nM was the IC50 for MOLM-13 cells, our ABT-199 sensitive AML cell line; 1.15μM is the maximally

tolerated clinical dose. Cell counts and the assessment of cell viability was performed by trypan blue dye exclusion at 72hrs in three primary AML samples (AML 1002, AML 013 and AML 022) with technical triplicates, Figure 5.3.10.1.

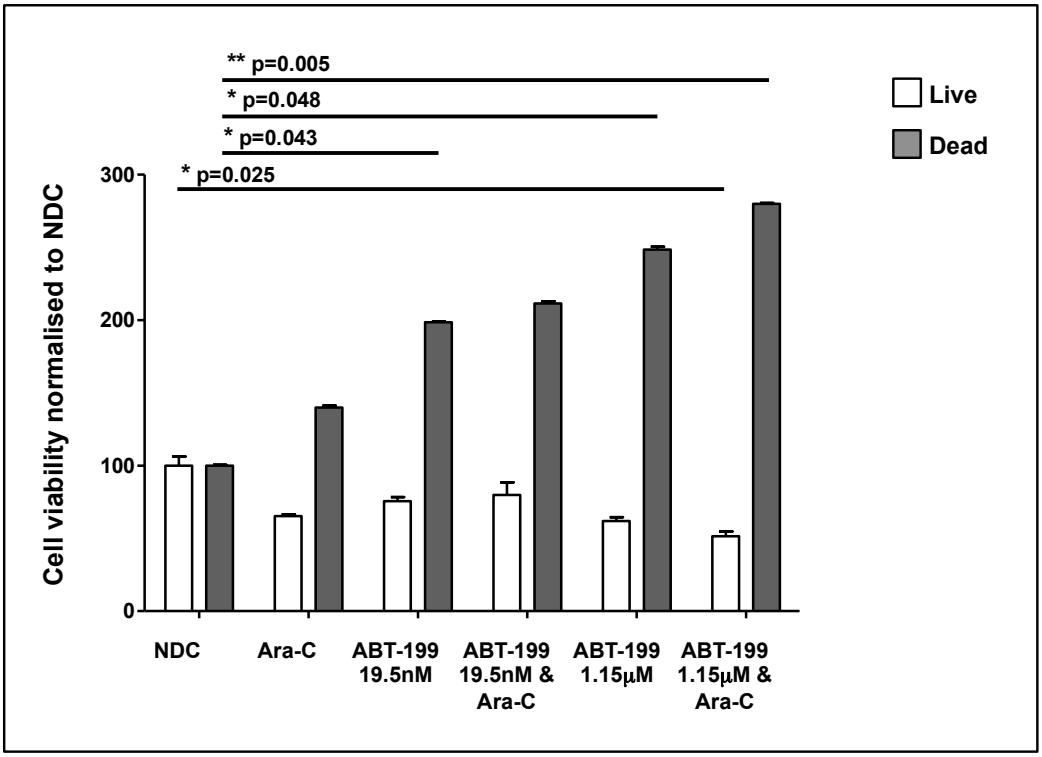

Figure 5.3.10.1: Proliferation, as determined by the trypan blue dye exclusion, following culture of an unselected cohort of primary *de novo* AML MNCs (n=3) with ABT-199 (19.5nM and 1.15μM) and Ara-C (100nM) alone, and in combination for 72hrs.
The primary samples AML 1002, AML 013 and AML 022 were recovered as described in Methods 2.2.1.2.5. Recovered cells were seeded at a concentration of $1.5x10^5$/ml then cultured for 72hrs with ABT-199 (19.5nM and 1.15μM), alone and in combination with Ara-C (100nM) as described in Methods 2.2.1.2.6. Each bar represents the mean cell number $x10^4$/ml (alive and dead) as determined by trypan blue dye exclusion with error bars indicating the SD. All statistically significant results are highlighted with p value to the nearest 3 decimal places, those not highlighted are not significant (ns).
ABT-199 alone (at both concentrations - 19.5nM and 1.15μM) caused an increase in the number of dead cells when results were normalised to the NDC (p=0.043 and p=0.048 respectively). There was no significant difference in the number of live cells. ABT-199 at a concentration of 1.15μM, in combination with Ara-C, caused a statistically significant reduction in live cells (p=0.025), with an increase in dead cells (p=0.005).

There was a statistically significant reduction in cell viability following culture with ABT-199 at a concentration of 1.15μM and Ara-C (p=0.025), with a statistically significant increase in the number of dead cells normalised to the NDC (p=0.005). ABT-199 alone, at both 19.5nM and 1.15mM, also caused a statistically significant increase in the number of dead cells when results were normalised to the NDC (p=0.043 and p=0.048 respectively). Whilst a reduction in live cells and increase in dead cells was demonstrated following culture with Ara-C alone, and in combination with ABT-199 at a concentration of 19.5nM, the results were not significant.

In keeping with absolute cell numbers as defined by trypan blue dye exclusion apoptosis was evidenced by Annexin V / 7AAD staining and flow cytometry analysis; Figure 5.3.10.2. There was a statistically significant reduction in the proportion of live cells following culture with Ara-C in combination with ABT-199 at 19.5nM (p=0.020), with an accompanying increase in apoptosis (p=0.025). There was an increase in apoptosis relative to the NDC following culture with Ara-C (100nM) and ABT-199 (19.5nM) as single agents though this was not significant (p=0.054 and p=0.051 respectively). A statistically significant difference in the proportion of apoptotic cells

was not reached following culture with ABT-199 at a concentration of 1.15μM alone, and in combination with Ara-C 100nM; this was considered due to significant variance between samples.

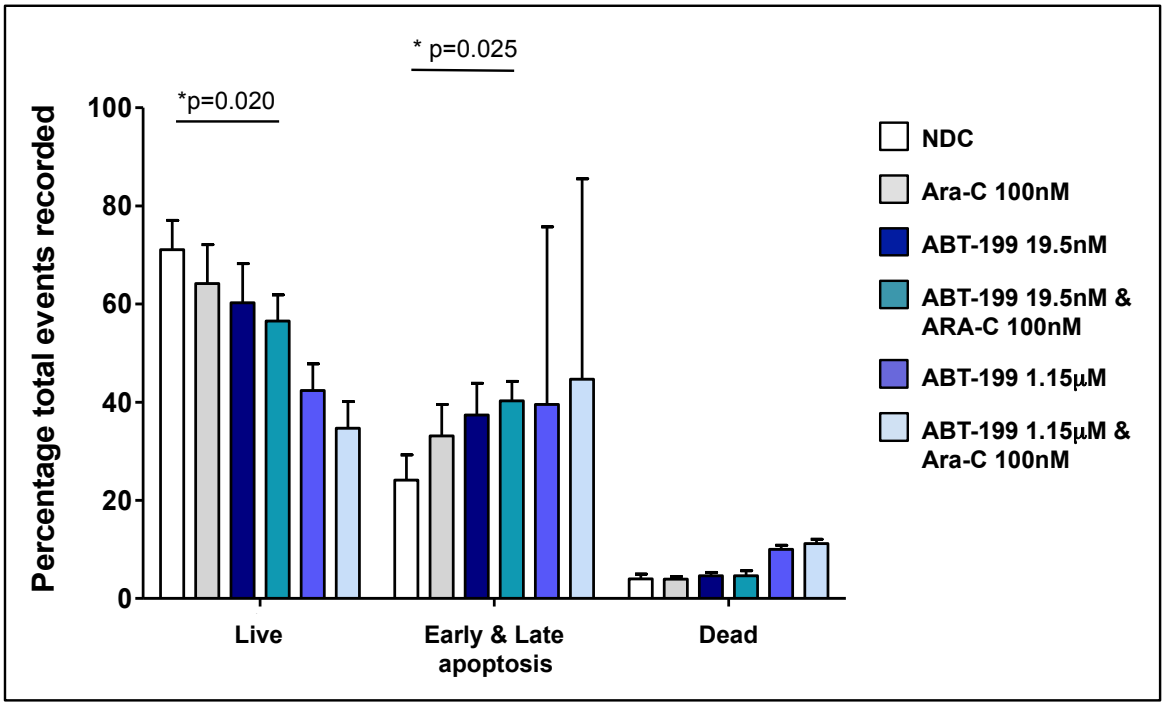

Figure 5.3.10.2: Apoptosis, as determined by Annexin V / 7AAD staining, following culture of an unselected cohort of primary de novo AML MNCs (n=3) with ABT-199 (19.5nM and 1.15μM) and Ara-C (100nM) alone, and in combination for 72hrs.
The primary samples AML 1002, AML 013 and AML 022 were recovered as described in Methods 2.2.1.2.5.Recovered cells were seeded at a concentration of $1.5x10^5$/ml, exposed to ABT-199 (19.5nM and 1.15μM), alone and in combination with Ara-C (100nM) and cultured for 72hrs, as described in Methods 2.2.1.2.6, prior to being stained with Annexin V / 7AAD and analysis by flow cytometry. The percentages shown indicate the proportion of total events gated as viable, apoptotic (early and late) and dead. Each bar represents the mean percentage from three independent experiments with error bars indicating SD. All statistically significant results are highlighted with p value to the nearest 3 decimal places, those not highlighted are not significant (ns).
A statistically significant reduction in live cells (p=0.02) with an increase in apoptosis was seen following culture with Ara-C in combination with ABT-199 at a concentration of 19.5nM (p=0.025). There was an increase in apoptosis relative to the NDC following culture with Ara-C (100nM) and ABT-199 (19.5nM) as single agents though this was not significant. Statistical significance was not reached following culture with ABT-199 (1.15μM alone and in combination with Ara-C 100nM) due to variance.

We also considered cell cycle kinetics assessed by PI staining and flow cytometry. ABT-199 at a concentration of 19.5nM and 1.15μM in combination with Ara-C led to a greater reduction in the proportion of quiescent 'resting' cells and increase in dying / dead cells compared to the effect seen following culture with Ara-C as a single agent. Statistical significance was reached following culture with ABT-199 (1.15μM) and Ara-C in combination with a reduction in the proportion of G0-G1 (p=0.025) and M (p=0.007) fractions and an increase in the Sub G0 fraction (p=0.021).

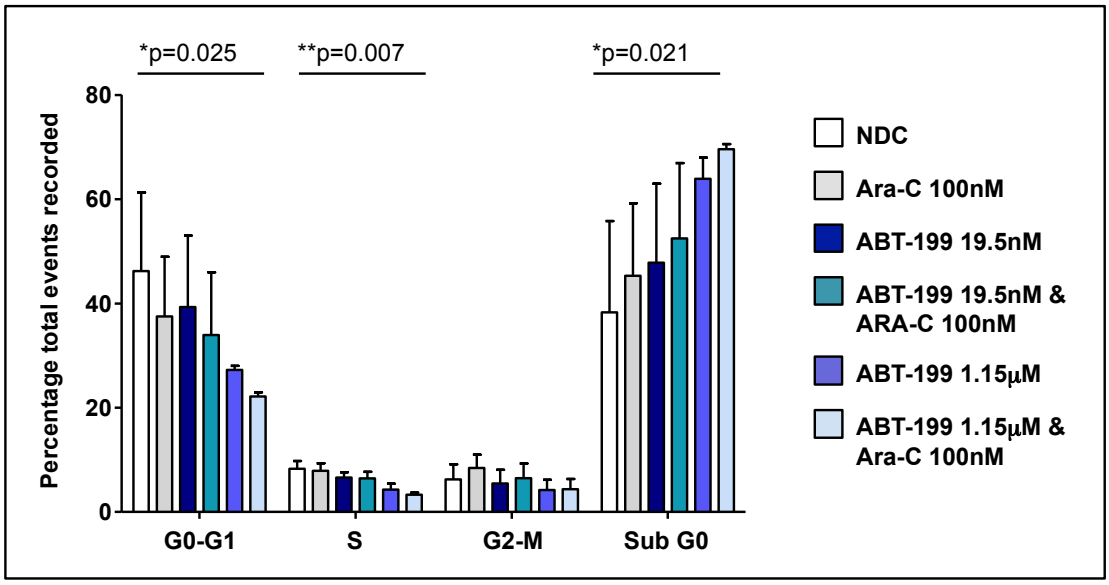

Figure 5.3.10.3: Culture of an unselected cohort of primary *de novo* AML cells with the combination of ABT-199 and Ara-C for 72hrs caused a statistically significant alteration in cell cycle kinetics (n=3).
The primary samples AML 1002, AML 013 and AML 022 were recovered as described in Methods 2.2.1.2.5. Recovered cells were seeded at a concentration of $1.5x10^5$/ml, exposed to ABT-199 (19.5nM and 1.15μM), alone and in combination with Ara-C (100nM) and cultured for 72hrs as described in Methods 2.2.1.2.6. Cells were harvested and stained with PI prior to analysis by flow cytometry. The proportion of cells within each cell cycle phase (G0-G1, S, G2-M and Sub G0) as determined by PI, and analysis by flow cytometry is shown in this bar graph. Each bar represents the mean percentage from three independent experiments with error bars indicating SD.
ABT-199 at both concentrations (19.5nM and 1.15μM) led to a greater reduction in the proportion of quiescent 'resting' cells and increase in dying / dead cells than Ara-C alone; the effect was more marked with the higher concentration of 1.15μM. Statistical significance was reached following culture with ABT-199 (1.15μM) and Ara-C with a reduction in the proportion of G0-G1 (p=0.025) and S (p=0.007) and increase in the Sub G0 fraction (p=0.021).

5.3.11 There was no evidence of synergism between glasdegib, at a concentration of 2.67μM and ABT-199 at a concentration of 19.5nM

Bcl-2 is a recognised downstream target of the Hh signalling pathway. We therefore sought to determine if the combination of a BH3 mimetic and Smo antagonist would be synergistic in a cohort of primary AML samples.

Experimental design was as described in section 5.1.10. Four samples (AML 1002, AML 013, AML 018 and AML 022) were cultured with ABT-199 (19.5nM), glasdegib (2.67μM) and the combination of ABT-199 (19.5nM) and glasdegib, (2.67μM) as described in Methods 2.2.1.2.6. We selected those samples used to analyse the effect of ABT-199 alone and in combination with Ara-C (section 5.3.10) to ensure selected samples were responsive to ABT-199. A response, whilst not significant had been shown with a concentration of 19.5nM. Considering our previous data (section 5.1) we hypothesised the addition of glasdegib would strengthen the response seen following culture with ABT-199 alone. A concentration of 2.67μM is representative of the recommended clinical dose [407]. Cell counts and the assessment of cell viability was performed by trypan blue dye exclusion at 72hrs. All experiments were performed in technical duplicate, Figure 5.3.11.1.

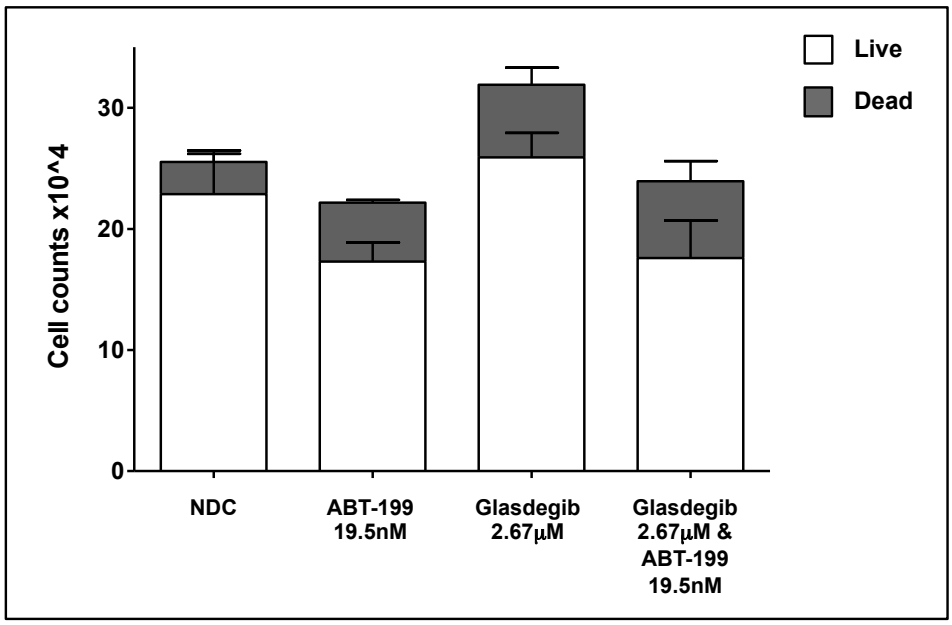

Figure 5.3.11.1: Proliferation, as determined by the trypan blue dye exclusion, following culture of an unselected cohort of primary, *de novo* AML MNCs (n=4) with ABT-199 (19.5nM) and glasdegib (2.67μM) alone, and in combination, for 72hrs.
The primary samples AML 1002, AML 13, AML 018, and AML 022 were recovered as described in Methods 2.2.1.2.5. Recovered cells were seeded at a concentration of $1.5x10^5$/ml and cultured with glasdegib (2.67μM), ABT-199 (19.5nM) and the combination of glasdegib (2.67μM) and ABT-199 (19.5nM) for 72hrs as described in Methods 2.2.1.2.6. Each bar represents the mean cell number $x10^4$/ml (alive and dead) as determined by trypan blue dye exclusion with error bars indicating the SD. All experiments were performed in technical duplicate.
There was a reduction in the number of live cells following culture with ABT-199 though this was not significant; the addition of glasdegib to ABT-199 did not enhance this effect. Glasdegib, as a single agent, did not affect cell proliferation within this cohort of primary *de novo* AML cells.

There was a reduction in the number of live cells following culture with ABT-199 though this was not significant (p=0.114); this was consistent with results obtained from this cohort in section 5.1.10, validating our previous results. In this instance whilst an increase in cell death was demonstrated the results were not significant (p=0.064). The addition of glasdegib, at our selected concentration, did not lead to a further reduction in live cells or dead cells (p=0.122 and p=0.074 respectively). We have previously shown the reduction in proliferation following culture with ABT-199 to be consequent to an increase in early and late apoptosis by Annexin V / 7AAD, Figure 5.3.10.2. We therefore sought to determine if the addition of glasdegib to ABT-199 affected the degree of cell apoptosis. As before apoptosis was assessed by Annexin V / 7AAD staining and flow cytometry analysis. Culture with ABT-199 alone and in combination with glasdegib led to a reduction in the proportion of live cells though the results were not significant, Figure 5.3.11.2. There was a statistically significant increase in the proportion of early apoptotic cells following culture with ABT-199 alone, with a statistically significant increase in the proportion of late apoptotic cells following culture with ABT-199 in combination with glasdegib. There was no difference in the proportion of dead cells across all experimental arms. We plan to repeat this to determine if the addition of glasdegib to ABT-199 causes an additive effect.

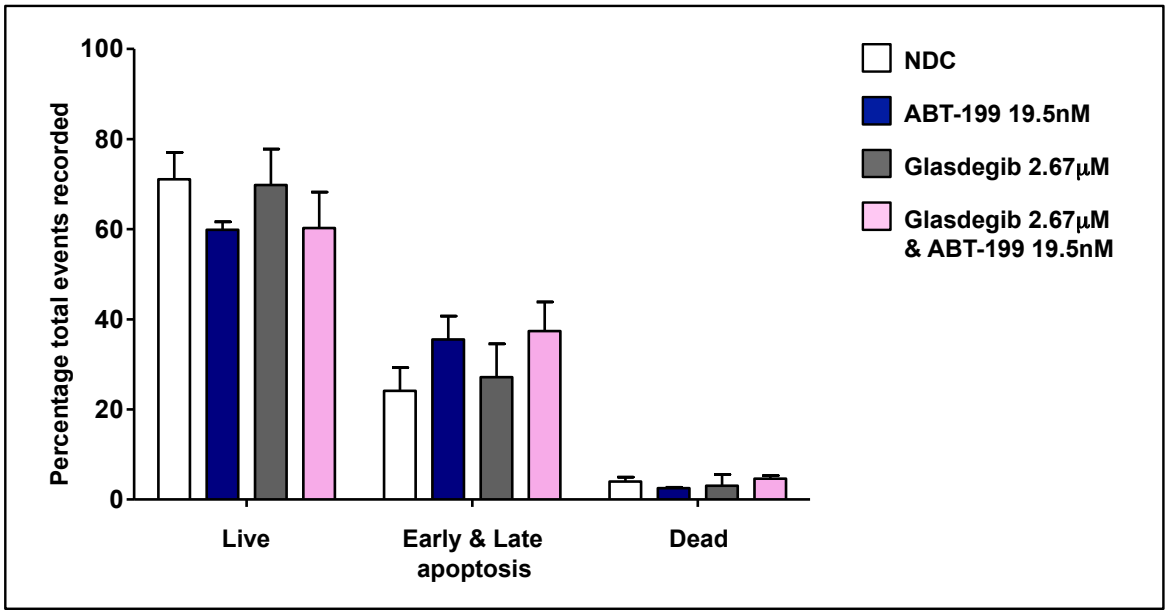

Figure 5.3.11.2: Apoptosis, as determined by Annexin V / 7AAD staining, following culture of an unselected cohort of primary, *de novo* AML MNCs (n=4) with ABT-199 (19.5nM) and glasdegib (2.67μM) alone, and in combination, for 72hrs.
The primary samples AML 1002, AML 13, AML 018, and AML 022 were recovered as described in Methods 2.2.1.2.5. Recovered cells were seeded at a concentration of $1.5x10^5$/ml and cultured with glasdegib (2.67μM), ABT-199 (19.5nM) and the combination of glasdegib (2.67μM) and ABT-199 (19.5nM) for 72hrs as described in Methods 2.2.1.2.6. Apoptosis was assessed by Annexin V / 7AAD staining and analysis by flow cytometry. The proportion of viable, apoptotic (early and late) and dead cells are shown. Each bar represents the mean total number of events with error bars indicating SD.
ABT-199, alone and in combination with glasdegib, resulted in an increase in apoptosis, with a reduction in the percentage of live cells though the results were not significant. The addition of glasdegib did not enhance the affect of ABT-199 alone. Glasdegib alone did not affect cell viability as measured by Annexin V / 7AAD.

Glasdegib and ABT-199, as single agents, had not affected cell cycle kinetics in our unselected cohorts of primary AML samples. We had however shown glasdegib to affect cell cycle kinetics in select AML cell lines. We therefore sought to determine if the combination of these two small molecule inhibitors would affect cell cycle kinetics, assessed by PI staining and flow cytometry.

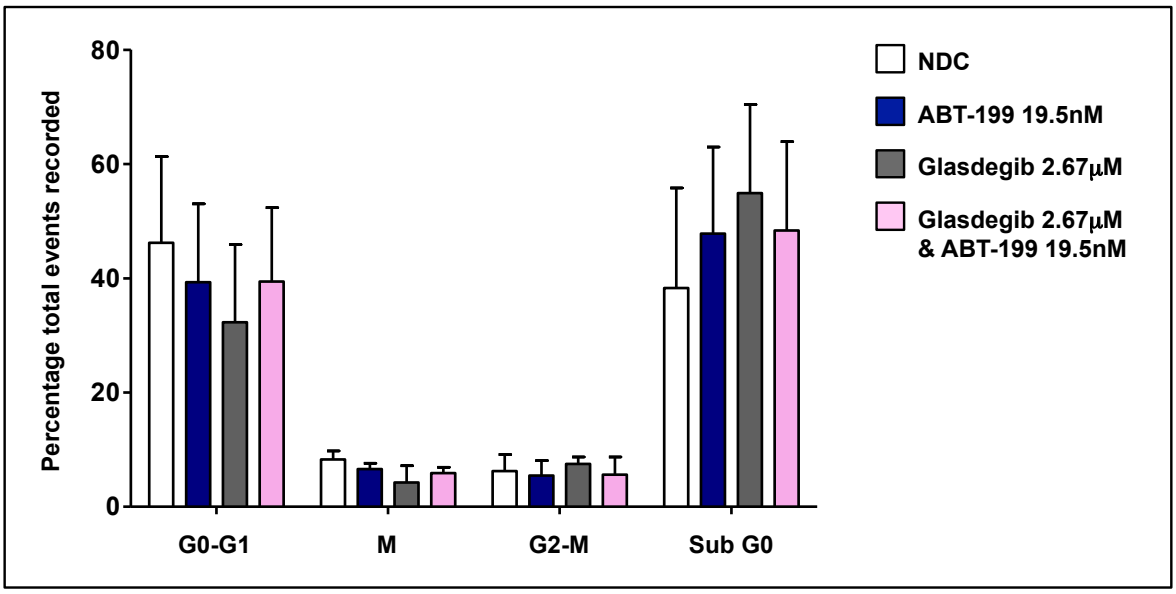

Figure 5.3.11.3: Cell cycle kinetics, as determined by the PI assay, following culture of an unselected cohort of primary, *de novo* AML MNCs (n=4) with ABT-199 (19.5nM) and glasdegib (2.67μM) alone, and in combination, for 72hrs.
The primary samples AML 1002, AML 013, AML 018, and AML 022 were recovered as described in Methods 2.2.1.2.5. Recovered cells were seeded at a concentration of $1.5x10^5$/ml and cultured with glasdegib (2.67μM), ABT-199 (19.5nM) and the combination of glasdegib (2.67μM) and ABT-199 (19.5nM) for 72hrs as described in Methods 2.2.1.2.6. Cells were subsequently harvested and stained with PI prior to analysis by flow cytometry. The proportion of cells within each cell cycle phase (G0-G1, S, G2-M and Sub G0) as determined by PI, and analysis by flow cytometry is shown in this bar graph. Each bar represents the mean percentage from four independent experiments with error bars indicating SD. Glasdegib led to a reduction in the percentage of 'resting' cell (G0-G1 fraction) with a consequent increase in dying cells (the sub G0 fraction) as determined by PI staining (p=ns). ABT-199 did not affect cell cycle kinetics within this cohort of primary AML samples. The combination of glasdegib and ABT-199 did not enhance this effect.

Glasdegib reduced the proportion of cells in the G0-G1 fraction with a consequent increase in the sub G0 fraction though the results were not significant. Interestingly this increase in the Sub G0 fraction, primarily consisting of dead and dying cells and consequent cell debris, was not evident by Annexin V / 7AAD though a non-significant increase in dead cells by trypan blue dye exclusion was seen (p=0.074). Consistent with previous results ABT-199 did not affect cell cycle kinetics. Interestingly the addition of ABT-199 to glasdegib was shown to reduce the effect of glasdegib alone on cell cycle kinetics. In the future, once our CFC and re-plate protocol has been optimised, it would be interesting to study the effect of these two small molecule inhibitors on colony-forming ability and subsequently their self-renewal capacity. Would an additive effect be demonstrated in long-term assays?

5.3.12 Discussion

BCL-2 is strongly associated with a wide range of malignancies; elevated expression thought to occur in approximately half of all malignancies [504-508]. Whilst its association with AML has long been recognised, BCL-2 is an independent prognostic factor and predictor of remission [517]. More recently, quiescent CD34+CD33-CD13- AML cells, in contrast to their normal counterparts, have been shown to highly express BCL-2 [519,520]. The increased functional reliance of leukaemic cells upon BCL-2, especially primitive cells, thought to be responsible for MRD, in comparison to normal haematopoietic cells makes it an exciting therapeutic target, and an area of intense research.

In accordance with published data, we have shown *BCL-2* and *MCL-1* to be up-regulated in select, genetically diverse AML cell lines. Interestingly, there was >100-fold difference between the highest and lowest expressers, suggesting a variable dependence on BCL-2. Further, the pro-apoptotic regulator *BAX* was also shown to be up-uegulated, indicating cell survival and maintenance results from a careful balance between the pro- and anti-apoptotic family members. Considering the variance in expression across each Bcl-2 family member it would be interesting to assess this expression alongside other important regulators of cell death such as p53, located upstream of BCL-2 [697]. Further, it is important to recognise these cell lines have been immortalised, with gene expression performed following culture of each cell line in optimal conditions. Had time allowed the impact of cellular stress and, in contrast, culture in the presence of supporting stromal cells would have been an interesting concept to explore further.

The heterogeneous response both between, and within, our selected cell lines following culture with each of the three Bcl-2 inhibitors is particularly interesting. Importantly, whilst these small molecule inhibitors are referred to as 'Bcl-2 inhibitors' they function by targeting the BH3-binding domain, blocking BH3-domain-mediated heterodimerisation, inducing apoptosis. It is the BH3 domain that is vital in the promotion of cell apoptosis [698]. ABT-199 was developed through reverse engineering of ABT-263; whilst ABT-199 retains the high-affinity interactions with two hydrophobic pockets within the BH3 domain it has been modified electrostatically to specifically interact with Arg103 (specific to BCL-2). All three of our selected inhibitors bind the BH3 domain of BCL-2, though with different potency: ABT-199 >> TW-37 > HA14-1 [559,681,699,700]. In addition, TW-37 binds MCL-1 and to a lesser degree BCL-xL. Whilst our IC_{50} data for the MOLM-13 and MV4-11 cell lines correlates with the inhibitory effect of each of the drugs on BCL-2, the response of the genetically diverse OCI-AML3 and THP-1 cell lines to ABT-199 and TW-37 suggests that, whilst less potent, the dual inhibitory action of TW-37, targeting both BCL-2 and MCL-1, may be more effective in some instances. The inhibitory effect of TW-37 must not be considered in isolation however, with consideration given to the knowledge that it binds Bcl-xL. Progression of ABT-737, a first generation BH3-mimetic, was prevented due to dose limiting toxicity - thrombocytopenia, seen as a consequence of its binding to Bcl-xL [232].

We showed expression of total BCL-2 protein to contrast with that of *BCL-2*, discussing potential explanations within the text. Perhaps, more interesting, is how this contrasts with the universal expression of BCL-2 in primary human AML samples, and marked up-regulation relative to our normal controls, as assesed by IHC on FFPE BMTs (section 3.1.8). It would be interesting to measure BCL-2 in primary human samples by western blotting and further, to correlate these results with gene expression to ascertain if the degree of discordancy seen in cell lines is mirrored by primary cells. It is important to consider this potential discrepancy when analysing cell line data and further, when translating *in vitro* cell line work – if ABT-199 sensitivity is determined by BCL-2 levels, primary AML cells may therefore be far more sensitive than cell line data might suggest.

It is interesting to consider the inhibitory effect of the BCL-2 inhibitors, in particular ABT-199, in parallel to the levels of expression of BCL-2 in our cell lines. Previous *in vitro* studies in diffuse large B cell lymphoma (DLBCL) had shown a positive correlation between BCL-2 levels and sensitivity to ABT-199 [701]. BCL-2 is also highly expressed in follicular lymphoma (FL); *in vitro* studies showing FL cell lines and primary cells to be highly sensitive to ABT-199 though, in contrast to results seen with DLBCL, no correlation with BCL-2 expression was seen, rather ABT-199 sensitivity was dependent upon expression of BIM [702]. In select AML cell lines, a positive correlation between BCL-2 and sensitivity to ABT-199 has been reported [682]; this same study showed levels of BCL-xL to inversely correlate with ABT-199 sensitivity and a non-significant trend to anti-correlation with MCL-1 [682]. We hypothesised BCL-2 expression would positively correlate with the degree of cell death. We showed the OCI-AML3 cell to be relatively resistant to ABT-199 and the MOLM-13 to be highly sensitive to ABT-199-mediated cell death. However BCL-2, as assessed by Western blot, suggested a potential threshold of effect, with those cell lines showing higher levels being relatively resistant to the effects of ABT-199, conflicting with

published data [682]. In this respect, the Bcl-2 family regulates cell survival, and apoptosis; a carefully controlled balance between the pro- and anti-apoptotic family members determining cell fate, rather than simply Bcl-2. Further, analysis of an ABT-199-resistant FL cell line found increased levels of MCL-1 and phosphorylation of BCL-2 to contribute to the resistant phenotype [702]. To further consider these discrepant results it would be important to assess expression of other Bcl-2 family members - MCL-1, BCL-xL and pBCL-2 (phosphorylation of Bcl-2 at serine 70 required for full and potent supprression of apoptosis [688,689,703]), to analyse expression ratios, and to correlate this with the levels of BCL-2 and inhibitory effect. This work would link with that to determine the mechanism underlying the heterogeneous response within select cell lines following culture with ABT-199 and TW-37.

The Bcl-2 family regulates all major types of cell death [468], Figure 1.12, though their core function is the regulation of MOMP, in turn regulating the release of proteolytic proteins [486]. We confirmed ABT-199 induced cell death through the mitochondria in the sensitive MOLM-13 cell line and not in the resistant OCI-AML3 cell line. Further ABT-199 was seen to target the G0-G1 fraction. It would be interesting to utilise agents such as Hoechst-33343^{low}/Pyronin-Y^{low} to separate the G0 and G1 stages to ascertain whether ABT-199 is capable of targeting this population; of particular importance considering LSCs are considered predominantly quiescent.

During the write up of this thesis, updated results from a phase I/II study analysing ABT-199 (venetoclax) with LDAC in those ineligible to receive intensive therapy were presented at EHA 2017 [704]. Subsequently, in July 2017 the FDA granted venetoclax breakthrough therapy designation for use in combination with LDAC in treatment-naïve elderly patients with AML who are ineligible for intensive chemotherapy. With an ORR of 61% (37/61 subjects) and a CR rate of 21% it will be interesting to see if a genetic subtype or molecular profile can indicate treatment response. I*n vivo,* will a positive correlation between BCL-2 and clinical response be seen? Or, is the association of BCL-2 with AML indicative of deregulated apoptosis (a causative mutation not currently recognised) - targeting the process at any level, thereby disrupting the balance towards apoptosis rather than cell survival? It will be interesting to see if these questions are addressed when clinical trial data is published.

In conclusion, whilst there is a clear rationale for the use of Bcl-2 inhibitors in cancer therapeutics, it is important to consider Bcl-2 is not unique to cancerous cells, indeed the apoptotic process is vital in maintaining normal tissue homeostasis. Further, whilst in theory ABT-199 should be highly active in FL, responses have been disappointing; a xenograft model showing acquired resistance developed easily [702]. Considering the mechanism driving increased BCL-2 in AML remains to be determined, it will be interesting to see responses out with the clinical trial setting, and longer follow up data from those trials already presented / published. Additionally the relative resistance of OCI-AML3 cells to ABT-199 requires further investigation, results of a phase II trial studying ABT-199 as a single agent in patients with AML unsuitable for intensive therapy or with R/R disease showed superior responses in those with mutations in genes regulating methylation [524]. The combination of decitabine and vorinostat, epigenetic agents, has been shown to overcome ABT-199 resistance in FL cell *in vitro* [702] and a phase I study of venetoclax with azacitidine or decitabine presented at ASCO in 2016 showed a response in 76% (26/34 subjects) [523]. Finally, whether Bcl-2 inhibitors will find a role in combination with intensive treatment remains to be determined - will concerns over the risk of unacceptable toxicity affecting regenerating normal tissues prove to be well founded [705]?

The ABC transporters similarly play an important role in normal physiology, responsible for the transport, or efflux, of a huge variety of compounds, across plasma and intracellular membranes. Drug resistance is one of the primary causes of treatment failure and disease relapse [215,532] with the ABC transporters representing a major mechanism of chemoresistance; increased expression of thirteen of the ABC transporters linked to chemoresistance [218,526,534].

Chemoresistance is well recognised in AML; members of ABC family confer an independent adverse prognostic factor, are up-regulated in poor prognostic WHO subtypes [540,544] and efflux

anthracyclines [218]. Despite these findings the role of the ABC transporters in AML remains contentious with debate surrounding expression patterns in normal and leukaemic CD34+CD38- haematopoietic cells [539,540,545]. We confirmed expression of five members of the ABC transporter family, each associated with chemoresistance, with select genetically diverse AML cell lines. Marked variation in expression, both within and across each ABC transporter, was shown. It would be interesting to evaluate expression following culture with cytotoxic agents such as Ara-C and following co-culture with supportive stromal cells. Further, to analyse expression of the ABC transporters in sorted cell populations, both normal and malignant – whilst minimal short-term effect is seen do these agents allow us to obtain superior drug concentrations within the CSC? Will long-term data find a reduction in disease relapse?

Within the clinic the first three generations of ABC inhibitors including cyclosporin, elacridar, verapamil and zosuquidar, have shown limited or no benefit, high doses being required to achieve effect with significant adverse effects and unwanted drug-drug interactions reported. Many of the toxicity issues are considered to arise due to abundant expression of the ABC transporters by normal tissues, in particular within the liver, kidney and brain, leading to the adverse accumulation of cytotoxic agents within these organs. The limited success has, in part, been considered to result from the broad, and overlapping, specificity of ABC transporters expressed by tumours. Our data is consistent, showing no additional benefit when select ABC transporter inhibitors were combined with Ara-C in genetically diverse AML cell lines. Expression did not correlate with response. Considering the importance of concentration ratios for many chemotherapeutic agents, in particular the ratio of cytarabine to daunorubicin in the intensive management of AML, it would be interesting to study the effect of the ABC transport inhibitors in combination with both agents. Further, given the difficulties translating *in vitro* data into the clinic it would be interesting to perform the assays in, perhaps more reliable, preclinical assays such as those utilizing supportive stromal cells; with positive results needing to be tested within an *in vivo* model.

6 Final conclusions and future directions

AML originates from a CSC, the term encompassing a group of aggressive haematological neoplasms. AML is a clinically, morphologically and genetically heterogeneous disease [1,150,154,162]. It is this complexity which, whilst ensuring AML is a fascinating disease to study, means despite huge advances in our knowledge and understanding, obtained through extensive research and international trials, with molecularly and immunologically targeted therapies now available [706], clinicians still face the challenge of curing only the minority [707]. Indeed our understanding of the molecular biology of AML has far-outpaced the development of new and effective therapeutics though with the FDA approving five new agents in 2017 this may, excitingly, be about to change. Advances in both technology and our understanding are however not only shaping the future for AML but far wider, forging the way for cancer research.

The hedgehog signalling pathway is highly complex, and is intricately involved in developmental processes. Aberrant activity has been demonstrated in a variety of malignancies [259,262,367,368], linked to tumour growth, progression and drug resistance; in myeloid malignancies it has been shown to be vital in the maintenance and expansion of the CSC [252,344,375–377]. Components of the pathway, Smo and Gli, considered as promising targets for cancer therapeutics - sonidegib and vismodegib (Smo inhibitors) both receiving FDA approval for the treatment of advanced or metastatic BCC [708] [709]. To date however, out with BCC, these small molecule inhibitors have shown limited efficacy though results of a Phase I study combining sonidegib with conventional chemotherapy (etoposide and cisplatin) in patients with extensive small cell lung cancer has shown promising results [710]. To translate knowledge of the Hh signalling pathway into AML and, further, to determine whether it represents a clinically effective therapeutic target careful consideration must first be given to the clinical trial setting.

The UK national trial, NCRI AML 19 [711], highlights how our advancing knowledge and technology is being translated into clinical practice. Building upon data from previous trials [712,713] it aims to: (1) refine the current standard of care, and improve outcome whilst reducing treatment-related morbidity and mortality; (2) risk stratify according to the calculated risk index [204], adjusting treatment accordingly; (3) determine the relevance of MRD, detected molecularly and immunophenotypically; and (4) identify potential molecular markers, correlating these with clinical outcome.

To risk stratify is to seek to tailor management to both the disease, by considering response to first cycle of chemotherapy and cytogenetics, and the patient, by considering patient-specific factors such as age, presenting white cell count and performance status. This approach recognises the marked inter- and intra-patient heterogeneity, importantly classifing many more patients as poor risk than the MRC classification [158] with significant implications to the patient's prognosis and potential treatment journey. In essence, on a national scale, it seeks to 'personalise' medicine.

Whilst the NCRI AML trials have sought, and continue to seek, to improve outcomes by risk stratifying those younger, fitter patients, new, novel agents have been notably lacking from these and other intensive trials. Investigators seeking to incorporate newer agents into current standard-of-care regimens are faced with many challenges: the comparatively low incidence of AML, its intrinsic heterogeneity and, often, its aggressiveness, dictating a clinical urgency for treatment initiation and not infrequently patients dying before a measurable benefit can be determined. Intense effort does however continue. There are currently 271 open phase I-III trials listed by the EU Clinical Trials register [223] with an exciting armourary of new, and in some cases, novel agents being utilised. Five drugs were approved by the FDA in 2017 – venetoclax [704], enasidenib [714], CPX-351 [715], midostaurin [716] and gemtuzumab ozogamacin [709]. Indeed, whilst the newest agent included in the NCRI AML 17 trial was Gemtuzumab ozogamacin, first used in the treatment of AML in 2000 [717] the current NCRI AML 19 trial incorporates CPX-351. CPX-351 a liposomal formulation of Ara-C and daunorubicin, delivers these drugs in a 5:1 molar ratio direct

to the cell, optimising synergy and minimising drug antagonism [718]. A phase III study comparing CPX-351 to DA in newly diagnosed t-AML and AML-MRC recently published an improvement in OS to 9.56 months with CPX-351 versus 5.95 months with DA [715].

Further, a new model, "pick-a-winner", has recently been brought into trial design, enabling a larger number of agents to be investigated within a given period [719,720]; this template is used in the current NCRI Low Intensity (LI)-1 trial. This trial is important to consider for another reason pertinent to the field of AML clinical research and targeted therapies. It has moved away from the single agent approach, instead combining novel therapies with current standard-of-care in a bid to improve patient outcome. The rationale for combinational therapies is substantial [707,721], the complex and progressive genetic landscape of AML enabling the disease to bypass molecular targets and become resistant to single-agent therapy [722].

Another challenge for investigators is eligibility criteria or patient selection. By focusing on those unable to tolerate intensive treatment as in the NCRI LI-1 trial or those with R/R disease, there is the potential to lose or negate any beneficial effect that might be seen in a broader patient cohort. AML of the elderly, in many respects considered a distinct entity [723], whilst R/R disease has demonstrated a more resistant phenotype [724] by virtue of the clinical history, and further been exposed to the selective pressure of treatment. This patient cohort should however not be ignored.

Although it is an exciting time for translational medicine the attrition of experimental therapies, and the associated time and resources, raises concerns over current experimental, preclinical, models. Whilst the limitations of immortalised cell lines and *in vitro* liquid culture are well recognised, increasingly the limitations of primary, patient-derived leukaemia cells are becoming apparent. Most notable is the concern of subpopulation or 'clonal' selection, deriving a population of cells not wholly representative of AML, defined by its genomic complexity and the presence often of multiple coexisting molecularly defined clones [151]. Another concern regarding *in vitro* models is the absence of a supporting microenvironment. Whilst assays utilising supporting stroma cells and xenotransplantation models may provide more reliable results, the limitations must be recognised and considered when interpreting results. Our unique observation that haematopoietic cells possess primary cilia within the BM microenvironment yet loose / disassemble or 'switch off' these organelles once they leave the BM environment beautifully illustrating this point.

Technology has allowed us to begin to unravel and appreciate the genetic complexity of AML. AML does not derive from a single "driver" mutation as seen in CML, transformed from a 'fatal cancer to a manageble chronic disease' by the small molecule inhibitor imatinib. Rather AML has been shown to develop after normal HSPCs acquire a relatively small number of "driver" mutations, additional mutations stochastically acquired. In this respect it will be interesting to see how next-generation sequencing is incorporated into clinical practice, will it enable selection of small molecule inhibitors or further enable targeted combinational therapies, 'precision medicine'? Mutational profile and burden, however, is clearly not the sole factor in determining AML cell behaviour; on average five pathogenic mutations and an additional eight mutations are identified in *de novo* AML at diagnosis [721], far fewer than seen in solid tumours [725]. A significant proportion of AML appear cytogenetically and genetically normal, yet gene expression signatures tell a different story [721]. The Cancer Genome Atlas described 16 distinct subgroups of AML. These subgroups were classified according to unsupervised analyses using Pearson's correlation coefficient, 2856 probe sets (2008 annotated genes and 146 short sequences of unknown genes) utilised to define the gene-expression profiles [381]. Subsequent to this the NEJM published a study in 2016 analysing gene expression patterns and relationships, correlating these genotypes with clinical data [726]. '5234 driver mutations involving 76 genes, or regions, in 1540 patients were identified' with 96% of patients shown to harbor at least one driver mutation [726]. Utilising a Bayesian statistical model patients were classified according to their compound genotype, with 11 non-overlapping subgroups defined; three genomic categories

emerging beyond the existing WHO classification: chromatin–spliceosome, *TP53*–aneuploidy, and provisionally, *IDH2R172* mutations [726]. It will be interesting to see how these studies are incorporated into clinical practice; a sub study within the NCRI AML 17 trial highlighting how molecular results can drastically alter a patient's prognosis and thus the treatment offered and further, can be performed and available within an acceptable time frame to be useful clinically. This sub study focused on *NPM1* mutated AML, demonstrating that sequential assessment of this molecular marker provided treatment defining prognostic information. Ongoing positivity after cycle two predicting disease relapse, with a superior efficacy to that seen using current diagnostic molecular markers, influencing decisions regards treatment escalation to SC transplantation [727]. Nor does AML consistently express an immunological target as seen in B-cell lymphomas, the anti-CD20 monoclonal antibody rituximab radically improving prognosis for the majority of these patients. There is however intense efforts to further define the LSC, to differentiate it from its counterpart the HSC, with whom it shares the CD34+CD38− immunophenotype [112,121]. To date work has shown preferential expression of a number of cell surface proteins including CD25, CD32, CD41, CD44, CD47, CD93, CD96, CD123, CLL-1 and TIM-3 in LSCs relative to HSCs [133,600,728-733]; these markers defining subpopulations and potentially involved in the evolution of mutated 'pre-leukaemic' HSCs to LSCs [734]. Excitingly, CD44, CD47 and CD123 have been shown to be therapeutically targetable in *in vitro* and murine studies [600,731,735] and whilst the results of a phase I study in R/R AML using an anti-CD44 monoclonal antibody (NCT01641250) showed limited efficacy [736] evaluation of a CD123 x CD3 Dual Affinity Re-Targeting (DART®) Bi-Specific Antibody (NCT02152956) and the anti-CD47 monoclonal antibody Hu5F9-G4 (NCT02678338) in R/R AML and high risk MDS are ongoing, with the results eagerly awaited.

Single cell assays are rapidly developing, enabling 'genome-scale' molecular information to be studied at the individual cell level. Whilst significant challenges remain in the analysis, integration, and interpretation of single cell omic data the results are eagerly awaited. Will this technology enable us to begin to understand the genetic changes allowing the development of different dominant clones?

There is considerable evidence to support the role of the Hh signalling pathway in AML [381]. Data showing it to be active [69], associated with an inferior OS and poor prognostic markers [379-382] and to confer drug resistance [378,379]. Whilst its role in normal haematopoiesis remains controversial [253,362-364] importantly genetic inhibition of canonical signalling through a *SMO* knockout did not adversely affect normal haematopoiesis [363,366] affording Smo inhibition a therapeutic window. In 2016, serial transplantation studies using the NOD/SCID/IL2rγ^{null} mouse model showed the Smo inhibitor PF-04449913 to reduce the leukaemic potential of AML cells [618]. Interestingly, whilst *in vitro* work using the Marimo cell line demonstrated minimal cell death the quiescent population was reduced. Further, PF-04449913 sensitised primary AML cells and two genetically distinct AML cell lines cells (Marimo and MOLM-14) to Ara-C. This demonstration of a synergistic action is particularly exciting; knowledge of the complex interplay between the intrinsic and extrinsic signals governing CSC behaviour and the genomic complexity and clonal heterogeneity seemingly suggesting combinational therapies will be required to translate these insights into clinically effective interventions. Whilst a number of questions still remain unanswered, Pfizer recently reported promising results from its phase I/II trial studying the effect of glasdegib with LDAC in those ineligible to receive intensive therapy presented at ASH 2016 [654].

Whether the new generation of molecularly and immunologically targeted therapies prove sufficiently beneficial, and tolerated, to be brought into mainstream treatment algorithms remains to be seen. Whether agents thought to offer little benefit were not fully explored clinically, due to the heterogeneity of AML, is an important question to raise, as is the concern that if we select certain subtypes do we risk missing a beneficial unexpected effect in other patients? With our increasing knowledge, will we see a return of some of these once shelved agents to the treatment of specific subtypes or categories of AML, such as arsenic trioxide in the management of APML, or the incorporation of non-chemotherapeutic agents such as antibiotics

alongside existing cytotoxic therapies?

In addition to future work discussed through the text in this section I wish to present some interesting preliminary results. We had considered work by the Copland group showing MSC co-culture to protect CD34+ CML cells against imatinib-induced apoptosis (unpublished) with recent studies indicating the importance of this microenvironment in AML [254]. Recognising the limitations of liquid culture, we therefore considered whether the effect of Smo inhibition would be abrogated when cells were co-cultured. In this respect we first considered a number of stromal cell lines. We found HS-5, M210-B4 and SL-SL cell lines to express all components of the Hh signalling pathway at a gene and protein level, and to possess primary cilia. The M210-B4 and SL-SL cell lines, both murine BM-derived stromal cell lines, were selected as they are frequently used in LTC-ICs whilst the HS-5 stromal cells are human-derived used, as described in Methods 2.2.1.2.5, by our group to support primary AML cells post thawing. Having demonstrated the Hh pathway to be present in stromal cells we sought to evaluate the effect of pharmacological Smo inhibition using cyclopamine with fascinating results. The stromal cell lines were >100-fold more sensitive to cyclopamine than our selected AML cell lines when cyclopamine was added during cell passage with all cells dead at 24hrs following culture with concentrations as low as 500nM. In contrast all stromal cell lines were able to tolerate cyclopamine, up to a concentration of 20μM, with no evidence of cell death by trypan blue dye exclusion, once >75% confluent. This preliminary data clearly shows the Hh pathway to be present, and functionally active, in our selected stromal cell lines and to be fundamentally dependent upon cellular dynamics. In future work we plan to build upon these observations and to determine whether stroma induced Hh signalling plays a role in supporting AML cell lines and primary AML cells in short and long-term culture. Additionally, as previously discussed, whilst cell lines serve as useful experimental models they may not always accurately represent primary cells [627]. We therefore sought to further develop the existing primary MSC bank within the Copland laboratory. MSCs were derived by the plastic adherence method as discussed in methods 2.2.1.2.7. MSCs were derived from the BM of 9 primary *de novo* AML samples, 4 CP-CML samples, 5 BC-CML samples and 3 normal samples. A cell bank with cells cryopreserved from passage 2 through 6 for each sample with paired RNA, protein and CM is now available for further evaluation. CML MSCs were generated for a colleague, Dr G A Horne. In the future it would be interesting to determine the:

(1) Expression of the Hh pathway at a gene and protein level in all MSCs both normal and AML
(2) Presence or absence of the Hh ligands in CM, and if present to determine the concentration secreted by AML in comparison to normal MSCs
(3) Effect of cyclopamine on MSCs both normal and AML
(4) Effect of cyclopamine on primary human AML cells co-cultured with primary MSCs

We had hypothesised co-culture would abrogate the effect of Smo inhibition, implying either a regulatory role of the microenvironment or a different mode of pathway activity in the presence of stromal cells. A result that would mirror previously published work in mature B cell malignancies [363]. Further, it would lend a potential explanation to the conflicting results seen when using Smo antagonists *in vitro* and *in vivo* [618]. Interestingly, and in keeping with our hypothesis, during the write up of this PhD glasdegib was reported to nullify resistance to Ara-C in AML cell lines co-cultured with HS-5 stromal cells, sensitising these cells to Ara-C induced apoptosis [618].

All forms of cancer arise from abnormal growth, when the balance between cell death and survival is disturbed. In AML both increased proliferation and decreased cell death are well recognised. Whilst standard treatment results in remission rates of 60-80% in younger patients, only 30-40% survive 5 years [205]. Disease relapse and progression is largely attributed to the LSCs, extensive work showing these cells to be innately less sensitive to treatment [23,126]. We have considered the Hh signalling pathway, one of the self-renewal pathways, seeking to further

understand its role in the pathogenesis of AML. Fascinatingly we have shown inhibition of Smo *in vitro* to seemingly shift the balance between cellular self-renewal and differentiation properties. Further, we have sought to understand the relationship between pro- and anti-apoptosis, in a situation in which the balance clearly favours cell survival, seeking to determine if components of the apoptotic pathway can be targeted to shift the balance to favour apoptosis.

Whilst the role of small molecule inhibitors in such a heterogeneous and aggressive disease as AML remains to be determined, personally I consider myself fortunate to be involved in the care of these patients during this new and immensely exciting era.

References

1. Döhner H, Estey E, Grimwade D, et al. Diagnosis and management of AML in adults: 2017 ELN recommendations from an international expert panel. *Blood*. 2017;129(424–447):424–447.

2. Nguyen L V., Vanner R, Dirks P, Eaves CJ. Cancer stem cells: an evolving concept. *Nat Rev Cancer*. 2012;12(February):133-143. doi:10.1038/nrc3184.

3. Serafini M, Verfaillie CM. Pluripotency in adult stem cells: state of the art. *Semin Reprod Med*. 2006;24(5):379-388. doi:10.1055/s-2006-952153.

4. Till JE, McCulloch EA. A direct measurement of the radiation sensitivity of normal mouse bone marrow cells. *Radiat Res*. 1961;14(2):213-222. doi:10.2307/3570892.

5. Obokata H, Kojima K, Westerman K, et al. The potential of stem cells in adult tissues representative of the three germ layers. *Tissue Eng Part A*. 2011;17(5-6):607-615. doi:10.1089/ten.TEA.2010.0385.

6. McClay DR. Gastrulation. *Curr Opin Genet Dev*. 1991;1:191-195.

7. Cairns J. The origin of human cancers. *Nature*. 1981;289:353-357. doi:10.1038/nature13748.

8. Morrison SJ, Kimble J. Asymmetric and symmetric stem-cell divisions in development and cancer. *Nature*. 2006;441(7097):1068-1074. doi:10.1038/nature04956.

9. Morrison SJ, Qian D, Jerabek L, et al. A genetic determinant that specifically regulates the frequency of hematopoietic stem cells. *J Immunol*. 2002;168(2):635-642. http://www.ncbi.nlm.nih.gov/pubmed/11777956.

10. Zhu a J, Haase I, Watt FM. Signaling via beta1 integrins and mitogen-activated protein kinase determines human epidermal stem cell fate in vitro. *Proc Natl Acad Sci U S A*. 1999;96(12):6728-6733. doi:10.1073/pnas.96.12.6728.

11. Zon LI. Intrinsic and extrinsic control of haematopoietic stem-cell self-renewal. *Nature*. 2008;453(7193):306-313. doi:10.1038/nature07038.

12. Mendelson A, Frenette PS. Hematopoietic stem cell niche maintenance during homeostasis and regeneration. *Nat Med*. 2014;20(8):833-846. doi:10.1038/nm.3647.

13. Birbrair A, Frenette PS. Niche heterogeneity in the bone marrow. *Ann N Y Acad Sci*. 2016;1370(1):82-96. doi:10.1111/nyas.13016.

14. Morrison SJ, Scadden DT. The bone marrow niche for haematopoietic stem cells. *Nature*. 2014;505(7483):327-334. doi:10.1038/nature12984.

15. Gailani MR and AEB. Acquired and inherited basal cell carcinomas and the patched gene. *Adv Dermatol*. 1999;14:261-283.

16. Polakis P. Wnt signaling and cancer. *Genes Dev*. 2000;14(15):1837-1851. doi:10.1038/nature03319.

17. Wechsler-Reya R, Scott MP. The developmental biology of brain tumors. *Annu Rev Neurosci*. 2001;24:385-428. doi:10.1146/annurev.neuro.24.1.385.

18. Moignard V, Woodhouse S, Haghverdi L, et al. Decoding the regulatory network of early blood development from single-cell gene expression measurements. *Nat Biotechnol*. 2015;33(3):269-276. doi:10.1038/nbt.3154.

19. Wilson NK, Kent DG, Buettner F, et al. Combined Single-Cell Functional and Gene Expression Analysis Resolves Heterogeneity within Stem Cell Populations. *Cell Stem Cell*. 2015;16(6):712-724. doi:10.1016/j.stem.2015.04.004.

20. Kokkaliaris KD, Lucas D, Beerman I, Kent DG, Perié L. Understanding hematopoiesis from a single-cell standpoint. *Exp Hematol*. 2016;44(6):447-450. doi:10.1016/j.exphem.2016.03.003.

21. Zhou Y, Basu S, Laue E, Seshia A. Single cell studies of mouse embryonic stem cell (mESC) differentiation by electrical impedance measurements in a microfluidic device. *Biosens Bioelectron*. 2016;15(81):249-258.

22. Göttgens B. Creating cellular diversity through transcription factor competition. *EMBO J*. 2015;34(6):691-694. doi:10.15252/embj.201591017.

23. Tannishtha R, Morrison SJ, Clarke MF, Weissman IL. Stem cells, cancer, and cancer stem cells. *Nature*. 2001;414(November):105-111. doi:10.1007/978-1-60327-933-8.

24. Pardal R, Clarke MF, Morrison SJ. Applying the principles of stem-cell biology to cancer. *Nat Rev Cancer*. 2003;3(12):895-902. doi:10.1038/nrc1232.

25. Balmain A, Gray J, Ponder B. The genetics and genomics of cancer. *Nat Genet*. 2003;33(3s):238-244. doi:10.1038/ng1107.

26. Friedenstein AJ, Petrakova KV, Kurolesova AI FG. Heterotopic of bone marrow. Analysis of precursor cells for osteogenic and hematopoietic tissues. *Transplantation*. 1968;6(2):230-247.

27. Friedenstein A. Osteogenic stem cells in bone marrow. *Bone Miner Res*. 1990:243–272.

28. Schofield R. The relationship between the spleen colony-forming cell and the haemopoietic stem cell. *Blood Cells*. 1978;4(1-2):7-25. doi:Chronic ischaemic mitral regurgitation. Current treatment results and new mechanism-based surgical approaches☆.

29. Tavassoli, M CWH. Transplantation of Marrow to Extramedullary Sites. *Science (80-)*. 1968;161(3836):54-56.

30. Tavassoli M, Weiss L. The structure of developing bone marrow sinuses in extramedullary autotransplant of the marrow in rats. *Anat Rec*. 1971;171(4):477–493.

31. Tavassoli M, Friedenstein A. Hemopoietic stromal microenvironment. *Haematology*. 1983;15(2):195–203.

32. Friedenstein AJ, Chailakhyan RK, Latsinik NV, Panasyuk AF K-BI. Stromal cells responsible for transferring the microenvironment of the hemopoietic tissues. Cloning in vitro and retransplantation in vivo. *Transplantation*. 1974;17(4):331-340.

33. Brockbank KGM, van Peer CMJ. Colony-Stimulating Activity Production by Hemopoietic Organ Fibroblastoid Cells in vitro. *Acta Haematol*. 1983;69(6):369-375.

34. Zucali, J. Dinarello C.A., Oblon D.J., Gross M.A., Anderson L. WRS. Interleukin 1 stimulates fibroblasts to produce ganulocyte macrophage colony-stimulating activity and prostaglandin E2. *J Clin Invest*. 1986;78:1306-1323.

35. Lee, M.; Segal, G.M.; Bagby GC. Interleukin 1 induces human bone marrow-derived fibroblasts to produce mulit-lineage hemopoietic growth factors. *Exp Hematol*. 1987;15:983-988.

36. Brockbank K.G.M.; De Jong J.P.; Piersma A.H., Voerman JSA. Hemopoiesis on purified bone-marrow-derived reticular fibroblasts in vitro. *Exp Hematol*. 1986;14:386-394.

37. Dominici M, Le Blanc K, Mueller I, et al. Minimal criteria for defining multipotent mesenchymal stromal cells. The International Society for Cellular Therapy position statement. *Cytotherapy*. 2006;8(4):315-317. doi:10.1080/14653240600855905.

38. Martinez C, Hofmann TJ, Marino R, Dominici M, Horwitz EM. Human bone marrow mesenchymal stromal cells express the neural ganglioside GD2: a novel surface marker for the identification of MSCs. *Blood*. 2007;109(10):4245-4248. doi:10.1182/blood-2006-08-039347.

39. Anjos-Afonso F, Bonnet D. Flexible and dynamic organization of bone marrow stromal compartment. *Br J Haematol*. 2007;139(3):373-384. doi:10.1111/j.1365-2141.2007.06827.x.

40. Anjos-Afonso F, Bonnet D. Nonhematopoietic/endothelial SSEA-1+ cells define the most primitive progenitors in the adult murine bone marrow mesenchymal compartment. *Blood*. 2007;109(3):1298-1306. doi:10.1182/blood-2006-06-030551.

41. Anjos-Afonso F, Bonnet D. Prospective identification and isolation of murine bone marrow derived multipotent mesenchymal progenitor cells. *Best Pr Res Clin Haematol*. 2011;24(1):13-24. doi:S1521-6926(10)00132-5 [pii]\r10.1016/j.beha.2010.11.003.

42. Anjos-Afonso F, Bonnet D. Isolation, culture, and differentiation potential of mouse marrow stromal cells. *Curr Protoc Stem Cell Biol*. 2008;Chapter 2:Unit 2B 3. doi:10.1002/9780470151808.sc02b03s7.

43. Gang EJ, Bosnakovski D, Figueiredo CA, Visser JW, Perlingeiro RCR. SSEA-4 identifies mesenchymal stem cells from bone marrow. *Blood*. 2007;109(4):1743-1751. doi:10.1182/blood-2005-11-010504.

44. Morrison SJ, Spradling AC. Stem Cells and Niches: Mechanisms That Promote Stem Cell Maintenance

throughout Life. *Cell*. 2008;132(4):598-611. doi:10.1016/j.cell.2008.01.038.

45. Scadden DT. The stem-cell niche as an entity of action. *Nature*. 2006;441(7097):1075-1079. doi:10.1038/nature04957.

46. Park D, Sykes DB, Scadden DT. The hematopoietic stem cell niche. *Front Biosci (Landmark Ed*. 2012;17:30-39. doi:10.3824/stembook.1.28.1.

47. Rocheteau P, Vinet M, Chretien F. Dormancy and Quiescence of Skeletal Muscle Stem Cells. *Results Probl Cell Differ*. 2015;56:191-213. doi:10.1007/978-3-662-44608-9.

48. Teitell MA, Mikkola HKA. Transcriptional activators, repressors, and epigenetic modifiers controlling hematopoietic stem cell development. *Pediatr Res*. 2006;59(4 PART. 2). doi:10.1203/01.pdr.0000205155.26315.c7.

49. Dzierzak E, Speck NA. Of lineage and legacy: the development of mammalian hematopoietic stem cells. *Nat Immunol*. 2008;9(2):129-136. doi:ni1560 [pii]\r10.1038/ni1560.

50. Dzierzak E. Embryonic beginnings of definitive hematopoietic stem cells. In: *Annals of the New York Academy of Sciences*. Vol 872. ; 1999:256-264. doi:10.1111/j.1749-6632.1999.tb08470.x.

51. Eaves CJ. Hematopoietic stem cells: Concepts, definitions, and the new reality. *Blood*. 2015;125(17):2605-2613. doi:10.1182/blood-2014-12-570200.

52. Notta F, Zandi S, Takayama N, et al. Distinct routes of lineage development reshape the human blood hierarchy across ontogeny. *Science*. 2016;351(6269):aab2116. doi:10.1126/science.aab2116.

53. Woolthuis CM, Park CY. Hematopoietic stem/progenitor cell commitment to the megakaryocyte lineage. *Blood*. 2016;127(10):1242-1248. doi:10.1182/blood-2015-07-607945.

54. Copley MR, Beer PA, Eaves CJ. Hematopoietic stem cell heterogeneity takes center stage. *Cell Stem Cell*. 2012;10(6):690-697. doi:10.1016/j.stem.2012.05.006.

55. Ema, H. YM and TS. Heterogeneity and hierarchy of hematopoietic stem cells. *Exp Hematol*. 2014;42(2):72-82 e72.

56. Sieburg HB, Cho RH, Muller-Sieburg CE. Limiting dilution analysis for estimating the frequency of hematopoietic stem cells: uncertainty and significance. *Exp Hematol*. 2002;30(12):1436-1443. doi:S0301472X02009633 [pii].

57. Muller-Sieburg, C. E.; Sieburg HB. The GOD of hematopoietic stem cells: a clonal diversity model of the stem cell compartment. *Cell Cycle*. 2006;5(4):394-398.

58. Sieburg, H. B., R. H. Cho, B. Dykstra, N. Uchida CJE and CEM-S. The hematopoietic stem compartment consists of a limited number of discrete stem cell subsets. *Blood*. 2006;107(6):2311-2316.

59. Dykstra B, Kent D, Bowie M, et al. Long-Term Propagation of Distinct Hematopoietic Differentiation Programs In Vivo. *Cell Stem Cell*. 2007;1(2):218-229. doi:10.1016/j.stem.2007.05.015.

60. Muller-Sieburg CE, Cho RH, Thoman M, Adkins B, Sieburg HB. Deterministic regulation of hematopoietic stem cell self-renewal and differentiation. *Blood*. 2002;100(4):1302-1309.

61. Moignard, V., S. Woodhouse JF and BG. Transcriptional hierarchies regulating early blood cell development. *Blood Cells Mol Dis*. 2013;51(4):239-247.

62. Ramos CA, Bowman TA, Boles NC, et al. Evidence for diversity in transcriptional profiles of single hematopoietic stem cells. *PLoS Genet*. 2006;2(9):1487-1499. doi:10.1371/journal.pgen.0020159.

63. Pina C, Fugazza C, Tipping A, et al. Inferring rules of lineage commitment in haematopoiesis. *Nat Publ Gr*. 2012;14(3):287-294. doi:10.1038/ncb2442.

64. Hanoun M, Frenette PS. This niche is a maze; An amazing niche. *Cell Stem Cell*. 2013;12(4):391-392. doi:10.1016/j.stem.2013.03.012.

65. Boulais PE, Frenette PS. Making sense of hematopoietic stem cell niches. *Blood*. 2015;125(17):2621-2629. doi:10.1182/blood-2014-09-570192.

66. Kunisaki Y, Bruns I, Scheiermann C, et al. Arteriolar niches maintain haematopoietic stem cell quiescence. *Nature*. 2013;502(7473):637-643. doi:10.1038/nature12612.

67. Zhang J, Niu C, Ye L, et al. Identification of the haematopoietic stem cell niche and control of the niche size. *Nature*. 2003;425(6960):836-841.

68. Nombela-Arrieta C, Pivarnik G, Winkel B, et al. Quantitative imaging of haematopoietic stem and progenitor cell localization and hypoxic status in the bone marrow microenvironment. *Nat Cell Biol*. 2013;15(5):533-543.

69. Lo Celso C, Fleming H, Wu J, et al. Live-animal tracking of individual haematopoietic stem/progenitor cells in their niche. *Nature*. 2009;457(7225):92-96.

70. Sugiyama T, Kohara H, Noda M, Nagasawa T. Maintenance of the Hematopoietic Stem Cell Pool by CXCL12-CXCR4 Chemokine Signaling in Bone Marrow Stromal Cell Niches. *Immunity*. 2006;25(6):977-988. doi:10.1016/j.immuni.2006.10.016.

71. Kiel M, Radice G, Morrison S. Lack of evidence that hematopoietic stem cells depend on N-cadherin-mediated adhesion to osteoblasts for their maintenance. *Cell Stem Cell*. 2007;1(2):204-217.

72. Zhu J, Garrett R, Jung Y, et al. Osteoblasts support B-lymphocyte commitment and differentiation from hematopoietic stem cells. *Blood*. 2007;109(9):3706-3712.

73. Lymperi S, Horwood N, Marley S, Gordon M, Cope A, Dazzi F. Strontium can increase some osteoblasts without increasing hematopoietic stem cells. *Blood*. 2008;111(3):1173-1181.

74. Raaijmakers M. Regulating traffic in the hematopoietic stem cell niche. *Haematologica*. 2010;95(9):1439-1441.

75. Kiel M, Iwashita T, Yilmaz O, Morrison S. Spatial differences in hematopoiesis but not in stem cells indicate a lack of regional patterning in definitive hematopoietic stem cells. *Dev Biol*. 2005;283(1):29-39.

76. Kiel M, Yilmaz O, Iwashita T, Yilmaz O, Terhorst C, Morrison S. SLAM family receptors distinguish hematopoietic stem and progenitor cells and reveal endothelial niches for stem cells. *Cell*. 2005;121(7):1109-1121.

77. Guezguez B, Campbell C, Boyd A, et al. Regional localization within the bone marrow influences the functional capacity of human HSCs. *Cell Stem Cell*. 2013;13(2):175-189.

78. Sacchetti B, Funari A, Michienzi S, et al. Self-renewing osteoprogenitors in bone marrow sinusoids can organize a hematopoietic microenvironment. *Cell*. 2007;131(2):324-336.

79. Chan C, Chen C, Luppen C, et al. Endochondral ossification is required for haematopoietic stem-cell niche formation. *Nature*. 2009;457(7228):490-494.

80. Ding L, Saunders T, Enikolopov G, Morrison S. Endothelial and perivascular cells maintain haematopoietic stem cells. *Nature*. 2012;481(7382):457-462.

81. Omatsu Y, Sugiyama T, Kohara H, et al. The essential functions of adipo-osteogenic progenitors as the hematopoietic stem and progenitor cell niche. *Immunity*. 2010;33(3):387-399.

82. Noda M, Omatsu Y, Sugiyama T, Oishi S, Fujii N, Nagasawa T. CXCL12-CXCR4 chemokine signaling is essential for NK-cell development in adult mice. *Blood*. 2011;117(2):451-458.

83. Méndez-Ferrer S, Michurina T, Ferraro F, et al. Mesenchymal and haematopoietic stem cells form a unique bone marrow niche. *Nature*. 2010;466(7308):829-834.

84. Li W, Johnson SA, Shelley WC, Yoder MC. Hematopoietic stem cell repopulating ability can be maintained in vitro by some primary endothelial cells. *Exp Hematol*. 2004;32(12):1226-1237. doi:10.1016/j.exphem.2004.09.001.

85. Butler J, Nolan D, Vertes E, et al. Endothelial cells are essential for the self-renewal and repopulation of Notch-dependent hematopoietic stem cells. *Cell Stem Cell*. 2010;6(3):251-264.

86. Kobayashi H, Butler J, O'Donnell R, et al. Angiocrine factors from Akt-activated endothelial cells balance self-renewal and differentiation of haematopoietic stem cells. *Nat Cell Biol*. 2010;12(11):1046-1056.

87. Winkler I, Barbier V, Nowlan B, et al. Vascular niche E-selectin regulates hematopoietic stem cell dormancy, self renewal and chemoresistance. *Nat Med*. 2012;18(11):1651-1657.

88. Kiel M, Morrison S. Maintaining hematopoietic stem cells in the vascular niche. *Immunity*.

2006;25(6):862-864.

89. Méndez-Ferrer S, Lucas D, Battista M, Frenette P. Haematopoietic stem cell release is regulated by circadian oscillations. *Nature*. 2008;452(7186):442-447.

90. Katayama Y, Battista M, Kao WM, et al. Signals from the sympathetic nervous system regulate hematopoietic stem cell egress from bone marrow. *Cell*. 2006;124(2):407-421. doi:10.1016/j.cell.2005.10.041.

91. Nakada D, Levi BP, Morrison SJ. Integrating Physiological Regulation with Stem Cell and Tissue Homeostasis. *Neuron*. 2011;70(4):703-718. doi:10.1016/j.neuron.2011.05.011.

92. Ding L, Morrison S. Haematopoietic stem cells and early lymphoid progenitors occupy distinct bone marrow niches. *Nature*. 2013;495(7440):231-235.

93. O'Brien C, Kreso A, Dick J. Cancer stem cells in solid tumors: an overview. *Semin Radiat Oncol*. 2009;19(2):71-77.

94. BRUCE WR, VAN DER GAAG H. A QUANTITATIVE ASSAY FOR THE NUMBER OF MURINE LYMPHOMA CELLS CAPABLE OF PROLIFERATION IN VIVO. *Nature*. 1963;199:79-80. doi:10.1038/199079a0.

95. Fialkow P, Jacobson R, Papayannopoulou T. Chronic myelocytic leukemia: clonal origin in a stem cell common to the granulocyte, erythrocyte, platelet and monocyte/macrophage. *Am J Med*. 1977;63(1):125-130.

96. Potter V. Summary of discussion on neoplasms. *Cancer Res*. 1968;28(9):1901-1907.

97. Potter V. Phenotypic diversity in experimental hepatomas: the concept of partially blocked ontogeny. The 10th Walter Hubert Lecture. *Br J Cancer*. 1978;38(1):1-23.

98. Pierce G, Wallace C. Differentiation of malignant to benign cells. *Cancer Res*. 1971;31(2):127-134.

99. Heppner GH. Tumor Heterogeneity. *Cancer Res*. 1984;44(6):2259-2265.

100. Shouval, R., L. I. Shlush, S. Yehudai-Resheff, S. Ali, N. Pery, E. Shapiro, M. Tzukerman JMR and TZ. Single cell analysis exposes intratumor heterogeneity and suggests that FLT3-ITD is a late event in leukemogenesis. *Exp Hematol*. 2014;42(6):457-463.

101. Allison KH, Sledge GW. Heterogeneity and Cancer. *Oncology (Williston Park)*. 2014;28(9):1-9. http://www.ncbi.nlm.nih.gov/pubmed/25224475.

102. Yap TA, Gerlinger M, Futreal PA, et al. Intratumor heterogeneity: seeing the wood for the trees. *Sci Transl Med*. 2012;4(127):127ps10. doi:10.1126/scitranslmed.3003854.

103. Sun X-X, Yu Q. Intra-tumor heterogeneity of cancer cells and its implications for cancer treatment. *Acta Pharmacol Sin*. 2015;36(10):1219-1227. doi:10.1038/aps.2015.92.

104. Fidler IJ and IRH. The development of biological diversity and metastatic potential in malignant neoplasms. *Oncodev Biol Med*. 1982;4(1-2):161-176.

105. Fidler IJ, Hart IR. Biological diversity in metastatic neoplasms: origins and implications. *Science (80-)*. 1982;217(4564):998-1003.

106. Grady W, Markowitz S. Genomic instability and colorectal cancer. *Curr Opin Gastroenterol*. 2000;16(1):62-67.

107. Dontu G, Abdallah WM, Foley JM, et al. In vitro propagation and transcriptional profiling of human mammary stem/progenitor cells. *Genes Dev*. 2003;17(10):1253-1270. doi:10.1101/gad.1061803.

108. Hamburger AW and SES. Primary bioassay of human tumor stem cells. *Science (80-)*. 1977;197(4302):461-463.

109. Hamburger A, Salmon S. Primary bioassay of human myeloma stem cells. *J Clin Invest*. 1977;60(4):846-854.

110. Bayani J, Selvarajah S, Maire G, et al. Genomic mechanisms and measurement of structural and numerical instability in cancer cells. *Semin Cancer Biol*. 2007;17(1):5-18.

111. Lobo, N. A., Y. Shimono DQ and MFC. The biology of cancer stem cells. *Annu Rev Cell Dev Biol*. 2007;23:675-699.

112. Bonnet D and JED. Human acute myeloid leukemia is organized as a hierarchy that originates from a primitive hematopoietic cell. *Nat Med*. 1997;3(7):730-737.

113. Goardon, N., E. Marchi, A. Atzberger, L. Quek, A. Schuh, S. Soneji, P. Woll, A. Mead, K. A. Alford, R. Rout, S. Chaudhury, A. Gilkes, S. Knapper, K. Beldjord, S. Begum, S. Rose, N. Geddes, M. Griffiths, G. Standen, A. Sternberg, J. Cavenagh, H. Hunter, D. CP and PV. Coexistence of LMPP-like and GMP-like leukemia stem cells in acute myeloid leukemia. *Cancer Cell*. 2011;19(1):138-152.

114. Garza-Treviño EN, Said-Fernández SL, Martínez-Rodríguez HG. Understanding the colon cancer stem cells and perspectives on treatment. *Cancer Cell Int*. 2015;15(1):2. doi:10.1186/s12935-015-0163-7.

115. Bozorgi A, Khazaei M, Khazaei MR. New findings on breast cancer stem cells: A review. *J Breast Cancer*. 2015;18(4):303-312. doi:10.4048/jbc.2015.18.4.303.

116. Collins AT, Berry PA, Hyde C, Stower MJ, Maitland NJ. Prospective identification of tumorigenic prostate cancer stem cells. *Cancer Res*. 2005;65(23):10946-10951. doi:10.1158/0008-5472.CAN-05-2018.

117. Buglino JA, Resh MD. Palmitoylation of Hedgehog Proteins. *Vitam Horm*. 2012;88:229-252. doi:10.1016/B978-0-12-394622-5.00010-9.

118. O'Flaherty, J. D., M. Barr, D. Fennell, D. Richard, J. Reynolds JO and KO. The cancer stem-cell hypothesis: its emerging role in lung cancer biology and its relevance for future therapy. *J Thorac Oncol*. 2012;7(12):1880-1890.

119. Singh SK, Clarke ID, Terasaki M, et al. Identification of a Cancer Stem Cell in Human Brain Tumors. *Cancer Res*. 2003;63(18):5821-5828. doi:10.1038/nature03128.

120. Fialkow PJ. Stem cell origin of human myeloid blood cell neoplasms. *Verh Dtsch Ges Pathol*. 1990;74:43-47.

121. Lapidot T, Sirard C, Vormoor J, et al. A cell initiating human acute myeloid leukaemia after transplantation into SCID mice. *Nature*. 1994;367(6464):645-648. doi:10.1038/367645a0.

122. Cozzio A, Passegué E, Ayton PM, Karsunky H, Cleary ML, Weissman IL. Similar MLL-associated leukemias arising from self-renewing stem cells and short-lived myeloid progenitors. *Genes Dev*. 2003;17(24):3029-3035. doi:10.1101/gad.1143403.

123. Krivtsov A V, Twomey D, Feng Z, et al. Transformation from committed progenitor to leukaemia stem cell initiated by MLL-AF9. *Nature*. 2006;442(7104):818-822. doi:10.1038/nature04980.

124. Somervaille T, Cleary M. Identification and characterization of leukemia stem cells in murine MLL-AF9 acute myeloid leukemia. *Cancer Cell*. 2006;10(4):257-268.

125. Jamieson C, Ailles L, Dylla S, et al. Granulocyte-macrophage progenitors as candidate leukemic stem cells in blast-crisis CML. *N Engl J Med*. 2004;351(7):657-667.

126. Alison, M. R. SML and LJN. Cancer stem cells: problems for therapy. *J Pathol*. 2011;223(2):147-161.

127. Baum CM, Weissman IL, Tsukamoto AS, Buckle AM, Peault B. Isolation of a candidate human hematopoietic stem-cell population. *Proc Natl Acad Sci U S A*. 1992;89(7):2804-2808. doi:10.1073/pnas.89.7.2804.

128. Spangrude GJ, Heimfeld S, Weissman IL. Purification and characterization of mouse hematopoietic stem cells. *Science*. 1988;241(4861):58-62. doi:10.1126/science.2898810.

129. Hope KJ, Jin L, Dick JE. Acute myeloid leukemia originates from a hierarchy of leukemic stem cell classes that differ in self-renewal capacity. *Nat Immunol*. 2004;5(7):738-743. doi:10.1038/ni1080.

130. Blair A, Sutherland H. Primitive acute myeloid leukemia cells with long-term proliferative ability in vitro and in vivo lack surface expression of c-kit (CD117). *Exp Hematol*. 2000;28(6):660-671.

131. Blair A, Hogge D, Ailles L, Lansdorp P, Sutherland H. Lack of expression of Thy-1 (CD90) on acute myeloid leukemia cells with long-term proliferative ability in vitro and in vivo. *Blood*. 1997;89(9):3104-12.

132. Sutherland H, Blair A, Zapf R. Characterization of a hierarchy in human acute myeloid leukemia progenitor cells. *Blood*. 1996;87(11):4754-4761.

133. Jordan CT, Upchurch D, Szilvassy SJ, et al. The interleukin-3 receptor alpha chain is a unique

marker for human acute myelogenous leukemia stems cells. *Leukemia*. 2000;14(10).

134. Lane SW, Gilliland DG. Leukemia stem cells. *Semin Cancer Biol*. 2010;20(2):71-76. doi:10.1016/j.semcancer.2009.12.001.

135. Buss EC, Ho AD. Leukemia stem cells. *Int J Cancer*. 2011;129(10):2328-2336. doi:10.1002/ijc.26318.

136. Blair A, Hogge D, Sutherland H. Most acute myeloid leukemia progenitor cells with long-term proliferative ability in vitro and in vivo have the phenotype CD34(+)/CD71(-)/HLA-DR-. *Blood*. 1998;92(11):325-335.

137. Brendel C, Mohr B, Schimmelpfennig C, et al. Detection of cytogenetic aberrations both in CD90 (Thy-1)-positive and (Thy-1)-negative stem cell (CD34) subfractions of patients with acute and chronic myeloid leukemias. *Leukemia*. 1999;13(11):1770-1775.

138. Huntly BJP, Gilliland DG. Leukaemia stem cells and the evolution of cancer-stem-cell research. *Nat Rev Cancer*. 2005;5(4):311-321. doi:10.1038/nrc1592.

139. Miyamoto T, Weissman IL, Akashi K. AML1/ETO-expressing nonleukemic stem cells in acute myelogenous leukemia with 8;21 chromosomal translocation. *Proc Natl Acad Sci U S A*. 2000;97(13):7521-7526. doi:10.1073/pnas.97.13.7521.

140. Martino V, Tonelli R, Montemurro L, et al. Down-regulation of MLL-AF9, MLL and MYC expression is not obligatory for monocyte-macrophage maturation in AML-M5 cell lines carrying t(9;11)(p22;q23). *Oncol Rep*. 2006;15(1):207-211.

141. Zeisig BB, Garca-Cullar MP, Winkler TH, Slany RK. The oncoprotein MLL-ENL disturbs hematopoietic lineage determination and transforms a biphenotypic lymphoid/myeloid cell. *Oncogene*. 2003;22(11):1629-1637. doi:10.1038/sj.onc.1206104.

142. Kindle KB, Collins HM, Heery DM. MOZ-TIF2-mediated destruction of CBP/p300 is blocked by calpain inhibitor 2. *Leukemia*. 2010;24(7):1359-1361. doi:10.1038/leu.2010.92.

143. Deguchi K, Ayton P, Carapeti M, et al. MOZ-TIF2-induced acute myeloid leukemia requires the MOZ nucleosome binding motif and TIF2-mediated recruitment of CBP. *Cancer Cell*. 2003;3(3):259-271.

144. Kindle K, Troke P, Collins H, et al. MOZ-TIF2 inhibits transcription by nuclear receptors and p53 by impairment of CBP function. *Mol Cell Biol*. 2005;25(3):988-1002.

145. Salesse S, Verfaillie C. BCR/ABL: from molecular mechanisms of leukemia induction to treatment of chronic myelogenous leukemia. *Oncogene*. 2002;21(56):8547-8559.

146. Huntly BJP, Shigematsu H, Deguchi K, et al. MOZ-TIF2, but not BCR-ABL, confers properties of leukemic stem cells to committed murine hematopoietic progenitors. *Cancer Cell*. 2004;6(6):587-596. doi:10.1016/j.ccr.2004.10.015.

147. Jordan CT. Searching for leukemia stem cells-Not yet the end of the road? *Cancer Cell*. 2006;10(4):253-254. doi:10.1016/j.ccr.2006.09.010.

148. Minami Y, Stuart S, Ikawa T, et al. BCR-ABL-transformed GMP as myeloid leukemic stem cells. *Proc Natl Acad Sci U S A*. 2008;105(46):17967-17972.

149. Goardon N, Marchi E, Atzberger A, et al. Coexistence of LMPP-like and GMP-like leukemia stem cells in acute myeloid leukemia. *Cancer Cell*. 2011;19(1):138-152. doi:10.1016/j.ccr.2010.12.012.

150. Estey E and HD. Acute myeloid leukaemia. *Lancet*. 2006;368(9550):1894-1907.

151. Welch J, Ley T, Link D, et al. The origin and evolution of mutations in acute myeloid leukemia. *Cell*. 2012;150(2):264-278.

152. https://www.ons.gov.uk.

153. Vardiman JW, Harris NL, Brunning RD. The World Health Organization (WHO) classification of the myeloid neoplasms. *Blood*. 2002;100(7):2292-2302. doi:10.1182/blood-2002-04-1199.

154. Arber DA, Orazi A, Hasserjian R, et al. The 2016 revision to the World Health Organization classification of myeloid neoplasms and acute leukemia. *Blood*. 2016;127(20):2391-2405. doi:10.1182/blood-2016-03-643544.

155. Kumar CC. Genetic abnormalities and challenges in the treatment of acute myeloid leukemia.

Genes Cancer. 2011;2(2):95-107. doi:10.1177/1947601911408076.

156. Mrózek K, Bloomfield CD. Chromosome aberrations, gene mutations and expression changes, and prognosis in adult acute myeloid leukemia. *Hematology Am Soc Hematol Educ Program*. 2006:169-177. doi:10.1182/asheducation-2006.1.169.

157. Grimwade D, Ivey A, Huntly BJP. Molecular landscape of acute myeloid leukemia in younger adults and its clinical relevance. *Blood*. 2016;127(1):29-41. doi:10.1182/blood-2015-07-604496.

158. Grimwade D, Hills R, Moorman A, et al. Refinement of cytogenetic classification in acute myeloid leukemia: determination of prognostic significance of rare recurring chromosomal abnormalities among 5876 younger adult patients treated in the United Kingdom Medical Research Council trials. Grimw. *Blood*. 2010;116((3):354-365.

159. Chuang L, Ito K, Ito Y. RUNX family: regulation and diversification of roles through interacting proteins. *Int J Cancer*. 2013;132:1260–1271.

160. Lam K, Zhang D. RUNX1 and RUNX1-ETO: roles in hematopoiesis and leukemogenesis. *Front Biosci*. 2012;17:1120–1139.

161. deLima M, Strom SS, Keating M, et al. Implications of potential cure in acute myelogenous leukemia: Development of subsequent cancer and return to work. *Blood*. 1997;90(12):4719-4724.

162. Estey EH. Acute myeloid leukemia: 2012 update on diagnosis, risk stratification, and management. *Am J Hematol*. 2012;87(1):89-99. doi:10.1002/ajh.22246; 10.1002/ajh.22246.

163. Coombs CC, Tavakkoli M, Tallman MS. Acute promyelocytic leukemia: where did we start, where are we now, and the future. *Blood Cancer J*. 2015;5(4):e304. doi:10.1038/bcj.2015.25.

164. Burnett AK, Russell NH, Hills RK, et al. Arsenic trioxide and all-trans retinoic acid treatment for acute promyelocytic leukaemia in all risk groups (AML17): Results of a randomised, controlled, phase 3 trial. *Lancet Oncol*. 2015;16(13):1295-1305. doi:10.1016/S1470-2045(15)00193-X.

165. Mrozek K, Heinonen K, de la Chapelle A, Bloomfield CD. Clinical significance of cytogenetics in acute myeloid leukemia. *Semin Oncol*. 1997;24(1):17-31. http://www.ncbi.nlm.nih.gov/pubmed/9045301.

166. Caligiuri M, Strout M, Lawrence D, et al. Rearrangement of ALL1 (MLL) in acute myeloid leukemia with normal cytogenetics. *Cancer Res*. 1998;58(1):55-59.

167. Lugthart S, Gröschel S, Beverloo HB, et al. Clinical, molecular, and prognostic significance of WHO type inv(3)(q21q26.2)/t(3;3)(q21;q26.2) and various other 3q abnormalities in acute myeloid leukemia. *J Clin Oncol*. 2010;28(24):3890-3898. doi:10.1200/JCO.2010.29.2771.

168. Martinelli G, Ottaviani E, Buonamici S, et al. Association of 3q21q26 syndrome with different RPN1/EVI1 fusion transcripts. *Haematologica*. 2003;88(11):1221-1228.

169. Bernstein J, Dastugue N, Haas O, et al. Nineteen cases of the t(1;22)(p13;q13) acute megakaryblastic leukaemia of infants/children and a review of 39 cases: report from a t(1;22) study group. *Leukemia*. 2000;14(1):216-218.

170. Martinez-Climent J, Lane N, Rubin C, et al. Clinical and prognostic significance of chromosomal abnormalities in childhood acute myeloid leukemia de novo. *Leukemia*. 1995;9(1):95-101.

171. Wouters BJ, Löwenberg B, Delwel R. A decade of genome-wide gene expression profiling in acute myeloid leukemia: Flashback and prospects. *Blood*. 2009;113(2):291-298. doi:10.1182/blood-2008-04-153239.

172. Falini B, Martelli MP, Bolli N, et al. Acute myeloid leukemia with mutated nucleophosmin (NPM1): Is it a distinct entity? *Blood*. 2011;117(4):1109-1120. doi:10.1182/blood-2010-08-299990.

173. Verhaak RGW, Goudswaard CS, Van Putten W, et al. Mutations in nucleophosmin (NPM1) in acute myeloid leukemia (AML): Association with other gene abnormalities and previously established gene expression signatures and their favorable prognostic significance. *Blood*. 2005;106(12):3747-3754. doi:10.1182/blood-2005-05-2168.

174. Liu Y, He P, Liu F, et al. Prognostic significance of NPM1 mutations in acute myeloid leukemia: A meta-analysis. *Mol Clin Oncol*. 2014;2:275-281. doi:10.3892/mco.2013.222.

175. Colombo E, Marine J-C, Danovi D, Falini B, Pelicci PG. Nucleophosmin regulates the stability and

transcriptional activity of p53. *Nat Cell Biol*. 2002;4(7):529-533. doi:10.1038/ncb814.

176. Okuda M, Horn HF, Tarapore P, et al. Nucleophosmin/B23 Is a Target of CDK2/Cyclin E in Centrosome Duplication. *Cell*. 2000;103(1):127-140. doi:10.1016/S0092-8674(00)00093-3.

177. Wouters B, Löwenberg B, Erpelinck-Verschueren C, van Putten W, Valk P, Delwel R. Double CEBPA mutations, but not single CEBPA mutations, define a subgroup of acute myeloid leukemia with a distinctive gene expression profile that is uniquely associated with a favorable outcome. *Blood*. 2009;113(13):3088-3091.

178. Li H-Y, Deng D-H, Huang Y, et al. Favorable prognosis of biallelic CEBPA gene mutations in acute myeloid leukemia patients: a meta-analysis. *Eur J Haematol*. 2015;94(5):439-448. doi:10.1111/ejh.12450.

179. Fasan a, Haferlach C, Alpermann T, et al. The role of different genetic subtypes of CEBPA mutated AML. *Leukemia*. 2014;28(4):794-803. doi:10.1038/leu.2013.273.

180. Levis M, Small D. FLT3: ITDoes matter in leukemia. *Leuk Off J Leuk Soc Am Leuk Res Fund, UK*. 2003;17(9):1738-1752. doi:10.1038/sj.leu.2403099.

181. Patel J, Levine R. How do novel molecular genetic markers influence treatment decisions in acute myeloid leukemia? *Ash …*. 2012;2012:28-34. doi:10.1182/asheducation-2012.1.28.

182. Griffith J, Black J, Faerman C, et al. The Structural Basis for Autoinhibition of FLT3 by the Juxtamembrane Domain. *Mol Cell*. 2004;13(2):169-178. doi:10.1016/S1097-2765(03)00505-7.

183. Yamamoto Y, Kiyoi H, Nakano Y, et al. Activating mutation of D835 within the activation loop of FLT3 in human hematologic malignancies. *Blood*. 2001;97(8):2434-2439. doi:10.1182/blood.V97.8.2434.

184. Gale RE, Green C, Allen C, et al. The impact of FLT3 internal tandem duplication mutant level, number, size, and interaction with NPM1 mutations in a large cohort of young adult patients with acute myeloid leukemia. *Blood*. 2008;111(5):2776-2784. doi:10.1182/blood-2007-08-109090.

185. Pratcorona M, Brunet S, Nomdedéu J, et al. Favorable outcome of patients with acute myeloid leukemia harboring a low-allelic burden FLT3-ITD mutation and concomitant NPM1 mutation: relevance to post-remission therapy. *Blood*. 2013;121(14):2734-2738. doi:10.1182/blood-2012-06-431122.

186. ISRCTN - ISRCTN78449203; http://www.isrctn.com/ISRCTN78449203.

187. Metzeler KH, Hummel M, Bloomfield CD, et al. An 86-probe-set gene-expression signature predicts survival in cytogenetically normal acute myeloid leukemia. *Blood*. 2008;112(10):4193-4201. doi:10.1182/blood-2008-02-134411.

188. Meshinchi S. Prevalence and prognostic significance of Flt3 internal tandem duplication in pediatric acute myeloid leukemia. *Blood*. 2001;97(1):89-94. doi:10.1182/blood.V97.1.89.

189. Mead AJ, Linch DC, Hills RK, Wheatley K, Burnett AK, Gale RE. FLT3 tyrosine kinase domain mutations are biologically distinct from and have a significantly more favorable prognosis than FLT3 internal tandem duplications in patients with acute myeloid leukemia. *Blood*. 2007;110(4):1262-1270. doi:10.1182/blood-2006-04-015826.

190. Kindler T, Lipka DB, Fischer T. FLT3 as a therapeutic target in AML: Still challenging after all these years. *Blood*. 2010;116(24):5089-5102. doi:10.1182/blood-2010-04-261867.

191. Muñoz L, Nomdedéu JF, Villamor N, et al. Acute myeloid leukemia with MLL rearrangements: clinicobiological features, prognostic impact and value of flow cytometry in the detection of residual leukemic cells. *Leuk Off J Leuk Soc Am Leuk Res Fund, UK*. 2003;17(1):76-82. doi:10.1038/sj.leu.2402708.

192. Wiederschain D, Kawai H, Shilatifard A, Yuan Z. Multiple mixed lineage leukemia (MLL) fusion proteins suppress p53-mediated response to DNA damage. *J Biol Chem*. 2005;280(26):24315-24321.

193. Krauth MT, Alpermann T, Bacher U, et al. WT1 mutations are secondary events in AML, show varying frequencies and impact on prognosis between genetic subgroups. *Leukemia*. 2015;29(3):660-667. doi:10.1038/leu.2014.243.

194. Liedtke M, Cleary ML. Therapeutic targeting of MLL. *Blood*. 2009;113(24):6061-6068. doi:10.1182/blood-2008-12-197061.

195. Wander SA, Levis MJ, Fathi AT. The evolving role of FLT3 inhibitors in acute myeloid leukemia: quizartinib and beyond. *Ther Adv Hematol*. 2014;5(3):65-77. doi:10.1177/2040620714532123.

196. Di Stasi A, Jimenez AM, Minagawa K, Al-Obaidi M, Rezvani K. Review of the results of WT1 peptide vaccination strategies for myelodysplastic syndromes and acute myeloid leukemia from nine different studies. *Front Immunol*. 2015;6(FEB). doi:10.3389/fimmu.2015.00036.

197. Godley LA, Larson RA. Therapy-Related Myeloid Leukemia. *Semin Oncol*. 2008;35(4):418-429. doi:10.1053/j.seminoncol.2008.04.012.

198. Qian Z, Fernald A a, Godley L a, Larson R a, Le Beau MM. Expression profiling of CD34+ hematopoietic stem/ progenitor cells reveals distinct subtypes of therapy-related acute myeloid leukemia. *Proc Natl Acad Sci U S A*. 2002;99:14925-14930. doi:10.1073/pnas.222491799.

199. Smith SM, Le Beau MM, Huo D, et al. Clinical-cytogenetic associations in 306 patients with therapy-related myelodysplasia and myeloid leukemia: The University of Chicago series. *Blood*. 2003;102(1):43-52. doi:10.1182/blood-2002-11-3343.

200. Walter RB, Othus M, Burnett AK, et al. Significance of FAB subclassification of "acute myeloid leukemia, NOS" in the 2008 WHO classification: analysis of 5848 newly diagnosed patients. *Blood*. 2013;121(13):2424-2431. doi:10.1182/blood-2012-10-462440.

201. Burnett AK. Treatment of acute myeloid leukemia: are we making progress? *Hematology Am Soc Hematol Educ Program*. 2012;2012(Table 1):1-6. doi:10.1182/asheducation-2012.1.1.

202. Burnett AK. The Challenge of AML in Older Patients.". *Mediterr J Hematol Infect Dis*. 2013;5(1):e2013038.

203. Cheson, B. D., J. M. Bennett, K. J. Kopecky, T. Buchner, C. L. Willman, E. H. Estey, C. A. Schiffer, H. Doehner, M. S. Tallman, T. A. Lister, F. Lo-Coco, R. Willemze, A. Biondi, W. Hiddemann, R. A. Larson, B. Lowenberg, M. A. Sanz, D. R. Head, R. Ohno, C. S o. RCTOIWG for D and LRS for TT in AM. Revised recommendations of the International Working Group for Diagnosis, Standardization of Response Criteria, Treatment Outcomes, and Reporting Standards for Therapeutic Trials in Acute Myeloid Leukemia. *J Clin Oncol*. 2003;21(24):4642-4649.

204. Burnett A. Blood 2006;108;11:10a (Abstract 18). *Blood*. 2006;108(11):10a (Abstract 18).

205. De Kouchkovsky I, Abdul-Hay M. "Acute myeloid leukemia: a comprehensive review and 2016 update." *Blood Cancer J*. 2016;6(7):e441. doi:10.1038/bcj.2016.50.

206. Beerman I, Maloney WJ, Weissmann IL, Rossi DJ. Stem cells and the aging hematopoietic system. *Curr Opin Immunol*. 2010;22(4):500-506. doi:10.1016/j.coi.2010.06.007.

207. http://asheducationbook.hematologylibrary.org.

208. Corces-Zimmerman MR, Majeti R. Pre-leukemic evolution of hematopoietic stem cells: the importance of early mutations in leukemogenesis. *Leukemia*. 2014;28(12):2276-2282. doi:10.1038/leu.2014.211.

209. Corces-Zimmerman MR, Hong W-J, Weissman IL, Medeiros BC, Majeti R. Preleukemic mutations in human acute myeloid leukemia affect epigenetic regulators and persist in remission. *Proc Natl Acad Sci U S A*. 2014;111(7):2548-2553. doi:10.1073/pnas.1324297111.

210. Shlush LI, Zandi S, Mitchell A, et al. Identification of pre-leukaemic haematopoietic stem cells in acute leukaemia. *Nature*. 2014;506(7488):328-333. doi:10.1038/nature13038.

211. Gale K, Ford A, Repp R, et al. Backtracking leukemia to birth: identification of clonotypic gene fusion sequences in neonatal blood spots. *Proc Natl Acad Sci U S A*. 1997;94(25):13950-4.

212. Papaemmanuil, E., M. Gerstung, L. Bullinger, V. I. Gaidzik, P. Paschka, N. D. Roberts, N. E. Potter, M. Heuser, F. Thol, N. Bolli, G. Gundem, P. Van Loo, I. Martincorena, P. Ganly, L. Mudie, S. McLaren, S. O'Meara, K. Raine, D. R. Jones, J. W. Teague, A. HD and PJC. Genomic Classification and Prognosis in Acute Myeloid Leukemia. *N Engl J Med*. 2016;374(23):2209-2221.

213. Genovese, G., A. K. Kahler, R. E. Handsaker, J. Lindberg, S. A. Rose, S. F. Bakhoum, K. Chambert, E. Mick, B. M. Neale, M. Fromer, S. M. Purcell, O. Svantesson, M. Landen, M. Hoglund, S. Lehmann, S. B. Gabriel, J. L. Moran, E. S. Lander, P. F. Sullivan, P CMH and SAM. Clonal hematopoiesis and blood-cancer risk inferred from blood DNA sequence. *N Engl J Med*. 2014;371(26):2477-2487.

214. Jaiswal, S., P. Fontanillas, J. Flannick, A. Manning, P. V. Grauman, B. G. Mar, R. C. Lindsley, C. H.

Mermel, N. Burtt, A. Chavez, J. M. Higgins, V. Moltchanov, F. C. Kuo, M. J. Kluk, B. Henderson, L. Kinnunen, H. A. Koistinen, C. Ladenvall, G. Getz, A. C DA and BLE. Age-related clonal hematopoiesis associated with adverse outcomes. *N Engl J Med*. 2014;371(26):2488-2498.

215. Longley D, Johnston P. Molecular mechanisms of drug resistance. *J Pathol*. 2005;205(2):275-292. doi:10.1002/path.1706.

216. Abdullah LN, Chow EK-H. Mechanisms of chemoresistance in cancer stem cells. *Clin Transl Med*. 2013;2(1):3. doi:10.1186/2001-1326-2-3.

217. Chow E. Implication of cancer stem cells in cancer drug development and drug delivery. *J Lab Autom*. 2013;18(1):6-11.

218. Fletcher JI, Haber M, Henderson MJ, Norris MD. ABC transporters in cancer: more than just drug efflux pumps. *Nat Rev Cancer*. 2010;10(2):147-156. doi:10.1038/nrc2789.

219. Cripe L, Uno H, Paietta E, et al. Zosuquidar, a novel modulator of P-glycoprotein, does not improve the outcome of older patients with newly diagnosed acute myeloid leukemia: a randomized, placebo-controlled trial of the Eastern Cooperative Oncology Group 3999. *Blood*. 2010;116(20):4077-4085.

220. Dalton WS, Crowley JJ, Salmon SS, et al. A phase III randomized study of oral verapamil as a chemosensitizer to reverse drug resistance in patients with refractory myeloma: A Southwest Oncology Group study. *Cancer*. 1995;75(3):815-820. doi:10.1002/1097-0142(19950201)75:3<815::AID-CNCR2820750311>3.0.CO;2-R.

221. Chow EK, Zhang X-Q, Chen M, et al. Nanodiamond therapeutic delivery agents mediate enhanced chemoresistant tumor treatment. *Sci Transl Med*. 2011;3(73):73ra21. doi:10.1126/scitranslmed.3001713.

222. Shapira A, Livney YD, Broxterman HJ, Assaraf YG. Nanomedicine for targeted cancer therapy: Towards the overcoming of drug resistance. *Drug Resist Updat*. 2011;14(3):150-163. doi:10.1016/j.drup.2011.01.003.

223. https://www.clinicaltrialsregister.eu.

224. Kelly PN, Strasser a. The role of Bcl-2 and its pro-survival relatives in tumourigenesis and cancer therapy. *Cell Death Differ*. 2011;18(9):1414-1424. doi:10.1038/cdd.2011.17.

225. Krajewski S, Bodrug S, Gascoyne R, Berean K, Krajewska M, Reed JC. Immunohistochemical analysis of Mcl-1 and Bcl-2 proteins in normal and neoplastic lymph nodes. *Am J Pathol*. 1994;145(3):515-525. http://www.ncbi.nlm.nih.gov/pubmed/8080035.

226. Mehta S V., Shukla SN, Vora HH. Overexpression of Bcl2 protein predicts chemoresistance in acute myeloid leukemia: Its correlation with FLT3. *Neoplasma*. 2013;60(6):666-675. doi:10.4149/neo_2013_085.

227. Mortenson MM, Galante JG, Gilad O, et al. BCL-2 functions as an activator of the AKT signaling pathway in pancreatic cancer. *J Cell Biochem*. 2007;102(5):1171-1179. doi:10.1002/jcb.21343.

228. Marinov M, Ziogas A, Pardo OE, et al. AKT/mTOR pathway activation and BCL-2 family proteins modulate the sensitivity of human small cell lung cancer cells to RAD001. *Clin Cancer Res*. 2009;15(4):1277-1287. doi:10.1158/1078-0432.ccr-08-2166.

229. Ruvolo PP, Deng X, Carr BK, May WS. A functional role for mitochondrial protein kinase Calpha in Bcl2 phosphorylation and suppression of apoptosis. *J Biol Chem*. 1998;273(39):25436-25442. doi:10.1074/jbc.273.39.25436.

230. Deng X, Ruvolo P, Carr B, May WS. Survival function of ERK1/2 as IL-3-activated, staurosporine-resistant Bcl2 kinases. *Proc Natl Acad Sci U S A*. 2000;97:1578-1583. doi:10.1073/pnas.97.4.1578.

231. Cammareri P, Scopelliti A, Todaro M, et al. Aurora-A is essential for the tumorigenic capacity and chemoresistance of colorectal cancer stem cells. *Cancer Res*. 2010;70(11):4655-4665. doi:10.1158/0008-5472.CAN-09-3953.

232. van Delft MF, Wei AH, Mason KD, et al. The BH3 mimetic ABT-737 targets selective Bcl-2 proteins and efficiently induces apoptosis via Bak/Bax if Mcl-1 is neutralized. *Cancer Cell*. 2006;10(5):389-399. doi:10.1016/j.ccr.2006.08.027.

233. Roberts AW, Davids MS, Pagel JM, et al. Targeting BCL2 with Venetoclax in Relapsed Chronic

Lymphocytic Leukemia. *N Engl J Med*. 2016;374(4):311-322. doi:10.1056/NEJMoa1513257.

234. Kalluri R. EMT: When epithelial cells decide to become mesenchymal-like cells. *J Clin Invest*. 2009;119(6):1417-1419. doi:10.1172/JCI39675.

235. Kalluri R, Weinberg RA. The basics of epithelial-mesenchymal transition. *J Clin Invest*. 2009;119(6):1420-1428. doi:10.1172/JCI39104.

236. Ayala F, Dewar R, Kieran M, Kalluri R. Contribution of bone microenvironment to leukemogenesis and leukemia progression. *Leukemia*. 2009;23(12):2233-2241. doi:10.1038/leu.2009.175.

237. Sund M, Kalluri R. Tumor stroma derived biomarkers in cancer. *Cancer Metastasis Rev*. 2009;28(1-2):177-183. doi:10.1007/s10555-008-9175-2.

238. Heerboth S, Housman G, Leary M, et al. EMT and tumor metastasis. *Clin Transl Med*. 2015;4(1):6. doi:10.1186/s40169-015-0048-3.

239. Singh A, Settleman J. EMT, cancer stem cells and drug resistance: an emerging axis of evil in the war on cancer. *Oncogene*. 2010;29(34):4741-4751. doi:10.1038/onc.2010.215.

240. C-C C, J-Y Y, J-P G, et al. Favorable clinical outcome and unique characteristics in association with Twist1 overexpression in de novo acute myeloid leukemia. *Blood Cancer J*. 2015;5(e339).

241. Cosset E, Hamdan G, Jeanpierre S, et al. Deregulation of TWIST-1 in the CD34+ compartment represents a novel prognostic factor in chronic myeloid leukemia. *Blood*. 2011;117(5):1673-1676. doi:10.1182/blood-2009-11-254680.

242. Chowdhury M, Mihara K, Yasunaga S, Ohtaki M, Takihara Y, Kimura A. Expression of Polycomb-group (PcG) protein BMI-1 predicts prognosis in patients with acute myeloid leukemia. *Leukemia*. 2007;21(5):1116-1122.

243. Pérez-Mancera PA, González-Herrero I, Pérez-Caro M, et al. SLUG in cancer development. *Oncogene*. 2005;24(19):3073-3082. doi:10.1038/sj.onc.1208505.

244. Pérez-Mancera PA, Pérez-Caro M, González-Herrero I, et al. Cancer development induced by graded expression of Snail in mice. *Hum Mol Genet*. 2005;14(22):3449-3461. doi:10.1093/hmg/ddi373.

245. Barrallo-Gimeno A, Nieto MA. The Snail genes as inducers of cell movement and survival: implications in development and cancer. *Development*. 2005;132(14):3151-3161. doi:10.1242/dev.01907.

246. Vega S, Morales A V, Ocaña OH, Valdés F, Fabregat I, Nieto MA. Snail blocks the cell cycle and confers resistance to cell death. *Genes Dev*. 2004;18(10):1131-1143. doi:10.1101/gad.294104.

247. Percio S, Coltella N, Grisanti S, Bernardi R, Pattini L. A HIF-1 network reveals characteristics of epithelial-mesenchymal transition in acute promyelocytic leukemia. *Genome Med*. 2014;6(12):84. doi:10.1186/s13073-014-0084-4.

248. Song Z, Yue W, Wei B, et al. Sonic hedgehog pathway is essential for maintenance of cancer stem-like cells in human gastric cancer. *PLoS One*. 2011;6(3). doi:10.1371/journal.pone.0017687.

249. Zhao C, Chen A, Jamieson CH, et al. Killing Hedgehog to treat CML. *Nature*. 2009;458(7239):776-779. doi:10.1038/nature07737.

250. Flis K, Irvine D, Copland M, Bhatia R, Skorski T. Chronic myeloid leukemia stem cells display alterations in expression of genes involved in oxidative phosphorylation. *Leuk Lymphoma*. 2012;53(May):1-5. doi:10.3109/10428194.2012.696313.

251. Alonso-Dominguez JM, Grinfeld J, Alikian M, et al. PTCH1 expression at diagnosis predicts imatinib failure in chronic myeloid leukaemia patients in chronic phase. *Am J Hematol*. 2015;90(1):20-26. doi:10.1002/ajh.23857.

252. Zhao C, Chen A, Jamieson CH, et al. Hedgehog signalling is essential for maintenance of cancer stem cells in myeloid leukaemia. *Nature*. 2009;458(7239):776-779. doi:10.1038/nature07737.

253. Dierks C, Beigi R, Guo G-R, et al. Expansion of Bcr-Abl-positive leukemic stem cells is dependent on Hedgehog pathway activation. *Cancer Cell*. 2008;14(3):238-249. doi:10.1016/j.ccr.2008.08.003.

254. Irvine, D. A., B. Zhang, E. K. Allan, T. L. Holyoake, M. Dorsch, P. W. Manley RB and MC. Combination of the Hedgehog Pathway Inhibitor LDE225 and Nilotinib Eliminates Chronic Myeloid

Leukemia Stem and Progenitor Cells. *Blood*. 2009;114(22):580581.

255. Campbell V, Copland M. Hedgehog signaling in cancer stem cells: a focus on hematological cancers. *Stem cells cloning*. 2015;8:27-38. doi:10.2147/SCCAA.S58613.

256. Wan J, Zhou J, Zhao H, et al. Sonic hedgehog pathway contributes to gastric cancer cell growth and proliferation. *Biores Open Access*. 2014;3(2):53-59. doi:10.1089/biores.2014.0001.

257. Katoh Y, Katoh M. Hedgehog target genes: mechanisms of carcinogenesis induced by aberrant hedgehog signaling activation. *Curr Mol Med*. 2009;9(7):873-886. doi:10.2174/156652409789105570.

258. Martin, S. T., N. Sato, S. Dhara, R. Chang, S. R. Hustinx, T. Abe AM and MG. Aberrant methylation of the Human Hedgehog interacting protein (HHIP) gene in pancreatic neoplasms. *Cancer Biol Ther*. 2005;4(7):728-733.

259. Thayer SP, di Magliano MP, Heiser PW, et al. Hedgehog is an early and late mediator of pancreatic cancer tumorigenesis. *Nature*. 2003;425(6960):851-856. doi:10.1038/nature02009.

260. Lonardo E, Hermann PC, Heeschen C. Pancreatic cancer stem cells - update and future perspectives. *Mol Oncol*. 2010;4(5):431-442. doi:10.1016/j.molonc.2010.06.002.

261. Mueller M-T, Hermann PC, Heeschen C. Cancer stem cells as new therapeutic target to prevent tumour progression and metastasis. *Front Biosci (Elite Ed)*. 2010;2:602-613. http://www.ncbi.nlm.nih.gov/pubmed/20036905.

262. Park, K. S., L. G. Martelotto, M. Peifer, M. L. Sos, A. N. Karnezis, M. R. Mahjoub, K. Bernard, J. F. Conklin, A. Szczepny, J. Yuan, R. Guo, B. Ospina, J. Falzon, S. Bennett, T. J. Brown, A. Markovic, W. L. Devereux, C. A. Ocasio, J. K. Chen, T. Stearns, CDP and JS. A crucial requirement for Hedgehog signaling in small cell lung cancer. *Nat Med*. 2011;17(11):1504-1508.

263. Watkins DN, Berman DM, Burkholder SG, Wang B, Beachy PA, Baylin SB. Hedgehog signalling within airway epithelial progenitors and in small-cell lung cancer. *Nature*. 2003;422(6929):313-317. doi:10.1038/nature01493.

264. Szkandera J, Kiesslich T, Haybaeck J, Gerger A, Pichler M. Hedgehog signaling pathway in ovarian cancer. *Int J Mol Sci*. 2013;14(1):1179-1196. doi:10.3390/ijms14011179.

265. Theunissen J-W, de Sauvage FJ. Paracrine Hedgehog signaling in cancer. *Cancer Res*. 2009;69(15):6007-6010. doi:10.1158/0008-5472.CAN-09-0756.

266. Karhadkar SS, Bova GS, Abdallah N, et al. Hedgehog signalling in prostate regeneration, neoplasia and metastasis. *Nature*. 2004;431(7009):707-712. doi:10.1097/01.ju.0000156734.69186.57.

267. Chen M, Carkner R, Buttyan R. The hedgehog/Gli signaling paradigm in prostate cancer. *Expert Rev Endocrinol Metab*. 2011;6(3):453-467. doi:10.1586/EEM.11.2.

268. Gonnissen A, Isebaert S, Haustermans K. Hedgehog signaling in prostate cancer and its therapeutic implication. *Int J Mol Sci*. 2013;14(7):13979-14007. doi:10.3390/ijms140713979.

269. Noda T, Nagano H, Takemasa I, et al. Activation of Wnt/β-catenin signalling pathway induces chemoresistance to interferon-α/5-fluorouracil combination therapy for hepatocellular carcinoma. *Br J Cancer*. 2009;100(10):1647–1658.

270. Flahaut M, Meier R, Coulon A, et al. The Wnt receptor FZD1 mediates chemoresistance in neuroblastoma through activation of the Wnt/beta-catenin pathway. *Oncogene*. 2009;28(23):2245-2256. doi:10.1038/onc.2009.80; 10.1038/onc.2009.80.

271. Chau WK, Ip CK, Mak a SC, Lai H-C, Wong a ST. c-Kit mediates chemoresistance and tumor-initiating capacity of ovarian cancer cells through activation of Wnt/β-catenin–ATP-binding cassette G2 signaling. *Oncogene*. 2012;(May):1-15. doi:10.1038/onc.2012.290.

272. Capaccione KM, Pine SR. The Notch signaling pathway as a mediator of tumor survival. *Carcinogenesis*. 2013;34(7):1420-1430. doi:10.1093/carcin/bgt127.

273. Weng AP, Aster JC. Multiple niches for Notch in cancer: Context is everything. *Curr Opin Genet Dev*. 2004;14(1):48-54. doi:10.1016/j.gde.2003.11.004.

274. Xu X, Zhao Y, Xu M, et al. Activation of Notch signal pathway is associated with a poorer prognosis in acute myeloid leukemia. *Med Oncol*. 2011;28 Suppl 1:S483-9. doi:10.1007/s12032-010-9667-0.

275. Donnem T, Andersen S, Al-shibli K, Al-Saad S, Busund L-T, Bremnes RM. Prognostic impact of Notch ligands and receptors in nonsmall cell lung cancer: coexpression of Notch-1 and vascular endothelial growth factor-A predicts poor survival. *Cancer*. 2010;116(24):5676-5685. doi:10.1002/cncr.25551.

276. Westhoff B, Colaluca IN, D'Ario G, et al. Alterations of the Notch pathway in lung cancer. *Proc Natl Acad Sci U S A*. 2009;106(52):22293-22298. doi:10.1073/pnas.0907781106.

277. Reedijk M. Notch signaling and breast cancer. *Adv Exp Med Biol*. 2012;727:241-257. doi:10.1007/978-1-4614-0899-4_18.

278. Stylianou S, Clarke RB, Brennan K. Aberrant activation of Notch signaling in human breast cancer. *Cancer Res*. 2006;66(3):1517-1525. doi:10.1158/0008-5472.CAN-05-3054.

279. McAuliffe SM, Morgan SL, Wyant GA, et al. Targeting Notch, a key pathway for ovarian cancer stem cells, sensitizes tumors to platinum therapy. *Proc Natl Acad Sci U S A*. 2012;109(43):E2939-48. doi:10.1073/pnas.1206400109.

280. Ulasov I V, Nandi S, Dey M, Sonabend AM, Lesniak MS. Inhibition of Sonic hedgehog and Notch pathways enhances sensitivity of CD133(+) glioma stem cells to temozolomide therapy. *Mol Med*. 2011;17(1-2):103-112. doi:10.2119/molmed.2010.00062.

281. Purow BW, Haque RM, Noel MW, et al. Expression of Notch-1 and its ligands, Delta-like-1 and Jagged=1, is critical for glioma cell survival and proliferation. *Cancer Res*. 2005;65(6):2353-2363. doi:10.1158/0008-5472.CAN-04-1890.

282. Meng RD, Shelton CC, Li YM, et al. ??-secretase inhibitors abrogate oxaliplatin-induced activation of the Notch-1 signaling pathway in colon cancer cells resulting in enhanced chemosensitivity. *Cancer Res*. 2009;69(2):573-582. doi:10.1158/0008-5472.CAN-08-2088.

283. Liu C, Li Z, Bi L, et al. NOTCH1 signaling promotes chemoresistance via regulating ABCC1 expression in prostate cancer stem cells. *Mol Cell Biochem*. 2014;393(1-2):265-270. doi:10.1007/s11010-014-2069-4.

284. Yu HG, Ai YW, Yu LL, et al. Phosphoinositide 3-kinase/Akt pathway plays an important role in chemoresistance of gastric cancer cells against etoposide and doxorubicin induced cell death. *Int J Cancer*. 2008;122(2):433-443. doi:10.1002/ijc.23049.

285. Zuolo G, Minoia M, Gentilin E, et al. GH induces chemoresistance in human endometrial cancer cell lines involving ERK 1/2 and PKCdelta. *Endocr Abstr*. 2014;35.

286. Li B, Li J, Wen Xu W, et al. Suppression of esophageal tumor growth and chemoresistance by directly targeting the PI3K/AKT pathway. *Oncotarget*. 2014;5(22):11576-11587. doi:10.18632/oncotarget.2596.

287. Xiao ZM, Wang XY, Wang AM. Periostin induces chemoresistance in colon cancer cells through activation of the PI3K/Akt/survivin pathway. *Biotechnol Appl Biochem*. 2015;62(3):401-406. doi:10.1002/bab.1193.

288. Liu SQ, Yu JP, Yu HG, Lv P, Chen H l. Activation of Akt and ERK signalling pathways induced by etoposide confer chemoresistance in gastric cancer cells. *Dig Liver Dis*. 2006;38(5):310-318. doi:10.1016/j.dld.2006.01.012.

289. Chen D, Xie D, Guo S, et al. ERK signaling pathway may induce gemcitabine chemoresistance in pancreatic cancer cell line SW1990 by regulating the expression of mdr-1 and RRM1 gene. *Chinese-German J Clin Oncol*. 2009;8(37).

290. Yip NC, Fombon IS, Liu P, et al. Disulfiram modulated ROS-MAPK and NFκB pathways and targeted breast cancer cells with cancer stem cell-like properties. *Br J Cancer*. 2011;104(10):1564-1574. doi:10.1038/bjc.2011.126.

291. Perkins ND. The diverse and complex roles of NF-κB subunits in cancer. *Nat Rev Cancer*. 2012;12(2):121-132. doi:10.1038/nrc3204.

292. Alvero AB, Chen R, Fu H-H, et al. Molecular phenotyping of human ovarian cancer stem cells unravels the mechanisms for repair and chemoresistance. *Cell Cycle*. 2009;8(1):158-166. doi:10.4161/cc.8.1.7533.

293. Leizer AL, Alvero AB, Fu HH, et al. Regulation of inflammation by the NF-κB pathway in ovarian cancer stem cells. *Am J Reprod Immunol*. 2011;65(4):438-447. doi:10.1111/j.1600-0897.2010.00914.x.

294. Gallmeier E, Hermann PC, Mueller MT, et al. Inhibition of ataxia telangiectasia- and Rad3-related function abrogates the in vitro and in vivo tumorigenicity of human colon cancer cells through depletion of the CD133+ tumor-initiating cell fraction. *Stem Cells*. 2011;29(3):418-429. doi:10.1002/stem.595.

295. Venkatesha VA, Parsels LA, Parsels JD, et al. Sensitization of pancreatic cancer stem cells to gemcitabine by Chk1 inhibition. *Neoplasia*. 2012;14(6):519-525. doi:10.1593/neo.12538.

296. Sakurikar N, Eastman A. Will targeting Chk1 have a role in the future of cancer therapy? *J Clin Oncol*. 2015;33(9):1075-1077.

297. Sakurikar N, Thompson R, Montano R, Eastman A. A subset of cancer cell lines is acutely sensitive to the Chk1 inhibitor MK-8776 as monotherapy due to CDK2 activation in S phase. *Oncotarget*. 2016;7(2):1380-1394. doi:10.18632/oncotarget.6364.

298. Thompson R, Eastman A. The cancer therapeutic potential of Chk1 inhibitors: How mechanistic studies impact on clinical trial design. *Br J Clin Pharmacol*. 2013;76(3):358-369. doi:10.1111/bcp.12139.

299. Haidar M a, Kantarjian H, Manshouri T, et al. ATM gene deletion in patients with adult acute lymphoblastic leukemia. *Cancer*. 2000;88:1057-1062. doi:10.1002/(SICI)1097-0142(20000301)88:5<1057::AID-CNCR16>3.0.CO;2-6.

300. Ripolles L, Ortega M, Ortuno F, et al. Genetic abnormalities and clinical outcome in chronic lymphocytic leukemia. *Cancer Genet Cytogenet*. 2006;171(1):57-64. doi:10.1016/j.cancergencyto.2006.07.006.

301. Salimi M, Mozdarani H, Majidzadeh K. Expression pattern of ATM and cyclin D1 in ductal carcinoma, normal adjacent and normal breast tissues of Iranian breast cancer patients. *Med Oncol*. 2012;29(3):1502-1509. doi:10.1007/s12032-011-0043-5.

302. Seshagiri S. The burden of faulty proofreading in colon cancer. *Nat Genet*. 2013;45(10):121-122. doi:10.1038/ng.2540.

303. Ding L, Getz G, Wheeler DA, et al. Somatic mutations affect key pathways in lung adenocarcinoma. *Nature*. 2008;455(7216):1069-1075. doi:10.1038/nature07423.

304. Bertoni F, Codegoni AM, Furlan D, Tibiletti MG, Capella C, Broggini M. CHK1 frameshift mutations in genetically unstable colorectal and endometrial cancers. *Genes Chromosom Cancer*. 1999;26(2):176-180. doi:10.1002/(SICI)1098-2264(199910)26:2<176::AID-GCC11>3.0.CO;2-3.

305. Vassileva V, Millar A, Briollais L, Chapman W, Bapat B. Genes involved in DNA repair are mutational targets in endometrial cancers with microsatellite instability. *Cancer Res*. 2002;62(14):4095-4099.

306. Menoyo A, Alazzouzi H, Espín E, Armengol M, Yamamoto H, Schwartz S. J. Somatic mutations in the DNA damage-response genes ATR and CHK1 in sporadic stomach tumors with microsatellite instability. *Cancer Res*. 2001;61(21):7727-7730.

307. Zighelboim I, Schmidt AP, Gao F, et al. ATR mutation in endometrioid endometrial cancer is associated with poor clinical outcomes. *J Clin Oncol*. 2009;27(19):3091. doi:10.1200/JCO.2008.19.9802.A.

308. Guarini A, Marinelli M, Tavolaro S, et al. Atm gene alterations in chronic lymphocytic leukemia patients induce a distinct gene expression profile and predict disease progression. *Haematologica*. 2012;97(1):47-55. doi:10.3324/haematol.2011.049270.

309. Khatib Z, Matsushime H, Valentine M, Shapiro D, Sherr C, Look A. Coamplification of the CDK4 gene with MDM2 and GLI in human sarcomas. *Cancer Res*. 1993;53(22):5535-5541.

310. Knudsen ES, Knudsen KE. Tailoring to RB: tumour suppressor status and therapeutic response. *Nat Rev Cancer*. 2008;8(9):714-724. doi:10.1038/nrc2401.

311. Kollareddy M, Dzubak P, Zheleva D, Hajduch M. Aurora kinases: structure, functions and their association with cancer. *Biomed Pap Med Fac Univ Palack??, Olomouc, Czechoslov*. 2008;152(1):27-33. doi:10.5507/bp.2008.004.

312. Kollareddy M, Zheleva D, Dzubak P, Brahmkshatriya PS, Lepsik M, Hajduch M. Aurora kinase inhibitors: Progress towards the clinic. *Invest New Drugs*. 2012;30(6):2411-2432. doi:10.1007/s10637-012-9798-6.

313. Tanaka T, Kimura M, Matsunaga K, Fukada D, Mori H, Okano Y. Centrosomal kinase AIK1 is overexpressed in invasive ductal carcinoma of the breast. *Cancer Res*. 1999;59(9):2041-2044.

314. Sakakura C, Hagiwara A, Yasuoka R, et al. Tumour-amplified kinase BTAK is amplified and overexpressed in gastric cancers with possible involvement in aneuploid formation. *Br J Cancer*. 2001;84(6):824-831. doi:10.1054/bjoc.2000.1684.

315. Goepfert TM, Adigun YE, Zhong L, Gay J, Medina D, Brinkley WR. Centrosome amplification and overexpression of aurora A are early events in rat mammary carcinogenesis. *Cancer Res*. 2002;62(14):4115-4122.

316. Bavetsias V, Linardopoulos S. Aurora Kinase Inhibitors: Current Status and Outlook. *Front Oncol*. 2015;5. doi:10.3389/fonc.2015.00278.

317. Egger G, Liang G, Aparicio A, Jones P a. Epigenetics in human disease and prospects for epigenetic therapy. *Nature*. 2004;429(6990):457-463. doi:10.1038/nature02625.

318. Abdel-Wahab O, Levine RL. Mutations in epigenetic modifiers in the pathogenesis and therapy of acute myeloid leukemia. *Blood*. 2013;121(18):3563-3572. doi:10.1182/blood-2013-01-451781.

319. Fong CY, Gilan O, Lam EYN, et al. BET inhibitor resistance emerges from leukaemia stem cells. *Nature*. 2015;525(7570):538-+. doi:10.1038/nature14888.

320. Ley TJ, Ding L, Walter MJ, et al. DNMT3A mutations in acute myeloid leukemia. *N Engl J Med*. 2010;363(25):2424-2433. doi:10.1056/NEJMoa1005143.

321. Guryanova OA, Shank K, Luciani L, et al. Leukemia-associated DNMT3A R882 mutations and their role in anthracycline-induced DNA damage response and therapeutic resistance. In: *Proceedings of the AACR Special Conference: Cancer Susceptibility and Cancer Susceptibility Syndromes; Jan 29-Feb 1, 2014; San Diego, CA. Philadelphia (PA): AACR; Cancer Res*. Vol 74. ; 2014:Abstract 44. doi:10.1158/1538-7445.CANSUSC14-44.

322. Metzeler KH, Maharry K, Radmacher MD, et al. TET2 mutations improve the new European LeukemiaNet risk classification of acute myeloid leukemia: a Cancer and Leukemia Group B study. *J Clin Oncol*. 2011;29(10):1373-1381. doi:JCO.2010.32.7742 [pii]\r10.1200/JCO.2010.32.7742.

323. Marcucci G, Maharry K, Wu YZ, et al. IDH1 and IDH2 gene mutations identify novel molecular subsets within de novo cytogenetically normal acute myeloid leukemia: A cancer and leukemia group B study. *J Clin Oncol*. 2010;28(14):2348-2355. doi:10.1200/JCO.2009.27.3730.

324. Marcucci G, Haferlach T, Dohner H. Molecular genetics of adult acute myeloid leukemia: prognostic and therapeutic implications. *J Clin Oncol*. 2011;29(5):475-486. doi:JCO.2010.30.2554 [pii]\r10.1200/JCO.2010.30.2554.

325. Abbas S, Lugthart S, Kavelaars FG, et al. Acquired mutations in the genes encoding IDH1 and IDH2 both are recurrent aberrations in acute myeloid leukemia: Prevalence and prognostic value. *Blood*. 2010;116(12):2122-2126. doi:10.1182/blood-2009-11-250878.

326. Song WF, Wang L, Huang WY, Cai X, Cui JJ, Wang LW. MiR-21 upregulation induced by promoter zone histone acetylation is associated with chemoresistance to gemcitabine and enhanced malignancy of pancreatic cancer cells. *Asian Pacific J Cancer Prev*. 2013;14(12):7529-7536. doi:10.7314/APJCP.2013.14.12.7529.

327. Alzoubi S, Brody L, Rahman S, et al. Synergy between histone deacetylase inhibitors and DNA-damaging agents is mediated by histone deacetylase 2 in colorectal cancer. *Oncotarget*. 2016;7(28):44505-44521.

328. Ali M, Cacan E, Liu Y, et al. Transcriptional Suppression, DNA Methylation, and Histone Deacetylation of the Regulator of G-Protein Signaling 10 (RGS10) Gene in Ovarian Cancer Cells. *PLoS One*. 2013;8(3):e60185.

329. Nusslein-Volhard C and EW. Mutations affecting segment number and polarity in Drosophila. *Nature*. 1980;287(5785):795-801.

330. Ingham PW and APM. Hedgehog signaling in animal development: paradigms and principles. *Genes Dev*. 2001;15(23):3059-3087.

331. Ingham PW and MP. Orchestrating ontogenesis: variations on a theme by sonic hedgehog. *Nat Rev Genet*. 2006;7(11):841-850.

332. Cridland SO, Keys JR, Papathanasiou P, Perkins AC. Indian hedgehog supports definitive erythropoiesis. *Blood Cells, Mol Dis*. 2009;43(2):149-155. doi:10.1016/j.bcmd.2009.04.004.

333. Bitgood MJ, Shen L, McMahon a P. Sertoli cell signaling by Desert hedgehog regulates the male germline. *Curr Biol*. 1996;6(3):298-304. doi:10.1016/S0960-9822(02)00480-3.

334. Lee JJ, Ekker SC, von Kessler DP, Porter J a, Sun BI, Beachy P a. Autoproteolysis in hedgehog protein biogenesis. *Science*. 1994;266(5190):1528-1537. doi:10.1126/science.7985023.

335. Porter J a, von Kessler DP, Ekker SC, et al. The product of hedgehog autoproteolytic cleavage active in local and long-range signalling. *Nature*. 1995;374(6520):363-366. doi:10.1038/374363a0.

336. Porter J a, Young KE, Beachy P a. Cholesterol modification of hedgehog signaling proteins in animal development. *Science*. 1996;274(5285):255-259. doi:10.1126/science.274.5285.255.

337. Rohatgi R, Milenkovic L, Scott MP. Patched1 regulates hedgehog signaling at the primary cilium. *Science (80-)*. 2007;317(5836):372-376. doi:10.1126/science.1139740.

338. Taipale J, Cooper MK, Maiti T, Beachy PA. Patched acts catalytically to suppress the activity of Smoothened. *Nature*. 2002;418(6900):892-897. doi:10.1038/nature00989.

339. Tukachinsky H, Lopez L V., Salic A. A mechanism for vertebrate Hedgehog signaling: Recruitment to cilia and dissociation of SuFu-Gli protein complexes. *J Cell Biol*. 2010;191(2):415-428. doi:10.1083/jcb.201004108.

340. Humke EW, Dorn K V., Milenkovic L, Scott MP, Rohatgi R. The output of Hedgehog signaling is controlled by the dynamic association between Suppressor of Fused and the Gli proteins. *Genes Dev*. 2010;24(7):670-682. doi:10.1101/gad.1902910.

341. Barzi M, Berenguer J, Menendez A, Alvarez-Rodriguez R, Pons S. Sonic-hedgehog-mediated proliferation requires the localization of PKA to the cilium base. *J Cell Sci*. 2010;123:62-69. doi:10.1242/jcs.060020.

342. Ruiz i Altaba A, Mas C, Stecca B. The Gli code: an information nexus regulating cell fate, stemness and cancer. *Trends Cell Biol*. 2007;17(9):438-447. doi:10.1016/j.tcb.2007.06.007.

343. Dai P, Akimaru H, Tanaka Y, Maekawa T, Nakafuku M, Ishii S. Sonic hedgehog-induced activation of the Gli1 promoter is mediated by GLI3. *J Biol Chem*. 1999;274(12):8143-8152. doi:10.1074/jbc.274.12.8143.

344. Bhardwaj, G., B. Murdoch, D. Wu, D. P. Baker, K. P. Williams, K. Chadwick, L. E. Ling FNK and MB. Sonic hedgehog induces the proliferation of primitive human hematopoietic cells via BMP regulation. *Nat Immunol*. 2001;2(2):172-180.

345. Sasaki H, Nishizaki Y, Hui C, Nakafuku M, Kondoh H. Regulation of Gli2 and Gli3 activities by an amino-terminal repression domain: implication of Gli2 and Gli3 as primary mediators of Shh signaling. *Development*. 1999;126(17):3915-3924. doi:10.1038/386735a0.

346. Chuang PT, McMahon AP. Vertebrate Hedgehog signalling modulated by induction of a Hedgehog-binding protein. *Nature*. 1999;397(6720):617-621. doi:10.1038/17611.

347. Chen MH, Wilson CW, Li YJ, et al. Cilium-independent regulation of Gli protein function by Sufu in Hedgehog signaling is evolutionarily conserved. *Genes Dev*. 2009;23(16):1910-1928. doi:10.1101/gad.1794109.

348. Irvine DA, Copland M. Targeting hedgehog in hematologic malignancy. *Blood*. 2012;119(10):2196-2204. doi:10.1182/blood-2011-10-383752.

349. Jenkins D. Hedgehog signalling: emerging evidence for non-canonical pathways. *Cell Signal*. 2009;21(7):1023-1034.

350. Brennan D, Chen X, Cheng L, Mahoney M, Riobo NA. Noncanonical Hedgehog Signaling. *Vitam Horm*. 2012;88:55-72. doi:10.1016/B978-0-12-394622-5.00003-1.

351. Chinchilla P, Xiao L, Kazanietz M, Riobo N. Hedgehog proteins activate pro-angiogenic responses in endothelial cells through non-canonical signaling pathways. *Cell Cycle*. 2010;9(3):570-579.

352. Bredesen DE, Mehlen P, Rabizadeh S. Apoptosis and dependence receptors: a molecular basis for cellular addiction. *Physiol Rev*. 2004;84(2):411-430. doi:10.1152/physrev.00027.2003.

353. Thibert C, Teillet M-A, Lapointe F, Mazelin L, Le Douarin NM, Mehlen P. Inhibition of neuroepithelial patched-induced apoptosis by sonic hedgehog. *Science*. 2003;301(5634):843-846. doi:10.1126/science.1085405.

354. Barnes E a, Kong M, Ollendorff V, Donoghue DJ. Patched1 interacts with cyclin B1 to regulate cell cycle progression. *EMBO J*. 2001;20(9):2214-2223. doi:10.1093/emboj/20.9.2214.

355. Jiang X, Yang P, Ma L. Kinase activity-independent regulation of cyclin pathway by GRK2 is essential for zebrafish early development. *Proc Natl Acad Sci U S A*. 2009;106(25):10183-10188. doi:10.1073/pnas.0812105106.

356. Renault MA, Roncalli J, Tongers J, et al. The hedgehog transcription factor Gli3 modulates angiogenesis. *Circ Res*. 2009;105(8):818-826. doi:10.1161/CIRCRESAHA.109.206706.

357. Charron F, Tessier-Lavigne M. Novel brain wiring functions for classical morphogens: a role as graded positional cues in axon guidance. *Development*. 2005;132(10):2251-2262. doi:10.1242/dev.01830.

358. Nybakken K, Vokes S a, Lin T-Y, McMahon AP, Perrimon N. A genome-wide RNA interference screen in Drosophila melanogaster cells for new components of the Hh signaling pathway. *Nat Genet*. 2005;37(12):1323-1332. doi:10.1038/ng1682.

359. Varjosalo M, Björklund M, Cheng F, et al. Application of Active and Kinase-Deficient Kinome Collection for Identification of Kinases Regulating Hedgehog Signaling. *Cell*. 2008;133(3):537-548. doi:10.1016/j.cell.2008.02.047.

360. Lum L, Yao S, Mozer B, et al. Identification of Hedgehog pathway components by RNAi in Drosophila cultured cells. *Science (80-)*. 2003;299(5615):2039-2045.

361. Kuo G, Arnaud L, Kronstad-O'Brien P, Cooper JA. Absence of Fyn and Src causes a reeler-like phenotype. *J Neurosci*. 2005;25:8578–8586.

362. Trowbridge JJ, Scott MP, Bhatia M. Hedgehog modulates cell cycle regulators in stem cells to control hematopoietic regeneration. *Proc Natl Acad Sci U S A*. 2006;103:14134-14139. doi:10.1073/pnas.0604568103.

363. Gao, J., S. Graves, U. Koch, S. Liu, V. Jankovic, S. Buonamici, A. El Andaloussi, S. D. Nimer, B. L. Kee, R. Taichman FR and IA. Hedgehog signaling is dispensable for adult hematopoietic stem cell function. *Cell Stem Cell*. 2009;4(6):548-558.

364. Dierks C, Grbic J, Zirlik K, et al. Essential role of stromally induced hedgehog signaling in B-cell malignancies. *Nat Med*. 2007;13(8):944-951. doi:10.1038/nm1614.

365. Cohen DJ. Targeting the hedgehog pathway: role in cancer and clinical implications of its inhibition. *Hematol Oncol Clin North Am*. 2012;26(3):565-588, viii.

366. Hofmann, I., E. H. Stover, D. E. Cullen, J. Mao, K. J. Morgan, B. H. Lee, M. G. Kharas, P. G. Miller, M. G. Cornejo, R. Okabe, S. A. Armstrong, N. Ghilardi, S. Gould, F. J. de Sauvage APM and DGG. Hedgehog signaling is dispensable for adult murine hematopoietic stem cell function and hematopoiesis. *Cell Stem Cell*. 2009;4(6):559-567.

367. Xie J, Murone M, Luoh SM, et al. Activating Smoothened mutations in sporadic basal-cell carcinoma. *Nature*. 1998;391(January):90-92. doi:10.1038/34201.

368. Berman, D. M., S. S. Karhadkar, A. R. Hallahan, J. I. Pritchard, C. G. Eberhart, D. N. Watkins, J. K. Chen, M. K. Cooper, J. Taipale JMO and PAB. Medulloblastoma growth inhibition by hedgehog pathway blockade. *Science (80-)*. 2002;297(5586):1559-1561.

369. Slade, I., A. Murray, S. Hanks, A. Kumar, L. Walker, D. Hargrave, J. Douglas, C. Stiller LI and NR. Heterogeneity of familial medulloblastoma and contribution of germline PTCH1 and SUFU mutations to sporadic medulloblastoma. *Fam Cancer*. 2011;10(2):337-342.

370. Shahi, M. H. AL and JSC. Hedgehog signalling in medulloblastoma, glioblastoma and neuroblastoma. *Oncol Rep*. 2008;19(3):681-688.

371. Car, D., M. Sabol, V. Musani PO and SL. Epigenetic regulation of the Hedgehog-Gli signaling pathway in cancer. *Period Biol*. 2010;112(4):419-423.

372. Ochs, M., J. Farrar, M. Considine, R. E. Ries, L. R. Trevino, T. A. Alonzo, J. Guidry-Auvil, T. M. Davidsen, P. Gesuwan, D. M. Muzny, A. S. Gamis, D. A. Wheeler, H. L. Helton, M. A. Smith, D. S.

Gerhard SM and RJA. Genome Wide Promoter Methylation Patterns Predict AML Subtype Outcomes and Identify Novel Pathways Characterizing Diagnostic and Relapsed Disease in Children. *Blood*. 2012;120(21).

373. Scales SJ and FJ de S. Mechanisms of Hedgehog pathway activation in cancer and implications for therapy. *Trends Pharmacol Sci*. 2009;30(6):303-312.

374. Blotta S, Jakubikova J, Calimeri T, et al. Canonical and noncanonical hedgehog pathway in the pathogenesis of multiple myeloma. *Blood*. 2012;120(25):5002-5013. doi:10.1182/blood-2011-07-368142.

375. Kobune, M., Y. Ito, Y. Kawano, K. Sasaki, H. Uchida, K. Nakamura, H. Dehari, H. Chiba, R. Takimoto, T. Matsunaga, T. Terui, J. Kato YN and HH. Indian hedgehog gene transfer augments hematopoietic support of human stromal cells including NOD/SCID-beta2m-/- repopulating cells. *Blood*. 2004;104(4):1002-1009.

376. Kobune, M., J. Kato, Y. Kawano, K. Sasaki, H. Uchida, K. Takada, S. Takahashi RT and YN. Adenoviral vector-mediated transfer of the Indian hedgehog gene modulates lymphomyelopoiesis in vivo. *Stem Cells*. 2008;26(2):534-542.

377. Kobune M, Takimoto R, Murase K, et al. Drug resistance is dramatically restored by hedgehog inhibitors in CD34+ leukemic cells. *Cancer Sci*. 2009;100(5):948-955. doi:10.1111/j.1349-7006.2009.01111.x.

378. Wellbrock J, Latuske E, Kohler J, et al. Expression of hedgehog pathway mediator GLI represents a negative prognostic marker in human acute myeloid leukemia and its inhibition exerts Antileukemic effects. *Clin Cancer Res*. 2015;21(10):2388-2398. doi:10.1158/1078-0432.CCR-14-1059.

379. Zahreddine HA, Culjkovic-Kraljacic B, Assouline S, et al. The sonic hedgehog factor GLI1 imparts drug resistance through inducible glucuronidation. *Nature*. 2014;511(7507):90-93. doi:10.1038/nature13283.

380. Campbell, V., E. Tholouli, M. T. Quigley, J. Keilty, P. Kelly, K. McGovern, M. Read JLK and RB. Evidence That Activated Hedgehog Signaling Predicts for Poor Clinical Outcome in Acute Myeloid Leukemia. *Blood*. 2012;120(21).

381. Valk, P. J., R. G. Verhaak, M. A. Beijen, C. A. Erpelinck, S. Barjesteh van Waalwijk van Doorn-Khosrovani, J. M. Boer, H. B. Beverloo, M. J. Moorhouse, P. J. van der Spek BL and RD. Prognostically useful gene-expression profiles in acute myeloid leukemia. *N Engl J Med*. 2004;350(16):1617-1628.

382. Stirewalt DL, Meshinchi S, Kopecky KJ, et al. Identification of genes with abnormal expression changes in acute myeloid leukemia. *Genes, Chromosom {&} Cancer*. 2008;47(1):8-20. doi:10.1002/gcc.20500.

383. Fukushima, N., Y. Minami, F. Hayakawa, H. Kiyoi, A. Sadarangani CHMJ and TN. Treatment With Hedgehog Inhibitor, PF-04449913, Attenuates Leukemia-Initiation Potential In Acute Myeloid Leukemia Cells. *Blood*. 2013;122(21).

384. Kim J, Lee JJ, Kim J, Gardner D, Beachy P a. Arsenic antagonizes the Hedgehog pathway by preventing ciliary accumulation and reducing stability of the Gli2 transcriptional effector. *Proc Natl Acad Sci U S A*. 2010;107(30):13432-13437. doi:10.1073/pnas.1006822107.

385. Cooper MK, Porter JA, Young KE, Beachy PA. Teratogen-mediated inhibition of target tissue response to Shh signaling. *Science (80-)*. 1998;280(5369):1603-1607. doi:10.1126/science.280.5369.1603.

386. Firestone AJ, Weinger JS, Maldonado M, et al. Small-molecule inhibitors of the AAA+ ATPase motor cytoplasmic dynein. *Nature*. 2012;484(7392):125-129. doi:10.1038/nature10936.

387. Chen JK, Taipale J, Cooper MK, Beachy PA. Inhibition of Hedgehog signaling by direct binding of cyclopamine to Smoothened. *Genes Dev*. 2002;16(21):2743-2748. doi:10.1101/gad.1025302.

388. Lauth M, Bergström Å. Inhibition of GLI-mediated transcription and tumor cell growth by small-molecule antagonists. *Proc …*. 2007;104(20):8455-8460. doi:10.1073/pnas.0609699104.

389. Hyman JM, Firestone AJ, Heine VM, et al. Small-molecule inhibitors reveal multiple strategies for Hedgehog pathway blockade. *Proc Natl Acad Sci U S A*. 2009;106(33):14132-14137. doi:10.1073/pnas.0907134106.

390. Kim J, Tang JY, Gong R, et al. Itraconazole, a Commonly Used Antifungal that Inhibits Hedgehog Pathway Activity and Cancer Growth. *Cancer Cell*. 2010;17(4):388-399. doi:10.1016/j.ccr.2010.02.027.

391. Lee J, Wu X, Di Magliano MP, et al. A small-molecule antagonist of the Hedgehog signaling pathway. *ChemBioChem*. 2007;8(16):1916-1919. doi:10.1002/cbic.200700403.

392. Manetti F, Faure H, Roudaut H, et al. Virtual screening-based discovery and mechanistic characterization of the acylthiourea MRT-10 family as smoothened antagonists. *Mol Pharmacol*. 2010;78(4):658-665. doi:10.1124/mol.110.065102.

393. Rohner a., Spilker ME, Lam JL, et al. Effective Targeting of Hedgehog Signaling in a Medulloblastoma Model with PF-5274857, a Potent and Selective Smoothened Antagonist That Penetrates the Blood-Brain Barrier. *Mol Cancer Ther*. 2012;11(1):57-65. doi:10.1158/1535-7163.MCT-11-0691.

394. Stanton BZ, Peng LF. Small-molecule modulators of the Sonic Hedgehog signaling pathway. *Mol Biosyst*. 2010;6(1):44-54. doi:10.1039/b910196a.

395. Petrova E, Rios-Esteves J, Ouerfelli O, Glickman JF, Resh MD. Inhibitors of Hedgehog acyltransferase block Sonic Hedgehog signaling. *Nat Chem Biol*. 2013;9(4):247-249. doi:10.1038/nchembio.1184.

396. Wang Y, Arvanites AC, Davidow L, et al. Selective identification of hedgehog pathway antagonists by direct analysis of smoothened ciliary translocation. *ACS Chem Biol*. 2012;7(6):1040-1048. doi:10.1021/cb300028a.

397. Incardona JP, Gaffield W, Lange Y, et al. Cyclopamine inhibition of Sonic hedgehog signal transduction is not mediated through effects on cholesterol transport. *Dev Biol*. 2000;224(2):440-452. doi:10.1006/dbio.2000.9775.

398. http://mct.aacrjournals.org/cgi/content/meeting_abstract/8/12_MeetingAbstracts/B192.

399. Wong H, Alicke B, West KA, et al. Pharmacokinetic-pharmacodynamic analysis of vismodegib in preclinical models of mutational and ligand-dependent Hedgehog pathway activation. *Clin Cancer Res*. 2011;17(14):4682-4692. doi:10.1158/1078-0432.CCR-11-0975.

400. Peluso MO, Campbell VT, Harari JA, et al. Impact of the smoothened inhibitor, IPI-926, on smoothened ciliary localization and hedgehog pathway activity. *PLoS One*. 2014;9(3). doi:10.1371/journal.pone.0090534.

401. Pan S, Wu X, Jiang J, et al. Discovery of NVP-LDE225, a Potent and Selective Smoothened Antagonist. *ACS Med Chem Lett*. 2010;1(3):130-134.

402. http://cancerres.aacrjournals.org/cgi/content/short/71/8_MeetingAbstracts/2819.

403. Munchhof MJ, Li Q, Shavnya A, et al. Discovery of PF-04449913, a potent and orally bioavailable inhibitor of smoothened. *ACS Med Chem Lett*. 2012;3(2):106-111. doi:10.1021/ml2002423.

404. Shah NP, Cortes JE, Martinelli G, et al. Dasatinib Plus Smoothened (SMO) Inhibitor BMS-833923 in Chronic Myeloid Leukemia (CML) with Resistance or Suboptimal Response to a Prior Tyrosine Kinase Inhibitor (TKI): Phase I Study CA180323. *Blood*. 2014;124(21):4539. http://www.bloodjournal.org/content/124/21/4539.abstract.

405. Trudel G, Paliwal P, Lainas I. Dasatinib plus SMO antagonist versus dasatinib alone for treating patients (pts) with newly diagnosed Philadelphia chromosome-positive (Ph+) chronic myeloid leukemia in chronic phase (CML-CP): Design of CA180-363, a phase II, open-label randomized trial. *J Clin Oncol*. 2012.

406. Sasaki K, Gotlib JR, Mesa RA, et al. Phase II evaluation of IPI-926, an oral Hedgehog inhibitor, in patients with myelofibrosis. *Leuk Lymphoma*. 2015;56(7):2092-2097. doi:10.3109/10428194.2014.984703.

407. Martinelli G, Oehler VG, Papayannidis C, et al. Treatment with PF-04449913, an oral smoothened antagonist, in patients with myeloid malignancies: A phase 1 safety and pharmacokinetics study. *Lancet Haematol*. 2015;2(8):e339-e346. doi:10.1016/S2352-3026(15)00096-4.

408. Assouline S, Culjkovic B, Cocolakis E, et al. Molecular targeting of the oncogene eIF4E in acute myeloid leukemia (AML): A proof-of-principle clinical trial with ribavirin. *Blood*. 2009;114(2):257-260. doi:10.1182/blood-2009-02-205153.

409. Migden M, Guminski A, Gutzmer R, et al. Phase 2 randomized, double-blind study of sonidegib (LDE225) in patients with locally advanced basal cell carcinoma and metastatic basal cell carcinoma. *Br J Dermatol*. 2014;171:66-67. doi:http://dx.doi.org/10.1111/bjd.13282.

410. Migden MR, Guminski A, Gutzmer R, et al. Treatment with two different doses of sonidegib in patients with locally advanced or metastatic basal cell carcinoma (BOLT): a multicentre, randomised, double-blind phase 2 trial. *Lancet Oncol*. 2015;16(6):716-728. doi:10.1016/S1470-2045(15)70100-2.

411. Migden M, Lear J, Gutzmer R, et al. Inhibition of the hedgehog pathway with sonidegib (LDE225) in advanced basal cell carcinoma. *J Am Acad Dermatol*. 2015;72(5 suppl. 1):Ab186. doi:10.1016/j.jaad.2015.02.759.

412. Irvine DA, Zhang B, Kinstrie R, et al. Deregulated hedgehog pathway signaling is inhibited by the smoothened antagonist LDE225 (Sonidegib) in chronic phase chronic myeloid leukaemia. *Sci Rep*. 2016;6:25476. doi:10.1038/srep25476.

413. Tibes R, Al-Kali A, Oliver GR, et al. The Hedgehog pathway as targetable vulnerability with 5-azacytidine in myelodysplastic syndrome and acute myeloid leukemia. *J Hematol Oncol*. 2015;8(1):114. doi:10.1186/s13045-015-0211-8.

414. Kowalevsky A. Entwickelungsgeschichte des Amphioxus lanceolatus. *Mem l'Academie Imp des Sci St-petersbg*. 1867;VII(11,):1-17.

415. Dobell C. Antony van Leeuwenhoek and his "Little Animals." *New York Harcourt, Brace Co*. 1932:435.

416. Wheatley DN, Wang a M, Strugnell GE. Expression of primary cilia in mammalian cells. *Cell Biol Int*. 1996;20(1):73-81. doi:10.1006/cbir.1996.0011.

417. Goetz SC and KVA. The primary cilium: a signalling centre during vertebrate development. *Nat Rev Genet 1*. 2010;1(5):331-344.

418. Hoey DA, Downs ME, Jacobs CR. The mechanics of the primary cilium: An intricate structure with complex function. *J Biomech*. 2012;45(1):17-26. doi:10.1016/j.jbiomech.2011.08.008.

419. Rosenbaum JL, Witman GB. Intraflagellar transport. *Nat Rev Mol Cell Biol*. 2002;3(11):813-825. doi:10.1038/nrm952.

420. Pedersen LB and JLR. Intraflagellar transport (IFT) role in ciliary assembly, resorption and signalling. *Curr Top Dev Biol*. 2008;85:23-61.

421. Reiter JF, Blacque OE, Leroux MR. The base of the cilium: roles for transition fibres and the transition zone in ciliary formation, maintenance and compartmentalization. *EMBO Rep*. 2012;13(7):608-618. doi:10.1038/embor.2012.73.

422. Marshall WF. Basal bodies platforms for building cilia. *Curr Top Dev Biol*. 2008;85:1-22. doi:10.1016/S0070-2153(08)00801-6.

423. Scholey JM. Intraflagellar transport. *Annu Rev Cell Dev Biol*. 2003;19:423-443. doi:10.1146/annurev.cellbio.19.111401.091318.

424. Pedersen, L. B., I. R. Veland JMS and STC. Assembly of primary cilia. *Dev Dyn*. 2008;237(8):1993-2006.

425. Silverman MA, Leroux MR. Intraflagellar transport and the generation of dynamic, structurally and functionally diverse cilia. *Trends Cell Biol*. 2009;19(7):306-316. doi:10.1016/j.tcb.2009.04.002.

426. de la Roche M, Ritter AT, Angus KL, et al. Hedgehog signaling controls T cell killing at the immunological synapse. *Science*. 2013;342(6163):1247-1250. doi:10.1126/science.1244689.

427. Oh EC, Katsanis N. Cilia in vertebrate development and disease. *Development*. 2012;139(3):443-448. doi:10.1242/dev.050054.

428. Wheatley D. Primary cilia in normal and pathological tissues. *Pathobiology*. 1995;63(4):222-238. doi:10.1159/000163955.

429. Veland IR, Awan A, Pedersen LB, Yoder BK, Christensen ST. Primary cilia and signaling pathways in mammalian development, health and disease. *Nephron - Physiol*. 2009;111(3). doi:10.1159/000208212.

430. Satir P, Christensen ST. Overview of structure and function of mammalian cilia. *Annu Rev Physiol*. 2007;69:377-400. doi:10.1146/annurev.physiol.69.040705.141236.

431. Satir P. Controlling the direction of division. *Stem Cell Res Ther*. 2010;1(3):21. doi:10.1186/scrt21.

432. Satir P, Pedersen LB, Christensen ST. The primary cilium at a glance. *J Cell Sci*. 2010;123(Pt 4):499-503. doi:10.1242/jcs.050377.

433. Tasouri E, Tucker KL. Primary cilia and organogenesis: Is Hedgehog the only sculptor? *Cell Tissue Res*. 2011;345(1):21-40. doi:10.1007/s00441-011-1192-8.

434. Badano JL, Mitsuma N, Beales PL, Katsanis N. The ciliopathies: an emerging class of human genetic disorders. *Annu Rev Genomics Hum Genet*. 2006;7:125-148. doi:10.1146/annurev.genom.7.080505.115610.

435. Lancaster MA and JGG. The primary cilium as a cellular signaling center: lessons from disease.". *Curr Opin Genet Dev*. 2009;19(3):220-229.

436. Hassounah NB, Bunch TA, McDermott KM. Molecular pathways: The role of primary cilia in cancer progression and therapeutics with a focus on hedgehog signaling. *Clin Cancer Res*. 2012;18(9):2429-2435. doi:10.1158/1078-0432.CCR-11-0755.

437. Wood LD, Parsons DW, Jones S, et al. The genomic landscapes of human breast and colorectal cancers. *Science (80-)*. 2007;318(5853):1108-1113. doi:10.1126/science.1145720.

438. Sjoblom T, Jones S, Wood LD, et al. The consensus coding sequences of human breast and colorectal cancers. *Science (80-)*. 2006;314(5797):268-274. doi:1133427 [pii]\r10.1126/science.1133427.

439. Bowers AJ, Boylan JF. Nek8, a NIMA family kinase member, is overexpressed in primary human breast tumors. *Gene*. 2004;328(1-2):135-142. doi:10.1016/j.gene.2003.12.002.

440. Habbig S, Bartram MP, Sägmüller JG, et al. The ciliopathy disease protein NPHP9 promotes nuclear delivery and activation of the oncogenic transcriptional regulator TAZ. *Hum Mol Genet*. 2012;21(26):5528-5538. doi:10.1093/hmg/dds408.

441. Santos N, Reiter JF. Building it up and taking it down: The regulation of vertebrate ciliogenesis. *Dev Dyn*. 2008;237(8):1972-1981. doi:10.1002/dvdy.21540.

442. Mans DA, Voest EE, Giles RH. All along the watchtower: Is the cilium a tumor suppressor organelle? *Biochim Biophys Acta - Rev Cancer*. 2008;1786(2):114-125. doi:10.1016/j.bbcan.2008.02.002.

443. Kim J, Dabiri S, Seeley ES. Primary cilium depletion typifies cutaneous melanoma in situ and malignant melanoma. *PLoS One*. 2011;6(11). doi:10.1371/journal.pone.0027410.

444. Yuan K, Frolova N, Xie Y, et al. Primary cilia are decreased in breast cancer: analysis of a collection of human breast cancer cell lines and tissues. *J Histochem Cytochem*. 2010;58(10):857-870. doi:jhc.2010.955856 [pii]\r10.1369/jhc.2010.955856.

445. Seeley ES, Carri??re C, Goetze T, Longnecker DS, Korc M. Pancreatic cancer and precursor pancreatic intraepithelial neoplasia lesions are devoid of primary cilia. *Cancer Res*. 2009;69(2):422-430. doi:10.1158/0008-5472.CAN-08-1290.

446. Egeberg DL, Lethan M, Manguso R, et al. Primary cilia and aberrant cell signaling in epithelial ovarian cancer. *Cilia*. 2012;1(1):15. doi:10.1186/2046-2530-1-15.

447. Wong SY, Seol AD, So P-L, et al. Primary cilia can both mediate and suppress Hedgehog pathway-dependent tumorigenesis. *Nat Med*. 2009;15(9):1055-1061. doi:10.1038/nm.2011.

448. Han Y-G, Kim HJ, Dlugosz AA, Ellison DW, Gilbertson RJ, Alvarez-Buylla A. Dual and opposing roles of primary cilia in medulloblastoma development. *Nat Med*. 2009;15(9):1062-1065. doi:10.1038/nm.2020.

449. Brancati F, Dallapiccola B, Valente EM. Joubert Syndrome and related disorders. *Orphanet J Rare Dis*. 2010;5:20. doi:10.1186/1750-1172-5-20.

450. Huangfu, D., A. Liu, A. S. Rakeman, N. S. Murcia LN and KVA. Hedgehog signalling in the mouse requires intraflagellar transport proteins. *Nature*. 2003;426(6962):83-87.

451. Haycraft, C. J., B. Banizs, Y. Aydin-Son, Q. Zhang EJM and BKY. Gli2 and Gli3 localize to cilia and

require the intraflagellar transport protein polaris for processing and function. *PLoS Genet*. 2005;1(4):e53.

452. Eggenschwiler JT, Anderson K V. Cilia and developmental signaling. *Annu Rev Cell Dev Biol*. 2007;23:345-373. doi:10.1146/annurev.cellbio.23.090506.123249.

453. Aanstad P, Santos N, Corbit KC, et al. The Extracellular Domain of Smoothened Regulates Ciliary Localization and Is Required for High-Level Hh Signaling. *Curr Biol*. 2009;19(12):1034-1039. doi:10.1016/j.cub.2009.04.053.

454. Corbit KC, Aanstad P, Singla V, Norman AR, Stainier DYR, Reiter JF. Vertebrate Smoothened functions at the primary cilium. *Nature*. 2005;437(October):1018-1021. doi:10.1038/nature04117.

455. Hsiao Y-C, Tuz K, Ferland RJ, et al. Trafficking in and to the primary cilium. *Cilia*. 2012;1(1):4. doi:10.1186/2046-2530-1-4.

456. Huangfu D and KVA. Cilia and Hedgehog responsiveness in the mouse. *Proc Natl Acad Sci U S A*. 2005;102(32):11325-11330.

457. Liu, A. BW and LAN. Mouse intraflagellar transport proteins regulate both the activator and repressor functions of Gli transcription factors. *Development*. 2005;132(13):3103-3111.

458. Ray, K., S. E. Perez, Z. Yang, J. Xu, B. W. Ritchings HS and LSG. Kinesin-II is required for axonal transport of choline acetyltransferase in Drosophila.". *J Cell Biol*. 1999;147(3):507-518.

459. Levine RL, Wadleigh M, Cools J, et al. Activating mutation in the tyrosine kinase JAK2 in polycythemia vera, essential thrombocythemia, and myeloid metaplasia with myelofibrosis. *Cancer Cell*. 2005;7(4):387-397. doi:10.1016/j.ccr.2005.03.023.

460. Fliegauf M, Benzing T, Omran H. When cilia go bad: cilia defects and ciliopathies. *Nat Rev Mol Cell Biol*. 2007;8(11):880-893. doi:10.1038/nrm2278.

461. Kuzhandaivel A, Schultz SW, Alkhori L, Alenius M. Cilia-Mediated Hedgehog Signaling in Drosophila. *Cell Rep*. 2014;7(3):672-680. doi:10.1016/j.celrep.2014.03.052.

462. Ling V. Charles F. Kettering Prize. P-glycoprotein and resistance to anticancer drugs. *Cancer*. 1992;69(10):2603-2609.

463. Reed JC. Bcl-2 family proteins: strategies for overcoming chemoresistance in cancer. *Adv Pharmacol*. 1997;41:501-532.

464. Kurinna, S., M. Konopleva, S. L. Palla, W. Chen, S. Kornblau, R. Contractor, X. Deng, W. S. May MA and PPR. Bcl2 phosphorylation and active PKC alpha are associated with poor survival in AML. *Leukemia*. 2006;20(7):1316-1319.

465. Cleary ML, Smith SD, Sklar J. Cloning and structural analysis of cDNAs for bcl-2 and a hybrid bcl-2/immunoglobulin transcript resulting from the t(14;18) translocation. *Cell*. 1986;47(1):19-28. doi:10.1016/0092-8674(86)90362-4.

466. Tsujimoto Y, Croce CM. Analysis of the structure, transcripts, and protein products of bcl-2, the gene involved in human follicular lymphoma. *Proc Natl Acad Sci U S A*. 1986;83(14):5214-5218.

467. Reed, J. C., M. Cuddy, T. Slabiak CMC and PCN. Oncogenic potential of bcl-2 demonstrated by gene transfer. *Nature*. 1988;336(6196):259-261.

468. Kroemer G, Galluzzi L, Vandenabeele P, et al. Classification of cell death: recommendations of the Nomenclature Committee on Cell Death 2009. *Cell Death Differ*. 2009;16(1):3-11. doi:10.1038/cdd.2008.150.

469. Pellegrini M, Strasser A. A portrait of the Bcl-2 protein family: life, death, and the whole picture. *J Clin Immunol*. 1999;19(6):365-377. http://www.ncbi.nlm.nih.gov/pubmed/10634210.

470. Muchmore SW, Sattler M, Liang H, et al. X-ray and NMR structure of human Bcl-xL, an inhibitor of programmed cell death. *Nature*. 1996;381(6580):335-341.

471. Kvansakul M, Yang H, Fairlie W, et al. Vaccinia virus anti-apoptotic F1L is a novel Bcl-2-like domain-swapped dimer that binds a highly selective subset of BH3-containing death ligands. *Cell Death Differ*. 2008;1583(10):1564-1571. doi:10.1038/cdd.2008.83.

472. Hinds, M. G., C. Smits, R. Fredericks-Short, J. M. Risk, M. Bailey DCH and CLD. Bim, Bad and Bmf:

intrinsically unstructured BH3-only proteins that undergo a localized conformational change upon binding to prosurvival Bcl-2 targets. *Cell Death Differ 1*. 2007;14(1):128-136.

473. Certo M, Moore VDG, Nishino M, et al. Mitochondria primed by death signals determine cellular addiction to antiapoptotic BCL-2 family members. *Cancer Cell*. 2006;9(5):351-365. doi:10.1016/j.ccr.2006.03.027.

474. Willis SN, Fletcher JI, Kaufmann T, et al. Apoptosis initiated when BH3 ligands engage multiple Bcl-2 homologs, not Bax or Bak. *Science*. 2007;315(February):856-859. doi:10.1126/science.1133289.

475. Willis SN, Chen L, Dewson G, et al. Proapoptotic Bak is sequestered by Mcl-1 and Bcl-xL, but not Bcl-2, until displaced by BH3-only proteins. *Genes Dev*. 2005;19(11):1294-1305. doi:10.1101/gad.1304105.

476. Simmons MJ, Fan G, Zong W-X, Degenhardt K, White E, Gélinas C. Bfl-1/A1 functions, similar to Mcl-1, as a selective tBid and Bak antagonist. *Oncogene*. 2008;27:1421-1428. doi:10.1038/sj.onc.1210771.

477. Fletcher, J. I., S. Meusburger, C. J. Hawkins, D. T. Riglar, E. F. Lee, W. D. Fairlie DCH and JMA. Apoptosis is triggered when prosurvival Bcl-2 proteins cannot restrain Bax. *Proc Natl Acad Sci U S A*. 2008;105(47):18081-18087.

478. Lindsten, T., A. J. Ross, A. King, W. X. Zong, J. C. Rathmell, H. A. Shiels, E. Ulrich, K. G. Waymire, P. Mahar, K. Frauwirth, Y. Chen, M. Wei, V. M. Eng, D. M. Adelman, M. C. Simon, A. Ma, J. A. Golden, G. Evan, S. J. Korsmeyer GRM and CBT. The combined functions of proapoptotic Bcl-2 family members bak and bax are essential for normal development of multiple tissues. *Mol Cell*. 2000;6(6):1389-1399.

479. Cory S, Huang DCS, Adams JM. The Bcl-2 family: roles in cell survival and oncogenesis. *Oncogene*. 2003;22(53):8590-8607. doi:10.1038/sj.onc.1207102.

480. Adams JM, Cory S. The Bcl-2 apoptotic switch in cancer development and therapy. *Oncogene*. 2007;26(9):1324-1337. doi:10.1038/sj.onc.1210220.

481. Chen, L., S. N. Willis, A. Wei, B. J. Smith, J. I. Fletcher, M. G. Hinds, P. M. Colman, C. L. Day JMA and DCH. Differential targeting of prosurvival Bcl-2 proteins by their BH3-only ligands allows complementary apoptotic function. *Mol Cell*. 2005;17(3):393-403.

482. Kuwana, T., L. Bouchier-Hayes, J. E. Chipuk, C. Bonzon, B. A. Sullivan DRG and DDN. BH3 domains of BH3-only proteins differentially regulate Bax-mediated mitochondrial membrane permeabilization both directly and indirectly. *Mol Cell*. 2005;17(4):525-535.

483. Kim, H., M. Rafiuddin-Shah, H. C. Tu, J. R. Jeffers, G. P. Zambetti JJH and EHC. Hierarchical regulation of mitochondrion-dependent apoptosis by BCL-2 subfamilies. *Nat Cell Biol*. 2006;8(12):1348-1358.

484. Llambi, F., T. Moldoveanu, S. W. Tait, L. Bouchier-Hayes, J. Temirov, L. L. McCormick CPD and DRG. A unified model of mammalian BCL-2 protein family interactions at the mitochondria. *Mol Cell*. 2011;44(4):517-531.

485. Graupner V, Alexander E, Overkamp T, et al. Differential regulation of the proapoptotic multidomain protein Bak by p53 and p73 at the promoter level. *Cell Death Differ*. 2011;18(7):1130-1139. doi:10.1038/cdd.2010.179.

486. Kluck RM, Bossy-Wetzel E, Green DR, Newmeyer DD. The release of cytochrome c from mitochondria: a primary site for Bcl-2 regulation of apoptosis. *Science (80-)*. 1997;275(5303):1132-1136. doi:10.1126/science.275.5303.1132.

487. Lapidot, T., C. Sirard, J. Vormoor, B. Murdoch, T. Hoang, J. Caceres-Cortes, M. Minden B., Li, P., D. Nijhawan, I. Budihardjo, S. M. Srinivasula, M. Ahmad ESA and XW. Cytochrome c and dATP-dependent formation of Apaf-1/caspase-9 complex initiates an apoptotic protease cascade. *Cell*. 1997;91(4):479-489.

488. Zou H, Yang R, Hao J, et al. Regulation of the Apaf-1/caspase-9 apoptosome by caspase-3 and XIAP. *J Biol Chem*. 2003;278(10):8091-8098. doi:10.1074/jbc.M204783200.

489. Zou H, Henzel WJ, Liu X, Lutschg A, Wang X. Apaf-1, a human protein homologous to C. elegans CED-4, participates in cytochrome c-dependent activation of caspase-3. *Cell*. 1997;90(3):405-413. doi:10.1016/S0092-8674(00)80501-2.

490. Du C, Fang M, Li Y, Li L, Wang X. Smac, a mitochondrial protein that promotes cytochrome c-dependent caspase activation by eliminating IAP inhibition. *Cell*. 2000;102(1):33-42. doi:10.1016/S0092-8674(00)00008-8.

491. Srinivasula SM, Datta P, Fan XJ, Fernandes-Alnemri T, Huang Z, Alnemri ES. Molecular determinants of the caspase-promoting activity of Smac/DIABLO and its role in the death receptor pathway. *J Biol Chem*. 2000;275(46):36152-36157. doi:10.1074/jbc.C000533200.

492. Korsmeyer SJ, Wei MC, Saito M, Weiler S, Oh KJ, Schlesinger PH. Pro-apoptotic cascade activates BID, which oligomerizes BAK or BAX into pores that result in the release of cytochrome c. *Cell Death Differ*. 2000;7(12):1166-1173. doi:10.1038/sj.cdd.4400783.

493. Baines CP. Role of the mitochondrion in programmed necrosis. *Front Physiol*. 2010;1:156.

494. Tsujimoto Y, Shimizu S, Eguchi Y, Kamiike W, Matsuda H. Bcl-2 and Bcl-xL block apoptosis as well as necrosis: possible involvement of common mediators in apoptotic and necrotic signal transduction pathways. *Leukemia*. 1997;11 Suppl 3:380-382. http://www.ncbi.nlm.nih.gov/pubmed/9209397.

495. Levine B, Sinha S, Kroemer G. Bcl-2 family members: Dual regulators of apoptosis and autophagy. *Autophagy*. 2008;4(5):600-606. doi:10.1016/j.biotechadv.2011.08.021.Secreted.

496. Hockenbery, D. M., M. Zutter, W. Hickey MN and SJK. BCL2 protein is topographically restricted in tissues characterized by apoptotic cell death. *Proc Natl Acad Sci U S A*. 1991;88(16):6961-6965.

497. Adams JM, Cory S. The Bcl-2 protein family: arbiters of cell survival. *Science (80-)*. 1998;281(5381):1322-1326. doi:10.1126/science.281.5381.1322.

498. Adams JM, Cory S. Life-or-death decisions by the Bcl-2 protein family. *Trends Biochem Sci*. 2001;26(1):61-66. doi:10.1016/S0968-0004(00)01740-0.

499. Reed JC. Double identity for proteins of the Bcl-2 family. *Nature*. 1997;387(6635):773-776. doi:10.1038/42867.

500. Reed JC. Bcl-2 family proteins. *Oncogene*. 1998;17(25):3225-3236. doi:10.1038/sj.onc.1202591.

501. Krajewski S, Krajewska M, Reed JC. Immunohistochemical analysis of in vivo patterns of Bak expression, a proapoptotic member of the bcl-2 protein family. *Cancer Res*. 1996;56(12):2849-2855.

502. Peters R, Leyvraz S, Perey L. Apoptotic regulation in primitive hematopoietic precursors. *Blood*. 1998;92(6):2041-2052. http://www.ncbi.nlm.nih.gov/pubmed/9731062.

503. Krajewska, M., S. Krajewski, J. I. Epstein, A. Shabaik, J. Sauvageot, K. Song SK and JCR. Immunohistochemical analysis of bcl-2, bax, bcl-X, and mcl-1 expression in prostate cancers. *Am J Pathol*. 1996;148(5):1567-1576.

504. Weyhenmeyer B, Murphy AC, Prehn JHM, Murphy BM. Targeting the anti-apoptotic Bcl-2 family members for the treatment of cancer. *Exp Oncol*. 2012;34(3):192-199.

505. Placzek WJ, Wei J, Kitada S, Zhai D, Reed JC, Pellecchia M. A survey of the anti-apoptotic Bcl-2 subfamily expression in cancer types provides a platform to predict the efficacy of Bcl-2 antagonists in cancer therapy. *Cell Death Dis*. 2010;1(5):e40.

506. Beverly LJ, Varmus HE. MYC-induced myeloid leukemogenesis is accelerated by all six members of the antiapoptotic BCL family. *Oncogene*. 2009;28(9):1274-1279. doi:10.1038/onc.2008.466.

507. Yip KW, Reed JC. Bcl-2 family proteins and cancer. *Oncogene*. 2008;27(50):6398-6406. doi:10.1038/onc.2008.307.

508. Reed JC. Bcl-2-family proteins and hematologic malignancies: History and future prospects. *Blood*. 2008;111(7):3313-3321. doi:10.1182/blood-2007-08-110114.

509. Hanada M, Delia D, Aiello A, Stadtmauer E, Reed JC. bcl-2 gene hypomethylation and high-level expression in B-cell chronic lymphocytic leukemia. *Blood*. 1993;82(6):1820-1828. http://www.bloodjournal.org/content/82/6/1820.abstract.

510. Cimmino A, Calin GA, Fabbri M, et al. miR-15 and miR-16 induce apoptosis by targeting BCL2. *PNAS*. 2005;102(39):13944-13949. doi:10.1073/pnas.0506654102.

511. Krajewska M, Moss SF, Krajewski S, Song K, Holt PR, Reed JC. Elevated expression of Bcl-X and reduced Bak in primary colorectal adenocarcinomas. *Cancer Res*. 1996;56(10):2422-2427.

512. Reed, J. C., T. Miyashita, S. Krajewski, S. Takayama, C. Aime-Sempe, S. Kitada, T. Sato, H. G. Wang, M. Harigai, M. Hanada, M. Krajewska, K. Kochel JM and HK. Bcl-2 family proteins and the regulation of programmed cell death in leukemia and lymphoma. *Cancer Treat Res*. 1996;84:31-72.

513. Hermann P, Bhaskar S, Cioffi M, Heeschen C. Cancer stem cells in solid tumors. *Semin Cancer Biol*. 2010;20(2):77-84.

514. Bensi L, Longo R, Vecchi A, et al. BCL-2 oncoprotein expression in acute myeloid leukemia. *Haematologica*. 1995;80(2):98-102.

515. Campos L, Rouault JP, Sabido O, et al. High expression of bcl-2 protein in acute myeloid leukemia cells is associated with poor response to chemotherapy. *Blood*. 1993;81(11):3091-3096. doi:10.1038/sj.onc.1210097.

516. Lauria F, Raspadori D, Rondelli D, et al. High bcl-2 expression in acute myeloid leukemia cells correlates with CD34 positivity and complete remission rate. *Leukemia*. 1997;11(12):2075-2078. doi:10.1038/sj.leu.2400854.

517. Kornblau SM, Thall PF, Estrov Z, et al. The prognostic impact of BCL2 protein expression in acute myelogenous leukemia varies with cytogenetics. *Clin Cancer Res*. 1999;5(7):1758-1766. http://www.ncbi.nlm.nih.gov/pubmed/10430080.

518. Moore VDG, Brown JR, Certo M, Love TM, Novina CD, Letai A. Chronic lymphocytic leukemia requires BCL2 to sequester prodeath BIM, explaining sensitivity to BCL2 antagonist ABT-737. *J Clin Invest*. 2007;117(1):112-121. doi:10.1172/JCI28281.

519. Konopleva M, Contractor R, Tsao T, et al. Mechanisms of apoptosis sensitivity and resistance to the BH3 mimetic ABT-737 in acute myeloid leukemia. *Cancer Cell*. 2006;10(5):375-388. doi:10.1016/j.ccr.2006.10.006.

520. Lagadinou ED, Sach A, Callahan K, et al. BCL-2 inhibition targets oxidative phosphorylation and selectively eradicates quiescent human leukemia stem cells. *Cell Stem Cell*. 2013;12(3):329-341. doi:10.1016/j.stem.2012.12.013.

521. Andreeff M, Jiang S, Zhang X, et al. Expression of Bcl-2-related genes in normal and AML progenitors: changes induced by chemotherapy and retinoic acid. *Leuk Off J Leuk Soc Am Leuk Res Fund, UK*. 1999;13(11):1881-1892. http://www.ncbi.nlm.nih.gov/pubmed/10557066.

522. DiNardo C, Pollyea D, Pratz K, et al. A Phase 1b Study of Venetoclax (ABT-199/GDC-0199) in Combination with Decitabine or Azacitidine in Treatment-Naive Patients with Acute Myelogenous Leukemia Who Are ≥ to 65 Years and Not Eligible for Standard Induction Therapy. 2015.

523. Pollyea, D.A., Dinardo, D., Thirman, M.J., Letai, A., Wei, A.H., Wei, A.H., Jonas, B.A., Arellano, M.L., Frattini, M.G., Kantarjian, H.M., Chyla, B., Zhu, M. Potluri, J. Humerickhouse, R., Mabry, M.H., Konopleva, M., Pratz KW. Results of a phase 1b study of venetoclax plus decitabine or azacitidine in untreated acute myeloid leukemia patients ≥ 65 years ineligible for standard induction therapy. *J Clin Oncol*. 2016;34(suppl; abs 7009):poster presentation. http://meetinglibrary.asco.org/content/168695-176.

524. Konopleva M, Pollyea DA, Potluri J, et al. Efficacy and Biological Correlates of Response in a Phase II Study of Venetoclax Monotherapy in Patients with Acute Myelogenous Leukemia. *Cancer Discov*. 2016;6(10):1106-1117. doi:10.1158/2159-8290.CD-16-0313.

525. Potluri J, Xu T, Hong W, MH M. Phase 3, randomized, double-blind, placebo-controlled study of venetoclax combined with azacitidine versus azacitidine in treatment-naïve patients with acute myeloid leukemia. *J Clin Oncol*. 2017;35,:TPS7069.

526. Szakács G, Annereau J-P, Lababidi S, et al. Predicting drug sensitivity and resistance: Profiling ABC transporter genes in cancer cells. *Cancer Cell*. 2004;6(2):129-137. doi:10.1016/j.ccr.2004.06.026.

527. Albrecht C, Viturro E. The ABCA subfamily--gene and protein structures, functions and associated hereditary diseases. *Pflugers Arch*. 2007;453(5):581-589. doi:10.1007/s00424-006-0047-8.

528. Dean M, Hamon Y, Chimini G. The human ATP-binding cassette (ABC) transporter superfamily. *J Lipid Res*. 2001;42(7):1007-1017. doi:10.1101/gr.GR-1649R.

529. Hlava V, Sou ek P. Role of family D ATP-binding cassette transporters (ABCD) in cancer. *Biochem Soc Trans*. 2015;43(5):937-942. doi:10.1042/BST20150114.

530. Kerr ID, Haider AJ, Gelissen IC. The ABCG family of membrane-associated transporters: You don't

have to be big to be mighty. *Br J Pharmacol*. 2011;164(7):1767-1779. doi:10.1111/j.1476-5381.2010.01177.x.

531. Tang L, Bergevoet SM, Gilissen C, et al. Hematopoietic stem cells exhibit a specific ABC transporter gene expression profile clearly distinct from other stem cells. *BMC Pharmacol*. 2010;10:12. doi:10.1186/1471-2210-10-12.

532. Fukuda Y, Lian S, Schuetz JD. Leukemia and ABC Transporters. *Adv Cancer Res*. 2015;125:171-196. doi:10.1016/bs.acr.2014.10.006.

533. Maier S, Strasser S, Saiko P, et al. Analysis of mechanisms contributing to AraC-mediated chemoresistance and re-establishment of drug sensitivity by the novel heterodinucleoside phosphate 5-FdUrd-araC. *Apoptosis*. 2006;11(3):427-440. doi:10.1007/s10495-006-4066-x.

534. Marzac C, Garrido E, Tang R, et al. ATP Binding Cassette transporters associated with chemoresistance: Transcriptional profiling in extreme cohorts and their prognostic impact in a cohort of 281 acute myeloid leukemia patients. *Haematologica*. 2011;96(9):1293-1301. doi:10.3324/haematol.2010.031823.

535. Ueda K, Clark DP, Chen CJ, Roninson IB, Gottesman MM, Pastan I. The human multidrug resistance (mdr1) gene. cDNA cloning and transcription initiation. *J Biol Chem*. 1987;262(2):505-508. doi:Base Sequence *Cloning, Molecular Colchicine/toxicity Doxorubicin/toxicity *Drug Resistance DNA/*metabolism DNA Restriction Enzymes Gene Amplification *Genes Human KB Cells Nucleic Acid Hybridization Support, Non-U.S. Gov't Support, U.S. Gov't, P.H.S. *Transcription, Genetic Vinblastine/toxicity.

536. Yasuhisa K, Shin-ya M, Michinori M, Kazumitsu U. Mechanism of multidrug recognition by MDR1/ABCB1. *Cancer Sci*. 2007;98(9):1303-1310. doi:10.1111/j.1349-7006.2007.00538.x.

537. Steinbach D, Legrand O. ABC transporters and drug resistance in leukemia: was P-gp nothing but the first head of the Hydra? *Leukemia*. 2007;21(6):1172-1176. doi:10.1038/sj.leu.2404692.

538. Robey RW, To KKK, Polgar O, et al. ABCG2: A perspective. *Adv Drug Deliv Rev*. 2009;61(1):3-13. doi:10.1016/j.addr.2008.11.003.

539. van der Kolk DM, de Vries EG, Koning JA, van den Berg E, Muller M, Vellenga E. Activity and expression of the multidrug resistance proteins MRP1 and MRP2 in acute myeloid leukemia cells, tumor cell lines, and normal hematopoietic CD34+ peripheral blood cells. *Clin Cancer Res*. 1998;4(7):1727-1736. http://www.ncbi.nlm.nih.gov/pubmed/9676848.

540. Van Der Kolk DM, De Vries EG, Noordhoek L, et al. Activity and expression of the multidrug resistance proteins P-glycoprotein, MRP1, MRP2, MRP3 and MRP5 in de novo and relapsed acute myeloid leukemia. *Leuk Off J Leuk Soc Am Leuk Res Fund UK*. 2001;15(10):1544-1553. doi:10.1038/sj.leu.2402236.

541. Munoz M, Henderson M, Haber M, Norris M. Role of the MRP1/ABCC1 Multidrug Transporter Protein in Cancer. *IUBMB Life*. 2007;59(12):752-757. doi:10.1080/15216540701736285.

542. Yin J, Zhang J. Multidrug resistance-associated protein 1 (MRP1/ABCC1) polymorphism: from discovery to clinical application. *Zhong Nan Da Xue Xue Bao Yi Xue Ban*. 2011;36(10):927-938. doi:10.3969/j.issn.1672-7347.2011.10.002.

543. Van Meer G, Halter D, Sprong H, Somerharju P, Egmond MR. ABC lipid transporters: Extruders, flippases, or flopless activators? *FEBS Lett*. 2006;580(4):1171-1177. doi:10.1016/j.febslet.2005.12.019.

544. Tellingen O Van, Buckle T, Jonker JW, et al. P-glycoprotein and Mrp1 collectively protect the bone marrow from vincristine-induced toxicity in vivo. *Br J Cancer*. 2003;89(9):1776-1782. doi:10.1038/sj.bjc.6601363.

545. de Grouw E, Raaijmakers M, Boezeman J, et al. Preferential expression of a high number of ATP binding cassette transporters in both normal and leukemic CD34+CD38- cells. *Leukemia*. 2006;20(750-4):750-754.

546. Gallagher R, Collins S, Trujillo J, et al. Characterization of the continuous, differentiating myeloid cell line (HL-60) from a patient with acute promyelocytic leukemia. *Blood*. 1979;54(3):713-733.

547. Asou H, Tashiro S, Hamamoto K, Otsuji A, Kita K, Kamada N. Establishment of a human acute myeloid leukemia cell line (Kasumi-1) with 8;21 chromosome translocation. *Blood*. 1991;77(9):2031-2036.

548. Furley AJJ, Reeves BRR, Mizutani S, et al. Divergent molecular phenotypes of KG1 and KG1a myeloid cell lines. *Blood*. 1986;68(5):1101-1107.

549. Matsuo Y, MacLeod RAF, Uphoff CC, et al. Two acute monocytic leukemia (AML-M5a) cell lines (MOLM-13 and MOLM-14) with interclonal phenotypic heterogeneity showing MLL-AF9 fusion resulting from an occult chromosome insertion, ins(11;9)(q23;p22p23). *Leukemia*. 1997;11(9):1469-1477. doi:10.1038/sj.leu.2400768.

550. Lange B, Valtieri M, Santoli D, et al. Growth factor requirements of childhood acute leukemia: establishment of GM-CSF-dependent cell lines. *Blood*. 1987;70:192-199.

551. Wang C, Curtis JE, Minden MD, McCulloch EA. Expression of a retinoic acid receptor gene in myeloid leukemia cells. *Leukemia*. 1989;3:264-269. http://www.ncbi.nlm.nih.gov/entrez/query.fcgi?cmd=Retrieve&db=PubMed&dopt=Citation&list_uids=2538684.

552. Tsuchiya S, Yamabe M, Yamaguchi Y, Kobayashi Y, Konno T, Tada K. Establishment and characterization of a human acute monocytic leukemia cell line (THP-1). *Int J Cancer*. 1980;26(2):171-176. doi:10.1002/ijc.2910260208.

553. Roecklein BA, Torok-Storb B. Functionally distinct human marrow stromal cell lines immortalized by transduction with the human papilloma virus e6/e7 genes. *Blood*. 1995;85(4):997-1005. http://www.ncbi.nlm.nih.gov/pubmed/7849321.

554. Lemoine FM, Humphries RK, Abraham SD, Krystal G, Eaves CJ. Partial characterization of a novel stromal cell-derived pre-B-cell growth factor active on normal and immortalized pre-B cells. *Exp Hematol*. 1988;16(8):718-726. http://www.ncbi.nlm.nih.gov/pubmed/3261251.

555. Hogge DE, Lansdorp PM, Reid D, Gerhard B, Eaves CJ. Enhanced detection, maintenance, and differentiation of primitive human hematopoietic cells in cultures containing murine fibroblasts engineered to produce human steel factor, interleukin-3, and granulocyte colony-stimulating factor. *Blood*. 1996;88(10):3765-3773.

556. Sutherland HJ, Eaves CJ, Lansdorp PM, Thacker JD, Hogge DE. Differential regulation of primitive human hematopoietic cells in long-term cultures maintained on genetically engineered murine stromal cells. *Blood*. 1991;78(3):666-672. http://eutils.ncbi.nlm.nih.gov/entrez/eutils/elink.fcgi?dbfrom=pubmed&id=1713512&retmode=ref&cmd=prlinks%5Cnpapers2://publication/uuid/F7EAE3B7-7626-47F3-B3DB-FA8F6837DA6E.

557. Mather JP. Establishment and Characterization of Two Distinct Mouse Testicular Epithelial Cell Lines. *Biol Reprod*. 1980;23(1):243-252.

558. Frank-Kamenetsky M, Zhang XM, Bottega S, et al. Small-molecule modulators of Hedgehog signaling: identification and characterization of Smoothened agonists and antagonists. *J Biol*. 2002;1(2):10. doi:10.1186/1475-4924-1-10.

559. Souers AJ, Leverson JD, Boghaert ER, et al. ABT-199, a potent and selective BCL-2 inhibitor, achieves antitumor activity while sparing platelets. *Nat Med*. 2013;19(2):202-208. doi:10.1038/nm.3048.

560. Keeler RF, Binns W. Teratogenic compounds of Veratrum californicum (Durand). V. Comparison of cyclopian effects of steroidal alkaloids from the plant and structurally related compounds from other sources. *Teratology*. 1968;1(1):5-10. doi:10.1002/tera.1420010103.

561. Drexler H, MacLeod R. Leukemia-lymphoma cell lines as model systems for hematopoietic research. *Ann Med*. 2003;35(6):404-412. doi:10.1080/07853890310012094.

562. Drexler HG, Minowada J. History and classification of human leukemia-lymphoma cell lines. *Leuk Lymphoma*. 1998;31(3-4):305-316. doi:10.3109/10428199809059223.

563. Drexler HG. Establishment and culture of leukemia-lymphoma cell lines. *Methods Mol Biol*. 2011;731:181-200. doi:10.1007/978-1-61779-080-5_16.

564. Drexler HG, Quentmeier H, MacLeod RAF. Cell line models of leukemia. *Drug Discov Today Dis Model*. 2005;2(1):51-56. doi:10.1016/j.ddmod.2005.05.010.

565. Kohlmann A, Kipps TJ, Rassenti LZ, et al. An international standardization programme towards the application of gene expression profiling in routine leukaemia diagnostics: The Microarray Innovations in LEukemia study prephase. *Br J Haematol*. 2008;142(5):802-807. doi:10.1111/j.1365-2141.2008.07261.x.

566. Singh M, Chaudhry P, Ramsingh G, Merchant A. Presence of Primary Cilia in Human Hematopoietic System. *Blood*. 2015;126(23):4762.

567. Long B, Wang LX, Zheng FM, et al. Targeting GLI1 suppresses cell growth and enhances chemosensitivity in CD34+ enriched acute myeloid leukemia progenitor cells. *Cell Physiol Biochem*. 2016;38(4):1288-1302. doi:10.1159/000443075.

568. Bai LY, Weng JR, Lo WJ, et al. Inhibition of hedgehog signaling induces monocytic differentiation of HL-60 cells. *Leuk Lymphoma*. 2012;53(6):1196-1202. doi:10.3109/10428194.2011.639877.

569. Frenette PS, Pinho S, Lucas D, Scheiermann C. *Mesenchymal Stem Cell: Keystone of the Hematopoietic Stem Cell Niche and a Stepping-Stone for Regenerative Medicine*. Vol 31.; 2013. doi:doi:10.1146/annurev-immunol-032712-095919.

570. Kfoury Y, Scadden DT. Mesenchymal cell contributions to the stem cell niche. *Cell Stem Cell*. 2015;16(3):239-253. doi:10.1016/j.stem.2015.02.019.

571. Kuhn NZ, Tuan RS. Regulation of stemness and stem cell niche of mesenchymal stem cells: Implications in tumorigenesis and metastasis. *J Cell Physiol*. 2010;222(2):268-277. doi:10.1002/jcp.21940.

572. Irvine DA. Defining novel therapeutic targets in chronic myeloid leukaemia stem cells : targeting self-renewal through hedgehog pathway inhibition. 2013.

573. Chou TC. Drug combination studies and their synergy quantification using the chou-talalay method. *Cancer Res*. 2010;70(2):440-446. doi:10.1158/0008-5472.CAN-09-1947.

574. Coulombel L. Identification of hematopoietic stem/progenitor cells: strength and drawbacks of functional assays. *Oncogene*. 2004;23(43):7210-7222. doi:10.1038/sj.onc.1207941.

575. Wognum B, Yuan N, Lai B, Miller CL. Colony Forming Cell Assays for Human Hematopoietic Progenitor Cells. *Methods Mol Biol*. 2013;(946):267-283.

576. Livak KJ, Schmittgen TD. Analysis of relative gene expression data using real-time quantitative PCR and the 2(-Delta Delta C(T)) Method. *Methods*. 2001;25(4):402-408. doi:10.1006/meth.2001.1262.

577. Cramer-Morales K, Nieborowska-Skorska M, Scheibner K, et al. Personalized synthetic lethality induced by targeting RAD52 in leukemias identified by gene mutation and expression profile. *Blood*. 2013;122(7):1293-1304. doi:10.1182/blood-2013-05-501072.

578. Flis K, Irvine D, Copland M, Bhatia R, Skorski T. Chronic myeloid leukemia stem cells display alterations in expression of genes involved in oxidative phosphorylation. *Leuk Lymphoma*. 2012;53(12):2474-2478. doi:10.3109/10428194.2012.696313.

579. Sanger F, Nicklen S, Coulson AR. DNA sequencing with chain-terminating inhibiters. *Proc Natl Acad Sci U S A*. 1977;74:5463-5467. doi:10.1073/pnas.74.12.5463.

580. Reifenberger J, Wolter M, Weber RG, et al. Missense mutations in SMOH in sporadic basal cell carcinomas of the skin and primitive neuroectodermal tumors of the central nervous system. *Cancer Res*. 1998;58(9):1798-1803. http://www.ncbi.nlm.nih.gov/pubmed/9581815.

581. Epstein EH. Basal cell carcinomas: attack of the hedgehog. *Nat Rev Cancer*. 2008;8(10):743-754. doi:10.1038/nrc2503.

582. Sweeney RT, McClary AC, Myers BR, et al. Identification of recurrent SMO and BRAF mutations in ameloblastomas. *Nat Genet*. 2014;46(7):722-725. doi:10.1038/ng.2986.

583. Network TCGAR. Genomic and epigenomic landscapes of adult de novo acute myeloid leukemia. *N Engl J Med*. 2013;368(22):2059-2074.

584. https://www.illumina.com/systems/sequencing-platforms/miseq/products-services/miseq-reporter.html.

585. Fedchenko N, Reifenrath J. Different approaches for interpretation and reporting of immunohistochemistry analysis results in the bone tissue - a review. *Diagn Pathol*. 2014;9:221. doi:10.1186/s13000-014-0221-9.

586. Alberts B. *Molecular Biology of the Cell, 5th Edition.*; 2008. http://books.google.com/books?id=obVmGQAACAAJ&printsec=frontcover.

587. Quah BJC, Warren HS, Parish CR. Monitoring lymphocyte proliferation in vitro and in vivo with the intracellular fluorescent dye carboxyfluorescein diacetate succinimidyl ester. *Nat Protoc*. 2007;2(9):2049-2056. doi:10.1038/nprot.2007.296.

588. Quah BJC, Parish CR. New and improved methods for measuring lymphocyte proliferation in vitro and in vivo using CFSE-like fluorescent dyes. *J Immunol Methods*. 2012;379(1):1-14. doi:10.1016/j.jim.2012.02.012.

589. Eisen MB, Spellman PT, Brown PO, Botstein D. Cluster analysis and display of genome-wide expression patterns. *Proc Natl Acad Sci USA*. 1998;95(25):14863-14868. doi:10.1073/pnas.95.25.14863.

590. Legras S, Günthert U, Stauder R, et al. A strong expression of CD44-6v correlates with shorter survival of patients with acute myeloid leukemia. *Blood*. 1998;91(9):3401-3413. http://www.bloodjournal.org/content/91/9/3401.abstract.

591. Alharbi RA, Pettengell R, Pandha HS, Morgan R. The role of HOX genes in normal hematopoiesis and acute leukemia. *Leukemia*. 2013;27(5):1000-1008. doi:10.1038/leu.2012.356.

592. Skvarova Kramarzova K, Fiser K, Mejstrikova E, et al. Homeobox gene expression in acute myeloid leukemia is linked to typical underlying molecular aberrations. *J Hematol Oncol*. 2014;7(1):94. doi:10.1186/s13045-014-0094-0.

593. Sengupta A, Banerjee D, Chandra S, et al. Deregulation and cross talk among Sonic hedgehog, Wnt, Hox and Notch signaling in chronic myeloid leukemia progression. *Leukemia*. 2007. doi:10.1038/sj.leu.2404657.

594. http://www.proteinatlas.org/.

595. Lindemann RK. Stroma-initiated Hedgehog signaling takes center stage in B-cell lymphoma. *Cancer Res*. 2008;68(4):961-964. doi:10.1158/0008-5472.CAN-07-5500.

596. Tabe Y, Konopleva M. Advances in understanding the leukaemia microenvironment. *Br J Haematol*. 2014;164(6):767-778. doi:10.1111/bjh.12725.

597. Tabe Y, Konopleva M. Role of Microenvironment in Resistance to Therapy in AML. *Curr Hematol Malig Rep*. 2015;10(2):96-103. doi:10.1007/s11899-015-0253-6.

598. Bigelow RLH, Chari NS, Undén AB, et al. Transcriptional Regulation of bcl-2 Mediated by the Sonic Hedgehog Signaling Pathway through gli-1. *J Biol Chem*. 2004;279(2):1197-1205. doi:10.1074/jbc.M310589200.

599. Kawai S, Sugiura T. Characterization of human bone morphogenetic protein (BMP)-4 and -7 gene promoters: Activation of BMP promoters by Gli, a sonic hedgehog mediator. *Bone*. 2001;29(1):54-61. doi:10.1016/S8756-3282(01)00470-7.

600. Jin L, Hope KJ, Zhai Q, Smadja-Joffe F, Dick JE. Targeting of CD44 eradicates human acute myeloid leukemic stem cells. *Nat Med*. 2006;12(10):1167-1174. doi:nm1483 [pii]; 10.1038/nm1483 [doi].

601. Jian-Hui C, Er-Tao Z, Si-Le C, et al. CD44, Sonic Hedgehog, and Gli1 Expression Are Prognostic Biomarkers in Gastric Cancer Patients after Radical Resection. *Gastroenterol Res Pract*. 2016;2016:1013045. doi:https://dx.doi.org/10.1155/2016/1013045.

602. Kenney AM, Rowitch DH. Sonic hedgehog Promotes G1 Cyclin Expression and Sustained Cell Cycle Progression in Mammalian Neuronal Precursors. *Mol Cell Biol*. 2000;20(23):9055-9067. doi:10.1128/MCB.20.23.9055-9067.2000.

603. Lin Z, Sheng H, You C, et al. Inhibition of the CyclinD1 promoter in response to sonic hedgehog signaling pathway transduction is mediated by Gli1. *Exp Ther Med*. 2016:307-314. doi:10.3892/etm.2016.3969.

604. Zhang J, Tian X, Xing J. Signal Transduction Pathways of EMT Induced by TGF-β, SHH, and WNT and Their Crosstalks. *J Clin Med*. 2016;5(4):41. doi:10.3390/jcm5040041.

605. Liang H, Chen Q, Coles AH, et al. Wnt5a inhibits B cell proliferation and functions as a tumor suppressor in hematopoietic tissue. *Cancer Cell*. 2003;4(5):349-360. doi:10.1016/S1535-6108(03)00268-X.

606. Reya T, O'Riordan M, Okamura R, et al. Wnt signaling regulates B lymphocyte proliferation through a LEF-1 dependent mechanism. *Immunity*. 2000;13(1):15-24. doi:S1074-7613(00)00004-2 [pii].

607. Nemeth MJ, Topol L, Anderson SM, Yang Y, Bodine DM. Wnt5a inhibits canonical Wnt signaling in hematopoietic stem cells and enhances repopulation. *PNAS*. 2007;104(39):15436-15441.

608. Battula VL, Le PM, Sun J, et al. Acute myeloid leukemia cells induce osteogenic differentiation in mesenchymal stem cells through bone morphogenetic protein-and RUNX-2-mediated signaling. *Cancer Res*. 2015;75(15). http://www.embase.com/search/results?subaction=viewrecord&from=export&id=L72195531%0Ahttp://cancerres.aacrjournals.org/content/75/15_Supplement/5085.abstract?sid=45ef3f66-15bc-44b8-81ec-f8f455864d9d%0Ahttp://dx.doi.org/10.1158/1538-7445.AM2015-5085.

609. Laperrousaz B, Jeanpierre S, Sagorny K, et al. Primitive CML cell expansion relies on abnormal levels of BMPs provided by the niche and on BMPRIb overexpression. *Blood*. 2013;122(23):3767-3777. doi:10.1182/blood-2013-05-501460.

610. Coughlin TR, Voisin M, Schaffler MB, Niebur GL, McNamara LM. Primary cilia exist in a small fraction of cells in trabecular bone and marrow. *Calcif Tissue Int*. 2014;96(1):65-72. doi:10.1007/s00223-014-9928-6.

611. Singh M, Chaudhry P, Merchant AA. Primary cilia are present on human blood and bone marrow cells and mediate Hedgehog signaling. *Exp Hematol*. 2016;44(12):1181-1187. doi:10.1016/j.exphem.2016.08.009.

612. imagej@nih.gov.

613. Zeng X, Zhao H, Li Y, et al. Targeting Hedgehog signaling pathway and autophagy overcomes drug resistance of BCR-ABLpositive chronic myeloid leukemia. *Autophagy*. 2015;11(2):355-372. doi:10.4161/15548627.2014.994368.

614. Marchant J. Phase contrast and electron microscope studies of the appearance and behaviour of the white cells of normal human blood. *Q J Microsc Sci*. 1952;93(4):395-411.

615. http://lcresearchcenter.tumblr.com/post/78676163547/signal-corps.

616. https://www.utsouthwestern.edu/labs/emcf/services/.

617. Wang X De, Inzunza H, Chang H, et al. Mutations in the Hedgehog Pathway Genes SMO and PTCH1 in Human Gastric Tumors. *PLoS One*. 2013;8(1). doi:10.1371/journal.pone.0054415.

618. Fukushima N, Minami Y, Kakiuchi S, et al. Small-molecule Hedgehog inhibitor attenuates the leukemia-initiation potential of acute myeloid leukemia cells. *Cancer Sci*. 2016;107(10):1422-1429. doi:10.1111/cas.13019.

619. Kool M, Jones DTW, Jäger N, et al. Genome sequencing of SHH medulloblastoma predicts genotype-related response to smoothened inhibition. *Cancer Cell*. 2014;25(3):393-405. doi:10.1016/j.ccr.2014.02.004.

620. Atwood SX, Sarin KY, Whitson RJ, et al. Smoothened Variants Explain the Majority of Drug Resistance in Basal Cell Carcinoma. *Cancer Cell*. 2015;27(3):342-353. doi:10.1016/j.ccell.2015.02.002.

621. Rombouts WJ, Blokland I, Lowenberg B, Ploemacher RE. Biological characteristics and prognosis of adult acute myeloid leukemia with internal tandem duplications in the Flt3 gene. *Leukemia*. 2000;14(4):675-683. http://www.ncbi.nlm.nih.gov/entrez/query.fcgi?cmd=Retrieve&db=PubMed&dopt=Citation&list_uids=10764154.

622. Stirewalt DL. FLT3, RAS, and TP53 mutations in elderly patients with acute myeloid leukemia. *Blood*. 2001;97(11):3589-3595. doi:10.1182/blood.V97.11.3589.

623. Kottaridis PD, Gale RE, Linch DC. Prognostic Implications of the Presence of FLT3 Mutations in Patients with Acute Myeloid Leukemia. *Leuk Lymphoma*. 2003;44(6):905-913. doi:10.1080/1042819031000067503.

624. Thol F, Damm F, Lüdeking A, et al. Incidence and prognostic influence of DNMT3A mutations in acute myeloid leukemia. *J Clin Oncol*. 2011;29(21):2889-2896. doi:10.1200/JCO.2011.35.4894.

625. Bai, L. Y., C. F. Chiu, C. W. Lin, N. Y. Hsu, C. L. Lin WJL and MCK. Differential expression of Sonic hedgehog and Gli1 in hematological malignancies. *Leukemia*. 2008;22(1):226-228.

626. Haferlach T, Kohlmann A, Wieczorek L, et al. Clinical utility of microarray-based gene expression

profiling in the diagnosis and subclassification of leukemia: Report from the international microarray innovations in leukemia study group. *J Clin Oncol*. 2010;28(15):2529-2537. doi:10.1200/JCO.2009.23.4732.

627. Kaur G, Dufour JM. Cell lines: Valuable tools or useless artifacts. *Spermatogenesis*. 2012;2(1):1-5. doi:10.4161/spmg.19885.

628. Del Álamo D, Rouault H, Schweisguth F. Mechanism and significance of cis-inhibition in notch signalling. *Curr Biol*. 2011;21(1). doi:10.1016/j.cub.2010.10.034.

629. Binns W, James LF, Shupe JL. Toxicosis Of Veratrum Californicum In Ewes And Its Relationship To A Congenital Deformity In Lambs. *Ann N Y Acad Sci*. 1964;111(2):571-576.

630. Binns W, Keeler RF, Dellball.L. Congenital Deformities in Lambs, Calves, and Goats Resulting from Maternal Ingestion of Veratrum californicum: Hare Lip, Cleft Palate, Ataxia, and Hypoplasia of Metacarpal and Metatarsal Bones. *Clin Toxicol*. 1972;5(2):245-261. doi:10.3109/15563657208991003.

631. Lipinski RJ, Hutson PR, Hannam PW, et al. Dose- and route-dependent teratogenicity, toxicity, and pharmacokinetic profiles of the hedgehog signaling antagonist cyclopamine in the mouse. *Toxicol Sci*. 2008;104(1):189-197. doi:10.1093/toxsci/kfn076.

632. Sarma NJ, Takeda A, Yaseen NR. Colony forming cell (CFC) assay for human hematopoietic cells. *J Vis Exp*. 2010;(46):3-7. doi:10.3791/2195.

633. Hengartner MO. The biochemistry of apoptosis. *Nature*. 2000;407(6805):770-776. doi:10.1038/35037710.

634. Kristensen AR, Gsponer J, Foster LJ. Protein synthesis rate is the predominant regulator of protein expression during differentiation. *Mol Syst Biol*. 2013;9(689):689. doi:10.1038/msb.2013.47.

635. Heretsch P, Tzagkaroulaki L, Giannis A. Modulators of the hedgehog signaling pathway. *Bioorg Med Chem*. 2010;18(18):6613-6624. doi:10.1016/j.bmc.2010.07.038.

636. Varjosalo M, Taipale J. Hedgehog: Functions and mechanisms. *Genes Dev*. 2008;22(18):2454-2472. doi:10.1101/gad.1693608.

637. Roy S, Ingham PW. Hedgehogs tryst with the cell cycle. *J Cell Sci*. 2002;115(Pt 23):4393-4397. doi:10.1242/jcs.00158.

638. Murrow L, Debnath J. Autophagy as a Stress-Response and Quality-Control Mechanism: Implications for Cell Injury and Human Disease. *Annu Rev Pathol Mech Dis*. 2012;8(1):121016121742000. doi:10.1146/annurev-pathol-020712-163918.

639. Glick D, Barth S, Macleod KF. Autophagy: cellular and molecular mechanisms. *J Pathol*. 2010;221(1):3-12. doi:10.1002/path.2697.

640. Auberger P, Puissant A. Autophagy, a key mechanism of oncogenesis and resistance in leukemia. *Blood*. 2017;129(5):547-552.

641. Jimenez-Sanchez M, Menzies FM, Chang Y-Y, Simecek N, Neufeld TP, Rubinsztein DC. The Hedgehog signalling pathway regulates autophagy. *Nat Commun*. 2012;3(1200):1-11. doi:10.1038/ncomms2212.

642. Wang Y, Han C, Lu L, Magliato S, Wu T. Hedgehog signaling pathway regulates autophagy in human hepatocellular carcinoma cells. *Hepatology*. 2013;58(3):995-1010. doi:10.1002/hep.26394.

643. Monastyrska I, Rieter E, Klionsky DJ, Reggiori F. Multiple roles of the cytoskeleton in autophagy. *Biol Rev*. 2009;84(3):431-448. doi:10.1111/j.1469-185X.2009.00082.x.

644. Satir P, Mitchell DR, Jékely G. Chapter 3 How Did the Cilium Evolve? *Curr Top Dev Biol*. 2008;85:63-82. doi:10.1016/S0070-2153(08)00803-X.

645. Davis RJ. Signal Transduction by the JNK Group of MAP Kinases. *Cell*. 2000;103(2):239-252. doi:10.1016/S0092-8674(00)00116-1.

646. Karin M. Nuclear factor-kappaB in cancer development and progression. *Nature*. 2006;441(7092):431-436. doi:10.1038/nature04870.

647. Herriott A, Tudhope SJ, Junge G, et al. PARP1 expression, activity and ex vivo sensitivity to the

PARP inhibitor, talazoparib (BMN 673), in chronic lymphocytic leukaemia. *Oncotarget*. 2015;6(41):43978-43991. doi:10.18632/oncotarget.6287.

648. Rouleau M, Patel A, Hendzel MJ, Kaufmann SH, Poirier GG. PARP inhibition: PARP1 and beyond. *Nat Rev Cancer*. 2010;10(4):293-301. doi:10.1038/nrc2812.

649. Curtin N. PARP inhibitors for anticancer therapy. *Biochem Soc Trans*. 2014;42(1):82-88. doi:10.1042/BST20130187.

650. Liu JF, Konstantinopoulos PA, Matulonis UA. PARP inhibitors in ovarian cancer: Current status and future promise. *Gynecol Oncol*. 2014;133(2):362-369. doi:10.1016/j.ygyno.2014.02.039.

651. Mullard A. European regulators approve first PARP inhibitor. *Nat Rev Drug Discov*. 2014;13:877-877. doi:10.1038/nrd4508.

652. Bhalla A, Saif MW asif. PARP-inhibitors in BRCA-associated pancreatic cancer. *JOP*. 2014;15(4):340-343. doi:10.6092/1590-8577/2690.

653. Davar D, Beumer JH, Hamieh L, Tawbi H. Role of PARP Inhibitors in Cancer Biology and Therapy. *Curr Med Chem*. 2012;19:3907-3921. doi:10.1016/j.biotechadv.2011.08.021.Secreted.

654. Cortes JE, Heidel FH, Heuser M, et al. A Phase 2 Randomized Study of Low Dose Ara-C with or without Glasdegib (PF-04449913) in Untreated Patients with Acute Myeloid Leukemia or High-Risk Myelodysplastic Syndrome. In: *58th ASH Annual Meeting*. ; 2016:99.

655. https://clinicaltrials.gov/ct2/show/NCT01826214.

656. Leonard SM, Perry T, Woodman CB, Kearns P. Sequential treatment with cytarabine and decitabine has an increased anti-leukemia effect compared to cytarabine alone in xenograft models of childhood acute myeloid leukemia. *PLoS One*. 2014;9(1). doi:10.1371/journal.pone.0087475.

657. Dos Santos C, Mcdonald T, Ho YW, et al. The Src and c-Kit kinase inhibitor dasatinib enhances p53-mediated targeting of human acute myeloid leukemia stem cells by chemotherapeutic agents. *Blood*. 2013;122(11):1900-1913. doi:10.1182/blood-2012-11-466425.

658. Walter RB, Laszlo GS, Lionberger JM, et al. Heterogeneity of clonal expansion and maturation-linked mutation acquisition in hematopoietic progenitors in human acute myeloid leukemia. *Leukemia*. 2014;28(10):1969-1977. doi:10.1038/leu.2014.107.

659. Saito Y, Uchida N, Tanaka S, et al. Induction of cell cycle entry eliminates human leukemia stem cells in a mouse model of AML. *Nat Biotechnol*. 2010;28(3):275-280. doi:10.1038/nbt.1607.

660. Feuring-Buske M, Gerhard B, Cashman J, Humphries RK, Eaves CJ, Hogge DE. Improved engraftment of human acute myeloid leukemia progenitor cells in beta 2-microglobulin-deficient NOD/SCID mice and in NOD/SCID mice transgenic for human growth factors. *Leukemia*. 2003;17(4):760-763. doi:10.1038/sj.leu.2402882.

661. Zhou J, Quinlan M, Hurh E, Sellami D. Exposure-Response Analysis of Sonidegib (LDE225), an Oral Inhibitor of the Hedgehog Signaling Pathway, for Effectiveness and Safety in Patients With Advanced Solid Tumors. *J Clin Pharmacol*. 2016:1406-1415. doi:10.1002/jcph.749.

662. Yoshida H, Kondo M, Ichihashi T, et al. A novel myeloid cell line, Marimo, derived from therapy-related acute myeloid leukemia during treatment of essential thrombocythemia: Consistent chromosomal abnormalities and temporary C-MYC gene amplification. *Cancer Genet Cytogenet*. 1998;100(1):21-24. doi:10.1016/S0165-4608(97)00017-4.

663. https://www.ucl.ac.uk/ich/services/lab-services/FCCF/protocols/g0_g1_separation.

664. Watt SM, Chan JY-H. CD164 - A novel sialomucin on CD34+ cells. *Leuk Lymphoma*. 2000;37(1-2):1-25. doi:10.3109/10428190009057625.

665. Kollmann K, Nangalia1 J, Warsch W, et al. MARIMO cells harbor a CALR mutation but are not dependent on JAK2/STAT5 signaling. *Leukemia*. 2015;(29):494–497.

666. van der Kolk DM, de Vries EG, van Putten WJ, et al. P-glycoprotein and multidrug resistance protein activities in relation to treatment outcome in acute myeloid leukemia. *Clin Cancer Res*. 2000;6(8):3205-3214.

667. de Jonge-Peeters SD, Kuipers F, de Vries EG, Vellenga E. ABC transporter expression in hematopoietic stem cells and the role in AML drug resistance. *Crit Rev Oncol Hematol*.

2007;62(3):214-226. doi:S1040-8428(07)00036-4 [pii]\r10.1016/j.critrevonc.2007.02.003.

668. Li HY, Appelbaum FR, Willman CL, Zager RA, Banker DE. Cholesterol-modulating agents kill acute myeloid leukemia cells and sensitize them to therapeutics by blocking adaptive cholesterol responses. *Blood*. 2003;101(9):3628-3634. doi:10.1182/blood-2002-07-2283.

669. Banker DE, Mayer SJ, Li HY, Willman CL, Appelbaum FR, Zager RA. Cholesterol synthesis and import contribute to protective cholesterol increments in acute myeloid leukemia cells. *Blood*. 2004;104(6):1816-1824. doi:10.1182/blood-2004-01-0395.

670. Peeters SDPWM, van der Kolk DM, de Haan G, et al. Selective expression of cholesterol metabolism genes in normal CD34+CD38- cells with a heterogeneous expression pattern in AML cells. *Exp Hematol*. 2006;34(5):622-630. doi:10.1016/j.exphem.2006.01.020.

671. Opferman JT, Iwasaki H, Ong CC, et al. Obligate role of anti-apoptotic MCL-1 in the survival of hematopoietic stem cells. *Sci (New York, NY)*. 2005;307(5712):1101-1104. doi:10.1126/science.1106114.

672. Jamil S, Mojtabavi S, Hojabrpour P, Cheah S, Duronio V. An essential role for MCL-1 in ATR-mediated CHK1 phosphorylation. *Mol Biol Cell*. 2008;19(8):3212-3220. doi:10.1091/mbc.E07-11-1171.

673. JAMIL S, SOBOUTI R, HOJABRPOUR P, RAJ M, KAST J, DURONIO V. A proteolytic fragment of Mcl-1 exhibits nuclear localization and regulates cell growth by interaction with Cdk1. *Biochem J*. 2005;387(3):659-667. doi:10.1042/BJ20041596.

674. Eimani BG, Sanati MH, Houshmand M, Ataei M, Akbarian F, Shakhssalim N. Expression and prognostic significance of Bcl-2 and Bax in the progression and clinical outcome of transitional bladder cell carcinoma. *Cell J*. 2014;15(4):356-363.

675. Khodapasand E, Jafarzadeh N, Farrokhi F, Kamalidehghan B, Houshmand M. Is Bax/Bcl-2 ratio considered as a prognostic marker with age and tumor location in colorectal cancer? *Iran Biomed J*. 2015;19(2):69-75. doi:10.6091/ibj.1366.2015.

676. Catz SD, Johnson JL. Transcriptional regulation of bcl-2 by nuclear factor kappa B and its significance in prostate cancer. *Oncogene*. 2001;20(50):7342-7351. doi:10.1038/sj.onc.1204926.

677. Willimott S, Wagner SD. Post-transcriptional and post-translational regulation of Bcl2. *Biochem Soc Trans*. 2010;38(6):1571-1575. doi:10.1042/BST0381571.

678. Vogel C, Marcotte EM. Insights into the regulation of protein abundance from proteomic and transcriptomic analyses. *Nat Rev Genet*. 2012;13(4):227-232. doi:10.1038/nrg3185.

679. Doshi JM, Tian D, Xing C. Structure−Activity Relationship Studies of Ethyl 2-Amino-6-bromo-4-(1-cyano-2-ethoxy-2-oxoethyl)-4 *H* -chromene-3-carboxylate (HA 14-1), an Antagonist for Antiapoptotic Bcl-2 Proteins To Overcome Drug Resistance in Cancer. *J Med Chem*. 2006;49(26):7731-7739. doi:10.1021/jm060968r.

680. Zeitlin BD, Joo E, Dong Z, et al. Antiangiogenic effect of TW37, a small-molecule inhibitor of Bcl-2. *Cancer Res*. 2006;66(17):8698-8706. doi:10.1158/0008-5472.CAN-05-3691.

681. Wang G, Nikolovska-Coleska Z, Yang C-Y, et al. Structure-based design of potent small-molecule inhibitors of anti-apoptotic Bcl-2 proteins. *J Med Chem*. 2006;49(21):19-22. doi:10.1021/jm060460o.

682. Pan R, Hogdal LJ, Benito JM, et al. Selective BCL-2 inhibition by ABT-199 causes on-target cell death in acute myeloid Leukemia. *Cancer Discov*. 2014;4(3):362-675. doi:10.1158/2159-8290.CD-13-0609.

683. Lin, T., Strickland, S. A., Fiedler, W., Walter, R.B., Hou, J.-Z., Roboz, G.J., Enjeti, A., Fakhoui, K.M., Darden D.e., Dunbar, M., Zhu, M., Hayslip, J.W., Wei AH. Phase Ib/2 study of venetoclax with low-dose cytarabine in treatment-naive patients age ≥ 65 with acute myelogenous leukemia. *J Clin Oncol*. 2016;34(suppl; abstr 7007):oral presentation. doi:10.1200/JCO.2016.34.15_suppl.7007.

684. Kaufmann SH, Karp JE, Svingen PA, et al. Elevated expression of the apoptotic regulator Mcl-1 at the time of leukemic relapse. *Blood*. 1998;91(3):991-1000. doi:10.1002/1097-0142(19940415)73:8<2013::aid-cncr2820730802>3.0.co.

685. Khaw SL, Mérino D, Anderson MA, et al. Both leukaemic and normal peripheral B lymphoid cells are highly sensitive to the selective pharmacological inhibition of prosurvival Bcl-2 with ABT-199.

Leukemia. 2014;28(6):1207-1215. doi:10.1038/leu.2014.1.

686. Al-harbi S, Hill BT, Mazumder S, et al. An antiapoptotic BCL-2 family expression index predicts the response of chronic lymphocytic leukemia to ABT-737. *Blood*. 2011;118(13):3579-3590. doi:10.1182/blood-2011-03-340364.

687. Merino D, Khaw SL, Glaser SP, et al. Bcl-2, Bcl-x L, and Bcl-w are not equivalent targets of ABT-737 and navitoclax (ABT-263) in lymphoid and leukemic cells. *Blood*. 2012;119(24):5807-5816. doi:10.1182/blood-2011-12-400929.

688. Blagosklonny M V. Unwinding the loop of Bcl-2 phosphorylation. *Leukemia*. 2001;15(6):869-874. doi:10.1038/sj.leu.2402134.

689. Ruvolo PP, Deng X, May WS. Phosphorylation of Bcl2 and regulation of apoptosis. *Leuk Off J Leuk Soc Am Leuk Res Fund, UK*. 2001;15:515-522. doi:10.1038/sj.leu.2402090.

690. Song T, Chai G, Liu Y, Yu X, Wang Z, Zhang Z. Bcl-2 phosphorylation confers resistance on chronic lymphocytic leukaemia cells to the BH3 mimetics ABT-737, ABT-263 and ABT-199 by impeding direct binding. *Br J Pharmacol*. 2016;173(3):471-483. doi:10.1111/bph.13370.

691. Cang S, Iragavarapu C, Savooji J, Song Y, Liu D. ABT-199 (venetoclax) and BCL-2 inhibitors in clinical development. *J Hematol Oncol*. 2015;8:129. doi:10.1186/s13045-015-0224-3.

692. Chao JR, Wang JM, Lee SF, et al. mcl-1 is an immediate-early gene activated by the granulocyte-macrophage colony-stimulating factor (GM-CSF) signaling pathway and is one component of the GM-CSF viability response. *Mol Cell Biol*. 1998;18(8):4883-4898. http://www.pubmedcentral.nih.gov/articlerender.fcgi?artid=109073&tool=pmcentrez&rendertype=abstract.

693. Jourdan M, De Vos J, Mechti N, Klein B. Regulation of Bcl-2-family proteins in myeloma cells by three myeloma survival factors: interleukin-6, interferon-alpha and insulin-like growth factor 1. *Cell Death Differ*. 2000;7:1244-1252. doi:10.1038/sj.cdd.4400758.

694. Wang JM, Chao JR, Chen W, Kuo ML, Yen JJ, Yang-Yen HF. The antiapoptotic gene mcl-1 is up-regulated by the phosphatidylinositol 3-kinase/Akt signaling pathway through a transcription factor complex containing CREB. *Mol Cell Biol*. 1999;19(9):6195-6206. doi:10.1128/MCB.19.9.6195.

695. Akgul C, Turner PC, White MR, Edwards SW. Functional analysis of the human MCL-1 gene. *Cell Mol Life Sci*. 2000;57(4):684-691. doi:10.1007/PL00000728.

696. Eghtedar A, Verstovsek S, Estrov Z, et al. Phase 2 study of the JAK kinase inhibitor ruxolitinib in patients with refractory leukemias, including postmyeloproliferative neoplasm acute myeloid leukemia. *Blood*. 2012;119(20):4614-4618. doi:10.1182/blood-2011-12-400051.

697. Hemann MT, Lowe SW. The p53–Bcl-2 connection. *Cell Death Differ*. 2006;13(8):1256-1259. doi:10.1038/sj.cdd.4401962.

698. Lessene G, Czabotar PE, Colman PM. BCL-2 family antagonists for cancer therapy. *Nat Rev Drug Discov*. 2008;7(12):989-1000. doi:10.1038/nrd2658.

699. Mohammad RM, Goustin AS, Aboukameel A, et al. Preclinical studies of TW-37, a new nonpeptidic small-molecule inhibitor of Bcl-2, in diffuse large cell lymphoma xenograft model reveal drug action on both Bcl-2 and Mcl-1. *Clin Cancer Res*. 2007;13(7):2226-2235. doi:10.1158/1078-0432.CCR-06-1574.

700. Wang JL, Liu D, Zhang ZJ, et al. Structure-based discovery of an organic compound that binds Bcl-2 protein and induces apoptosis of tumor cells. *Proc Natl Acad Sci U S A*. 2000;97(13):7124-7129. doi:10.1073/pnas.97.13.7124.

701. Klanova M, Andera L, Soukup J, et al. MCL1 targeting agent homoharringtonine exerts strong cytotoxicity towards diffuse large B-cell lymphoma (DLBCL) cells and synergizes with BCL2 targeting agent ABT199 in eliminating BCL2-positive DLBCL cells. *Blood*. 2014;124(21):3645–5.

702. Bodo J, Zhao X, Smith MR, Hsi ED. Activity of ABT-199 and Acquired Resistance in Follicular Lymphoma Cells. *Blood*. 2014;124(21):3635-3635. http://www.bloodjournal.org/content/124/21/3635%0Ahttp://www.bloodjournal.org/content/124/21/3635?sso-checked=true.

703. Ito T, Deng X, Carr B, May WS. Bcl-2 phosphorylation required for anti-apoptosis function. *J Biol Chem*. 1997;272(18):11671-11673. doi:10.1074/jbc.272.18.11671.

704. Wei A, Strickland SA, Roboz GJ, et al. Safety and Efficacy of Venetoclax Plus Low-Dose Cytarabine in Treatment-Naive Patients Aged ≥65 Years with Acute Myeloid Leukemia. *Blood*. 2016;128(22):102 LP-102. http://www.bloodjournal.org/content/128/22/102.abstract.

705. Cragg MS, Harris C, Strasser A, Scott CL. Unleashing the power of inhibitors of oncogenic kinases through BH3 mimetics. *Nat Rev Cancer*. 2009;9(5):321-326. doi:10.1038/nrc2615.

706. Longo DL. Cancer-Drug Discovery — Let's Get Ready for the Next Period. *N Engl J Med*. 2014;371(23):2227-2228. doi:10.1056/NEJMe1412624.

707. Lancet JE. New agents: Great expectations not realized. *Best Pract Res Clin Haematol*. 2013;26(3):269-274. doi:10.1016/j.beha.2013.10.0076.

708. https://www.fda.gov/newsevents/newsroom/pressannouncements/ucm455862.htm.

709. http://www.fda.gov/NewsEvents/Newsroom/PressAnnouncements/ucm289545.htm.

710. Pietanza MC, Litvak AM, Varghese AM, et al. A phase I trial of the Hedgehog inhibitor, sonidegib (LDE225), in combination with etoposide and cisplatin for the initial treatment of extensive stage small cell lung cancer. *Lung Cancer*. 2016;99:23-30. doi:10.1016/j.lungcan.2016.04.014.

711. http://www.isrctn.com/ISRCTN78449203.

712. Burnett AK, Russell NH, Hills RK, et al. Optimization of chemotherapy for younger patients with acute myeloid leukemia: results of the medical research council AML15 trial. *J Clin Oncol*. 2013;31(27):3360-3368. doi:10.1200/JCO.2012.47.4874.

713. Burnett AK, Russell NH, Hills RK, et al. A randomized comparison of daunorubicin 90 mg/m^2 vs 60 mg/m^{2}in AML induction: Results from the UK NCRI AML17 trial in 1206 patients. *Blood*. 2015;125(25):3878-3885. doi:10.1182/blood-2015-01-623447.

714. https://www.fda.gov/Drugs/InformationOnDrugs/ApprovedDrugs/ucm569482.htm.

715. Lancet JE, Uy GL, Cortes JE, et al. Final results of a phase III randomized trial of CPX-351 versus 7+3 in older patients with newly diagnosed high risk (secondary) AML. *J Clin Oncol*. 2016;34(15_suppl):7000. doi:10.1200/JCO.2016.34.15_suppl.7000.

716. Stone RM, Mandrekar SJ, Sanford BL, et al. *Midostaurin plus Chemotherapy for Acute Myeloid Leukemia with a FLT3 Mutation*.; 2017. doi:10.1056/NEJMoa1614359.

717. Godwin CD, Gale RP, Walter RB. Gemtuzumab ozogamicin in acute myeloid leukemia. *Leukemia*. 2017. doi:10.1038/leu.2017.187.

718. Tardi P, Johnstone S, Harasym N, et al. In vivo maintenance of synergistic cytarabine:daunorubicin ratios greatly enhances therapeutic efficacy. *Leuk Res*. 2009;33(1):129-139. doi:10.1016/j.leukres.2008.06.028.

719. Estey EH, Thall PF. New designs for phase 2 clinical trials. *Blood*. 2003;102(2):442-448. doi:10.1182/blood-2002-09-2937.

720. Hills RK, Burnett AK. Applicability of a "Pick a Winner" trial design to acute myeloid leukemia. *Blood*. 2011;118(9):2389-2394. doi:10.1182/blood-2011-02-337261.

721. The Cancer Genome Atlas Research Network. Genomic and epigenomic landscapes of adult de novo acute myeloid leukemia. *N Engl J Med*. 2013;368(22):2059-2074.

722. Schmitt MW, Loeb LA, Salk JJ. The influence of subclonal resistance mutations on targeted cancer therapy. *Nat Rev Clin Oncol*. 2015;13(6):335-347. doi:10.1038/nrclinonc.2015.175.

723. Almeidaa A, Ramosb F. Acute myeloid leukemia in the older adults. *Leuk Res Rep*. 2016;6:1–7.

724. Thol F, Schlenk RF, Heuser M, Ganser A. How I treat refractory and early relapsed acute myeloid leukemia. *Blood*. 2015;126(3):319-327. doi:10.1182/blood-2014-10-551911.

725. Kandoth C, McLellan MD, Vandin F, et al. Mutational landscape and significance across 12 major cancer types. *Nature*. 2013;502(7471):333-339. doi:10.1038/nature12634.

726. Papaemmanuil E, Gerstung M, Bullinger L, et al. Genomic Classification and Prognosis in Acute Myeloid Leukemia. *N Engl J Med*. 2016;374(23):2209-2221. doi:10.1056/NEJMoa1516192.

727. Grimwade D, Vyas P, Freeman S. Assessment of minimal residual disease in acute myeloid leukemia. *Curr Opin Oncol*. 2010;22(6):656-663. doi:10.1097/CCO.0b013e32833ed831.

728. Van Rhenen A, Van Dongen GAMS, Kelder A Le, et al. The novel AML stem cell-associated antigen CLL-1 aids in discrimination between normal and leukemic stem cells. *Blood*. 2007;110(7):2659-2666. doi:10.1182/blood-2007-03-083048.

729. Hosen N, Park CY, Tatsumi N, et al. CD96 is a leukemic stem cell-specific marker in human acute myeloid leukemia. *Proc Natl Acad Sci U S A*. 2007;104(26):11008-11013. doi:10.1073/pnas.0704271104.

730. Jaiswal S, Jamieson CHM, Pang WW, et al. CD47 Is Upregulated on Circulating Hematopoietic Stem Cells and Leukemia Cells to Avoid Phagocytosis. *Cell*. 2009;138(2):271-285. doi:10.1016/j.cell.2009.05.046.

731. Majeti R, Chao MP, Alizadeh AA, et al. CD47 Is an Adverse Prognostic Factor and Therapeutic Antibody Target on Human Acute Myeloid Leukemia Stem Cells. *Cell*. 2009;138(2):286-299. doi:10.1016/j.cell.2009.05.045.

732. Kikushige Y, Shima T, Takayanagi SI, et al. TIM-3 is a promising target to selectively kill acute myeloid leukemia stem cells. *Cell Stem Cell*. 2010;7(6):708-717. doi:10.1016/j.stem.2010.11.014.

733. Iwasaki M, Liedtke M, Gentles AJ, Cleary ML. CD93 Marks a Non-Quiescent Human Leukemia Stem Cell Population and Is Required for Development of MLL-Rearranged Acute Myeloid Leukemia. *Cell Stem Cell*. 2015;17(4):412-421. doi:10.1016/j.stem.2015.08.008.

734. Jan M, Snyder TM, Corces-Zimmerman MR, et al. Clonal evolution of preleukemic hematopoietic stem cells precedes human acute myeloid leukemia. *Sci Transl Med*. 2012;4(149):149ra118. doi:10.1126/scitranslmed.3004315.

735. Kikushige Y, Miyamoto T. TIM-3 as a novel therapeutic target for eradicating acute myelogenous leukemia stem cells. *Int J Hematol*. 2013;98(6):627-633. doi:10.1007/s12185-013-1433-6.

736. Vey N, Delaunay J, Martinelli G, et al. Phase I clinical study of RG7356, an anti-CD44 humanized antibody, in patients with acute myeloid leukemia. *Oncotarget*. 2016;7(22):32532-32542. doi:10.18632/oncotarget.8687\r8687 [pii].

Appendix 1

UPN	Sex	Age	WHO Subtype	Mut^{n}	Gene	IHC	*SMO* Seq	NGS	ICC
1A	F	57	AML NOS	*FLT3-ITD*	Y	Y	Y	Y	Y
1B	F	43	AML NOS	*FLT3-ITD, NPM1*	Y	Y	Y	Y	Y
1E	M	75	AML NOS	N/A	Y	Y	Failed	Failed	Y
1F	F	60	AML NOS	*FLT3-ITD, NPM1*	Y	Y	Y	Y	Y
1G	M	72	AML NOS	NONE	Y	Y			Y
1H	F	26	AML NOS	N/A	Y	Y	Y		Y
1K	F	81	AML NOS	NONE	Y	Y	Y	Y	Y
1L	F	84	AML NOS	N/A	Y	Y	Y	Y	Y
1N	M	87	AML NOS	NONE	Y	Y	Y	Y	Y
31	M	34	AML NOS	*BCR-ABL*	Y	Y	Y	Y	Y
32	F	49	AML NOS	*FLT3-ITD, NPM1*	Y	Y	Y	Y	Y
33	M	80	AML NOS	*NPM1, CEBPa*	Y	Y			Y
6	F	63	AML NOS	NONE	Y	Y	Y		
7	M	43	AML NOS	*FLT3-D835*	Y	Y	Y	Y	
8	M	51	AML NOS	NONE	Y	Y	Y		Y
15	M	71	AML NOS	*NPM1*	Y	Y	Y		
16	M	57	AML NOS	*FLT3-ITD*	Y	Y	Y	Y	
18	F	46	AML NOS	*FLT3-D835*	Y	Y	Y	Y	
1J	F	60	AML - MDS	NONE	Y	Y	Y	Y	Y
1	F	72	AML - MDS	NONE	Y	Y	Y	Y	Y
4	M	65	AML - MDS	NONE	Y	Y		Y	
5	F	73	AML - MDS	*FLT3-ITD*	Y	Y	Failed	Failed	
19	F	72	t-AML	NONE	Y	Y	Y	Y	Y
20	F	86	t-AML	N/A	Y	Y	Y	Y	
22	F	75	t-AML	NONE	Y	Y	Y		
23	M	79	t-AML	N/A	Y	Y	Y	Y	
1M	M	73	AML - R	*PML-RARA*	Y	Y			Y
27	M	72	AML - R	*PML-RARA*	Y	Y	Y	Y	
28	M	76	AML - R	*PML-RARA*	Y	Y	Y	Y	
29	F	63	AML - R	*PML-RARA*	Y		Y	Y	
34	F	42	AML - R	*inv16*	Y	Y	Y	Y	
1D	M	57	AML - R	*MLLT3-KMT2A*	Y	Y	Y	Y	Y
1C	F	37	AML MLL	N/A	Y		Y	Y	Y
1E	F	30	AML MLL	N/A	Y	Y			Y
36	F	60	AML – R	*PML-RARA*	Y		Y	Y	
10	F		AML NOS	N/A	Y		Y		
12	M	67	AML NOS	N/A	Y		Y		
25	M	52	AML – R	*BCR-ABL, RUNX1/RUNXT1*	Y		Y		
1M	F	65	N/A	N/A	Y	Y			Y
14	M	84	AML NOS	N/A	Y		Y	Y	Y
30	M	65	AML NOS	N/A	Y	Y	Y	Y	Y
34	F	57	AML – R	*RUNX1/RUNXT1*	Y	Y	Y	Y	Y
36	M	43	AML NOS	N/A	Y		Y	Y	Y
1P	F	75	AML – R	*CBFB-MYH11*	Y		Y		
AML36	M	78	AML – R	*RUNX1/RUNXT1*	Y			Y	
AML51	M	59	AML NOS	N/A				Y	
AML40	F	66	AML NOS	N/A	Y			Y	
AML53	N/A	N/A	AML NOS	N/A				Y	
AML47	M	58	N/A	N/A				Y	
AML35	M	44	N/A	N/A	Y			Y	
AML12	F	66	AML - MDS	N/A	Y			Y	
AML009	N/A	N/A	N/A	N/A	Y				
AML31	F	57	t-AML	N/A	Y				
AML18	N/A	N/A	AML NOS	N/A	Y			Y	
AML005	N/A	N/A	AML NOS	N/A	Y				
AML43	M	67	AML NOS	N/A	Y				
AMLAMcG	N/A	N/A	N/A	N/A	Y			Y	
AML27	N/A	N/A	AML NOS	N/A	Y				
AMLAG50	N/A	N/A	N/A	N/A	Y			Y	
AML22	N/A	N/A	N/A	N/A	Y				

AML1002	N/A	N/A	AML NOS	N/A	Y				
AML008	N/A	N/A	AML NOS	N/A	Y				
AML011	N/A	N/A	N/A	N/A	Y			Y	
AML013	N/A	N/A	AML NOS	FLT3-ITD	Y			Y	
AML014	N/A	N/A	AML NOS	N/A	Y				
AML015	N/A	N/A	AML NOS	N/A	Y				
AML016	N/A	N/A	N/A	N/A	Y			Y	
AML017	N/A	N/A	N/A	N/A	Y			Y	
AML019	F	47	AML – R	PML-RARA	Y				
AML020ER	N/A	N/A	N/A	N/A	Y				
AML021	N/A	N/A	AML NOS	N/A	Y			Y	
AML020WM	N/A	N/A	AML NOS	N/A	Y				
AML023	N/A	N/A	AML - MDS	N/A	Y			Y	
AML024	N/A	N/A	N/A	N/A	Y			Y	
AML025	N/A	N/A	AML - MDS	N/A	Y			Y	
AML027DA	N/A	N/A	N/A	N/A					
AML028RR	N/A	N/A	N/A	N/A					
AML029LB	F	52	AML NOS	N/A					
AML030	F	35	AML – R	RUNX1/RUNX1T1	Y			Y	
AML032	N/A	N/A	AML NOS	N/A	Y				
AML034	N/A	N/A	N/A	N/A	Y			Y	
AML037	N/A	N/A	N/A	N/A					
AML044JR	N/A	N/A	AML NOS	N/A	Y				
AML045JS	F	82	AML NOS	N/A					

UPN	Treatment	Cytogenetics-diagnosis	Cytogenetics - relapse
1A	AML 17 – DA (90) cytarabine - remission after #1. Died 28/05/14 multi organ failure - liver/neuro/resp/sepsis	46,XX,add(11)(?p15)[3]/46,XX[17]	N/A
1B	AML 17 - DA (90) cytarabine - remission after #1. CEP 701 randomisation. VUD allogeneic PBSCT 08/12. Chronic GVHD - extracorporeal photophoresis. In remission.	46,XX	N/A
1E	2003- prostate Ca - treated with radiotherapy, then zoladex - bony mets 2011. DA - suboptimal response, switched to low dose cytarabine (20mg BD) - completed 6 cycles - dx grew threw - palliative. Died 05/2012.	46,XY,del(8)(p?21),add(21)(q22)[12]/46,XY[3]	N/A
1F	AML 17 - high-risk arm (ADE) - RIC allogeneic PBSCT 27/1/11 relapsed D100 (20/5/2011). Died 05/2011.	46,XX	46,XX,?der(4)?t(4;15)(?p16;?q21),del(9)?(?q13)[3]/46,XX[17]
1G	AML 16 trial - DA + Gemtuzomab - CR after #1. Died.	48~50,XY,+6,del(11)(q23),add(16)(?p),+2~3mar[cp7]	N/A
1H	AML 17 - ADE + Myelotarg 6 - CR #1. Remission 3 years out.	47,XX,+8. Additional 5'MLL signal	N/A
1K	Not fit for treatment. Died 07/2010.	49,XX,+8,+8,+20[21]	N/A
1L	Supportive care - spontaneous remission 07/2014. Remains in remission.	46,XX	N/A
1N	Supportive care. Died 04/2012.	46,XY	N/A
31	AML 17 - high dose DA (90) then consented to high-risk arm - CR #1. VUD allo PBSCT 03/2012. Remains in remission.	51,XY,+4,+6,+8,t(9;22)(q34;q11.2),+10,+13	N/A
32	AML 17 - 2xDA60; 2high dose AraC - CR#1. Relapsed 5/12 - FLAG-IDA, VUD PBSCT 05/2014 - relapsed during transplant. Died 07/2014.	46,XX	46,XX,ins(15;17)(q22;q21q2?3)
33	Declined palliative chemotherapy. Died 05/2013.	45,X,-Y[7]/46,XY[13]	N/A
6	AML 17 – DA (90) - CR #1 (4% blasts) subsequently stratified as high risk (DCLO). VUD PBSCT 12/2012. Remains in remission.	46,XY	N/A
7	AML 17 - DA - CR #1. Relapsed 8/12 - FLAG-IDA, MIDA - second CR. VUD PBSCT 04/2014. 07/2014 PTLPD - Rituximab.	46,XX	46,XX,add(3)(p1?),add(11)(p15.?)[cp6]/46,XX[24]
8	AML 17 - high-risk arm (ADE) + Gemtuzimab (6) - CR #1 (5%balsts). Metastatic colorectal Ca 05/2011. Died 06/2011.	46,XY,?i(1)(q10),-8,add(11)(q2?1),add(12)(q2?1),add(17)(q25),del(19)(p13),+mar	N/A
15	AML 16 - intensive (ADE + ATRA) - failed to obtain CR after #2. Died large intracranial bleed - 02/2012.	46,XY	N/A
16	Died 12/2011 sepsis/multiorgan failure.	39~41,XY,del(1)(q?21q?42),?t(1;2)(q?13;q33),add(2)p?23),?t(3;21)(p1?4;q?21),add(4)(q?22),-5,add(6)(q?24),-	N/A

		7,?add(8)(p?21),add(9)(p?13),add(11)(p1?),-14,add(14)(p1?),-16,-17,?t(17;22)(p?11;q?11),-18,add(18)(q?22),-20,-21,-22,add(22)(q?22),+2~4mar,+dm[12]	
18	Off trial - 2xADE; high dose cytarabine - CR#1. RIC PBSCT 11/2010. Remission 4 years out.	46,XY	N/A
1J	Off trial - DA - failed to obtain CR after #1 - palliative. Died 05/2010.	49,XX,+8,+12,?del(18)(q?) +20,-21,+mar[3]	N/A
1	DA - CR#1. Marked cardiac toxicity - maintenance chemo - low dose AraC (30 # to date)	46,XX	N/A
4	DA - failed to obtain CR after #1. Matched PBSCT 12/2010. Died 01/2011 - multiorgan failure.	47,XX,+8[20]	N/A
5	Evolved from CMML-2. Low dose AraC. Died 04/2013.	46,XY[20]	47,XY,+X[9]/46,XY[11]
19	AML 17 - DA (60) - CR #1. Very frail post #1 - long delay - started low dose AraC 11/2012. Died 04/2014.	46,XX[20]	46,XX,del(7)(q32)[5]/46,XX[15
20	Died, no further information available.	45~46,XX,-7,del(7)(q22q35),i(17)(q10)[cp17]/46,XX[3]	N/A
22	Azacitidine (7#). Died 09/2013.	46,XX	N/A
23	No information available.	47,XY +8[1] /46,XY[19]	N/A
1M	AML 17 - Idarubicin + ATRA - CR #1. Remains in remission.	46,XY,t(15;17)(q22;q21)[10]/47,XY,t(15;17)(q22;q21),+8[3]/46,XY[4]	N/A
27	AML 17 - Idarubicin + ATRA. Died.	Sample failed	N/A
28	AML 17 - ATRA + arsenic trioxide - CR #1. Remains in remission.	46,XY,t(15;17)(q22;q1?)[3]/46,XY[17]	N/A
29	No information available.	46,XY,t(15;17)(q22;q21)[4]/46,XY[16]	N/A
34	AML 17 - DA - CR #1. Remains in remission.	46~48,XX,del(7)(q3?),inv(16)(p13.1q22),+20,+22[cp20]	N/A
1D	AML 17 - CR #1 - ADE, DClo. Sibling donor allogeneic PBSCT 03/2011. Increasing percentage host derived T cells - 05/2012 - relapsed 06/2012 - chemo + DLI 11/2012 second CR. GVHD lungs. Died GVHD 12/2013.	46,XY,add(11)(q23)[5]/46,XY[15]	N/A
1C	2xDA, 2x high dose AraC, ICE - morphological remission #1; FISH remission #3. VUD 11/2009 (not in MR at time of transplant) - MR and 100% donor chimerism. cGVHD. Relapse 5/12 post transplant. Supportive care. Died 08/2010.	46,XX,t(6;11)(q27;q23)[7]/46,XX[13]	N/A
1E	AML 17 – DA (90) - CR #1. (2xDA, 1xhigh dose AraC) - MR but unquantifiable levels AML ETO transcript. Remains in remission.	46,XX,t(8;21)(q22;q22)[14]/46,XX[6]	N/A
36	AML 17 - DA + Gemtuzumab - CR #1. Completed tx 12/2013. Remains in remission.	N/A	N/A
10	AML 17 – DA (90) - 10% after #1; CR#2.	46,XX	N/A
12	AML 17 - ATRA + arsenic - CR #1. Remains in remission 4 years out.	46,XY,del(7)(q3?5),t(15;17)(q22;q2?1)[12]/46,XY[2]	N/A
25	CR #1.	46,XY	N/A
1M	Died 08/2011 with sepsis.	46,XX,del(5)(q1?3),der(11)t(11;13)(q2?3;q1?2),del(12)(p13),-13,-17,-18,+21,+2~6mar,inc[cp10]	N/A
14	AML 16 intensive - DA - CR #1. Stopped after 2# (06/2010) due to sepsis and poor count recovery. Relapsed 11/2010. Died 12/2010.	46,XY	N/A
30	AML 17 - CR #1 but +RTPCR. Relapsed 10/2012 - int chemo (?FLAG-IDAx3). Sib allo RIC PBSCT 04/2013 - CR, low level + RTPCR. Cranial relapse - IT chemo - stopped 04/2014 due to progression. Died 05/2014 - intracerebral AML.	46,XY,t(8;21)(q22;q22),del(9)(q2?1.11q2?2)[cp14]	N/A
34	AML 15 - CR. CNS Relapse 05/2006 MUD PBSCT 09/2006. Died 12/2006.	46,XY,t(8;21)(q22;q22)[14]	N/A
36	AML 15 - CR #1. Relapsed 2005 post all PBSCT. Died	49,XY,+9,+14,inv(16)	46,XY,inv(16)(p13;q2

	11/2005.	(p13;q22),+22[18]/46,XY[3]	2)[3]/46,XY[27]
1P	Died 01/2006 - multi organ failure.	N/A	
AML36	I cycle azacitidine. Died sepsis.	47 XY, +11[4]/46, XY[6].	N/A
AML51	DA, 1 cycle, no CR, then supportive care.	N, 46 XY, del(12)(p?11.2),add(14)(p11.1)	N/A
AML40	DA x1, WCC fell to 0.8, died during induction.	**46 XX**	N/A
AML53	N/A	N/A	N/A
AML47	RAvVA study, Aza+ vori. Alive.	46 XY	N/A
AML35	N/A	N/A	N/A
AML12	Previous MDS. FLAG IDA x1 – failed to achieve CR – died AML	46 XX	N/A
AML009	N/A	N/A	N/A
AML31	N/A	47 XX, +4[2]/48, idem, +10[3]/48, idem, der (2)?t(2,17(q37;q21), +10[8]/46,XX[2]	N/A
AML18	N/A	46 XY	N/A
AML005	N/A	N/A	N/A
AML43	Supportive care. Dead (AML and sepsis)	trisomy 9	N/A
AMLAMcG	N/A	N/A	N/A
AML27	N/A	N/A	N/A
AMLAG50	N/A	N/A	N/A
AML22	N/A	N/A	N/A
AML1002	N/A	N/A	N/A
AML008	N/A	N/A	N/A
AML011	N/A	N/A	N/A
AML013	N/A	N/A	N/A
AML014	N/A	N/A	N/A
AML015	N/A	N/A	N/A
AML016	N/A	N/A	N/A
AML017	AML 15 - CR #1. Relapsed 2005 post all PBSCT. Died 11/2005.	49,XY,+9,+14,inv(16)(p13;q22),+22[18]/46,XY[3]	46,XY,inv(16)(p13;q22)[3]/46,XY[27]
AML019	AML 17, Myelotarg, Arsenic and Atra, x4. CR 1. Alive	t(15,17)	N/A
AML020ER	N/A	N/A	N/A
AML021	N/A	N/A	N/A
AML020WM	AML 17 - CR #1 but +RTPCR. Relapsed 10/2012 - int chemo (?FLAG-IDAx3). Sib allo RIC PBSCT 04/2013 - CR, low level + RTPCR. Cranial relapse - IT chemo - stopped 04/2014 due to progression. Died 05/2014 - intracerebral AML.	46,XY,t(8;21)(q22;q22),del(9)(q2?1.11q2?2)[cp14]	N/A
AML023	N/A	N/A	N/A
AML024	N/A	N/A	N/A
AML025	N/A	N/A	N/A
AML027DA	AML 15 - CR. CNS Relapse 05/2006 MUD PBSCT 09/2006. Died 12/2006.	46,XY,t(8;21)(q22;q22)[14]	N/A
AML028RR	N/A	N/A	N/A
AML029LB	DAx2, HD AraC x1, AML17. CR1. Alive		N/A
AML030	FLAGX2, HD AraC x2, not in trial. CR1. Alive	45,X,-X, t(8,21)	N/A
AML032	AML17, DAx2, HD AraC x1. CR1. Alive	46 XX	N/A
AML034	N/A	N/A	N/A
AML037	N/A	N/A	N/A
AML044JR	N/A	N/A	N/A
AML045JS	Supportive care. Died.	46 XY	N/A

UPN, unique patient number; Mut^{n}, mutation(s) present at diagnosis; Gene, gene expression performed; IHC, IHC performed; *SMO* Seq, SMO Sequencing performed; NGS, Next-generation sequencing performed; ICC, ICC performed; AML-NOS, AML not otherwise specified; AML-MDS, AML with MDS related changes; t-AML, therapy related AML; AML-R, AML with recurrent abnormalities; N/A not available; Y, analysis performed.